

Talanta

The International Journal of Pure and Applied Analytical Chemistry

Editors-in-Chief

Professor G.D. Christian, University of Washington, Department of Chemistry, 36 Bagely Hall, P.O. Box 351700, Seattle, WA 98195-1700, U.S.A.

Professor J.-M. Kauffmann, Université Libre de Bruxelles, Institut de Pharmacie, Campus de la Plaine, C.P. 205/6, Boulevard du Triomphe, B-1050 Bruxelles, Belgium

Associate Editors

Professor J.-H. Wang, Research Center for Analytical Sciences, Northeastern University, Box 332, Shenyang 110004, China

Professor J.L. Burguera, Los Andes University, IVAQUIM, Faculty of Sciences, P.O. Box 542, 5101-A Mérida, Venezuela.

Assistant Editors

Dr R.E. Synovec, Department of Chemistry, University of Washington, Box 351700, Seattle, WA 98195-1700, U.S.A.

Professor J.-C. Vire, Université Libre de Bruxelles, Institut de Pharmacie, Campus de la Plaine, C.P. 205/6, Boulevard du Triomphe, B-1050 Bruxelles, Belgium

Talanta

R. Apak (Istanbul, Turkey)
E. Bakker (Auburn, AL, U.S.A.)
D. Barceló (Barcelona, Spain)
B. Birch (Luton, UK)
K. S. Booksh (Tempe, AZ, U.S.A.)
J.-L. Capelo-Martinez (Caparica, Portugal)
Z. Cai (Kowloon, Hong Kong)
S. Cosnier (Grenoble, France)
D. Diamond (Dublin, Ireland)
W. Frenzel (Berlin, Germany)
A.G. Gonzales (Seville, Spain)
E.H. Hansen (Lyngby, Denmark)
P. de B. Harrington (OH, U.S.A.)

A. Ho (Hsin-chu, Taiwan)
J. Kalivas (Pocatella, ID, U.S.A.)
B. Karlberg (Stockholm, Sweden)
J.-M. Lin (Beijing, China)
Y. Lin (Richland, WA, U.S.A.)
M.D. Luque de Castro (Cordoba, Spain)
I.D. McKelvie (Victoria, Australia)
S. Motomizu (Okayama, Japan)
D. Nacapricha (Bangkok, Thailand)
J.-M. Pingarron (Madrid, Spain)
E. Pretsch (Zürich, Switzerland)
W. Schuhmann (Bochum, Germany)
M. Shamsipur (Kermanshah, Iran)

M. Silva (Porto Alegre, Brazil)
P. Solich (Hradec Králové, Czech Republic)
K. Suzuki (Yokohama, Japan)
D.G. Themelis (Thessaloniki, Greece)
D.L. Tsalev (Sofia, Bulgaria)
Y. van der Heyden (Belgium)
B. Walczak (Katowice, Poland)
J. Wang (Tempe, AZ, U.S.A.)
J.D. Winefordner (Gainesville, U.S.A.)
Xiu-Ping Yan (Tianjin, China)
E.A.G. Zagatto (Piracicaba, SP, Brazil)

Copyright © 2008 Elsevier B.V. All rights reserved

Publication information: *Talanta* (ISSN 0039-9140). For 2008, volumes 74–76 are scheduled for publication. Subscription prices are available upon request from the Publisher or from the Regional Sales Office nearest you or from this journal's website (<http://www.elsevier.com/locate/talanta>). Further information is available on this journal and other Elsevier products through Elsevier's website: (<http://www.elsevier.com>). Subscriptions are accepted on a prepaid basis only and are entered on a calendar year basis. Issues are sent by standard mail (surface within Europe, air delivery outside Europe). Priority rates are available upon request. Claims for missing issues should be made within six months of the date of dispatch.

Orders, claims, and journal enquiries: please contact the Customer Service Department at the Regional Sales Office nearest you:

Orlando: Elsevier, Customer Service Department, 6277 Sea Harbor Drive, Orlando, FL 32887-480 USA; phone: (+1) (877) 8397126 [toll free number for US customers], or (+1) (407) 3454020 [customers outside US]; fax: (+1) (407) 3631354; e-mail: usjcs@elsevier.com

Amsterdam: Elsevier, Customer Service Department, PO Box 211, 1000 AE Amsterdam, The Netherlands; phone: (+31) (20) 4853757; fax: (+31) (20) 4853432; e-mail: nlinfo-f@elsevier.com

Tokyo: Elsevier, Customer Service Department, 4F Higashi-Azabu, 1-Chome Bldg, 1-9-15 Higashi-Azabu, Minato-ku, Tokyo 106-0044, Japan; phone: (+81) (3) 5561 5037; fax: (+81) (3) 5561 5047; e-mail: jp.info@elsevier.com

Singapore: Elsevier, Customer Service Department, 3 Killiney Road, #08-01 Winsland House I, Singapore 239519; phone: (+65) 63490222; fax: (+65) 67331510; e-mail: asiainfo@elsevier.com

USA mailing notice: *Talanta* (ISSN 0039-9140) is published monthly by Elsevier B.V. (P.O. Box 211, 1000 AE Amsterdam, The Netherlands). Annual subscription price in the USA US\$ 4,085 (valid in North, Central and South America), including air speed delivery. Application to mail at periodical postage rate is paid at Rathway, NJ and additional mailing offices.

USA POSTMASTER: Send address changes to *Talanta*, Publications Expediting Inc., 200 Meacham Avenue, Elmont, NY 11003.

AIRFREIGHT AND MAILING in the USA by Publications Expediting Inc., 200 Meacham Avenue, Elmont, NY 11003.

Short communication

Distinction and identification of lignins based on their volatile headspace composition

Silvia Maria Rocha^{a,*}, Virginia Gonçalves^a,
Dmitry Evtuguin^b, Ivonne Delgadillo^a

^a *Department of Chemistry, University of Aveiro, 3810-193 Aveiro, Portugal*

^b *CICECO, University of Aveiro, 3810-193 Aveiro, Portugal*

Received 29 June 2007; received in revised form 18 October 2007; accepted 7 November 2007

Available online 17 November 2007

Abstract

A new non-degradation methodology is proposed for the distinction and identification of lignins, according to their biological origin and/or isolation methodology, using an electronic aroma sensing system. The system, once trained with representative lignins, could quickly and objectively be used as a simple tool by providing, in real-time, information about the lignin origin, based on their headspace volatile composition. In order to understand which kind of volatile compounds are responsible to the different sensors response present in the headspace, lignins were also analysed by headspace-solid phase microextraction followed by gas chromatography–mass spectrometry detection mode (HS-SPME/GC–MS). Among volatile compounds in the lignin headspace were identified a series of aromatic compounds, C₁₄ to C₁₈ fatty acids and an isoprenoid, squalene. It was proposed that a small proportion of volatile degradation products emerged during the lignin partial degradation during the technogenic process (i.e. delignification) play a key role regarding the aroma sensor response.

© 2007 Elsevier B.V. All rights reserved.

Keywords: Electronic aroma sensing system; Lignin; Volatile components; Solid phase microextraction (SPME)

1. Introduction

The identification of the biological origin (structural type) of the lignins is a rather common task in the lignin chemistry. The distinction of the lignins based on the isolation methodology (technogenic origin) may be also important when this information is unavailable. Traditionally these tasks are resolved applying a series of labour and time-consuming analyses involving degradation techniques such as nitrobenzene [1], permanganate oxidation [2], and thioacidolysis [3]. The non-degradation techniques, such as NMR [4], RAMAN [5], and FTIR [6] are also widely applied. However, the researchers in the area know that different lignins, depending on their biological and technogenic origins, possess a characteristic aroma profile (smell). The aroma perceived by the olfactory system is due to the presence of volatile/semi-volatile molecules in the sample headspace, if they are in concentrations above their sen-

sory perception limit [7]. This fact stimulated our study on the identification and distinction of lignins based on their volatile headspace composition.

Nowadays, the electronic aroma sensing systems are widely used in the research aroma studies, by providing real-time analysis of a sample overall aroma and may also be applied as a simple quality control tool incorporated into the normal quality control procedures in the industry [8,9]. Solid phase microextraction (SPME) also appears as a suitable method for investigating volatile compounds. SPME is a sample preparation technique that is simple to use, relatively fast and does not require solvent extraction [10]. It has been successfully applied to a wide variety of compounds, in particular for the extraction of volatile and semi-volatile compounds from environmental, biological and food samples, since SPME is available with various sorbent materials and various coating thickness. Headspace (HS)-SPME coupled with a gas chromatography–mass spectrometry detection (GC–MS) was applied to the analysis of volatile organic compounds emitted from a lignin-containing materials [11], being vanillin and phenol reported as a volatile markers of the lignin degradation [11–13].

* Corresponding author. Tel.: +351 234401508; fax: +351 234370084.
E-mail address: smrocha@ua.pt (S.M. Rocha).

In this work was studied the electronic aroma sensing system (EASS) response to dioxane lignin preparations isolated from gymnosperm (spruce) and angiosperm (eucalypt) woods, as well as to gymnosperm (spruce) and angiosperm (poplar) lignins isolated from the liquors after the oxygen–organosolv delignification. The principal component analysis (PCA) was used to study the main sources of variability between the different lignins and to establish relationships between the sensors response and the lignins biological and/or technogenic origins. In order to explain the aroma profiles defined by EASS analyses, headspace volatile components of each lignin were identified using HS-SPME followed by GC–MS analyses.

2. Experimental

2.1. Materials

Dioxane lignins were isolated from *Eucalyptus globulus* L. (EGDL) and *Picea abies* L. (PADL) according to the procedure developed previously [14]. The aspen (*Populus tremula* L.—PTOAS) and spruce (*P. abies* L.—PAOAS) lignin samples were isolated from pulping liquor after the oxygen–organosolv pulping according to the published fractionation scheme [15]. Lignin samples contained low sugars content (<1.5%, w/w). The conditions for the pulping of spruce and aspen chips in the acetone–water (60:40, v/v) were as follows: temperature, 150 °C for spruce and 140 °C for aspen chips; time-to-temperature, 60 min; time-at-temperature, 230 min; liquor-to-wood ratio, 10; initial oxygen pressure, 1.5 MPa. All lignins were extracted with diethyl ether (liquor-to-ether ratio, 100) under reflux followed by the washing of samples with distilled water and vacuum drying at room temperature for 72 h.

2.2. Electronic aroma sensing system analysis

An AromaScan A32S/8S Labstation System (AromaScan plc., Crewe, UK) was used. This system comprises an analyzer (A32S) unit with a 32-element sensor array of conducting polymers, and a sample station (A8S). The latter generates reference air of known quality and humidity that is used to fill the vials containing the sample. The sensors are made of a polymer that changes its electrical resistance when a volatile compound adheres. The change in electrical resistance ($\Delta R/R$) of each sensor element is measured and all responses are converted into a normalized pattern of responses. Each sensor has a different characteristic response. The relative responses of individual sensors reflect the range of volatile compounds given off by a sample [8]. In order to promote the transference of the volatile and/or semi-volatile compounds from the sample to the headspace, each lignin (*ca.* 150 mg) was introduced in a glass vial and than was left to equilibrate for 90 min at 25 °C, in the A8S sample station. This procedure was repeated for all samples. The samples were then analysed on the unit A32S, using the 32 sensors. The following protocol for the valve sequence was established: reference 10 s, sample 90 s, wash 30 s and reference 30 s. The reference consisted of 10–12% RH air passed directly from the A8S sample station to the analyser (A32S). The purpose of this part of

the cycle is to avoid cross-contamination between successive samples. The effectiveness of the wash with butanol/water in the reduction of the cross-contamination of the sensors is controlled during the second reference step when the response of the sensors has to return to zero. The sample station provides a wash (vapour) source through the wash line at the rear of the instrument. A data set was produced for a period of acquisition of 30–60 s from the start of the acquisition. Three replicates were carried out for each sample. The system software includes data mapping tools and PCA. PCA, as an exploratory technique, allows the study of the main sources of variability present in the data sets [16], to detect clustering, and to establish relations between and among samples and sensors response.

2.3. HS-SPME/GC–MS analysis

The SPME holder for manual sampling and fibre used in the analyses were purchased from Supelco (Aldrich, Bellefonte, PA). The SPME fibre coated with 100 μm polydimethylsiloxane (PDMS) from Supelco (Bellefonte, PA, USA) was used. Polydimethylsiloxane is a liquid-type polymer, which extracts analytes via absorption [17]. The principle advantage of absorption extraction (partitioning) is a linear isotherm over a wide range of analyte and interference concentrations [18]. Fibre was conditioned at 260 °C during 2 h, prior to use. For headspace sampling, *ca.* 0.5 g of lignin was inserted into a 20 ml glass vial, which corresponds to a ratio of the volume of the liquid phase to the headspace volume ($1/\beta$) of 0.5. The vial was capped with a Teflon septum and an aluminium cap (Chromacol LTD), and was placed in a thermostated bath adjusted to 40 °C. The SPME fibre was manually inserted into the sample vial headspace for 90 min. Since headspace volume can be a critical factor determining the precision of the results in three-phase systems—liquid sample-headspace-fibre coating, vials from the same producer and lot were used. The SPME coating fibre containing the headspace volatile compounds was inserted into the GC injection port at 250 °C and kept for 15 min for the desorption. The injection port was lined with a 0.75 mm I.D. splitless glass liner. The desorbed volatile compounds were separated in a GC–MS Agilent Technologies 6890N Network gas chromatograph, equipped with a 30 m \times 0.32 mm I.D., 0.25 μm film thickness DB-FFAP fused silica capillary column (J&W Scientific Inc., Folsom, CA, USA), connected to an Agilent 5973 quadrupole mass selective detector. Splitless injection mode was used (5 min). The oven temperature was programmed from 35 °C (3 min) to 220 °C at 2 °C min^{-1} . The injector and the transfer line were heated at 250 °C and the He carrier gas had a flow of 1.7 mL min^{-1} . The mass spectrometer was operated in the electron impact mode (EI) at 70 eV scanning the range 30–300 m/z in a 1-s cycle. Identification of volatile compounds was achieved comparing the GC retention times and mass spectra with those, when available, of the pure standard compounds. All mass spectra were also compared with the data system library (Wiley 275). Blanks, corresponding to the analysis of the coating fibre not submitted to any extraction procedure, were run between a set of three analyses. All measurements were made with, at least, four replicates and the reproducibility was expressed as relative

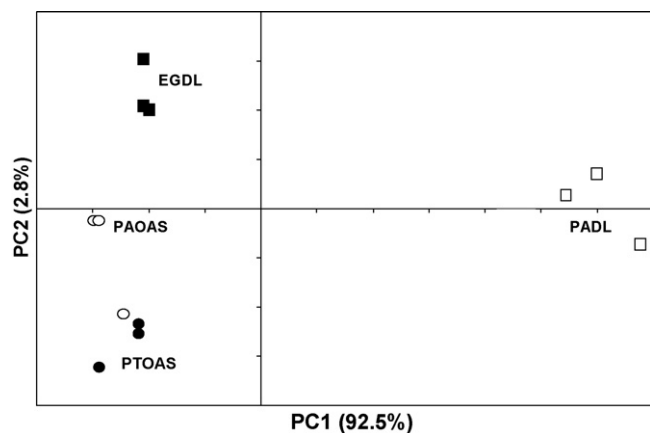


Fig. 1. Scores scatter plot (PC1 vs. PC2) of the electronic aroma sensing system data for the lignins PADL, EGDL, PAOAS and PTOAS (30–60 s). Three replicates were carried out for each sample.

standard deviation (R.S.D.) in the tables. The relative abundance of each compound was estimated based on its GC peak area.

3. Results and discussion

3.1. Electronic aroma sensing system analysis

Dioxane lignins from *E. globulus* L. (EGDL) and *P. abies* L. (PADL) woods, oxygen–organosolv lignins isolated after pulping of *P. tremula* L. (PTOAS) and *P. abies* L. (PAOAS) woods were subjected to the analysis by EASS. EGDL and PADL represent, respectively, hardwood (SG type) and softwood (G type) lignin samples isolated by preparative acidolytic technique and PTOAS and PAOAS are technical hardwood (SG type) and softwood (G type) lignin samples, respectively, isolated from pulping liquors after the oxygen–organosolv delignification. The analysis conditions were pre-selected in order to acquire the optimal sensor responses (data not shown). The sensor array responded to the presence of volatile compounds by changes in their electrical properties.

Fig. 1 shows the scores scatter plot (PC1 vs. PC2) of the EASS data for the lignins EGDL, PADL, PTOAS and PAOAS, which account for 95.3% of the total variability. PADL, a lignin from

Picea abies, located in PC1 positive are clearly distinguished from the others; EGDL in PC1 negative and PC2 positive, and PAOAS and PTOAS in PC1 and PC2 negative. Data obtained clearly showed the possibility of reliable distinction of lignin samples of different biological (SG and G types) origin isolated by the same method (pare EGDL–PADL) or the lignin samples of the same biological origin but isolated by different techniques (pare PADL–PAOAS) based on their headspace composition. However, the distinction of lignin samples from different kind of wood species suffered the same technogenic affect (such as oxygen delignification) may be more difficult (pare PAOAS–PTOAS). Overall results obtained showed the potential of EASS as a tool for the lignins distinction and potential identification. These objectives may be accomplished through the creation of databases corresponding to different lignin groups of interest.

3.2. HS-SPME/GC–MS analysis

In order to assess the aroma profiles defined by the EASS analyses, headspace volatile components of each lignin were identified using HS-SPME followed by GC–MS. Table 1 shows the proportion of volatile compounds identified in the lignin headspace, which comprises aromatic compounds, C₁₄ to C₁₈ fatty acids and an isoprenoid, squalene. PADL lignin exhibited a total GC peak area 5–9 times higher than the other three lignins, which may explain the distinction obtained by EASS–PCA between PADL and others lignins (Fig. 1). The PADL lignin presented a GC peak area higher than the other three lignins for all compounds, with the exception of vanillin.

The presence of a small proportion of extractive compounds in lignins is not surprising. In spite of exhaustive wood extraction with toluene–ethanol (2:1, v/v) solution before the lignin isolation, some amount of extractives still remained in the lignocellulosic material being imbibed or even chemically linked in cell wall matrix. The precipitation of lignin in water from dioxane solution after the acidolytic procedure or from aqueous acetone solution after the organosolv pulping led to co-precipitation of dissolved extractives together with lignin. These low molecular weight compounds could not be com-

Table 1
Peak area ($\times 10^{-5}$) of the compounds of PADL, EGDL, PAOAS and PTOAS obtained by HS-SPME/GC–MS analysis

Compound	Ident. ^a	Peak area ($\times 10^5$)			
		PADL (n=4)	EGDL (n=4)	PAOAS (n=4)	PTOAS (n=4)
Phenol	A–C	9.29 (7) ^b	0.55 (11)	0.95 (10)	0.29 (11)
Benzoic acid	A–C	36.2 (4)	1.12 (4)	3.05 (6)	0.62 (9)
Vanillin	A–C	0.71 (14)	0.35 (9)	1.96 (8)	1.51 (5)
Myristic acid (C14:0)	A–C	6.82 (3)	0.97 (8)	1.58 (4)	1.00 (5)
Pentadecanoic acid (C15:0)	A–C	21.73 (3)	–	4.67 (5)	2.65 (6)
Palmitic acid (C16:0)	A–C	7.45 (11)	2.98 (8)	1.46 (5)	–
Squalene	B,C	9.73 (7)	5.2 (7)	5.77 (9)	6.38 (8)
Stearic acid (C18:0)	A–C	3.3 (14)	–	–	–
Total area		95.23	11.17	19.44	12.45

^a The reliability of the identification or structural proposal is indicated by the following: (A) mass spectrum and retention time consistent with those of an authentic standard; (B) structural proposals given on the basis of mass spectral data (Wiley 275); (C) mass spectrum consistent with spectra found in the literature.

^b Relative standard deviation, R.S.D.% in parentheses.

pletely removed from lignin by washing/extraction with diethyl ether due to their affinity.

The most marked differences among EGDL, PAOAS and PTOAS samples were found in the amount of aromatic volatile organic compounds. Particularly, the amount of benzoic acid and vanillin in the headspace might be decisive in the distinction of former three lignins. Vanillin has a characteristic vanilla and sweet aroma descriptor, with a very low odour threshold ($20 \mu\text{g kg}^{-1}$) [19] that potentially may contribute to the lignin aroma. Vanillin could emerge in EGDL and PADL samples as the result of acidolytic degradation of terminal benzaldehyde type units detected both in EGDL [14] and PADL [20]. EGDL, being a lignin with high proportion of syringyl (S) structural units, revealed smaller amounts of vanillin in headspace than PADL, which is built essentially by guaiacyl (G) units. Hence, the electronic sensor response is sensitive to the proportion of S/G structural units in lignin. The increase of vanillin concentration in PAOAS, when compared to PADL, is the result of the oxidative degradation of guaiacyl structures [14]. Therefore, vanillin formed in the oxidative delignification was adsorbed onto the lignin. The low molecular degradation products are very difficult to eliminate from the lignin surface even by it washing with diethyl ether. The relative amounts of vanillin were less abundant in PTOAS than in PAOAS for the reason of smaller proportion of guaiacyl units in aspen than in spruce lignin. Thus, the specific low molecular weight products emerged in the technological processes and adsorbed on lignins can facilitate their distinction by the electronic aroma sensing system. These low molecular weight degradation products are impossible to eliminate completely by simple extraction of lignin with low polar organic solvent [19].

It seems some very small amounts of low molecular weight aromatics adsorbed on lignin may also serve as the specific volatile markers. Thus, in the case of spruce lignin samples (both PADL and PAOAS) the presence of phenol was significantly higher in the headspace than in the case of other analysed lignin samples. This fact certainly favoured the better discrimination of spruce lignin analytes. It is difficult, however, to define clearly the phenol origin, but its presence is related more to the wood nature rather than to the method of lignin isolation (Table 1).

3.3. Concluding remarks

The results of this work clearly showed the possibility for the distinction and identification of lignins of different biological

and technogenic origins using an electronic aroma sensing system. Particularly, this methodology was successfully applied for the distinction of gymnosperm and angiosperm lignins isolated by conventional acidolytic procedure, whereas the distinction between oxygen–organosolv lignins from softwood and hardwood was more difficult. It was suggested that minor amounts of volatile lignin degradation products emerged from the isolation procedure play a key role regarding the aroma sensor response.

References

- [1] C.-L. Chen, in: S.Y. Lin, C.W. Dence (Eds.), *Methods in Lignin Chemistry*, Springer-Verlag, Berlin, 1992, pp. 301–319.
- [2] G. Gellerstedt, in: S.Y. Lin, C.W. Dence (Eds.), *Methods in Lignin Chemistry*, Springer-Verlag, Berlin, 1992, pp. 322–333.
- [3] C. Rolando, B. Monties, C. Lapierre, in: S.Y. Lin, C.W. Dence (Eds.), *Methods in Lignin Chemistry*, Springer-Verlag, Berlin, 1992, pp. 334–350.
- [4] C.-L. Chen, D. Robert, in: W.A. Wood, S.T. Kellogg (Eds.), *Methods in Enzymology*, vol. 161, Academic Press, Inc., New York, 1988, pp. 137–158.
- [5] U.P. Agarwal, in: D.S. Argyropoulos (Ed.), *Advances in Lignocellulosics Characterization*, TAPPI Press, Atlanta, 1999, pp. 201–225.
- [6] O. Faix, in: S.Y. Lin, C.W. Dence (Eds.), *Methods in Lignin Chemistry*, Springer-Verlag, Berlin, 1992, pp. 83–107.
- [7] S. Rocha, V. Ramalheira, A. Barros, I. Delgadillo, M.A. Coimbra, *J. Agric. Food Chem.* 49 (2001) 142.
- [8] S. Rocha, I. Delgadillo, A.J. Ferrer Correia, A. Barros, P. Wells, *J. Agric. Food Chem.* 46 (1998) 145.
- [9] R. Aparicio, S. Rocha, I. Delgadillo, M.T. Morales, *J. Agric. Food Chem.* 48 (2000) 853.
- [10] C.L. Arthur, J. Pawliszyn, *Anal. Chem.* 62 (1990) 2145–2148.
- [11] A. Lattuati-Derieux, S. Bonnassies-Termes, B. Lavedrine, *J. Cult. Herit.* 7 (2006) 123.
- [12] A. Espert, L.A. de las Heras, S. Karlsson, *Polym. Degrad. Stab.* 90 (2005) 555.
- [13] A. Regert, V. Alexandre, N. Thomas, A. Lattuati-Derieux, *J. Chromatogr. A* 1101 (2006) 245.
- [14] D.V. Evtuguin, C. Pascoal Neto, A.M.S. Silva, P.M. Domingues, F.M.L. Amado, D. Robert, O. Faix, *J. Agric. Food Chem.* 49 (2001) 4252.
- [15] M.Ya. Zarubin, I.P. Deineko, D.V. Evtuguin, A. Robert, *TAPPI J.* 72 (1989) 163.
- [16] I.T. Jolliffe, *Principal Component Analysis*, Springer-Verlag, New York, 1986.
- [17] T. Górecki, X. Yu, J. Pawliszyn, *Analyst* 124 (1999) 643.
- [18] J. Pawliszyn, *J. Chromatogr. Sci.* 38 (2000) 270.
- [19] H.-D. Belitz, W. Grosch, P. Schieberle, *Food Chemistry*, 3rd ed., Springer-Verlag, Berlin-Heidelberg, 2004, pp. 973–974.
- [20] D.V. Evtugin, D. Robert, M.Ya. Zarubin, *Russ. J. Appl. Chem. (Engl. Transl.)* 67 (1994) 1486.

Short communication

Anion concentration-dependent partitioning mechanism in the extraction of uranium into room-temperature ionic liquids

Mark L. Dietz^{*}, Dominique C. Stepinski

Chemical Sciences & Engineering Division, Argonne National Laboratory, Argonne, IL 60439, United States

Received 18 September 2007; received in revised form 19 November 2007; accepted 20 November 2007

Available online 31 December 2007

Abstract

The mode of partitioning of uranyl ion between nitrate-containing aqueous phases and various *N,N'*-dialkylimidazolium-based room-temperature ionic liquids (RTILs) in the presence of tri-*n*-butyl phosphate (TBP) is shown to change from an ion-exchange process to one involving extraction of a neutral uranyl–TBP–nitrate complex as the aqueous nitrate concentration is increased. Increasing the hydrophobicity of the RTIL cation eventually leads to nitrate complex extraction as the predominant mode of partitioning, regardless of nitrate concentration.

Published by Elsevier B.V.

Keywords: Uranium; Extraction; Tri-*n*-butyl phosphate; Ionic liquids

1. Introduction

Considerable attention has recently been devoted to the application of ionic liquids (ILs) in chemical separations, often as replacements for the conventional organic solvents employed in traditional liquid–liquid (L–L) or membrane-based systems for the separation of metal ions or organic solutes [1–40]. Ionic liquids exhibit a number of properties that make them appealing alternatives to ordinary molecular solvents in these applications, including negligible vapor pressure, a wide liquid range, and good thermal stability. Most importantly, ILs are extraordinarily tunable; an enormous range of structural variations in both the anionic and cationic constituents are possible, and even minor changes in either have been shown to yield often significant alterations in the physicochemical properties of the IL [41]. Such tunability, while offering many opportunities for the design of improved separations, also poses an immense challenge. That is, given the present limited state of knowledge regarding the fundamental chemical aspects of separation systems employing ionic liquids, identification of the ionic liquid best suited to a particular purpose remains largely a matter of trial and error, a clear impediment to their more widespread adoption [42].

Recent work in this laboratory concerning the use of ionic liquids has sought to determine their utility in the liquid–liquid extraction of metal ions, particularly of actinides and fission products from acidic media, a separation problem of importance in the development of both analytical-scale systems for radiochemical separations and large-scale processes for the treatment of nuclear wastes [43]. In a series of earlier studies [44–47], we showed that the extraction of strontium ion from acidic nitrate media by the macrocyclic polyether dicyclohexano-18-crown-6 (DCH18C6) into various short-chain 1-alkyl-3-methylimidazolium-based room-temperature ionic liquids (RTILs), in contrast to its extraction into molecular organic solvents (*e.g.*, 1-octanol), involves the exchange of a cationic strontium–crown ether complex for the cationic constituent of the ionic liquid. Such a mode of ion transfer, in that it implies a gradual dissolution of the organic phase as metal extraction proceeds, has obvious negative implications for the use of ILs in L–L extraction. Clearly then, it is important to establish the prevalence of ion-exchange as a mechanism of metal ion partitioning into these solvents. With this in mind, we have examined the extraction of uranium from nitric acid by the well-known neutral extractant tributyl phosphate (TBP) into various 1-alkyl-3-methylimidazolium bis[(trifluoromethylsulfonyl)]imides (abbreviated hereafter as $C_n\text{mim}^+\text{Tf}_2\text{N}^-$, where $n=5-10$). Although the extraction of uranium into ionic liquids has been considered previously [30,33,37,40], these studies employed either

^{*} Corresponding author. Tel.: +1 630 252 3647; fax: +1 630 252 7501.
E-mail address: mdietz@anl.gov (M.L. Dietz).

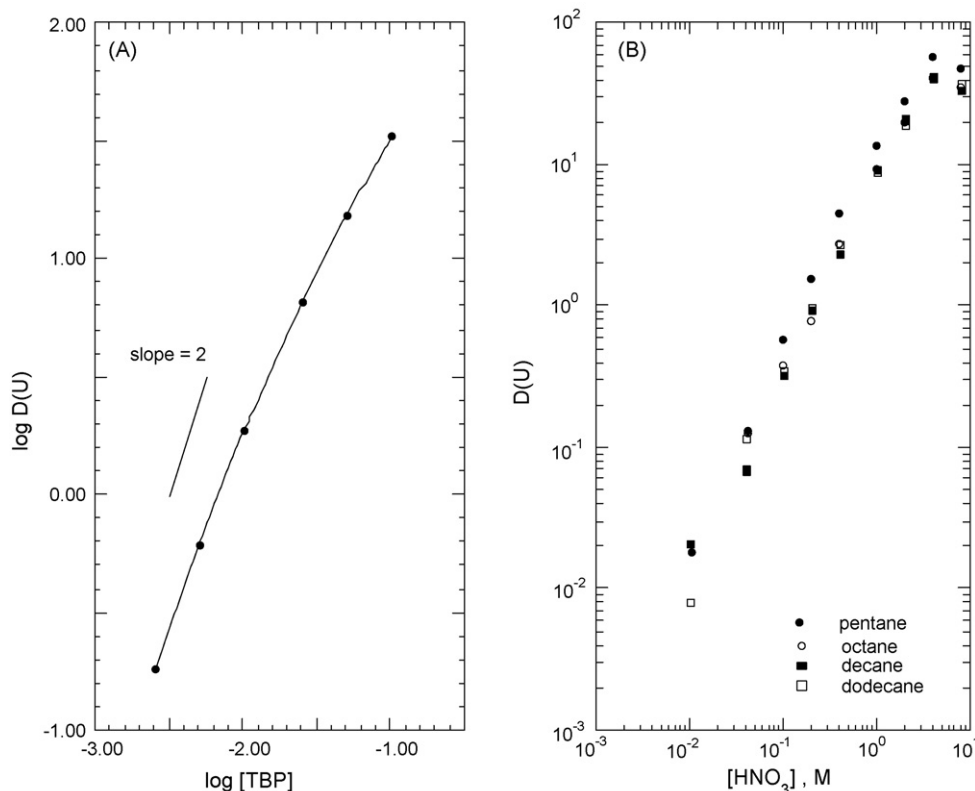


Fig. 1. (A) Dependency of the uranium distribution ratio, D_U , on TBP concentration in dodecane at constant (3 M) nitric acid concentration ($T = 23 \pm 2^\circ C$). (B) Dependency of the uranium distribution ratio, D_U , on HNO_3 concentration at constant (1.2 M) TBP concentration in several *n*-alkanes ($T = 23 \pm 2^\circ C$).

hexafluorophosphate-based ILs [30,33,40] (solvents about which increasing concerns have arisen as a result of their possible decomposition to yield hydrogen fluoride [6,48]) or acidic (rather than neutral) extractants [37]. The removal of uranium from various matrices, in addition to its continuing relevance to nuclear materials processing [49], remains a separation of importance in a variety of geological, biological, and environmental analyses [50–54].

2. Experimental

2.1. Materials

The 1-alkyl-3-methylimidazolium ionic liquids were prepared and purified according to published methods [55]. The tributyl phosphate was obtained from Aldrich Chemical Company (Milwaukee, WI) and distilled prior to use. Aqueous acid solutions were prepared using Milli-Q2 water and UltrexTM nitric acid (Mallinckrodt Baker Inc., Phillipsburg, NJ). All other reagents were ACS reagent grade and were used as received.

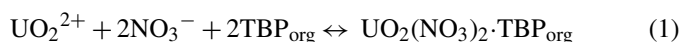
2.2. Methods

All uranium distribution ratios were determined radiometrically using a U-233 tracer obtained from Argonne National Laboratory stocks, assayed by liquid scintillation counting on a Packard Model 2000 CA counter according to standard procedures. A 1:1 phase ratio was employed for all measurements,

and all determinations were carried out at ambient temperature ($23 \pm 2^\circ C$). Preconditioning of the organic phase prior to distribution ratio measurements was accomplished *via* two contacts with twice the volume of water or an appropriate aqueous nitric acid solution.

3. Results and discussion

In a pair of earlier reports [44,45], we demonstrated that comparison of the metal ion extraction behavior of a given reagent in a conventional solvent and an ionic liquid can provide important insights into the mode of metal ion transfer into the IL. For this reason, our efforts to understand the partitioning of uranium between acidic nitrate media and the various $C_n\text{mim}^+\text{Tf}_2\text{N}^-$ ionic liquids in the presence of TBP began with an examination of its extraction into a series of alkanes. Prior work [56] has established that the extraction of uranium(VI) from acidic aqueous nitrate solutions into conventional solvents proceeds *via* partitioning of a neutral uranyl–TBP–nitrate complex according to the following reaction:



Such a mode of partitioning, in that it allows for efficient extraction of uranium from solutions containing high concentrations of nitric acid (such as are encountered in nuclear fuel and waste reprocessing and, for analytical-scale uranium recovery, in soil leachates, for example) and its ready recovery in dilute acid or water, represents an optimal route for uranium extrac-

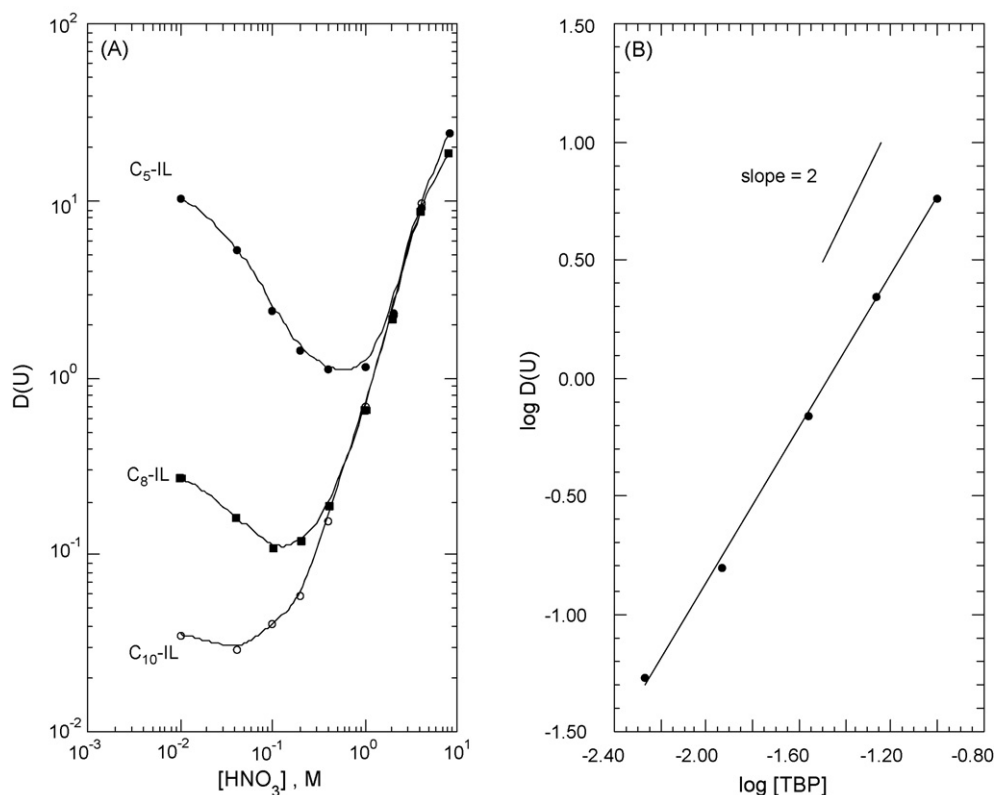


Fig. 2. (A) Dependency of the uranium distribution ratio, D_U , on HNO_3 concentration at constant (1.2 M) TBP concentration in several $C_nmim^+Tf_2N^-$ ionic liquids ($T=23 \pm 2^\circ C$). (B) Dependency of the uranium distribution ratio, D_U , on TBP concentration in $C_{10}mim^+Tf_2N^-$ at constant (3 M) nitric acid concentration ($T=23 \pm 2^\circ C$).

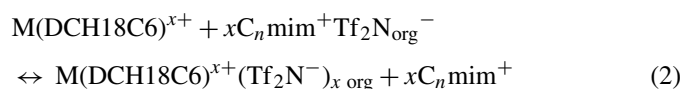
tion. As expected from this equation, the extraction of uranium at constant acidity into, for example, dodecane (as reflected in the uranium distribution ratio, D_U , defined as $[U]_{org}/[U]_{aq}$ at equilibrium) is seen to increase markedly with TBP concentration (Fig. 1A). The slight downward curvature of the plot (*i.e.*, the deviation from the theoretically expected line of slope 2) at the highest extractant concentrations is consistent with system non-ideality, as has been noted previously in, for example, the TBP extraction of rare earth ions [57]. Fig. 1B depicts the corresponding nitric acid dependency of uranium extraction at a constant TBP concentration (1.2 M), along with that observed for three other n -alkanes: pentane, octane, and decane under the same conditions. As can be seen, the extraction of uranium into each solvent rises (nearly linearly) with increasing acid (hence, nitrate) concentration. (At sufficiently high acidities, however, competition between the acid and the metal ion for extractant eventually leads to decreasing uranium extraction efficiency.) Of particular note in the context of this discussion is that variations in the hydrocarbon chain length of the alkane have little effect on the extraction of uranium at a given acidity.

In contrast, as shown in Fig. 2A, the shape of the acid dependency of uranium extraction into the ionic liquids varies considerably as the alkyl chain length of the IL cation is changed over much the same range (*i.e.*, from C_5 to C_{10}). For $C_{10}mim^+Tf_2N^-$, the overall shape of the dependency (*i.e.*, rising D_U with increasing acidity) approximates that observed in the alkanes (aside from some flattening of the dependency in the

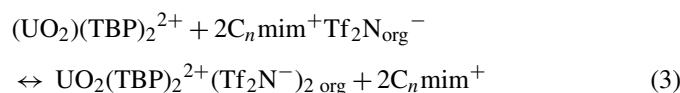
IL at the lowest acidities), indicating that uranium extraction into the $C_{10}mim^+Tf_2N^-$ also primarily involves partitioning of the neutral uranyl–TBP–nitrate complex (Eq. (1)). This is supported by the results of measurements of the dependence of D_U on TBP concentration at constant acidity (here, 3 M HNO_3) for the same IL (Fig. 2B), which as a line of slope ~ 2 , again resembles the dependency obtained for dodecane. This observation, that the behavior of a neutral extractant in ionic liquids comprising relatively hydrophobic cations (*i.e.*, C_nmim^+ , with $n \geq 10$) parallels its behavior in conventional organic solvents, is consistent with results obtained previously comparing the extraction of strontium ion by dicyclohexano-18-crown-6 (DCH18C6) into various $C_nmim^+Tf_2N^-$ ILs and aliphatic alcohols [46].

As the hydrophobicity of the IL cation is reduced, a significant upward deviation from linearity becomes evident in the D_U acid dependency at nitric acid concentrations less than *ca.* 0.2–0.3 M. As a result, the dependencies for the C_5 and C_8 ILs comprise two distinct regions, one in which rising acidity (hence, nitrate concentration) is accompanied by falling uranium extraction and a second, higher acidity region, in which (as is the case for dodecane and $C_{10}mim^+Tf_2N^-$) D_U rises with nitric acid concentration. The close correspondence of the uranium distribution ratios obtained in the three ILs in the latter region indicates that the same process, namely, extraction of the neutral uranium–TBP–nitrate complex, occurs in all three solvents at sufficiently high acidities (*i.e.*, nitrate concentrations).

As we have noted in our previous studies of the extraction of strontium [44] and sodium [36] by DCH18C6, a decrease in metal ion partitioning with increasing nitrate concentration is inconsistent with the extraction of a neutral metal–nitrate complex. For this reason, the upward deviation in the low-acidity region of the nitric acid dependencies for the C₅ and C₈ ILs must signal a contribution to the observed D_U values from another partitioning process. That its prevalence (as reflected in the magnitude of the upward deviation in the acid dependency) increases as the IL cation chain length falls (*i.e.*, as the cation becomes more hydrophilic) is indicative of a process involving the exchange of a cationic uranyl–TBP complex for the cationic constituent of the ionic liquid, in analogy to the ion-exchange reaction observed previously in the partitioning of strontium [46] and sodium [36] into C_{*n*}mim⁺Tf₂N⁻ ILs (with $n \leq 8$) containing DCH18C6:



where $x = 1$ (for sodium ion) or 2 (for strontium ion). Because a log–log plot of the TBP dependence of D_U for C₅mim⁺Tf₂N⁻ exhibits a slope of ~ 2 and because measurements of nitrate ion transfer indicate that little or no nitrate ion (*ca.* 10% or less of that required to maintain electroneutrality) accompanies extracted uranium from aqueous phases containing low (≤ 0.4 M) nitrate concentrations, the following mode of uranium partitioning is indicated:



Although a contribution to the observed D_U values from a second type of ion-exchange process, one in which a protonated TBP molecule serves as a cation exchanger (so-called “extractant-mediated” ion-exchange [36]), cannot be entirely ruled out, several facts argue against it. First, nitric acid extraction data obtained for TBP in a wide variety of solvents consistently demonstrate that a neutral (*i.e.*, unionized) 1:1 HNO₃ adduct represents the predominant extracted species [57]. Next, the significant differences in the low-acid D_U values at a given acidity among the various ILs are inconsistent with the occurrence of the same partitioning process (*i.e.*, extractant-mediated ion-exchange) in all three solvents in this region. Finally, as shown in Fig. 3, the dependence of the distribution of uranium between water and C₅mim⁺Tf₂N⁻ on uranyl nitrate concentration exhibits the same shape as the nitric acid dependence of D_U in the same solvent (Fig. 2). Thus, the presence of acid is not required to explain the decrease in D_U observed in the low-acid region. Taken together, these observations rule out all but a minor contribution from extractant-mediated ion-exchange.

These results provide an interesting (and encouraging) contrast to those observed in the partitioning of certain other metal cations into C_{*n*}mim⁺Tf₂N⁻ ionic liquids in the presence neutral extractants. That is, as noted in a prior study [36], in the

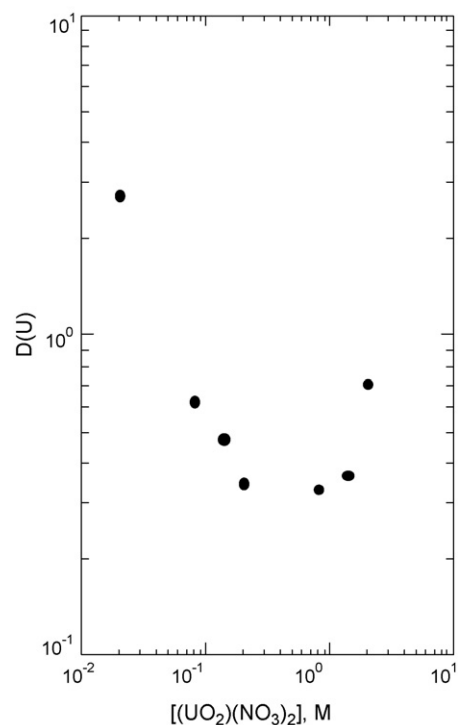


Fig. 3. Dependency of the uranium distribution ratio, D_U , on uranyl nitrate concentration at constant (1.2 M) TBP concentration in C₅mim⁺Tf₂N⁻ ($T = 23 \pm 2$ °C).

extraction of sodium ion by DCH18C6, an increase in nitric acid concentration is accompanied by a gradual shift in the predominant mode of ion partitioning, from exchange of the cationic metal–extractant complex for the IL cation to extractant-mediated ion-exchange (Fig. 4A), neither of which is regarded (from a practical point of view) as a desirable pathway for metal ion extraction [36]. In the present system, however, exchange of the cationic (here, uranyl–TBP) complex for the C_{*n*}mim⁺ cation gradually gives way to partitioning of a neutral nitrate complex as the nitric acid (*i.e.*, nitrate) concentration rises (Fig. 4B). (This difference is a likely consequence of both the facile formation of a hydronium ion–extractant complex by DCH18C6 [36,58] and the greater stability (*vs.* sodium ion) of the uranyl nitrate complex(es) [59].) From a practical perspective, this difference is a significant one, as it indicates that by simply increasing the aqueous phase acidity (*i.e.*, nitrate concentration), an undesirable pathway for the partitioning of uranium (and by analogy, other metal ions) can be suppressed in certain systems.

Two other practical aspects of the present results are less encouraging, however. First, the use of ionic liquids has been suggested as an approach to achieving metal ion extraction efficiencies far higher than those achievable in conventional solvent systems [4]. The results presented here, however, which show that uranium extraction into dodecane is actually more efficient than into the C_{*n*}mim⁺Tf₂N⁻ ILs examined, call into question the notion of the superiority of ILs as extraction solvents. Along these same lines, although interesting from a fundamental perspective, the unusual nitric acid

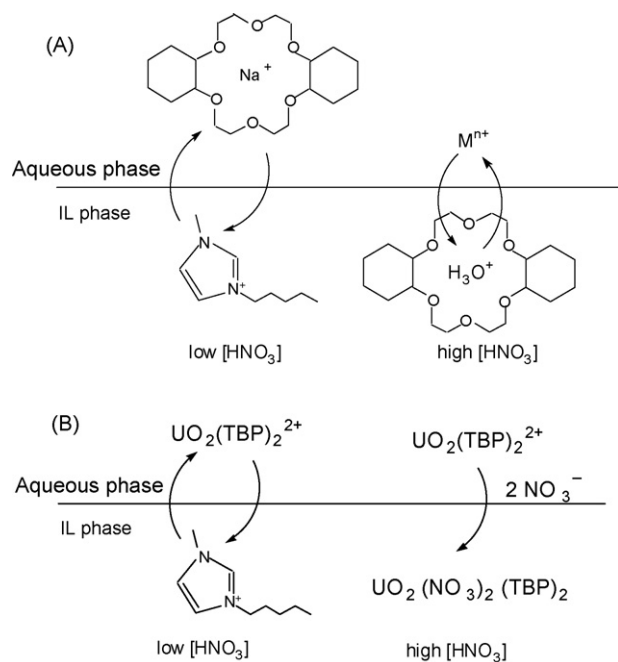


Fig. 4. Schematic diagram illustrating the effect of increasing aqueous phase nitric acid concentration on the partitioning into C₁₀mim⁺Tf₂N⁻ of (A) sodium ion in the presence of DCH18C6 and (B) uranyl ion in the presence of TBP.

dependency of uranium partitioning into C₅mim⁺Tf₂N⁻ and its C₈ analog poses practical problems in terms of the recovery of extracted uranium. That is, as noted above, the ideal L–L system is one permitting extraction from aqueous phases containing relatively high concentrations of acid and facile recovery in dilute acid or water, something clearly not feasible for ILs for which extraction is equally efficient from solutions containing either high or low nitric acid concentrations. Resolution of these issues, while beyond the scope of the present study, clearly warrants additional investigation.

4. Conclusions

The rational design of ionic liquid-based systems for the separation of metal ions requires a thorough understanding of the fundamental aspects of ion transfer into these solvents. The results presented in this study, by clarifying the factors governing the transfer of uranium in the presence of a neutral extractant, represent a step toward this goal. At the same time, the results provide information of practical significance in efforts to evaluate the viability of ionic liquids as substitutes for conventional organic solvents in the separation and preconcentration of uranium and other metal ions by liquid–liquid extraction and related techniques. Most notably, they indicate that in certain systems, the ion-exchange pathway for metal ion partitioning, which is undesirable from the perspective of process “greenness”, can be eliminated by careful control of the aqueous phase composition. Work to determine the generality of this observation and its significance to IL-based separations is now underway in this laboratory.

Acknowledgments

This work was performed under the auspices of the Office of Basic Energy Sciences, Division of Chemical Sciences, Geosciences, and Biosciences, United States Department of Energy, under contract number DE-AC02-06CH11357.

References

- [1] J.G. Huddleston, H.D. Willauer, R.P. Swatloski, A.E. Visser, R.D. Rogers, *Chem. Commun.* (1998) 1765.
- [2] D.W. Armstrong, L. He, Y.-S. Liu, *Anal. Chem.* 71 (1999) 3873.
- [3] R.D. Rogers, A.E. Visser, R.P. Swatloski, D.H. Hartman, in: K.C. Lid-dell, D.J. Chaiko (Eds.), *Metal Separation Technologies Beyond 2000*, The Minerals, Metals & Materials Society, Warrendale, PA, 1999, pp. 139–147.
- [4] S. Dai, Y.H. Ju, C.E. Barnes, *J. Chem. Soc., Dalton Trans.* (1999) 1201.
- [5] A.E. Visser, R.P. Swatloski, D.H. Hartman, J.G. Huddleston, R.D. Rogers, in: G.J. Lumetta, R.D. Rogers, A.S. Gopalan (Eds.), *Calixarenes for Separations*, American Chemical Society, Washington, DC, 2000, pp. 223–236.
- [6] A.E. Visser, R.P. Swatloski, W.M. Reichert, S.T. Griffin, R.D. Rogers, *Ind. Eng. Chem. Res.* 39 (2000) 3596.
- [7] E.G. Yanes, S.R. Gratz, M.J. Baldwin, S.E. Robison, A.M. Stalcup, *Anal. Chem.* 73 (2001) 3838.
- [8] S. Chun, S.V. Dzyuba, R.A. Bartsch, *Anal. Chem.* 73 (2001) 3737.
- [9] A.E. Visser, R.P. Swatloski, S.T. Griffin, D.H. Hartman, R.D. Rogers, *Sep. Sci. Technol.* 36 (2001) 785.
- [10] R.A. Bartsch, S. Chun, S.V. Dzyuba, in: R.D. Rogers, K.R. Seddon (Eds.), *Ionic Liquids: Industrial Applications for Green Chemistry*, American Chemical Society, Washington, DC, 2002, pp. 58–68.
- [11] A.E. Visser, J.D. Holbrey, R.D. Rogers, in: K.C. Sole, P.M. Cole, J.S. Preston, D.J. Robinson (Eds.), *Proceedings of the International Solvent Extraction Conference, ISEC 2002*, South African Institute of Mining and Metallurgy, Marshalltown, South Africa, 2002, pp. 474–480.
- [12] L.C. Branco, J.G. Crespo, C.A.M. Alfonso, *Angew. Chem. Int. Ed.* 41 (2002) 2771.
- [13] L.C. Branco, J.G. Crespo, C.A.M. Alfonso, *Chem. Eur. J.* 8 (2002) 3865.
- [14] M.H. Abraham, A.M. Zissimos, J.G. Huddleston, H.D. Willauer, R.D. Rogers, W.E. Acree Jr., *Ind. Eng. Chem. Res.* 42 (2003) 413.
- [15] K. Nakashima, F. Kubota, T. Maruyama, M. Goto, *Anal. Sci.* 19 (2003) 1097.
- [16] A.E. Visser, R.D. Rogers, *J. Solid State Chem.* 171 (2003) 109.
- [17] A.E. Visser, M.P. Jensen, I. Laszak, K.L. Nash, G.R. Choppin, R.D. Rogers, *Inorg. Chem.* 42 (2003) 2197.
- [18] G.-T. Wei, J.-C. Chen, Z. Yang, *J. Chin. Chem. Soc.* 50 (2003) 1123.
- [19] G.-T. Wei, Z. Yang, J.-C. Chen, *Anal. Chim. Acta* 488 (2003) 183.
- [20] M.P. Jensen, J. Neuefeind, J.V. Beitz, S. Skanthakumar, L. Soderholm, *J. Am. Chem. Soc.* 125 (2003) 15466.
- [21] M.L. Dietz, M.P. Jensen, J.V. Beitz, J.A. Dzielawa, in: C.A. Young, A.M. Alfantazi, C.G. Anderson, D.B. Dreisinger, B. Harris, A. James (Eds.), *Hydrometallurgy 2003. Proceedings of the Fifth International Conference in Honor of Prof. Ian Ritchie*, vol. 1: Leaching and Solution Purification, The Minerals, Metals, and Materials Society, Warrendale, PA, 2003, pp. 929–939.
- [22] J. Liu, Y. Chi, J. Peng, G. Jiang, A. Jonsson, *J. Chem. Eng. Data* 49 (2004) 1422.
- [23] M. Matsumoto, K. Mochiduki, K. Fukunishi, K. Kondo, *Sep. Purif. Technol.* 40 (2004) 97.
- [24] J. Liu, Y. Chi, G. Jiang, C. Tai, J. Peng, J.-T. Hu, *J. Chromatogr. A* 1026 (2004) 143.
- [25] S. Smirnova, I.I. Torocheshnikova, A.A. Formanovsky, I.V. Pletnev, *Anal. Chem. Biochem.* 378 (2004) 1369.
- [26] K. Shimojo, M. Goto, *Chem. Lett.* 33 (2004) 320.
- [27] K. Shimojo, M. Goto, *Anal. Chem.* 76 (2004) 5039.
- [28] H. Luo, S. Dai, P.V. Bonnesen, *Anal. Chem.* 76 (2004) 2773.
- [29] H. Luo, S. Dai, P.V. Bonnesen, A.C. Buchanan III, J.D. Holbrey, N.J. Bridges, R.D. Rogers, *Anal. Chem.* 76 (2004) 3078.

- [30] P. Giridhar, K.A. Venkatesan, T.G. Srinivasan, P.R. Vasudeva Rao, *J. Nucl. Radioanal. Sci.* 5 (2004) 21.
- [31] J. Wang, Y. Pei, Y. Zhao, Z. Hu, *Green Chem.* 7 (2005) 196.
- [32] K. Nakashima, F. Kubota, T. Maruyama, M. Goto, *Ind. Eng. Chem. Res.* 44 (2005) 4368.
- [33] P. Giridhar, K.A. Venkatesan, T.G. Srinivasan, P.R. Vasudeva Rao, *J. Radioanal. Nucl. Chem.* 265 (2005) 31.
- [34] N. Hirayama, M. Deguchi, H. Kawasumi, T. Honjo, *Talanta* 65 (2005) 255.
- [35] D.C. Stepinski, M.P. Jensen, J.A. Dzielawa, M.L. Dietz, *Green Chem.* 7 (2005) 151.
- [36] M.L. Dietz, D.C. Stepinski, *Green Chem.* 7 (2005) 747.
- [37] V.A. Cocalia, M.P. Jensen, J.D. Holbrey, S.K. Spear, D.C. Stepinski, R.D. Rogers, *Dalton Trans.* (2005) 1966.
- [38] H. Heitzman, B.A. Young, D.J. Rausch, P. Rickert, D.C. Stepinski, M.L. Dietz, *Talanta* 69 (2006) 527.
- [39] M.L. Dietz, *Sep. Sci. Technol.* 41 (2006) 2047.
- [40] T. Chu, L. Qin, X. Liu, X. Wang, *J. Nucl. Radiochem.* 29 (2007) 146.
- [41] S.A. Forsyth, J.M. Pringle, D.R. MacFarlane, *Aust. J. Chem.* 57 (2004) 113.
- [42] M.L. Dietz, J.A. Dzielawa, M.P. Jensen, J.V. Beitz, M. Borkowski, in: R.D. Rogers, K.R. Seddon (Eds.), *Ionic Liquids IIIB: Fundamentals, Progress, Challenges and Opportunities*, American Chemical Society, Washington, DC, 2005, pp. 2–18.
- [43] D.C. Stepinski, B.A. Young, M.P. Jensen, P.G. Rickert, J.A. Dzielawa, A.A. Dilger, D.J. Rausch, M.L. Dietz, in: G.J. Lumetta, K.L. Nash, S.B. Clark, J.I. Friese (Eds.), *Separations for the Nuclear Fuel Cycle in the 21st Century*, American Chemical Society, Washington, DC, 2006, pp. 233–247.
- [44] M.L. Dietz, J.A. Dzielawa, *Chem. Commun.* (2001) 2124.
- [45] M.P. Jensen, J.A. Dzielawa, P. Rickert, M.L. Dietz, *J. Am. Chem. Soc.* 124 (2002) 10664.
- [46] M.L. Dietz, J.A. Dzielawa, I. Laszak, B.A. Young, M.P. Jensen, *Green Chem.* 5 (2003) 682.
- [47] M.L. Dietz, J.A. Dzielawa, M.P. Jensen, M.A. Firestone, in: R.D. Rogers, K.R. Seddon (Eds.), *Ionic Liquids as Green Solvents: Progress and Prospects*, American Chemical Society, Washington, DC, 2003, pp. 526–543.
- [48] R.P. Swatloski, J.D. Holbrey, R.D. Rogers, *Green Chem.* 5 (2003) 361.
- [49] K.L. Nash, in: G.J. Lumetta, K.L. Nash, S.B. Clark, J.I. Friese (Eds.), *Separations for the Nuclear Fuel Cycle in the 21st Century*, American Chemical Society, Washington, DC, 2006, pp. 21–40.
- [50] S.K. Sahu, V. Chakravorty, M.L.P. Reddy, T.R. Ramamohan, *Talanta* 51 (2000) 523.
- [51] M.H. Lee, C.W. Lee, *Talanta* 54 (2001) 181.
- [52] M.L. Dietz, E.P. Horwitz, L.R. Sajdak, R. Chiarizia, *Talanta* 54 (2001) 1173.
- [53] A.M. Starvin, T.P. Rao, *Talanta* 63 (2004) 225.
- [54] M.A. Maheswari, M.S. Subramanian, *Talanta* 64 (2004) 202.
- [55] P. Bonhôte, A.-P. Dias, N. Papageorgiou, K. Kalyanasundaram, M. Gratzel, *Inorg. Chem.* 35 (1996) 1168.
- [56] J.H. Cavendish, in: W.W. Schulz, J.D. Navratil, T. Bess (Eds.), *Science and Technology of Tributyl Phosphate*, vol. II, Part A, CRC Press, Boca Raton, FL, 1987, pp. 1–41.
- [57] D.A. Orth, R.M. Wallace, D.G. Karraker, in: W.W. Schulz, J.D. Navratil (Eds.), *Science and Technology of Tributyl Phosphate*, vol. I, CRC Press, Boca Raton, FL, 1984, pp. 161–219.
- [58] R.M. Izatt, B.L. Haymore, J.S. Bradshaw, J.J. Christensen, *Inorg. Chem.* 14 (1975) 3132.
- [59] R.M. Smith, A.E. Martell, *Critical Stability Constants*, vol. 4: *Inorganic Complexes*, Plenum Press, New York, 1976, p. 48.

Liquid chromatographic–electrospray mass spectrometric determination (LC–ESI–MS) of phase II metabolites of flobufen in rat liver microsomes—Chiral discrimination

Yogeeta N. Babú^a, Michal Němec^a, Petr Solich^{b,*}, Vladimír Wsól^a

^a Department of Biochemical Sciences, Charles University, Faculty of Pharmacy, Heyrovského 1203, CZ-500 05 Hradec Králové, Czech Republic

^b Department of Analytical Chemistry, Charles University, Faculty of Pharmacy, Heyrovského 1203, CZ-500 05 Hradec Králové, Czech Republic

Received 17 July 2007; received in revised form 8 November 2007; accepted 14 November 2007

Available online 22 November 2007

Abstract

Glucuronidation of the non-steroidal anti-inflammatory chiral drug flobufen and its major metabolite M17203 has been implicated as an important mechanism of flobufen elimination. To characterize flobufen metabolism by *O*-glucuronidation, new liquid chromatographic method (LC) coupled with ESI–MS was developed to detect the conjugates of flobufen and its metabolites formed *in vitro* in rat liver microsomes. Discovery DSC–18 LT cartridge columns were utilized for solid phase extraction (SPE) and Discovery C18 column (150 mm × 2.1 mm, 5 μm particle size) was used for LC separation. Chiral inversion of flobufen and its metabolites enantiomers was checked by special 1-allyl-(5*R*,8*S*,10*R*)-terguride column (150 mm × 4.6 mm). *O*-Glucuronidation of the *S*-enantiomer displayed a typical Michaelis–Menten kinetics, whereas the *R*-enantiomer exhibited a substrate inhibition type of kinetics. The study of glucuronidation of M17203 led to kinetics with sigmoidal characteristics.

© 2007 Elsevier B.V. All rights reserved.

Keywords: Flobufen; Chiral; Enantiomer; LC–MS/MS; Enzyme kinetics; Microsomes

1. Introduction

Non-steroidal anti-inflammatory drugs are among the most widely used drugs and the great majority belongs to the class of 2-arylpropionic acids (2-APAs) or profens. Their mechanism of action consists predominantly of the inhibition of both forms of cyclooxygenase (COX) – COX-1, constitutive, and COX-2, induced during inflammation – and, therefore, they inhibit the synthesis of prostaglandins and thromboxanes [1].

2-APAs are chiral compounds and their racemic forms can be resolved into *R*- and *S*-enantiomers with different pharmacokinetic and pharmacological behaviour [2]. A particular characteristic of the metabolism of this class of compounds is the ability to undergo unidirectional inversion of the *R*- to the *S*-enantiomer, via the formation of an acyl-coenzyme A thioester, a reaction which is both species and drug dependent [3–5]. This can be associated with an important pharmacological implica-

tion: it is suggested that the *S*-enantiomer is responsible for the anti-inflammatory activity, whilst the *R*-enantiomer has a minor (if any) contribution [6]. Nevertheless, the clinically used 2-APAs are marketed as racemates, being naproxen the exception and, more recently, ibuprofen and ketoprofen, which have been marketed as *S*-enantiomer formulations [7].

Flobufen (FLO, Fig. 1), 4-(2',4'-difluorobiphenyl-4-yl)-2-methyl-4-oxobutanoic acid, belongs to the group of arylpropionic acids, which are structurally related to the arylpropionic acids [8]. FLO can be characterized as a drug with combined inhibitory effect on 5-lipoxygenase and COX, although antagonist effects on LTB₄ receptors can also be observed [9]. For this reason, FLO is considered to be an anti-rheumatic drug. It displays intermediate to strong efficacy and lengthened effect, which enables a single daily administration.

Phase I biotransformation studies of FLO have been carried out from both achiral and chiral point of view. *In vitro* experiments concerning different species – mouse, rat, guinea pig, rabbit, mini-pig and dog – found 4-dihydroflobufen, 4-(2',4'-difluorobiphenyl-4-yl)-2-methyl-4-hydroxybutanoic acid (DHF) to be its major metabolite [10,11]. DHF is fur-

* Corresponding author. Tel.: +420 495 067 294; fax: +420 495 067 164.
E-mail address: Petr.Solich@faf.cuni.cz (P. Solich).

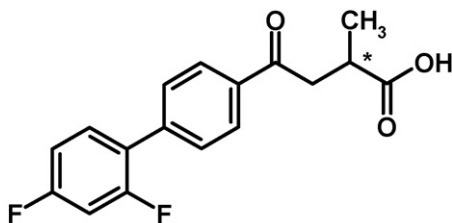


Fig. 1. Chemical structure of flobufen. The * denotes the stereogenic centre.

ther metabolised to a higher or lesser extent in hepatocytes [11–13] and *in vivo* [11,14] into the final metabolite 2-(2',4'-difluorobiphenyl-4-yl)-acetic acid (M17203) by a process similar to the β -oxidation of fatty acids [12], being this metabolite much more potent than FLO itself [15].

The metabolism of FLO in man is distinct from that observed in other animal species, as the final metabolite is DHF, which does not undergo the transformation into M17203 [13]. From this point of view, the complex metabolic study of FLO concerning human use differs from the studies in rat. While the use of FLO in human medicine is still open, its unique properties are being applied in veterinary medicine for several years, since the Virbac Company from Carros, France, obtained the license for commercialisation of FLO.

Stereoselective pharmacokinetics of FLO in rat [16] and guinea pig [17] was assessed and significant unidirectional inversion of (+)-(R)-FLO into (–)-(S)-FLO was found, in similarity with the majority of 2-APAs.

The different disposition of the individual enantiomers also influences other aspects of the metabolic pathways of these drugs, like the phase II biotransformation. Glucuronidation is a biotransformation pathway, which plays an important role in the metabolism of most profens [18,19]. Glucuronidation of chiral compounds was also found to be enantioselective, as reported for several drugs [20–23].

Till now, no information about phase II biotransformation of flobufen is known. The aim of the present study was to find if FLO enantiomers are conjugated with glucuronic acid and if the process is enantioselective. For these goals, new liquid chromatographic (LC) method for separation of glucuronides in connection with ESI-MS and ESI-MS/MS methods was used to separate and consequently to identify the respective metabolites. *In vitro* experiments using isolated microsomes from male Wistar rats were performed and significantly different glucuronidation of FLO in rat was found for both its enantiomers.

2. Experimental

2.1. Chemicals

Rac-FLO (R/S:50/50), (+)-(R)-FLO and (–)-(S)-FLO (optical purity >99%) were obtained from the Research Institute for Pharmacy and Biochemistry (Prague, Czech Republic). Uridine diphosphoglucuronic acid (UDPGA) and magnesium chloride ($MgCl_2$) were purchased from Sigma–Aldrich (Prague, Czech Republic). Methanol and acetonitrile (ACN), HPLC grade were acquired from Merck (Prague, Czech Republic). Water from

the Milli-Q-RG Ultra-Pure Water System was from Millipore (Prague, Czech Republic), in all cases. All the other chemicals were of the highest purity commercially available.

2.2. Animals

Male Wistar rats (*Rattus norvegicus* var. *Alba*, 12–14 weeks, 280–320 g, BioTest, Konárovice, Czech Republic) were housed under a 12 h light/dark cycle, on a standard rat chow with free access to tap water. Experiments with the animals were carried out according to the *Guide for the care and use of laboratory animals* (Protection of Animals against Cruelty Act. No. 246/92 Coll., Czech Republic).

2.3. Isolation of microsomes

Liver was homogenized with cold Na-phosphate buffer (pH 7.4; 0.1 M) in a 1:6 (w/v) ratio. The sub-cellular fractions were obtained by fractional ultra-centrifugation of the homogenates [24]. A re-washing step (followed by a second ultra-centrifugation) was added at the end of the microsomes preparation procedure. Microsomes were finally resuspended in the homogenising buffer containing 20% glycerol (v/v) and were stored at $-80^\circ C$. Protein contents were determined by bicinchoninic acid (BCA) method [25].

2.4. Microsomal incubations

To achieve maximal activity of UDP-glucuronosyltransferases (UGTs), the microsomes were pre-incubated with alamethicin, 50 $\mu g/mg$ of microsomal protein, at $4^\circ C$ for 20 min [26]. Standard incubation mixtures (total volume 300 μL) consisted of *rac*-FLO, (+)-(R)-FLO, (–)-(S)-FLO or M17203, 10 mM UDPGA, 1.0 mM $MgCl_2$ and Na-phosphate buffer (pH 7.4; 0.1 M). After pre-incubation of the medium at $37^\circ C$ for 2 min, the reaction started with the addition of the activated microsomal proteins, 1.0 mg/mL of reaction mixture. The assays were performed in triplicate. Total incubation time was 60 min and after this times the reaction was stopped with 0.1 mL H_3PO_4 (pH 2; 1 M) and cooling to $0^\circ C$. All the samples were centrifuged for 10 min at $3500 \times g$. The resulting supernatant was subjected to cleanup by solid phase extraction (SPE). Control reactions were also run and consisted of assays without UDPGA.

2.5. Solid phase extraction

The extraction procedure was conducted as follows: the SPE cartridges (Discovery[®] DSC-18 LT 1.0 mL tube, 100 mg, Supelco, Bellefonte, PA, USA) were conditioned with 1.0 mL of methanol and 1.0 mL of monopotassium phosphate buffer (KH_2PO_4 ; pH 3.0; 25 mM). After loading the samples, the cartridges were rinsed with 1 mL of KH_2PO_4 (pH 3.0; 25 mM) and the retained compounds were eluted with 1 mL of methanol. The eluents were then evaporated to dryness (Concentrator 5103 from Eppendorf, Medesa, Policka, Czech Republic) and reconstituted in 10% ACN and 90% water in a total volume of 150 μL .

Table 1
LC conditions for the analysis of FLO-glucuronide and M17203-glucuronide

Column	C18 150 mm × 2.1 mm, 5 μm
Flow rate (μL/min)	
0 min	300
4 min	200
10 min	200
Wavelength (nm)	275 for FLO and its conjugates 240 for M17203 and its conjugates
Column temperature (°C)	25
Injection volume (μL)	10
Gradient ^a	
0 min	70% A and 30% B
2 min	70% A and 30% B
4 min	10% A and 90% B
10 min	10% A and 90% B
Total run time (min)	10.0

^a Mobile phase A: 10 mM formic acid (pH 5.0, NH₄OH); mobile phase B: ACN.

2.6. Analytical assessment

The analytical assessments were conducted on a Surveyor LC system equipped with a quaternary gradient pump, an autosampler, a PDA detector and a LCQ Advantage ion trap mass spectrometer (ThermoFinnigan, San Jose, CA, USA). For semi-quantification analysis, the PDA detector was used whereas, the LCQ Advantage ion trap mass spectrometer was used for identification of the conjugates. Mass spectrometry experiments were performed using electrospray ionization (ESI) operated in negative ion mode. The electrospray voltage was set at −4.5 kV. The capillary voltage was set at −10 V and the temperature was maintained at 200 °C. The LC column effluent was nebulized using N₂ as sheath gas at the flow rate of 50 arbitrary units. The product ion spectra were produced by collision-induced dissociation (CID) of the selected precursor ions with He with the relative collision energy set at 25%. Separations were obtained on a Discovery[®] C18 150 mm × 2.1 mm i.d., 5 μm achiral column (Supelco, Bellefonte, PA, USA) coupled with a guard column Discovery[®] C18 20 mm × 2.1 mm i.d., 5 μm (Supelco, Bellefonte, PA, USA). The remaining LC conditions are detailed in Table 1. Data were collected with Xcalibur Software, version 1.2 (Vienna, VA, USA).

Stereoselective HPLC analysis was employed to establish if there was no conversion of (−)-(S)-FLO to (+)-(R)-FLO, and

vice versa, at all conditions tested. The measurements were performed using a non-commercially available 150 mm × 4.6 mm i.d. 1-allyl-(5*R*,8*S*,10*R*)-terguride column (Institute of Microbiology, Academy of Sciences of the Czech Republic, Prague, Czech Republic). A mixture of potassium acetate (10 mM) adjusted to pH 3.0 with acetic acid (1 M and 0.1 M, respectively) and ACN in a ratio 60:40 (v/v) was used as mobile phase. Retention times were 8.57 min for (−)-(S)-FLO and 9.71 min for (+)-(R)-FLO (Fig. 2). The calibration curve was linear up to 0.8 mg/mL for both (−)-(S)-FLO and (+)-(R)-FLO [16].

2.7. Kinetic parameters estimation

The kinetic parameters were estimated using a non-linear least-square regression fit to the Michaelis–Menten equation or to the modified Hill-substrate inhibition equation and the best model for each substrate was found on the basis of *F*-test comparison (*P* < 0.05), by GraphPad Prism 4.00 for Windows, GraphPad Software (San Diego, CA, USA, www.graphpad.com).

3. Results

3.1. HPLC analysis

It is known that for the great majority of 2-APAs unidirectional chiral inversion of the *R*-enantiomer to the *S*-enantiomer occurs. This reaction involves the participation of CoA, where it plays a major role and it is thought to be catalyzed by long chains acyl-CoA synthetases [3–5].

In preliminary studies using stereoselective conditions of HPLC analysis of FLO glucuronidation it was shown that no chiral inversion occurs between its enantiomers under the incubation conditions above mentioned. For this reason, it was chosen to perform all measurements under the achiral conditions referred in section 2.

3.2. Identification of glucuronides by LC–MS/MS

The glucuronides were eluted within 5–6 min (Figs. 3 and 4). Due to a lack of reference material, relative glucuronidation rates were determined as LC–UV peak areas. *Rac*-FLO, (+)-(R)-FLO, (−)-(S)-FLO and M17203 as substrates were used in the microsomal incubations in the range 0.01–0.50 mM. All the four substrates were found to be glucuronidated.

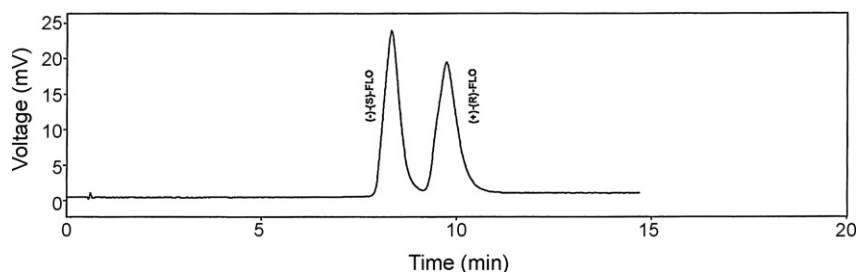


Fig. 2. Chiral separation of flobufen enantiomers on terguride column.

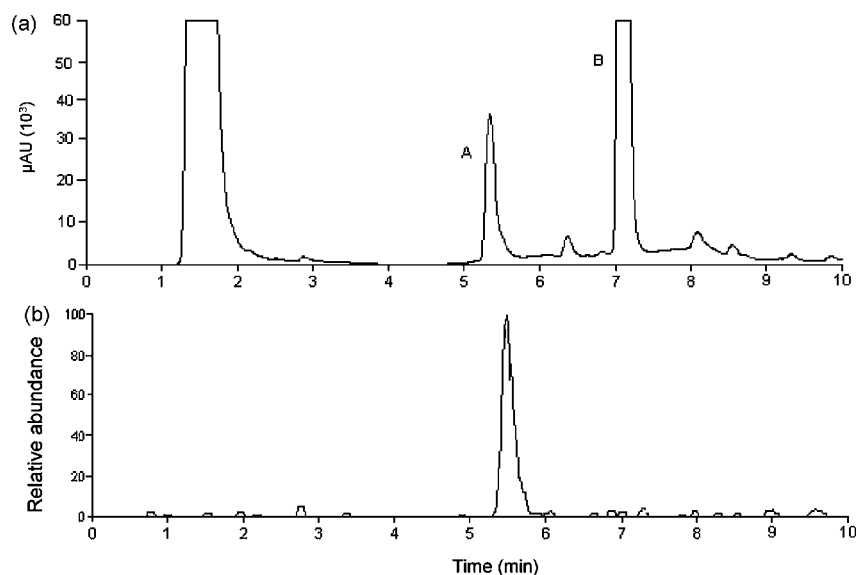


Fig. 3. (a) Chromatographic record of microsomal incubation of FLO with UDPGA—peak A (RT 5.34 min); FLO-glucuronide: peak B (RT 7.08 min); FLO; (b) MS record of extracted ion m/z 479, corresponding to FLO-glucuronide.

The ESI mass spectra of the peak typically formed after incubation of flobufen or M17203 with UDP-glucuronic acid in rat liver microsomes (Figs. 5 and 6) showed a deprotonated molecule at m/z 479 and m/z 423 ($[M - H]^-$), respectively, indicating the molecular weight of the metabolites as 480 and 424, respectively, corresponding to flobufen and M17203 glucuronides. The product ion spectrum of m/z 479 showed ions at m/z 303 and m/z 193 corresponding to deprotonated flobufen and deprotonated glucuronic acid, respectively. The single product ion at m/z 193 corresponding to deprotonated glucuronic acid was observed in the product ion spectrum of m/z 423.

Glucuronidation of all four diastereoisomers of DHF was also studied at different incubation conditions, but no glucuronide formation for any diastereoisomer was detected under the analytical conditions used.

3.3. Glucuronidation of FLO enantiomers: empirical kinetic model

Glucuronidation of (–)-(*S*)-FLO and *rac*-FLO followed a Michaelis–Menten model and the kinetic parameters were calculated using the following equation:

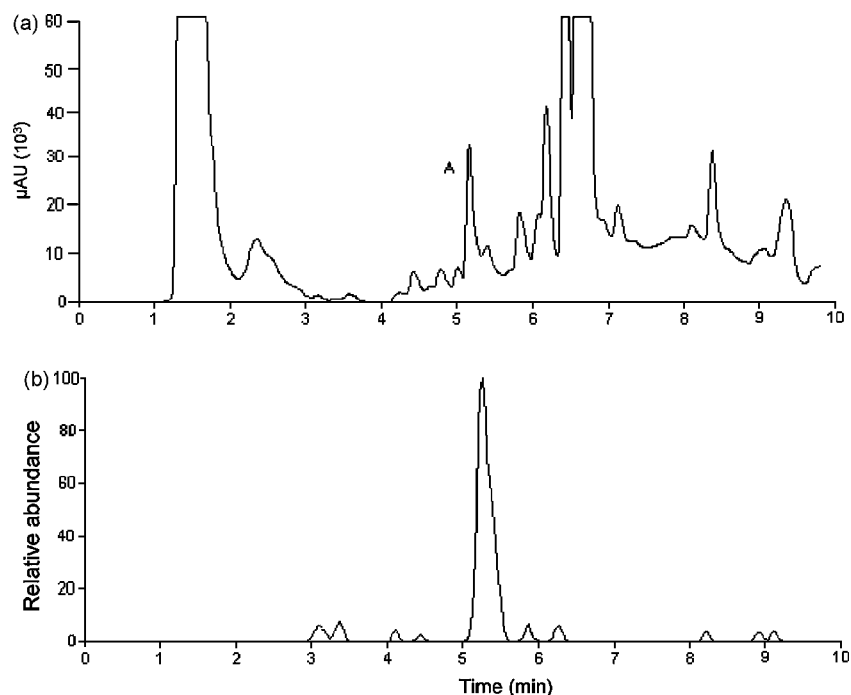


Fig. 4. (a) Chromatographic record of microsomal incubation of M17203 with UDPGA—peak A (RT 5.28 min); M17203-glucuronide. (b) MS record of extracted ion m/z 423, corresponding to M17203-glucuronide.

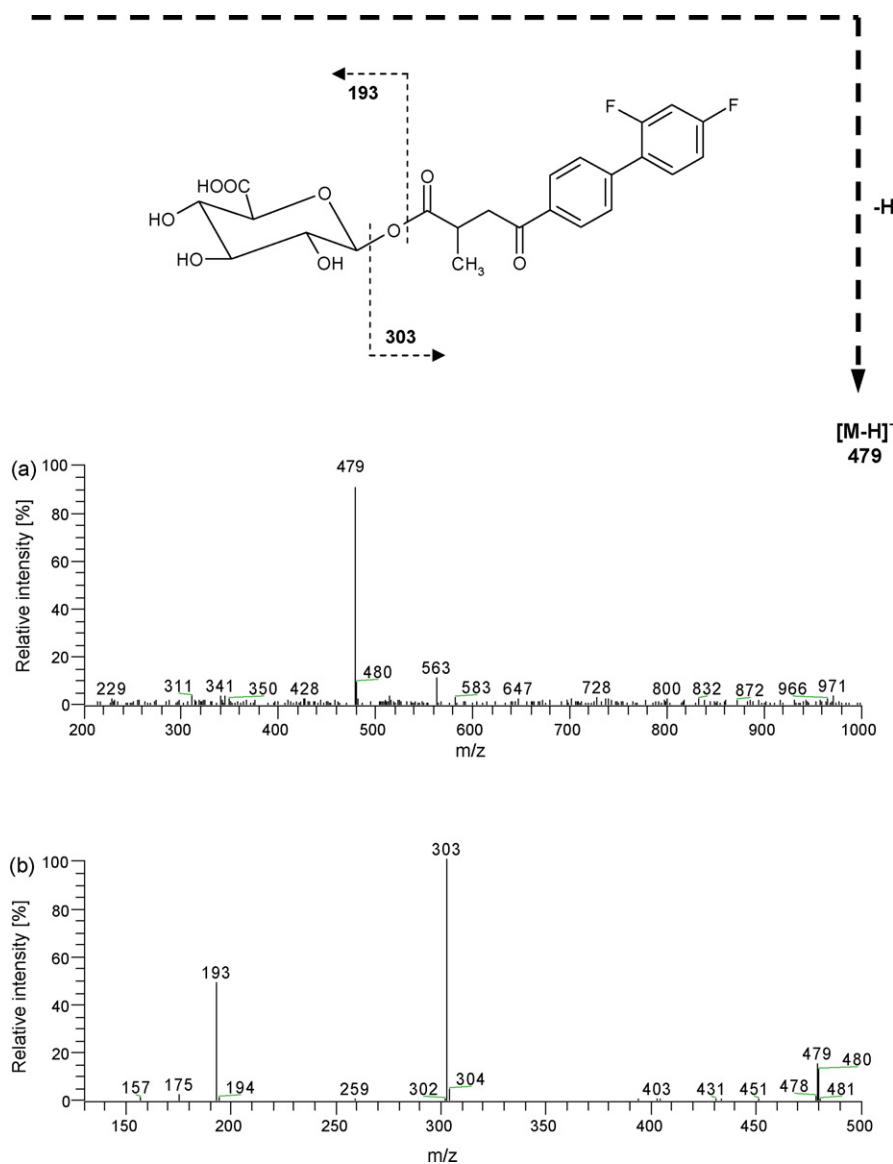


Fig. 5. Product ion spectra and proposed fragmentation scheme of the $[M-H]^-$ ion at m/z 479 of flobufen glucuronide; (a) ESI-MS spectrum and (b) ESI-MS/MS spectrum.

$$v = \frac{V_{\max}[S]}{K_m + [S]} \quad (1)$$

where v is the rate of the reaction, V_{\max} is the maximum velocity, K_m is the Michaelis constant (substrate concentration at $V_{\max}/2$) and $[S]$ is the substrate concentration. The calculated kinetic parameters are summarized in Table 2.

The glucuronidation of (+)-(*R*)-FLO, on the other hand, exhibited atypical kinetics, namely substrate inhibition kinetics. In this type of inhibition, high concentrations of substrate lead to a decrease in the rate of product formation (Fig. 7). The model of substrate inhibition kinetics is described by the following equation [27]:

$$v = \frac{V_{\max}[S]}{K_m + [S](1 + ([S]/K_s))} \quad (2)$$

where K_s is the constant describing the substrate inhibition interaction. At low concentrations of substrate, i.e., when

$[S] \ll K_s$, the $[S]/K_s$ term becomes negligible and this equation changes into Eq. (1), and therefore Michaelis–Menten kinetics is observed for the first part of the plot.

However, using this model, it was not possible to obtain a good fit of the data (based on 95% confidence intervals, r^2), yielding physically unrealistic values for all kinetic parameters.

For this reason, it was necessary to explore other models and find a suitable equation which could give a good fit to the experimental data for this type of substrate inhibition.

The Hill equation [28],

$$v = \frac{V_{\max}[S]^{nH}}{S_{50}^{nH} + [S]^{nH}} \quad (3)$$

where S_{50} is the substrate concentration resulting in 50% of V_{\max} (analogous to K_m in the previous equations) and nH is the Hill coefficient, describes sigmoidal kinetics, typical for allosteric enzymes.

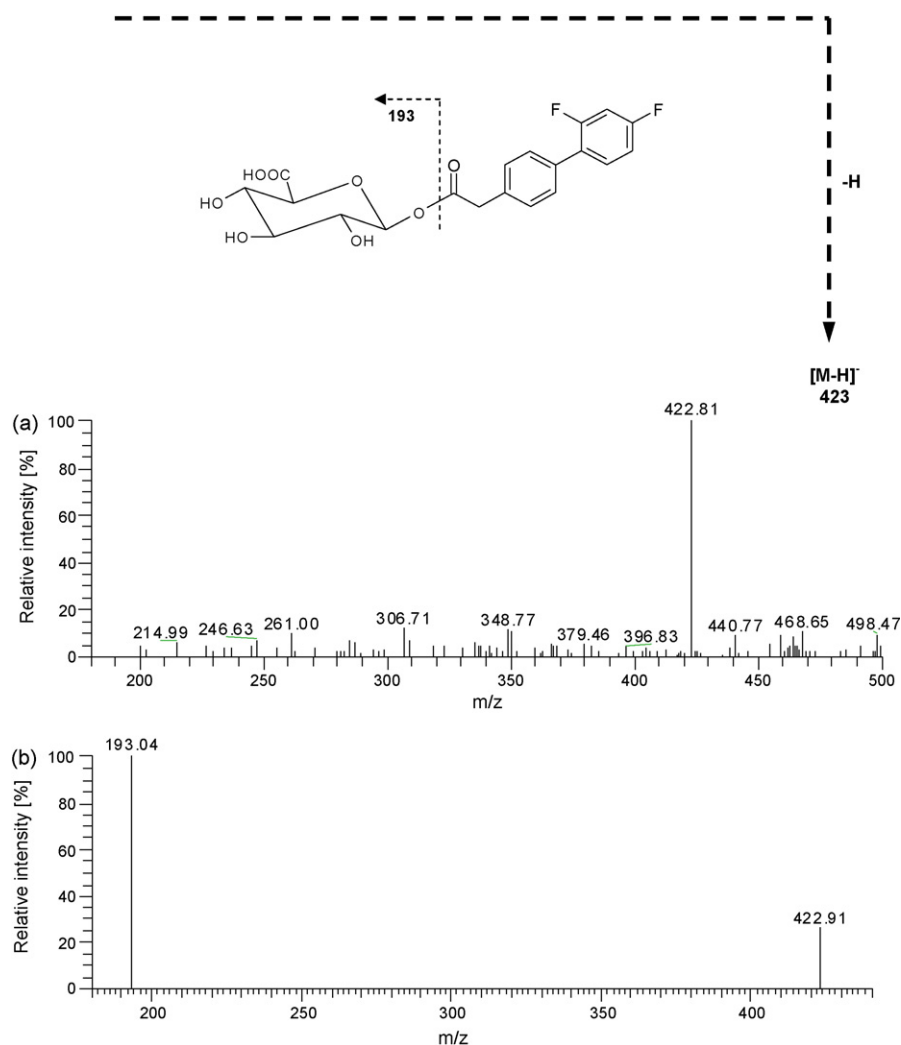


Fig. 6. Product ion spectra and proposed fragmentation scheme of the $[M - H]^-$ ion at m/z 423 of M17203 glucuronide; (a) ESI-MS spectrum and (b) ESI-MS/MS spectrum.

Evaluating the experimental data and truncating the data to the lower substrate concentrations, it was possible to verify that the Hill equation displayed the best fit, with a value of $nH = 3.2$.

Based on this assumption and relating to the inter-conversion of Eq. (1) into Eq. (2), a combined Hill-substrate inhibition equation was generated, which ultimately obtained the best fit for the experimental data:

$$v = \frac{V_{\max}[S]^{nH}}{K_m^{nH} + [S]^{nH}(1 + ([S]^{nH}/K_s^{nH}))} \quad (4)$$

The fitted parameters for this model closely match the values that would be derived by visual inspection. $K_m = 16.5 \pm 0.5 \mu\text{M}$ and $K_s = 192.0 \pm 30.3 \mu\text{M}$ are comparable to the $[S]/2$ values for the ascending and descending arms of the curve, respectively. The fitted Hill coefficient ($nH = 4.0$) also agrees with the one obtained from the Hill plot. All calculated kinetic parameters are resumed in Table 2.

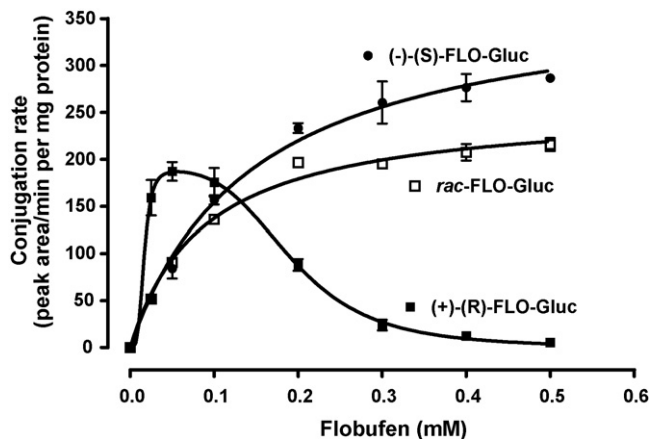


Fig. 7. Kinetic profiles of FLO-glucuronide formation from *rac*-FLO, (+)-(R)-FLO and (-)-(S)-FLO catalyzed by rat liver microsomes. Values are given as mean \pm S.D. of triplicates.

Table 2
Apparent kinetic parameters for *O*-glucuronidation of *rac*-FLO, (+)-(*R*)-FLO, (–)-(*S*)-FLO and M17203 in rat liver microsomes

	(–)-(<i>S</i>)-FLO-Gluc	<i>rac</i> -FLO-Gluc	(+)-(<i>R</i>)-FLO-Gluc	M17203-Gluc
Michaelis–Menten				
V_{\max}	380.5 ± 15.8	257.3 ± 9.7	–	–
K_m	146.0 ± 16.7	87.2 ± 11.2	–	–
r^2	0.995	0.992	–	–
Hill equation ^a				
V_{\max}	–	–	194.4 ± 8.2	38.0 ± 4.3
nH	–	–	3.2 ± 0.4	1.6 ± 0.4
S_{50}	–	–	16.3 ± 0.7	378.0 ± 44.3
r^2	–	–	0.997	0.991
Empirical model				
V_{\max}	–	–	189.6 ± 2.5	–
nH	–	–	4.0 ± 0.2	–
K_m	–	–	16.5 ± 0.5	–
K_s	–	–	192.0 ± 30.4	–
r^2	–	–	0.999	–

Values of V_{\max} are given in peak area/min per mg of protein; K_m , K_s and S_{50} in μM .

^a Fits to the Hill equation for (+)-(*R*)-FLO using truncated data.

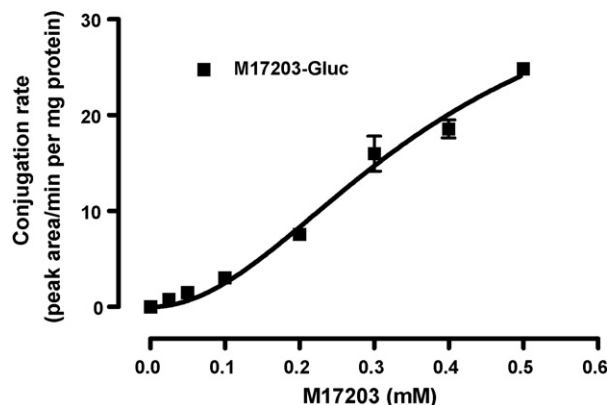


Fig. 8. Kinetic profile of M17203 glucuronide formation catalyzed by rat liver microsomes. Values are given as mean ± S.D. of triplicates.

3.4. Glucuronidation of M17203

Glucuronidation of M17203 also displayed atypical kinetics and best fitted to the Hill model – Eq. (3) – with a value of $nH = 1.6$ (Fig. 8). The calculated kinetic parameters are summarized in Table 2.

4. Discussion

The purpose of this work was to determine if FLO and/or its metabolites could undergo glucuronidation *in vitro* and, in the case of flobufen, if the reaction could be enantioselective.

The stereoselectivity of glucuronidation *in vitro* of 2-arylpropionic acids has been previously studied and concluded that the enantioselectivity was both substrate and species dependent. For instance, considering naproxen, the *S*-enantiomer is preferentially glucuronidated in rabbits, opposite to rat and monkey, where the *R*-enantiomer was selectively conjugated. In humans, the ratio of *S/R*-naproxen glucuronidation was close to 1 [18,19]. Other authors have reported that

the formation of *S*-glucuronide of different profens *in vivo* (benoxaprofen, carprofen, and flunixinaprofen) was more than two times higher than the formation of the *R*-glucuronide [29,30].

The assays performed in this study determined that, with the exception of DHF, all the other substrates are conjugated *in vitro* with glucuronic acid. However, but interestingly, the conjugation of the different substrates followed different kinetics, determining not only stereoselective glucuronidation of the different enantiomers, but suggesting also a possible implication of different UGT isoforms catalyzing the glucuronidation of the different substrates.

(–)-(*S*)-FLO displayed a typical Michaelis–Menten kinetics, whereas (+)-(*R*)-FLO exhibited substrate inhibition kinetics. This type of deviation is not so uncommon, although its mechanism is still unclear. Several models of substrate inhibition have been proposed, which include allosteric mechanisms [31], enzymatic chemical oscillations [32] and the recovery model [33]. Nevertheless, the experimental data obtained did not fit to any of the known models and it was necessary to derive an equation that could interpret the data.

The generated equation (Eq. (4)) combines a Hill equation with substrate inhibition model.

When truncating the data for (+)-(*R*)-FLO to the lower concentrations, it was possible to verify that this part of the plot assumed a sigmoidal shape, i.e., followed the Hill equation. This equation is a useful mathematical tool to describe the degree of sigmoidicity of the substrate concentration/enzyme activity relationship. It was originally proposed to provide an indication of the number of subunits in a multimeric enzyme that bound successive ligands in a cooperative manner [34]. The Hill coefficient value for the UGT isoform responsible for glucuronidation of (+)-(*R*)-FLO in the current set of experiments was around 4.0. Some authors have demonstrated that some isoforms of UGT exist as tetramers [35] and as dimers [36]. Moreover, other studies suggest that some isoforms possess more than one

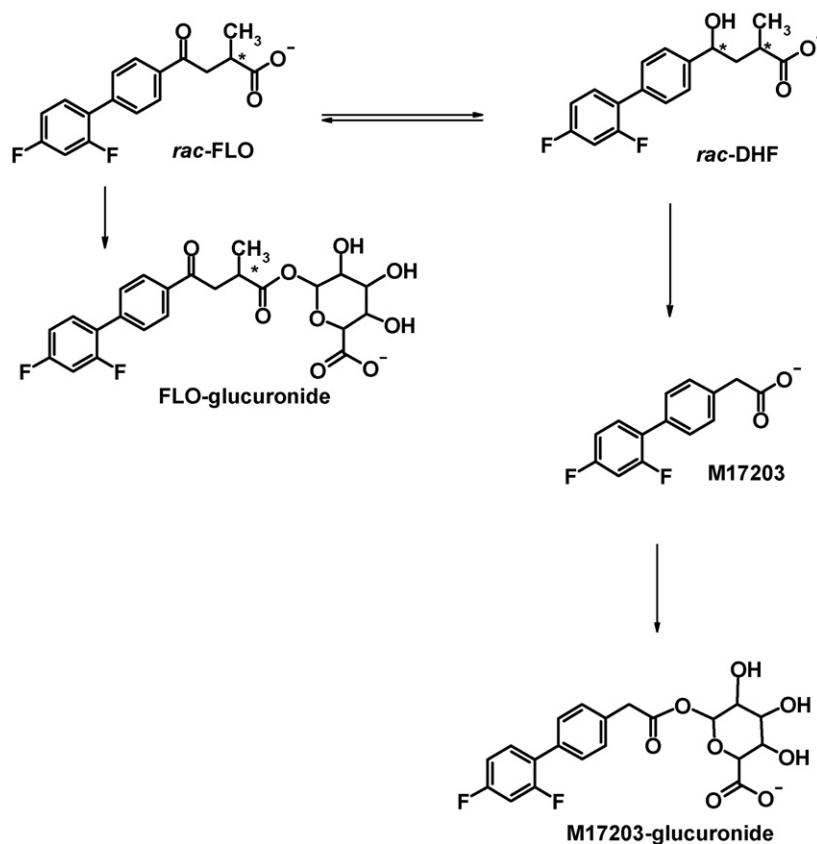


Fig. 9. Metabolic pathway of FLO and M17203 glucuronidation *in vitro* in rat liver microsomes.

active site [37]. Based on these studies, it can be assumed that the UGT isoform implicated in (+)-(*R*)-FLO glucuronidation behaves as a cooperative ligand-binding multisubunit enzyme. When analysing the set of data as a whole, in opposition to a cooperative behaviour for lower substrate concentrations, substrate inhibition was observed for higher concentrations of substrate.

As it was not in the scope of this work, the empirical model here exposed needs further investigations in order to better explain the mechanisms of this particular type of substrate inhibition.

Analysing the kinetic parameters values for both enantiomers of flobufen, and considering only the truncated fitted values for (+)-(*R*)-FLO, it should be said that the *R*-enantiomer is the preferential substrate for glucuronidation, at lower concentrations, as its S_{50} (analogous to K_m) is about ninefold higher than the K_m for the *S*-enantiomer. However, the overall view clearly suggests (–)-(*S*)-FLO as the elected substrate for glucuronidation, as for higher concentrations, the *R*-enantiomer exhibits substrate inhibition, as already referred. The fitted kinetic values for *rac*-FLO are, in fact, about the average of the kinetic values of both enantiomers.

Glucuronidation of M17203 occurs to a lesser extent when compared to the other substrates studied, nevertheless it can be assumed that another UGT isoform different from the ones catalyzing the enantiomers of flobufen is implicated in this reaction, as it follows the Hill model with $nH=1.6$. The

same explanation earlier given for the kinetics at lower concentration of (+)-(*R*)-FLO can be extended to the kinetics of M17203.

5. Conclusions

New analytical LC method for separation of flobufen glucuronides was developed. ESI-MS and ESI-MS/MS were used to confirm structure of the respective glucuronides. The present work demonstrated that flobufen, like many other known NSAIDs, is selectively glucuronidated in rat *in vitro* (Fig. 9). The fitted kinetic values suggest that, for lower concentrations, (+)-(*R*)-FLO is the primary substrate for glucuronidation and following the increase of its concentration, where inhibition is exhibited, (–)-(*S*)-FLO is taken as substrate. M17203, the main metabolite of FLO, is likewise glucuronidated, although to a lesser extent.

All these glucuronide structures were proved by MS/MS method. The study was performed with pure individual enantiomers employing achiral chromatographic conditions because no chiral inversion was observed when using chiral chromatography. Furthermore, a unique feature was found as the individual enantiomers of flobufen followed different kinetic profiles; while (–)-(*S*)-FLO displayed Michaelis–Menten type of kinetics, (+)-(*R*)-FLO followed a particular type of substrate inhibition model.

These results are important for flobufen as a veterinary drug itself and should be followed by testing in other species but can

be equally useful in the study of new xenobiotics, especially those which are structurally related to 2-arylpropionic acids.

Acknowledgements

The authors would like to thank Dr. Miroslav Kuchar for providing the standards of *rac*-FLO, its pure enantiomers, M17203 and pure DHF stereoisomers. We would also like to thank Dr. Radim Kral for his excellent assistance regarding MS analysis. We also gratefully acknowledge the Ministry of Education, Youth and Sports of Czech Republic through its Grant No. MSM 0021620822.

References

- [1] J.R. Vane, R.M. Botting, *Am. J. Med.* 104 (1998) 2S.
- [2] N. Muller, E. Payan, F. Lapicque, B. Bannwarn, P. Netter, *Fundam. Clin. Pharmacol.* 4 (1990) 617.
- [3] J. Caldwell, A.J. Hutt, S. Fournel-Gigleux, *Biochem. Pharmacol.* 37 (1988) 105.
- [4] D.S. Hall, Q. Xiaotao, *Chem-Biol. Interact.* 90 (1994) 235.
- [5] R. Brugger, C. Reichel, B.G. Alia, K. Brune, T. Yamamoto, I. Tegeder, G. Geisslinger, *Biochem. Pharmacol.* 61 (2001) 651.
- [6] W. Rhys-Williams, F. McCarthy, J. Baker, Y.F. Hung, M.J. Thomason, A.W. Lloyd, G.W. Hanlon, *Enzyme Microb. Technol.* 22 (1998) 281.
- [7] M. Glowka, J. Karazniewicz, *Pharm. Biomed. Anal.* 35 (2004) 807.
- [8] P.A. Insel, in: J.G. Hardman, L.E. Limbird, P.B. Molinoff, R.W. Ruddon, A.G. Gilman (Eds.), *The Pharmacological Basis of Therapeutics*, McGraw-Hill, New York, 1996, pp. 617–658.
- [9] M. Kuchar, V. Vosatka, M. Poppova, E. Knezova, V. Panajotovova, H. Tomkova, J. Taimr, *Collect. Czech Chem. Commun.* 60 (1995) 1026.
- [10] E. Kvasnickova, B. Szotakova, V. Wsol, F. Trejtnar, L. Skalova, I.M. Hais, M. Kuchar, M. Poppova, *Exp. Toxic. Pathol.* 51 (1999) 88.
- [11] V. Wsol, R. Kral, B. Szotakova, F. Trejtnar, F. Flieger, *Chirality* 13 (2001) 754.
- [12] R. Kral, L. Skalova, B. Szotakova, J. Velik, L. Schroterova, Y.N. Babu, V. Wsol, *BMC Pharmacol.* 3 (5) (2003) 1.
- [13] L. Skalova, R. Kral, B. Szotakova, Y.N. Babu, L. Pichard-Garcia, V. Wsol, *Chirality* 15 (2003) 433.
- [14] R. Kral, L. Skalova, B. Szotakova, Y.N. Babu, V. Wsol, *Chirality* 16 (2004) 1.
- [15] M. Kuchar, A. Jandera, V. Panajotova, V. Wsol, E. Kvasnickova, A. Jegorov, *Chem. Papers* 52 (1998) 436.
- [16] F. Trejtnar, V. Wsol, B. Szotakova, L. Skalova, P. Pavek, M. Kuchar, *Chirality* 11 (1999) 781.
- [17] F. Trejtnar, R. Kral, P. Pavek, V. Wsol, *Chirality* 15 (2003) 724.
- [18] M. El Mouelhi, H.W. Ruelius, C. Fenselau, D.M. Dulik, *Drug Metab. Dispos.* 15 (1987) 767.
- [19] M. El Mouelhi, S. Beck, K.W. Bock, *Biochem. Pharmacol.* 46 (1993) 1298.
- [20] G.S. Yost, L.P. Johnson, S. Pallante, M. Colvin Jr., C. Fenselau, *Fed. Proc.* 40 (1981) 650.
- [21] B. Silber, N.H.G. Holford, S. Riegelman, *J. Pharm. Sci.* 71 (1982) 699.
- [22] S.F. Sisenwine, C.O. Tio, F.V. Hadley, A.L. Liu, H.B. Kimmel, H.W. Ruelius, *Drug Metab. Dispos.* 10 (1982) 605.
- [23] B.K. Wilson, J.A. Thompson, *Drug Metab. Dispos.* 12 (1984) 161.
- [24] J.R. Gillete, in: B.N. La Du, H.G. Mandel, E.L. Way (Eds.), *Fundamentals of Drug Metabolism and Drug Disposition*, Williams and Wilkins, Baltimore, 1971, pp. 400–418.
- [25] P.K. Smith, R.I. Krohn, G.T. Hermanson, A.K. Mallia, F.H. Gartner, M.D. Provenzano, E.K. Fujimoto, N.M. Goeke, B.J. Olson, D.C. Klenk, *Anal. Biochem.* 150 (1985) 76.
- [26] M.B. Fisher, K. Campanale, B.L. Ackermann, M. Vandenbranden, S.A. Wrighton, *Drug Metab. Dispos.* 28 (2000) 560.
- [27] A. Gangloff, A. Garneau, Y.-W. Huang, F. Yang, S.-X. Lin, *Biochem. J.* 356 (2001) 269.
- [28] A. Cornish-Bowden, *Fundamentals of Enzyme Kinetics*, Portland Press, London, 1995, pp. 203–216.
- [29] H. Spahn, S. Iwakawa, E.T. Lin, L.Z. Benet, *Pharm. Res.* 6 (1989) 125.
- [30] S. Iwakawa, H. Spahn, L.Z. Benet, E.T. Lin, *J. Pharm. Pharmacol.* 19 (1991) 853.
- [31] V.J. LiCata, N.M. Allewell, *Biophys. Chem.* 64 (1997) 225.
- [32] P. Shen, R. Larter, *Biophys. Chem.* 67 (1994) 1414.
- [33] P.W. Kuhl, *Biochem. J.* 298 (1994) 171.
- [34] J.A. Williams, B. Ring, V.E. Cantrell, K. Campanale, D.R. Jones, S.D. Hall, S.A. Wrighton, *Drug Metab. Dispos.* 30 (2002) 1266.
- [35] W.H. Peters, P.L. Jansen, *J. Hepatol.* 2 (1986) 182.
- [36] R. Meech, P.I. Mackenzie, *J. Biol. Chem.* 272 (1997) 26913.
- [37] G.R. Rios, T.R. Tephly, *Drug Metab. Dispos.* 30 (2002) 1364.

A rapid and reliable size-exclusion chromatographic method for determination of kojic dipalmitate in skin-whitening cosmetic products

Angel Balaguer^a, Amparo Salvador^a, Alberto Chisvert^{b,*}

^a *Departamento de Química Analítica, Facultad de Química, Universidad de Valencia, 46100 Burjassot, Valencia, Spain*

^b *Departamento de Química Analítica, Nutrición y Bromatología, Facultad de Ciencias, Universidad de Alicante, P.O. Box 99, E-03080 Alicante, Spain*

Received 24 July 2007; received in revised form 31 October 2007; accepted 8 November 2007

Available online 17 November 2007

Abstract

A size-exclusion chromatographic method has been developed to determine the relatively novel skin-whitening agent called kojic dipalmitate (KDP) in skin-whitening cosmetic products.

Preliminary experiments were carried out in order to select the solvent for standard and sample solution, and also for mobile phase composition. A PLGel Mixed-D (polystyrene/divinylbenzene co-polymer) column and isocratic mobile phase of pure tetrahydrofuran (at 1.5 mL min⁻¹ flow rate) were used. Detection was carried out by means of an UV/vis spectrometry detector set at 248 nm.

A study of interferences reveals that KDP can be determined without interferences coming from cosmetic matrices. Most other cosmetic ingredients usually employed in skin-whitening cosmetic products, such as other whitening agents and common UV filters, do not interfere.

The accuracy and precision of the proposed method was tested by the analysis of six laboratory-made and five commercial skin-whitening cosmetic samples.

The sensitivity and limit of detection (3 µg mL⁻¹) obtained are suitable for the analysis of this type of samples. The chromatographic run takes less than 8 min to complete.

All these features make the method easy to apply to quality control in the cosmetic industry.

© 2007 Elsevier B.V. All rights reserved.

Keywords: Kojic dipalmitate; Skin-bleaching agent; Skin-whitening agent; Cosmetic; Size-exclusion chromatography

1. Introduction

The appearance of brown-spots on skin, as a consequence of hyperpigmentation, is one of the most common aesthetic problems [1]. This skin disorder is a consequence of melanin excess, produced by hyperactivity of melanocytes, which are the cells responsible for skin pigmentation. This could be caused by over-exposure to solar radiation, ageing, hormone disorders, genetic predisposition, etc. [2,3].

This disorder can be reduced with cosmetic treatment based on the use of so-called skin-whitening (also referred to as skin-bleaching) cosmetic products [4], although the most serious cases could require medical assistance. These products contain different chemicals called skin-whitening (or skin-bleaching)

agents that produce a whitening effect on the skin, based on the inhibition that they produce in melanin biosynthesis via different mechanisms [4–6].

Most of the commercially available skin-whitening cosmetic products found elsewhere are based on the use of the active called kojic acid, whose skin-whitening efficacy has been proven [5,7]. However, due to its labile oxidative properties, which can be accelerated in presence of light and heat [8,9], recently, kojic acid is added to cosmetics by means of its dipalmitic ester, that is, as kojic dipalmitate (KDP) (see Fig. 1), which is hydrolyzed by means of esterases located in skin cells producing an *in situ* liberation of kojic acid [10].

Although no adverse effects have been reported concerning cosmetics containing KDP, it should be controlled in this type of products in order to assure their efficacy. However, as with other cosmetic ingredients, there are no official analytical methods; moreover, in contrast to other cosmetic ingredients, no published papers have been found reporting KDP determination,

* Corresponding author. Tel.: +34 96 590 34 00x3117; fax: +34 96 590 35 27.
E-mail address: alberto.chisvert@ua.es (A. Chisvert).

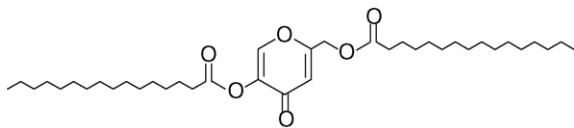


Fig. 1. Molecular structure of kojic dipalmitate (KDP).

as recently reviewed by the authors of this article [11], probably owing to the fact that it is a very recent cosmetic ingredient. Therefore, analytical methods to determine KDP must be developed for accurate and precise determination of this cosmetic ingredient, thus assuring the efficacy of this type of cosmetic products. Furthermore, it should be borne in mind that cosmetic industry demands rapid analytical methods.

In this respect, the aim of this paper focuses on developing a reliable and rapid analytical method based on liquid chromatography (LC), which is able to carry out the determination of KDP in cosmetic products. The method is based on the use of size-exclusion chromatography (SEC) with ultraviolet/visible spectrometry (UV/vis) detection.

2. Experimental

2.1. Apparatus

A Hitachi LC system equipped with a Hitachi L-7100 high-pressure pump and a Hitachi L7420 diode array detector (DAD) (Tokyo, Japan) was employed. The injections were carried out by means of a 7725i Rheodyne® (Rohnert Park, CA, USA) manual injector equipped with a 20 μL loop. A personal computer equipped with a LC System Manager software connected to the LC system was used to process all chromatographic data.

A PLGel Mixed-D (polystyrene/divinylbenzene co-polymer) (300 mm \times 7.5 mm i.d., 5 μm particle size) analytical column from Polymer Laboratories (Church Stretton, Shropshire, UK) and a PLGel Guard (50 mm \times 7.5 mm i.d. 5 μm particle size) guard column made up of the same stationary phase were used in the proposed method.

An ultrasonic water bath from Torrecilla (Valencia, Spain) was used to improve KDP extraction.

2.2. Reagents and samples

Kojic dipalmitate (KDP) 98% from Chengdu Wonho Biology Engineering Co., Ltd. (Mainland, China) was used as standard.

LC-grade tetrahydrofuran (THF) from Scharlau Chemie (Barcelona, Spain) was used as solvent to prepare standard and sample solutions and mobile phase.

Five commercial samples (A–E) purchased in local markets containing different amounts of KDP were analysed. They were from different laboratories: Sesderma S.L. (Rafelbunyol, Valencia, Spain), Interpharma (Sta. Coloma de Gramanet, Barcelona, Spain), SVR Laboratoires (Bondoufle, France) and Industrial Farmacéutica Cantabria (Santander, España).

Six laboratory-made skin-whitening creams (LM1–LM6) containing different amounts of the target skin-whitening agent (1.52%, 0.49%, 2.16%, 2.66%, 1.05% and 2.84%, respectively)

were prepared in our laboratory. These formulations also contained different usual cosmetic ingredients employed in this type of cosmetics (emollients, surfactants, smoothing agents, UV filters, moisturizing agents, preservatives) (see Table 1), which were of cosmetic-grade and were provided by Guinama S.L. (Valencia, Spain).

2.3. Proposed method

Each sample was homogenized and, in triplicate, 0.02–0.07 g was weighed into a 10 mL volumetric flask, and dissolved in 5 mL approx. of THF. In order to accelerate the solubility, an ultrasonic water bath was used for 10 min. Next, the mixture was left to reach room temperature and diluted to the mark with the same solvent. Finally, the solution was filtered through a 0.45 μm nylon membrane filter.

A 1000 $\mu\text{g mL}^{-1}$ KDP stock standard solution was prepared in the same solvent as samples, and adequately diluted using the same solvent to prepare a set of standard solutions ranging from 20 to 100 $\mu\text{g mL}^{-1}$.

Both sample and standard solutions were injected into the LC system through a 0.45 μm nylon membrane filter, and each run was performed by using THF at 1.5 mL min^{-1} as mobile phase. The UV detection was carried out at 248 nm.

3. Results and discussion

3.1. Preliminary studies

In order to select a suitable solvent to dissolve and dilute the analyte, 11 solvents of different polarity were assayed; namely heptane, dichloromethane, ethyl acetate, acetonitrile, tetrahydrofuran (THF), isobutyl methyl ketone, dimethylformamide, isopropanol, ethanol, methanol and water.

Only dichloromethane and THF were suitable for KDP solubilization. Samples were soluble in both solvents.

The addition of water to solutions of KDP in these two solvents was also assayed. Water is not miscible with dichloromethane, but when water was added (10% approx.) to THF, KDP precipitation occurred.

As its toxicity levels are lower, THF was chosen for further experiments.

Pure THF was chosen as mobile phase in order to avoid KDP precipitation inside the LC system. When reversed-phase chromatography was assayed, by means of a LiChrospher® RP-18 (250 mm \times 4 mm i.d., 5 μm particle size) column, KDP was not retained in the column, since pure THF (at 1 mL min^{-1} flow rate) has a considerable elution strength for reversed-phase chromatography, and thus, KDP eluted at dead time jointly with the rest of the unretained components of the sample, which interfered in the determination. Therefore, this chromatographic retention mechanism was rejected.

Thus, SEC (size-exclusion chromatography) was tested using a PLGel Mixed-D (polystyrene/divinylbenzene co-polymer) column, giving suitable retention by employing THF at 1 mL min^{-1} flow rate. Owing to the large molecular structure of KDP (see Fig. 1) compared with other usual ingredients

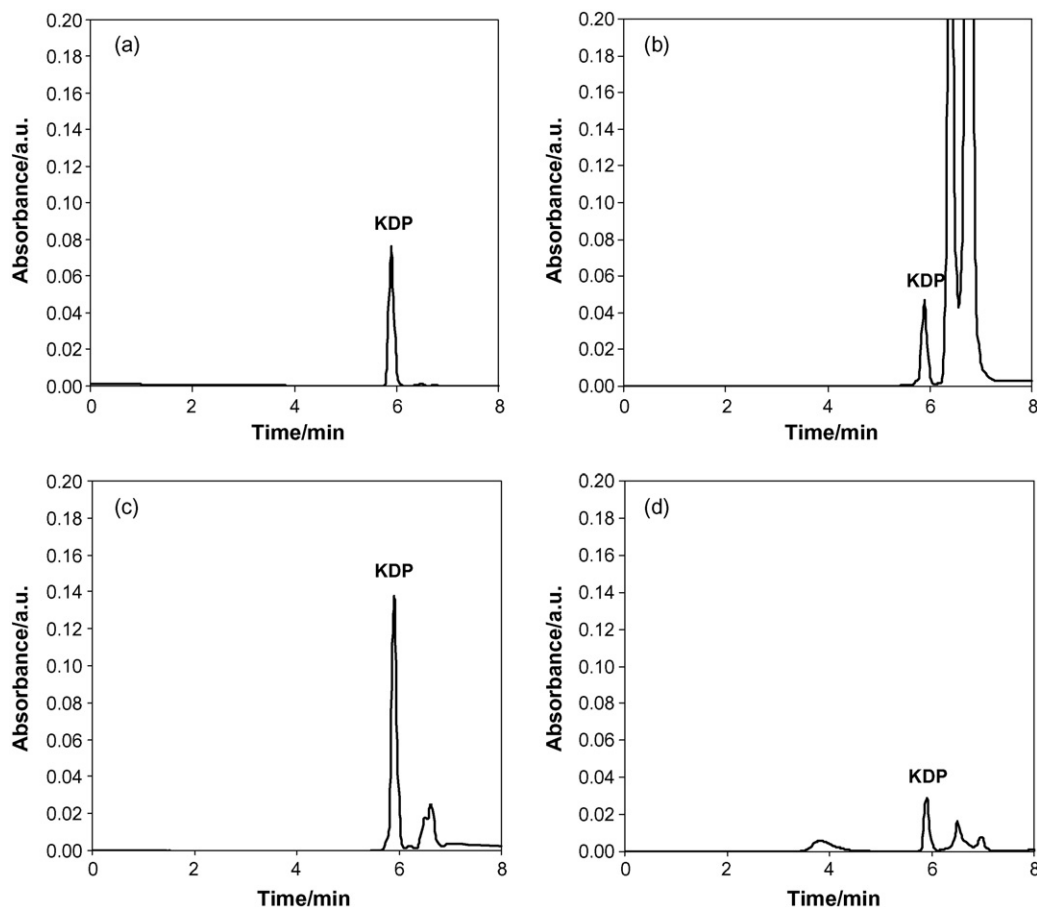


Fig. 2. Chromatograms of (a) KDP $40 \mu\text{g mL}^{-1}$ standard solution, (b) laboratory-made sample LM1, (c) laboratory-made sample LM3 and (d) commercial sample D, obtained by using the proposed method.

employed in skin-whitening cosmetic products containing KDP, they were separated effectively. This study is further described in Section 3.2.

The effect of flow rate was studied over the range $0.5\text{--}1.5 \text{ mL min}^{-1}$. Higher flow rates were not possible because they caused pump pressures over the safety limit. Obviously, KDP retention time decreased when flow rate increased, but in any case the separation from other assayed ingredients changed significantly. A flow rate of 1.5 mL min^{-1} was chosen, since it provided a retention time for KDP of 5.90 min approx. and a suitable run time analysis of less than 8 min, as shown in Fig. 2.

3.2. Study of interferences

Different compounds that may commonly be present in skin-whitening cosmetic products, and thus, could interfere in determining the target analyte, were assayed at the conditions selected in the proposed method.

Thus, seven other common skin-whitening agents were assayed, namely arbutine, hydroquinone, kojic acid, ascorbic acid, ascorbyl glucoside, ascorbyl phosphate (sodium salt) and ascorbyl palmitate. Three of them, namely ascorbic acid, ascorbyl glucoside, ascorbyl phosphate (sodium salt) were not soluble in THF owing to their water-solubility behaviour, and were retained in the filter step. The other four were eluted after KDP

(retention time of 5.90 min) (6.21, 6.50, 6.51 and 6.53 min approx.), as expected given the smaller molecular size, and did not interfere.

Furthermore, the presence of UV filters was assayed. These compounds are added to skin-whitening cosmetics to protect users' skin from sunlight to avoid tanning [12]. Thus, five water-soluble UV filters, namely disodium phenyldibenzimidazole tetrasulphonate, PABA (*p*-aminobenzoic acid), phenylbenzimidazole sulphonic acid, benzophenone-4 and PEG-25 PABA were tested. All of them eluted after KDP, owing to their smaller size, except PEG-25 PABA (i.e. polyoxyethylene ethyl-4-aminobenzoate), whose molecular structure is quite large, and which interfered in the determination of KDP. Moreover, 14 fat-soluble UV filters were assayed, namely benzophenone-3, isoamyl methoxycinnamate, 4-methylbencyliden camphor, octocrylene, ethylhexyl dimethyl PABA, ethylhexyl methoxycinnamate, butyl methoxydibenzoylmethane, homosalate, ethylhexyl salicylate, diethylhexyl butamido triazone, ethylhexyl triazone, drometrisole trisiloxane, bis-ethylhexyloxyphenol methoxyphenyl triazine and polysilicone-15. All of them also eluted after KDP, except polysilicone-15, which eluted before KDP (5.04 min approx.), and diethylhexyl butamido triazone, ethylhexyl triazone and drometrisole trisiloxane which interfered in KDP determination.

Table 1
Composition in percentage terms of the analysed laboratory-made samples

Ingredient	Laboratory-made samples					
	LM1	LM2	LM3	LM4	LM5	LM6
Base o/w ^a	19.6	20.7	19.2	17.4	17.8	17.2
KDP	1.52	0.49	2.16	2.66	1.05	2.84
Dimethicone 350	5.1	5.2	5.1	5.0	5.3	5.4
Avocado pear oil	5.1	5.7	0	0	0	0
Wheat germ oil	0	0	5.2	5.2	0	0
Coconut oil	0	0	0	0	5.2	5.6
Aloe vera	0	0	0	0	0.8	0.5
Propylene glycol	5.2	5.3	4.9	5.0	5.0	5.4
Hydroviton ^{®b}	4.3	3.8	4.1	4.0	3.9	3.9
Phenonip ^{®c}	0.5	0.5	0.5	0.5	0.5	0.5
Benzophenone-3 ^d	5.2	4.8	0	0	0	0
Butyl methoxydibenzoyl methane ^d	2.6	2.4	0	0	0	0
Ethylhexyl methoxycinnamate ^d	5.0	5.2	0	0	5.3	5.2
Ethylhexyl salicylate ^d	0	0	0	0	2.7	2.8
Glycolic acid	0	0	0	0	4.9	5.0
Lactic acid	0	0	1.3	1.4	0	0
Resorcinol	0	0	0.5	0.5	0	0
Arbutin ^e	0	0	2.4	2.2	0	0
Azelaic acid ^e	0	0	1.9	2.1	0	0
Kojic acid ^e	0	0	1.6	0.9	0	0
Phytic acid ^e	0	0	0	0	1.1	1.1
Hydroquinone ^e	0	0	0.9	1.0	0	0
Water	Up to 100	Up to 100	Up to 100	Up to 100	Up to 100	Up to 100

^a Base for production of oil/water emulsions, made up of fatty substances, such as myristyl myristate, cetyl alcohol, glyceryl laurate, cetearyl ethylhexanoate, isopropyl myristate, among others.

^b Moisturizing cosmetic preparation made up of urea, sodium chloride, glycerine, sodium lactate, allantoin, amino acids and water, among others.

^c Cosmetic preparation containing a mixture of preservatives such as: phenoxyethanol, methyl-, ethyl-, propyl-, butyl- and isobutylparaben.

^d Common UV filters combined with KDP in cosmetics.

^e Other cosmetic ingredients employed as skin-whitening agents.

Fortunately, these four UV filters, which coelute with KDP when the proposed method is used, have not been found mixed with KDP in the present commercial skin-whitening products. Nevertheless, this limitation should be taken into account for the analysis of further formulations.

3.3. Analytical figures of merit of the proposed method

The repeatability of the measurements was tested by injecting a 50 $\mu\text{g mL}^{-1}$ KDP standard solution five times. Retention time and its standard deviation was 5.90 ± 0.01 min. Relative standard deviation (R.S.D.) in area was 0.9%. Results indicate suitable precision in both cases.

The upper linearity limit ($650 \mu\text{g mL}^{-1}$) was established by injecting standard solutions of KDP in THF (from 10 to $1000 \mu\text{g mL}^{-1}$). Nevertheless, the working range was set from 20 to $100 \mu\text{g mL}^{-1}$ (number of calibration points, $N=5$), showing a calibration line such as $A_{\text{KDP}} = (6050 \pm 40)C_{\text{KDP}} - (0 \pm 2000)$; $R^2 = 0.99998$, where A_{KDP} is the KDP peak area expressed in $\mu\text{V s}$, C_{KDP} is KDP concentration expressed in $\mu\text{g mL}^{-1}$ and R^2 is the regression coefficient.

Thus, the sensitivity of the instrumental measurements estimated by means of the slope of the calibration line was 6050 ± 40 ($\mu\text{V s})/(\mu\text{g mL}^{-1})$.

The limit of detection estimated as $3s_{y/x}/b$ (where $s_{y/x}$ is the standard deviation of the calibration curve and b is the slope) was $3 \mu\text{g mL}^{-1}$, which is suitable for the analysis of this type of samples.

In order to evaluate the accuracy of the method, six laboratory-made skin-whitening cosmetic products containing known amounts of the analyte, whose composition is shown in Table 1, were analysed. Fig. 2 shows the chromatograms of laboratory-made samples LM1 and LM3. The results are shown in Table 2. The obtained R.S.D. in concentration values ranged from 0.1% to 2.5%, demonstrating precise results. The method has a low relative error (<4%), thus results are accurate. The data obtained using the proposed method (Y) were compared to the nominal values (X) by using a linear regression model.

Table 2
Results obtained in the analysis of six laboratory-made skin-whitening samples by using the proposed method

Sample	Real content (% w/w)	Found content $\pm s^a$ (% w/w)	Error (%)
LM1	1.52	1.46 ± 0.02	-3.9
LM2	0.49	0.490 ± 0.008	0.0
LM3	2.16	2.08 ± 0.01	-3.7
LM4	2.66	2.692 ± 0.002	1.2
LM5	1.05	1.028 ± 0.002	-2.1
LM6	2.84	2.81 ± 0.07	-1.1

^a Average values of three determinations \pm standard deviation (s).

Table 3

Results (and recoveries) obtained in the analysis of commercial skin-whitening cosmetic products by using the proposed method

Sample	Found content \pm s ^a (% w/w)	Recovery (%)
A	1.11 \pm 0.01	99 \pm 2
B	1.79 \pm 0.08	101 \pm 2
C	1.58 \pm 0.03	102 \pm 2
D	2.14 \pm 0.08	102 \pm 2
E	0.34 \pm 0.01	100 \pm 2

^a Average values of three determinations \pm standard deviation (s).

The equation obtained was: $Y = (1.00 \pm 0.02)X - (0.03 \pm 0.04)$; $R^2 = 0.998$; $N = 6$, where Y and X are expressed in % KDP (w/w). The theoretical t -value for a 5% significance level and $N - 2$ degrees of freedom is 2.78, and the experimental t -values for the slope and the intercept were 0.01 and 0.61, respectively, which statistically proves the accuracy of the proposed method.

Finally, the robustness was proven by analyzing the six laboratory-made samples with small changes in the mobile phase flow rate (± 0.1 ml min⁻¹) and in the monitoring wavelength (± 1 nm). The results were compared by an ANOVA test [13], showing the comparability for a 5% confidence level, and thus showing the robustness of the method.

3.4. Application of the proposed method to the analysis of commercial skin-whitening cosmetic products

The method was employed to determine the target skin-whitening agent in five commercial samples (data given in Table 3). A chromatogram obtained for one of these samples is shown in Fig. 2.

On the other hand, according to the results obtained, the R.S.D. in concentration is obviously in the same order as that obtained in the analysis of laboratory-made samples.

As no methods have been published for KDP determination, it was not possible to evaluate the accuracy of the obtained values, since the nominal values were unknown. Therefore, solutions of the five commercial samples were spiked with known amounts of the target analyte and the recoveries were evaluated. Excellent recoveries were obtained, as shown in Table 3.

4. Conclusions

A rapid and reliable analytical method to determine the relatively novel skin-whitening agent called kojic dipalmitate (KDP)

is proposed here for the first time. The method is based on size-exclusion chromatography with conventional UV/vis detection.

The chromatographic run takes less than 8 min to complete, with good resolution.

The study of interferences reveals that KDP can be determined without interferences coming from cosmetic matrices. Most of other cosmetic ingredients usually employed in skin-whitening cosmetic products, such as other whitening agents and common UV filters, do not interfere.

Thus, the proposed method has been proven accurate and precise, and its sensitivity and limit of detection are suitable for the analysis of this type of samples. It has been validated by analysing laboratory-made and commercial skin-whitening products.

All these features make the method easy to apply to quality control in the cosmetic industry.

Acknowledgements

The authors acknowledge the financial support of the Spanish Government (Project CTQ2006-00296), especially A. Balaguer for his predoctoral grant.

References

- [1] M.D. Pawaskar, P. Parikh, T. Markowski, A.J. McMichael, S.R. Feldman, R. Balkrishnan, *J. Dermatol. Treat.* 18 (2007) 5.
- [2] M.I. Pérez, *Cutis* 75 (2005) 217.
- [3] P. Grimes, J.J. Nordlund, A.G. Pandya, S. Taylor, M. Rendon, J.P. Ortonne, *J. Am. Acad. Dermatol.* S255 (54) (2006).
- [4] S. Briganti, E. Camera, M. Picardo, *Pigment Cell Res.* 16 (2003) 101.
- [5] J. Cabanes, S. Chazarra, F. Garcíacarmona, *J. Pharm. Pharmacol.* 46 (1994) 982.
- [6] L. Petit, G.E. Piérard, *Int. J. Cosmet. Sci.* 25 (2003) 169.
- [7] K. Maeda, M. Fukuda, *J. Soc. Cosmet. Chem.* 42 (1991) 361.
- [8] T. Nishimura, T. Kometani, H. Takii, Y. Terada, S. Okada, *J. Jpn. Soc. Food Sci. Technol.* 42 (1995) 602.
- [9] M. Gallarate, M.E. Carlotti, M. Trotta, A.E. Grande, C. Talarico, *J. Cosmet. Sci.* 55 (2004) 139.
- [10] M. Aparecida-Nicoletti, E.M. Almeida-Orsine, A.C. Nogueira-Duarte, G. Arbex-Buono, *Cosmet. Toilet (Ed. Portuguese)* 14 (2002) 46.
- [11] A. Chisvert, A. Balaguer, A. Salvador, in: A. Salvador, A. Chisvert (Eds.), *Analysis of Cosmetics Products*, Elsevier, Amsterdam, 2007, pp. 128–140.
- [12] T. Piamphongsant, *Int. J. Dermatol.* 37 (1998) 897.
- [13] J.C. Miller, J.N. Miller, *Statistics and Chemometrics for Analytical Chemistry*, 4th ed., Prentice Hall, Harlow, UK, 2000, p. 57.

Selective solid-phase extraction of a triterpene acid from a plant extract by molecularly imprinted polymer

Bérengère Claude^a, Philippe Morin^{a,*}, Michel Lafosse^a,
Anne-Sophie Belmont^b, Karsten Haupt^b

^a Institut de Chimie Organique et Analytique, CNRS FR 2708 UMR 6005, Université d'Orléans, 45067 Orléans, France

^b Université de Technologie de Compiègne, UMR CNRS 6022, 60205 Compiègne, France

Received 26 June 2007; received in revised form 1 October 2007; accepted 7 November 2007

Available online 21 November 2007

Abstract

A molecularly imprinted polymer (MIP) has been prepared by a thermal polymerisation method using methacrylic acid as functional monomer, ethylene glycol dimethacrylate as cross-linking agent, chloroform as porogenic solvent and an oleanane triterpene compound (18- β -glycyrrhetic acid) as imprinted molecule (template).

Equilibrium ligand binding experiments were done to assess the performance of the MIP relative to non-imprinted polymer (NIP).

After optimisation of SPE protocol (CHCl₃ as washing solvent and MeOH as elution solvent), successful imprinting was confirmed by comparison of the recoveries between NIP (5%) and MIP (97%) cartridges. The binding capacity of the MIP for 18- β -glycyrrhetic acid was determined to be 0.94 mg g⁻¹.

Four structurally related oleanane triterpenes (18- α -glycyrrhetic acid, oleanolic acid, echinocystic acid, erythrodiol) were selected to assess the MIP selectivity. Experimental data illustrated the influence of functional groups on the triterpene skeleton.

The MIP was applied to the solid-phase extraction of triterpenoids from a plant extract prior HPLC analysis. However, CHCl₃ was replaced by ACN during the washing step in order to suppress non-specific interactions due to polar matrix components. A selective extraction of 18- β -glycyrrhetic acid from hydrolyzed extract of liquorice roots was achieved with a good extraction yield (98%).

© 2007 Elsevier B.V. All rights reserved.

Keywords: Molecularly imprinted polymer; Triterpene; Plant extract; Glycyrrhetic acid; Natural compounds

1. Introduction

Liquorice roots (*Glycyrrhiza glabra*) are used in herbal medicines for their anti-inflammatory, gastroprotective and anti-allergic properties. After treating dried liquorice roots with boiling water and evaporation until dryness a solid liquorice extract is obtained. The main active compound of liquorice is glycyrrhizic acid (3-*O*-(2-*O*- β -D-glucopyranuronosyl)- α -D-glucopyranurosyl)-3 β -hydroxy-11-oxo-18 β , 20 β -olean-12-en-29-oic acid). Its therapeutic potential is mainly ascribed to the action of the steroid-like structure aglycone (18- β -glycyrrhetic acid, see Fig. 1) having immunomodulatory properties. Otherwise, traces of the α -form of glycyrrhetic acid

are also present in liquorice roots but have no pharmacological activity.

A reversed-phase liquid chromatography method (HPLC) with UV detection has been previously reported for the determination of 18- β - and 18- α -glycyrrhetic acids in pharmaceutical formulations [1]. Sample preparation methods such as liquid–liquid extraction [2] or solid-phase extraction [3] have been used during the analysis of 18- β -glycyrrhetic acid in plasma with concentration recoveries higher than 85%. However, plant extracts are complex mixtures with a large variety of chemical compounds and efficient sample preparation methods are required to selectively extract 18- β -glycyrrhetic acid from hydrolyzed extract of liquorice roots. 18- β -Glycyrrhetic acid has already been analyzed by capillary electrophoresis with UV detection after a SPE (Oasis HLB cartridges) of liquorice roots extracts [4]. A good selectivity has been obtained and no matrix component has been found in the retention range of the

* Corresponding author. Tel.: +33 238 494 590; fax: +33 238 417 281.

E-mail address: philippe.morin@univ-orleans.fr (P. Morin).

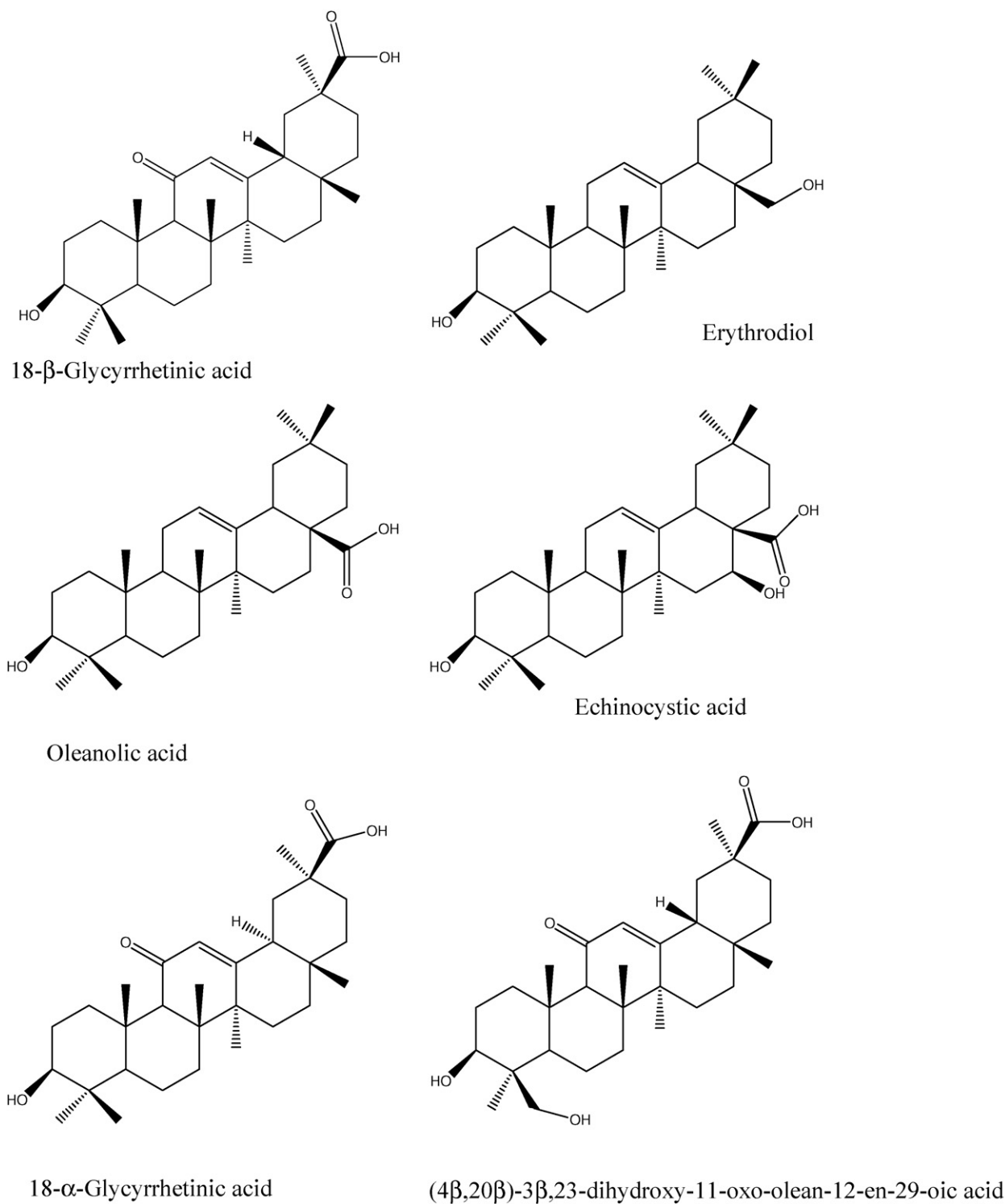


Fig. 1. Chemical structures of 18-β-glycyrrhetic acid and related triterpene compounds.

target analyte. Satisfactory recoveries (higher than 75%) were obtained with spiked liquorice roots extracts with or without hydrolysis. However, no comment has been mentioned about the interference of fatty acids which are often present in plant extracts. Indeed, conventional supports, like reversed-phase or anion exchange phases, cannot selectively extract triterpenoid acid fraction versus fatty acid fraction.

One of the most promising separation techniques that have emerged during the last decade is based on the use of molecularly imprinted polymers (MIPs). These tailor-made materials possess a high selectivity for a target molecule, similar to immunosorbents. Most of the studies have concerned the extraction of analytes from biological samples. These highly cross-linked polymers display binding sites which are able to recognize tem-

plate molecule and some of its structural analogues. These sites are complementary both sterically and chemically to the template molecule, similarly to antibodies and enzymes having sites complementary to their antigens and substrates, respectively [5]. The advantage of MIPs over such biomacromolecules is, however, their stability under hard conditions such as organic solvents or extreme pH values.

Molecularly imprinted solid-phase extraction (MISPE) has already been used to extract analyte from complex samples like plant extracts [6–9]. Good results were obtained thanks to the selective recognition by the MIP of specific analytes and related compounds.

In this study, a MIP was prepared for 18- β -glycyrrhetic acid (target molecule) using a non-covalent imprinting approach, which is based on non-covalent interactions (electrostatic, hydrogen, π - π and Van der Waals bonds) between template and monomer molecules. Numerous reports on the use of MIPs for solid-phase extraction [10] have shown that the structure, the functionalities of the template, and also the polymerisation method [11], define the selectivity and the capacity of a MIP. The experimental conditions are not straightforward as steroids imprinted polymers performances testify [12,13]. Nevertheless, a satisfactory selective rebinding was obtained for any MIP prepared from a steroid as template.

Here we report the synthesis and characterisation of a 18- β -glycyrrhetic acid MIP, by using methacrylic acid as functional monomer, ethylene glycol dimethacrylate as cross-linker and chloroform as porogenic solvent. The usefulness of the MIP for the quantification of 18- β -glycyrrhetic acid in liquorice roots extract was evaluated.

2. Experimental

2.1. Materials

Methacrylic acid (MAA), ethylene glycol dimethacrylate (EDMA), azobisisobutyronitrile (AIBN) and chloroform (>99.9% HPLC grade, CHCl_3) were from Aldrich (St. Quentin Fallavier, France). 18- α -Glycyrrhetic acid, oleanolic acid, echinocystic acid and erythrodiol (Fig. 1) were purchased from ExtraSynthèse (Genay, France). 18- β -Glycyrrhetic acid was obtained from LVMH, Parfums Christian Dior, France.

Before use, EDMA and MAA were distilled under vacuum and AIBN was recrystallized from methanol.

Methanol (MeOH), acetonitrile (MeCN) were HPLC grade and obtained from SDS (Carlo-Erba, Val de Reuil, France), glacial acetic acid was from Merck (Darmstadt, Germany). Phosphoric acid (85%) and sodium hydroxide were of analytical grade.

Deionized water (18 M Ω) was prepared with an Elgastat UHQ II system (Elga, Antony, France).

The phosphoric acid–sodium hydroxide buffer solution was prepared at pH 3.5 and at fixed ionic strength (20 mM) with the help of Phoebus software (Analis, Namur, Belgium).

The extract of liquorice roots (LVMH, Parfums Christian Dior, France) was hydrolyzed following French Pharmacopoeia before SPE extraction.

2.2. Preparation of the molecularly imprinted polymer

A 18- β -glycyrrhetic acid imprinted polymer was synthesized as follows: in an 8 mL glass test tube, 0.326 mmol 18- β -glycyrrhetic acid (template), 1.6 mmol MAA (functional monomer), 8 mmol EDMA (cross-linker) were dissolved in 2.55 mL CHCl_3 . The mixture was stirred and sonicated for 5 min. As soon as the solution became clear, 0.17 mmol AIBN was added. The solution was cooled in an ice bath and purged with nitrogen during 10 min. Then, the tube was sealed. The polymerisation was carried out at 60 °C in a water bath for 20 h, until the polymerisation was complete. The monolith polymer was ground with a pestle in a mortar and wet-sieved through a 45 μm metal sieve. The fine particles were removed by repeated sedimentation using acetone. The remaining particles were washed with MeOH–acetic acid (80:20, v/v) mixture, then with MeOH. The recovered polymer particles were dried under vacuum and stored at ambient temperature. The non-imprinted polymer (NIP) was prepared by the same procedure without adding the template to the initial polymerisation mixture.

2.3. Binding experiments

Increasing amounts of MIP particles were thoroughly mixed with 1 mL of chloroform solution of 18- β -glycyrrhetic acid (20 $\mu\text{g mL}^{-1}$). The mixtures were thermostated at 25 °C for 3 h under continuous stirring and filtered through a 0.2 μm syringe filter (Gelman Laboratory, Ann Arbor, USA). The concentration of free 18- β -glycyrrhetic acid in the filtrate was determined by HPLC–UV. The same procedure was followed for NIP particles.

2.4. SPE for assessment of MIP and NIP performances

For the SPE experiments, 60 mg of the polymer were packed in 1 mL extraction cartridges. Each cartridge was conditioned with MeOH (3 mL) and CHCl_3 (10 mL) before use. A triterpene sample (0.5 mL) dissolved in CHCl_3 was loaded on the sorbent cartridge. The cartridge was washed with CHCl_3 (2 mL) to eliminate molecules retained by non-specific interactions with the polymer. The elution of the extracted analytes was performed using MeOH (1.5 mL). Each collected fraction was evaporated to dryness under a stream of nitrogen at 25 °C and then redissolved in 0.5 mL MeOH before analysis by HPLC. The extraction procedure was done in triplicate.

2.5. Evaluation of the MIP cartridge capacity

Following the previously described SPE procedure, 0.5 mL of 18- β -glycyrrhetic acid solutions at different concentrations (42–744 $\mu\text{mol L}^{-1}$) was loaded on the MIP cartridge. Eluted fractions were collected and analyzed by HPLC. The amount of eluted 18- β -glycyrrhetic acid was plotted versus the amount of 18- β -glycyrrhetic acid loaded on the SPE cartridge. Each assay was done in duplicate. The same experiments were realized with NIP.

2.6. Extraction of 18- β -glycyrrhetic acid from extract of liquorice roots preparation by MIP-SPE

A 3 mL-volume SPE cartridge was packed with 200 mg MIP. The sorbent was successively conditioned with MeOH (6 mL) and MeCN (12 mL). The hydrolyzed extract of liquorice roots (1 mg) was dissolved in 3 mL MeCN and the obtained solution was spiked with linoleic acid ($50 \mu\text{g mL}^{-1}$). The SPE extraction was performed on a 12-Port Visiprep vacuum manifold (Supelco, Sigma–Aldrich, St. Quentin Fallavier, France). A small sample volume (0.5 mL) was loaded on the MIP cartridge until dryness and 1.5 mL MeCN were percolated through the cartridge. Then, the elution was carried out with 2 mL MeOH. Every fraction was evaporated under a gentle stream of nitrogen until dryness, and further dissolved in 0.5 mL MeOH.

Following this procedure, the loading capacities of MIP and NIP cartridges were evaluated. Three fractions of 0.5 mL liquorice extract were loaded on MIP and NIP sorbents. The breakthrough as well as the washing (1.5 mL MeCN) and elution (2 mL MeOH) fractions were analyzed by HPLC. Each extraction was made in duplicate.

In order to compare MIP versus classical reversed-phase sorbent performances, a 3 mL-volume DSC-18 (500 mg, Supelco, Sigma–Aldrich, St. Quentin Fallavier, France) solid-phase extraction was also applied on a liquorice roots extract spiked with linoleic acid. The SPE procedure included four steps: conditioning with 4 mL MeOH, 4 mL H_2O , 4 mL MeOH/ H_2O (85/15, v/v); load of 2 mL sample (obtained from dry extract roots (1 mg) dissolved in MeOH/ H_2O 85/15 (v/v) (3 mL)), then wash with MeOH/ H_2O 75/25 (v/v) (4 mL) and elution with MeOH (4 mL).

2.7. Quantification of 18- β -glycyrrhetic acid by HPLC

The separation was performed on a 150 mm \times 4.6 mm i.d., 5 μm particle size Platinum EPS- C_{18} HPLC column (Alltech France, Templemars, France). The mobile phase was MeCN/phosphate buffer (pH 3.5, 20 mM ionic strength) 80:20 (v/v). The flow rate was set at 1 mL min^{-1} . The 18- β -glycyrrhetic acid was detected at 254 nm, while other triterpene compounds and linoleic acid were detected at 210 nm.

The solvent was delivered using a programmable Solvent 126 HPLC pump (Beckman, Fullerton, USA). UV detection was done with an ABI 785A programmable Absorbance Detector (Applied Biosystem, Les Ulis, France). A Rheodyne (Cotati, CA, USA) Model 7125 injection valve fitted with a 20 μL loop was used for injection. Data were collected and analyzed using Gold software (Gold V810).

3. Results and discussion

3.1. Preparation and evaluation of the molecularly imprinted polymer

Methacrylic acid has been selected as functional monomer to interact with 18- β -glycyrrhetic acid. This monomer has

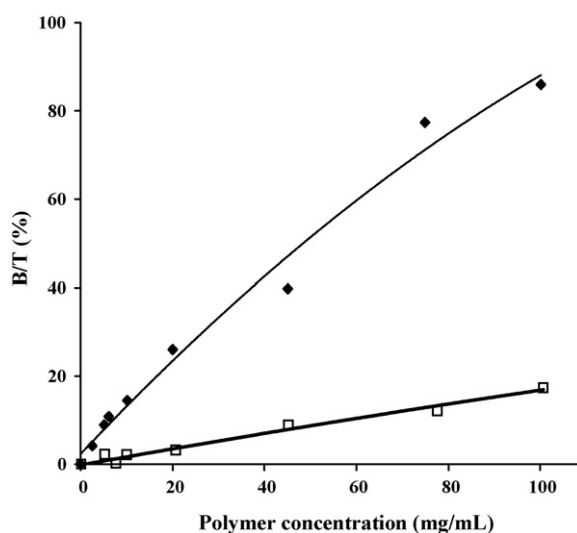


Fig. 2. Binding of 18- β -glycyrrhetic acid ($20 \mu\text{g mL}^{-1}$ in CHCl_3) to MIP (◆) and NIP (□) as a function of polymer concentration. B/T (%) is the ratio of the amount of analyte bound at equilibrium to the amount of analyte initially introduced into the vial.

already been successfully used with other steroids [4]. Otherwise, 4-vinylpyridine has also been tested as functional monomer in preliminary experiments, to benefit of electrostatic interactions between acidic and basic functions of 18- β -glycyrrhetic acid and 4-vinylpyridine, respectively. However, the obtained polymer revealed too numerous non-specific interactions and was not further studied. The proportions of template/monomer/cross-linker were fixed to 1:4.9:24.5. The monomer/porogenic solvent ratio was 3:5 (v/v) [14]. The porogenic volume was a compromise between the solubility of template–monomer mixture and the porosity of the polymer. Indeed, an increase of porogenic solvent volume induces higher pore diameter and better accessibility of the analyte into the imprinted cavities [15], but a decrease of particle size. Thus, the composition of pre-polymerisation mixture should favour the formation of particles whose diameter is higher than 20 μm in order to avoid the loss of particles through the frits of the SPE cartridge [10].

After MIP synthesis, equilibrium binding experiments were performed at 25 °C with MIP and NIP. Incubations of 18- β -glycyrrhetic acid with polymers particles were carried out in the same solvent as used during MIP synthesis. Indeed, it has been often reported that the recognition of template molecules by imprinted polymer was better in the porogenic solvent [16–18]. Fig. 2 shows experimental binding isotherms of MIP (and NIP) versus 18- β -glycyrrhetic acid concentration. In the 5–100 mg mL^{-1} polymer concentration range, the binding capacity of the MIP was always higher than that of the NIP. For example, with a 100 mg amount of polymer, 88% of template molecules were bound to MIP compared to 18% to NIP, highlighting the presence of specific cavities into the imprinted polymer. The weak adsorption of template on NIP is due to non-specific interactions with the polymer matrix.

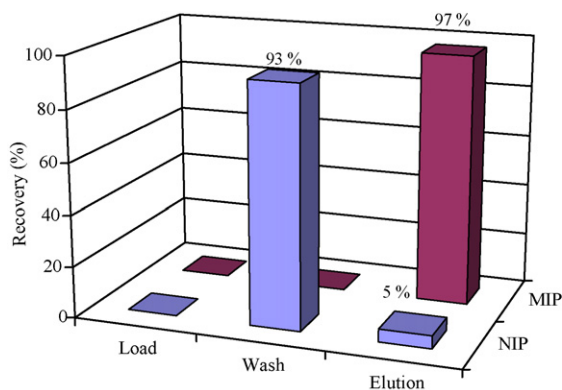


Fig. 3. Recoveries (%) obtained from MIP and NIP-SPE of 18- β -glycyrrhetic acid ($50 \mu\text{g mL}^{-1}$) in CHCl_3 .

3.2. Solid-phase extraction protocol on MIP

Binding experiments show that 60% of target molecules, initially loaded on a 60 mg MIP cartridge, were adsorbed whereas the same amount of NIP only adsorbed 11% of template molecule amount. The imprint parameter (IP) has been calculated for 60 and 100 mg polymer. IP is the relative difference of analyte quantities adsorbed, respectively, on MIP and NIP that corresponds to the assessment of the ratio of the number of specific interactions versus the number of non-specific interactions. As 60 and 100 mg batches induced equivalent IP values (4.4 and 3.9, respectively), the SPE cartridges were further filled with 60 mg polymer to reduce the amount of sorbent. Moreover, it has been reported that when the analyte is bound in non-equilibrium conditions the affinity of MIP may be higher than that obtained in equilibrium batch conditions [12].

A 18- β -glycyrrhetic acid solution (0.5 mL , $50 \mu\text{g mL}^{-1}$ in CHCl_3) was loaded on MIP and NIP (Fig. 3). During the washing step a 2 mL chloroformic solution eliminated 18- β -glycyrrhetic acid from NIP by suppression of non-specific interactions. The chloroform is able to disrupt Van der Waals interactions and, probably, a part of the hydrogen bonds thanks to its hydrogen bond donor properties. The washing step is the most crucial point during SPE protocol as the washing solvent must decrease non-specific interactions to discard matrix components.

Then, 18- β -glycyrrhetic acid was eluted from MIP by 1.5 mL MeOH with a high recovery of 97%. Indeed, MeOH is a protic and polar solvent able to break hydrogen bonds between functional groups of 18- β -glycyrrhetic acid and carboxyl groups present in MIP cavities.

3.3. Evaluation of MIP capacity

Capacity curves were plotted for MIP and NIP polymers in order to evaluate the maximum amount of 18- β -glycyrrhetic acid retained on a 60 mg MIP-SPE cartridge. The sample volume loaded was fixed (0.5 mL); then, the amount of 18- β -glycyrrhetic acid recovered during the elution step was plotted against the amount of 18- β -glycyrrhetic acid loaded on SPE cartridge (Fig. 4).

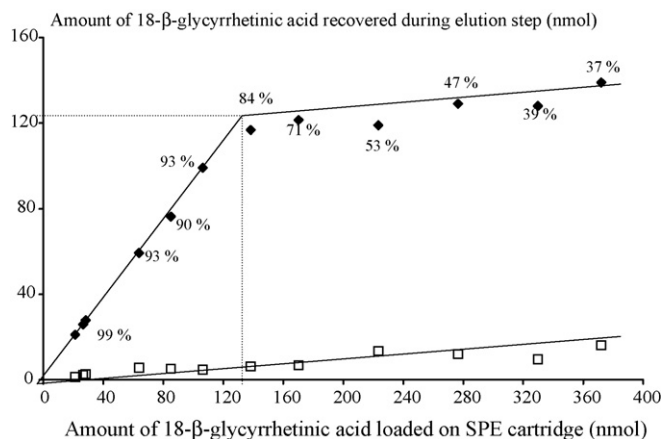


Fig. 4. Curve of capacity obtained after the loading of 0.5 mL CHCl_3 spiked with increasing amounts of 18- β -glycyrrhetic acid onto the MIP (\blacklozenge) and NIP (\square) SPE cartridges (60 mg). MIP and NIP-SPE elution recoveries (%) are reported on the graph.

Firstly, it is noteworthy that MIP elution recoveries for 18- β -glycyrrhetic acid are always higher than 84% for amounts of loaded analyte lower than 130 nmol. Only 2.5 nmol of 18- β -glycyrrhetic acid are retained on the NIP which proves the suitability of the washing step to eliminate non-specific interactions.

Otherwise, the capacity curve reaches a limit when the amount of loaded β -glycyrrhetic acid is higher than 130 nmol. Taking into account template–monomer ratio during MIP preparation, the theoretical number of imprints was $189 \mu\text{mol g}^{-1}$ of polymer. However, experimental data show weak specific retention of 18- β -glycyrrhetic acid ($2 \mu\text{mol g}^{-1}$ of MIP), which means that only 1% of the theoretical number of sites was formed. Such behaviour is coherent with previous data [8,9] with MIP capacities ranged from 1 to $40 \mu\text{mol g}^{-1}$.

For higher triterpenic acid amounts (higher than 160 nmol), a slight increase of retained 18- β -glycyrrhetic acid was observed on both MIP and NIP capacity curves with the same slope. As all the accessible specific cavities of the MIP are saturated, the retention of the analyte is only due to non-specific interactions which are identical for MIP and NIP polymers.

3.4. Study of MIP selectivity

The MIP's ability of extracting other oleanane triterpenes, having the same carbon skeleton (Fig. 1), has been investigated. Each triterpene has an hydroxyl group in position 3 but did not possess a carbonyl group. Oleanolic and echinocystic acids display a carboxyl group in position 28, while erythrodiol and echinocystic acid have an hydroxyl group in positions 28 and 16, respectively. Otherwise, 18- α -glycyrrhetic acid is a diastereoisomer of 18- β -glycyrrhetic acid.

The previous SPE protocol was applied to these triterpene molecules on MIP and NIP (Fig. 5). In the case of 18- α -glycyrrhetic acid, a quantitative extraction and an excellent MIP/NIP selectivity were obtained; indeed, mean recoveries obtained, respectively, for NIP and MIP were 5 and 100%. On the other hand, oleanolic acid, echinocystic acid and erythrodiol

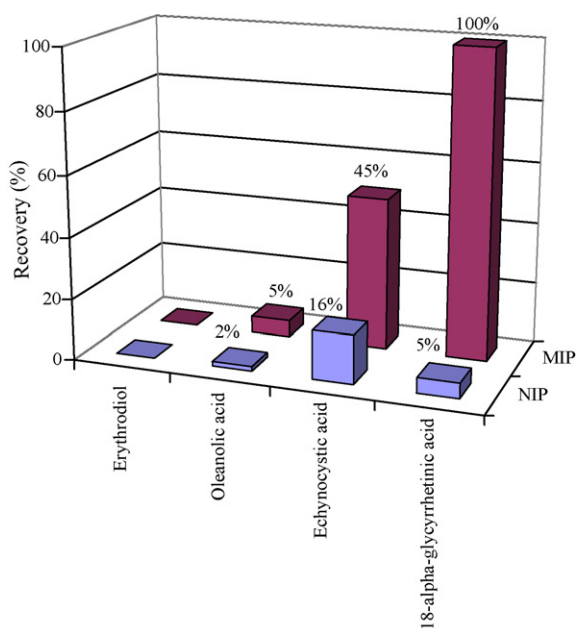


Fig. 5. Elution recoveries of four oleanane triterpene compounds from MIP and NIP. Solute concentration: $50 \mu\text{g mL}^{-1}$ in CHCl_3 .

recoveries obtained for the MIP were low (5, 50 and 0%, respectively). These compounds are quantitatively eliminated during the washing step and sometimes during the loading step (erythrodiol). As recently reported [19], the spatial orientation of functional groups in the imprinted binding sites is an important factor for the molecular recognition in non-covalent molecularly imprinted polymers. Thus, the MIP of 18- β -glycyrrhetic acid shows limited capacity to rebind triterpenes other than the original template.

3.5. Application of MIP-SPE protocol to hydrolyzed extract of liquorice roots

The previous SPE method has been applied to an hydrolyzed extract of liquorice roots. We found that polar matrix components were not fully eliminated (except for fatty acids) during the washing step (CHCl_3). However, using a more polar solvent (MeCN) yielded better results. The values of partial polarity from Snyder and Rohrschneider indicate that MeCN displays higher hydrogen bond acceptor properties (p_e) and more dipole–dipole interactions (p_n) than CHCl_3 (MeCN/ CHCl_3 : $p_e = 1.798/1.025$, $p_n = 2.436/1.353$) [20]. Similar results have already been reported with an atrazine–MIP based on MAA as functional monomer [21].

Initially, we used a 60 mg MIP cartridge but the capacity was not high enough to quantitatively retain 18- β -glycyrrhetic acid during the MeCN washing step. A 200 mg MIP cartridge was thus used in order to increase the number of available binding sites. During the washing step, 93% of polar matrix components was discarded and the elution recovery of 18- β -glycyrrhetic acid was 98%. Recoveries were calculated as the ratio of peaks areas obtained before and after MISPE (Fig. 6). According to the specifications given by the supplier concerning the liquorice extract, peak 2 has been tentatively attributed to (4 β ,20 β)-3 β ,23-

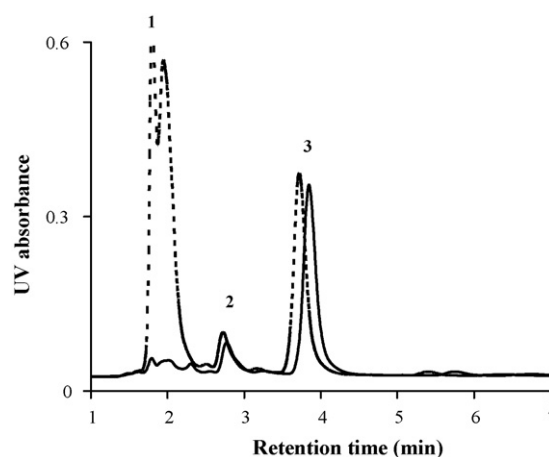


Fig. 6. Chromatograms of liquorice roots extract before (dotted line) and after (continuous line) MIP-SPE. HPLC column: Platinum EPS- C_{18} ; mobile phase: MeCN/phosphate buffer (pH 3.5, 20 mM ionic strength) 80:20 (v/v); flow rate: 1 mL min^{-1} ; detection wavelength: 254 nm; solute: (1) polar matrix component, (2) (4 β ,20 β)-3 β ,23-dihydroxy-11-oxo-olean-12-en-29-oic acid, and (3) 18- β -glycyrrhetic acid.

dihydroxy-11-oxo-olean-12-en-29-oic acid (Fig. 1), a structural and functional analogue of the template. HPLC chromatograms of liquorice roots extracts with and without MISPE are shown in Fig. 6.

The selectivity of MIP highlighted because 53% of 18- β -glycyrrhetic acid was eliminated during the washing step from NIP and only 2% from MIP.

The MIP capacity was assessed with an hydrolyzed extract of liquorice roots. Experimental results are reported in Table 1. The maximum amount of 18- β -glycyrrhetic acid specifically retained by 200 mg MIP is equal to 100.7 nmol (139.7–39). Thus, the MIP capacity is equal to $0.5 \mu\text{mol g}^{-1}$. Although the volume of the sample percolated is higher than the volume used with standard solution, the decrease of the capacity (0.5 versus $2 \mu\text{mol g}^{-1}$ obtained with the standard solution) is mainly attributed to the complex matrix and to the higher eluent strength of acetonitrile versus chloroform. Nevertheless, most of the polar matrix was eliminated from MIP and NIP cartridges during the washing step.

At last, the liquorice extract solution was spiked with a fatty acid (linoleic acid), slightly more hydrophobic than 18- β -glycyrrhetic acid. A SPE extraction performed with a reversed-phase C18 sorbent failed to selectively extract this pentacyclic triterpene from the fatty acids fractions (Fig. 7).

Table 1
Capacity evaluation of MIP and NIP SPE cartridges (200 mg) with hydrolyzed liquorice roots

18- β -Glycyrrhetic acid amount (nmol)	MIP	NIP
Loaded on the cartridge	251.5	251.5
Lost during load	$251.5 - 244.2 = 7.3$	$251.5 - 238.5 = 13$
Lost during wash	107.4	206.4
Eluted	139.7	39
Overall recovery (%)	101	102.7

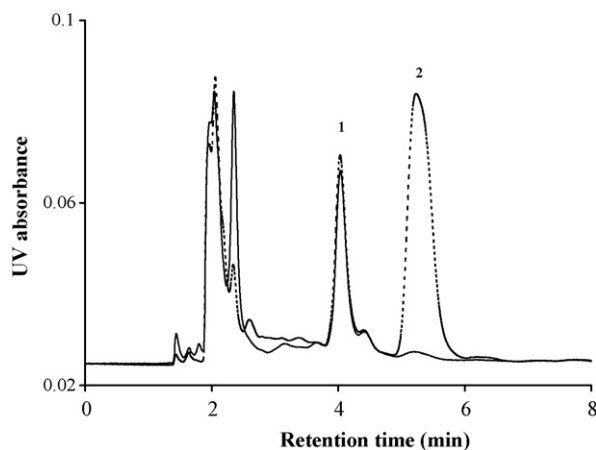


Fig. 7. Chromatograms of liquorice roots extract after C18 silica SPE (dotted line) and after (continuous line) MISPE. HPLC column: Platinum EPS-C₁₈; mobile phase: MeCN/phosphate buffer (pH 3.5, 20 mM ionic strength) 80:20 (v/v); flow rate: 1 mL min⁻¹; detection wavelength: 210 nm; solute: (1) 18- β -glycyrrhetic acid and (2) linoleic acid.

On the other hand, the chromatogram of the elution fraction underscores specific extraction of 18- β -glycyrrhetic acid; indeed, linoleic acid was totally eliminated during the washing step (ACN).

4. Conclusion

A molecular imprinting polymer has been synthesized for the extraction of an oleanane triterpene (18- β -glycyrrhetic acid) from a plant roots extract. After optimisation of SPE protocol, the selectivity of the MIP for the original template over related oleanane triterpenes was demonstrated. MIP-SPE constitutes a useful tool for selective clean-up of the liquorice roots extracts and 18- β -glycyrrhetic acid quantification. The successful SPE protocol (ACN washing and MeOH elution) achieved the elimi-

nation of the matrix (93%) and also of fatty acid fraction during the washing step. The recovery of 18- β -glycyrrhetic acid was 98% during the elution step.

References

- [1] V. Andrisano, D. Bonazzi, V. Cavrini, J. Pharm. Biomed. Anal. 13 (1995) 597–605.
- [2] M. Song, T.J. Hang, Y. Wang, L. Jiang, X.L. Wu, Z. Zhang, J. Shen, I. Zhang, J. Pharm. Biomed. Anal. 40 (2006) 190–196.
- [3] F.G.M. Russel, S. van Uum, Y. Tan, P. Smits, J. Chromatogr. B 710 (1998) 223–226.
- [4] C. Sabbioni, R. Mandrioli, A. Ferranti, F. Bugamelli, M. Addolotata Saracino, G. Cantelli Forti, S. Fanali, M. Augusta Raggi, J. Chromatogr. A 1081 (2005) 65–71.
- [5] O. Ramström, L. Ye, K. Mosbach, Chem. Biol. 3 (1996) 471–477.
- [6] X. Dong, W. Wang, S. Ma, H. Sun, Y. Li, J. Guo, J. Chromatogr. A 1070 (2005) 125–130.
- [7] J. Xie, L. Zhu, H. Luo, L. Zhou, C. Li, X. Xu, J. Chromatogr. A 934 (2001) 1–11.
- [8] L. Zhu, X. Xu, J. Chromatogr. A 991 (2003) 151–158.
- [9] J.-P. Lai, X.-W. He, Y. Jiang, F. Chen, Anal. Bioanal. Chem. 375 (2003) 264–269.
- [10] V. Pichon, J. Chromatogr. A 1152 (2007) 41–53.
- [11] C. Alexander, H.-S. Andersson, L.-I. Andersson, R.-J. Ansell, N. Kirsch, I.-A. Nicholls, J. O'Mahony, M.-J. Whitcombe, J. Mol. Recognit. 19 (2006) 106–180.
- [12] S. Wei, B. Mizaikoff, Biosens. Bioelectron. 23 (2007) 201–209.
- [13] H. Dong, A.-J. Tong, L.-D. Li, Spectrochim. Acta Part A 59 (2003) 279–284.
- [14] B. Sellergren, K.J. Shea, J. Chromatogr. 635 (1993) 31–49.
- [15] K. Farrington, E. Magner, F. Regan, Anal. Chim. Acta 566 (2006) 60–68.
- [16] D. Spivak, M.A. Gilmore, K.J. Shea, J. Am. Chem. Soc. 119 (1997) 4388–4393.
- [17] C. Yu, K. Mosbach, J. Chromatogr. A 888 (2000) 63–72.
- [18] Q.Z. Zhu, K. Haupt, D. Knopp, R. Niesser, Anal. Chim. Acta 468 (2002) 217–227.
- [19] Y. Lu, C. Li, X. Liu, W. Huang, J. Chromatogr. A 950 (2002) 89–97.
- [20] R. Rosset, M. Caude, A. Jardey, Chromatographies en phase liquide et supercritique, third ed., Masson, Paris, 1991.
- [21] M.T. Muldoon, L.H. Stanker, Anal. Chem. 69 (1997) 803–808.

Advantages of hydride generation interface for selenium speciation in waters by high performance liquid chromatography–inductively coupled plasma mass spectrometry coupling

Jérôme Darrouzès^a, Maité Bueno^{a,*}, Stéphane Simon^b,
Florence Pannier^a, Martine Potin-Gautier^a

^a *Laboratoire de Chimie Analytique Bio-Inorganique et Environnement, Université de Pau et des Pays de l'Adour, UMR CNRS 5254, Hélioparc Pau-Pyrénées, 2 avenue du Président Pierre Angot, 64053 PAU Cedex, France*

^b *Laboratoire des Sciences de l'Eau et de l'Environnement, Faculté des Sciences et Techniques, 123 avenue Albert Thomas, 87060 Limoges, France*

Received 20 July 2007; received in revised form 17 October 2007; accepted 7 November 2007

Available online 17 November 2007

Abstract

This paper focuses on the analytical performance improvement of the coupled technique HPLC–ICPMS using on-line collision/reaction cell technology for selenium elemental and speciation analyses at the ng (Se) l⁻¹ level in aquatic environment. Collision/reaction cell operating parameters were optimised, resulting in selected conditions of 5.5 ml min⁻¹ H₂ and 0.5 ml min⁻¹ He mixture. The detection limits obtained were around 5 ng (Se) l⁻¹ for total analysis, and between 7 and 15 ng (Se) l⁻¹ depending on the species for speciation analysis.

The capability of UV irradiation-hydride generation interfacing to increase detector sensitivity was also evaluated for speciation analysis. The detection limits obtained were in the range 2–8 ng (Se) l⁻¹ depending on the species. Moreover, such interface allowed to prevent bromine introduction to the ICPMS which is particularly convenient for selenium trace analysis in natural waters as ⁸⁰Se is preserved free from BrH interferences. The developed method was validated using certified water with low selenium content (TM Rain 95, NWRI, Canada) and applied to the analysis of different waters.

© 2007 Elsevier B.V. All rights reserved.

Keywords: ICPMS; Selenium; Speciation; Collision/reaction cell; Water; Hydride generation

1. Introduction

The hyphenation of HPLC and ICPMS is nowadays commonly used for selenium speciation analysis. Nevertheless, when applied to aquatic systems, such method is steeply limited due to detection limits close to total selenium concentrations in natural waters (generally below 1 μg (Se) l⁻¹) [1–3]. Indeed, Se detection using ICPMS suffers from two main difficulties. The first one is linked to the high first ionisation potential (9.75 eV) of this element, responsible of low ionisation in Ar plasma. Secondly, as the most abundant selenium isotope, ⁸⁰Se (49.6%), is interfered by ⁴⁰Ar⁴⁰Ar⁺ dimer, a less interfered but also less abundant selenium isotope (⁸²Se, 9.2%) is commonly monitored.

The development of ICPMS equipped with collision/reaction cell (C/RC) has offered an interesting solution to overcome polyatomic interferences. By adding a gas, or a mixture of gases, inside the cell, i.e. a multipole inserted between the ionic lenses and the quadrupole analyser, the polyatomic interferences can be removed by gas phase collisions and/or reactions [4]. Thus, ⁸⁰Se and ⁷⁸Se can be monitored resulting in increased ICPMS sensitivity. Different optimisations, depending principally on ICPMS instrument have been published with detection limits in the 40–600 ng (Se) l⁻¹ (based on ⁸⁰Se) range, depending on the species and the chromatographic system used [5–7]. Such detector performance is still not sufficient to determine selenium species at their naturally occurring concentrations in aquatic systems. The use of larger injection volumes (500 μl) has been proposed by Mazan et al. [8] to lower detection limits down to 12 and 24 ng (Se) l⁻¹ respectively for selenite (SeIV) and selenate (SeVI). Wallschlager and London [9] have combined injection volume of 1 ml and efficient introduction system to reach

* Corresponding author. Tel.: +33 559 407 753; fax: +33 559 407 781.
E-mail address: maité.bueno@univ-pau.fr (M. Bueno).

detection limits lower than $0.2 \text{ ng (Se) l}^{-1}$ for speciation analysis of SeIV, SeVI and selenocyanate (SeCN^-). Such low detection limits allow inorganic selenium speciation in many water systems. However, assessment of selenium biogeochemical cycle requires the knowledge of complete selenium speciation, i.e. including organic species which were not considered in these studies.

Moreover, the analysis of real samples with ICPMS equipped with C/RC indicated new possible interferences such as $^{79}\text{BrH}^+$ and $^{81}\text{BrH}^+$, selenium quantification based on ^{80}Se and ^{82}Se is therefore unusable directly [7,9–12]. For elemental analysis, correction equation of m/z 80 signal taking into account bromine hydridation should be applied to remove this bias [7]. In the case of speciation analysis, if bromine species coelute with Se species, ^{80}Se is no more adapted for quantitation. The signal of ^{78}Se isotope should then be preferably used even being twofold less abundant than ^{80}Se [7]. Wallschläger and London have added a second reaction gas (NH_3) in the C/RC system to remove BrH^+ interferences created by the reaction gas (CH_4) dedicated to remove $^{40}\text{Ar}^{40}\text{Ar}^+$ dimer [9]. Another solution consists in modifying chromatographic conditions to reach separation of bromine from selenium species but can lead to higher backgrounds [13].

Changing sample introduction system from classical nebulisation to hydride generation (HG) represents an interesting alternative. Indeed, this chemical volatilization process offers high introduction efficiency and limits matrix based interferences since hydridation conditions are generally species specific. In the case of selenium, only SeIV undergoes a quantitative on-line volatilization [14]. For other species, especially for SeVI, several procedures have been proposed to allow on-line conversion into SeIV before the HG step. These systems are mainly based on microwave heating [15–17] or ultraviolet (UV) photodecomposition [18–20]. Detection is commonly realised with atomic absorption spectrometry or atomic fluorescence spectrometry and more rarely with ICPMS [9,21]. The present paper details the optimisation of recent ICPMS equipped with on-line octopole collision/reaction cell for selenium analysis. Then, UV–HG interface operating conditions previously optimised in our laboratory for HPLC–AFS coupling have been expanded to be coupled with an ICPMS detector. Capability of such interface to increase sensitivity and remove, or at least lower, bromine interferences using ICP–C/RC–MS detection is evaluated. Detection limits are reported and compared to those obtained with conventional pneumatic nebulisation as introduction system. Advantages of UV–HG interface are demonstrated with applications to freshwaters, including commercial mineral waters and certified reference rainwater (TM Rain 95, National Water Research Institute, Canada).

2. Experimental

2.1. Reagents

Ultrapure water was obtained from a Milli-Q System (Millipore Co., Bedford, MA, USA). L-Selenocystine (SeCyst) and D,L-selenomethionine (SeMet) (both from Sigma–Aldrich,

Steinheim, Germany), sodium selenite (SeIV) and selenate (SeVI) (both from Merck, Darmstadt, Germany) were used without further purification. Stock standard solutions containing $1000 \text{ mg (Se) l}^{-1}$ of each compound in ultrapure water were stored in the dark at 4°C . Working standard solutions were prepared daily by dilution in ultrapure water.

Citric acid (Analytical grade, Prolabo, Paris, France), triammonium citrate, ammonium nitrate (both from Sigma–Aldrich, Steinheim, Germany), di ammonium hydrogen phosphate (Merck, Darmstadt, Germany), nitric acid, sodium hydroxide and methanol (J.T. Baker, Deventer, Holland) were used for mobile phases preparation. The pH was adjusted by drop wise addition of 30% ammonia solution (Merck, Darmstadt, Germany). Mobile phase was continuously degassed while delivered.

A 0.1% (w/v) KI (J.T. Baker) solution containing 0.01% (w/v) NaOH (Merck, pro analysis) was used for photo-decomposition. Hydride-generation was performed with 3 mol l^{-1} HCl (J.T. Baker, 37%) and 2.5% (w/v) NaBH_4 (Sigma–Aldrich, 98%) stabilised by 1% (w/v) NaOH.

Glassware was decontaminated by soaking overnight in 10% (v/v) nitric acid solution and rinsed with ultrapure water before use.

A certified reference material, the TM Rain 95 (National Water Research Institute, Canada), was chosen to validate optimised working conditions, due to its low level of selenium ($740 \pm 290 \text{ ng (Se) l}^{-1}$).

2.2. Instrumentation for ICPMS and HPLC system

The ICPMS instrument was the 7500ce from Agilent technologies (Tokyo, Japan), equipped with on-line octopole collision/reaction cell. Recommended gases are helium and hydrogen of 99.995% purity (Air Liquide, Paris, France). Operating conditions were optimised daily using a $1 \mu\text{g l}^{-1}$ solution of Li, Y, Tl and Ce solution, and a $1 \mu\text{g (Se) l}^{-1}$ as SeIV solution.

The HPLC system consisted of Agilent 1100 series HPLC pump, equipped with an autosampler and variable volume sample loop. Injection volume was fixed at $100 \mu\text{l}$.

For conventional sample introduction using concentric nebuliser (Meinhard Associates, CA, USA), the interface between HPLC and ICPMS was simply realised with a polyetheretherketone (PEEK) tube. The chromatographic separation of SeCyst, SeMet, SeIV and SeVI was adapted from Ge et al. [22] and performed using a Hamilton PRP-X100 column ($250 \text{ mm} \times 4.1 \text{ mm}$, $10 \mu\text{m}$) and guard column. Mobile phase, i.e. 5 mmol l^{-1} ammonium citrate buffer with pH adjusted to 5.2, was delivered at 1 ml min^{-1} . Low percentage of methanol (2%, v/v) was added in the mobile phase to improve sensitivity in the case of direct HPLC–ICPMS coupling [23].

A schematic representation of HPLC–ICPMS coupling with UV–HG interface is presented in Fig. 1. UV–HG operating conditions were adapted from a precedent work developed in our laboratory for HPLC–AFS coupling [24]. At the outlet of the chromatographic column, the reductant solution (KI stabilised with NaOH), is added using a T-connection by a peristaltic pump (Gilson Minipuls 2) at 0.5 ml min^{-1} . Mixed solutions were intro-

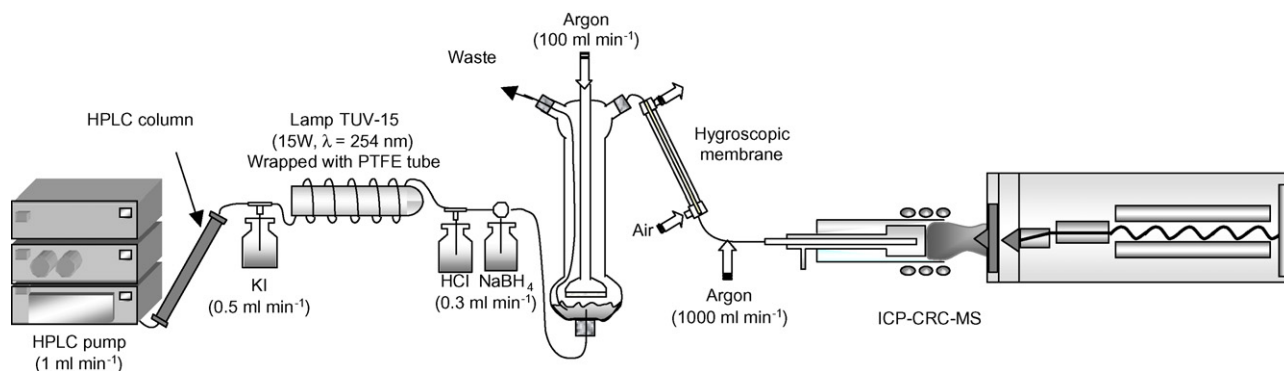


Fig. 1. General scheme of HPLC–UV–HG–ICPMS coupling.

duced into a PTFE tube (0.5 mm i.d., length corresponding to 60 s irradiation time) wrapped around a Philips TUV-15 lamp ($\lambda = 253.7$ nm, 15 W, 44 cm long) for UV photoconversion. HCl and NaBH₄ solutions, allowing hydride generation, were added at the UV lamp outflow at a flow rate of 0.3 ml min⁻¹ using a peristaltic pump (Labcraft) through a T-joint and a mixing valve, respectively. Another channel of this pump was required for removing waste from the gas–liquid separator developed in our laboratory. The connection between the gas–liquid separator and the ICPMS was realised using a drying membrane followed by a Teflon tube directly connected to the torch. As shown in Fig. 1, two additional argon flow rates were inserted to carry the gaseous effluent to ICPMS: Ar_{GLS} was added to the gas liquid separator, and Ar_{Torch} was affixed, via a T-piece, to the end of drying membrane.

Mobile phases, i.e. 0.1 mol l⁻¹ NH₄NO₃, HNO₃, NaOH and (NH₄)₂HPO₄, were tested for their compatibility with HG–UV interface.

Operating conditions are summarized in Table 1.

2.3. Analytical figures of merit

Instrumental performances were evaluated in terms of detection limits (DL), repeatability and linearity. Limits of detection were calculated using IUPAC recommendations [25]:

$$DL = \frac{t \times S.D.}{S}$$

with: DL: detection limit in ng (Se) l⁻¹; t : student coefficient ($t = 3$ for a confidence interval of 99.86%); S.D.: standard deviation of the background signal (10 blanks measurements) in counts; S : slope of the calibration curve (net signal) in (counts s⁻¹) (ng (Se) l⁻¹)⁻¹ for total analysis and (peak height) (ng (Se) l⁻¹)⁻¹ for speciation analysis.

3. Results and discussion

3.1. Optimisation of C/RC system

Optimisation was realised using simplex methodology and measuring successively $m/z = 80$ signals given for a blank solution (ultrapure water) and for a solution spiked with 1 μg (Se) l⁻¹ as SeIV. Plasma power was settled at 1500 W. Preliminary experiments have shown that optimum flow rates ranged between 3.5

and 6 ml min⁻¹ for H₂, and between 0 and 1 ml min⁻¹ for He. In order to find optimal conditions, several combinations of both flow rates were tested. The effect of gases flow rates was checked by measuring signal to background ratio at m/z 80 (⁸⁰SBR). As shown in Fig. 2, the combination of 5.5 ml min⁻¹ of H₂ and 0.5 ml min⁻¹ of He, corresponding to the best compromise as the maximum signal to background ratio, was selected. For lower flow rates, interferent is not completely removed, resulting in lower SBR. For upper values, sensitivity falls (data not shown). The small addition of helium is likely to increase focalisation of the ion beam [26]. Optimum values for gas flow rates are slightly superior to the ones previously reported in the literature

Table 1
ICPMS operating conditions

Sample introduction via concentric nebuliser	
Plasma power (W)	1500 (1600 in HPLC)
Cooling gas flow rate (l min ⁻¹)	15
Auxiliary gas flow rate (l min ⁻¹)	0.9
Nebulisation gas flow rate (l min ⁻¹)	1–1.1
Extract lens 1 (V)	4
Extract lens 2 (V)	–140
Sample introduction via UV–HG interface	
Plasma power (W)	1100
Ar _{GLS} (l min ⁻¹)	0.1
Ar _{Torch} (l min ⁻¹)	1
Collision/reaction cell (values in brackets correspond to standard mode)	
H ₂ flow rate (ml min ⁻¹)	5.5 (0)
He flow rate (ml min ⁻¹)	0.5 (0)
Ω bias ce (V)	–26
Ω lens ce (V)	0
CEn (V)	–46
QP Focus (V)	–20 (0)
CEx (V)	–50
PB (V)	200
OB (V)	–20 (–6)
QB (V)	–19 (–3)
Total analysis mode	
Isotopes	From $m/z = 72$ to $m/z = 83$
Integration time (s per isotope)	0.3
HPLC analysis mode	
Isotopes	⁷⁸ Se, ⁷⁹ Br, ⁸⁰ Se, ⁸¹ Br
Integration time (s per isotope)	0.4 for Se and 0.1 for Br
Total time analysis (min)	15

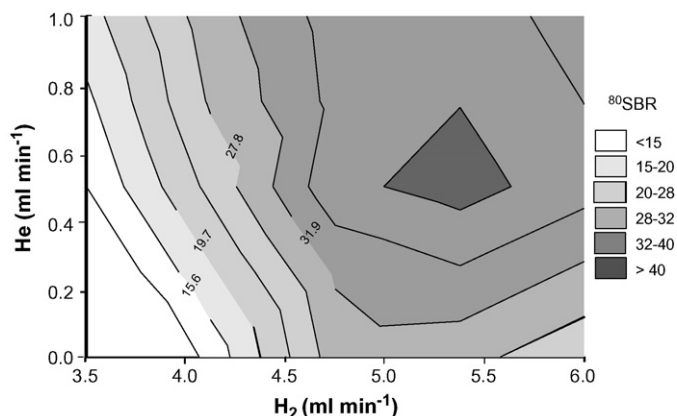


Fig. 2. Optimisation of hydrogen and helium flow rates: sensitivity to background ratio at $m/z=80$ (^{80}SBR).

for selenium speciation with the preceding version of this instrument [7,11]. In the new configuration of the instrument, the C/R/C system is disposed on-line probably resulting in a better transmission of the ion beam and more energetic ions.

Insuring better focalisation of the ion beam and kinetic energy discrimination, the voltages of the different lenses around the C/R/C system were also investigated according to constructor advices. Common settings are presented in Table 1. The most critical adjustment is the difference between the voltage of the octopole (OB) and the quadrupole bias (QB). The dc bias of the quadrupole is set at a less negative value to the one of the octopole, i.e. $\text{OB} = -20\text{ V}$ and $\text{QB} = -19\text{ V}$ when C/R/C is activated in order to keep the maximum sensitivity.

Using optimised conditions, analytical performances were calculated for total and speciation analyses. Results are reported in Table 2. Calibration curves for total and speciation analyses are linear up to the highest studied concentration, i.e. $10\text{ }\mu\text{g (Se) l}^{-1}$. For total analysis, detection limits are close to 5 ng (Se) l^{-1} for ^{78}Se and ^{80}Se , which represents a 10-fold improvement in comparison with the preceding version of this instrument [7]. Using 10 consecutive measurements of 50 ng (Se) l^{-1} solution, repeatability was calculated close to 5%. For higher concentrations ($200\text{ ng (Se) l}^{-1}$ or $1000\text{ ng (Se) l}^{-1}$), repeatability is in the range 2–4%. For speciation analysis, detection limits based on ^{80}Se are in the range 7–15 ng (Se) l^{-1} depending on the species. These values are close to those required for determination of selenium species at their natural occurrence level in many

Table 2
Compared detection limits (in ng (Se) l^{-1}) for total selenium and speciation analyses as a function of sample introduction system

	Concentric nebuliser		UV–HG interface	
	^{78}Se	^{80}Se	^{78}Se	^{80}Se
Total	6	4	nd	nd
SeIV	14	7	3	2
SeVI	28	15	10	5
SeMet	28	14	15	8
SeCyst	16	8	11	6

aquatic systems. Repeatability is less than 8% at 50 ng (Se) l^{-1} level, and in the range 1–4% for 200 and $1000\text{ ng (Se) l}^{-1}$.

Creation of new interferences using C/R/C system such as AsH^+ , SeH^+ and BrH^+ has been previously reported [7,10–12]. The hydration rates of As, Se and Br were evaluated, respectively to 1.2, 3.4 and 15.0% under our operating conditions. BrH^+ formation is particularly critical when dealing with natural waters analyses. Indeed, bromine is generally much more abundant than selenium, resulting in misuse of m/z 80 and 82 signals for Se quantitation if signal correction taking into account Br hydration is not applied. The use of an introduction system which prevents bromine introduction in the ICPMS such as hydride generation interface was then evaluated and is described in the following paragraphs.

3.2. Interfacing HPLC and ICPMS with on-line UV–HG

On-line UV–HG interface between HPLC and ICPMS was firstly optimised with the C/R/C switched off. Hence, signals of ^{82}Se were measured in blank solution (ultrapure water) and in $1\text{ }\mu\text{g (Se) l}^{-1}$ as SeIV solution. Incident plasma power and additional flow rates of argon, i.e. Ar_{GLS} and Ar_{Torch} , were optimised as shown respectively in Figs. 3 and 4. Background signal was found to be constant in the tested range and these parameters were thus adjusted to obtain maximum sensitivity. Incident plasma power was settled at 1100 W which is much lower than the one used with pneumatic nebulisation. This is probably due to H_2 generated with HG process and introduced inside the plasma, which has higher thermal conductivity than argon. The flow rates of Ar_{GLS} and Ar_{Torch} transfer the gaseous effluent to the ICPMS and support the plasma. They were respectively settled at 100 and 1000 ml min^{-1} to obtain maximum sensitivity.

The coupling of ion exchange chromatography with ICPMS detection and pneumatic nebulisation as introduction system is mainly limited by salt concentration of the mobile phase. With UV–HG interface, the critical point rather depends on mobile phase nature since it has to show no reactivity towards UV irradiation. The compatibility of the mobile phase was tested by separate injections of $100\text{ }\mu\text{l}$ of each species (SeIV, SeVI, SeMet and SeCyst) in different mobile phases, without chromatographic column. Mobile phases tested were the ones

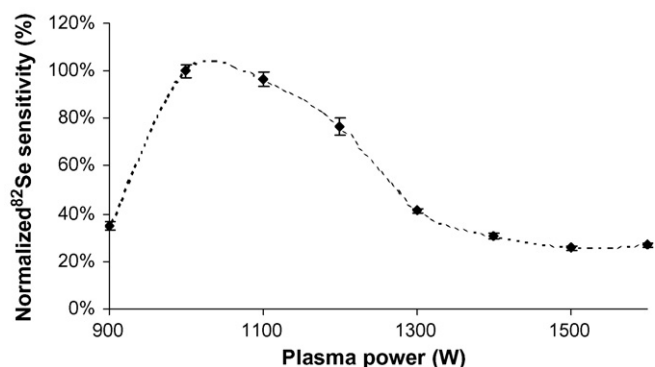


Fig. 3. Influence of plasma power on ^{82}Se signal (normalized on ^{82}Se signal for 1000 W plasma power).

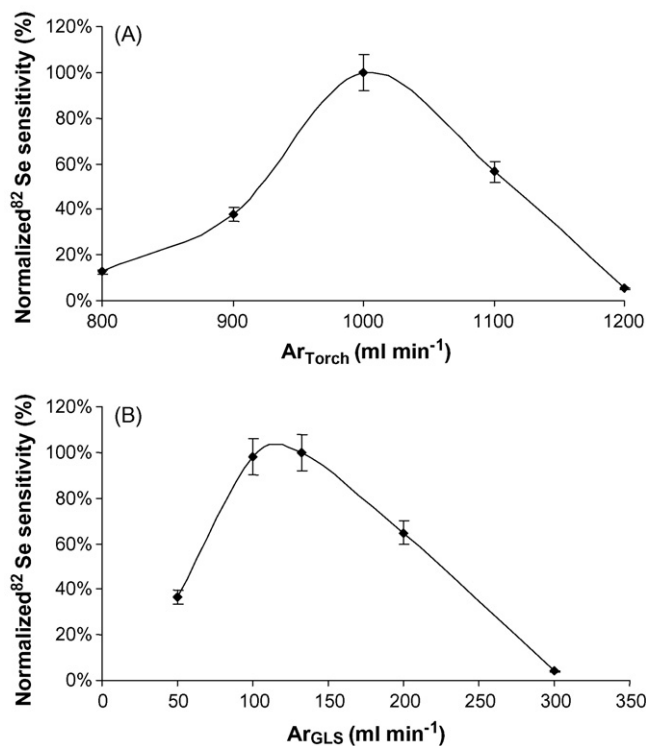


Fig. 4. Influence of Ar_{Torch} and Ar_{GLS} flow rates on ^{82}Se signal (normalized respectively on ^{82}Se signal for $\text{Ar}_{\text{GLS}} = 100 \text{ ml min}^{-1}$ and $\text{Ar}_{\text{Torch}} = 1000 \text{ ml min}^{-1}$): (A) influence of Ar_{Torch} with $\text{Ar}_{\text{GLS}} = 100 \text{ ml min}^{-1}$ and (B) influence of Ar_{GLS} with $\text{Ar}_{\text{Torch}} = 1000 \text{ ml min}^{-1}$.

commonly used in anion exchange chromatography (0.1 mol l^{-1} NH_4NO_3 , HNO_3 , NaOH and $(\text{NH}_4)_2\text{HPO}_4$). Organic mobile phases are not commonly used due to possible absorption at the UV wavelength used and disruption of hydride generation. In ultrapure water, a similar response is observed for the four compounds. Mobile phase containing nitrate ions were found not suitable probably due to oxidative properties of nitrate which were emphasized under UV irradiation [27]. With NaOH mobile phase, a salt deposit, conducting to signal drift, was observed in the gas–liquid separator after few minutes. Significant increase of the background was observed at $m/z = 80$ when phosphate buffer was used, probably due to the creation of interferences such as $^{31}\text{P}^{16}\text{O}_3^1\text{H}$. Citrate buffer previously used (see above) was tested and finally selected as only a 15% decrease of SeVI , SeCyst and SeMet signals was observed.

Keeping these conditions and switching on the C/R system (with the conditions previously defined), solutions containing increasing bromine concentrations (from $0.1 \mu\text{g (Br)} \text{ l}^{-1}$ to $1000 \text{ mg (Br)} \text{ l}^{-1}$) were analysed by monitoring m/z 79, 80, 81 and 82 signals. Comparison with signals obtained in ultrapure water, as reported in Fig. 5, shows no significant differences. This result suggests that bromine is not introduced in the ICPMS with our HG conditions. Hence, the creation of BrH interferences inside the C/R system is prevented. This result was confirmed by the analysis of different samples, including mineral waters and urine, using the complete system (HPLC–UV–HG–ICP–C/R–MS). Using pneumatic nebulisation, a bromine-containing species was shown to elute at the

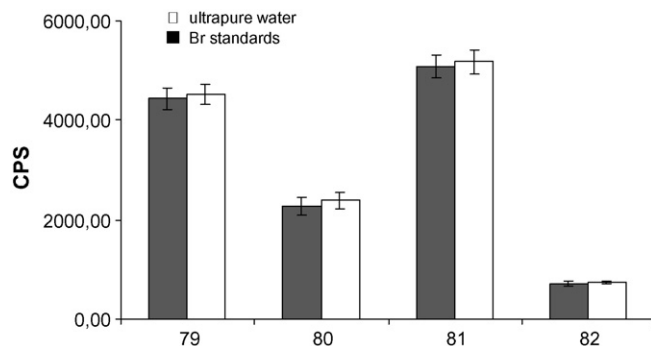


Fig. 5. Comparison of mean signals (CPS) monitored at $m/z = 79, 80, 81, 82$ in ultrapure water and bromine standards from $0.1 \mu\text{g (Br)} \text{ l}^{-1}$ to $1000 \text{ mg (Br)} \text{ l}^{-1}$.

same retention time than SeVI whereas, with UV–HG interface, this signal could not be observed at m/z 79 and 81. This result is different from the one published by Wallschlag and London [9] who observed bromine hydridation using similar introduction system, i.e. hydride generation interface. In this study, BrH interferent was removed by adding a second reactive gas, i.e. NH_3 , in the collision/reaction cell system. We suppose that such opposite observations may be due to the different conditions of hydride generation used in both studies.

3.3. Analytical figures of merit

Analytical performances with both introduction systems were compared for speciation analysis. As reported in Table 2, with HG as introduction system, detection limits, based on ^{80}Se , vary between 2 and $11 \text{ ng (Se)} \text{ l}^{-1}$ depending on the species. This represents a 2–4 times improvement factor compared to pneumatic nebulisation. Indeed, as shown in Fig. 6, sensitivity is 10-fold increased thanks to efficient sample introduction achieved with HG, but at the same time, standard deviation is slightly damaged due to interface complexity. With high resolution ICPMS and hydride generation following microwave digestion, Gonzalez La Fuente et al. [21] also observed higher

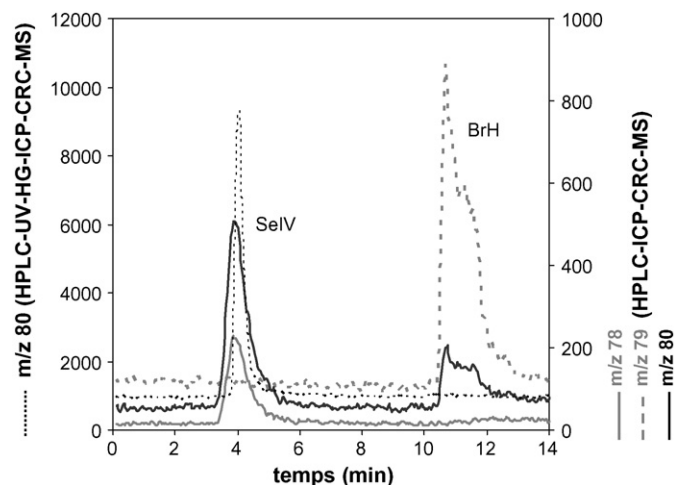


Fig. 6. Example chromatograms of TM Rain 95 obtained with both sample introduction systems.

Table 3
Selenium concentrations for different water samples

		Se _{Total}	Concentric nebuliser		UV–HG interface	
			SeIV	SeVI	SeIV	SeVI
TM Rain 95	⁷⁸ Se	622 ± 19	629 ± 7	nd	620 ± 19	nd
	⁸⁰ Se		615 ± 8	nd	606 ± 19	nd
A	⁷⁸ Se	467 ± 17	nd	475 ± 4	nd	478 ± 11
	⁸⁰ Se		nd	492 ± 5	nd	513 ± 13
B	⁷⁸ Se	240 ± 20	nd	232 ± 13	nd	230 ± 2
	⁸⁰ Se		nd	267 ± 13	nd	221 ± 2
C	⁷⁸ Se	67 ± 1	nd	69 ± 2	nd	69 ± 3
	⁸⁰ Se		nd	72 ± 6	nd	70 ± 5
S	⁷⁸ Se	1890 ± 160	55 ± 2	1840 ± 30	57 ± 3	1790 ± 40
	⁸⁰ Se		57 ± 6	1920 ± 20	54 ± 4	1840 ± 40

Results in ng (Se) l⁻¹ for total selenium and speciation analyses (uncertainty represents the standard deviation of three replicates).

sensitivity (23- to 59-fold) in comparison to pneumatic nebulisation, but only a 8.7-fold lowered detection limits due to background noise. Repeatability was estimated to be around 6% at 50 ng (Se) l⁻¹ level and around 2% at 1000 ng (Se) l⁻¹ which is close to the values obtained using pneumatic nebulisation.

As previously discussed, the use of ⁸⁰Se isotope should be avoided with pneumatic nebulisation sample introduction, with the exception of samples free from bromine. Thus, for real samples, an appropriate comparison of analytical performances should be between those obtained for ⁷⁸Se isotope with pneumatic nebulisation coupling, and for ⁸⁰Se isotope with UV–HG interface. In this case, detection limits are lowered up to a factor of 7 with the help of HG introduction system.

Our last attempt to improve detection limits was to estimate the maximum injectable volume. In this part, only SeIV and SeVI species were considered since SeMet and SeCyst peaks were distorted from the very first larger injected volume tested. The maximum injectable volume was evaluated on the basis of peak height versus peak area for 100, 500, 1000 and 2000 µl injection volumes. Peak height was found linearly correlated to peak area up to a maximum injectable volume of 2 ml, that represent a further 20-fold improvement of detection limits. Such large injection volume is thus well adapted for samples with really low Se levels, and/or for complex matrices which have to be diluted before analysis.

3.4. Application to natural waters

Different mineral and spring waters were analysed to test the suitability of the method for natural samples. Results for some of them are summarized in Table 3. For total analysis, results for ⁷⁸Se are reported as this isotope is free from interferences and does not require the use of correction equations.

A certified simulated rain water (TM Rain 95 from National Water Research Institute) was analysed. Concentrations found in total and speciation analyses are in complete agreement, as well as with previous results [7]. SeIV was the only species identified, which could be explained by the 0.2% HCl stabilisation medium [28].

In the different waters (A–C), only SeVI was identified. Selenate is the common species found in oxygenated waters. Concentrations found in elemental and speciation analysis are in complete agreement. Using pneumatic nebulisation, elution of bromine-containing compound creates interference on ⁸⁰Se. This peak does not overlap with SeVI but extend the chromatogram for about 5 min. The low Se level of water C implied a 2 ml injection. Even with this large volume, only SeVI was quantified at 69 ± 2 ng (Se) l⁻¹ with ⁷⁸Se and ⁸⁰Se isotopes.

The groundwater S was analysed 5 years ago in a previous study of our group. Analytical methodology used was HPLC–ICPMS (without CRC) after preconcentration by solid-phase extraction [29]. At that time, total selenium was quantified at 900 ± 100 ng (Se) l⁻¹, and SeIV, SeVI and SeCyst were identified following speciation analysis. The present level of selenium determined in this water is higher than previously obtained and the presence of SeIV and SeVI was confirmed. SeCyst was not detected, its level being previously determined to be between 2 and 10 ng (Se) l⁻¹ [29].

4. Conclusion

Selenium analysis in non-polluted waters still presents a number of challenges. The use of ICPMS detector equipped with on-line octopole collision/reaction cell allowed reduction of argon polyatomics interferences, decreasing detection limits to 5–15 ng (Se) l⁻¹ with *m/z* = 80 monitoring. While such instrumental performances seem well adapted to selenium analyses at its natural occurrence level in many aquatic systems, interferences from BrH⁺ caused by bromine presence in water samples and the use of a reactive gas into the C/RC impair direct quantification of selenium on *m/z* = 80.

Changing direct nebulisation ICPMS to UV irradiation-hydride generation interfacing resulted in (i) lowered detection limits (i.e. 2–8 ng (Se) l⁻¹ depending on the species) and (ii) no introduction of bromine in the ICPMS eliminating BrH⁺ creation. This improved detection power is likely to significantly facilitate selenium quantification in specific applications (ultra-trace concentration, high level of bromine compounds).

Such sensitive analytical methods are necessary to better understand biogeochemical cycle of selenium in the aquatic environment. Other applications dealing with more complex matrices, such as urine and marine waters, are actually in progress in our laboratory.

Acknowledgment

The authors would like to thanks Agilent Technologies (Tokyo, Japan) for the technical support provided.

References

- [1] G. Kolb, K. Kalcher, K.J. Irgolic, R.J. Magee, *Appl. Organomet. Chem.* 7 (1993) 443.
- [2] H. Robberecht, R. Van Grieken, *Talanta* 29 (1982) 823.
- [3] J.E. Conde, M. Sanz Alaejos, *Chem. Rev.* 97 (1997) 1979.
- [4] S.D. Tanner, V.I. Baranov, D.R. Bandura, *Spectrochim. Acta Part B* 57 (2002) 1362.
- [5] J.M. Marchante-Gayon, C. Thomas, I. Feldmann, N. Jakubowski, *J. Anal. Atom. Spectrom.* 15 (2000) 1093.
- [6] V. Diaz-Huerta, L. Hinojosa-Reyes, J.M. Marchante-Gayon, M.L. Fernandez-Sanchez, A. Sanz-Medel, *J. Anal. Atom. Spectrom.* 18 (2003) 1243.
- [7] J. Darrouzès, M. Bueno, G. Lespès, M. Potin-Gautier, *J. Anal. Atom. Spectrom.* 20 (2005) 88.
- [8] S. Mazan, N. Gilon, G. Crétier, J.L. Rocca, J.M. Mermet, *J. Anal. Atom. Spectrom.* 17 (2002) 366.
- [9] D. Wallschlager, *J. London, J. Anal. Atom. Spectrom.* 19 (2004) 1119.
- [10] S.F. Boulyga, J.S. Becker, *Fresenius J. Anal. Chem.* 370 (2001) 618.
- [11] L. Hinojosa-Reyes, J.M. Marchante-Gayon, J.I. Garcia-Alonso, A. Sanz-Medel, *J. Anal. Atom. Spectrom.* 18 (2003) 11.
- [12] J.J. Sloth, E.H. Larsen, *J. Anal. Atom. Spectrom.* 15 (2000) 669.
- [13] J. Darrouzès, M. Bueno, G. Lespes, M. Holeman, M. Potin-Gautier, *Talanta* 71 (2007) 2080.
- [14] I. Ipolyi, Z. Stefanka, P. Fodor, *Anal. Chim. Acta* 435 (2001) 367.
- [15] M.E. Moreno, C. Perez-Conde, C. Camara, *J. Anal. Atom. Spectrom.* 15 (2000) 681.
- [16] M. Johansson, G. Bordin, A.R. Rodriguez, *Analyst* 125 (2000) 273.
- [17] J.L. Gomez-Ariza, M.A. Caro De La Torre, I. Giraldez, D. Sanchez-Rodas, A. Velasco, E. Morales, *Appl. Organomet. Chem.* 16 (2002) 265.
- [18] R. Rubio, A. Padro, G. Rauret, *Anal. Chim. Acta* 353 (1997) 91.
- [19] M. Vilano, R. Rubio, *J. Anal. Atom. Spectrom.* 15 (2000) 177.
- [20] I. Ipolyi, W. Corns, P. Stockwell, P. Fodor, *J. Autom. Methods Manage. Chem.* 23 (2001) 167.
- [21] J.M. Gonzalez LaFuente, J. Marchante-Gayon, M.L. Fernandez-Sanchez, A. Sanz-Medel, *Talanta* 50 (1999) 207.
- [22] H. Ge, X.J. Cai, J.F. Tyson, P.C. Uden, E.R. Denoyer, E. Block, *Anal. Commun.* 33 (1996) 279.
- [23] E.H. Larsen, S. Stürup, *J. Anal. Atom. Spectrom.* 9 (1994) 1099.
- [24] S. Simon, A. Barats, F. Pannier, M. Potin-Gautier, *Anal. Bioanal. Chem.* 383 (2005) 562.
- [25] G.L. Long, J.D. Winefordner, *Anal. Chem.* 55 (1983) 712A.
- [26] D.J. Douglas, J.B. French, *J. Am. Soc. Mass Spectrom.* 3 (1992) 398.
- [27] J. Golimowski, K. Golimowska, *Anal. Chim. Acta* 325 (1996) 111.
- [28] I. Heninger, M. Potin-gautier, I. De Gregori, H. Pinochet, *Fresenius J. Anal. Chem.* 357 (1997) 600.
- [29] M. Bueno, M. Potin-Gautier, *J. Chromatogr. A* 963 (2002) 185.

Vanadium doped tin dioxide as a novel sulfur dioxide sensor

S. Das^a, S. Chakraborty^a, O. Parkash^b, D. Kumar^b, S. Bandyopadhyay^c,
S.K. Samudrala^c, A. Sen^{a,*}, H.S. Maiti^a

^a *Sensor and Actuator Division, Central Glass and Ceramic Research Institute,
Kolkata 700032, India*

^b *Department of Ceramic Engineering, Institute of Technology, Banaras Hindu University,
Varanasi 221005, India*

^c *School of Materials Science and Engineering, University of New South Wales, Sydney, Australia*

Received 22 August 2007; received in revised form 7 November 2007; accepted 7 November 2007
Available online 17 November 2007

Abstract

Considering the short-term exposure limit of SO₂ to be 5 ppm, we first time report that semiconductor sensors based on vanadium doped SnO₂ can be used for SO₂ leak detection because of their good sensitivity towards SO₂ at concentrations down to 5 ppm. Such sensors are quite selective in presence of other gases like carbon monoxide, methane and butane. The high sensitivity of vanadium doped tin dioxide towards SO₂ may be understood by considering the oxidation of sulfur dioxide to sulfur trioxide on SnO₂ surface through redox cycles of vanadium–sulfur–oxygen adsorbed species.

© 2008 Published by Elsevier B.V.

Keywords: Gas sensor; Sulfur dioxide; Tin dioxide

1. Introduction

Due to growing concern on environmental issues, much attention has been focused on the monitoring of air pollutants. Sulfur dioxide is one of the major gases that cause a serious air pollution problem [1,2]. An exposure to SO₂ can cause irritation to the eyes, skin and respiratory system. SO₂ is also toxic to plants and animals and can damage structures and historical monuments. Sulfur dioxide may be produced naturally from the decay of vegetation and volcanic emissions and also as a by-product from metal smelting, processing and combustion of coal or oil, manufacture of sulfuric acid, fertilizer plants, petrochemical industry and other processes such as food preservation, wine making and bleaching. The long-term exposure limit and the short-term exposure limit of sulfur dioxide gas are 2 ppm and 5 ppm, respectively, through the acceptable limit of SO₂ in ambient air is much less. Nevertheless, the monitoring of SO₂ leakage at the source may be helpful to contain not only the accidental exposure at the source but

also environmental pollution in general. Though very low concentration (order of 10 ppb) of SO₂ in ambience is normally measured by West and Gaeke method [3] or ultraviolet fluorescence [4], a relatively high concentration (order of 1 ppm) can be measured by electrochemical sensors [5]. However, electrochemical sensors have a short life [6]. On the other hand, metal oxide based semiconductor sensors have a long life and are also cheap and rugged. However, till date, no such semiconductor sensor for detection of SO₂ is available in the market [5].

Semiconductor sensors for detection of toxic and combustible gases like carbon monoxide, methane, hydrogen, LPG, CNG appeared in the market more than 30 years ago [7–9]. One of the problems of such sensors is to engineer selectivity towards a particular gas. Incidentally, information on tin dioxide (and other semiconducting oxides) based sensors for detection of sulfur dioxide is available as a few publications [10–12] only, and in the reported papers the studies have been restricted to detection of high concentration (1000 ppm and in one case 200 ppm) of SO₂. Also nothing has been reported about the selectivity of such SO₂ sensors in presence of other interfering gases.

In this study, we show that it is possible to develop highly sensitive and selective SO₂ sensors based on nanostructured

* Corresponding author.

E-mail address: asen@cgcri.res.in (A. Sen).

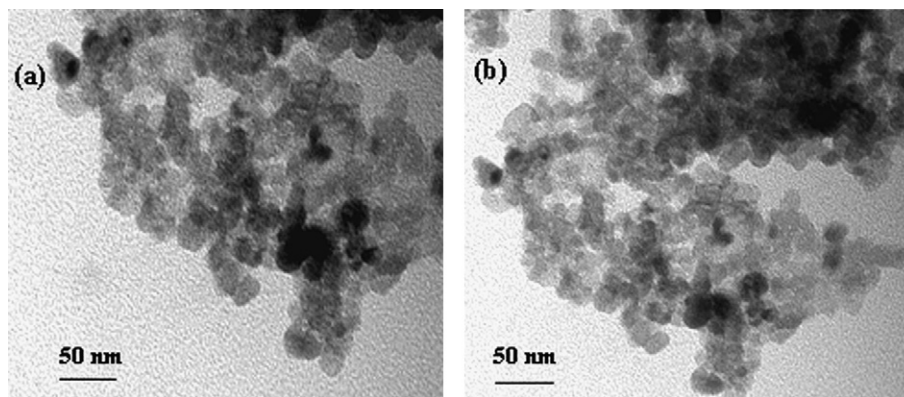


Fig. 1. Transmission electron micrographs showing the morphology of (a) tin dioxide and (b) vanadium doped (1 wt.%) tin dioxide powder prepared by simultaneous precipitation followed by calcination at 950 °C.

vanadium doped SnO₂ and for such sensors, the detection level of SO₂ can go down to 5 ppm.

2. Experimental

Powders containing SnO₂ doped with vanadium (added as 0–1 wt.% V₂O₅ with respect to SnO₂) were prepared by simultaneous precipitation technique [13]. In this technique, stannous chloride (SnCl₂·2H₂O) solution was made in distilled water containing a small amount of hydrochloric acid (1–2%). Vanadium pentoxide (V₂O₅) was dissolved in distilled water containing a small amount of hydrochloric acid (2–5 wt.%) at 60–80 °C for 1 h under constant stirring. The above solutions were added to ammonium hydroxide solution (maintaining a pH of 10) under stirring so that all the hydroxides were precipitated simultaneously. The precipitates were washed, made chloride free and finally calcined at 950 °C for 2 h to get the oxide powders.

The particle morphology of the powders was observed using a scanning electron microscope (Leo, 30i) after ultrasonically dispersing the powder in acetone. The phase identification of the calcined powders was carried out by X-ray diffraction (Philips, PW 1710 diffractometer). For infrared spectroscopic analysis, the powder was mixed with dried KBr. The mixture was pressed to make pellets of about 0.3 mm thickness. The fourier transform infrared spectra of the samples were recorded using Bruker Tensor-27 in the wave number range of 400–4000 cm⁻¹. Chemical species absorbed on the thick film sensors were determined on an EPR (Electron Paramagnetic Resonance, Bruker series) instrument. Thick pastes of the powders were prepared in an aqueous medium containing a small amount of PVA binder. The pastes were painted on the outer surface of alumina tubes (length 3 mm, outer diameter 2 mm and thickness 0.5 mm). Gold electrodes and platinum lead wires were attached at the ends of the tubes (by curing at a higher temperature) before applying the paste. The consistency of the pastes and the processing variables were optimized to get final coatings of around 100 μm thickness. After painting, the coated alumina tubes were cured at 600 °C for 1 h. Kanthal heating coils were placed inside the tubes and the leads were bonded to nickel pins. The details of the packaging arrangement have been given elsewhere [14,15]. The electrical resistance and sensitivity of the sensors were measured

in 100 ppm methane, butane, carbon monoxide and 5 ppm and 100 ppm sulfur dioxide at different temperatures (250–450 °C) in an ambient of 50–60% relative humidity using a digital multimeter (Solartron), a constant voltage–current source (Kiethley 228A) and an X-Y recorder (Yokogawa). All the samples were initially aged at 350 °C for 7 days to achieve the desired stability before the measurements.

3. Results and discussion

Fig. 1 depicts typical transmission electron micrographs of pure tin dioxide and vanadium doped (1 wt.%) tin dioxide powders prepared by simultaneous precipitation method followed by calcination at 950 °C for 2 h. The particle sizes of the tin dioxide and vanadium doped (1 wt.%) tin dioxide powders, as observed from the micrographs, were in the range of 40–50 nm and the crystallite sizes turned out to be 14 nm and 17 nm, respectively when calculated from the X-ray diffraction patterns (Fig. 2) using Scherrer formula [16]:

$$D = \frac{0.9\lambda}{\beta \cos \theta} \quad (1)$$

where D is the average crystallite size, $\lambda = 1.54 \text{ \AA}$ [X-ray wavelength (Cu K_α)] and $\beta = \sqrt{(B^2 - b^2)}$, B being the width of the

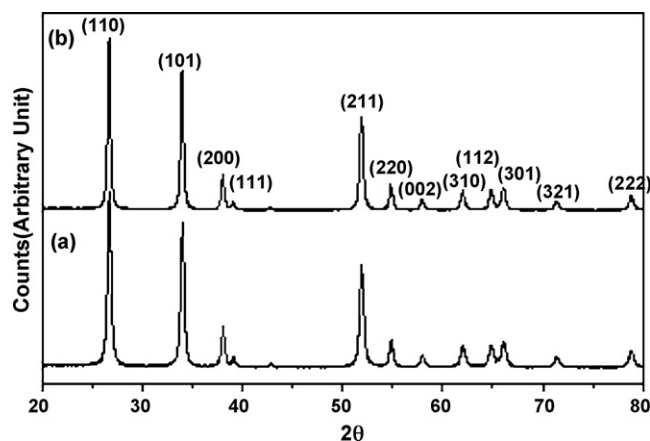


Fig. 2. XRD patterns for pure and vanadium doped tin dioxide powders (after calcination at 950 °C) (a) pure SnO₂ and (b) SnO₂ + 1 wt.% V₂O₅.

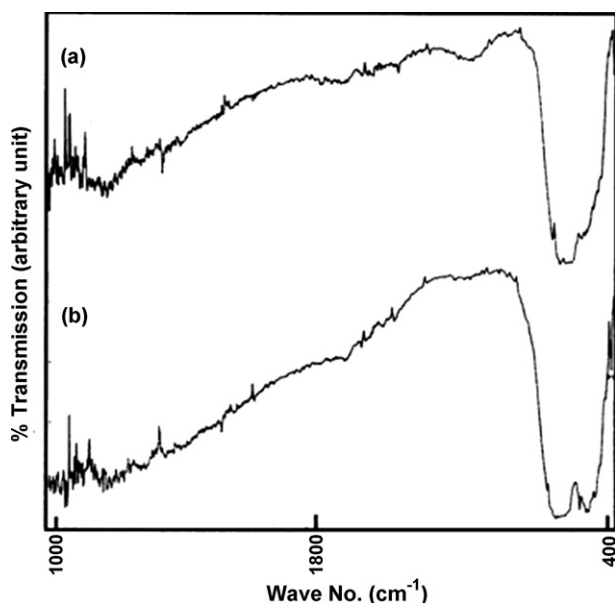


Fig. 3. FTIR spectra for (a) SnO₂ and (b) SnO₂ + 1 wt.% V₂O₅ powders.

diffraction peak at half maximum for the diffraction angle 2θ and b is the same for very large crystallites. The value of b was determined from XRD of a large-grained sample prepared by calcining the powder at a high temperature. Also from the XRD patterns, the solid solution of vanadium in tin dioxide was indicated from the slight shift of SnO₂ peaks for the powder containing 1 wt.% vanadium oxide.

Fig. 3(a) shows the FTIR spectrum of the undoped SnO₂ powder. From this spectrum a strong band associated with the anti-symmetric Sn–O–Sn stretching mode of the surface binding oxide can be observed apparently at 600 cm⁻¹ [17]. Fig. 3(b) shows the FTIR spectrum of vanadium doped (1 wt.%) tin

dioxide powder. The stretching-bond peak-shift with the V₂O₅ doping may be attributed to the incorporation of vanadium ions in the lattice site of tin dioxide.

In order to reveal the adsorbed oxygen species on the thick film of SnO₂, EPR measurement was carried out (Fig. 4). In n-type semiconductors like SnO₂, oxygen species are adsorbed on the sensor surface as O⁻ and O₂⁻ species and their concentration depends on the temperature [18,19]. In the EPR traces (both tin dioxide and vanadium doped (1 wt.%) tin dioxide sample), the peaks from O₂⁻ and O⁻ were found at 3382.3 G and 3597.8 G, respectively. The sharp peak of O₂⁻ indicates that the major species adsorbed on the SnO₂ powder at room temperature is O₂⁻. It may be noted that the O₂⁻ is not detectable by EPR because of its diamagnetic character. As vanadium is incorporated into SnO₂ (Fig. 4(b)), the peak due to O⁻ gradually increases and the peak from O₂⁻ remains nearly unchanged. The line broadening in Fig. 4(b) may be brought about by the magnetic interaction of O₂ with surface paramagnetic species [20]. However, further studies are required to understand why more O⁻ species are formed on SnO₂ surface in presence of vanadium and the exact mechanism behind the line broadening.

The effect of V₂O₅ doping on sulfur dioxide sensitivity of SnO₂ samples has been depicted in Fig. 5, where the percent sensitivity (percent response) is given by:

$$S = \left[\frac{R_A - R_G}{R_A} \right] \times 100 \quad (2)$$

where R_A and R_G are the sensor resistance in air and gas (at the operating temperature), respectively. It is found that SnO₂ sensor containing 0.15 wt.% V₂O₅ shows the highest sensitivity and the optimum operating temperature is around 350 °C. Interestingly, the SO₂ sensitivity of vanadium doped tin dioxide decreases (Fig. 5) with the increase in vanadium doping above 0.15%. It

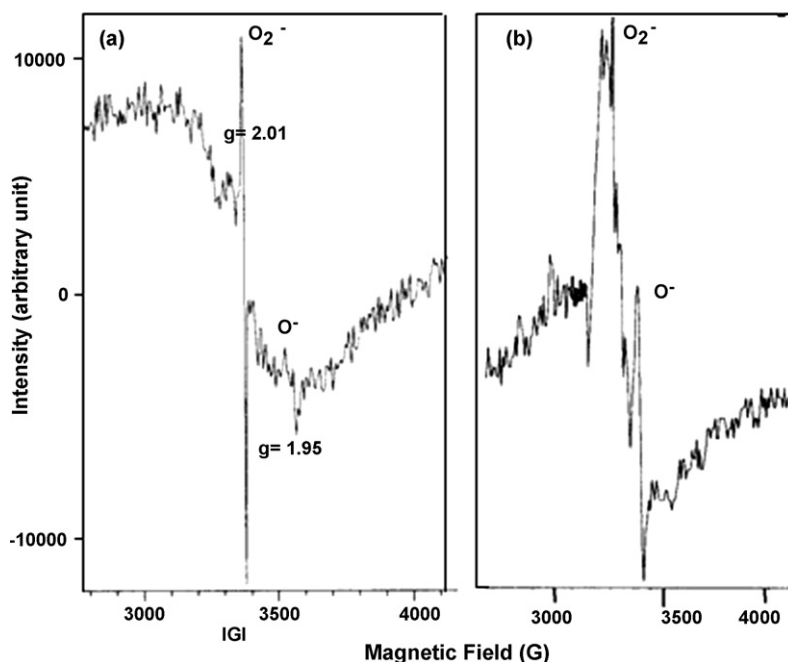


Fig. 4. EPR trace for (a) tin dioxide and (b) vanadium doped tin dioxide powders.

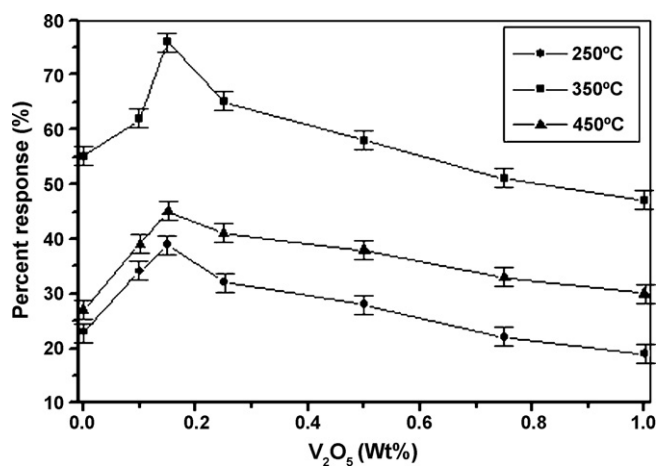


Fig. 5. Effect of vanadium concentration on sulfur dioxide (100 ppm) sensitivity of tin dioxide sensors at different temperatures.

is known that V^{5+} in Sn^{4+} site acts as a donor dopant [21] and hence, should increase the conductivity of n-type SnO_2 . The latter has been actually observed (at $350^\circ C$, the typical resistance of a sensor coating containing SnO_2 and a coating containing SnO_2 doped with 0.15 wt.% vanadium are $2.0 M\Omega$ and $0.9 M\Omega$, respectively) and the increase in free carrier concentration (for vanadium doped SnO_2) should reduce the depletion layer thickness [22,23] and in effect, should lower the gas sensitivity for higher vanadium doping. Fig. 6 shows the sensitivity of the 0.15 wt.% V_2O_5 doped SnO_2 sensor towards different gases. It is clear from Fig. 6 that V_2O_5 doped SnO_2 shows high sensitivity towards SO_2 (even at a concentration of 5 ppm) over CO , CH_4 and C_4H_{10} . Indeed, this differential sensitivity of vanadium doped SnO_2 can be exploited to make sensors selective to SO_2 in presence of CO , CH_4 and C_4H_{10} by properly modifying the electronic circuitry. It may be noted that SnO_2 without vanadium addition does not show such prominent differential sensitivity. We also studied the sensitivity of 0.15 wt.% V_2O_5 doped SnO_2 sensors at different concentrations of sulfur dioxide, which is of much importance for making real-life devices. We found (Fig. 7) the sensitivity of our sensors vs. plot to be linear at higher sulfur dioxide concentration (above 100 ppm), which is of much

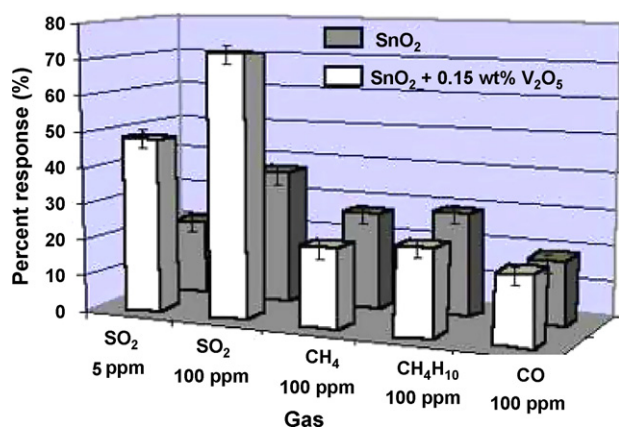


Fig. 6. Differential sensitivity of SnO_2 and $SnO_2 + 0.15$ wt.% V_2O_5 sensors in different gases (working temperature $350^\circ C$).

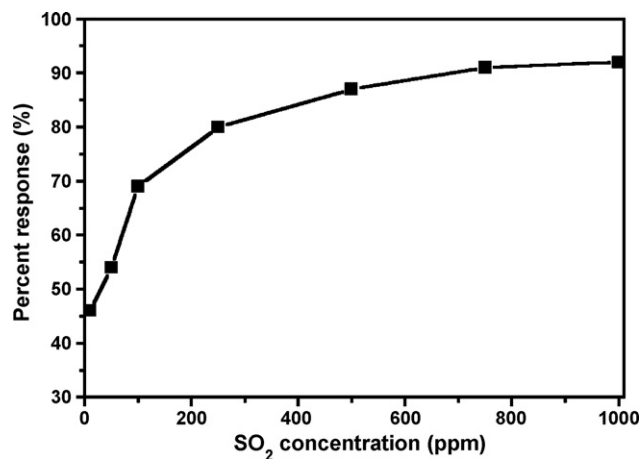


Fig. 7. Percent response vs. sulfur dioxide plot of $SnO_2 + 0.15$ wt.% V_2O_5 sensors (working temperature $350^\circ C$).

practical importance. Stability is an important requirement of any type of sensor. To begin the investigation in this area, the resistance as a function of time with sulfur dioxide exposure was examined for a period of 20 days sensitivity of 0.15 wt.% V_2O_5 doped SnO_2 sensors, as shown in Fig. 8. During the first day or so there is a small steady increase in resistance, which eventually leveled out. After this, the resistance reached steady state, with a standard deviation of $\sim 0.01 M\Omega$. This resulted in a signal to noise ratio of ~ 400 (average value/standard deviation).

To understand the role of vanadium doping in SnO_2 for obtaining sensors selective to SO_2 , we have to first appreciate the features of SO_2 sorption on SnO_2 surface. Sulfur dioxide chemisorption on tin dioxide can proceed in two forms [24]: reversible and irreversible. Their ratio depends on temperature and dopant content in SnO_2 . Indeed, SO_2 sorption on semiconductor metal oxides is a complex temperature- and time-dependent surface reaction and electronic interactions between the SO_2 related adsorbates and SnO_2 , which are far from being clearly understood [25]. The resistance of SnO_2 decreases on exposure to SO_2 up to $400^\circ C$, but it does not recover to the original value (air level) after removal of SO_2 indicating [10] the

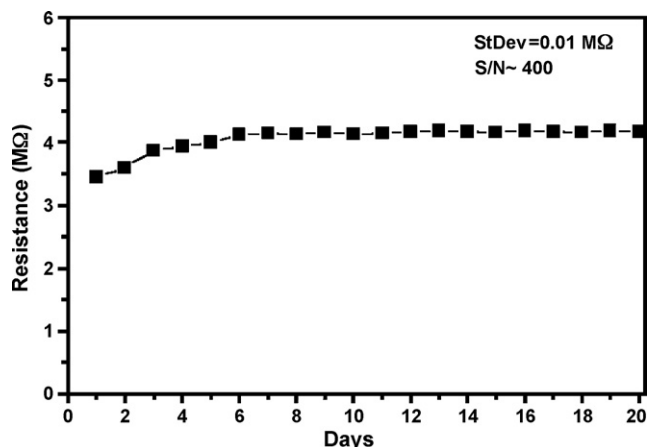


Fig. 8. Long-term stability results over a 20-day time frame of $SnO_2 + 0.15$ wt.% V_2O_5 sensors (working temperature $350^\circ C$).

irreversible formation of positively charged SO₂-related adsorbates on SnO₂. It has been observed that [26] two types of OH groups are formed on SnO₂ surface. Hydroxide ions, doubly bonded to Sn⁺⁴, have their O–H bonding weakened by polarization of adjacent metal ions. These OH groups exhibit acidic properties and tend to donate protons. The other OH groups simply bonded to metal cations conversely exhibit basic properties. Sulfur dioxide reacts with the basic OH groups to form chemisorbed sulfate species and according to Berger et al. [12], the irreversible chemisorption of SO₂ on SnO₂ surface is due to the formation of sulfate groups on basic OH groups on SnO₂.

Quantum chemical simulation of SO₂ chemisorption on SnO₂ surface [24] showed that several adsorption SO₂ species can exist which differ by their coordination, geometry and charge. The reversible decrease in resistance in presence of SO₂ may be understood as oxidation of SO₂ to SO₃ on SnO₂ surface like that of a reducing gas. Indeed, thermodesorption studies of SnO₂ surface in presence of SO₂ by Bukun et al. [25] showed the spectral features of SO₃ confirming oxidation of at least some SO₂ to SO₃ on SnO₂ surface above 300 °C. Donor chemisorption of SO₂ proceeds on surface oxygen ions to form surface SO₃ complexes. It can be assumed that further reaction of SO₃ complexes with the sorbed oxygen or gas phase oxygen yields SO₄ complexes.

Incidentally, supported vanadia [27] is a known catalyst for oxidation of SO₂. Sulfur dioxide is adsorbed and coordinated onto the basic V–O–Sn bond [28] to form (V⁺⁵)·SO₂-ads or the (V⁺³)·SO₃-ads state [29]. Such surface species take part in redox cycles [29] and oxidize sulfur dioxide to sulfur trioxide resulting in the lowering of the resistance of V doped tin dioxide in presence of sulfur dioxide. The lowering of sensitivity with increasing vanadium concentration may be understood by considering the formation of V₂O₅-crystallites [30] at higher vanadium concentration (instead of molecularly dispersed form of V₂O₅ at low vanadium concentration), which is not very active for redox reaction.

4. Conclusion

It has been found that vanadium doped tin dioxide can detect sulfur dioxide at concentrations down to 5 ppm. Such sensors are quite selective in presence of other gases like carbon monoxide, methane and butane. The high sensitivity of vanadium doped tin dioxide towards SO₂ may be understood by considering the oxidation of sulfur dioxide to sulfur trioxide on SnO₂ sur-

face through redox cycles of vanadium–sulfur–oxygen adsorbed species.

Acknowledgement

The authors are grateful to the Council of Scientific and Industrial Research, Government of India, for financial support (Networked Programme) during these investigations.

References

- [1] J.S. Pandey, R. Kumar, S. Devotta, *Atmos. Environ.* 39 (2005) 6868–6874.
- [2] L. Trasande, G.D. Thurston, *J. Allergy Clin. Immunol.* 115 (2005) 689–699.
- [3] E.H. Adema, V. Mejstřík, B. Binek, *Air Soil Poll.* 69 (1993) 321–335.
- [4] F. Cappellani, A. Bielli, *Environ. Monit. Assess.* 35 (1995) 77–84.
- [5] S.R. John, H.L. Michael, D.H. Darryl, Electrochemical sensor for determining analyte in the presence of interferent, US Patent No. 20020027086.
- [6] M. Stoytcheva, R. Zlatev, B. Valdez, J.P. Magnin, Z. Velkova, *Biosens. Bioelectron.* 22 (2006) 1–9.
- [7] W. Gopel, D. Schierbaum, *Sens. Actuators B* 26 (1995) 1–12.
- [8] H.X. Li, J.H. Liu, Y.H. Zhang, *Sens. Actuators B* 14 (1993) 675–676.
- [9] S.S. Park, J.D. Mackenzie, *J. Am. Ceram. Soc.* 78 (1995) 2669–2672.
- [10] Y. Shimizu, N. Matsunaga, T. Hyodo, M. Egashira, *Sens. Actuators B* 77 (2001) 35–40.
- [11] D. Girardin, F. Berger, A. Chambaudet, R. Planade, *Sens. Actuators B* 43 (1997) 147–153.
- [12] F. Berger, M. Fromm, A. Chambaudet, R. Planade, *Sens. Actuators B* 45 (1997) 175–181.
- [13] K. Chatterjee, S. Chatterjee, A. Banerjee, M. Raut, N.C. Paul, A. Sen, H.S. Maiti, *Mater. Chem. Phys.* 81 (2003) 33–38.
- [14] S. Chakraborty, A. Sen, H.S. Maiti, *Sens. Actuators B* 119 (2006) 431–434.
- [15] S. Chakraborty, A. Sen, H.S. Maiti, *Sens. Actuators B* 115 (2006) 610–613.
- [16] A. Taylor, *X-Ray Metallography*, Wiley, New York, 1961, pp. 678–86.
- [17] K. Nakamoto, *Infrared and Raman Spectra of Inorganic and Coordination Compounds*, fifth ed., John Wiley & Sons, Inc., NY, 1997.
- [18] S.C. Chang, *IEEE Trans. Electron. Dev.* ED-26 (1979) 1875–1880.
- [19] S.C. Chang, *J. Vac. Sci. Technol.* 17 (1979) 366–369.
- [20] M. Che, A.J. Tench, *Adv. Catal.* 32 (1983) 1.
- [21] S.D. Han, H. Yang, L. Wang, J.W. Kim, *Sens. Actuators B* 66 (2000) 112–115.
- [22] G. Zhang, M. Liu, *Sens. Actuators B* 69 (2000) 144–152.
- [23] L. Bruno, C. Pijolat, R. Lalauze, *Sens. Actuators B* 18 (1994) 195–199.
- [24] Y. Dobrovolsky, T. Zyubina, *Electrokhimia* 28 (1992) 1558–1566 (in Russian).
- [25] N. Bukun, A. Vinokurov, M. Vinokurova, L. Derlyukova, Y. Dobrovolsky, A. Levchenko, *Sens. Actuators B* 106 (2005) 153–157.
- [26] H.P. Boehm, *Discuss. Faraday Soc.* 52 (1971) 264–275.
- [27] J.P. Dunn, H.G. Sterger Jr., I.E. Wachs, *Catal. Today* 51 (1999) 301–318.
- [28] J.P. Dunn, P.R. Koppla, H.G. Stenger, I.E. Wachs, *Appl. Catal. B* 19 (1998) 103–117.
- [29] L. Lietti, P. Forzatti, F. Bregani, *Ind. Eng. Chem. Res.* 35 (1996) 3884.
- [30] I.E. Wachs, B.M. Weckhuysen, *Appl. Catal. A* 157 (1997) 67–90.

Analytical investigations of phenyl arsenicals in groundwater

B. Daus*, J. Mattusch, R. Wennrich, H. Weiss

UFZ Helmholtz Centre for Environmental Research, Permoserstrasse 15, 04318 Leipzig, Germany

Received 27 July 2007; received in revised form 17 October 2007; accepted 7 November 2007

Available online 17 November 2007

Abstract

Phenylic arsenic compounds are the main contaminants in groundwater at abandoned sites with a history of arsenic containing chemical warfare agents (CWA). A fast and sensitive HPLC–ICP–MS method was developed to determine inorganic arsenic compounds like arsenite and arsenate as well as the degradation products of the arsenic containing warfare agents (phenylarsonic acid, phenylarsine oxide, diphenylarsinic acid). Beside these arsenic species the groundwater samples contained also high iron contents (up to 23 mg/l as Fe(II)) which led to precipitates in the samples after coming into contact with the atmosphere. Preservation immediately after sampling by phosphoric acid has shown that a successful avoidance of any losses of any arsenic species between sampling and analysis was possible. The suggested analytical method was applied to groundwater samples taken from different depths at a polluted site. The main contaminant in the water samples was diphenylarsinic acid (up to 2.1 mg/l) identified by ESI–MS, but also elevated concentrations of inorganic arsenic (up to 240 µg/l) were found.

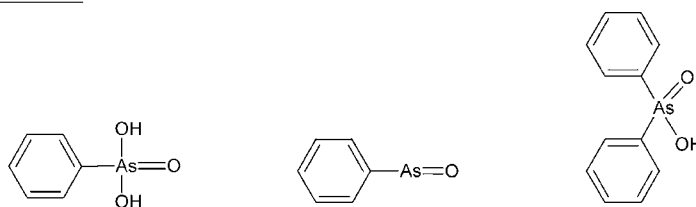
© 2007 Elsevier B.V. All rights reserved.

Keywords: Degraded warfare agents; Groundwater; Speciation analysis; Arsenic

1. Introduction

The variety of arsenicals in the environment is wide and a range of analytical tools can be used to analyze them [1]. One group of arsenic containing compounds is characterized by a phenylic moiety originating from synthetic arsenic compounds

hydrolysis and oxidation/reduction reactions (perhaps forced by the use of calcium hypochlorite for destruction during the time after World War II). Consequently, there remained compounds such as phenylarsonic acid (PhAs), phenylarsine oxide (PhAsO), diphenylarsinic acid (DPhAs), which are to be expected primarily in contaminated groundwater samples with a warfare history.



Phenylarsonic acid (PhAs) Phenylarsine oxide (PhAsO) Diphenylarsinic acid (DPhAs)

such as warfare agents. The original compounds are diphenylarsine chloride (Clark I), diphenylarsine cyanide (Clark II) phenylarsine dichloride (Pfiffikus), which are subjected to the degradation over time into some other compounds. The main reactions under environmental conditions that occur there, are

Usually the analysis of warfare agents and their degradation products is performed by gas chromatography (GC), after derivatization for the most part (e.g. [1–3]). The disadvantage of this method is that the inorganic arsenic compounds (arsenite and arsenate) cannot be detected simultaneously.

Some HPLC separations have also been suggested in the literature. The advantages of these methods are to be found in less effort for sample preparation and higher sensitivity by applying the ICP–MS as detector. For example, Hirano et al. [4] proposed a separation by using a reverse phase column and an ion pair

* Corresponding author at: UFZ Helmholtz Centre for Environmental Research, Department of Groundwater Remediation, Permoserstrasse 15, 04318 Leipzig, Germany. Tel.: +49 341 2352058; fax: +49 341 2352126.

E-mail address: birgit.daus@ufz.de (B. Daus).

mechanism to selectively detect the phenylarsonic acid and the phenylarsine oxide. Another method was described by Ishizaki and coworkers [6] who used a gel column to separate phenylarsonic and diphenylarsinic acid. Kinoshita et al. [5] proposed an Intersil C4 column using an acetonitrile/water eluent to separate arsenite, phenylarsonic acid, phenylarsine oxide and diphenylarsinic acid and applied it to well-water. However, due to the use of acetonitrile additional water was necessary as mobile-phase modifier.

The aim of the study was to develop an HPLC–ICP–MS method to analyze inorganic arsenicals as well as the main phenylic arsenicals originated from warfare agents in ground-water samples in one chromatographic run.

2. Experimental

2.1. Determination of total amounts of As and Fe

To determine the total concentrations of As and Fe ICP–atomic emission spectrometry was used. ICP–AES measurements (CIROS, Spectro A.I.) were performed using cross-flow nebulization. Calibrations were carried out using diluted ICP multi-element standard solution IV (CertiPUR, Merck) as well as arsenic single-element standard solutions (Merck, Darmstadt, Germany). The linear range was found to be between a few $\mu\text{g/l}$ and 10 mg/l. Limit of detection was 80 $\mu\text{g/l}$ for arsenic.

The anions (SO_4^{2-} , Cl^- , NO_3^-) were determined using an ion-chromatograph (DX 500, Dionex) with an IonPac AS12A/AG12A column and a conductivity detector. Details about these methods are given elsewhere [7].

2.2. Speciation of arsenic

Based on the findings of Ishizaki and coworkers [6] an HPLC separation with ICP–MS detection was developed using a Shodex RSpak NN-614 column (150 mm \times 6 mm; Shodex, Japan). The separation was optimized according to the analytes, which can be expected to assume a gradient program (for details see Table 1).

The chromatographic system (BECKMAN, System Gold, Fullerton, USA) equipped with an autosampler and a binary pump was coupled via a Peek capillary with a Meinhard nebulizer of an inductively coupled plasma mass spectrometer (ICP–MS, PQ ExCell, THERMO) for elemental selective detection.

Table 1
Details of the chromatographic separation

Flow	1 ml/min
Injection volume	50 μl
Eluent A	5 mM HNO_3 (Merck, Germany)
Eluent B	5 mM HNO_3 + 50 mM NH_4NO_3 (Merck, Germany)
Gradient program	0–10 min: 94% A + 6% B 10–20 min \rightarrow 50% B (linear) 20–20.2 min \rightarrow 6% B (linear) 20.2–30 min: 94% A + 6% B

A 0.05 mol/l As stock solution as arsenite (Merck, Germany), a 1000 mg/l As stock solution as arsenate (Titrisol[®], Merck, Germany), 1000 mg/l As as phenylarsonic acid ($\text{C}_6\text{H}_7\text{AsO}_3$, Fluka, Germany), 1000 mg/l As as 4-hydroxy-3-nitrobenzenearsonic acid (roxarsone, Fluka, Germany), 1000 mg/l As as monomethylarsonic acid, 1000 mg/l As as trimethylarsine oxide (courtesy of Prof. W. Goessler, University of Graz, Austria) and a 1000 mg/l As as phenylarsine oxide (Sigma, Switzerland) were diluted to get the mixed standards with the appropriate concentrations. Stock solutions prepared from solids were checked by ICP–AES.

2.3. Peak identification by ESI–MS

The structural information was obtained with a MSD G 1946 B (Agilent) coupled to the Beckman–HPLC using the atmosphere pressure electro-spray ionization (ESI). The detection conditions were the following: drying gas flow 9 l/min, nebulizer pressure 40 psi, drying gas temperature 350 $^\circ\text{C}$, capillary voltage 1500–3000 V, positive mode, and cycle time 1.86 s/cycle. The fragmentor voltage for additional fragmentation was fixed at 80 V. The detection was performed in the TIC (total ion current) and SIM (single ion monitoring) mode, alternatively. The mass calibration was repeated monthly.

2.4. Sampling site and sampling

The contaminated site of an abandoned chemical warfare agent filling station (active until 1945) was cleaned up by soil excavation in 2005. The contamination of the groundwater still exists and was therefore subject of the present investigations.

Water samples were taken by direct-push technology [8] from 15 m below ground up to the groundwater level in each 1.2 m steps and filter range 1 m. The samples (100 ml) were filled in polyethylene bottles and acidified for preservation with phosphoric acid to a final concentration of 10 mM.

3. Results and discussion

The chromatographic method was optimized to achieve a separation of the two inorganic arsenic compounds (arsenite (As(III)) and arsenate (As(V))) and to distinguish between the pentavalent phenylarsonic acid (PhAs) and the three-valent phenylarsine oxide (PhAsO) from other potential groundwater contaminations such as monomethylarsonic acid (MMA) or roxarsone. A chromatogram of a mixed standard (10 $\mu\text{g/l}$ As of each compound) is shown in Fig. 1. As can be seen in the peak pairs As(V)/MMA and As(III)/PhAs, respectively, a complete baseline separation of the arsenic species under investigation could not be achieved. However, the peak resolution is sufficient to quantify the arsenic species of interest.

The limit of quantification for all arsenic species under investigation varies between 0.2 $\mu\text{g/l}$ (narrow peaks) and 0.8 $\mu\text{g/l}$ (broad peaks).

In the groundwater sample some additional peaks were detected. One of them (at retention time of 1130 s, see Fig. 2) was identified by ESI–MS to be diphenylarsinic acid (DPhAs) with $m/z = 263$ as molecular mass of the $[\text{DPhAs} + \text{H}]^+$. An additional

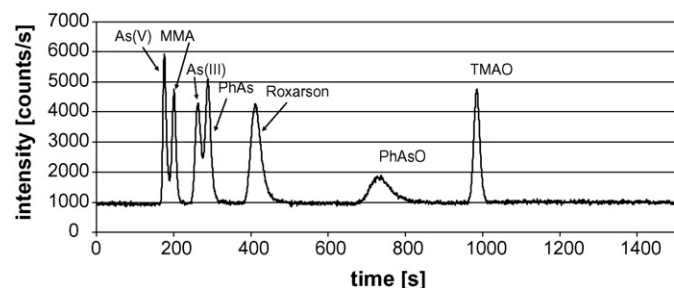


Fig. 1. HPLC-ICP-MS chromatogram obtained by the developed method ($10 \mu\text{g/l}$ each compound, As(III), arsenite; As(V), arsenate; MMA, monomethylarsenic acid; PhAs, phenylarsonic acid; roxarsone, 4-hydroxy-3-nitrobenzenearsonic acid; PhAsO, phenylarsine oxide; TMAO, trimethylarsine oxide).

small peak at 335 s has a signal at $m/z = 219$ and was suggested to be a thiophenylarsonic acid $[\text{C}_6\text{H}_5\text{AsO}_2\text{SH}_2 + \text{H}]^+$. Because of the low peak intensities the identification of the molecular structure was problematic, so that the peak will be named 335 s. Quantification of the unknown compounds was done by application of the regression with compounds (arsenate, arsenite, phenylarsonic acid and phenylarsine oxide) commercially available. The variation between these calibrations was less than 4%.

The groundwater samples contain iron in concentrations of about 10–20 mg/l. An oxidation of Fe^{2+} to Fe^{3+} in the groundwater samples after sampling is likely associated with a precipitation of iron(oxy)hydroxides. The influence of this reaction is demonstrated in Fig. 2. The preservation of inorganic arsenic species with phosphoric acid shown before [9,10] seems to be successful also for these kinds of samples. A groundwater sample was divided into two sub-samples immediately on-site. One of them was acidified with phosphoric acid to a final concentration of 10 mM. Both samples were measured after 24 h. As can be seen from Fig. 2, almost all arsenite, arsenate and phenylarsonic acid disappeared without adding a preservation agent to the sample. In comparison to the phenylarsonic acid the more nonpolar compounds such as phenylarsine oxide and diphenylarsinic acid were less affected by coprecipitation with iron.

Consequently, all groundwater samples, standards and blank solutions were acidified by phosphoric acid prior to analysis to get a final concentration of 10 mM.

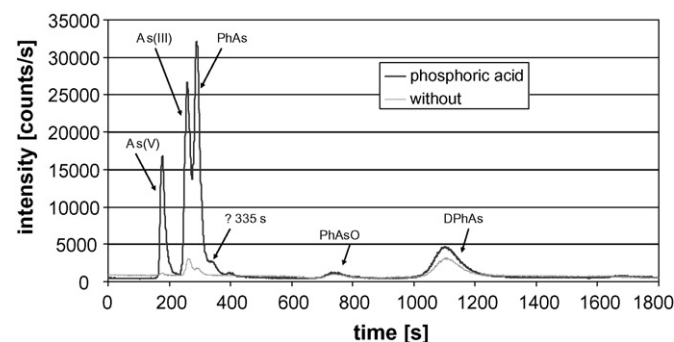


Fig. 2. Chromatogram of a groundwater sample with a preservation agent (10 mM phosphoric acid) and without preservation.

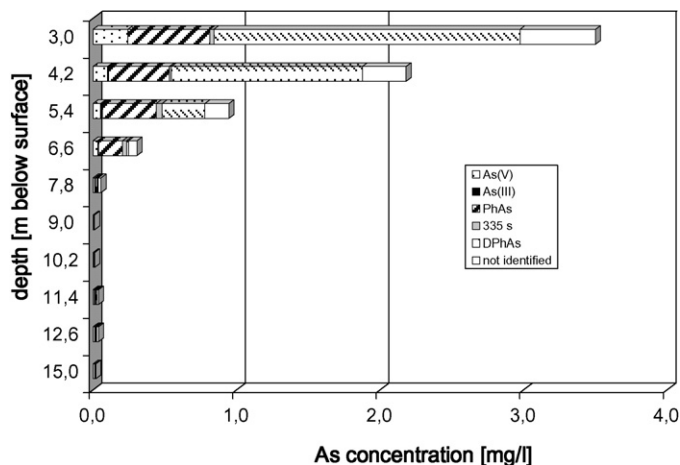


Fig. 3. Depth profile (m below surface) of arsenic species in groundwater samples at a contaminated site.

The method was applied to groundwater samples taken from different depths to investigate the extension of the contamination as well as the species distribution. Fig. 3 shows one typical depth profile from this contaminated area. The total iron and arsenic concentration of this series of samples are summarized in Table 2. It was found that the total arsenic concentration had its highest value near the groundwater table with 3.5 mg/l and decreased to less than $50 \mu\text{g/l}$ in samples collected at deeper levels. The pH of the samples varied between 6.2 and 7.4. Generally the water samples showed reducing properties (average Eh = 30 mV with no clear trend).

The results of arsenic speciation of the groundwater samples are presented in Fig. 3. The species are depicted in relation to the measured total As concentration. The difference between total concentration and the sum of all measured species is named “not identified”.

The “not identified” part is about 15% in the highly polluted samples, which may include measuring errors (keep in mind the mean calibration for DPhAs), or may be a not detectable species.

Generally, the DPhAs is the main contaminant in the samples taken from the upper 3 m of the groundwater followed by the phenylarsonic acid (PhAs). However, inorganic arsenic is also present in concentrations up to $240 \mu\text{g/l}$. The peak at 335 s has

Table 2

Total concentrations of As and Fe in the groundwater samples taken at different depths

Depth (m)		pH	Fe (mg/l)	As (mg/l)
From	To			
15.0	14.0	6.63	17.3	0.019
12.6	11.6	6.63	22.8	0.042
11.4	10.4	6.40	18.8	0.043
10.2	9.2	6.24	10.5	0.013
9.0	8.0	6.85	8.6	0.011
7.8	6.8	6.25	14.8	0.056
6.6	5.6	6.54	8.9	0.306
5.4	4.4	6.54	6.5	0.958
4.2	3.2	6.98	3.3	2.183
3.0	2.0	7.44	1.7	3.505

its highest value with 40 $\mu\text{g/l}$ in the sample taken at 5.4 m below surface.

The high content of diphenylarsinic acid in the groundwater samples is in accordance with the findings of Ishizaki and coworkers [6]. They have found that 4.3 mg/l As of total 4.5 mg/l As in Japanese well-water was in the form of diphenylarsinic acid. In these well-water samples, a condensation product of diphenylarsinic acid namely bis(diphenylarsine)oxide was also detected. The here suggested method is presumably not able to detect this compound. Due to the lack of a commercially available standard for this compound, we are not able to check this. It is possible that not analyzing this compound might also provide an explanation for getting somewhat low recovery rates of the total arsenic.

4. Conclusion

A method for the determination of arsenate and arsenite as well as the phenylic arsenicals (phenylarsonic acid, phenylarsine oxide and diphenylarsinic acid) is suggested and was proven to analyze more than 80% of the species in groundwater samples from an abandoned site with handling of chemical warfare agents more than 60 years ago. The fast method (one run: 30 min) without a sample preparation such as derivatization, allows a sensitive detection of the arsenicals.

The high iron content of the waters makes a preservation procedure necessary. Phosphoric acid seems to be a suitable agent to preserve the species in the samples.

The complete analyzing procedure suggested include the addition of phosphoric acid immediately after sampling, stor-

ing at 6 °C, and determination of the arsenic species by HPLC–ICP–MS within 1 week. In this way, a precipitation of iron hydroxides can be avoided in order to prevent losses of any arsenic compounds. Changes between the different arsenic compounds were not observed applying this preservation method. A determination of total arsenic by ICP–AES or ICP–MS is advisable to get information about the recovery.

References

- [1] M. Leermakers, W. Baeyens, M. De Gieter, B. Smedts, C. Meert, H.C. De Bisschop, R. Moarbitoa, P. Quevauviller, *Trends Anal. Chem.* 25 (2006) 1–10.
- [2] F.-A. Pitten, G. Müller, P. König, D. Schmidt, K. Thurow, A. Kramer, *Sci. Total Environ.* 226 (1999) 237–245.
- [3] S. Hanaoka, E. Nagasawa, K. Nomura, M. Yamazawa, M. Ishizaki, *Appl. Organomet. Chem.* 19 (2005) 265–275.
- [4] S. Hirano, Y. Kobayashi, T. Hayakawa, X. Cui, M. Yamamoto, S. Kanno, A. Shraim, *Arch. Toxicol.* 79 (2005) 54–61.
- [5] M. Ishizaki, T. Yanaoka, M. Nakamura, T. Hakuta, U. Seicho, M. Komuro, M. Shibata, T. Kitamura, A. Honda, M. Doy, K. Ishii, A. Tamaoka, N. Shimojo, T. Ogata, E. Nagasawa, S. Hanaoka, *J. Health Sci.* 51 (2005) 130–137.
- [6] K. Kinoshita, Y. Shida, C. Sakuma, M. Ishizaki, K. Kiso, O. Shikino, H. Ito, M. Morita, T. Ochi, T. Kaise, *Appl. Organomet. Chem.* 19 (2005) 287–293.
- [7] R. Wennrich, J. Mattusch, P. Morgenstern, K. Freyer, H.-C. Treutler, H.-J. Stärk, L. Brüggemann, A. Paschke, B. Daus, H. Weiss, *Environ. Geol.* 45 (2004) 818–833.
- [8] P. Dietrich, C. Leven, in: R. Kirsch (Ed.), *Groundwater Geophysics. A Tool for Hydrogeology*, Springer, Berlin, 2006, pp. 321–340.
- [9] B. Daus, J. Mattusch, R. Wennrich, H. Weiss, *Talanta* 58 (2002) 57–65.
- [10] B. Daus, H. Weiss, J. Mattusch, R. Wennrich, *Talanta* 69 (2006) 430–434.

Zircaloy-2 secondary phase precipitate analysis by X-ray microspectroscopy

C. Degueldre^{a,*}, J. Raabe^b, G. Kuri^a, S. Abolhassani^a

^a LWV, NES, Paul Scherrer Institute, 5232 Villigen, Switzerland

^b SYN, SLS, Paul Scherrer Institute, 5232 Villigen, Switzerland

Received 10 July 2007; received in revised form 5 November 2007; accepted 8 November 2007

Available online 4 January 2008

Abstract

Secondary phase precipitates of a Zircaloy sample have been characterised by X-ray microspectroscopy. In Zircaloy-2 X-ray microscopy reveals pictures with a 40 nm resolution identifying Fe, Cr and to a lower occurrence Ni phases up to size of the micrometer. Analysis by X-ray spectroscopy defines the structure of specific secondary phase precipitates. The feasibility tests demonstrate that the characterisation of Fe and Cr can be performed on 100 nm size phases allowing the analysis of the Fe or Cr atoms environment in these secondary phase precipitates.
© 2008 Elsevier B.V. All rights reserved.

Keywords: Zircaloy; Secondary phases precipitate; X-ray microspectroscopy

1. Introduction

Zirconium based alloys are used as structural material in light water reactors (LWR) and also as pressure tubes in the CANDU reactors. Zirconium has two allotropic phases, a hexagonal close packed (hcp) phase stable from low temperatures to 863 °C and a body-centred cubic (bcc) phase stable at higher temperatures. The alloying elements used for nuclear applications such as O, Cr, Fe, Ni, Nb and Sn, have an influence on the material mechanical properties as well as corrosion resistance and irradiation growth of the material in reactor e.g. [1]. Most of these elements stabilise the high temperature β phase whereas Sn and O stabilise the low temperature α phase. The commercially available alloys Zircaloy-2 (Zry-2) and Zircaloy-4 (Zry-4) are made of: (Sn,Zr)–(Zr,Fe,Cr)–(Zr,Ni,Fe) and (Sn,Zr)–(Zr,Fe,Cr), respectively [2,3]. Intermetallic phases are formed because they are above their solubility limits in zirconium. They are called secondary phase precipitates or particles (SPP). These phases have specific crystallographic structures and chemical stoichiometries that need to be well established. The composition of these intermetallics depends on the exact heat treatment of the alloy. In general two types of intermetallics are reported.

In Zry-4 SPP's are made of $Zr(Fe,Cr)_2$ [4]. The SPP's in Zircaloy-2 consist of $Zr_2(Ni, Fe)$ e.g. $Zr_2(Ni_{0.6-0.5}Fe_{0.4-0.5})_2$ phases with a body-centred tetragonal structure and of hexagonal $Zr(Fe_{0.45-0.43}Cr_{0.55-0.57})_2$ phases; both SPP's are sized $\leq 1 \mu m$ with smaller $Zr_2(Ni,Fe)$ precipitates [5,6]. The mean particle sizes ranged from about 0.07–0.4 μm in commercial products [7]. The trend towards increased fuel burn-up and higher operating temperatures in order to achieve more economic operation of nuclear power plants places demands on a better understanding of the role of SPP's on Zircaloy corrosion. As reported in the literature, when Zircaloy-2 and Zircaloy-4 are irradiated at intermediate temperatures with high-energy neutrons, a crystalline to amorphous phase transition occurs. It will be important to analyse their structure and the way they behave during irradiation and during propagation of the corrosion front.

The analytical methods used to characterise SPP's are ex situ or in situ. The ex situ methods are called extraction techniques. The two methods for SPP extractions are found in the literature. The first one, the extractive carbon replica method, allows determining the chemical composition of the SPP's. The second one, an anodic dissolution procedure of the matrix, is an interesting way of isolating SPP's from the surrounding α -Zr matrix, giving access to a precise determination of the crystallographic structure and lattice parameters of the SPP by X-ray diffraction. This procedure was validated for Zry-4 by comparing the SPP size distribution obtained by extraction with that directly measured

* Corresponding author. Tel.: +41 56 3104176; fax: +41 56 3103565.
E-mail address: claude.degueldre@psi.ch (C. Degueldre).

on a massive Zry-4 alloy. The SPP size distributions may be measured by this method [8].

The in situ analysis is primarily performed by microscopic techniques. Transmission electron microscopy (TEM) and energy dispersive X-ray spectroscopy (EDS) have been widely used to observe SPP in the Zircaloy matrix. Several aspects of the SPP's are revealed in these experiments coupled with scanning electron microscopy (SEM) while analysis may be subsequently completed by atomic force microscopy (AFM) on chemically resolved SPP's [9,10].

ToF-E ERD with a 60 MeV $^{127}\text{I}^{11+}$ ion beam was used to determine the oxygen content and chemical composition in Zr corroded samples resolving the analysis in depth profile. In Zry-2, the concentration of SPP elements (Fe,Cr,Ni) in relation to Zr was the same in oxide as in the same thickness of metal [11].

The ^{18}O -SIMS technique was used to evaluate the transport of oxygen and hydrogen in oxidation of Zr-based materials. At 400 °C, it is found that oxygen dissociation efficiency decreases in the order: Pt > Zr₂Fe > Zr₂Ni > ZrCr₂ ≥ Zry-2. It was suggested that a proper choice of the SPP's composition and size distribution can lead to reduced hydrogen uptake during oxidation of Zr-based materials in water [12].

XAFS of Zry has already been performed earlier [13], however, nothing is reported about XAFS of the SPP's. The present study explores the potential of the use of X-ray microspectroscopy for the characterisation of SPP's in a Zry-2 metal sample.

2. Experimental and modelling background

2.1. Sample preparation

Zircaloy 2 samples were originally recrystallized for 1 h at 800 °C. Zircaloy is in essence a solid substitutional solution of Sn (1.2–1.7 wt.%) in a Zr hexagonal closed packed structure (-phase) with a mean grain size of about 10 μm in our case. Oxygen is another alloy element (about 1000 ppm) found in solution as an interstitial. Zircaloy also possesses smaller amounts of Fe, Cr and Ni in the form of small intragranular intermetallic precipitates (i.e., not in solution). The last ones have very low solubility in the Zr matrix (see composition in Table 1).

Transmission electron microscope (TEM) samples were prepared from Zry-2 material. The desired sample was ground to a thickness of 200–300 μm. The material was ultrasonically cleaned in order to remove all the traces of silica particles used in the last stages of polishing. A 3 mm disc was subsequently punched out of the bulk material. It was then further thinned by double-jet electropolishing using a solution of 10% perchloric, 90% methanol as electrolyte. The electropolishing voltage was 20 V, the temperature of electrolyte was held below 30 °C.

2.2. Scanning X-ray micro-spectroscopy

Measurements were made on PoLux, the new soft X-ray micro-spectroscopy beam line dedicated to studies in polymer physics, environmental science and magnetism at the Swiss Light Source (SLS) of the Paul Scherrer Institute. This approach

to measure XAS spectra has been developed on scanning transmission X-ray microscope (STXM) (Jacobsen et al. [14,15]; Zhang et al. [16]). In principle, this method could also be used with a full-field transmission X-ray microscope, such instruments have sufficient energy resolution for quantitative XAS analysis. It is also conceptually quite similar to spectrum imaging in the STEM or energy-filtered TEM.

The scanning X-ray microscope has a tunable energy ranging from 200 to 1200 eV and is optimized for very low background and low detection limits. A spherical grating monochromator (SGM) is located upstream of the microscope and provides an energy resolution of $\Delta E/E \approx 3 \times 10^{-4}$. The sample is mounted vertically on a high-precision piezoelectric stage and scanned horizontally and vertically, perpendicular to the X-ray microprobe, which remains fixed, to produce a two-dimensional image. Fresnel zone plates are used as focusing optics to generate a submicrometer X-ray probe (~40 nm) by geometrical demagnification of the exit slit. The transmitted signal is collected by using a small-area detector, consisting of a phosphorous screen coupled to a photomultiplier. The image acquisition is done by a computer controlled processing electronics. The instrument is operated under vacuum in order (i) to minimize the X-ray absorption in air, which is significant for soft X-rays, (ii) to avoid scattering from air, and (iii) to prevent sample contamination.

X-ray absorption spectroscopy analyses were performed at the L-edges of Fe, Cr and tested at the Ni L-edge.

2.3. Modelling spectra

FEFF calculations were carried out with the code FEFF8 to quantify the Extended X-ray-Absorption Fine Structure (EXAFS) and the X-ray-Absorption Near Edge Structure (XANES). FEFF8 uses an ab initio self-consistent real space multiple scattering approach for clusters of atoms ($Z < 99$), including polarization dependence e.g. see Ankudinov and Rehr [17,18]. Calculations are based on an all-electrons approach and a real space relativistic Green's function formalism with no symmetry requirements. The method combines both full multiple scattering based on Lu or Lanczos algorithms and a high-order path expansion based on the Rehr–Albers multiple scattering formalism. Calculation of the X-ray elastic scattering amplitude (f) is performed using the ATOMS program to provide the crystallographic functionality for the X-ray absorption spectroscopy. Its primary function is to generate input files for the FEFF8 from crystallographic data (e.g. Table 2a–d).

X-ray diffraction data for ZrFe₂ was reported by Brueckner et al. [19] from powder. The unit cell data as well as the atomic coordinates are given in Table 2a. The crystal symmetry is cubic, the space group $Fd\bar{3}m$ S2, and the structure type is Cu₂Mg. The volume of the cell is 355.95 Å³ and for the 8 atoms the density is 7.57 g cm⁻³.

Neutron powder diffraction data for Zr(Fe_{0.6}Cr_{0.4})₂ was reported by Canet et al. [20]. The unit cell data as well as the atomic coordinates are given in Table 2b. The crystal symmetry is hexagonal closed packed, the space group $P63/m$ m c, and the structure type is MgZn₂. The volume of the cell is 179.45 Å³ and the density is 7.39 g cm⁻³.

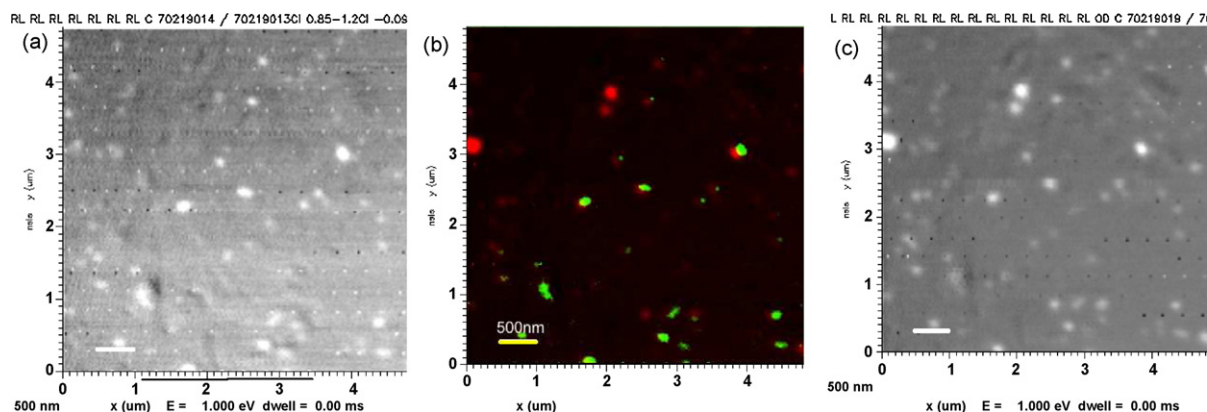


Fig. 1. X-ray microscopy photo of Zry-2 revealing the secondary phase precipitates. (a and c) Black-white are the element distributions according to the filename (Cr and Fe). (b) A combined image with red representing Fe and green Cr ((Fe,Cr) phases). Note the Fe phase may be associated with Ni, since Ni is not detected. Selected SPP for XAFS spectrum in Fig. 2: the ($x=2.1 \mu\text{m}$, $y=3.9 \mu\text{m}$) red spot in (b).

X-ray diffraction data for Zr_2Fe was reported by Havinga et al. [21]. The unit cell data as well as the atomic coordinates are given in Table 2c. The crystal symmetry is tetragonal and the space group $I4/mcm$. The volume of the cell is 228.14 \AA^3 and the density is 6.94 g cm^{-3} .

X-ray diffraction data for Zr_3Fe was reported by Matkovic et al. [22]. The unit cell data as well as the atomic coordinates are given in Table 2d. The crystal symmetry is orthorhombic, the space group $Cmcm$, and the structure type is Re_3B . The volume of the cell is 321.39 \AA^3 and the density is 6.81 g cm^{-3} .

It must be noted that Ni form with Fe solid solution in these intermetallic phases.

3. Results and discussion

3.1. Microscopy investigations

The X-ray microscopy investigations on SPP's in Zry-2 were performed on a TEM sample using the SLS PolLux BL. An area of $25 \mu\text{m}^2$ was scanned during 2 h for energy ranging around the L edges of the investigated elements.

The Cr and Fe elemental distribution maps, obtained at energies of 700–750 eV and 560–610 eV respectively, from the Zry-2 specimen are shown in Fig. 1(a and c). The images were collected at room temperature with a beam spot focused to a size of $\sim 40 \text{ nm}$ and scanned across the sample. The SPP's are easily recorded for Fe and rather well identified for Cr, how-

ever, Ni detection was more difficult because of the lower Ni concentration (see Table 1). The images of Ni doped phases are consequently not contrasted and are not shown. The result depicted in Fig. 2b represents the combined images of Cr and Fe mappings which defines the points of interest that encompassed both population of Cr and Fe. The measured XANES spectrum at the Fe $L_{2,3}$ edge for the selected SSP (see Fig. 1b) is presented in Fig. 2(b).

3.2. Spectroscopic data evaluation

A XANES spectrum obtained for a Fe rich SPP is shown in Fig. 2. XANES calculations at Fe $L_{2,3}$ edges were carried out for a set of model (Zr,Fe,Cr) intermetallic compounds and are presented Fig. 2a. The description of their possible crystallographic configurations used in the simulations is provided in Table 2. For a direct comparison of the experimental data with the computed ones, the measured XANES spectrum (shown in Fig. 2b) was processed using the ATHENA analysis program [23]. The background in the pre-edge as well as post-edge regions were removed by spline polynomial approximations and normalized to the edge jump value of unity at a higher photon energy range than the L_2 edge (740–748 eV).

The calculated spectra at the Fe L_3 edge for the cubic ZrFe_2 , hcp $\text{Zr}(\text{Fe,Cr})_2$, bct Zr_2Fe and orthorhombic Zr_3Fe compounds are shown in Fig. 2(a). It can be clearly noticed that the line-shape of the computed spectra are quite different from

Table 1
Zry-2 and SPP compositions and densities

a							
Element	Zr	Sn	O	Fe	Cr	Ni	
Fraction (wt.%)*	98.55–97.63	1.20–1.70	0.10–0.14	0.07–0.20	0.05–0.15	0.03–0.08	
Phases	Zry-2 Bulk			Secondary phase precipitates			
b							
Element	Zr	Sn	O	Zr	Fe	Cr	Ni
Fraction (at%)**	98.53–97.89	0.92–1.31	0.55–0.80	~ 33.3	~ 30.5	~ 24.0	~ 12.2
Density (g cm^{-3})**	6.50			~ 7.0			

(a) Data for the material. (b) Data for the phases, note in secondary phase composition (Zr and SPP's with $\text{Zr}(\text{Fe,Cr,Ni})_2$ stoichiometry).

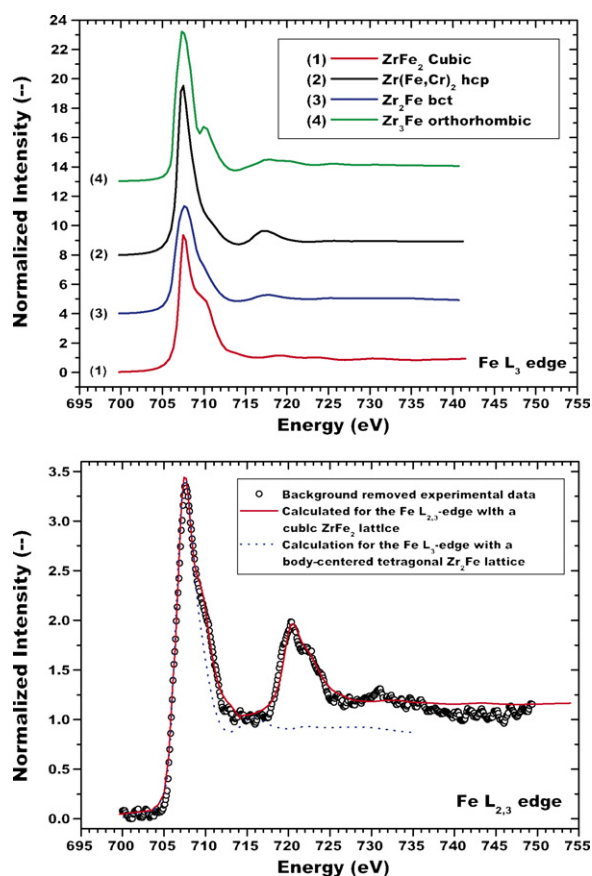


Fig. 2. X-ray microscopy XANES spectra of intermetallic phases and the experimental XANES of a secondary phase precipitates. Note the Fe L edges. (Top) Calculated spectra with the structures given in Table 1a–d ($\text{Zr}(\text{Fe},\text{Cr})_2$ is added for information). (Bottom) Comparison of the experimental spectrum (for selected SPP in Fig. 1) and the calculated spectra for cubic ZrFe_2 (partially substitute with Cr) and for Zr_2Fe (bct) structures.

each other. The L_3 XANES of Fe in the hcp $\text{Zr}(\text{Fe},\text{Cr})_2$ compound exhibits a single prominent absorption peak. Similarly, the white line of the XANES spectrum from bct Zr_2Fe structure is also characterised mainly by one peak with a small shoulder (tail) observed above the edge. However, the cubic- ZrFe_2 and orthorhombic- Zr_3Fe provide more pronounced secondary XANES feature above the edge. Although, the peaks normalised (to post-edge intensity) intensities in all cases range from 7 to 11; they are not correlated to Fe ratio or material density. Incidentally, these results help to explain the experimental Fe $L_{2,3}$ -edge XANES data that was measured. Qualitatively, the additional XANES feature appearing in the cases of cubic- ZrFe_2 or bct- Zr_2Fe structures, more closely resemble the measured XANES spectrum.

The calculated Fe $L_{2,3}$ XANES spectra using the cubic- ZrFe_2 structure together with the background corrected and normalized experimental XANES spectrum are shown in Fig. 2b.

The theoretical spectra were normalized to the experimental data at the peak of Fe L_3 edge. The calculations are performed using the full multiple scattering method [17,18] and in the absence of a core hole, followed by a convolution by the experimental resolution of 0.5 eV (using the CORRECTIONS card in FEFF). A statistical structural disorder in the atomic layers was

Table 2

Unit cell data as well as the atomic coordinate of (a) ZrFe_2 face centred cubic (fcc), (b) $\text{Zr}(\text{Fe},\text{Cr})_2$ hexagonal close packed (hcp), (c) Zr_2Fe body-centred tetragonal (bct), (d) Zr_3Fe orthorhombic

	a (Å)	b (Å)	c (Å)	α (°)	β (°)	γ (°)
(a) ZrFe_2						
Unit cell	7.087	7.087	7.087	90.00	90.00	90.00
Atom	#	OX	Site	x	y	z
Fe	1	+0	16d	0.625	0.625	0.625
Zr	1	+0	8a	0	0	0
	a (Å)	b (Å)	c (Å)	α (°)	β (°)	γ (°)
(b) $\text{Zr}(\text{Fe},\text{Cr})_2$						
Unit cell	5.019	5.019	8.266	90.00	90.00	120.00
Atom	#	OX	Site	x	y	z
Cr	1	+0	2a	0	0	0
Fe	1	+0	2a	0	0	0
Cr	2	+0	6h	0.8304	0.6608	0.250
Fe	2	+0	6h	0.8304	0.6608	0.250
Zr	1	+0	4f	0.3333	0.6667	0.063
	a (Å)	b (Å)	c (Å)	α (°)	β (°)	γ (°)
(c) Zr_2Fe						
Unit cell	6.385	6.385	5.596	90.00	90.00	90.00
Atom	#	OX	Site	x	y	z
Fe	1	+0	4c	0	0	0
Zr	1	+0	8h	0.1728	0.6728	0
	a (Å)	b (Å)	c (Å)	α (°)	β (°)	γ (°)
(d) Zr_3Fe						
Unit cell	3.321	10.966	8.825	90.00	90.00	90.00
Atom	#	OX	Site	x	y	z
Fe	1	+0	4c	0	0.7610	0.2500
Zr	1	+0	4c	0	0.4307	0.2500
Zr	2	+0	8f	0	0.1373	0.0581

furthermore incorporated with the help of the SIG2 card (a value of 0.002). In this way it was possible to obtain a very reasonable agreement between experiment and simulation, in terms of both absolute magnitudes and the line-shape. Past work conducted on Zr_2 identified two different intermetallic compounds present in three structural forms: bct $\text{Zr}_2(\text{Fe},\text{Ni})$ and hcp as well as cubic $\text{Zr}(\text{Fe},\text{Cr})_2$. Clearly Fe on the analysed SPP should be associated with Ni. In the analysis simulation tests have been made with $\text{Zr}(\text{Fe},\text{Cr})_2$ with various fractions of Cr, however no significant changes in the spectra can be found as Cr and Fe are practically indistinguishable as backscatters.

Fig. 3 completes the picture with an X-ray microscopy XANES spectrum of four similar intermetallic SPP's loaded with Cr. The experimental XANES spectrum of this SPP is compared with the Cr L_3 edges calculated with the structures given in Table 1a: the cubic ZrFe_2 with Fe partially substituted by Cr.

The role of other alloy elements such as tin or oxygen does not need to be mentioned at this level. Both elements are soluble

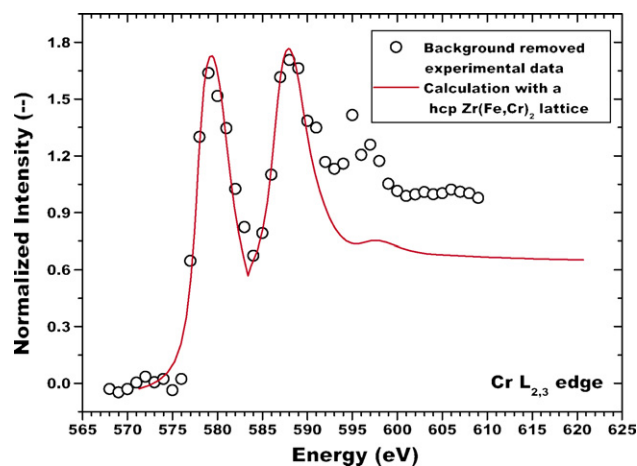


Fig. 3. Indicative X-ray microscopy XANES spectra of intermetallic phases, the experimental XANES and the Cr $L_{2,3}$ edges calculated with the structures given in Table 1a (cubic $ZrFe_2$ with Fe partially substituted with Cr) compared with the experimental spectra.

in the Zr matrix. Since Zr is more electropositive than Fe or the other transition metals, it is currently accepted that oxygen stays in the matrix. Tin is also expected to stay in the Zr matrix as no effect on SPP has been recorded.

Comparing the performance between TEM/EDS and XANES microscopy it may be sketched that TEM and electron energy loss spectrometry (EELS) allow morphology and chemical analysis around 1 nm, EDS around 10 nm, X-ray microscopy can identify feature around 40 nm and XANES microscopy allows analysis of phases of around 100 nm. The sample thickness for EELS need to be 30–60 nm in general while STXM allows analysis of samples of 20–200 nm (depending of the matrix). Clearly STXM is more flexible from this point of view). Finally, the impact of the doses is more devastating with the electrons than with the photons making the organic/bioorganic nanophases analysis easier with the STXM than with the TEM/EELS.

4. Conclusion

Secondary phase precipitates of a Zircaloy sample have been successfully investigated by X-ray microspectroscopy. X-ray microscopy reveals in Zircaloy-2 Fe and Cr phases with a 40 nm resolution up to size of about 500 nm. Ni could be present but it was not possible to produce well defined micrographs for this element may be because its concentration is lower than the other. The structures of $ZrFe_2$ or $Zr(Fe,Cr)_2$, Zr_3Fe and Zr_2Fe or $Zr_2(Ni,Fe)$ phases were used to calculate the X-ray absorption spectra recorded for selected secondary phase precipitates. The cubic structure gave the best results for Fe rich phases, however,

Cr doped phases are likely to be hexagonal. The feasibility tests demonstrate that the characterisation of the Fe and Cr can be performed on 100 nm size phases allowing the analysis of these metal atoms environment in a Fe or Cr rich secondary phase precipitates. Further studies at the nanoscopic scale in systems with precipitates, dispersoids and vacancies clusters are foreseen coupling techniques such as XAFS as well as TEM/EELS. The later technique is more powerful from a spatial resolution point of view, however, more difficult to fully on fra.

Acknowledgements

This study has been performed in the frame of the Core Material Behaviour program at PSI. Swissnuclear is acknowledged for the partial funding of this program.

References

- [1] P. Rudling, G. Wikmark, *J. Nucl. Mater.* 265 (1999) 44–59.
- [2] B. Cox, *J. Nucl. Mater.* 170 (1990) 1–23.
- [3] D.O. Northwood, *Mater. Des.* 6 (1985) 58–70.
- [4] C. Rodríguez, D.A. Barbiric, M.E. Pepe, J.A. Kovacs, J.A. Alonso, R. Hojvat de Tendler, *Intermetallics* 10 (2002) 205–216.
- [5] D.O. Xianying Meng, *J. Nucl. Mater.* 168 (1989) 125–136.
- [6] P. Chemelle, D.B. Knorr, J.B. Van Der Sand, R.M. Pelloux, *J. Nucl. Mater.* 113 (1983) 58–64.
- [7] S. Shimada, Y. Etoh, K. Tomida, *J. Nucl. Mater.* 248 (1997) 275–280.
- [8] C. Toffolon-Masclat, J.-Ch. Brachet, G. Jago, *J. Nucl. Mater.* 305 (2002) 224–231.
- [9] S. Abolhassani, M. Dadras, M. Leboeuf, D. Gavillet, *J. Nucl. Mater.* 321 (2003) 70–77.
- [10] S. Abolhassani, D. Gavillet, F. Groeschel, P. Jourdain, H.U. Zwicky, *Proceedings of the International Topical Meeting on Light-Water-Reactor Fuel Performance*, IAEA, Park-City, Utah, April 10–13, 2000, p. 470.
- [11] H.J. Whitlow, Y. Zhang, Y. Wang, T. Winzell, N. Simic, E. Ahlberg, M. Limbäck, G. Wikmark, *Nucl. Instrum. Methods B* 161–163 (2000) 584–589.
- [12] Cl. Anghel, G. Hultquist, M. Limbäck, *J. Nucl. Mater.* 340 (2005) 271–283.
- [13] C. Degueldre, St. Conradson, A. Amato, E. Campitelli, *J. Nucl. Mater.* 352 (2006) 126–135.
- [14] Ch. Jacobsen, J. Kirz, S. Williams, *Ultramicroscopy* 47 (1992) 55–79.
- [15] Ch. Jacobsen, *Trends Cell Biol.* 9 (1999) 44–47.
- [16] X. Zhang, H. Ade, C. Jacobsen, J. Kirz, S. Lindaas, S. Williams, S. Wirick, *Nucl. Instrum. Methods B* 347 (1994) 431–435.
- [17] A.L. Ankudinov, B. Ravel, J.J. Rehr, S.D. Conradson, *Phys. Rev. B* 58 (1998) 7565–7576.
- [18] A.L. Ankudinov, J.J. Rehr, *Phys. Rev. B* 62 (2000) 2437–2445.
- [19] W. Brueckner, K. Kleinstueck, G.E.R. Schulze, *Phys. Status Solidi* 23 (1967) 475–480.
- [20] O. Canet, M. Latroche, F. Bouree-Vigneron, A. Percheron-Guegan, *J. Alloys Compd.* 210 (1994) 129–134.
- [21] E.E. Havinga, H. Damsma, P. Hokkeling, *J. Less Com. Met.* 27 (1927) 169–186.
- [22] P. Matkovic, T. Matkovic, I. Vickovic, *Metalurgija Croatia* 29 (1990) 3–6.
- [23] B. Ravel, M. Newville, *J. Synchrotron Rad.* 12 (2005) 537–541.

Study on the resonance Rayleigh scattering, second-order scattering and frequency doubling scattering spectra of the interactions of palladium(II)–ceftriaxone chelate with anionic surfactants and their analytical applications

Shenghui Fu, Zhongfang Liu, Shaopu Liu*, Aoer Yi

School of Chemistry and Chemical Engineering, Southwest University, Chongqing 400715, China

Received 24 July 2007; received in revised form 14 November 2007; accepted 16 November 2007

Available online 24 November 2007

Abstract

In pH 1.8–2.9 Britton–Robinson (BR) buffer medium, ceftriaxone (CTRX) can react with palladium(II) (Pd(II)) to form 1:2 cationic chelate, which can further react with anionic surfactants (AS) such as sodium lauryl sulfonate (SLS), sodium dodecyl sulfate (SDS) and sodium dodecylbenzene sulfonate (SDBS) to form 1:3 ion-association complexes. As a result, the resonance Rayleigh scattering (RRS), second-order scattering (SOS) and frequency doubling scattering (FDS) were enhanced greatly. The maximum RRS, SOS and FDS wavelengths of three ion-association complexes were located at 335 nm, 560 nm and 390 nm, respectively. The increments of scattering intensity (ΔI) were directly proportional to the concentrations of CTRX in certain ranges. The detection limits (3σ) of CTRX for SLS, SDBS and SDS systems were 1.8 ng ml^{-1} , 2.3 ng ml^{-1} and 2.3 ng ml^{-1} (RRS method), 4.9 ng ml^{-1} , 7.4 ng ml^{-1} and 4.7 ng ml^{-1} (SOS method) and 6.8 ng ml^{-1} , 7.3 ng ml^{-1} and 9.1 ng ml^{-1} (FDS method), separately. The sensitivity of RRS method was higher than those of SOS and FDS methods. The optimum conditions of RRS method and the influence factors were investigated, and the composition of ion-association complexes and the reaction mechanism were discussed also. The effects of foreign substances were tested and it showed that the method has a good selectivity. Based on the ion-association reaction, the sensitive, simple and rapid methods for the determination of CTRX have been developed.

© 2007 Elsevier B.V. All rights reserved.

Keywords: Resonance Rayleigh scattering; Second-order scattering; Frequency doubling scattering; Ceftriaxone; Palladium(II); Anionic surfactants

1. Introduction

Ceftriaxone (CTRX) is one of the long-efficient and broad-spectrum third generation cephalosporin antibiotics, which is widely used in the clinical at present. It has the strongest activity against gonorrhoeae and chlamydia trachomatis. The drug can penetrate quickly into tissue culter and fast distribute to inflammatory lesions after mainline. It possesses a half life of more than 8 h so that it belongs one of the longest half life cephalosporin. Clinically, it is often used to treat respiratory tract infection, skin tissue infection, urinary tract infection,

osteoarthritis infection and bacteroidal septicemia, and remarkable curative effects have been achieved. It has been used in the front line of treating gonorrhoea [1,2]. To the study of the pharmacokinetics and recommendation of suitable dosage, it is significant to quantitatively determine the drug both in the pharmaceutical preparations and in body fluids.

Presently, methods in the literatures reported for the determination of CTRX consist of HPLC [3], high-performance capillary electrophoresis [4], microbiology [5], chemiluminescence [6], etc. A very few literatures for the determination of CTRX by fluorimetry have been reported. It mainly bases on Tb(III) [7] reacting with CTRX. But its sensitivity is not high because its detection limit is $0.34 \mu\text{g ml}^{-1}$. Spectrophotometry is more popular because of its low cost, simple manipulation and high accuracy. The reaction of spectrophotometric method mainly based on the formation of chelates of CTRX with Pd(II)

* Corresponding author. Tel.: +86 23 68252748; fax: +86 23 68254000.
E-mail address: liusp@swu.edu.cn (S. Liu).

[8–10] and Fe(III) [11], which result in the change of absorption spectra. However, their sensitivities are not high enough to determine trace amount of CTRX. Therefore, it is still a worthwhile subject to develop more sensitive, simple and selective methods for the determination of trace CTRX.

Over these years, resonance Rayleigh scattering (RRS), second-order scattering (SOS) and frequency doubling scattering (FDS) have been paid more and more attention because of their high sensitivities and simplicities [12]. And these techniques have been applied to determine macromolecules such as inorganic ions [13–16], organic compounds [17,18], nucleic acids [19–21], proteins [22–24] and heparin [25,26], and some drugs [27–29].

It is known that in the weak acid medium, Pd(II) can react with CTRX in the presence of sodium lauryl sulfonate (SLS) to form a chelate. The color reaction was used to spectrophotometric determination of determine CTRX [30]. However, the completion of this reaction required keep heating for a long time (about 45 min) in the boiling water bath, and the sensitivity was not high and the molar absorptivity (ϵ) was $3.39 \times 10^4 \text{ l mol}^{-1} \text{ cm}^{-1}$. Our experiments found that in the pH 1.8–2.9 Britton–Robinson (BR) buffer medium, at room temperature, Pd(II) reacted with CTRX to form 1:2 cationic chelate $[\text{Pd}_2 \cdot \text{CTR X}]^{3+}$, which can result in a little enhancements of intensities of RRS, SOS and FDS. Then $[\text{Pd}_2 \cdot \text{CTR X}]^{3+}$ further reacted with anionic surfactants (AS) such as sodium lauryl sulfonate (SLS), sodium dodecyl sulfate (SDS) and sodium dodecylbenzene sulfonate (SDBS) to form 1:3 ternary ion-association complexes $[\text{Pd}_2 \cdot \text{CTR X}] (\text{AS})_3$. The intensities of RRS, SOS and FDS were all enhanced greatly. Three ion-association complexes have similar spectral characteristics and the maximum RRS, SOS and FDS wavelengths of three ion-association complexes were located at 335 nm, 560 nm and 390 nm, respectively. The increments of scattering intensity (ΔI) were directly proportional to the concentrations of CTRX in certain ranges. Under the same experiment conditions, other third generation cephalosporin antibiotics such as ceftazidime (CZD), cefoperazone (CPZ) and cefotaxime (CFTM) did not interfere the reactions. So, all three methods above can selectively determine CTRX. Their sensitivities are very high and the lowest detection limit (3σ) is 1.8 ng ml^{-1} . The sensitivities of three methods are not only higher by one to three order of magnitude than those of common spectrophotometric methods, but also higher than those of common HPLC [4], chemiluminescence [6] and fluorimetry [7]. So they are more suitable for the determination of trace CTRX. In this work, the effects of ternary ion-association complexes on RRS, SOS and FDS spectra were studied. Because the sensitivity of RRS method is higher than those of SOS and FDS, the optimum conditions of the reactions and influence factors were mainly investigated by RRS method. The effects of foreign substances were tested and it showed that the RRS method has a good selectivity. A sensitive, simple, selective and rapid method was developed for the determination of CTRX in the human serum and urine. In this paper, the mechanism for the ion-association reactions and the reasons of RRS enhancement were also discussed.

2. Experimental

2.1. Apparatus and reagents

A Hitachi F-2500 spectrofluorophotometer (Tokyo, Japan) was used to record the RRS, SOS and FDS spectra and to measure the scattering intensities. A UV-8500 spectrophotometer (Tianmei, Shanghai) was used to record the absorption spectra and measure absorbance intensity. A PHS-3C pH meter (Shanghai Dazhong Analytical Instrument Plant) was used to adjust pH.

CTR X standard solution was prepared by dissolving 0.0200 g CTR X (Hainan Hailing Pharmaceutical Co. Ltd.) in water, and diluting accurately with water to $200 \mu\text{g ml}^{-1}$ for stock solution. Then dilute to $50 \mu\text{g ml}^{-1}$ for working solution.

The concentration for working solution of Pd(II) ($100 \mu\text{g ml}^{-1}$) was prepared by dissolving 0.0420 g of PdCl_2 (Shanghai Reagent First Plant) in 5 ml of water, to which 0.5 ml of concentrated HCl had been added and warming the mixture in a water bath. The solution was cooled and diluted with water in a 250 ml calibrated flask.

Anionic surfactants solutions: SLS, SDS and SDBS (Shanghai Reagent First Plant) were $1.0 \times 10^{-3} \text{ mol l}^{-1}$, $1.0 \times 10^{-3} \text{ mol l}^{-1}$ and $1.0 \times 10^{-2} \text{ mol l}^{-1}$, respectively.

Britton–Robinson buffer solutions with different pH were prepared according to suitable proportion and adjusted pH values with a pH meter.

All reagents were analytical reagent grade and doubly distilled water was used.

2.2. General procedure

A 0.4 ml of AS solution was pipetted into a 10 ml calibrated flask followed by 0.5 ml of Pd(II) solution, suitable amount of CTR X solution and 1.0 ml of pH 1.8–2.9 BR buffer solution. Dilute the solution to the mark with water and shake thoroughly, then set aside for 5 min. The RRS intensity (I^{RRS}) of the systems were recorded with synchronous scanning at $\lambda_{\text{ex}} = \lambda_{\text{em}}$. The SOS intensity (I^{SOS}) and the FDS intensity (I^{FDS}) of the systems were recorded at $\lambda_{\text{em}} = 2\lambda_{\text{ex}}$ and $2\lambda_{\text{em}} = \lambda_{\text{ex}}$, respectively. The I^{SOS} and I^{FDS} were plotted versus the different wavelengths to get SOS and FDS spectra. Then, the scattering intensities (I^{RRS} , I^{SOS} and I^{FDS}) for the ion-association complexes, and I_0^{RRS} , I_0^{SOS} and I_0^{FDS} for the reagent blank at their own maximum were measured, $\Delta I^{\text{RRS}} = I^{\text{RRS}} - I_0^{\text{RRS}}$, $\Delta I^{\text{SOS}} = I^{\text{SOS}} - I_0^{\text{SOS}}$ and $\Delta I^{\text{FDS}} = I^{\text{FDS}} - I_0^{\text{FDS}}$.

3. Results and discussion

3.1. Spectral characteristics

3.1.1. RRS spectra

The RRS spectra of Pd(II)–CTR X–AS systems are shown in Fig. 1. From Fig. 1A, it can be seen that the RRS intensities of AS, Pd(II) and CTR X themselves are very weak. The binary chelate that Pd(II) and CTR X formed can only result in a little change of the RRS spectra. When the binary chelate further reacts with AS such as SLS, SDBS and SDS to form ternary com-

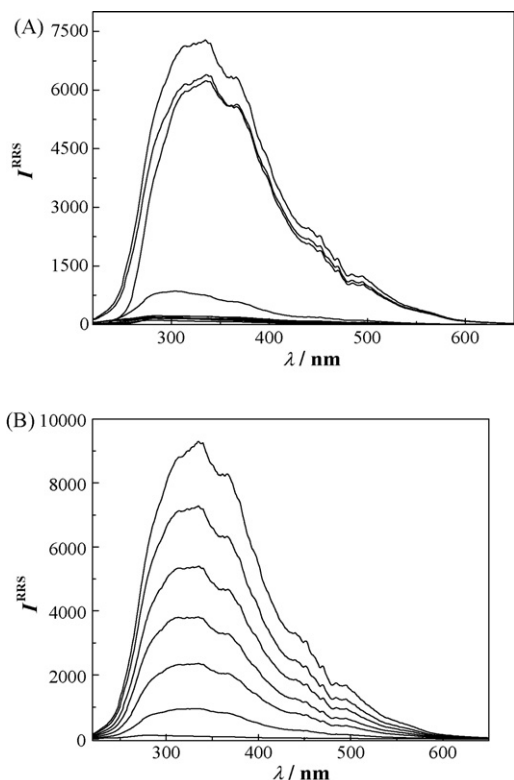


Fig. 1. RRS spectra of Pd(II)-CTR-X-AS systems. (A) Pd(II)-CTR-X-AS systems. From above to bottom: Pd(II)-CTR-X-SLS; Pd(II)-CTR-X-SDBS; Pd(II)-CTR-X-SDS; Pd(II)-CTR-X; Pd-SDBS; Pd(II)-SLS; Pd(II)-SDS; SDS; SLS; SDBS; CTR-X; Pd(II). The concentration of CTR-X: $2.5 \mu\text{g ml}^{-1}$; the concentration of Pd(II): $5.0 \mu\text{g ml}^{-1}$; the concentration of SLS and SDS: $4.0 \times 10^{-5} \text{ mol l}^{-1}$; the concentration of SDBS: $4.0 \times 10^{-4} \text{ mol l}^{-1}$. (B) Pd(II)-CTR-X-SLS system. From above to bottom: the concentration of CTR-X: 3.0, 2.5, 2.0, 1.5, 1.0, 0.5, 0 $\mu\text{g ml}^{-1}$; the concentration of Pd(II): $5.0 \mu\text{g ml}^{-1}$; the concentration of SLS: $4.0 \times 10^{-5} \text{ mol l}^{-1}$.

plexes, RRS intensities are enhanced greatly. The three reaction products have similar spectral characteristics as the maximum RRS peaks are all at 335 nm. The RRS intensity of the SLS system is the highest among the three systems, followed by the SDBS and SDS systems.

Fig. 1B shows that the enhancement of RRS intensity for the Pd(II)-CTR-X-SLS system is directly proportional to the concentration of CTR-X. So did the other two reaction systems. Hence, the RRS method can be applied to the determination of CTR-X.

3.1.2. SOS spectra

The SOS spectra of Pd(II)-CTR-X-AS systems are shown in Fig. 2. From Fig. 2A, it can be seen that the SOS intensities of AS, Pd(II) and CTR-X themselves are very weak. The binary chelate results a certain change of the SOS spectra. When the binary chelate further reacts with AS such as SLS, SDBS and SDS to form ternary complexes, SOS intensities are enhanced greatly. The three reaction products have similar spectral characteristics as the maximum SOS peaks are all at 560 nm. The scattering intensities (ΔI^{SOS}) of reaction products obey the order of SDS > SLS > SDBS.

Taking Pd(II)-CTR-X-SDS as an example, when the λ_{ex} is at 280 nm, the changes of SOS intensities with different concentration of CTR-X were investigated (Fig. 2B). It can be seen from Fig. 2B that the enhancement of SOS intensity is linear to an increased concentration of CTR-X. So did the other two reaction systems. Hence, the SOS method can be applied to determine CTR-X.

3.1.3. FDS spectra

The FDS spectra of Pd(II)-CTR-X-AS systems are shown in Fig. 3. From Fig. 3A, it can be seen that the FDS intensities of AS, Pd(II) and CTR-X themselves are very weak. The binary chelate results a little change of the FDS spectra. When the binary chelate reacts with AS such as SLS, SDBS and SDS to form ternary complexes, FDS intensities are enhanced greatly. The three reaction products have similar spectral characteristics as the maximum FDS peaks are all at 390 nm. The intensities of reaction products were different and their relative scattering intensities (ΔI^{FDS}) are in the order of SLS > SDBS > SDS.

Taking Pd(II)-CTR-X-SLS as an example, when the λ_{ex} is at 780 nm, the changes of FDS intensities with different concentration of CTR-X were investigated (Fig. 3B). It can be seen

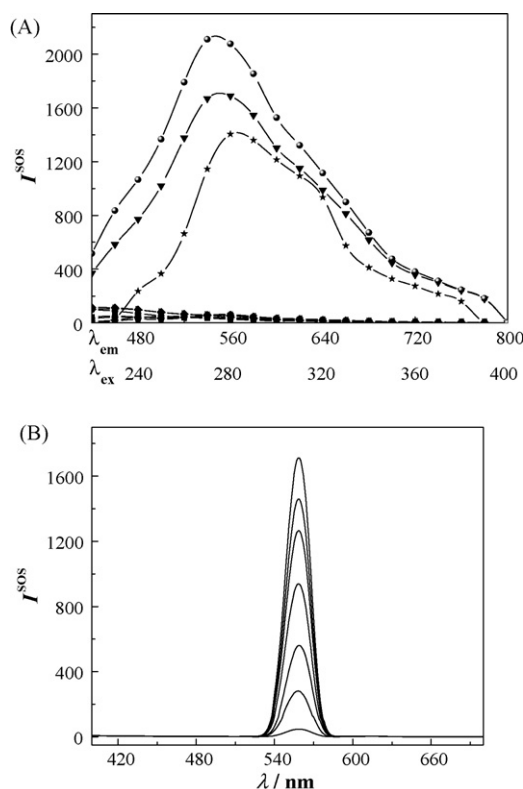


Fig. 2. SOS spectra of Pd(II)-CTR-X-AS systems. (A) Pd(II)-CTR-X-AS systems. From above to bottom: Pd(II)-CTR-X-SDS; Pd(II)-CTR-X-SLS; Pd(II)-CTR-X-SDBS; Pd-SDBS; Pd(II)-SLS; Pd(II)-SDS; SDS; SLS; SDBS; CTR-X; Pd(II). The concentration of CTR-X: $4.0 \mu\text{g ml}^{-1}$; the concentration of Pd(II): $5.0 \mu\text{g ml}^{-1}$; the concentration of SLS and SDS: $4.0 \times 10^{-5} \text{ mol l}^{-1}$; the concentration of SDBS: $4.0 \times 10^{-4} \text{ mol l}^{-1}$. (B) Pd(II)-CTR-X-SDS system ($\lambda_{\text{ex}} = 280 \text{ nm}$). From above to bottom: the concentration of CTR-X: 3.0, 2.5, 2.0, 1.5, 1.0, 0.5, 0 $\mu\text{g ml}^{-1}$; the concentration of Pd(II): $5.0 \mu\text{g ml}^{-1}$; the concentration of SDS: $2.0 \times 10^{-5} \text{ mol l}^{-1}$.

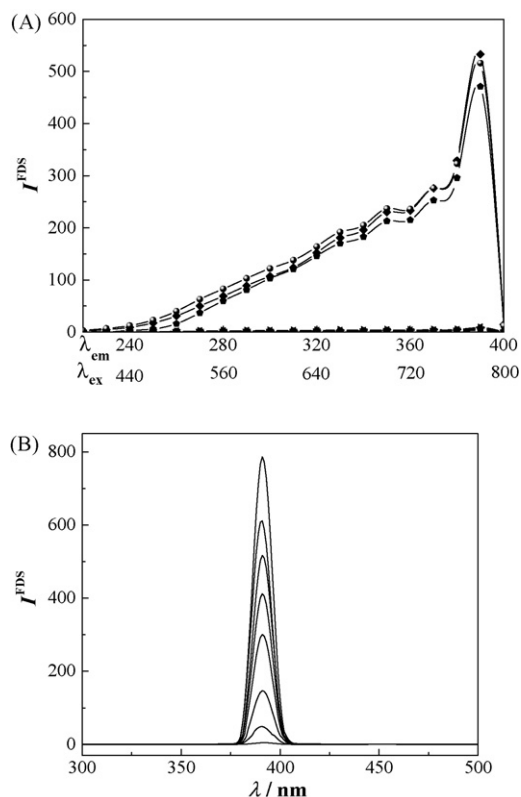


Fig. 3. FDS spectra of Pd(II)-CTRX-AS systems. (A) Pd(II)-CTRX-AS systems. From above to bottom: Pd(II)-CTRX-SLS; Pd(II)-CTRX-SDBS; Pd(II)-CTRX-SDS; Pd-SDBS; Pd(II)-SLS; Pd(II)-SDS; SDS; SLS; SDBS; CTRX; Pd(II). The concentration of CTRX: $4.0 \mu\text{g ml}^{-1}$; the concentration of Pd(II): $5.0 \mu\text{g ml}^{-1}$; the concentration of SLS and SDS: $4.0 \times 10^{-5} \text{ mol l}^{-1}$; the concentration of SDBS: $4.0 \times 10^{-4} \text{ mol l}^{-1}$. (B) Pd(II)-CTRX-SLS system ($\lambda_{\text{ex}} = 780 \text{ nm}$). From above to bottom: the concentration of CTRX: 6.5, 5.5, 4.5, 3.5, 2.5, 1.5, 0.5, $0 \mu\text{g ml}^{-1}$; the concentration of Pd(II): $5.0 \mu\text{g ml}^{-1}$; the concentration of SLS: $4.0 \times 10^{-5} \text{ mol l}^{-1}$.

from Fig. 3B that the enhancement of FDS intensity for system is linear to an increased concentration of CTRX. So did the other two reaction systems. Hence, the FDS method can be applied to the determination of CTRX.

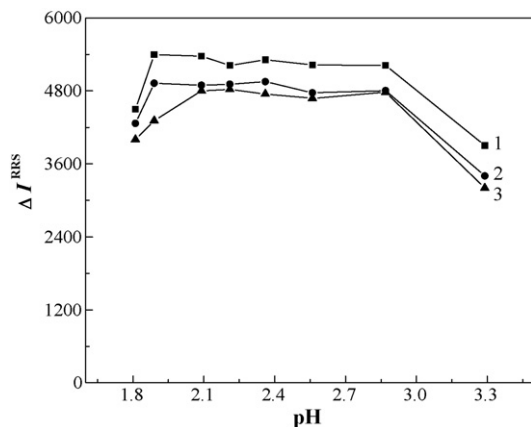


Fig. 4. Effects of acidity. (1) Pd(II)-CTRX-SLS; (2) Pd(II)-CTRX-SDBS; (3) Pd(II)-CTRX-SDS. The concentration of CTRX: $2.0 \mu\text{g ml}^{-1}$; the concentration of Pd(II): $5.0 \mu\text{g ml}^{-1}$; the concentration of SLS and SDS: $4.0 \times 10^{-5} \text{ mol l}^{-1}$; the concentration of SDBS: $4.0 \times 10^{-4} \text{ mol l}^{-1}$.

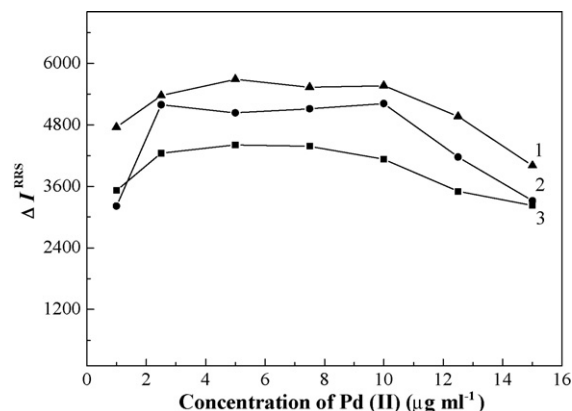


Fig. 5. Effect of the Pd(II) concentration. (1) Pd(II)-CTRX-SLS; (2) Pd(II)-CTRX-SDBS; (3) Pd(II)-CTRX-SDS. The concentration of CTRX: $2.0 \mu\text{g ml}^{-1}$; the concentration of SLS and SDS: $4.0 \times 10^{-5} \text{ mol l}^{-1}$; the concentration of SDBS: $4.0 \times 10^{-4} \text{ mol l}^{-1}$.

Because the sensitivity of RRS method is higher than those of SOS method and FDS method, the optimum conditions of the reactions, the effects of foreign substances were investigated taking RRS method as an example.

3.2. Optimum reactive conditions

3.2.1. Effects of acidity

The effects of different buffer solutions on RRS intensities of three reaction systems were tested with BR, HAc-NaAc and citrate sodium-HCl. The results showed that BR was better than other buffer solutions and the optimum pH ranges for the reaction were 1.8–2.9 for SLS system, 1.8–2.9 for SDBS system and 2.2–2.9 for SDS system, respectively (Fig. 4). So, pH 2.3 was chosen as reaction acidity for three systems and the appropriate amount was 1.0 ml.

3.2.2. Effect of the Pd(II) concentration

Fig. 5 shows the effect of the Pd(II) concentration on RRS intensities for three systems. From Fig. 5, it can be seen that RRS intensity reached the maximum and remained stable when the

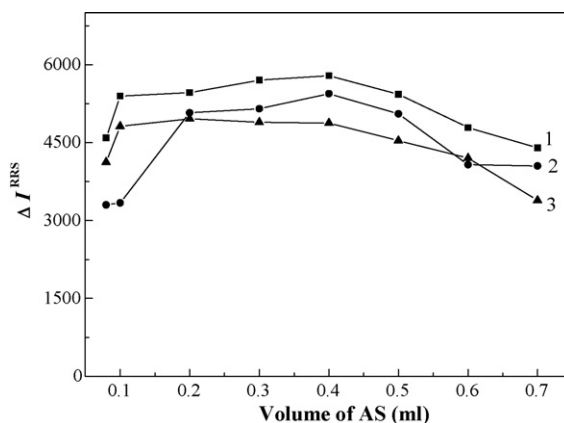
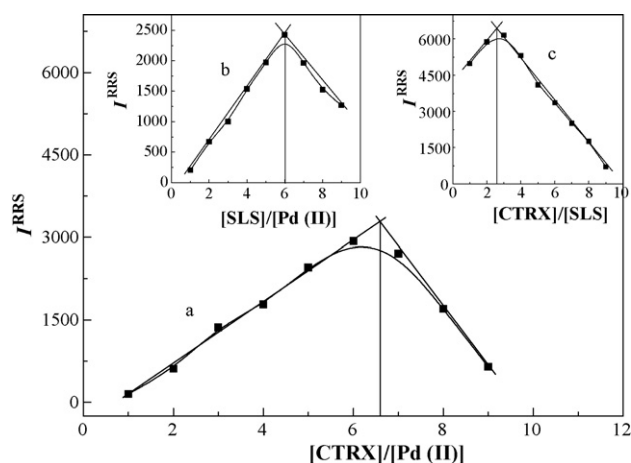


Fig. 6. Effects of the AS concentrations. (1) Pd(II)-CTRX-SLS; (2) Pd(II)-CTRX-SDBS; (3) Pd(II)-CTRX-SDS. The concentration of CTRX: $2.0 \mu\text{g ml}^{-1}$; the concentration of SLS and SDS: $4.0 \times 10^{-4} \text{ mol l}^{-1}$; the concentration of SDBS: $4.0 \times 10^{-3} \text{ mol l}^{-1}$.



Scheme 1. The composition ratio for ion-association complex of Pd(II)–CTRX–SLS system as established by Job's method of continuous variation: (a) SLS excess; (b) CTRX excess; (c) Pd(II) excess.

concentration of Pd(II) was from $2.5 \mu\text{g ml}^{-1}$ to $10 \mu\text{g ml}^{-1}$. So the experimental concentration was $5.0 \mu\text{g ml}^{-1}$ for Pd(II).

3.2.3. Effects of the AS concentrations

The influences of the concentrations of AS on the RRS intensity of Pd(II)–CTRX–AS systems were investigated. The results showed that the RRS intensity enhanced gradually with the increasing of AS concentration. When the concentrations of SLS, SDBS and SDS were $(1.0\text{--}5.0) \times 10^{-5} \text{ mol l}^{-1}$, $(2.0\text{--}5.0) \times 10^{-4} \text{ mol l}^{-1}$ and $(1.0\text{--}4.0) \times 10^{-5} \text{ mol l}^{-1}$, respectively, ΔI^{RRS} remained stable (Fig. 6). If AS is not adequate, the reactions would be incomplete. If AS is excessive, the intensities of RRS would decrease because of the formation of AS dimers by self-aggregation. So, $4.0 \times 10^{-5} \text{ mol l}^{-1}$, $4.0 \times 10^{-4} \text{ mol l}^{-1}$ and $2.0 \times 10^{-5} \text{ mol l}^{-1}$ were chosen as suitable SLS, SDBS and SDS concentrations, respectively.

3.2.4. Reaction speed and the stability of scattering intensity

At room temperature, the reaction completed in 5 min and RRS intensity can remain constant for 10 h at least.

3.2.5. Effect of ionic strength

The effect of ionic strength on the intensities of RRS for the three systems was investigated with NaCl. The result showed when the concentration of NaCl was lower than $2.0 \times 10^{-2} \text{ mol l}^{-1}$, ΔI^{RRS} kept constant, and with the increasing of the concentration of NaCl, ΔI^{RRS} decreased gradually. So, the ion-association reaction should be under a low ionic strength condition. The effect also indicated that the electrostatic interaction was a very important factor in this ion-association reaction.

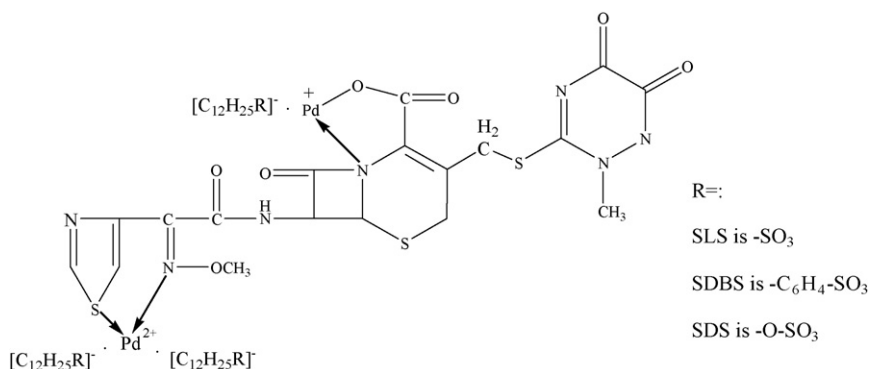
3.3. Sensitivity of method

Under optimum conditions, the different concentrations of CTRX reacted with Pd(II) and AS to form ternary complexes and the relative scattering intensities ΔI^{RRS} , ΔI^{SOS} and ΔI^{FDS} of the ternary complexes were measured at their maximum scattering wavelengths after 5 min, separately. The calibration graphs of ΔI^{RRS} , ΔI^{SOS} and ΔI^{FDS} against the concentrations of CTRX were constructed. The relevant parameters were listed in Table 1. From Table 1, it can be seen that the sensitivity of RRS method is higher than those of SOS and FDS methods though three methods all can be applied to determine CTRX. The detection limits (3σ) of CTRX by RRS method were 1.8 ng ml^{-1} for SLS system, 2.3 ng ml^{-1} for SDBS system and 2.3 ng ml^{-1} for SDS system, respectively. RRS method had much higher sensitivity than other common analytical methods (Table 2). The sensitivities of three methods were higher by one to three order of magnitude than those of common HPLC, capillary electrophoresis, chemiluminescence, spectrophotometry and fluorimetry. So they proved to be more suitable for the determination of trace amounts of CTRX.

3.4. Formation of ternary ion-association complex and its effect on the spectral characteristics

3.4.1. The ion-association reaction

We studied the ion-association reactions of CTRX with Pd(II) and AS. The composition ratio of the ternary complex for Pd(II)–CTRX–AS was 2:1:3 as established by using Job's method of continuous variation. Taking Pd(II)–CTRX–SLS as an example, the composition ratio for ion-association complex was shown in Scheme 1.



Scheme 2. The structure of $[\text{Pd}_2\text{-CTRX}](\text{AS})_3$.

Table 1
Analytical parameters for the determination of CTRX

Method	Analytical reagent	Linear range ($\mu\text{g ml}^{-1}$)	Regression equation C , ($\mu\text{g ml}^{-1}$)	Correlation coefficient (r)	Detection limit 3σ , (ng ml^{-1})
RRS	Pd(II)–SLS	0.0058–3.0	$\Delta I = -1076.9 + 3320.3C$	0.9971	1.8
	Pd(II)–SDBS	0.0076–2.5	$\Delta I = -247.0 + 2552.2C$	0.9997	2.3
	Pd(II)–SDS	0.0078–2.8	$\Delta I = -72.2 + 2498.9C$	0.9985	2.3
SOS	Pd(II)–SLS	0.016–4.5	$\Delta I = -37 + 560.7C$	0.9981	4.9
	Pd(II)–SDBS	0.025–5.5	$\Delta I = 2.8 + 367.4C$	0.9974	7.4
	Pd(II)–SDS	0.016–3.0	$\Delta I = -29.4 + 581.3C$	0.9952	4.7
FDS	Pd(II)–SLS	0.023–6.5	$\Delta I = -20.7 + 120.0C$	0.9972	6.8
	Pd(II)–SDBS	0.024–6.5	$\Delta I = -43.6 + 110.3C$	0.9985	7.3
	Pd(II)–SDS	0.030–2.0	$\Delta I = -18.3 + 88.7C$	0.9984	9.1

Therefore, the composition of ternary ion-association complex is $[\text{Pd}_2 \cdot \text{CTRX}](\text{AS})_3$. The structure of the complex and the reaction mechanism were shown as follows.

Pd(II) can react with CTRX to form 2:1 cationic chelate $[\text{Pd}_2 \cdot \text{CTRX}]^{3+}$. In the molecular structure of CTRX, there are several function groups which contain certain oxygen, nitrogen and sulfur as the coordinate atoms that can react with Pd(II) to form Pd(II)–CTRX chelate by virtue of coordinate bonds. Generally, the binding sites between CTRX and metal ion was supposed at sulfur atoms of the thiazole ring and nitrogen atoms on the β -lactam [24,35]. Therefore, CTRX reacts with Pd(II) to form chelate cation $[\text{Pd}_2 \cdot \text{CTRX}]^{3+}$.

AS such as SLS, SDBS and SDS, in a weak acidic medium and when their concentration are very low, exist as the mono-valent anions SLS^- , SDBS^- and SDS^- , respectively. They can react with $[\text{Pd}_2 \cdot \text{CTRX}]^{3+}$ to form ternary ion-association complexes through electrostatic attraction and hydrophobic forces:



The structure of $[\text{Pd}_2 \cdot \text{CTRX}](\text{AS})_3$ is as shown in Scheme 2.

Table 2
Comparison of sensitivities of RRS with other methods for the determination of CTRX

Method	Analytical reagent	Medium condition	Determination wavelength (nm)	Detection limits ($\mu\text{g ml}^{-1}$)	Literature
HPLC			270	0.019	[3]
LC		pH 7.0	280	0.02	[31]
HPCZE		pH 9.1	270	0.42	[4]
CZE		pH 7.0	254	5.21	[32]
CL	Ce(IV)–Rh 6G	$0.2 \text{ mol l}^{-1} \text{ H}_2\text{SO}_4$	560	0.039	[6]
OP		pH 4.5	–300 to 1300 mV	0.23	[33]
FL	Tb(III)	pH 8.0	$\lambda_{\text{em}} = 270$ $\lambda_{\text{em}} = 548$	0.34	[7]
SP	Fe(III)–1.10- <i>o</i> -phenanthroline	pH 4.2	510	80	[9]
	KIO ₃ and crystal violet	pH 4.0–4.2	588	0.08	[10]
	Metol-chromium(VI)	pH 2.9	520	0.05	[34]
RRS	Pd(II)–SLS	pH 1.8–2.9	335	0.0018	This work
	Pd(II)–SDBS	pH 1.8–2.9	335	0.0023	This work
	Pd(II)–SDS	pH 2.2–2.9	335	0.0023	This work

SP: spectrophotometry; FL: fluorimetry; CZE: capillary zone electrophoresis; CL: chemiluminescence; OP: oscillopolarography.

3.4.2. Effect on RRS spectra

It can be seen from 3.1 that the formation of the ion-association complexes can result in great enhancement of RRS, SOS and FDS. But the sensitivity of RRS method is higher than those of SOS and FDS methods. Therefore, RRS method is more suitable for the determination of trace amounts of CTRX.

The possible reasons for RRS enhancement included as follows:

- *Resonance enhanced Rayleigh scattering effect.* When the wavelength of Rayleigh scattering is located or is close to the molecular absorption band, the scattering can absorb the light energy and to produce a re-scattering process by resonance. As the result, the scattering intensity is greatly enhancement [36,37].
- *Enhancement of hydrophobicity.* Pd(II), $[\text{Pd}_2 \cdot \text{CTRX}]^{3+}$ and AS^- all have hydrophilicity and can easily dissolved in aqueous solution so that they cannot form an interface with water. When $[\text{Pd}_2 \cdot \text{CTRX}]^{3+}$ reacts with AS^- to form the neutral ion-association complexes $[\text{Pd}_2 \cdot \text{CTRX}](\text{AS})_3$, a hydrophobic liquid–solid interface appears owing to the presence of the hydrophobic aryl framework of the ternary complex. The formation of the hydrophobic interface is helpful to the enhancement of RRS signal [38].

Table 3
Results for the determination of CTRX in serum and urine samples

Sample	Found ($\mu\text{g ml}^{-1}$)	Added ($\mu\text{g ml}^{-1}$)	R.S.D. (%)	Recovery (%)
Serum no. 1	ND	0.50	2.3	97.2
Serum no. 2	ND	1.00	2.1	100.6
Serum no. 3	ND	1.50	0.98	100.5
Urine no. 1	ND	0.50	3.8	96.8
Urine no. 2	ND	1.00	2.7	99.2
Urine no. 3	ND	1.50	1.8	101.3

ND: not detected.

- *Enlargement of molecular volume.* It is known that when there is no change on other parameters the bigger of molecular volume, the higher of the RRS intensity. If molecular volume is not easy to calculate, it can be substituted by molecular weight, i.e. $I = KCMl_0$ [39]. When the binary chelate $[\text{Pd}_2\cdot\text{CTR}X]^{3+}$ reacts with AS^- such as SLS^- , SDBS^- and SDS^- to form the ternary complex $[\text{Pd}_2\cdot\text{CTR}X](\text{AS})_3$, the molecular weights increase from 851.4 to 1647.5, 1830.8 and 1599.5, respectively. The increase of the molecular volume (or weight) is a significant factor to the enhancement of RRS intensity.

Affected by all above factors, the RRS intensities of the productions enhanced notably.

3.5. Selectivity of RRS method and its analytical application

3.5.1. Effects of foreign substances

Under optimum conditions, we investigated the effects of some foreign substances on the determination of CTRX. The results show that when the relative error is about $\pm 5\%$, 20–100 times of common metal ions such as $\text{Mg}(\text{II})$, $\text{Ba}(\text{II})$, $\text{Zn}(\text{II})$, $\text{Fe}(\text{III})$ and $\text{Al}(\text{III})$, 36–96 times of general nonmetal ions such as NO_3^- , SO_4^{2-} and Cl^- , 300–1200 times of some saccharides such as glucose, sucrose, lactose and carbamide, 33–100 times of some amino acids such as L-histidine, glycine, L-tryptophan, L-isoleucine and threonine, 2–5 times of HSA and CtDNA, 1–3 times of other third generation cephalosporin antibiotics such as CZD, CPZ and CFTM do not interfere with the determination of CTRX. So, the RRS method has a good selectivity.

3.5.2. Analytical application

Determination of CTRX in serum: a 2.0-ml aliquot of fresh serum sample (healthy human) and 3.0 ml trichloroacetic acid were mixed thoroughly and centrifuged at 4500 rpm for 10 min. A 1.0-ml aliquot of the supernatant fluid was diluted to 20.0 ml and 1.0 ml of this solution was pipetted into a 10.0-ml volumetric flask for determination of CTRX concentration according to the general procedure. The relative standard deviation (R.S.D.) and recovery were examined by using the standard addition method. The results are shown in Table 3.

Determination of CTRX in urine: a 1.0 aliquot of fresh urine sample (healthy human) was filtrated and pipetted into a 10.0-ml volumetric flask for determination of CTRX accord-

ing to the general procedure. R.S.D. and recovery were tested by using the standard addition method. The results are listed in Table 3.

It can be seen from Table 3 that the RRS method has a good repeatability. The R.S.D. of human serum sample is between 0.98% and 2.3%, and the R.S.D. of the human urine sample is between 1.8% and 3.8%. The recovery of human serum is from 97.2% to 100.6% and the recovery of human urine is from 96.8% to 101.3%. Therefore, the method can be used for the determination of CTRX in serum and urine sample.

4. Conclusions

This paper shows three methods for the determination of the antibiotic CTRX. It is demonstrated that under the above mentioned conditions, CTRX reacts with $\text{Pd}(\text{II})$ and AS such as SLS, SDBS and SDS to form ternary ion-association complexes. As a result, the RRS, SOS and FDS intensities of complexes enhance remarkably. The increments (ΔI) are directly proportional to the concentrations of CTRX in certain ranges. Therefore, we have developed sensitive, rapid and simple methods for the determination of CTRX by RRS, SOS and FDS techniques. The proposed methods were successfully applied to the determination of trace amounts of CTRX in serum and urine samples.

Acknowledgements

This research was supported by the National Natural Science Foundation of China (No. 20475045) and all authors here express their deep thanks.

References

- [1] L.M. Qiu, Chin. Contemp. Med. Sci. 4 (2006) 107–108.
- [2] X.Q. Chen, Y.Y. Jin, G. Tang (Eds.), A New Material Medica, People's Health Press, Beijing, 2003, p. 57.
- [3] S. Eric-Jovanovic, D. Agbaba, D. Zivanov-Stakic, S. Vladimirov, J. Pharm. Biomed. Anal. 18 (1998) 893–898.
- [4] A. Melinda, G. Attila, K. Almos, J. Chromatogr. B 846 (2007) 355–358.
- [5] X.Q. Xiang, Q.N. Wang, Y.H. Liu, Chin. J. Antibiot. 12 (1987) 162–166.
- [6] J.D. Yang, Y.M. Huang, S.P. Liu, Chin. J. Pharm. Anal. 5 (2002) 352–357.
- [7] L.I. Bebawy a, K.E. Kelani b, L.A. Fattah, J. Pharm. Biomed. Anal. 32 (2003) 1219–1225.
- [8] A.F.M. El-Walily, A.A. Gazy, S.F. Belal, E.F. Khamis, J. Pharm. Biomed. Anal. 22 (2000) 385–392.
- [9] I.F. Al-Momani, J. Pharm. Biomed. Anal. 25 (2001) 751–757.
- [10] B. Franciszek, S.S. Barbara, Chem. Anal. 48 (2003) 145–149.
- [11] Z.Y. Zhang, Q. Ma, J. TaiYuan Univ. Technol. 36 (2005) 486–487.
- [12] E.K. Wang (Ed.), Advance in Analytical Chemistry, Science Press of China, Beijing, 2002, 280–288.
- [13] S.P. Liu, Q. Liu, Z.F. Liu, M. Li, C.Z. Huang, Anal. Chim. Acta 379 (1999) 53–61.
- [14] S.P. Liu, Z.F. Liu, H.Q. Luo, Anal. Chim. Acta 407 (2000) 255–260.
- [15] Z.L. Jiang, Q.Y. Liu, S.P. Liu, Talanta 58 (2002) 635–640.
- [16] M. Oshime, N. Goto, J.P. Susanto, S. Motorizo, Analyst 121 (1996) 1085–1088.
- [17] S.P. Liu, G.M. Zhou, Z.F. Liu, Fresenius J. Anal. Chim. 363 (1999) 651–654.
- [18] S.P. Liu, S. Chen, X.L. Hu, T.S. Li, Anal. Chim. Acta 535 (2005) 169–175.
- [19] R.F. Pasternach, C. Bustamante, P.J. Colling, A. Giannetto, E. Gibb, J. Am. Chem. Soc. 115 (1993) 5393–5399.

- [20] C.Z. Huang, K.A. Li, S.Y. Tong, *Anal. Chem.* 69 (1997) 514–520.
- [21] S.P. Liu, X.L. Hu, L. Fan, H.Q. Luo, *Sci. Chin. B: Chem.* 32 (2002) 18–25.
- [22] C.Q. Ma, K.A. Li, S.Y. Tong, *Anal. Biochem.* 239 (1996) 86–91.
- [23] S.P. Liu, Q. Liu, *Anal. Sci.* 17 (2001) 239–242.
- [24] X.F. Long, S.P. Liu, L. Kong, Z.F. Liu, S.P. Bi, *Talanta* 63 (2004) 279–286.
- [25] S.P. Liu, H.Q. Luo, N.B. Li, Z.F. Liu, *Anal. Chem.* 26 (2001) 3907–3914.
- [26] H.Q. Luo, S.P. Liu, Z.F. Liu, Q. Liu, N.B. Li, *Anal. Chim. Acta* 449 (2001) 267–270.
- [27] S.P. Liu, Z.Y. Zhang, H.Q. Luo, L. Kong, *Anal. Sci.* 18 (2002) 971–978.
- [28] X.L. Hu, S.P. Liu, N.B. Li, *Anal. Bioanal. Chem.* 376 (2003) 42–48.
- [29] S.P. Liu, P. Feng, *Mikrochim. Acta* 140 (2002) 189–193.
- [30] A.F.M. El Walily, A.A. Gazy, S.F. Belal, E.F. Khamis, *J. Pharm. Biomed. Anal.* 20 (1999) 643–653.
- [31] T.H. Tsai, F.C. Cheng, L.C. Hung, C.F. Chen, *Int. J. Pharm.* 193 (1999) 21–26.
- [32] L. Tu, C.Q. Hu, *Chin. J. Pharm. Anal.* 25 (2005) 303–307.
- [33] Z.Z. Shi, F.L. Wang, J.Z. Wang, *Phys. Testing Chem. Anal. B: Chem. Anal.* 42 (2006) 329–331.
- [34] A.S. Amina, G.H. Ragabb, *Spectrochim. Acta A* 60 (2004) 2831–2835.
- [35] N. Abo El-Maali, A.H. Osman, A.A.M. Aly, G.A.A. Al-Hazmi, *Bioelectrochem.* 65 (2005) 95–104.
- [36] J. Anglister, I.Z. Steinberg, *J. Chem. Phys.* 78 (1983) 5358–5368.
- [37] S.G. Stanton, *J. Chem. Phys.* 75 (1979) 5615–5626.
- [38] S.P. Liu, L. Kong, *Anal. Sci.* 19 (2003) 1055–1060.
- [39] Edition of Editorial Board of Chinese Macropaedia. *Chinese Macropaedia Biology (II)*, Chinese Macropaedia Press, Beijing, 1991, pp. 1374.

Determination of Pd, Pt and Rh in vehicles escape fumes by GF-AAS and ICP-OES

Antonio Goncalves, José R. Domínguez, José Alvarado*

*Laboratorio de Espectroscopía Atómica, Departamento de Química,
Universidad Simón Bolívar, Caracas 1080A, Venezuela*

Received 28 August 2007; received in revised form 14 November 2007; accepted 15 November 2007
Available online 7 January 2008

Abstract

Automotive exhaust gases from vehicles using catalytic converters were filtered through cellulose filter papers to collect suspended particles expelled along with the engine's escape fumes. A specially designed sample collector was used for supporting the filter papers during collection. The collector was manufactured from a new car's exhaust pipe. A cellulose circular paper filter, 11 cm diameter, was attached to one end of the pipe and kept centered by pressing it against the borders of the pipe by means of a perforated aluminum cap, slightly wider than the pipe, used to cover this end of the collector. Filter papers loaded with the solid particles were acid-digested using a modified domestic microwave oven to bring the solid material into solution. The resulting solutions were analyzed for Pt by graphite furnace atomic absorption spectrometry (GF-AAS) and for Pd and Rh by inductively coupled plasma (ICP-OES). Results indicate that concentration of these analytes in the particulate is higher for new vehicles, having new catalytic converters, than for old ones. Maximum Pd, Pt and Rh in the samples analyzed were found to be 5.36, 12.60 and 1.03 $\mu\text{g g}^{-1}$, respectively.

© 2007 Elsevier B.V. All rights reserved.

Keywords: Pd; Pt and Rh; GF-AAS; ICP-OES; Catalytic converters; Exhaust fumes

1. Introduction

In Venezuela, the use of unleaded gasoline was gradually adopted starting in 1997. Due to the existence of a considerable number of old cars being still in use in our larger cities, it was not until the year 2005 that leaded gasoline was totally eliminated from the market [1]. Adoption of unleaded gasoline for powering motor vehicles brought along the use of catalytic converters to reduce environmental contamination due to lead emission. Catalytic converters essentially consist of an inoxidable steel case which contains a high surface area body, usually of the honeycomb type, covered by aluminum oxide which supports layers of Pd, Pt and Rh. Catalytic converters help to transform nitrogen oxides into nitrogen and oxygen, NO_x , $\text{NO}_2 = \text{N}_2 + \text{O}_2$, in reactions catalyzed by Pt and Rh. Additionally, carbon monoxide and unburnt hydrocarbons are converted into carbon dioxide and water, CO , $\text{C}_x\text{H}_y = \text{CO}_2 + \text{H}_2\text{O}$, in reactions catalyzed by

Pt and Pd [2]. However, in spite of the benefit of their use, catalytic converters have been shown to expel Pd, Pt and Rh, as a very fine particulate, along with the car's exhaust fumes. Abrasion of the metals deposited on the catalytic substrate, produced by the hot gases coming from the car's engine, has been advocated as the main reason for expulsion of the metals [2]. To assess the extent of contamination due to the presence of Pd, Pt and Rh in the escape fumes of motor vehicles different approaches have been implemented. The analysis of samples such as air, soil dust, vegetation and even Greenland fresh snow and ancient ice, as well as a wide variety of analytical techniques and sample treatments have been proposed [3–7]. Zereini et al. [3] analyzed airborne particulate matter from urban and non-urban areas of two cities in Germany by total reflection X-ray fluorescence after high pressure asher digestion. A comparison between microwave-assisted digestion methods for the determination of Pd, Pt and Rh in dust samples by ICP-MS was reported by Niemela et al. [4]. Grass samples from U.S. roadsides were analyzed by ICP-MS to determine PGEs by Ely et al. [5] after conventional acid digestion. Barbante et al. [6] found Pd, Pt, and Rh in Greenland fresh snow and ancient ice using the

* Corresponding author. Fax: +58 212906 3981.
E-mail address: jalvar@usb.ve (J. Alvarado).

ultrasensitive inductively coupled plasma sector field mass spectrometry technique. Determination of the anthropogenic impact of PGE in soils along Austrian motorways was performed by Fristch and Meisel using isotope dilution ICP-MS coupled with chromatography [7]. Moldovan et al. [8,9] found Pd and Pt in particulate collected from automotive exhaust fumes and subsequently dissolved by acid digestion. Rh was not detectable. Sample collection in Moldovan's work was accomplished using a home made device which was directly attached to the car's exhaust pipe. The collector was connected to two vessels containing absorbent solutions able to retain the PGE released by the catalyst converter. After sampling, the absorbent solutions were filtered through a cellulose ester filter to obtain the soluble fraction of the PGE and to separate it from the insoluble particulate remaining in the filter, which was one of the main purposes of the work. Results showed that most of the Pd and Pt were found in the insoluble particulate. Since Pd, Pt and Rh and their halogenated compounds could be potent allergenic species [10] the determination of these metals in the emission fumes of combustion engines could provide information about the role catalytic converters could play as possible sources of environmental contamination. Taking into account that the vast majority of metals is found in the insoluble particulate coming out with the escape fumes of the motor vehicles, according to the work of Moldovan, we produced a simple, efficient and ease to implement collector device for retention of solid particulate expelled with the escape gases of motor vehicles. Since discrimination between soluble and insoluble particulates was not intended, the collection device did not require any absorbent solutions or filtration for separation of both types of particulate, making it much simpler than Moldovan's collecting system. The purpose of the present work is to describe this device, its direct application to car's exhaust pipes for particulate collection and the determination of Pd, Pt and Rh by GF-AAS and ICP-OES in the samples collected.

2. Experimental

2.1. Reagents

All reagents used were of analytical grade. Working solutions were prepared by appropriate dilution of Merck Titrisol® 1000 mg l⁻¹ standard solutions of the corresponding analyte using distilled-deionized, 18 M mhos resistivity, water from a Milli-Q-Water Purification System. Pro analysis quality hydrochloric acid (37%, v/v) nitric acid (65%, v/v) and sulphuric acid (95–97%, v/v) were from Riedel de Haën.

2.2. Instrumentation

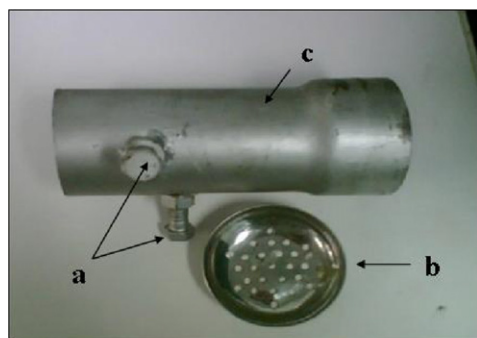
A sequential GBC Integra XL 100 model inductively coupled plasma emission spectrometer was used for Pd and Rh atomic emission measurements.

A PerkinElmer 5100 ZL model graphite furnace atomic absorption spectrometer with Zeeman effect background correction, a PerkinElmer Intensitron Pt hollow cathode lamp and a PerkinElmer AS-71 model autosampler were used for Pt peak height atomic absorption measurements.

2.3. Sampling

Twenty vehicles, all having three-way honeycomb type catalytic converters, were selected for this study. No attention was paid to car's brand, model or year of manufacture. Selection was based on odometer's readings including cars which had traveled distances between 19,997 and 148,245 Km.

Exhaust fumes were filtered through a Whatman No. 5 qualitative, 11 cm diameter, 0.06% (w/w) ash, cellulose paper filter, recommended for retention of fine particles held in a specially designed holder, as shown in Fig. 1. The holder consisted of a piece of a new exhaust pipe which was molded to accommodate



Sample collector assembly:

- a Fastening bolts
- b Perforated aluminum cap used to support the filter paper
- c Sample collector body



Sample collector coupled to motor vehicle's exhaust pipe

Fig. 1. Sample collector.

a slightly wider perforated metallic cap on one of its ends. A circular piece of paper filter, of a bigger diameter than the pipe, was kept in position by centering it in front of the molded end of the pipe and pressing the metallic cap to cover this end of the pipe. The whole assembly was then directly coupled to the car's exhaust pipe by means of the fastening bolts provided to this purpose (Fig. 1). For sampling engines were switched on with the car's gear stick in the Park position and allowed to run on idle. Visual inspection of the filters, as discussed later, showed that a 10-min collection period was enough to collect sufficient particulate for determination of the analytes of interest. The collector was robust enough to stand the high temperatures of the escape gases. Although changes in the exit speed of the exhaust fumes were somehow controlled by keeping the car's engine running on idle with the gear stick in the Park position, any increase in pressure due to changes in the amount of gases leaving the engine was not a cause of concern due to the fact that the aluminum cap used to keep the filters in position was perforated. Perforations in the cap allowed the filtered gases to go through with minimal restriction. The simplicity, ease of construction and ease of application of the collector means that several collectors could be used at the same time to collect several particulate samples at once.

2.4. Procedure

2.4.1. Sample collection

After fixing the sample holders to the automobile's exhaust pipes their engines were started to initiate filtration of the fumes with the gear stick in the Park position and the cars running on idle. The first experiments were used to optimize collection time as discussed in the corresponding section of the paper. At the end of the collection period the engine was turned off, the holder was allowed to cool down and the filter was dislodged from the holder by means of tweezers for sample treatment. This procedure was repeated three times for each car for a total of 60 samples collected.

2.4.2. Sample treatment

Paper filters loaded with samples were carefully folded to minimize sample losses during their introduction in the glass digestion tubes used for microwave-assisted acid dissolution. Twenty milliliters of aqua-regia were added to each tube and batches of four tubes were irradiated for 10 min at 50% maximum microwave power (700 W) as discussed later. After this time, digestion vessels were cooled down placing an electrical circular fan in front of the microwave's open door to speed up the cooling process. Solutions were then filtered through Whatman No. 5 paper filters, to eliminate undissolved carbon particles, taken to volume with distilled-deionized water in 100 ml flasks and kept refrigerated at approximately 4 °C until analysis.

2.4.3. Instrumental conditions

Tables 1 and 2 show the operating conditions used for quantification of Pd, and Rh by ICP-OES and Pt by GF-AAS, respectively.

Table 1
Instrumental conditions for ICP-OES determination of Pd and Rh

Parameter	Pd	Rh
Power (W)	1304	1304
Generator frequency (MHz)	40.06	40.06
Plasma gas flow rate (l min ⁻¹)	13	13
Auxiliary gas flow rate (l min ⁻¹)	0.6	0.6
Carrier gas flow rate (l min ⁻¹)	0.6	0.6
Observation height above coil (mm)	12	12
Slit width (mm)	0.1	0.1
Integration time (s)	0.24	0.40
Wavelength (nm)	Pd (I) 340.458	Rh (I) 343.489

3. Results and discussion

3.1. Collection time

Collection time was limited by two factors: mass of solid retained in the filter and temperature reached by the sample collector. We tried collection periods of 5, 10, 15, 20 and 25 min. Visual inspection of the paper filters after each collection time period showed that 5-min collection was insufficient. Although some spots of solid material could be easily seen on the surface of the paper there were many empty spaces, thus indicating the filter could retain some more solid material. Ten minutes collection time was enough to practically cover the whole surface of the paper with an apparently uniform layer of solid material. Subtraction of the weight of the clean paper filter from the paper plus sample after 10-min collection, rendered the amount of sample collected. Mass of sample collected was in the range 180–200 mg, which means that sample collection was reproducible within ± 20 mg. Longer collection times resulted in a series of lumps of solid material on the surface of the filter along with the presence of empty spaces probably due to dislodging of previously retained particles. Distribution of the solid on the filter looked totally uneven and mass of sample collected was highly variable. Additionally, at collection times longer than 15, 20 or 25 min, filters were partially burnt, mainly at the edges, which made it difficult to take them out from the holder in one piece for weighing. According to these findings collection time was set at 10 min.

Table 2
Instrumental conditions for GF-AAS determination of Pt

Step	Temperature (°C)	Ramp (s)	Hold (s)	Argon flow (ml min ⁻¹)
Drying 1	110	1	20	250
Drying 2	130	5	30	250
Ashing	1300	10	20	250
Atomization	2200	0	5	0
Cleaning	2400	1	5	250

Injection volume 10 μ l, wavelength 265.9 nm, slit width 0.7 nm, Zeeman effect background correction.

3.2. Sample treatment

Filters were carefully taken apart from the holder by means of tweezers, weighed and folded to allow their introduction into 150 ml glass digestion flasks for microwave-assisted acid dissolution. Microwave-assisted digestion was performed using a domestic microwave oven modified to digest four samples at a time in 150 ml glass digestion tubes. The bottom ends of the tubes containing the solid samples and the filters plus 20 ml of added sulphuric acid, nitric acid or aqua-regia, were placed right in front of the microwave radiation window of the oven cavity. Since the tubes were open their upper ends were water-cooled to avoid losses of volatile analytes or reagents. Under these conditions digestions were carried out at ambient pressure, as described in Ref. [11]. Sulphuric acid due to its comparatively stronger oxidizing power was the first choice for digestion of the filter papers and the solid samples. Twenty millilitres of 20% (v/v) aqueous solutions of the acid were added to each flask and microwave-assisted digestion was initiated at low, 30% irradiation power for 10 min. Samples thus treated developed substantial amounts of carbonaceous residues which did not disappear neither by addition of more acid nor by increasing time or irradiation power. Hence sulphuric acid was not longer considered for sample digestion. Nitric acid and aqua-regia were then assayed under variable conditions of microwave irradiation power and time. Twenty millilitres of 20% (v/v) aqueous solutions of nitric acid or aqua-regia were added to each flask. Results showed that 10 min irradiation time at 50% of the maximum oven power (700 W) was sufficient for dissolution of samples attacked with either reagent although some scattered, suspended carbon particles remained after treatment no matter how high the irradiation power or how large the heating time. Since aqua-regia-treated samples were clearer and presented lesser carbon particles than the nitric acid-treated ones, aqua-regia was selected as the reagent for dissolution of the samples under study. After cooling, samples were filtered to get rid off the carbon particles taken to volume in 100 ml volumetric flasks with distilled-deionized water and kept at 4 °C until analysis.

3.3. Atomic emission measurements

Concentrations of Pd and Rh in the samples studied were determined by ICP-OES under the instrumental conditions shown in Table 1. Standard aqueous solutions containing 100, 200, 600, 800, 1200 and 1800 $\mu\text{g l}^{-1}$ of both analytes were used to obtain working curves. Correlation coefficients and linear equations obtained were $R^2 = 0.9989$, $y = 2.2028x + 30637$ for Pd and $R^2 = 0.9976$, $y = 4.2512x + 29369$ for Rh. Determination of detection limits (3 s) after ten replicate measurements of an aqueous 100 $\mu\text{g l}^{-1}$ standard solution of both analytes resulted in 3.4 and 5.9 $\mu\text{g l}^{-1}$ for Pd and Rh, respectively. Corresponding literature values are 4.0 and 7.0 $\mu\text{g l}^{-1}$ [12].

3.4. Atomic absorption measurements

Although the original idea was to measure the concentrations of the three elements Pd, Pt and Rh by ICP-OES, the plasma

Table 3

Average ($n=3$) Pd, Pt and Rh concentrations, $\mu\text{g g}^{-1}$, and relative standard deviations (% R.S.D.) determined in solid particulate collected by filtration of vehicle escape fumes

Vehicle number	Odometer reading (Km)	Pd	Pt	Rh
1	19,997	5.36 (1.59)	12.60 (0.27)	1.03 (0.97)
2	25,146	5.27 (1.14)	12.49 (0.27)	1.02 (0.98)
3	28,899	4.96 (0.47)	11.73 (0.43)	0.97 (1.03)
4	31,146	4.28 (1.01)	10.81 (0.09)	0.87 (1.15)
5	35,102	3.00 (0.33)	10.20 (0.33)	0.81 (2.46)
6	39,987	2.92 (1.07)	10.04 (0.34)	
7	42,156	2.70 (1.62)	9.72 (0.41)	
8	43,111	2.51 (1.98)	9.70 (0.41)	
9	48,879	2.34 (2.08)	9.63 (0.42)	
10	72,489		9.12 (0.55)	
11	78,642		8.37 (0.48)	
12	84,348		8.31 (1.08)	
13	99,486		7.67 (0.65)	
14	102,156		7.41 (0.68)	
15	105,003		6.68 (0.51)	
16	111,692		6.41 (1.56)	
17	123,488		3.13 (1.60)	
18	124,124			
19	131,013			
20	148,245			

instrument became inoperative shortly after finishing Pd and Rh readings. Hence, we decided to measure Pt concentrations by GF-AAS. Table 2 shows the heating program used for Pt measurements. Under these conditions a characteristic mass of 211 $\text{pg } 0.0044^{-1} \text{ A s}$ for Pt by GF-AAS was determined using the software of the spectrometer. A GF-AAS detection limit (3 s) of 6.2 $\mu\text{g l}^{-1}$ was determined for Pt after reading ten replicates of a 20 $\mu\text{g l}^{-1}$ Pt aqueous solution. Reported values are 220 $\text{pg } 0.0044^{-1} \text{ A s}$ and 3.5 $\mu\text{g l}^{-1}$ [13].

3.5. Content of Pd, Pt and Rh

Table 3 shows the average ($n=3$) concentrations of the metals of interest found in the samples analyzed. Nine, seventeen, and five samples out of the twenty samples analyzed, gave measurable concentration values for Pd, Pt and Rh, respectively.

Concentrations of the metals in the rest of the samples, blank spaces in the table, were below the detection limits of the techniques used for their measurement. It is clear from Table 3 that Pt exists in the samples analyzed at higher concentrations than Pd and Rh. This is in accordance with the fact that the original amount of platinum in three-way catalytic converters is larger than that corresponding to palladium and rhodium. This is due to the fact that Pt intervenes as a catalyst in all the catalytic reactions occurring in the converter whereas Pd and Rh play selective roles. According to literature information, the ratios Pt:Pd and Pt:Rh in three-way catalytic converters are 5:1 and 9:1, respectively [14]. The relatively large amount of Pt in the converters made it possible to determine this analyte in solid particulate of exhaust fumes of vehicles with considerably large odometer readings, for which there was not any atomic signal for Pd or Rh. Eighty-five percent of the samples analyzed gave measur-

able signals for Pt, while Pd and Rh were detectable in only 45 and 25% of the samples, respectively. There is a clear tendency for larger metal emissions from newer converters (Table 3). This is in agreement with the findings of Moldovan et al. [8,9]. For the metals to be efficient catalysts they have to be located on the surface of the substrate for better contact with the hot fumes coming from the engine. If the deposited metals are not strongly enough adhered to the substrate, metals will be removed by abrasion and lost along with the fumes. According to our results this sort of “cleaning mechanism” is clearly much more efficient for new converters. After approximately the first 120,000 Km for Pt, the first 72,000 Km for Pd and the first 35,000 Km for Rh, abrasion is no longer able to dislodge the metals from their substrate in amounts sufficient to be detected using the techniques applied in this work. This does not necessarily mean the converter has been depleted from its catalysts but what remains of the metals is so firmly attached to the substrate that the hot gases and the high temperature cannot remove them as easy as it happens during the first kilometers of use. This process along with catalysts poisoning could account for the continuous loss of efficiency of catalytic converters as a function of their usage.

3.6. Accuracy of the results

Our laboratory does not have any appropriate standard reference material for accuracy checking. Therefore we resorted to recovery tests to check how accurate our results were. Triplicate samples collected from “old” cars, which in their neat form did not produce any atomic emission or absorption signals, were spiked with exactly known amounts of the metals of interest. Appropriate volumes of aqueous solutions of the metals were carefully added to the solid particulate retained in the filter paper and the spiked samples were submitted to digestion and analyzed as previously described. Recovery percentages were 102.6 ± 0.5 ; 98.6 ± 1.1 and 99.4 ± 0.9 , for Pd, Pt and Rh, respectively. Further recovery tests, using different samples which were previously confirmed to contain the PGE and which were spiked so to duplicate their analytes content, resulted in percentage recoveries within the range 95–104%. These results attest for the negligible effect of the matrix of the sample on the emission and absorption signals of the analytes, indicating an efficient transference of the metals from the particulate to the solution during digestion. Therefore, the recovery test could be taken as an indication of the accuracy of the measurements performed using aqueous standards for calibration.

4. Conclusions

A simple, practical and inexpensive sample collector for trapping solid particulate coming along with motor vehicles exhaust fumes, has been developed. Samples are collected after filtration of the automobiles escape fumes. The solid particulate retained in the paper filter contains most of the Pd, Pt and Rh coming out with the fumes. Analysis of the particulate by GF-AAS and ICP-OES resulted in concentrations in the ranges 2.34 ± 2.08 to 5.36 ± 1.59 for Pd; 3.13 ± 1.60 to 12.60 ± 0.27 for Pt and 0.81 ± 2.46 to $1.03 \pm 0.97 \mu\text{g g}^{-1}$; for Rh. These results clearly show that catalytic converters expel Pd, Pt and Rh along with the escape fumes of the vehicles. It is also clear that there exists an inverse correlation among the Pd, Pt and Rh content in the collected samples and the usage of the catalytic converters: the newer the converter the larger the amount of metals expelled.

Acknowledgement

Authors are grateful to Fondo Nacional de Ciencia, Tecnología e Innovación, FONACIT, for funding this research through Grant S1-2000000558.

References

- [1] Ecoportal, <http://www.contaminacion.ecoport.net>.
- [2] B. Gómez, M.A. Palacios, M. Gómez, J.L. Sánchez, G. Morrison, S. Rauch, C. Malead, A. Alimonti, F. Petrucci, B. Bocca, P. Schramel, M. Zischka, C. Petterson, W. Wass, *Sci. Total Environ.* 299 (2002) 1.
- [3] F. Zereini, C. Zientek and H. Urban, *UWSF-Z Umweltchem Ökoox.*, 5 (1993) 130.
- [4] M. Niemela, H. Kola, P. Perámáki, J. Piispanen, J. Poikolainen, *Microchim. Acta* 150 (2005) 211.
- [5] J. Ely, C. Neal, C. Kulpa, M. Schneegurt, J. Seidler, J. Jain, *Environ. Sci. Technol.* 35 (2001) 3816.
- [6] C. Barbante, A. Veyseyre, C. Ferrari, K. Van de Velde, C. Morel, G. Capodaglio, P. Cescon, G. Scarponi, C. Bautron, *Environ. Sci. Technol.* 35 (2001) 835.
- [7] J. Fristche, T. Meisel, *Sci. Total Environ.* (2004) 325.
- [8] M. Moldovan, M. Gómez, J. Palacios, *J. Anal. Atom. Spectrom.* 14 (1999) 1163.
- [9] M. Moldovan, S. Rauch, M. Gómez, M.A. Palacios, G.M. Morrison, *Water Res.* 35 (2001) 4175.
- [10] R. Merget, G. Rosner, *Sci. Total Environ.* 270 (2001) 165.
- [11] D. Alizo, J.R. Domínguez, I. Morales Fuentes, J. Alvarado Durán, *Ciencia* 14 (2007) 516.
- [12] *Integra XL Inductively Coupled Plasma Operation Manual*, GBC Scientific Equipment Pty. Ltd., Australia, 1997.
- [13] *Perkin-Elmer 5100 ZL GF-AAS Software Operation Guide*, version 5, The Perkin-Elmer Corporation U.S.A., 1992.
- [14] K. Jarvis, S. Parry, J. Piper, *Environ. Sci. Technol.* 35 (2001) 1031.

Use of NIRS technology with a remote reflectance fibre-optic probe for predicting major components in cheese

Inmaculada González-Martín*, Claudio González-Pérez,
José Miguel Hernández-Hierro, José Miguel González-Cabrera

*Departamento de Química Analítica, Nutrición y Bromatología, Facultad de CC,
Químicas, C/ Plaza de la Merced s/n, 37008 Salamanca, Spain*

Received 5 July 2007; received in revised form 3 October 2007; accepted 7 November 2007
Available online 17 November 2007

Abstract

In the present work the potential of near infra-red spectroscopy technology (NIRS) together with the use of a remote reflectance fibre-optic probe for the analysis of fat, moisture, protein and chlorides contents of commercial cheeses elaborated with mixtures of cow's, ewe's and goat's milk and with different curing times was examined. The probe was applied directly, with no previous sample treatment.

The regression method employed was modified partial least squares (MPLS). The equations developed for the cheese samples afforded fat, moisture, protein, and chloride contents in the range 13–52%, 10–62%, 20–30%, and 0.7–2.9%, respectively. The multiple correlation coefficients (RSQ) and prediction corrected standard errors (SEP (C)) obtained were respectively 0.97 and 0.995% for fat; 0.96% and 1.640% for moisture; 0.78% and 0.760% for protein, and 0.89% and 0.112% for chlorides.

© 2007 Published by Elsevier B.V.

Keywords: Cheese; Fat; Moisture; Crude protein; Chlorides; Near infra-red spectroscopy; Fibre-optic probe; Analysis

1. Introduction

The chemical characterization of cheeses has traditionally been undertaken using different physico-chemical methods to determine pH, fat content, nitrogen fractions, organic acids, etc. These methods can be labour-intensive and expensive. Taking this into account, the development of new methods for the determination of these chemical parameters is of significant importance.

There is a need for the cheese processing industry to have tools available for real-time control of production lines to check whether in-process material, during a given processing step, meets the necessary compositional or functional specifications to reach a predetermined quality standard in the final product. In this context, spectroscopic techniques are fast and relatively inexpensive and they provide a great deal of information with only one test. They are considered to be sensitive, non-destructive, rapid, environmentally friendly and non-invasive,

making them suitable for on-line or at-line process control. In the dairy industry, near-infrared spectroscopy (NIRS) has been used for the determination of moisture [1], fat and protein in cheese [2–5], protein and lactose in cheese [6] and butter [7]. More recently [8] they have reported its application for the assessment of selected sensory properties in Emmental cheese. For the control of sensory characteristics during the curing of cheese, [9–11] used this measuring technique.

It has also been used visible-near infrared reflectance spectrophotometers to measure the colour of foods and agricultural products, and for the characterization of the geographical origin of buffalo milk and mozzarella cheese by means of analytical and spectroscopic determinations [12]. In this type of conventional measurement in reflectance mode, the samples must be ground and manipulated, with the consequent expenditure of time and money. However, an innovative aspect of the present work is the adaptation of NIRS and fibre-optic probes in production systems with a view to being able to conduct measurements directly.

The aim of the present study was to assess the potential of NIRS for the instantaneous and simultaneous prediction of fat, moisture, protein and chloride contents of commercially marketed cheeses made of mixtures of cow's, ewe's and goat's milk,

* Corresponding author. Tel.: +34 23 294483; fax: +34 23 294483.
E-mail address: inmaglez@usal.es (I. González-Martín).

and cured at different times. To do so, we used NIRS technology and a remote reflectance fibre-optic probe, applied directly onto the sample with no previous sample treatment or manipulation.

2. Material and methods

2.1. Samples

In the present study, 131 samples of commercial cheeses were purchased from local Spanish market. For this group, data on fat and moisture content were available for all of them; for protein in 99, and for chloride 48 (The distribution of samples in the calibration and external validation sets was as follows: in the case of fat and moisture content, 107 samples were used in the calibration set and 24 in the external validation set; for protein 81 and 18, and for chlorides 39 and 9, respectively) from mixtures of cow's, ewe's and goat's milk in different proportions (according to the manufacturers) and with different curing times. This means that there were visible differences not only in the physical aspect of the cheeses but also in the chemical composition of the samples. Recording of the NIR spectra was accomplished by direct application of the fibre-optic probe onto a slice of sample (Fig. 1). This had a minimum surface area sufficient to completely cover the probe window (5 cm × 5 cm).

2.2. Chemical analyses

The compositions in crude protein (Kjeldahl method, $N \times 6.38$) and moisture of the cheese samples were analysed using AOAC methods (1990) (984.13 and 963.22) [13,14]. Fat and chloride contents were determined to Gerber van Gulik, ISO (1975) [16] and AOAC (1990) (935.43) analytical methods [15], respectively. All determinations were carried out in duplicate and the results are expressed in % by weight.

2.3. NIR spectroscopy

A Foss NIRSystem 5000 with a standard 1.5 m 210/210 bundle fibre-optic probe, Ref no. R6539-A, was used. The probe

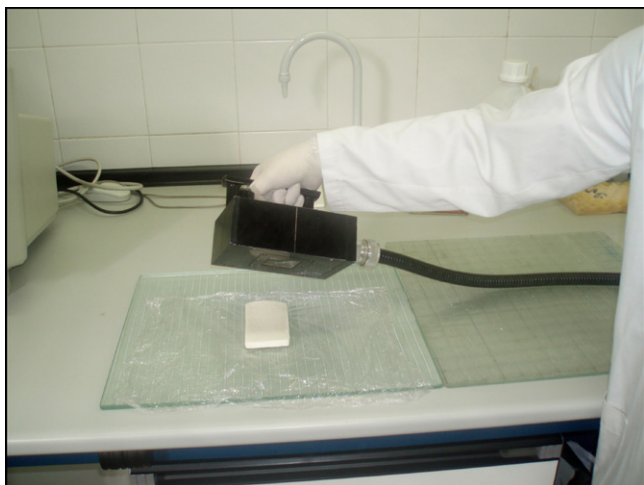


Fig. 1. Recording of the spectra of cheese samples with the probe.

employs a remote reflectance system and uses a ceramic plate as reference. The window is of quartz with a 5 cm × 5 cm surface area, measuring reflectance in the IR zone close to 1100–2000 nm. Spectra were recorded at intervals of 2 nm, performing 32 scans for both the reference and samples. The procedure was as follows: spectra were recorded in triplicate and the spectral mean was taken. Then, the calibration equations obtained during the work were applied and the predicted values were compared with those obtained later using the chemical method. The software used was Win ISI 1.50, installed on a Hewlett-Packard Pentium III computer.

2.4. Statistical analyses

The modified partial least squares (MPLS) regression method was used to obtain the NIR equations for all the parameters studied. Partial least squares (PLS) regression is similar to principal component regression (PCR), but uses both reference data (chemical, physical, etc.) and spectral information to form the factors useful for fitting purposes [17] (Martens and Naes). MPLS is often more stable and accurate than the standard PLS algorithm. In MPLS, the NIR residuals at each wavelength, obtained after each factor has been calculated, are standardised (dividing by the standard deviations of the residuals at each wavelength) before calculating the next factor. When developing MPLS equations, cross-validation is recommended in order to select the optimal number of factors and to avoid overfitting [18] (Shenk and Westerhaus). For cross-validation, the calibration set is divided into several groups; each group is then validated using a calibration developed on the other samples. Finally, validation errors are combined into a standard error of cross-validation (SECV) [19] (Davies and Williams). It has been reported that the SECV is the best single estimate for the prediction capability of the equation, and that this statistic is similar to the average standard error of prediction (SEP) from 10 randomly chosen prediction sets (Williams and Norris) [20]. The cross-validation groups used were 5 for fat and moisture; 6 for protein, and 7 for chlorides. With the exception of moisture, for which Standard Multiplicative Scatter Correction methods for scatter correction were used Geladi et al. [21], the remaining equations were obtained without scatter correction. Moreover, the mathematical treatments were tested in the development of the NIR calibrations: 1,4,4,1 where the first digit is the number of the derivative; the second is the gap over which the derivative is calculated; the third is the number of data points in a running average or smoothing, and the fourth is the second smoothing Shenk and Westerhaus [22]. The statistics used to select the best equations were RSQ (multiple correlation coefficients) and the standard error of cross-validation (SECV).

3. Results and discussion

3.1. Chemical analyses and spectral information

Table 1 shows the results of the chemical analyses of the samples of cheese and the contents of fat, protein, moisture, chloride, (the means, S.D. and range of values of chemical compositions

Table 1
Statistical overview of the chemical analyses of cheese (units in %)

Constituent	<i>N</i>	Minimum	Maximum	Mean	S.D.
Fat	107	16.3	42.3	32.5	6.6
Moisture	107	19.9	55.0	36.6	8.9
Crude protein	81	21.8	30.6	25.2	1.8
Chloride	39	1.10	2.61	1.81	0.4

N: number of samples; S.D.: standard deviation.

are included). The variability in the content of the constituents enables calibration equations to be developed for most commercial cheeses and such equations could thus be used to predict the contents of those constituents in unknown samples.

Fig. 2 shows the spectrum of a sample of cheese obtained directly with the fibre-optic probe and one of the mathematical treatments that afforded optimum values for the calibrations of moisture (using the Standard MSC). The effects of scattering were removed using MSC (multiplicative scatter correction), SNV (standard normal variate), DT (DeTrend) or SNV-DT, Geladi et al. [21] and Dhanoa et al. [23] have used the MSC mathematical treatment, in order to prevent the scattering in the samples from imposing itself on the chemical signals. Barnes et al. [24] indicated that SNV-DT should be introduced not only to reduce multicollinearity but also to calculate spectral differences by reducing the confounding effects of baseline shift and curvature.

3.2. Calibration equations

Calibration was carried out using NIR technology and a remote reflectance fibre-optic probe applied directly to the

cheese sample with no prior treatment or manipulation. To obtain the calibrations, a starting set of 107 cheese samples was used for fat and moisture; 81 for protein, and 39 for chlorides. Initially, a principal component analysis was carried out (PCA). In all cases, the spectral variability explained was above 99%, and 8 principal components were required for fat; 7 for moisture; 9 for protein and 5 for chlorides (Table 2). Anomalous spectra were detected by applying the Mahalanobis distance. Furthermore, the risk of there being mistakes in the equations under practical conditions is very low or almost null when the standardised H-statistic (Mahalanobis distance) is used during routine analysis of unknown samples. This tells us how different the spectrum of the unknown sample is from the average spectrum in the calibration set. Samples with an H-value greater than three may be considered as not belonging to the population from which the equations are developed, and in this case the equations should not be used to make any prediction. Two samples were removed for fat; 4 for moisture, 2 for protein, and none for chlorides. Calibrations were performed by modified partial least squares regression (MPLS). Using the $T \geq 2.5$ criterion, samples that were different from the population owing to chemical criteria were removed from the set. On the basis of this chemical criterion, 6 samples were removed for fat, 4 for moisture and protein, and 2 for chlorides.

The calibration process was implemented with the spectra of the resulting samples and their chemical data. The statistical parameters of the calibration were obtained for each of the components after removing the samples for spectral (H criterion) or chemical reasons (T criterion). The best of the different mathematical treatments, concentration range, and standard deviation for fat, moisture, protein and chlorides are also shown in (Table 3). The results obtained indicate that it is possible to

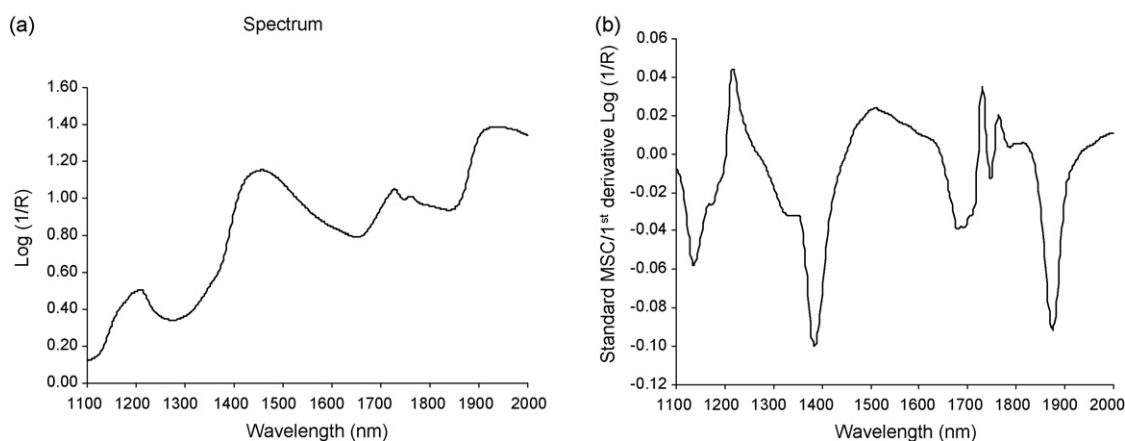


Fig. 2. Cheese NIR spectrum (a) and mathematical treatments for moisture (b) (using the Standard MSC).

Table 2
Selection of principal components in multivariate analysis

Constituent	<i>N</i>	Scatter correction	Mathematical treatment	Principal components	% expl.
Fat	107	None	2,10,10,1	8	99.77
Moisture	107	Detrend	1,4,4,1	7	99.71
Crude protein	81	SNV and Detrend	2,10,10,1	9	99.53
Chloride	39	Standard MSC	1,4,4,1	5	99.29

None: without treatment or correction of the spectrum; SNV: standard normal variate; MSC: multiplicative scatter correction; % expl. % of spectral variance explained.

Table 3
Calibration statistical descriptors for NIR determination in cheese

Constituent	N	Scatter correction	Mathematical treatment	RSQ	SEC	SECV	CV groups	Est. Min.	Mean	Est. Max.	S.D.
Fat	99	None	1,4,4,1	0.97	1.04	1.41	5	13.3	32.8	52.4	6.5
Moisture	99	Standard MSC	1,4,4,1	0.96	1.69	2.05	5	10.4	36.4	62.4	8.7
Crude protein	75	None	1,4,4,1	0.78	0.79	0.95	6	20.0	25.1	30.2	1.7
Chloride	37	None	1,4,4,1	0.89	0.12	0.20	7	0.71	1.8	2.9	0.4

N: number of samples; none: without treatment or correction of the spectrum; Standard MSC: standard multiplicative scatter correction; RSQ: multiple correlation coefficients; SEC: standard error of calibration; SECV: standard error of cross-validation; CV groups: groups of cross-validation; S.D.: standard deviation.

determine fat, moisture, protein and chlorides in commercial cheeses by direct application of a remote reflectance fibre-optic probe, and with broad parameter ranges (Table 3). The prediction capacity of the model obtained was evaluated with the RPD (ratio performance deviation), a capacity parameter that is defined as the relationship between the standard deviation of the chemical method (S.D. ref) and the standard prediction error encountered in the NIRS model (SEP); if the RPD value is greater than 2.5 the model is considered to be suitable. The RPD ratio for the calibration statistics of the properties was used to evaluate the prediction ability of reference methods for NIRS calibration, Williams and Sobering [25] based on the relationship between the error in analysis and the spread in composition. The RPD values obtained 6.6 for fat; 5.3 for moisture; 2.3 for protein and 3.4 for chlorides indicate that the NIRS equations obtained were applicable to unknown samples. These results reveal that the capacity of prediction is adequate for the fat, moisture and chlorides parameters, with some reservations for protein. This is reasonable since it is difficult to relate the results obtained by the reference analytical method to the spectroscopic data in the determination of bulk protein, considered as $\%N \times 6.38$, because nitrogen does not show a vibrational response in NIR. However, it is possible to measure the vibrations of N–H bonds – part of

the protein molecule – in the near IR. The NIR and the Kjeldahl reference methods do not measure the same type of species and the correlation between both methods may vary as a function of the type of sample involved.

3.3. Validation

3.3.1. Internal validation (prediction)

Fig. 3 shows a plot of the values predicted by the calibration equations and the reference values of cheese samples used in the development of the equations, together with the values of the most important statistics in prediction, the standard error of prediction and the standard error of prediction corrected by bias (SEP and SEP(C)) for fat, moisture, protein and chlorides in commercial cheeses.

3.3.2. External validation

The calibration equations obtained was assessed by applying the NIRS technology method to 24 new samples of cheeses in the case of fat and moisture, and 18 samples for protein and chlorides. The content ranges in the fat, moisture, protein and chloride parameters in the cheese samples used in the external validation and the differences (in %) found between the

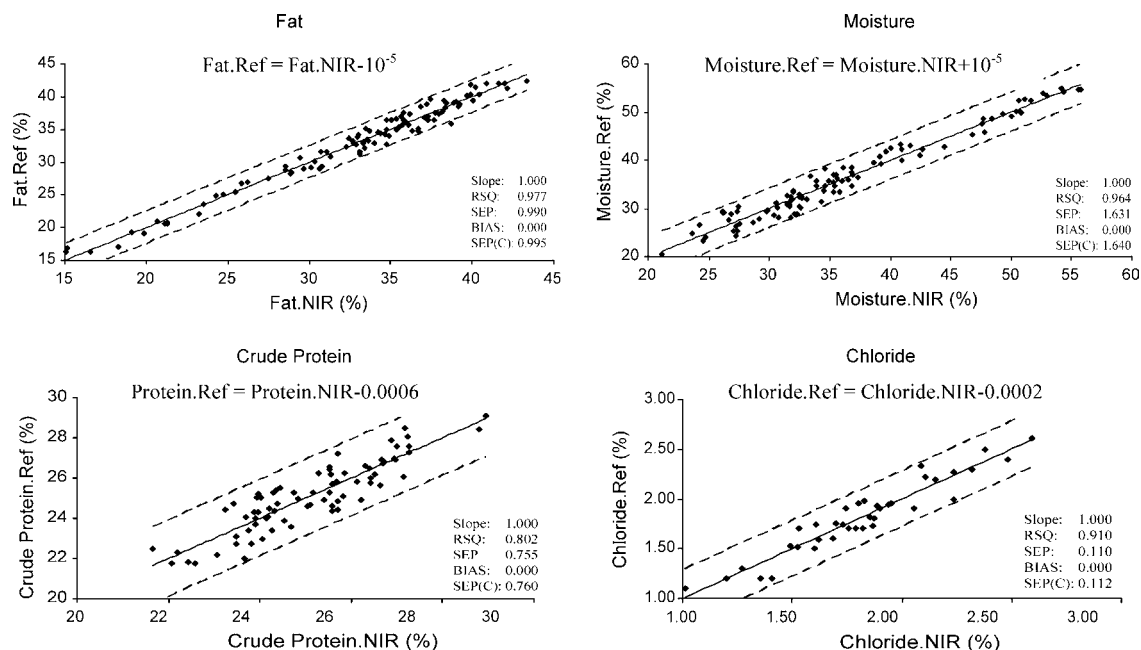


Fig. 3. Comparison of reference values with the values predicted by the calibration equations for fat, moisture, protein and chlorides. RSQ: multiple correlation coefficients; SEP: standard prediction error; SEP(C): standard prediction error corrected by the bias.

Table 4
External validation of the calibration model (units in %)

Constituent	<i>N</i>	Minimum	Maximum	Error (%)	<i>P</i> (level of significance)
Fat	24	17.5	42.0	4.5	0.87
Moisture	24	23.8	53.3	5.1	0.22
Crude protein	18	21.9	28.9	3.3	0.90
Chloride	9	1.2	2.3	11.5	0.98

reference chemical method and that obtained using NIRS technology are shown in Table 4. The NIRS and chemical methodologies were compared for the four constituents using Student's *t*-test for paired values with these samples. The levels of significance are shown in Table 4. The level of significance for all constituents was higher than 0.05 (chosen as the minimum); i.e., there were no differences among the results obtained. Our findings show that the analytical method discussed – employing a fibre-optic probe and measuring the samples by direct application of the probe – is rapid, does not require sample treatment and can be used to monitor the fat, moisture, protein and chloride parameters in commercial cheeses without prior knowledge of the type of milk (cow's, ewe's, goat's) or curing time of the sample.

4. Conclusions

Quantification of the major parameters (fat, protein, moisture, chlorides) in the cheese by means of NIRS technology with a remote reflectance fibre-optic probe in the present work as compared with the results reported by Rodríguez-Otero et al. [2] reveals a lower multiple regression coefficient (RSQ) in the protein parameter (0.98 against 0.78 in our case) and a greater standard error of calibration (SEC) (in fat, 0.39 against 1.04; and in protein, 0.40 against 0.79 in the present work.). Our work has the advantage of a broader range of application in the determination of fat (13–52 and protein (20–32%) in comparison with that of Rodríguez-Otero [2] (fat (17–32%) and protein (16–29%). Also, it permits the quantification of moisture and chlorides. The work of Karoui et al. (2007) [9] on emmental cheeses quantifies physico-chemical parameters such as non-protein nitrogen (NPN); total nitrogen (TN) and water-soluble nitrogen (WSN) but the quantification ranges of the fat and chloride parameters are narrower than those reported by us, and in our case the prediction capacity (RPD) is always higher, justifying its application in unknown samples. The work of McQueen et al. [3] determines the contents of protein (between 6% and 30%), fat (between 0% and 41%) and moisture (between 30% and 80%) in a very reduced number of samples (24), highlighting the characteristics of transform mid-infrared-attenuated total reflectance spectroscopy (FTIR-ATR) as compared with the optothermal method and wet chemistry, with prediction errors between 4% and 9%, which are higher than those found in other works. Additionally, our method is rapid, non-destructive and multiparametric.

From the present findings, it may be concluded that the NIRS technique with a fibre-optic probe is practical for the determination of fat, moisture, protein and chlorides in cheeses. Furthermore, use of the fibre-optic probe enables determinations to be made simply by placing the probe on the sample, with evident advantages as regards the possible speed of analysis.

Acknowledgement

The authors are grateful for funding from Project CTQ2006-04383 that enabled this work to be carried out.

References

- [1] R.L. Wehling, M.M. Pierce, J. AOAC Int. 71 (1988) 571.
- [2] J.L. Rodríguez-Otero, M. Hermida, A. Cepeda, J. AOAC Int. 78 (1995) 802.
- [3] D.H. McQueen, R. Wilson, A. Kinnunen, E.P. Jensen, Talanta 42 (1995) 2007–2015.
- [4] T.N. McCaig, Food Research Int. 35 (2002) 731.
- [5] J.L. Rodríguez-Otero, M. Hermida, J. Centeno, J. Agric. Food Chem. 45 (1997) 2815.
- [6] M.M. Pierce, R.L. Wehling, J. Agric. Food Chem. 42 (1994) 2830.
- [7] K. Molt, S. Kohn, Deut. Milchwirtschaft 44 (1993) 1104.
- [8] D. Brennan, J. Alderman, L. Sattler, B. O'Connor, C. O'Mathuna, Measurement 33 (2003) 67.
- [9] R. Karoui, L. Pillonel, E. Schaller, J.O. Bosset, J. De Baerdemaeker, Food Chem. 101 (3) (2007) 1121.
- [10] L.K. Sorensen, R. Jepsen, Int. Dairy J. 8 (1998) 863.
- [11] G. Downey, E. Sheehan, C. Delahunty, D. O'Callaghan, T. Guinee, V. Howard, Inter. Dairy J. 15 (2005) 701.
- [12] K.G. Adamopoulos, A.M. Goula, H.J. Petropakis, J. Food Compos. Anal. 14 (2001) 431.
- [13] T.N. McCaig, Food Res. Int. 35 (2002) 731–736.
- [14] M.A. Brescia, M. Monfreda, A. Buccolieri, C. Carrino, Food Chem. 89 (2005) 139.
- [15] A.O.A.C. Official Methods of Analysis, 15th ed., Vol I. In: K. Helrich (Ed.) AOAC, Inc. Arlington, VA, 1990.
- [16] ISO Standard 3433, International Standards Organisation, Geneva, Switzerland, 1975.
- [17] H. Martens, T. Naes, Multivariate Calibration, vol. 116, Wiley, Chichester, 2001.
- [18] J.S. Shenk, M.O. Westerhaus, Analysis of Agriculture and Food Products by Near Infrared Reflectance Spectroscopy, Monograph, NIRSystems, 1995.
- [19] A.M.C. Davies, P. Williams (Eds.), Near Infrared Spectroscopy: The Future Waves. Proceedings of the Seventh International Conference on Near Infrared Spectroscopy, NIR Publications, Chichester, West Sussex, UK, 1996.
- [20] P.C. Williams, K. Norris, Near Infrared Technology in the Agriculture and Food Industries, American Association of Cereal Chemists, Inc, St. Paul, Minnesota, USA, 1997.
- [21] P. Geladi, D. Mac Dougall, H. Martens, Appl. Spectrosc. 39 (1985) 491.
- [22] J.S. Shenk, M.O. Westerhaus, Routine Operation, Calibration, Development and Network System Management Manual, NIRSystems Inc., 12101 Tech Road, Silver Spring, MD 20904, USA, 1995.
- [23] M.S. Dhanoa, S.J. Lister, R.J. Barnes, Appl. Spectrosc. 49 (1995) 765.
- [24] R.J. Barnes, M.S. Dhanoa, S.L. Lister, Appl. Spectrosc. 43 (1989) 772.
- [25] P.C. Williams, D.C. Sobering, Near Infrared Spectrosc. 1 (1993) 25.

Gel-based immunoassay for non-instrumental detection of pyrene in water samples

Irina Yu. Goryacheva^{a,*}, Natalia V. Beloglazova^a, Sergei A. Eremin^b,
Dmitry A. Mikhirev^b, Reinhard Niessner^c, Dietmar Knopp^c

^a *Saratov State University, Chemistry Faculty, Department of Common and Inorganic Chemistry, Astrakhanskaya 83, 410012 Saratov, Russia*

^b *M.V. Lomonosov Moscow State University, Department of Chemical Enzymology, Leninskie hills 1, 119992 Moscow, Russia*

^c *Chair for Analytical Chemistry, Institute of Hydrochemistry and Chemical Balneology, Technische Universität München, Marchioninistrasse 17, D-81377 München, Germany*

Received 15 August 2007; received in revised form 12 November 2007; accepted 15 November 2007

Available online 22 November 2007

Abstract

A new qualitative immunologically based tube test for non-instrumental detection of pyrene (PYR) in water samples was developed. The method combines the pre-concentration of analyte by immunoextraction and its detection by immunoassay using Sepharose 4B-immobilized IgG-fraction of a polyclonal anti-PYR antiserum (immunoaffinity gel) and 1-pyrenebutyric acid-horseradish peroxidase conjugate (PYR-BA-HRP). The immunoaffinity gel was placed in a standard 1-ml SPE column through which a 10-ml aliquot of water sample spiked with 10% acetonitrile was passed. Following, free antibody binding sites were detected by application of PYR-BA-HRP. Four minutes after addition of the chromogenic substrate the results were visually evaluated by occurring or stayed away blue colour development for negative and positive samples, respectively. Total time for assay was about 15 min for six samples. Under optimized conditions a cut-off level for pyrene of 0.04 ng ml⁻¹ was found. At this defined concentration, a set of spiked samples ($n = 175$) was analyzed and very low rates of false negatives (1.2%) and false positives (4.6%) determined which fulfils the requirement set by Commission Decision 2002/657/EC for a screening method. No interference by other PAH compounds like naphthalene, fluoranthene, phenanthrene, anthracene, and benzo[*a*]pyrene at a concentration of 20 ng ml⁻¹, i.e., 500-fold excess compared to the defined cut-off level was observed. Different water types like surface water, tap water, bottled water, and melted snow were analyzed for PYR contamination by the proposed method and results confirmed by HPLC-FLD.

© 2007 Elsevier B.V. All rights reserved.

Keywords: Enzyme immunoassay; Immunoaffinity column; On-site method; Pyrene; Screening; Non-instrumental test; Visual detection

1. Introduction

Polycyclic aromatic hydrocarbons (PAHs) are a class of organic compounds consisting of two or more condensed aromatic rings. PAHs and derivatives are mainly formed during incomplete combustion of organic material arising, in part, from natural combustion such as fires and volcanic eruptions, but for most part from emissions of anthropogenic activities such as industrial manufacturing processes, the incinerating of solid waste, heating, automobile exhaust, but also cook-

ing and tobacco smoke. PAHs have generated considerable interest because of their toxicity and carcinogenicity potential. The most toxic members of this family known to-date are PAH molecules that have four to seven rings. These pollutants have a high persistence in the environment, low biodegradability and high lipophilicity. Natural waters can be heavily polluted with PAHs, which are either dissolved in water or adsorbed on colloids, depending on individual solubility. First of all, washout from the atmosphere by precipitation or runoff from streets and other surfaces are pathways bringing these chemicals into rivers and lakes [1]. In addition, oil and oil products can pollute waters accidentally. PAH compounds can also be found in groundwater, but usually at very low concentrations. As a result of their widespread presence, priority PAHs

* Corresponding author. Tel.: +7 88452 516959; fax: +7 88452 271491.
E-mail address: goryachevaiy@info.sgu.ru (I.Yu. Goryacheva).

were included in different Directives of the European Union and U.S. EPA. Pyrene constitutes one of the priority PAHs [2].

Generally, GC and HPLC are used for PAHs determination but these assays require pre-concentration of analyte, create large amounts of solvent waste, and are relatively time-consuming and difficult to perform on-site. As an alternative for the detection of PAHs in aqueous matrices non-invasive simpler methods were suggested, e.g., front-face fluorimetry on a solid sorbent and partial-least-square treatment [3]. In contrast, immunoassays are readily adapted to on-site screening. Commonly ELISA was used for PAH screening in different sample types such as surface water, potable water, sea water, sediments, and soil [4–7]. In addition, piezoelectric, electrochemical and optical immunosensors and fluorescent polarisation immunoassay were developed [8–13]. To our knowledge no non-instrumental tests were described for PAHs screening, probably due to problems in providing required sensitivity because of the very low concentration of PAHs in environmental samples. This study aimed at the development of a rapid qualitative non-instrumental immunochemical test which can be performed outside the laboratory for the screening of pyrene in water samples.

2. Experimental

2.1. Materials

Pyrene (PYR), naphthalene (NAPH), anthracene (ANT), phenanthrene (PHE), fluoranthene (FLA), benzo[*a*]pyrene (BAP), 1-pyrenebutyric acid (PYR-BA), Tween 20 and horseradish peroxidase (HRP) were purchased from Sigma (Bornem, Belgium). CNBr-activated Sepharose 4B (Sepharose) was obtained from Amersham Biosciences AB (Uppsala, Sweden). The substrate chromogenic solution used was ColorburstTMBlue TMB/Peroxide (ALerCHEK, Inc., Portland, ME, USA). All other chemicals and solvents were of analytical grade; doubly distilled water was used throughout. Tubes (Bond Elut reservoir, 1 ml) and polyethylene frits (1/4 in. diameter) were supplied by Varian Belgium NV/SA (Sint-Katelijn-Waver, Belgium). Phosphate-buffered saline (PBS) 0.01 M, pH 7.4, was used as assay buffer for the gel-based immunoassay. Proclin 300 (5-chloro-2-methyl-4-isothiazolin-3-one and 2-methyl-4-isothiazolin-3-one) was purchased from Supelco (Bellefonte, PA, USA) and was added to PBS as an antimicrobial preservative. PBS with 0.05% Tween 20 (PBS–Tween) was used as wash solution. Diapak C16M columns for solid-phase extraction (SPE) were supplied by BioChimMak (Moscow, Russia). Stock solutions of PAHs (100 $\mu\text{g ml}^{-1}$) were prepared in acetonitrile (ACN) and diluted in ACN to give standard solutions in the range of 0.01 ng ml^{-1} to 10 $\mu\text{g ml}^{-1}$.

2.2. Immunoreagents

The polyclonal rabbit antiserum 16.89 was obtained as previously described and IgG-fraction segregated by ammonium sulphate precipitation [14]. The pyrene derivative PYR-BA,

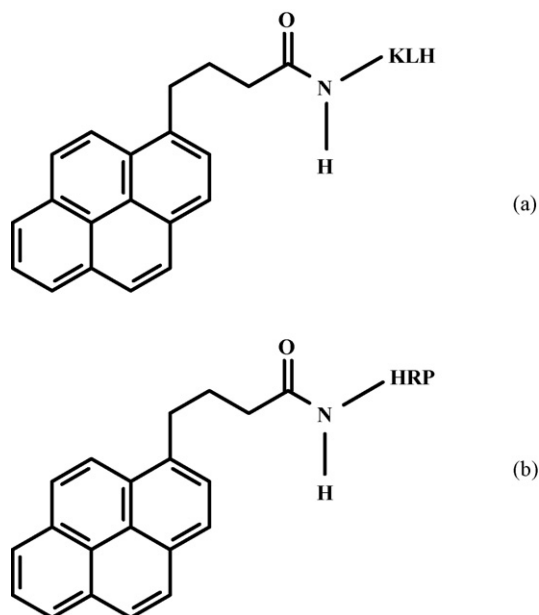


Fig. 1. Chemical structures of the immunogen (a) and conjugate PYR-BA-HRP (b).

which was used for the preparation of the hapten-KLH (key-hole limpet hemocyanine) conjugate (immunogen), was used for synthesis of the enzyme conjugate accordingly [14] (Fig. 1). In brief, 34.5 mg (300 μmol) of *N*-hydroxysuccinimide and 61 mg (300 μmol) of dicyclohexylcarbodiimide were dissolved in 1.5 ml of dimethylformamide. 0.5 ml of this solution was added dropwise under stirring to a solution of PYR-BA (28.8 mg, 100 μmol) in 500 μl of dimethylformamide. The reaction mixture was kept overnight at RT. Next day a small aliquot of activated hapten (5 μl) was added to a solution of 4 mg (0.1 μmol) of HRP in 2 ml of 0.05 M carbonate buffer (pH 9.6). The molar ratio of enzyme and hapten was 1:5. The reaction mixture was kept 1 h at RT followed by overnight incubation at 4 °C. The conjugate PYR-BA-HRP was purified by dialysis in distilled water (3 l) during 4 days with 2 times water change per day. It was stored at a concentration of 0.2 mg ml^{-1} in 50% glycerol at 4 °C.

2.3. Immunoaffinity gel preparation

The immunoaffinity gel was prepared as a mixture of coupled gel (Sepharose with bound rabbit anti-pyrene antibodies, diluted with PBS 1:3) and blocked gel (Sepharose with glycine blocked active groups, diluted with PBS 1:3). For coupled gel preparation 0.5 g of freeze-dried Sepharose (gave about 1.7 ml final gel volume) was washed on a sintered glass filter using 100 ml of 1 mM HCl. Then, 150 μl of the purified IgG-fraction and 50 μl PBS were added and this suspension was shaken for 2 h at RT. After incubation, the gel was washed with 5 ml of NaHCO_3 buffer, 0.1 M, pH 8.3 containing 0.5 M NaCl to remove excess antibody. For blocked gel preparation 2.5 g of Sepharose (gave about 8.5 ml final gel volume) was washed using 500 ml 1 mM HCl. For blocking of active groups five gel volumes of blocking agent (0.2 M glycine, pH 8.0) were added to both gels (cou-

pled with antibody and not coupled with antibody) and mixed for 2 h at RT. Blocking step was essential to reduce possible unspecific sorption of reagents and sample components on the immunoaffinity gel. Following, both gels were washed with 3 cycles of alternating pH and five gel volumes of each buffer. Each cycle consisted of a wash with 0.1 M acetate buffer, pH 4.0, containing 0.5 M NaCl followed by a wash with NaHCO₃ buffer, 0.1 M, pH 8.3 containing 0.5 M NaCl. Both gel types were suspended in PBS (1/3, v/v) and stored at 4 °C.

To prepare the immunoaffinity layer, gel with coupled specific antibody was mixed with blocked gel. Dilution of coupled gel was necessary to decrease the number of specific antibody binding sites and thus to increase sensitivity. An immunoaffinity gel solution (200 µl) was placed on the bottom frit in the 1 ml tube and then covered with the top frit. Prepared columns were stored at 4 °C and proved stable for at least 1 month.

2.4. Gel-based immunoassay

For the assay procedure a 10 ml aliquot of the standard solution ACN/H₂O (10/90, v/v) or water sample was drawn into the tube through the inlet means by pulling the plunger of a 10-ml syringe until air passed through the gel. Solid particles remained on the top frit and did not interfere with the immunoaffinity gel. PAHs, if present in the sample, were bound to the antibody binding sites in the immunoaffinity gel. Next, the PYR-BA-HRP conjugate solution (50 µl) at appropriate dilution was applied through the outlet means and excess of conjugate was removed with 5 ml of PBS-Tween by the inlet means. PYR-BA-HRP was bound by the non-occupied antibody binding sites. Finally, the chromogenic substrate was added by the inlet means. Colour was visually evaluated a few minutes after chromogenic substrate application.

2.5. Collection of water samples

For the investigation of matrix interferences on the developed immunoassay five types of water were used. The tap water was obtained from local water supply system using Volga river water as the source. The surface water samples were collected near the banks of the lake and the river Sazanka (both in Saratov region). Snow was collected at the central part of Saratov city. Bottled water “BonAqua” was purchased on the local market store. All tested types of water were directly used for the immunoassay, i.e., without any sample pretreatment like filtration or extraction.

2.6. HPLC-FLD

For the HPLC-FLD determination a preliminary clean-up and pre-concentration procedure was performed using Diapak C16M columns. A 50 ml of standard solution or appropriate volume of water sample (containing 10% ACN and 0.1% trifluoroacetic acid) were applied onto the SPE column. The column was dried and PAHs were eluted with 5 ml of acetone and 5 ml of dichloromethane. Eluates were combined, solvent evaporated and residue was redissolved in 250 µl of ACN/H₂O (80/20, v/v).

The Stayer HPLC system coupled to a fluorescent detector was used (Aquilon, Russia). The analytical column was a Phenomenex Luna C18, 5 µm, 150 mm × 4.6 mm. The column was kept at RT. The injection volume was 25 µl. The mobile phase consisted of ACN/water (80/20, v/v). For quantification of pyrene standard solutions of 0.05, 0.1, 0.25, 0.5 ng ml⁻¹ were prepared.

3. Results and discussion

3.1. Principle of the assay procedure

The gel-based immunoassay allows to combine pre-concentration with immunoaffinity column and direct competitive ELISA detection of an analyte within a single tube. In our previous work this approach was successfully used for ochratoxin A and aflatoxin B1 detection in high coloured food samples [15–18]. While the sample solution is drawing through the column the analyte, in the present investigation PYR, concentrates on the assay gel. This is followed by the addition of the enzyme-labelled conjugate (PYR-BA-HRP) which could only bind to PYR-specific antibodies if they are not occupied with the analyte. Consequently, quantity of bound conjugate and, therefore, intensity of developed colour are inversely proportional with the PYR concentration. As a positive result, i.e., PYR present, no colour development will be experienced. On the contrary, development of any colour at selected detection time can be interpreted as a negative result, i.e., absence of PYR. The cut-off level was defined as the lowest analyte concentration which results in no colour development at a fixed detection time.

3.2. Optimization of immunoreagents' concentration

As analytical signal for the presence of PAHs the colour development of the assay gel was used. Colour intensity and time of its development is influenced both by the concentration of specific antibodies and PYR-BA-HRP. Increasing the concentrations of immobilized antibodies and PYR-BA-HRP led to more intense colour development within shorter time. But, simultaneously the assay sensitivity decreased.

For optimization, the quantity of immobilized specific antibodies was varied by using 14 different ratios of antibody coupled and blocked gels (1 volume of coupled gel was diluted with $5-1 \times 10^7$ volumes of blocked gel). To check the assay sensitivity for each combination of antibody and PYR-BA-HRP concentration two columns were prepared. To these columns either 10 ml of blank solution or standard solution spiked with PYR at 0.5 ng ml⁻¹ (both solutions contained 10% of ACN to prevent unspecific PYR adsorption) were applied. It was shown that gel ratios up to 1:10⁵ resulted in the same intensity and time of colour development for both columns. Concluding, these dilutions were not high enough to detect PYR at the concentration of 0.5 ng ml⁻¹. On the contrary, ratios higher than 1:300 000 gave clear difference in colour development for blank and spiked samples. Regards to PYR-BA-HRP, the dilutions of 1:300, 1:500 and 1:1000 were tested. With dilution 1:500 (corresponds to 0.4 µg ml⁻¹) the most intense colour was obtained 10 min after

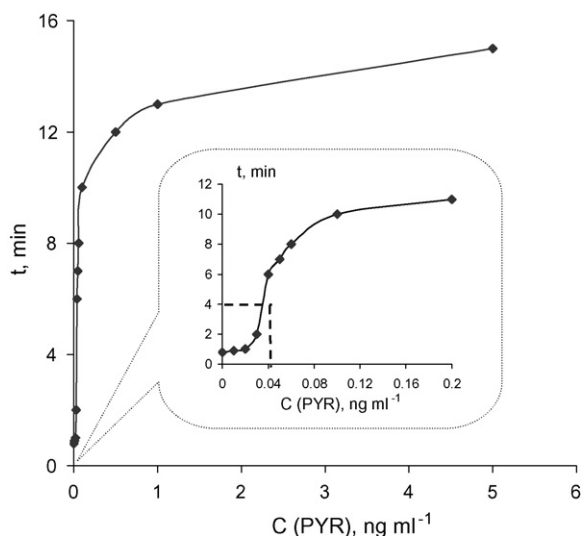


Fig. 2. The kinetics of colour development after the addition of the chromogenic substrate to the assay tube in dependence on the pyrene concentration.

application of the spiked sample. Therefore, this dilution was chosen as optimal for the evaluation of positive and negative samples.

3.3. Validation using spiked samples

To establish the assay sensitivity different PYR standard solutions in the concentration range 0–5 ng ml⁻¹ were prepared and the colour development observed after chromogenic substrate application (Fig. 2). With the blank, colour development started already after 1 min. With increase of the analyte concentration colouring of the assay gel was retarded. For defining the cut-off level both required sensitivity, speed of analysis and the visible evaluation of the test result must be considered. The latter means that a coloured assay gel which is a negative result must be clearly distinguishable from a non-coloured gel, i.e., a positive sample. Concluding from Fig. 2, if a detection time of 4 min after addition of the chromogenic substrate was cho-

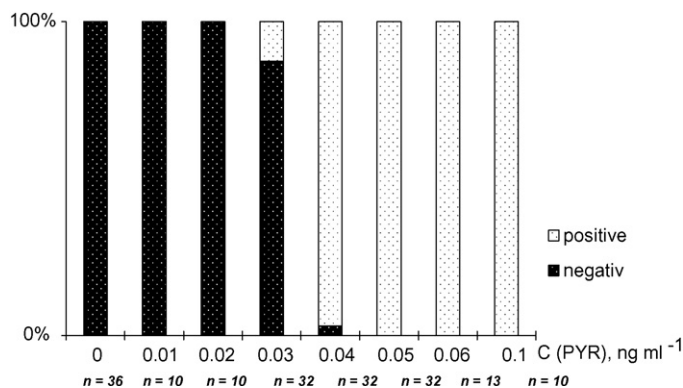


Fig. 4. Percentage rate of positive and negative results at different pyrene concentration levels. "n" refers to the number of determinations at corresponding concentration.

sen a cut-off level for PYR at 0.04 ng ml⁻¹ was obtained, i.e., no colour was developed at this and higher concentrations. Fig. 3 presents results for a set of different PYR concentrations (0–0.06 ng ml⁻¹) with gel ratio 1:10⁷ and PYR-BA-HRP dilution of 1:500 and visible evaluation 4 min after substrate application. In the absence of PYR an intense blue colour developed. The increase of PYR concentration resulted in a decrease of colour intensity. No blue colour appeared at PYR concentrations of 0.04 ng ml⁻¹ or higher. Following, with increasing analyte concentration a decrease of PYR-BA-HRP concentration in the gel was obtained, i.e., enzymatic activity was clearly diminished.

Sets of different PYR standards (range 0.01–0.1 ng ml⁻¹) were tested and probabilities of positive and negative results calculated for each concentration level (Fig. 4). In the optimized conditions all results for PYR concentrations of 0, 0.01 and 0.02 ng ml⁻¹ were correctly identified as negatives. At PYR levels of 0.03 and 0.04 ng ml⁻¹, 12.5% false positives and 3% false negatives were observed, respectively. All PYR levels of 0.05 ng ml⁻¹ or higher gave only positive results. Corresponding data were summarized in Table 1.

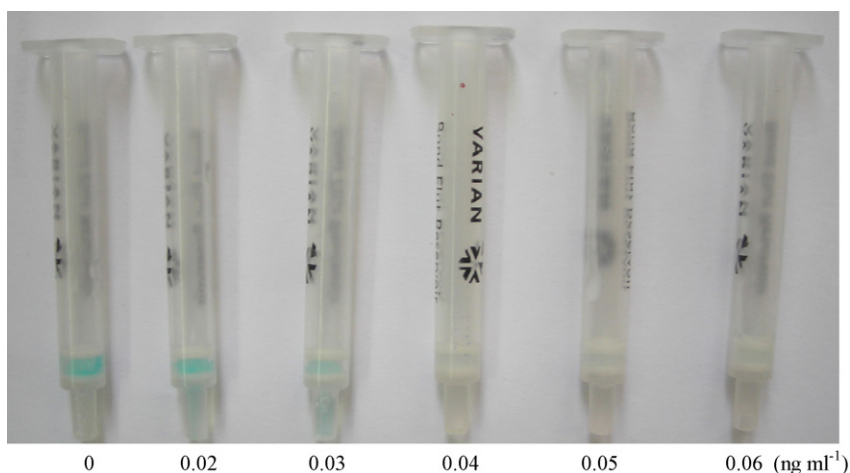


Fig. 3. Series of results for tube-test gel-based immunoassay. The pyrene concentrations are indicated below the tubes. Detection time was 4 min after chromogenic substrate application.

Table 1
Contingency table for positive and negative test results

Sample	Water samples fortified with pyrene		Total
	<0.04 ng ml ⁻¹	≥0.04 ng ml ⁻¹	
Positive	4 (N _{false positive})	86 (N _{positive})	90
Negative	84 (N _{negative})	1 (N _{false negative})	85
Total	88 (N ₋)	87 (N ₊)	175 (N)

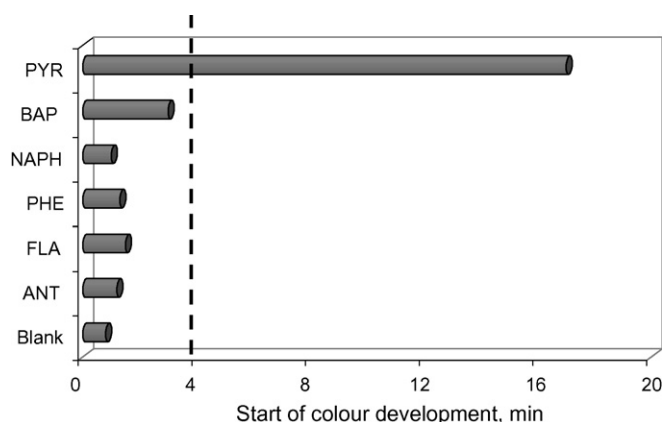


Fig. 5. Time of start of colour development for different PAH compounds: PYR, pyrene; BAP, benzo[*a*]pyrene; NAPH, naphthalene; PHE, phenanthrene; FLA, fluoranthene; ANT, anthracene; concentration of 20 ng ml⁻¹.

Performance parameters as indicators for the quality of the test were calculated and presented in Table 2. It becomes obvious that at defined cut-off level of 0.04 ng ml⁻¹ for PYR the rate of false negative results is very low (1.2%) and accuracy high (97%). This fulfils the requirement set by Commission Decision 2002/657/EC [19] for a screening method, i.e., a false compliant rate of <5% at the level of interest must be ensured.

3.4. Assay specificity

Among the PAH compounds which are regularly found at elevated levels in surface water samples are NAPH, FLA, PHE, and ANT. These compounds are much better water-soluble than higher annelated PAHs. Additionally, BAP was tested because a limit value of 10 ng l⁻¹ was set for this highly toxic compound in the new European water directive (Council Directive 98/83/EC). To control possible cross-reactivity of the gel-based immunoassay 10 ml of the 20 ng ml⁻¹ PAH standards containing 10% of ACN were passed through the columns and time of the beginning of colour development was recorded (Fig. 5). While for NAPH,

Table 2
Performance parameters of the gel-based immunoassay for determination of pyrene at the cut-off level of 0.04 ng ml⁻¹

Parameter	Formula	Percentage
False negative rate	(N _{false negative} /N ₋) × 100 (%)	1.2
False positive rate	(N _{false positive} /N ₊) × 100 (%)	4.6
Accuracy	[(N _{positive} + N _{negative})/N] × 100 (%)	97
Specificity rate	(N _{negative} /N ₋) × 100 (%)	95
Sensitivity rate	(N _{positive} /N ₊) × 100 (%)	99

Table 3
Pyrene determination in different water types by the gel-based immunoassay and HPLC-FLD

Water type	Gel-based immunoassay (n = 3)	HPLC-FLD (ng ml ⁻¹)
Lake water	+++	0.12
River water	--±	nd
Tap water	+++	0.09
Bottled water	---	nd
Melted snow	+++	0.22

(-) Blue coloured gel, negative result; PYR concentration <0.04 ng ml⁻¹; (±) weak blue coloured gel, negative result; PYR concentration <0.04 ng ml⁻¹; (+) Non-coloured gel, positive result; PYR concentration ≥0.04 ng ml⁻¹; (nd) non-detected.

FLA, PHE, and ANT colour development started already after about 1.5 min, it was about 3 min for BAP. With about 17 min it was significantly higher for PYR. Therefore, using the established detection time at 4 min, even a 500-fold excess of these PAHs would not interfere with the PYR detection at the defined cut-off level of 0.04 ng ml⁻¹. The observed high specificity of the used antiserum for PYR is based on the aimed immunization with a pyrene derivative.

3.5. Real sample analysis

For testing the usefulness of the developed gel-based immunoassay different water types like surface water, tap water, bottled water, and melted snow were analysed. As the main demand for a screening method is prevention of false negative results, a possible matrix effect was controlled by analysis of an additional portion of sample which was spiked with PYR at the cut-off level. Before analysis 1 ml ACN was added to 10 ml of sample to avoid PAH adsorption to the walls of syringe and column. This was passed through the column by the inlet means. Then 50 μl of PYR-BA-HRP solution was placed into the column through the outlet means and removed after 2 min. After washing step, 50 μl of chromogenic substrate was drawn into the column by the outlet means and after 4 min colour of the gel was evaluated. With all spiked samples no colour development was observed, i.e., no false negative results were obtained. Results for non-spiked real samples were summarized in Table 3. Comparison of the developed test outcomes and HPLC-FLD results showed good agreement both for positive and negative samples.

4. Conclusions

An approach for rapid non-instrumental detection of PYR was devised and optimized for qualitative screening of water samples. So far this approach was used only for mycotoxin detection in food samples. The described gel-based immunoassay has proved useful for screening of PYR in a fairly simple manner, and without any sample preparation like extraction, centrifugation, filtering, etc. The cut-off level for PYR was estimated at 0.04 ng ml⁻¹. With the optimized conditions, the developed assay revealed rather specific for PYR, i.e., lower annelated PAHs like NAPH, FLA, PHE and ANT and BAP did not interfere at a 500-fold excess compared to the defined cut-

off level. It is anticipated that both the cut-off level and the spectrum of targeted PAH compounds can be fine-tuned by careful selection of assay parameters, mainly the concentration of immunoreagents. This would allow the adaptation of the test to the required sensitivity and specificity. The immunoassay was applied for PYR detection in some real water samples like surface water, tap water, bottled water, and melted snow. The obtained positive and negative results could be confirmed by HPLC-FLD. High accuracy of the developed method makes it applicable for surveillance of surface and tap water quality.

Acknowledgement

The research was supported by NATO Collaborative Linkage Grant “New strategy for biodetection of explosive nitrochemicals in environmental samples”.

References

- [1] M. Grynkiewicz, Z. Polkowska, J. Namiesnik, *Atmos. Environ.* 36 (2002) 361.
- [2] K.A. Fährnich, M. Pravda, G.G. Guilbault, *Anal. Lett.* 35 (2002) 1269.
- [3] M. Algarra, V. Jiménez, P. Fournier de Violet, M. Lamotte, *Anal. Bioanal. Chem.* 382 (2005) 1103.
- [4] D. Barcelo, A. Oubina, J.S. Salau, S. Perez, *Anal. Chim. Acta* 376 (1998) 49.
- [5] D. Matschulat, A. Deng, R. Niessner, D. Knopp, *Analyst* 130 (2005) 1078.
- [6] K. Li, L.A. Woodward, A.E. Karu, Q.X. Li, *Anal. Chim. Acta* 419 (2000) 1.
- [7] M. Nording, K. Frech, Y. Persson, M. Forsman, P. Haglund, *Anal. Chim. Acta* 555 (2006) 107.
- [8] R.D. Vaughan, E. Geary, M. Pravda, G.G. Guilbault, *Int. J. Environ. Anal. Chem.* 83 (2003) 555.
- [9] K.V. Gobi, N. Miura, *Sens. Actuators B* 103 (2004) 265.
- [10] K.A. Fährnich, M. Pravda, G.G. Guilbault, *Biosens. Bioelectron.* 18 (2003) 73.
- [11] E.J. Moore, M.P. Kreuzer, M. Pravda, G.G. Guilbault, *Electroanalysis* 16 (2004) 1653.
- [12] J. Tschmelak, G. Proll, J. Riedt, J. Kaiser, P. Kraemmer, L. Bárzaga, J.S. Wilkinson, P. Hua, J.P. Hole, R. Nudd, M. Jackson, R. Abuknesha, D. Barceló, S. Rodriguez-Mozaz, M.J. López de Alda, F. Sacher, J. Stien, J. Slobodník, P. Oswald, H. Kozmenko, E. Korenková, L. Tóthová, Z. Krascenits, G. Gauglitz, *Biosens. Bioelectron.* 20 (2005) 1509.
- [13] I.Yu. Goryacheva, S.A. Eremin, E.A. Shutaleva, M. Suchanek, R. Niessner, D. Knopp, *Anal. Lett.* 40 (2007) 1445.
- [14] D. Knopp, M. Seifert, V. Väänänen, R. Niessner, *Environ. Sci. Technol.* 34 (2000) 2035.
- [15] M. Lobeau, S. De Saeger, L. Sibanda, I. Barna-Vetro, C. Van Peteghem, *Anal. Chim. Acta* 538 (2005) 57.
- [16] M. Lobeau, S. De Saeger, L. Sibanda, I. Barna-Vetro, C. Van Peteghem, *Food Addit. Contam.* 24 (2007) 398.
- [17] I.Yu. Goryacheva, S. De Saeger, M. Lobeau, S.A. Eremin, I. Barna-Vetro, C. Van Peteghem, *Anal. Chim. Acta* 577 (2006) 38.
- [18] I.Yu. Goryacheva, S. De Saeger, M. Lobeau, B. Delmulle, S.A. Eremin, I. Barna-Vetro, C. Van Peteghem, *Anal. Chim. Acta* 590 (2007) 118.
- [19] Commission Decision 657/2002 of 12 August 2002 implementing Council Directive 96/23/EC concerning the performance of analytical methods and the interpretation of results, *Off. J. Eur. Commun., L* 221/8 (August 17).

Direct determination of serotonin in gut lavage fluid by liquid chromatographic ion trap tandem mass spectrometry

Kine Gregersen^{a,b}, Livar Frøyland^a, Arnold Berstad^b, Pedro Araujo^{a,*}

^a National Institute of Nutrition and Seafood Research (NIFES), P.O. Box 2029, Nordnes, N-5817 Bergen, Norway

^b Institute of Medicine, Haukeland University Hospital, N-5021 Bergen, Norway

Received 11 June 2007; received in revised form 10 November 2007; accepted 14 November 2007

Available online 22 November 2007

Abstract

Direct determination of serotonin (5-HT) in gut lavage fluid from patients examined due to various gastrointestinal complaints has been achieved. The method involves addition of 5-methoxytryptamine (5-CH₃O-HT) internal standard, centrifugation, filtration and injection of the sample supernatant in a liquid chromatographic system coupled to an ion trap tandem mass detector. Electro-spray in positive mode was used to isolate and fragment the protonated ions [5-HT + H]⁺ and [5-CH₃O-HT + H]⁺ signals 177 and 191 *m/z*, respectively. Quantification was carried out by extracting the ion fragment chromatograms at 160 and 174 *m/z* for 5-HT and 5-CH₃O-HT, respectively. The relationship 5-HT/5-CH₃O-HT was modelled by using a simultaneous design in order to estimate the optimal amount of internal standard to be added to the samples prior to quantification.

© 2007 Elsevier B.V. All rights reserved.

Keywords: Serotonin; Liquid chromatography; Ion trap mass spectrometry; Uniform shell design; Gut lavage fluid

1. Introduction

Serotonin (5-hydroxytryptamine or 5-HT) is a monoamine known for its pivotal role in several aspects of gut function including secretion, motility and sensation. A large amount of 5-HT in the body (over 90%) is found in the enterochromaffin (EC) cells of the intestines, where most EC cells are of the “open” type with apical cytoplasmic extensions which project into the glandular lumen with short microvilli enabling the cells to respond to physical or chemical variations in luminal content. EC cells are believed to function as sensory transducers that activate mucosal processes of both intrinsic and extrinsic primary afferent neurons through their release of serotonin. Release or leakage of serotonin into the gut lumen has been demonstrated previously [1,2], but whether luminal serotonin has any physiological function or is just an overflow phenomenon is not clear.

Serotonin has also been implicated in several gastrointestinal disorders including irritable bowel syndrome [3,4], inflammatory bowel disease [4], food hypersensitivity [5], etc.

Determination of 5-HT in patients with different gastrointestinal conditions is carried out by obtaining mucosal specimens by means of biopsy forceps [3] and subsequent enzyme immunoassay determination of the tissue specimens. However, the main disadvantages of immunological assays are their lack of specificity for complex samples and liability to overestimate the levels of a determined analyte, especially in cases where multiple metabolically related products are present. High performance liquid chromatography and LC–MS (single or tandem) have been successfully used in the determination of 5-HT in a wide variety of biological samples such as tissues [6], brain [7], whole blood [8], serum [9], plasma [10], urine [11], cell culture [12], food [13], lachrymal glands [14], and intestine [15]. It has been suggested that the use of LC–MS/MS in the analysis of 5-HT offers advantages in terms of specificity and linear range, while permitting simultaneous determination of 5-HT metabolic related products [8]. Unfortunately in the majority of prior studies there is no description regarding the strategies behind the selection of an optimal amount of internal standard especially in cases where the analyte may have a wide span of concentrations. The potential applicability, in the analysis of biomedical samples, of a multivariate strategy to estimate an optimal concentration of internal standard and a robust response

* Corresponding author. Tel.: +47 95285039; fax: +47 55905299.

E-mail address: pedro.araujo@nifes.no (P. Araujo).

factor, which does not change with changes in the analyte and internal standard concentrations, has been recently suggested [16]. Aiming at proposing a new, simple, and less invasive sampling procedure in conjunction with a more precise and rapid technique for determination of 5-HT, gut lavage fluid (GLF) was collected and the levels of 5-HT were determined by LC–MS/MS, using a multivariate model for the estimation of an appropriate amount of internal standard. GLF is collected routinely during work-up of patients with suspected intestinal disorders. A review of the current literature revealed a lack of published studies on the analysis of 5-HT in GLF either by immunological assays or any other technique.

2. Experimental

2.1. Reagents

Serotonin hydrochloride (Cat No. H9523) and the internal standard 5-methoxytryptamine (Cat No. 286583) were purchased from Sigma–Aldrich Co. USA. Acetonitrile and ethanol HPLC-grade were from Merck (Darmstadt, Germany) and formic acid was from Fluka Chemie (Basel, Switzerland). De-ionized water was purified in a Milli-Q system (Milli-Q system Millipore, Milford, MA).

2.2. Samples

GLF was collected from fasting patients suffering various gastrointestinal complaints, after nasoduodenal intubation and duodenal administration of 2 l of an isotonic polyethylene glycol solution (PEG, MW 3350, Laxabon®, Tika, Sweden) containing 50 μCi of ^{51}Cr -labelled ethylenediaminetetra-acetic acid (^{51}Cr EDTA, Amersham, Little Chalfont, UK). ^{51}Cr EDTA was added to allow estimation of gut mucosal permeability [17]. The first clear fluid passed per rectum was collected and filtered through gauze, and a 4 ml aliquot was collected on tubes containing 0.5 ml of a solution with antiseptic and antiproteolytic activity prepared by adding 1 ml of 10% sodium azide (NaN_3) to 50 ml of soybean trypsin inhibitor (Sigma, Taufkirchen, Germany). The samples were stored at -80°C prior to analysis.

2.3. Experimental design to determine the optimal amount of internal standard

The validity of the internal standard method relies on the assumptions of linearity of the detector response towards the 5-HT and 5- CH_3O -HT. Studies on 5-HT analysis neither consider the linearity of the detector nor describe a rational way on how much internal standard should be added. In the present investigation, the aforementioned issues were addressed by using a uniform shell design proposed by Doehlert [18]. Fig. 1 described the generation of a uniform shell design for two factors. The main characteristics of this design are:

- The number of experiments is calculated by the general expression $X^2 + X + 1$, where X represents the number of vari-

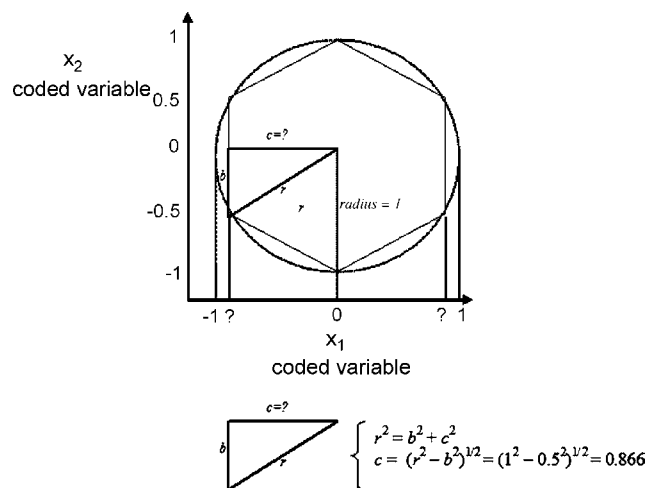


Fig. 1. Generation and characteristics of the uniform shell design proposed by Doehlert [18] for two variables.

ables studied. For instance, to investigate the effect of two variables ($X = 2$) seven experiments will be required.

- The experiments are allocated at the centre and at the vertexes of a hexagonal shape, circumscribed in a circle of radius 1, in this way the variances of the estimated responses are the same at all points on the circle centred at the origin.
- The variables are codified and equally spaced between -1 and 1 and by using basic geometric it is possible to determine the coded combination of the variables at each vertex of the hexagon. Fig. 1 described how the coded levels of the variable x_1 (represented by question marks) are calculated by using Pythagoras' theorem.
- The variables are simultaneously investigated at different numbers of levels. Fig. 1 shows how the coded variables X_1 and X_2 are studied at 3 and 5 levels ($-0.866, 0, 0.866$ and $-1, -0.5, 0, 0.5, 1$), respectively. The coded levels are then converted into the $\mu\text{g ml}^{-1}$ values described in Table 1.

The application of this particular design in the determination of the optimal amount of internal standard to be used in the quantitative determination of 5-HT is as follows:

Test tubes containing seven different concentration ratios of 5-HT:5- CH_3O -HT in 50 μl of ethanol (Table 1) were prepared in triplicates (7×3) and evaporated to dryness under a stream of nitrogen at room temperature. A GLF sample with no detectable levels of 5-HT was thawed at room temperature and centrifuged. The supernatant was collected and filtered by using a hydrophilic nylon membrane syringe filter, 4 mm diameter and 0.45 μm pore size (Chromacol Ltd., Trumbull, USA). Aliquots of 50 μl of the filtered supernatant were added into the aforementioned 21 test tubes. The tubes were vortex-mixed for 1 min, transferred to an autosampler vial and submitted to LC–MS/MS analysis. A GLF blank sample spiked with 3 $\mu\text{g ml}^{-1}$ of 5-HT and 16 $\mu\text{g ml}^{-1}$ of 5- CH_3O -HT was prepared in triplicate to check the prediction capability of the model to be proposed. The analytical signals recorded with this additional solution along with those obtained by applying the uniform shell design, were used for modelling purposes. Two set of GLF samples spiked with 0 and

Table 1

Concentrations of 5-HT and 5-CH₃O-HT dissolved in gut lavage fluid (GLF) according to a uniform shell design to study the behaviour of the response factor (RF) as a function of the analytical concentrations

Uniform shell design coded levels	Experiment number	Experimental levels dissolved in GLF (2–20 µg ml ⁻¹)		**RF (n = 3)
		5-HT	5-CH ₃ O-HT	
	I	11	20	0.037 ± 0.007
	II	3	16	0.029 ± 0.001
	III	19	16	0.036 ± 0.003
	IV	11	11	0.035 ± 0.001
	V	3	7	0.039 ± 0.003
	VI	19	7	0.048 ± 0.001
	VII	11	2	0.047 ± 0.007
	6*	16*	0.026 ± 0.003	

*Although these particular concentrations are not dictated by the design, the RF connected with them was considered for the purpose of modelling.

**RF calculated according to Eq. (1).

0.5 µg ml⁻¹ of 5-HT and a fixed concentration of internal standard (2 µg ml⁻¹) were prepared in triplicates and measured after proposing a suitable model in order to verify the robustness of the response factor (RF) in an experimental space not suggested by the design.

2.4. Samples quantification

After modelling the relationship 5-HT/5-CH₃O-HT an optimal concentration of internal standard (2 µg ml⁻¹) was selected. Gut lavage fluid samples (50 µl) from patients were spiked with the optimal concentration of 5-CH₃O-HT as described above and submitted to LC–MS quantification.

2.5. Liquid chromatography ion trap mass spectrometry

The LC–MSⁿ used in this study was an Agilent 1100 series LC/MSD trap, SL model with an electro-spray interface (ESI), a quaternary pump, degasser, autosampler, thermostated column compartment, variable-wavelength UV detector and 25 µl injection volume. The column, a Zorbax Eclipse-C₈ RP 150 mm × 4.6 mm, 5 µm (Agilent Technologies, Palo Alto, CA, USA) is a double endcapped column 100% water compatible which can be operated at maximum pH range of 2–9 and provides improved basic peaks of amines compounds (such as serotonin) due to the polar groups embedded in the stationary phase and fast conditioning of the column. The column was kept in the column compartment at 20 °C and the solvent system in gradient mode consisted of water with formic acid 0.1% (v/v) (A) and acetonitrile (B) and UV detection at 254 nm and 0.2 ml min⁻¹ flow rate. The initial condition 100% of A was ramped to 35%

of A in 20 min, returned immediately to 100% of A in 5 min and held there for 5 min. By using this gradient condition, reproducible retention times and peak areas from sample to sample were monitored. Nitrogen was used as nebulizing and drying gas at 300 °C. The ESI source was operated in positive ion mode and the ion optics responsible for getting the ions in the ion trap such as capillary exit, skimmer, lens and octapoles voltages were controlled by using the Smart View option with a resolution of 13000 m/z/s (FWHM/m/z = 0.6–0.7). Complete system control, data acquisition and processing were done using the ChemStation for LC/MSD version 4.2 from Agilent. The transitions monitored were 177 → 160 m/z for 5-HT and 191 → 174 m/z for 5-CH₃O-HT. The magnitude of the signals was recorded in ion counts per second (icps).

2.6. Statistics

Response factor (RF) data presented in Table 1 are expressed as mean values and standard deviations and calculated at every experimental point by the expression:

$$RF = \frac{[5\text{-CH}_3\text{O-HT}]}{[5\text{-HT}]} \times S_{5\text{-HT}/5\text{-CH}_3\text{O-HT}} \quad (1)$$

The terms in square brackets represent the 5-HT and 5-CH₃O-HT concentrations in µg ml⁻¹ and the term $S_{5\text{-HT}/5\text{-CH}_3\text{O-HT}}$ the signal ratio.

The behaviour of the two variables studied, namely [5-HT] and [5-CH₃O-HT] as a function of the parameter RF was studied by means of multiple regression analysis and the statistical significance of the coefficients and the correlation was determined by the *F*-test at a 95% confidence level. The regression analysis

was done by Statgraphics Plus 5.1 software package (Statistical Graphics Corp., Herndon, USA).

3. Results and discussion

3.1. Internal standard selection

The selection of the internal standard was based on the grounds that 5-CH₃O-HT is widely reported in the current scientific literature as a suitable internal standard for 5-HT analysis by LC–MS. In addition, a world reputed company specialized in supporting academic scientists and with a strong focus on neuroscience and analytical chemistry, has developed a commercial licensed kit for 5-HT that use 5-CH₃O-HT as internal standard [19].

3.2. Determination of the optimal amount of internal standard and a robust response factor

The GLF samples spiked with different concentrations of 5-HT and 5-CH₃O-HT were injected in the chromatographic system and detected by ion trap tandem MS. The total time required for the analysis of the 24 samples described in Table 1 was 12 h. During this time the chromatography pressure was monitored and no significant variations were observed. The pressure variation during the 12 h ranged from 56 to 63 bar. Protonated 5-HT and 5-CH₃O-HT signals at 177 and 191 *m/z* were isolated and the ion fragments 160 and 174 *m/z* corresponding to the loss of ammonia (NH₃)—monitored in both cases, respectively. Table 1 shows the experimental results obtained after applying the uniform shell design. The experiments were run in random order and every experimental point was replicated three times to provide sufficient degrees of freedom for the calculation of the pure error sum square. The response factors (RF) presented in Table 1 were calculated at every experimental point by using Eq. (1). The behaviour of the variables concentration of [5-HT] and [5-CH₃O-HT] as a function of the parameter RF was determined initially by using a full first-order polynomial model with 4 parameters (1 intercept, 2 linear and 1 interaction terms). Polynomial models and their representation through response surfaces are very powerful tools for optimizing and understanding the performance of many systems [20]. The significance of the initial 4 parameters model (*F*-test 95% confidence level) was checked and indicated that it was possible to simplify it to the reduced first-order polynomial model consisting of 2 linear and 1 interaction terms, described by the equation:

$$\text{RF} = 3.84 \times 10^{-3}[5\text{-HT}] + 2.03 \times 10^{-3}[5\text{-CH}_3\text{O-HT}] - 2.32 \times 10^{-4}[5\text{-CH}_3\text{O-HT}][5\text{-HT}]. \quad (2)$$

The statistical evaluation of Eq. (2) revealed that the coefficient of determination ($r^2 = 0.94$) of the fitted model explains confidently a considerable percentage of the variability of the RF. The contours of constant response generated by using Eq. (2) are depicted in Fig. 2. They represent an approximation to the true behaviour of the RF when the concentration of 5-HT and

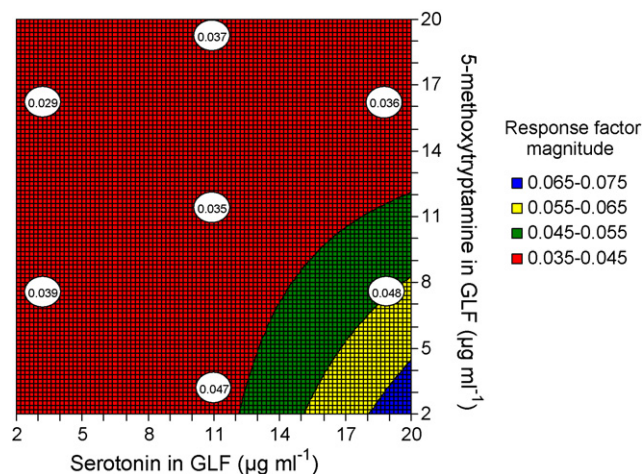


Fig. 2. Response factor contour plot estimated by using Eq. (2). The values inside the circles are the tabulated response factors calculated experimentally by using the concentration levels described in Table 1.

5-CH₃O-HT in GLF are varied simultaneously between 2 and 20 $\mu\text{g ml}^{-1}$. The delineated contours embodies regions where the RF remains constant and enables determining the optimal concentration of internal standard (5-CH₃O-HT) to be added to GLF samples. The red colour area in Fig. 2 shows that between 2 and 12 $\mu\text{g ml}^{-1}$ of 5-HT, a response factor that vary between 0.035 and 0.045 is obtained when the concentration of 5-CH₃O-HT is varied between 2 and 20 $\mu\text{g ml}^{-1}$ (the whole analytical range considered for internal standard in this study). Concentrations of 5-HT exceeding 12 $\mu\text{g ml}^{-1}$ cause a considerable variation of the RF with the concentration of internal standard and a remarkable lessening of the dynamic analytical range. For instance, the green, yellow and blue colour areas in Fig. 2, represent three different dynamic analytical ranges, namely 12–15, 15–18 and 18–20 $\mu\text{g ml}^{-1}$ of 5-HT with average RFs of 0.050, 0.060 and 0.070, respectively. By determining a wide span of analytical concentrations where the RF does not change considerably, then problem samples with unknown concentrations of 5-HT above the linear range and spiked with known concentrations of 5-CH₃O-HT can be diluted confidently into the range where RF remains constant with the concentration of the analytical species. This approach will assist the analyst in saving time and resources and avoiding further preparation, which is essential when the amount of sample is limited. The curvatures observed in Fig. 2 are the result of the interaction between 5-HT and 5-CH₃O-HT, which is ignored generally in quantification experiments, and could affect the accuracy of the determination. A visual inspection of the magnitude of experimental RFs (shown inside the white circles in Fig. 2) and the estimated RFs (see colour scale in Fig. 2) at the seven different concentration ratios of 5-HT:5-CH₃O-HT analysed, reveals clearly that the model as fitted predicts with a high degree of accuracy the experimental RFs as a function of the analytical concentrations. The estimation of concentration regions where the RF remains constant is vital in order to conform with the criteria of linearity of the detector towards the analyte and internal standard. Despite the fact that, the solution containing 0.5 $\mu\text{g ml}^{-1}$ of 5-HT and 2 $\mu\text{g ml}^{-1}$ of 5-CH₃O-HT was not considered in the

modelling of Eq. (2), the RF estimated from this solution (0.037) was similar to those predicted by the proposed model (0.040) in the analytical range 2–12 $\mu\text{g ml}^{-1}$ 5-HT, suggesting the robustness of the RF at low concentrations of 5-HT. The lower level of internal standard concentration (2 $\mu\text{g ml}^{-1}$) estimated from Fig. 2 was used for subsequent quantitative analyses of 5-HT in GLF samples collected from patients.

3.3. Traditional versus proposed method comparison

Studies on how simultaneous variations of the analyte and the internal standard affect RF and consequently the quantification process need to be undertaken, regardless of instrumental technique. The traditional method used for this purpose, the one-at-the-time methodology, is a tedious procedure that can give a wrong representation of the behaviour of the relationship analyte/internal-standard if there is a second-order interaction effect. A weak point in the majority of the literature on quantification is that it does not deal sufficiently with the strategies behind the selection of a particular amount of internal standard especially in cases where the analyte can have a wide span of concentrations.

This section intends to demonstrate that the approach described in this manuscript provides a distinct advantage over the more traditional approach of selecting an internal standard concentration. In this demonstration, the classical strategy of targeting the internal standard to the lower 1/3 of the working analytical range [21,22] in order to select an optimal concentration of 5-CH₃O-HT was used. A GLF sample was divided into nine equal portions and spiked in triplicates with 2, 11 and 20 $\mu\text{g ml}^{-1}$ of 5-HT at a fixed concentration of 5-CH₃O-HT (6 $\mu\text{g ml}^{-1}$) and submitted to LC–MS/MS analysis. The 5-HT/5-CH₃O-HT signal relationship at the different concentrations was recorded and regressed against the 5-HT/5-CH₃O-HT concentration ratios. The slope of the regression line, which represents the response factor (RF=0.052), was used to back-calculate the concentration of additional GLF test samples spiked with known concentrations of 5-HT and 6 $\mu\text{g ml}^{-1}$ of 5-CH₃O-HT. Table 2 shows the results when a RF=0.052 obtained by the classical methodology and the RF values of 0.040 and 0.050 estimated from Fig. 2 (red and green area of the graph, respectively) are

used in the calculation of the concentration of GLF test samples spiked with 10 and 15 $\mu\text{g ml}^{-1}$ of 5-HT and 6 $\mu\text{g ml}^{-1}$ of 5-CH₃O-HT. The accuracy of the results was quite low (78% on average) when the GLF sample containing 10 $\mu\text{g ml}^{-1}$ of 5-HT was analysed using the RF determined by the classical methodology (RF=0.052). However, by using this RF value a better accuracy (95% on average) was achieved at a nominal concentration of 15 $\mu\text{g ml}^{-1}$ of 5-HT. This variability in accuracy is a clear indication that the interaction between the amount of 5-HT and 5-CH₃O-HT has a strong influence on the quantitative results. It was mentioned above that the model proposed in this article allows selecting different RF values in accordance with the range of analytical concentrations investigated and the level of internal standard added. For instance, if the level of 5-CH₃O-HT is kept constant at 6 $\mu\text{g ml}^{-1}$ in Fig. 2, then it is possible to select the RF values of 0.040 (red area) and 0.050 (green area) and quantify the GLF test samples containing 10 and 15 $\mu\text{g ml}^{-1}$ of 5-HT with a high degree of accuracy (averages 103 and 100%, respectively). Table 2 shows unequivocally, that the approach described in this article provides a distinct advantage over the more traditional approach if the RF is affected by the interaction analyte/internal-standard. It is important to mention that the current literature on serotonin bears evidence that the aforementioned interaction could be a lurking factor which has been overlooked in the majority of the quantification analysis. For instance, in an investigation aimed at determining the concentration of serotonin in non-parasitic flatworms by HPLC [23], six different levels of 5-HT were prepared in triplicate at a fixed level of *N*_ω-methyl-5-HT internal standard. Although the variability of the RF was not of interest in this published study, it is possible to determine its magnitude at every concentration level by using the reported peak areas and Eq. (1) of the present article. By regressing the calculated RF against the concentration of serotonin, it is evident that the RF decreased logarithmically (RF = 1.034–0.049 × ln[5-HT]), $r^2 = 0.81$) as the concentration of serotonin was increased, indicating that among the possible variables affecting the accuracy, the interaction serotonin/internal-standard could be an important factor which was not considered and could not be estimated by the classical methodology used in this reported work. In a recent comparative study between the internal standard and

Table 2
Comparison between the response factor calculated by the classical and the proposed method in the quantification of serotonin in gut lavage fluid spiked with two different analytical concentrations and a fixed level of internal standard

GLF nominal concentration ($\mu\text{g ml}^{-1}$)		Signals (icps)		Concentration of 5-HT in the test sample ($\mu\text{g ml}^{-1}$) estimated by $[5\text{-HT}] = \frac{[5\text{-CH}_3\text{O-HT}]}{\text{RF}} \times \frac{S_{5\text{-HT}}}{S_{5\text{-CH}_3\text{O-HT}}}$			
5-HT	5-CH ₃ O-HT	5-HT	5-CH ₃ O-HT	RF=0.052 (from the classical methodology)		RF=0.040* and 0.050** (from the proposed model (Fig. 2))	
10	6	4327808	61973379	8.0	(80)	10.5*	(105)
10	6	4202876	62264834	7.7	(77)	10.1*	(101)
10	6	4228143	61875267	7.8	(78)	10.2*	(102)
15	6	7501117	61233608	14.0	(93)	14.7**	(98)
15	6	7796307	62017007	14.4	(96)	15.1**	(101)
15	6	7840061	62849956	14.3	(95)	15.0**	(100)

Values in round brackets represent percentage of accuracy.

* and ** indicate the RF values used in the calculation of [5-HT].

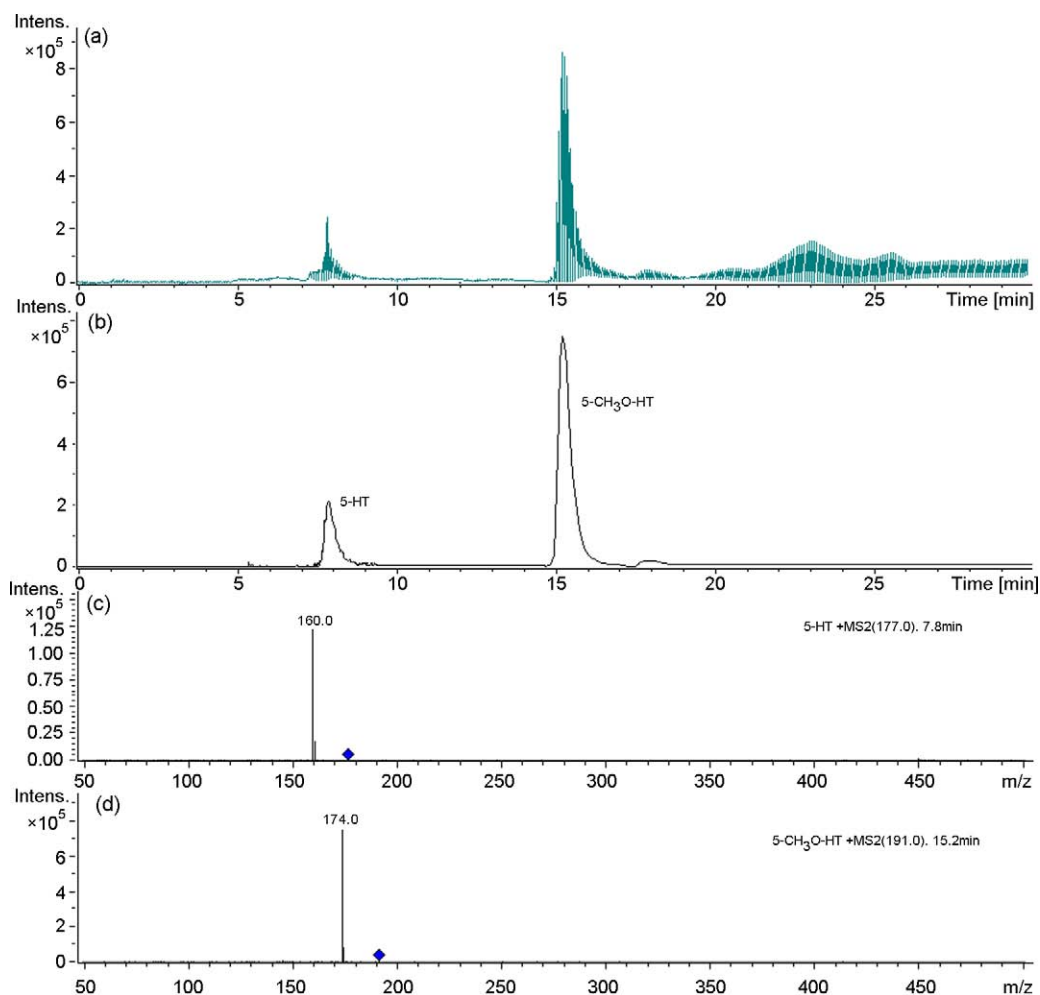


Fig. 3. (a) Representative ion chromatogram of a gut lavage fluid sample. (b) Extracted ion chromatograms at 160 and 174 m/z obtained by fragmenting $[5\text{-HT} + \text{H}]^+$ and $[5\text{-CH}_3\text{O-HT} + \text{H}]^+$ signals 177 and 191 m/z , respectively. (c) and (d) MS/MS product ion spectra for 177 and 191 m/z , respectively.

the traditional calibration method by using LC–MS/MS, it is highlighted that the degree of ionization in the electro-spray ion source is strongly dependent on the amount of molecules resulting in a non-linearity in the concentration/response ratio [24].

3.4. Gut lavage fluid quantification

The 5-HT quantification procedure applied on 6 GLF samples collected from different subjects with various gastrointestinal complaints was based on the method described in the Section 2 but using a fixed concentration of internal standard. The volume of sample was 50 μl and the concentration of internal standard selected from the model was 2 $\mu\text{g ml}^{-1}$. Six replicates of every sample were prepared and 25 μl injected and analysed. A representative ion chromatogram of one of the samples is shown in Fig. 3a. The ion chromatograms at 160 and 174 m/z obtained by fragmenting $[5\text{-HT} + \text{H}]^+$ and $[5\text{-CH}_3\text{O-HT} + \text{H}]^+$ signals 177 and 191 m/z , respectively, along with their mass spectra are shown in Fig. 3b–d. The limit of quantification and detection defined as the signal-to-noise ratio 10:1 and 3:1 were 97 and 29 ng of serotonin, respectively. The 5-HT content in the anal-

ysed GLF samples (Table 3) ranged from 0.167 to 0.367 $\mu\text{g ml}^{-1}$ with a mean of 0.258 $\mu\text{g ml}^{-1}$ and a median of 0.265 $\mu\text{g ml}^{-1}$.

The direct injection of the sample, might bring about a dependency of the 5-HT and 5-CH₃O-HT electro-spray signals on the GLF matrix which could significantly affect the signal reproducibility, detection sensitivity, and relative intensities of individual components in the sample. The recorded ion chromatograms and mass spectra revealed a significant mass discrimination and a low contribution of signals different to those of 5-HT and 5-CH₃O-HT, suggesting perhaps, that matrix effects

Table 3

Determination of serotonin in gut lavage fluid collected from different subjects with various gastrointestinal complaints

Patient	Instrumental replicates	Mean \pm S.D. ($\mu\text{g ml}^{-1}$)
1	6	0.367 \pm 0.033
2	6	0.263 \pm 0.010
3	6	0.267 \pm 0.009
4	6	0.185 \pm 0.009
5	6	0.167 \pm 0.012
6	3	0.299 \pm 0.009

S.D. = standard deviation.

are negligible at the analytical levels considered in this investigation. However, a more comprehensive study would be advisable considering that the analytical signals are the result of a competition between solvent polarity and volatility. The solvent polarity affects matrix–analytes interactions whereas solvent volatility affects the aerosol drying process.

4. Conclusions

This is the first LC–MS/MS method reported to directly measure serotonin in GLF from patients with various gastrointestinal complaints. Whether the determination of the serotonin levels in GLF will be useful as an indicator of condition or pathophysiology of the gastrointestinal tract remains to be shown.

The experimental design implemented enables to estimate the optimal amount of internal standard in quantification experiments and assess the significance of the polynomial terms as potential sources of uncertainty by performing a minimum of 7 experiments. The degree of information obtained with this minimum number of experiments cannot be outperformed by traditional methods such as the one-at-the-time strategy. Modelling and visualising a process under study are important tools that can assist the experimenter in analysing and interpreting complex experimental arrangements and data. Unfortunately, such tools are generally ignored in quantitative analysis. The reader interested in the implementation of the design described in this article or other type of design is referred to a comprehensive overview on experimental design in quantification experiments using the internal standard technique by Araujo et al. [16].

Acknowledgements

The authors are indebted to the patients for their participation and Kristine Lillestøl and Ragna Anne Lind for GLF collection.

References

- [1] M.D. Coates, C.R. Mahoney, D.R. Linden, J.E. Sampson, J. Chen, H. Blaszyk, M.D. Crowell, K.A. Sharkey, M.D. Gershon, G.M. Mawe, P.L. Moses, *Gastroenterology* 126 (2004) 1657.
- [2] R.J. Gilkin, *Clin. Ther.* 27 (2005) 1696.
- [3] R.J. Dearman, R.A. Skinner, N. Deakin, D. Shaw, I. Kimber, *Toxicology* 206 (2005) 195.
- [4] O. Nylander, L. Pihl, *Acta Physiol.* 186 (2006) 45.
- [5] D. Grundy, *J. Physiol.* 575 (2006) 1.
- [6] I.P. Kema, A.M.J. Schellings, C.J.M. Hoppenbrouwers, H.M. Rutgers, E.G.E. de Vries, F.A.J. Muskiet, *Clin. Chim. Acta* 221 (1993) 143.
- [7] S. Sasa, C.L. Blank, *Anal. Chim. Acta* 104 (1979) 29.
- [8] J.P. Danaceau, G.M. Anderson, W.M. McMahon, D.J. Crouch, *Anal. Toxicol.* 27 (2003) 440.
- [9] D. Bose, A. Durgbanshi, M.E. Capella-Peiró, M. Gil-Agustí, J. Esteve-Romero, S. Carda-Broch, *J. Pharm. Biomed. Anal.* 36 (2004) 357.
- [10] K.L. Locker, D. Morrison, A.P. Watt, *J. Chromatogr. B* 750 (2001) 13.
- [11] R.D. Johnson, R.J. Lewis, D.V. Canfield, C.L. Blank, *J. Chromatogr. B* 805 (2004) 223.
- [12] R.J. Slingerland, A.B.P. Van Kuilenburg, J.M. Bodlaender, H. Overmars, P.A. Voûte, A.H. Van Gennip, *J. Chromatogr. B* 716 (1998) 65.
- [13] P. Pastore, G. Favaro, D. Badocco, A. Tapparo, S. Cavalli, G. Saccani, *J. Chromatogr. A* 1098 (2005) 111.
- [14] M. Ruth, R.M. Williams, L. Bauce, W. Robert, R.W. Lea, J. Singh, A. Keith, K.A.S. Sharkey, *J. Autom. Nervous Syst.* 61 (1996) 37.
- [15] T. Huang, P. Kissinger, *Curr. Sep.* 14 (1996) 114.
- [16] P. Araujo, F. Couillard, E. Leirnes, K. Ask, A. Bøkevoll, L. Frøyland, *J. Chromatogr. A* 1121 (2006) 99.
- [17] A. Berstad, G. Arslan, G. Folvik, *Scand. J. Gastroenterol.* 1 (2000) 64.
- [18] D.H. Doehlert, *Appl. Stat.* 19 (1970) 231.
- [19] <http://www.picra.org/profiles/BASi.html>.
- [20] S.N. Deming, S.L. Morgan, *Experimental Design: A Chemometric Approach*, first ed., Elsevier, Amsterdam, 1987, p. 203.
- [21] W. Huber, A. Molero, C. Pereyra, E.M. de la Ossa, *J. Chromatogr. A* 715 (1995) 333.
- [22] Ion Source, <http://www.ionsource.com/tutorial/msquan/is.htm> (accessed November 2007).
- [23] S. Umeda, G.W. Stagliano, M.R. Borenstein, R.B. Raffa, *J. Pharmacol. Toxicol. Methods* 51 (2005) 73.
- [24] L.B. Nilsson, G. Eklund, *J. Pharm. Biomed. Anal.* 43 (2007) 1094.

Analytical advances in butyl-, phenyl- and octyltin speciation analysis in soil by GC-PFPD

Julien Heroult^{a,*}, Tea Zuliani^a, Maïté Bueno^a, Laurence Denaix^b, Gaëtane Lespes^a

^a *Equipe de Chimie Analytique Bio Inorganique et Environnement, UMR 5254, Université de Pau et des Pays de l'Adour, BP 1155, F-64013 PAU Cedex, France*

^b *UMR TCEM, Equipe Biogéochimie des Eléments Traces, INRA, Centre Bordeaux Aquitaine, Avenue E. Bourleaux, BP 81, F-33883 Villenave d'ornon Cedex, France*

Received 17 July 2007; received in revised form 12 November 2007; accepted 14 November 2007

Available online 30 January 2008

Abstract

The development and validation of a method for organotin analysis in soils, including butyl-, phenyl- and octyltins, are described in this study. The influence of pretreatment step based on sample lyophilisation was first studied. Different solid–liquid extraction techniques including mechanical stirring (MSAE), accelerated solvent (ASE), microwave (MAE) and ultrasound (UAE), were compared. MSAE gave the best recoveries and repeatability and was thus chosen for OTC extraction from soils. Then, ethylation/extraction step before GC-PFPD analysis was investigated and the best derivatisation conditions were assessed in order to achieve a simple, non-expensive and reliable routine procedure. Finally, the robustness of the method was tested by the analysis of several soils with different organic matter content allowing the validation of developed protocol. The method appears to be reliable and accurate for the OTC determination in a broad range of soils.

© 2007 Elsevier B.V. All rights reserved.

Keywords: Organotin compounds; Soil; Extraction; Speciation analysis; GC-PFPD

1. Introduction

For the last 30 years, organotin compounds (OTC) have been used for industrial, agricultural or domestic applications as fungicide, bactericide, insecticide, wood preservative or PVC stabilisers. Consequently, they have entered various ecosystems, being present in waters [1,2], sewage sludges [3,4], landfill leachates [5,6], sediments [7,8] and soils [9–11]. In agricultural soils, several sources of contamination have been identified. OTC may be introduced from the spreading of OTC-contaminated sludge [1], pulverization of biocide products [12], irrigation by OTC-contaminated water [13] or atmosphere deposition [10]. Their high toxicity for terrestrial and aquatic life is today recognized [9,14,15]. Some of them, i.e. tributyltin compounds, have been included in the European list as priority water pollutants [16].

Organotins behaviour has been extensively studied in marine environments [2,17,18], comparatively, only few results are reported concerning organotins in soils. Presence of butyl- and phenyltins up to 20–100 $\mu\text{g}(\text{Sn})\text{kg}^{-1}$ in soils has been mentioned [9,10,19–22]. Moreover analytical details related to development and validation of speciation methods for OTC determination in soil samples are generally not available in the literature. Some methods are reported but they are not applied for simultaneous OTC determination including butyl-, phenyl- and octyltins, or do not allow to reach satisfactory analytical performances for all the analytes [19–21]. Usually, same analytical procedure as for sediments is applied to soil samples, even though the matrices differ [19]. Most of time, recoveries, extraction yield and method accuracy are not evaluated with soil samples but with CRM sediments. Thus, the applicability of the analytical method cannot be justified to soil samples but only to sediment ones.

A pretreatment is necessary to prepare solid samples before analysis. Lyophilisation is often applied, allowing sample homogenization and ensuring improvement of analytical performances such as extraction yield or repeatability [8,10].

* Corresponding author. Tel.: +33 559 407 667; fax: +33 559 407 674.
E-mail address: jheroult@etud.univ-pau.fr (J. Heroult).

Then, analytes have to be extracted from the solid matrix. Mechanical stirring (MSAE) has been usually employed to accelerate extraction process [22–25], resulting in efficient, simple and non-expensive procedure. Accelerated solvent extraction (ASE) [26,27], microwave (MWAE) [6,25,28] and ultrasonic (UAE) assisted extractions [29,30] are also frequently used for butyltins extraction. They lead to a faster butyltins extraction but are seldom applied for simultaneous phenyl- and octyltins extraction. Recently, modern extraction techniques as solid-phase extraction (SPE) [31–33], solid-phase microextraction (SPME) [8,34], supercritical fluid extraction (SFE) [20,35] or molecularly imprinted solid-phase extraction (MISPE) [36,37] have been developed for organotin compound analysis [38]. Most of these techniques cannot be directly used for OTC extraction from solid samples [8,31–34,36,37]. Besides, they still need to be optimised to allow a satisfactory extraction of the whole OTC [20,36]. Some of these techniques can be used as a preconcentration step [31,36] or can be hyphenated to enhance the selectivity of the extraction and hence the performance of the analytical method (notably detection limit) [37].

Usually, OTC speciation analysis is performed via coupling between a separation technique, i.e. high performance liquid chromatography (HPLC) [39,40] or gas chromatography (GC) [41,42], with a specific detector such as pulsed flame photometric detector (PFPD) [2,24,42], atomic absorption (AAS) [43,44] or emission (AES) [45,46] as well as inductively coupled plasma mass spectrometry (ICP-MS) [6,47]. However GC-based couplings are widely used as they provide highly sensitive method. Among the different hyphenation possibilities, GC-PFPD offers a good compromise between analytical cost and satisfactory sensitivity and selectivity [48]. GC-based analysis involves a derivatisation step to convert dissolved OTC into volatile forms suitable for GC separation. The procedure commonly used is based on simultaneous ethylation by sodium tetraethylborate (NaBEt_4) and liquid–liquid extraction (LLE) with isooctane, as previously developed and validated [18,23,49].

OTC determination in soil samples is exposed to analytical difficulties, resulting from soil composition and the high heterogeneity between soils (differences in composition, pH or concentration in organic matter). Soil composition can lead to lower OTC extraction yield by inhibiting ethylation or isooctane extraction [19,24]. Besides, no analytical method for simultaneous OTC determination in soils has been still standardised or no exhaustive evaluation of such a method is available in the literature.

This paper focuses on the development of a simple, accurate and robust analytical method for the simultaneous determination of nine OTC in soils in order to be used as a routine procedure. This work is included in a current standardisation process and investigates from pretreatment sample to quantification. The benefit of lyophilisation was evaluated, and four extraction techniques, i.e. mechanical stirring (MSAE), accelerated solvent (ASE), microwave (MAE) and ultrasonic (UAE) were compared. Derivatisation conditions and quantification procedure were also optimised to enable the

cheapest and most repeatable process. Finally, robustness and accuracy were estimated in order to validate the analytical protocol.

2. Materials and methods

2.1. Instrumentation

A Varian 1079 split/splitless temperature programmable injector and a Varian 3800 gas chromatograph (Palo Alto, CA, USA) equipped with a pulsed flame photometric detector (PFPD) was used throughout the study. The separation was carried out on a capillary column (30 m \times 0.25 mm I.D.) coated with polydimethylsiloxane (0.25 μm film thickness) (Quadrex, New Heaven, CT, USA). Nitrogen was used as carrier gas, with a flow rate of 2 mL min^{-1} . The following temperature program was used to separate the nine organotin compounds: the column temperature was held at 80 $^\circ\text{C}$ for the first minute, increased to 160 $^\circ\text{C}$ at the rate of 10 $^\circ\text{C min}^{-1}$, then to 270 $^\circ\text{C}$ at 30 $^\circ\text{C min}^{-1}$, and finally held at this temperature for 5 min. The PFPD operating conditions were optimised elsewhere [50]. Briefly it was operated at 350 $^\circ\text{C}$ with an air/hydrogen flame. The gas flow rates were 23.4, 28.5 and 26.4 mL min^{-1} for Air 1, Air 2 and H_2 , respectively.

A Dionex ASE 200 (Sunnyvale, CA, USA) equipped with a solvent controller was used for accelerated solvent extraction from solid samples. Microwave assisted extraction was carried out with an open focused vessel microwave oven Prolabo A301 (Fontenay Sous Bois, France) and a Transsonic Digital S Elma (Singen, Germany) bath was used for ultrasonic extraction. Mechanical stirring was achieved on an elliptical table Fisher Bioblock Scientific (Illkirch, France).

2.2. Reagents and standards

Monobutyltin trichloride (MBT, 95%), dibutyltin dichloride (DBT, 96%), tributyltin chloride (TBT, 96%), triphenyltin chloride (TPhT, 95%), mono-octyltin trichloride (MOcT 97%), dioctyltin dichloride (DOcT 97%) and trioctyltin chloride (TOcT 95%) were purchased from Aldrich (Milwaukee, WI, USA). Monophenyltin trichloride (MPhT, 98%), diphenyltin dichloride (DPhT, 96%) and tripropyltin chloride (TPrT, 98%) were obtained from Strem chemicals (Bischoffshausen, France). Organotin stock solutions (1000 mg (Sn) L^{-1}) were prepared in methanol. Stored at +4 $^\circ\text{C}$ in the dark, they were stable for 1 year. Working standards solutions (10 mg (Sn) L^{-1}) were prepared weekly from stock standard solutions by dilution in Milli-Q water (18.2 M Ω) (Millipore, Bedford, MA, USA). Working 100 μg (Sn) L^{-1} standard solutions were prepared daily. They were also stored at +4 $^\circ\text{C}$ in the dark.

Nitric (65%) and ethanoic (99–100%) acids, sodium acetate (99%), ammonia (30%) and methanol (99.8%) were purchased from Atlantic Labo (Eysines, France). Isooctane was obtained from Fluka Chemie GmbH (Buchs, Switzerland). Sodium tetraethylborate (NaBEt_4 , min 98%) were purchased from Strem Chemicals (Bischoffshausen, France). NaBEt_4 was dissolved in Milli-Q water to provide a 2% (m/v) ethylating solution.

Glassware was rinsed with Milli-Q water, decontaminated for 7 days in 10% (v/v) nitric acid solution and then, rinsed three times again with water.

2.3. Soil samples

The soil samples used in this study, in optimisation and validation parts, were collected at the INRA Pierroton Experimental Unit, near Bordeaux (France), from the ploughed layer of a dense podzol [51]. This soil is sandy, acid (pH 4.6) and organic (4% total organic carbon). The 0–25 cm surface depth layer was collected and sieved (2 mm). The moisture level was 13% and it was found to be OTC-free.

Three additional soil samples were used in the last part of this work. The first one was clay-rich, poor in organic matter (0.9% total organic carbon) and with acidic pH (pH 3.5) [52]. The second one was slightly acid (pH 5.9), the third one slightly basic (pH 7.5) and both of them were very rich in organic matter (respectively 12.6 and 17% total organic carbon). All the soils showed to be under OTC limits of detection of applied analytical procedure. They were dried after collection and stored at +4 °C until analytical use.

2.4. Analytical procedure

The soil samples used for the optimisation of the analytical procedure were spiked in the range 0–200 $\mu\text{g (Sn) kg}^{-1}$.

2.4.1. Extraction from soil samples

2.4.1.1. Mechanical stirring and ultrasonic assisted extractions. Experimental conditions previously optimised for sediments were expanded to soil samples when extraction was assisted by mechanical stirring or ultrasound [23]. Briefly, 1 g of soil sample was precisely weighted and introduced in a capped 50 mL polycarbonate tube with 10 mL of ethanoic acid. When mechanical stirring was used (stirring rate adjusted to 400 rpm), the mixture was shaken during 15 h in the dark. When sonication was used, the mixture was placed into ultrasonic bath, under a 40 kHz frequency, during 5 or 30 min. Then, suspension was centrifuged at 4000 rpm for 15 min.

2.4.1.2. Accelerated solvent extraction. The ASE operating conditions were as follow [53]: 1 g of soil sample was mixed with 10 g of quartz sand and introduced in 11 mL stainless steel extraction cell. The cell was then transferred to the oven and automatically sealed under pressure. It was filled with extraction solution (20–21 mL of a 85% methanol/15% acetic acid mixture), heated and pressurized. After the set temperature was reached, the cell was held in the oven at constant temperature (100 °C) and pressure (90 bars). Extract was collected in a septum-topped 30 mL vial and the cell was flushed and purged by nitrogen gas. Three extraction cycles were runned per sample.

2.4.1.3. Microwave assisted extraction. A method previously optimised for organotins extraction from sediments and biological samples was expanded to soil samples [28]: 1 g of soil sample was mixed with 10 mL of ethanoic acid in the extraction

vessel. The mixture was placed in the open microwave cavity and extracted for 2 min at 20% of irradiation power (40 W). The sample was then cooled at room temperature and further introduced in a capped 50 mL polycarbonate tube for centrifugation at 4000 rpm for 15 min.

2.4.2. Derivatisation and extraction by isoctane

The derivatisation step involves the ethylation of organotins to obtain thermally stable volatile tetrasubstituted species for GC separation [17,50]. Briefly, 1 mL of the raw soil extract was introduced into the derivatisation reactor. Ethylation/extraction was performed in 20 mL of sodium ethanoate/ethanoic acid buffer (pH 4.8) with 0.2–1 mL of sodium tetraethylborate (NaBEt_4) (2% (w/v)) and 1 mL of isoctane. The mixture was shaken mechanically at 400 rpm on an elliptical table for 30 min. Organic phase (isoctane containing ethylated OTC) was separated from aqueous one for GC-PFPD analysis (2 μL injected).

2.4.3. Quantification

OTC quantification was performed by standard addition calibration method. TPrT was used as internal standard (I.S.) and added at 100 $\mu\text{g (Sn) kg}^{-1}$ level to soil sample before extraction procedure. OTC standards were added to soil sample either before extraction or after, i.e. into the acetic acid soil extract.

3. Results and discussion

3.1. Optimisation and validation

3.1.1. Pretreatment

3.1.1.1. Lyophilisation. Two aliquots of soil were individually spiked with TBT (70 $\mu\text{g (Sn) kg}^{-1}$ dry weight) or TPhT (50 $\mu\text{g (Sn) kg}^{-1}$ dry weight) as possible degradation due to lyophilisation could be readily detected for trisubstituted OTC [9]. Each spiked soil aliquot was divided into two sub-samples: the first one was directly submitted to mechanical stirring assisted extraction (MSAE), the second one was lyophilised for 16 h before MSAE. For each analysis, 3 extractions and 2 analyses per extraction were performed to ensure significant data. Results obtained from lyophilised and non-lyophilised samples are reported in Fig. 1. Mean values obtained for TBT and TPhT concentrations (dotted line in Fig. 1) are 66 ± 5 and $48 \pm 8 \mu\text{g (Sn) kg}^{-1}$ in lyophilised samples, respectively, and 66 ± 7 and $46 \pm 6 \mu\text{g (Sn) kg}^{-1}$ in non-lyophilised ones, indicating that no degradation of trisubstituted OTC occurred during lyophilisation. Moreover TBT and TPhT degradation products, i.e. DBT and MBT or, DPhT and MPhT, were never detected for both lyophilised and non-lyophilised sub-samples.

The repeatability (evaluated by Relative Standard Deviation, RSD) of the whole analytical process, i.e. from sample pretreatment to analysis, was calculated in the range 7.5–15% depending on the species for lyophilised samples, and was 10% for both species for non-lyophilised samples. Lyophilisation was expected to enhance soil samples homogenization and hence analytical repeatability. Nevertheless, it did not appear to improve repeatability, which was satisfactory without such pretreatment step. Finally, as lyophilisation did not show to have

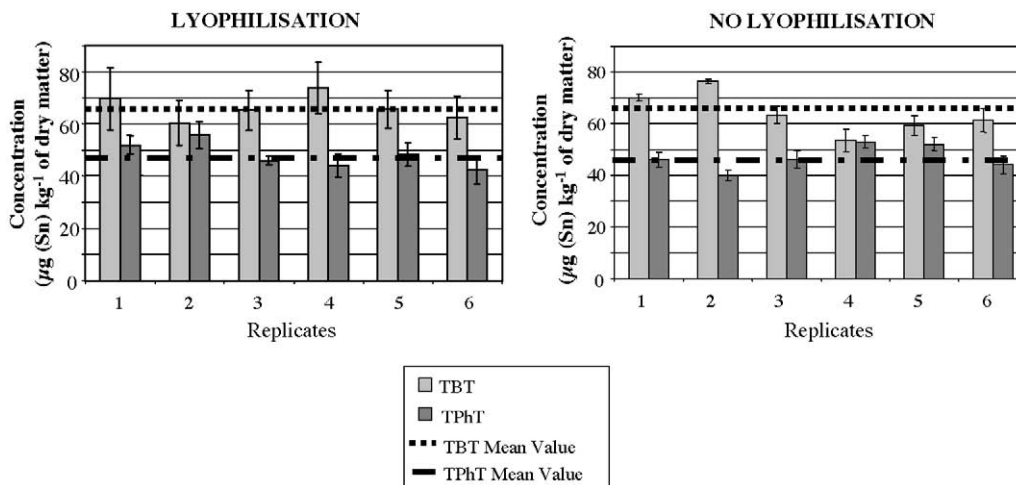


Fig. 1. Compared OTC quantification from lyophilised and non-lyophilised soil samples.

any effect neither on extraction quantitativity nor quality (i.e. respect of speciation and repeatability) it was not used later on.

3.1.1.2. *Extraction procedures.* Mechanical stirring (MSAE), accelerated solvent (ASE), microwave (MWAE) and ultrasonic (UAE) assisted extractions were compared in terms of accuracy, repeatability, limits of detection (LOD) and quantification (LOQ). The 9 OTC of interest, i.e. monobutyltin (MBT), dibutyltin (DBT), tributyltin (TBT), monophenyltin (MPHT), diphenyltin (DPHT), triphenyltin (TPhT), monoocetyl tin (MOcT), dioctyltin (DOcT) and trioctyltin (TOcT) were studied. Accuracy has been evaluated by the mean of OTC recoveries (Table 1). As no certified reference material is available, 50 µg (Sn) kg⁻¹ OTC spiked soil samples were used. LOD and LOQ were calculated according to IUPAC recommendations and are presented in Table 2 [54].

MSAE and ASE provide satisfactory recoveries, around 100% for all of the considered OTC, with no significant different extraction yields for the two techniques. MSAE leads to very satisfactory extraction repeatability (RSD), in the range 2–8%

except for TOcT. RSD obtained from ASE are acceptable. However, the values run from 7 to 15% depending on tin species. As a logical consequence of their highest efficiency in terms of recovery and repeatability, MSAE and ASE also present the lowest LOD and LOQ, even if the first technique gives slightly lower values than the second one.

Despite MWAE butyltins recoveries are acceptable, the values obtained for phenyl- and octyltins reflect bad extraction efficiency. Sonication leads to satisfactory recoveries with 5 min extraction time. In the case of 30 min extraction, low values are obtained for tri- and disubstituted species with poor repeatability (30–40%) for phenyl- and octyltins. More generally, recovery uncertainties obtained following MWAE and UAE are acceptable only for butyltins. Values corresponding to phenyl- and octyltins extraction, i.e. 20–40%, are not adequate for OTC spe-

Table 1
OTC recoveries (%) as a function of mechanical stirring (MSAE), accelerated solvent (ASE), microwave (MWAE) and ultrasonic (UAE) assisted extraction technique (n = 6)

	MSAE	ASE	MWAE	UAE	
				5 min	30 min
MBT	99 ± 3	82 ± 16	130 ± 10	90 ± 10	99 ± 3
DBT	106 ± 2	103 ± 7	90 ± 10	108 ± 6	72 ± 4
TBT	115 ± 5	108 ± 12	70 ± 20	120 ± 20	70 ± 8
Σ Butyltin	107 ± 3	98 ± 10	97 ± 10	107 ± 7	80 ± 7
MPHT	98 ± 3	72 ± 17	460 ± 30	110 ± 30	223 ± 20
DPHT	112 ± 7	120 ± 15	23 ± 5	104 ± 20	60 ± 10
TPhT	100 ± 7	103 ± 11	12 ± 3	110 ± 20	70 ± 40
Σ Phenyltin	103 ± 6	98 ± 10	165 ± 20	108 ± 20	118 ± 20
MOcT	101 ± 3	103 ± 12	80 ± 20	118 ± 5	90 ± 20
DOcT	108 ± 8	98 ± 10	20 ± 30	150 ± 20	40 ± 30
TOcT	93 ± 18	92 ± 14	160 ± 110	110 ± 40	190 ± 30
Σ Octyltin	101 ± 10	98 ± 10	90 ± 50	126 ± 20	110 ± 30

Table 2
Compared limits of detection (LOD) and quantification (LOQ) (µg (Sn) kg⁻¹) as a function of mechanical stirring (MSAE), accelerated solvent (ASE), microwave (MWAE) and ultrasonic (UAE) assisted extraction technique

		MSAE	ASE	MWAE	UAE	
					5 min	30 min
MBT	LOD	3	5	10	28	5
	LOQ	7	11	23	59	10
DBT	LOD	5	4	8	24	223
	LOQ	11	9	20	50	47
TBT	LOD	4	6	13	24	62
	LOQ	10	14	30	51	127
MPHT	LOD	3	6	35	40	26
	LOQ	8	13	80	84	54
DPHT	LOD	4	8	16	31	71
	LOQ	9	18	36	67	146
TPhT	LOD	4	4	28	26	72
	LOQ	9	10	64	55	148
MOcT	LOD	5	7	19	21	54
	LOQ	12	16	45	44	111
DOcT	LOD	5	8	36	31	77
	LOQ	12	19	83	66	158
TOcT	LOD	4	6	98	38	45
	LOQ	10	15	228	81	88

ciation analysis in soil. These different observations are clearly the result of important organotin degradation during MWAE and UAE, leading to monosubstituted OTC recoveries significantly above 100% while di- and trisubstituted OTC recoveries are all below 90%. Organometallic degradation (TBT, DPhT, TPhT and organomercuries) during UAE and MWAE extractions has been already reported in the literature [19,29]. In the case of organotins, the fast temperature increase of extracting solution induces desalkyl- and desarylations of analytes, especially the most thermolabile, i.e. trisubstituted ones, which is in agreement with the present results. Due to this significant degradation, microwave and ultrasonic extractions do not provide satisfactory results, with LOD and LOQ being between 2 and 10 times higher than those obtained after MSAE and ASE. These values are not convenient with regard to low-contaminated soil samples.

From these results, mechanical stirring assisted extraction appears to provide reliable simultaneous extraction of the nine OTC under study, as it showed higher extraction yields with suitable repeatability and preservation of the original speciation. So, to complete this study, MSAE robustness was evaluated according to the definition proposed by Green [55]. Extraction times of 7, 9, 11, 13 and 15 h were tested on soil samples spiked with TBT and TPhT at 10 and 50 $\mu\text{g (Sn) kg}^{-1}$. No influence of extraction time was observed neither on extraction yield nor repeatability in the studied range. Moreover, TBT and TPhT degradation products were never detected whatever be extraction time. An extraction time of 15 h was finally chosen for convenience as it allows extraction running during a whole night.

According to all these results, MSAE procedure was selected and thus applied later on in this study.

3.1.2. Derivatisation

OTC determination in complex environmental matrices following derivatisation with NaBEt_4 can suffer from interferences, which are mainly due to natural organic matter [19,24,56,57]. In order to detect such problems during derivatisation in soil extracts and have a reliable analysis, a convenient added amount of NaBEt_4 has to be determined. The influence of added volume of NaBEt_4 solution was thus studied to determine the best compromise between analysis cost and ethylation yield, this parameter being evaluated by recoveries. Soil sample was spiked with the nine OTC in high concentration in soil, i.e. 200 $\mu\text{g (Sn) kg}^{-1}$ (for the whole OTC, corresponding to $1.5 \times 10^{-9} \mu\text{mol (Sn) mL}^{-1}$ in the soil extract) which is twice the maximum contamination ever reported in soils [11]. Volumes of 200, 500 and 1000 μL of 2% NaBEt_4 aqueous solution, equivalent to 27, 67 and 133 μmol , respectively, were added to 1 mL soil extract. Results are presented in Fig. 2 pointing out the difference of OTC behaviour according to their substitution degree, as previously mentioned in the literature [58,59]. For trisubstituted species similar ethylation yields are obtained whatever the NaBEt_4 added volume. On the contrary, recoveries of mono- and di-substituted species are highly dependent on the amount of NaBEt_4 added: a significant enhancement of di- and monosubstituted OTC yields is observed when NaBEt_4 solution volume is increased from 200 to 500 μL . For a larger volume, i.e. 1000 μL , recoveries slightly or not significantly increase.

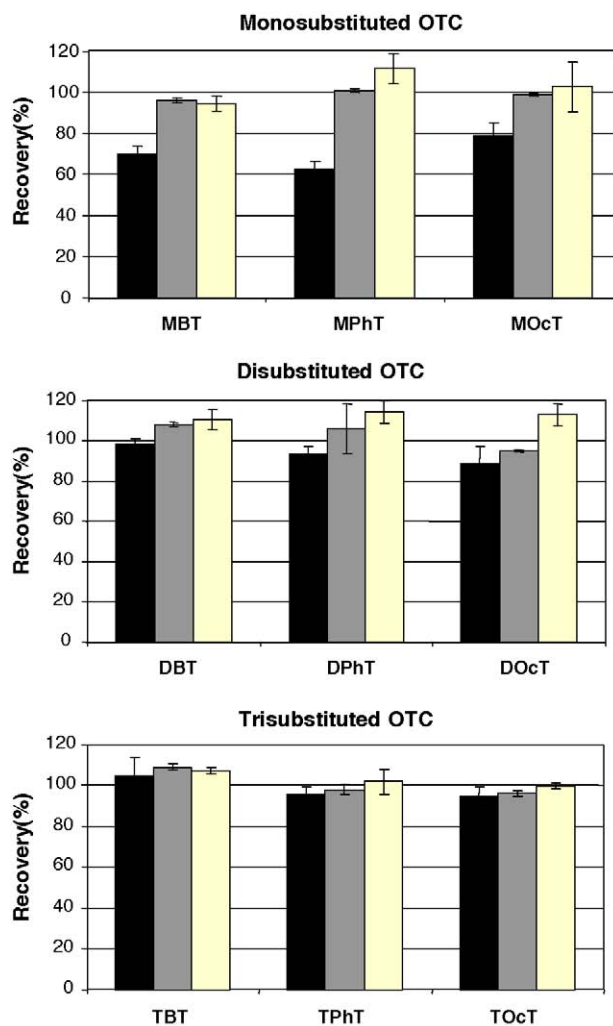


Fig. 2. Influence of added volume of 2% NaBEt_4 solution on OTC GC-PFPD signal. (■) $V = 200 \mu\text{L}$, (■) $V = 500 \mu\text{L}$ and (■) $V = 1000 \mu\text{L}$.

Ethylating yield appears to depend on NaBEt_4 amount according to substitution degree if this amount is not sufficiently in excess. However, all added volumes of 2% NaBEt_4 solution a priori correspond to a very large excess ($\text{NaBEt}_4/\text{OTC}$ ratio around $(9\text{--}44.4) \times 10^9$ by considering the stoichiometric of the reaction). Several reasons could explain these observations and have to be considered. The first one is the consumption of NaBEt_4 by organic matter (OM) coextracted with OTC, as previously noticed by several authors [19,24]. Other hypothesis lies on complexes formed between OM and OTC [24,57,60,61]. The presence of these complexes could decrease the ethylation reaction quantitatively. By using a large excess of NaBEt_4 , the reaction equilibrium could be shifted to the formation of ethylated OTC, leading to a satisfactory reaction quantitatively.

Finally, a 500 μL NaBEt_4 volume was selected for this type of sample, as a compromise between analysis cost and ethylating yield.

3.1.3. Analytical performances

OTC quantification can be performed by calibration curve-based method, adding OTC standards either into the soil sample,

Table 3

Comparison of analytical performances as a function of quantification method (LOD and LOQ in $\mu\text{g (Sn) kg}^{-1}$)

	Standard addition into soil sample				Standard addition into soil extract			
	LOD	LOQ	Recovery ^a (%)	R ²	LOD	LOQ	Recovery ^a (%)	R ²
MBT	4	10	96 ± 2	0.997	3	7	98 ± 3	0.997
DBT	4	10	108 ± 2	0.996	5	11	106 ± 2	0.992
TBT	7	16	109 ± 5	0.994	4	10	115 ± 5	0.995
MPhT	5	11	101 ± 3	0.993	3	8	98 ± 3	0.991
DPhT	4	9	106 ± 7	0.994	4	9	112 ± 7	0.993
TPhT	5	12	98 ± 6	0.996	4	9	100 ± 7	0.992
MOcT	5	11	97 ± 4	0.996	5	11	101 ± 3	0.980
DOcT	4	9	95 ± 4	0.996	5	12	108 ± 8	0.923
TOcT	4	10	96 ± 8	0.995	4	10	93 ± 18	0.880

^a Mean recovery and standard deviation from 3 different spiked concentrations (10, 50 and 100 $\mu\text{g (Sn) kg}^{-1}$, ($n = 14$)).

i.e. before extraction, or into soil extract. Both addition methods were compared in order to evaluate their accuracy in terms of LOD, LOQ and precision. This last parameter was estimated by both determination coefficient (R^2) of calibration curves and recovery uncertainty. The results are presented in Table 3.

For most OTC, analytical performances (i.e. LOD, LOQ or recoveries) obtained with both quantification methods are very similar, no statistically significant difference appearing. Only for DOcT and TOcT species, quantification based on standard additions onto soil sample seems to lead to better precision.

This quantification method was thus chosen for following applications.

3.2. Applicability to soils with varying organic matter content

Because there is no reference soil certified for its OTC content available, three OTC-free soils with different organic content were analysed after spiking with the nine OTC of interest. Six replicates were made to ensure significant data. The operating conditions and quantification method used were those previ-

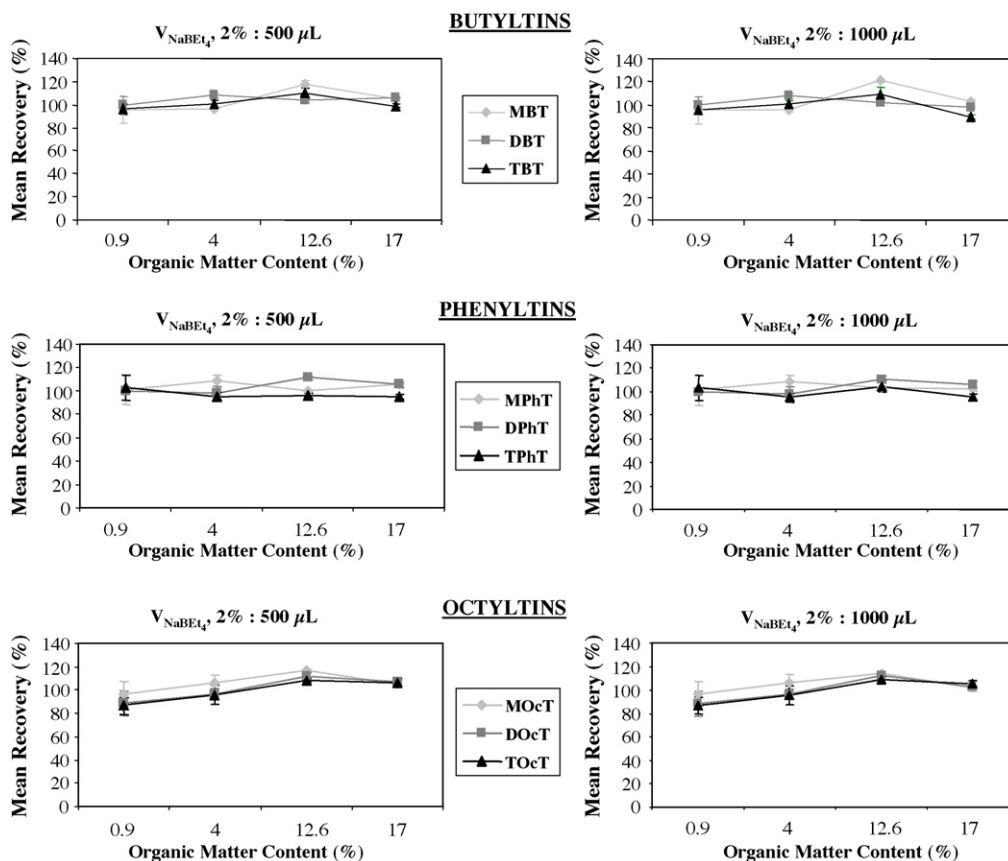


Fig. 3. OTC recoveries as a function of soil organic matter percentage.

ously selected in this work. However, as OTC ethylation has shown to be highly dependent on the organic matter content, different NaBEt₄ amounts (500 and 1000 μL of a 2% aqueous solution) were used in order to check the operating conditions previously selected. Thus, for both ethylating reagent amounts, OTC recoveries were studied as a function of soil organic matter content. Results were compared to those obtained with the soil used previously in this study and are presented in Fig. 3.

For the whole soils considered, OTC recoveries and repeatability remain satisfactory whatever the ethylating reagent quantity be. Thus, a 500 μL volume of a 2% NaBEt₄ solution was confirmed to be sufficient for a complete OTC ethylation.

Repeatability and recoveries of butyl- phenyl- and octyltins remain satisfactory for the whole range of studied soils. Variation of the organic matter content in range from 0.9 to 17% does not seem to prevent from a suitable OTC analysis in soils. The current method appears to be very reliable, sensitive, accurate and robust for OTC determination in various types of soils.

4. Conclusion

An analytical protocol has been defined and proposed in order to determine OTC speciation in soil samples in routine use. Lyophilisation appeared to be not necessary as pretreatment before extraction. Compared to accelerated solvent, microwave and ultrasonic assisted extractions, mechanical stirring assisted extraction with ethanoic acid showed higher extraction yields and repeatability for the nine organotins under study. A volume of 500 μL NaBEt₄ solution (2%) was found to be convenient whatever soil organic matter content in the range 0.9–17%. Quantification based on standard additions before extraction led to the best compromise between sensitivity and accuracy.

The first applications of the method have demonstrated the reliability and the accuracy of the procedure for the determination of organotin compounds in a wide field of soils and appeared to be suitable for routine organotin analysis in soils.

Acknowledgements

The authors gratefully acknowledge the financial support of ADEME (Agence De l'Environnement et de la Maîtrise de l'Energie) and the regional Council of Aquitaine.

References

- [1] K. Kannan, S. Tanabe, R. Tatsukawa, *Bull. Environ. Contam. Toxicol.* 55 (1995) 510.
- [2] C. Bancon Montigny, G. Lespes, M. Potin-Gautier, *Water Res.* 38 (2004) 933.
- [3] Y.K. Chau, *Sci. Total Environ.* 121 (1992) 271.
- [4] K. Fent, *Sci. Total Environ.* 185 (1996) 151.
- [5] I. Mersowsky, R. Brandsch, J. Ejlertsson, *J. Environ. Qual.* 30 (2001) 1604.
- [6] P. Pinel-Raffaitin, P. Rodriguez-Gonzalez, M. Ponthieu, D. Amouroux, I. Le Hecho, L. Mazeas, O.F.X. Donard, M. Potin-Gautier, *J. Anal. At. Spectrom.* 22 (2007) 258.
- [7] S. Diez, M. Abalos, J.M. Bayona, *Water Res.* 36 (2002) 905.
- [8] M. Bravo, G. Lespes, I. De Gregori, H. Pinochet, M. Potin-Gautier, *J. Chromatogr. A* 1046 (2004) 217.
- [9] M. Hoch, *Appl. Geochem.* 16 (2001) 719.
- [10] J.H. Huang, D. Schwesig, E. Matzner, *Environ. Pollut.* 130 (2004) 177.
- [11] C. Marcic, I. Le Hecho, L. Denaix, G. Lespes, *Chemosphere* 65 (2006) 2322.
- [12] K. Kannan, R.F. Lee, *Environ. Toxicol. Chem.* 15 (1996) 1492.
- [13] G. Lespes, C. Marcic, I. Le Hecho, M. Mench, M. Potin-Gautier, *Electron. J. Environ. Agric. Food Chem.* 3 (2003) 365.
- [14] H. Rüdél, *Ecotoxicol. Environ. Saf.* 56 (2003) 180.
- [15] WHO World Health Organization, Concise International Chemical Assessment Document 13: Triphenyltin compounds. United Nations Environment Program—World Health Organization, Geneva, Switzerland, 1999, p. 57, ISBN 92-4-153013-8.
- [16] O.J. (Official Journal 15/12/2001). Decision no. 2455/2001/ EC of the European Parliament and of the Council, on November 2001, the 20th, establishing the list of priority substances in the field of water policy and amending Directive 2000/ 60/EC (Text with EEA relevance). L 331, 0001-0005.
- [17] C. Carlier-Pinasseau, G. Lespes, M. Astruc, *Talanta* 44 (1997) 1163.
- [18] H. Rüdél, J. Müller, J. Steinhanses, C. Schröter-Kermani, *Chemosphere* 66 (2007) 1884.
- [19] J.H. Huang, G. Ilgen, E. Matzner, *Anal. Chim. Acta* 493 (2003) 23.
- [20] V. Lopez-Avila, Y. Liu, W.F. Beckert, *J. Chromatogr. A* 785 (1997) 279.
- [21] G.I. Paton, W. Cheewasedtham, I.L. Marr, J.J.C. Dawson, *Environ. Pollut.* 144 (2006) 746.
- [22] R. Gotz, O.H. Bauer, P. Friesel, T. Herrmann, E. Jantzen, M. Kutzke, R. Lauer, O. Paepke, K. Roch, U. Rohweder, R. Schwartz, S. Sievers, B. Stachel, *Chemosphere* 67 (2007) 592.
- [23] C. Bancon-Montigny, G. Lespes, M. Potin-Gautier, *Analyst* 819 (1999) 221.
- [24] T. Zuliani, G. Lespes, R. Milacic, J. Scancar, M. Potin-Gautier, *J. Chromatogr. A* 1132 (2006) 234.
- [25] M. Monperrus, O. Zuloaga, E. Krupp, D. Amouroux, R. Wahlen, B. Fairman, O.F.X. Donard, *J. Anal. At. Spectrom.* 18 (2003) 247.
- [26] S. Chiron, S. Roy, R. Cottier, R. Jeannot, *J. Chromatogr. A* 879 (2000) 137.
- [27] C. Marcic, G. Lespes, M. Potin-Gautier, *Anal. Bioanal. Chem.* 382 (2005) 1574.
- [28] J. Szpunar, V.O. Schmitt, R. Lobinski, *J. Anal. At. Spectrom.* 11 (1996) 193.
- [29] M. Abalos, J.M. Bayona, P. Quevauviller, *Appl. Organomet. Chem.* 12 (1998) 541.
- [30] D. Nguyen Van, S.R. Krishna Muppala, W. Frech, S. Tesfalidet, *Anal. Bioanal. Chem.* 386 (2006) 1505.
- [31] H. Serra, J.M.F. Nogueira, *J. Chromatogr. A* 1094 (2005) 130.
- [32] J. Munoz, J.R. Baena, M. Gallego, M. Valcarcel, *J. Chromatogr. A* 1023 (2004) 175.
- [33] J.L. Gomez-Ariza, R. Beltran, E. Morales, I. Giradlez, M. Ruiz-Benitez, *Appl. Organomet. Chem.* 8 (1994) 553.
- [34] N. Mzoughi, G. Lespes, M. Bravo, M. Dachraoui, M. Potin-Gautier, *Sci. Total Environ.* 349 (2005) 211.
- [35] J.M. Bayona, *Trends Anal. Chem.* 19 (2000) 107.
- [36] B.K. Puri, R. Munoz-Olivas, C. Camara, *Spectrochim. Acta B* 59 (2004) 209.
- [37] M. Gallego-Gallegos, M. Liva, R. Munoz Olivas, C. Camara, *J. Chromatogr. A* 1114 (2006) 82.
- [38] C. Dietz, J. Sanz, E. Sanz, R. Munoz-Olivas, C. Camara, *J. Chromatogr. A* 1153 (2007) 114.
- [39] Y. Inoue, K. Kawabata, Y. Suzuki, *J. Anal. At. Spectrom.* 10 (1995) 363.
- [40] S. Chiron, S. Roy, R. Cottier, R. Jeannot, *J. Chromatogr. A* 879 (2000) 137–145.
- [41] J. Ruiz-Encinar, J.I. Garcia-Alonso, A. Sanz-Medel, *J. Anal. At. Spectrom.* 15 (2000) 1233.
- [42] S. Simon, M. Bueno, G. Lespes, M. Mench, M. Potin-Gautier, *Talanta* 57 (2002) 31.
- [43] Y. Cai, S. Rapsomanikis, M.O. Andreae, *J. Anal. At. Spectrom.* 8 (1993) 119.
- [44] J. Szpunar, M. Ceulemans, V.O. Schmitt, F.C. Adams, R. Lobinski, *Anal. Chim. Acta* 332 (1996) 225.
- [45] M.S. Jimenez, R.E. Sturgeon, *J. Anal. At. Spectrom.* 12 (1997) 597.

- [46] S. Aguerre, G. Lespes, V. Desauziers, M. Potin-Gautier, *J. Anal. At. Spectrom.* 16 (2001) 263.
- [47] P. Rodriguez-Gonzalez, J. Ruiz Encinar, J.I. Garcia Alonso, A. Sanz-Medel, *J. Anal. At. Spectrom.* 17 (2002) 824.
- [48] H. Jing, A. Amirav, *J. Chromatogr. A* 805 (1998) 177.
- [49] P.W. Looser, M. Berg, K. Fent, J. Mühlemann, R.P. Schwarzenbach, *Anal. Chem.* 72 (2000) 5136.
- [50] C. Bancon-Montigny, G. Lespes, M. Potin-Gautier, *J. Chromatogr. A* 896 (2000) 149.
- [51] FAO, World Reference Base for Soil Resources, ISSS-AISS-IBG, ISRIC, FAO Ed, Rome, 2001.
- [52] M. Zupancic, P. Bukovec, R. Milacic, J. Scancar, *Waste Manage.* 26 (2006) 1392.
- [53] M. Le Gac, PhD thesis, Université de Pau et des Pays de l'Adour, 2003.
- [54] J. Mocak, A.M. Bond, S. Mitchell, G. Scollary, *Pure Appl. Chem.* 69 (1997) 297.
- [55] J.M. Green, *Anal. Chem.* 68 (1996) 305A.
- [56] C. Montigny, G. Lespes, M. Potin-Gautier, *J. Chromatogr. A* 819 (1998) 221.
- [57] S. Aguerre, G. Lespes, M. Potin Gautier, *J. Chromatogr. A* 999 (2003) 61.
- [58] J. Poerschmann, F.D. Kopinke, J. Pawliszyn, *Environ. Sci. Technol.* 31 (1997) 3629.
- [59] K.C. Bowles, M.D. Tiltman, S.C. Apte, L.T. Hales, J. Kalman, *Anal. Chim. Acta* 509 (2004) 127.
- [60] C.G. Arnold, A. Ciani, S.R. Müller, A. Amirbahman, R.P. Schwarzenbach, *Sci. Technol.* 32 (1998) 2976.
- [61] M. Berg, C.G. Arnold, S.R. Müller, J. Mühlemann, R.P. Schwarzenbach, *Sci. Technol.* 35 (2001) 3151.

Chiral analysis by multivariate regression modeling of spectral data using cyclodextrin guest–host complexes—Methods for determining enantiomeric composition with varying chiral analyte concentration

Jemima R. Ingle, Kenneth W. Busch, Marianna A. Busch*

Center for Analytical Spectroscopy, Department of Chemistry & Biochemistry, Baylor University, One Bear Place #97348, Waco, TX 76798, USA

Received 3 July 2007; received in revised form 20 November 2007; accepted 22 November 2007
Available online 15 January 2008

Abstract

The determination of the enantiomeric composition of samples by chemometric modeling of UV spectral data was investigated for samples of phenylalanine and norephedrine over a total concentration range of approximately 6–9 mM using β -cyclodextrin as a chiral auxiliary. Three different methods of compensating for variation in total analyte concentration were studied, and the results of all three are compared. This study shows that total analyte concentration need not be held constant during the analysis, as in previous studies, but can be allowed to vary within a given range and still give acceptable results. The choice of method depends on the analyte, and even raw data analysis without adjustment for concentration may be sufficient in some cases. Structural differences in the analytes may contribute to the degree of success for each of the three methods.

© 2007 Elsevier B.V. All rights reserved.

Keywords: Chiral analysis; Multivariate regression modeling; Cyclodextrin guest–host complexation; Enantiomeric purity; β -Cyclodextrin

1. Introduction

Chiral molecules play an important role in many biological processes [1,2], where enantiomeric pairs often demonstrate distinctly different physiological effects. While one member of the pair may have beneficial pharmaceutical properties, the other may be ineffective or even toxic [3–5]. Because of potential problems when racemic mixtures of drugs are administered [6,7], the pharmaceutical industry has significantly increased its production of single-enantiomer drugs [8,9]. Chiral molecules are also of interest to the agricultural industry [10]. Many pesticides and herbicides are chiral, and one form may persist longer in the environment than the other [11]. Optical isomers may also have very different tastes and smells [12].

Given our increased understanding of the different roles optical isomers play in biological systems, there is a need for rapid, accurate methods of determining the enantiomeric

composition of chiral molecules [13,14]. In a review of emerging high-throughput screening methods, Finn concludes that spectroscopic methods show the most promise for rapid determination of enantiomeric purity [15,16].

In 2003, we reported a method of chiral analysis by regression modeling of spectral data (CARMSD) using ordinary UV–vis spectral data and β -cyclodextrin (BCD) for the determination of the enantiomeric purity of amino acids [17]. Since this initial report, the technique has been used by a number of other research groups employing a variety of wavelength ranges and chiral auxiliaries [18–22]. Further work in our laboratory [23–28] has extended the technique with the use of additional cyclodextrins and surfactants to show that enantiomeric composition of a variety of chiral molecules can be determined with reasonable accuracy using multivariate regression modeling of UV–vis absorption [23,25,26,28] and fluorescence [24,27] spectra. The method is robust, and calibration models remain valid for up to 6 months or longer [29].

While analytical techniques such as chromatography and capillary electrophoresis, which also use chiral auxiliaries, may offer good selectivity, specificity and linear range, they may also require lengthy separation times [30–38]. In contrast to

* Corresponding author.

E-mail address: Marianna_Busch@baylor.edu (M.A. Busch).

such techniques, CARMSD does not require separation prior to analysis. CARMSD also differs from traditional chiroptical methods because polarized light is not required [39–48]. With CARMSD, the chiral auxiliary and optically active analyte appear to form *in situ*, transient, inclusion complexes, resulting in non-covalent, diastereomeric products with different physical and spectral properties. Although the spectral differences in the UV region are small, they can be readily correlated with enantiomeric composition using standard modeling techniques such as partial-least-squares regression (PLS-1) [23].

Although CARMSD has proven successful, some of its imposed limitations could prove problematic for more realistic analytical applications. Specifically, in all of the previous studies [17,23–28,49], the total analyte concentration was held constant, while only the ratio of enantiomers changed. This limitation is impractical for more realistic analytical situations where the total analyte concentration is likely to fluctuate around an average value.

If total analyte concentration is allowed to vary, one can envision three potential methods of accounting for the variation. Method I ignores variations in total concentration, relying on the statistical analysis to sort out any variations due to enantiomeric composition in the presence of variations due to total concentration differences. Method II includes the total concentration, along with spectral data, as a variable in the statistical analysis. Method III normalizes the spectra with respect to total concentration. Provided solution absorbance adheres to Beer's Law, normalization should eliminate variations in the spectra due to concentration differences, leaving only variations due to differences in enantiomeric composition. If the total concentration of both enantiomers is not known, Beer's Law can be used with whatever statistical program is employed for the regression analysis, and the total concentration of analyte can be calculated and used to normalize the spectra. Using Beer's Law to calculate total analyte concentration eliminates the requirement that the total concentration must be known in advance in order to normalize the data.

In this paper, the feasibility of determining the enantiomeric composition of samples with varying total analyte concentration through multivariate regression modeling of UV–vis spectral data is reported, and the results of all three methods are compared. For this study, we selected two analytes and a chiral auxiliary (β -cyclodextrin) used in previous investigations [25,27,28].

The first analyte studied was phenylalanine. The L isomer of phenylalanine (Fig. 1I) is one of 20 basic structural units making up human proteins and is relatively hydrophobic due to the delocalized π -electron cloud of its aromatic ring [50]. The L isomer is also used to make aspartame, a methyl ester of the dipeptide of the amino acids L-aspartic acid and L-phenylalanine. Aspartame is marketed as an artificial non-saccharide sweetener.

The second analyte studied was norephedrine (Fig. 1II). This drug, more commonly known as phenylpropanolamine or 2-amino-1-phenyl-1-propanol, has two chiral centers and therefore four optical isomers, two of which are an enantiomeric pair and are known as norephedrine. Norephedrine is a synthetic sympa-

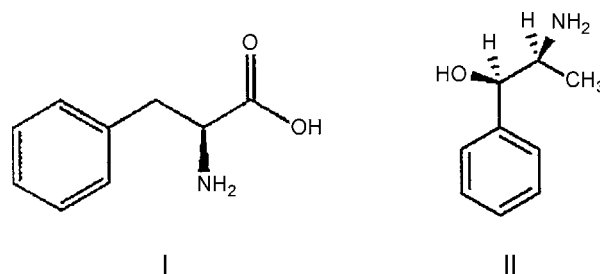


Fig. 1. Molecular structure of (I) L-(–)-phenylalanine and (II) (1*R*,2*S*)-(–)-norephedrine.

thomimetic amine, similar in structure to ephedrine and readily reduced to amphetamine. As a drug, norephedrine was used as a decongestant and an over-the-counter appetite suppressant until the 1990s, when studies indicated that it resulted in an increased risk of hemorrhagic stroke [51], especially in women. In 2000, the FDA issued a health advisory requesting drug companies to discontinue marketing products that contain any isomer of phenylpropanolamine.

2. Experimental

Enantiomerically pure D-(+)-phenylalanine, L-(–)-phenylalanine and β -cyclodextrin hydrate were obtained from Aldrich Chemical Co. and used without further modification. A stock solution of 15 mM β -cyclodextrin was prepared in deionized water by weighing the solid reagent and diluting to volume in a volumetric flask. Stock solutions of each enantiomer were prepared at five concentration levels, centered around 7.5 mM and varying $\pm 20\%$, as follows: 6.01 mM (X-Low), 6.74 mM (Low), 7.51 mM (Medium (Med)), 8.23 mM (High (Hi)), and 9.13 mM (X-High (X-Hi)). Carefully weighed quantities of each isomer were dissolved in the stock BCD solution. At each concentration level, solutions were then prepared that varied the enantiomeric composition (ϕ) in regular intervals; 20 solutions were prepared for X-Low, Low, Med and X-Hi and 10 solutions were prepared for Hi, giving a total of 90 samples.

Enantiomerically pure (1*R*,2*S*)-(–)-norephedrine and (1*S*,2*R*)-(+)-norephedrine were obtained from Aldrich Chemical Co. Stock solutions of each enantiomer were prepared at five concentration levels, centered around 7.5 mM and varying $\pm 20\%$, as follows: 6.03 mM (X-Low); 6.76 mM (Low), 7.49 mM (Med), 8.41 mM (Hi), and 9.01 mM (X-Hi). Carefully weighed quantities of each isomer were dissolved in the stock BCD solution described above. At each concentration level, solutions were then prepared that varied the enantiomeric composition (ϕ) in regular intervals; 20 solutions were prepared for the X-Low, Low and X-Hi, 19 solutions were prepared for the Med, and 10 solutions were prepared for the Hi, giving a total of 89 samples.

Spectra of the solutions were recorded with a Hewlett-Packard photodiode array UV–vis spectrometer (Model 8455) using a small-volume, 1.0-cm pathlength, quartz cell over the wavelength range of 190–1100 nm. Deionized water was used as a blank.

Spectral data were subjected to partial least-squares (PLS-1) multivariate regression analysis using The Unscrambler 7.6 (CAMO Inc., Woodbridge, NJ). Partial least squares regression (PLS-1) was performed on the spectral data using full cross validation of the calibration set. PLS-1 regression modeling is well established as an effective means of extracting information out of seemingly chaotic, uncontrolled systems by the use of statistical algorithms. In our study, PLS-1 was used to develop a mathematical model that correlates spectral data over many wavelengths with the enantiomeric composition, ϕ , expressed as a mole fraction. The process involves two steps: (1) calibration in which the computer is trained to predict ϕ from spectral data acquired for a set of samples (the calibration set) whose enantiomeric composition is known, and (2) validation in which a second, completely independent set of samples (the validation set), is analyzed over the same set of wavelengths. The statistically predicted enantiomeric compositions are then compared with known reference values obtained independently. PLS-1 has been thoroughly reviewed in earlier publications and will not be discussed further [23,52–60].

Mean-centered spectra were used in the multivariate analysis. A mean-centered plot, calculated by the Unscrambler statistical package, was obtained by first averaging the individual spectra on a wavelength-by-wavelength basis (i.e., adding the absorbances of each spectrum on a wavelength-by-wavelength basis and dividing each sum by the number of samples). This average spectrum was then subtracted from each individual spectrum on a wavelength-by-wavelength basis to give mean-centered spectra. Mean-centered spectra were useful in determining wavelengths in the spectrum that varied the most among different samples and were used as a guide in choosing spectral ranges that were the most likely candidates for PLS-1 analysis. In most cases, several wavelength ranges or combinations of wavelength ranges were tested in the calibration phase, and the range or ranges giving the lowest error were chosen for the analysis. Normalized spectra were calculated by dividing individual spectra by the total analyte concentration prior to mean centering.

A random number generator was used to select out a total of 20 samples from all five concentration levels. These 20 samples were used as the validation set, and the remaining samples were used as a calibration set. Regression models in the calibration phase were developed without the 20 samples in the validation set. The models were then used to predict the enantiomeric composition of the validation set, and the predicted values were compared with the known values as a measure of the predictability of the model.

The test of any regression model with CARMSD is its ability to accurately predict the enantiomeric composition of future samples. Both RMS absolute error and RMS percent relative error are reported. Because these samples have a very limited range, 0–1 mole fraction, RMS percent relative error can artificially make samples with a higher mole fraction, ϕ , appear more correct. Consequently, although both are reported, the RMS absolute error is preferred when making comparisons between different experimental protocols.

3. Results and discussion

3.1. Compliance with Beer's Law

In order for spectral normalization (Method III) and prediction of total analyte concentration to be successful, the analytes must obey Beer's Law. Data at four wavelengths (phenylalanine: 230, 252, 258 nm; norephedrine, 257 nm) were obtained, with and without BCD present, to demonstrate that this requirement was satisfied. Both analytes, with and without BCD, gave excellent correlations of 0.999 or better (ideal value of 1.000). The slopes at each wavelength, with and without BCD, were nearly identical, but the presence of the chiral auxiliary caused a distinct upward shift in the offset.

3.2. Studies with phenylalanine

Phenylalanine has one chiral center, is known to complex with β -cyclodextrin and has been studied by various analytical techniques [61–65]. Published studies report evidence for the formation of an inclusion complex, with the guest molecule penetrating inside the cavity in a 1:1 ratio [66–68]. This complexation is thought to form primarily through hydrophobic interactions between the cavity and the aromatic ring of the amino acid.

3.2.1. Method I: no correction for variation in concentration

In Method I, the spectral data from all five concentration levels were mean centered and then used without further modification in the regression model. Prior to regression modeling, the UV absorption spectra of all 90 solutions of phenylalanine containing a fixed BCD concentration (15 mM) were recorded over the wavelength range 220–300 nm, and the results are shown in Fig. 2.

These spectra represent five different concentration levels of phenylalanine having varying enantiomeric compositions within

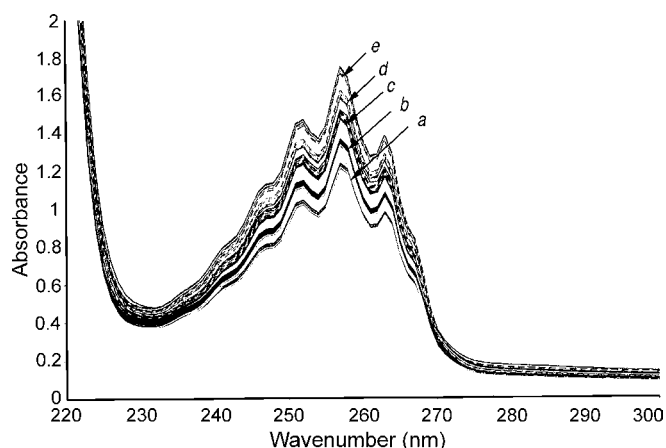


Fig. 2. UV-vis spectra of 90 solutions of phenylalanine and 15 mM BCD in deionized water with varying enantiomeric compositions and concentrations; 220–300 nm; without mean-centering. Total phenylalanine concentration: (a) 6.01 mM (X-Low), (b) 6.74 mM (Low), (c) 7.51 mM (Med), (d) 8.23 mM (Hi), and (e) 9.13 mM (X-Hi).

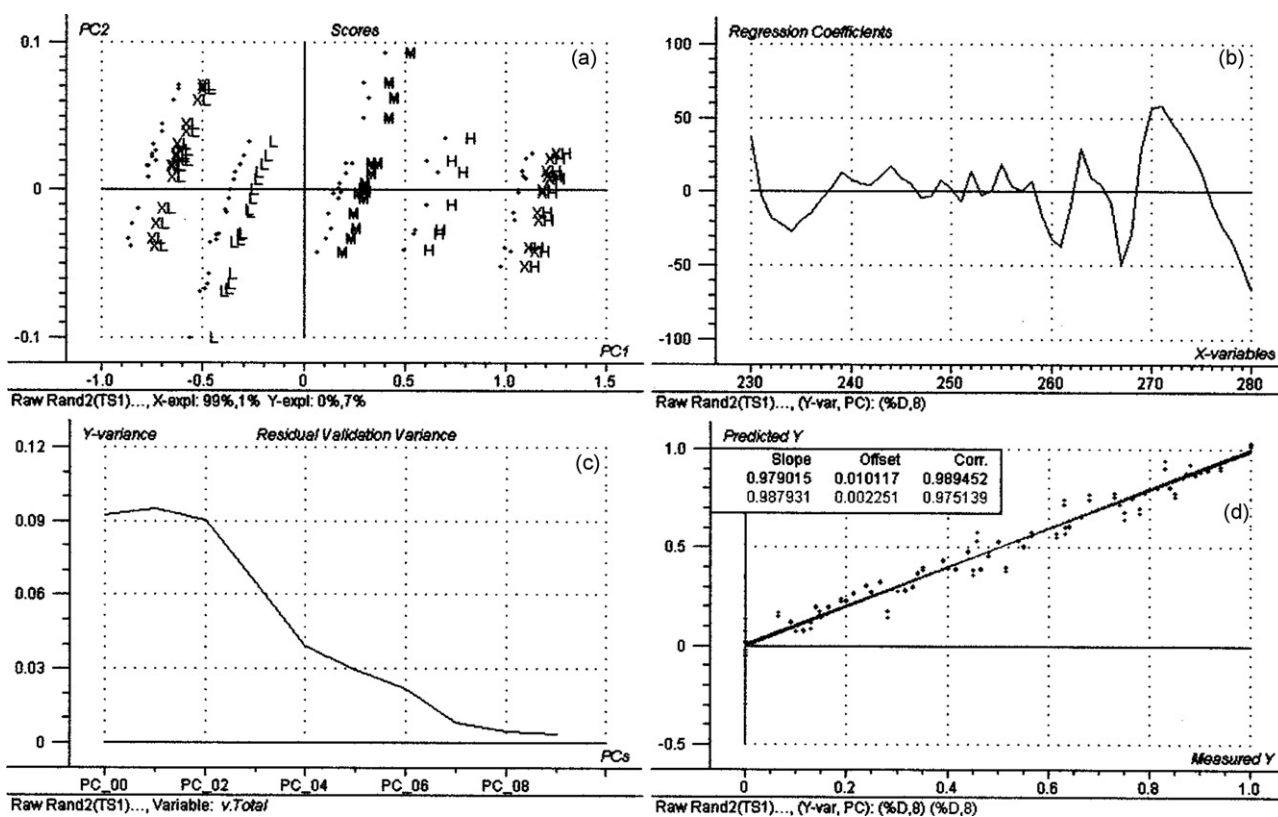


Fig. 3. Summary of regression results for 70 calibration samples of phenylalanine and 15 mM BCD in deionized water (230–280 nm); mean-centered spectral data with no concentration information included: (a) scores plot; (b) regression coefficients as a function of wavelength; (c) residual variance as a function of the number of PLS components (PC); (d) plot of the mole fraction of D-phenylalanine predicted by the model versus the known values.

each concentration level. Fig. 2 shows there are clear groupings of spectra that correspond to the five concentration levels, with spectral variations within each group due to differences in enantiomeric composition. All 90 samples were then modeled without any data treatment other than mean centering, and the regression analysis did not identify any outliers.

Fig. 3 shows a summary of the regression results for 70 samples, randomly selected from all five concentration levels and used in the calibration phase. Fig. 3a is a two-dimensional PLS-scores plot of the first PLS component versus the second PLS component for all 70 calibration samples. Scores plots often reveal relationships among samples. The distribution of the samples, marked by their concentration level, is clearly differentiated along the horizontal axis, indicating that the first PLS component is predominately concentration. Although the first two PLS components explain only 7% of the y-variable (in this case enantiomeric composition), the residual variance (Fig. 3c) indicates that the third, fourth, and fifth components explain 29%, 35%, and 6%, respectively. The sixth, seventh and eighth components contribute an additional 20%, bringing the total explained variance to 97%.

Fig. 3b is the plot of the regression coefficients versus wavelength. As can be seen, some wavelengths contribute positively to the model while others contribute negatively. Fig. 3c is a plot of the residual variance as a function of the number of PLS components. Here it can be seen that eight PLS components are needed in the model.

Fig. 3d shows two linear relationships. The line with the higher slope is the plot of predicted enantiomeric composition of phenylalanine by the PLS-1 regression model versus the known enantiomeric compositions of the calibration samples. The figures of merit for this regression model are given in Table 1 (phenylalanine, Method I). A perfect model would have a correlation coefficient of 1, a slope of 1, and an offset of 0.

The second line in Fig. 3d with the smaller correlation coefficient results from cross validation (leave-one-out) of the calibration model in which each sample in the calibration set is left out, one by one, and the remaining samples are used to predict the missing sample. After all samples in the calibration set have been treated in this way, the new predictions for each calibration sample are plotted. The Unscrambler statistical package automatically performs this calculation, but the results were not used except for comparison purposes. The more closely the two lines match, as observed in Fig. 3d, the better the calibration model.

With CARMSD, the test of any regression model is its ability to accurately predict the enantiomeric composition of future samples. To evaluate the performance and prediction capabilities of the model, the absorption spectra of the 20 independently prepared validation samples were recorded over the same wavelength range, and the enantiomeric compositions were predicted from the spectral data using the regression model. The validation samples did not include any samples used to prepare

Table 1
Summary of figures of merit for regression models made with phenylalanine and norephedrine in 15 mM β -cyclodextrin and deionized water

Analyte	Method	Correlation coefficient	Slope	Offset	Number of PCs used	Wavelength range (nm)	Total analyte (mM)
Phenylalanine	Method I	0.9895	0.9790	1.012×10^{-2}	8	230–280	6.01, 6.74, 7.51, 8.23, 9.13
Phenylalanine	Method II	0.9883	0.9768	1.121×10^{-2}	9	220–300	6.01, 6.74, 7.51, 8.23, 9.13
Phenylalanine	Method IIIA	0.9941	0.9881	5.722×10^{-3}	7	223–240, 268–285	6.01, 6.74, 7.51, 8.23, 9.13
Norephedrine	Method I	0.9837	0.9677	1.646×10^{-2}	5	230–280	6.03, 6.76, 7.49, 8.41, 9.01
Norephedrine	Method II	0.9849	0.9701	1.526×10^{-2}	6	230–280	6.03, 6.76, 7.49, 8.41, 9.01
Norephedrine	Method IIIA ^a	0.9894	0.9789	1.079×10^{-2}	5	230–280	6.03, 6.76, 7.49, 8.41, 9.01
Norephedrine	Method IIIA ^b	0.9981	0.9961	1.965×10^{-3}	5	230–280	6.76, 7.49, 8.41,
Norephedrine	Single concentration	0.9965	0.9929	3.787×10^{-3}	4	230–280	6.03
Norephedrine	Single concentration	0.9983	0.9965	1.902×10^{-3}	2	230–280	6.76
Norephedrine	Single concentration	0.9975	0.9951	2.505×10^{-3}	2	230–280	7.49
Norephedrine	Single concentration	0.9968	0.9937	2.945×10^{-3}	2	230–280	8.41
Norephedrine	Single concentration	0.9968	0.9937	2.941×10^{-3}	2	237–265	9.01

^a Five concentration levels.

^b Three concentration levels.

the model in the calibration phase. The prediction capability of the model was evaluated by calculating both the root-mean-square of the absolute error and the percent relative error. The results of the validation studies for data analysis by Method I are shown in Table 2. The root mean square absolute error was 0.0528, and the root mean square percent relative error was 21.8%.

3.2.2. Method II: concentration treated as an explicit variable

In Method II, total phenylalanine concentration was entered as an explicit variable along with the mean-centered spectral data in the regression model. Concentrations were entered in millimolar units to bring the numerical values up to an order of magnitude comparable to mean-centered spectral absorbances.

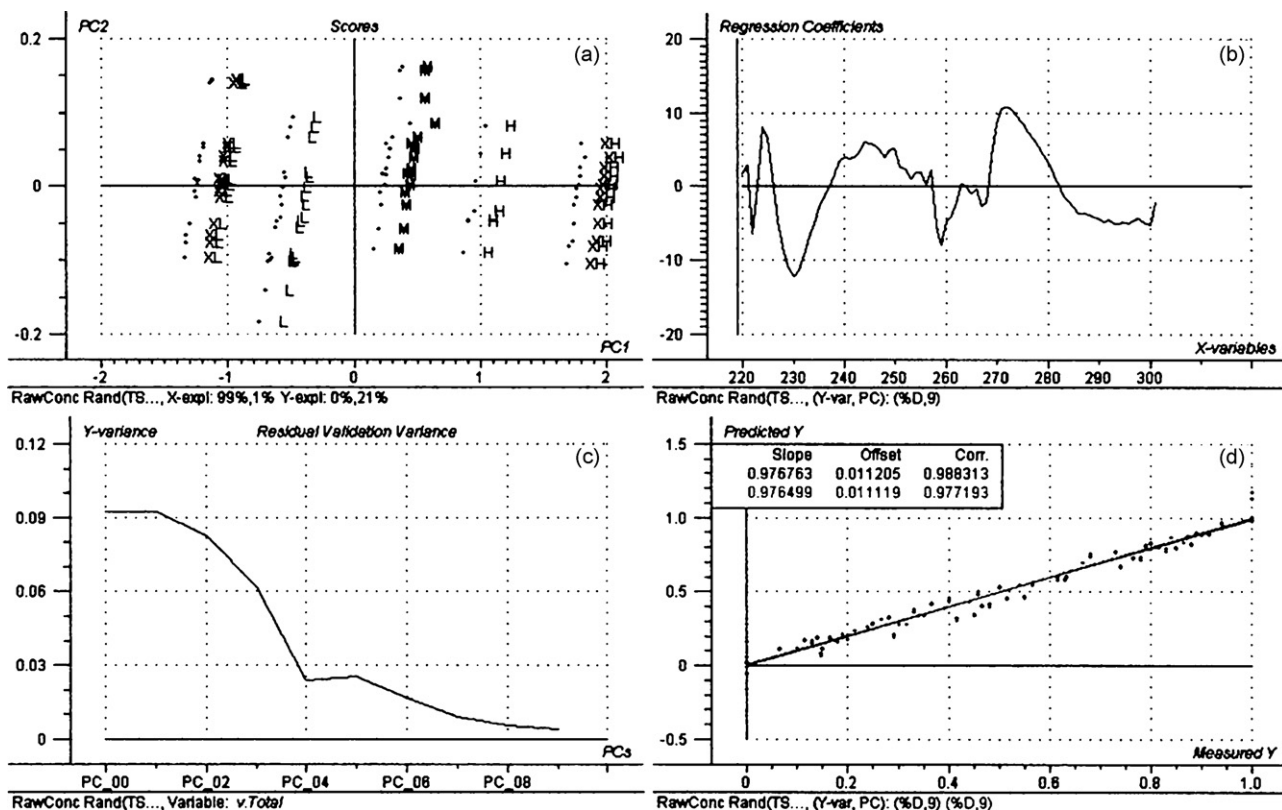


Fig. 4. Summary of regression results for 70 calibration samples of phenylalanine and 15 mM BCD in deionized water (220–300 nm); mean-centered spectral data with total phenylalanine concentration in millimolar units entered as an explicit variable: (a) scores plot; (b) regression coefficients as a function of wavelength; (c) residual variance as a function of the number of PLS components (PC); (d) plot of the mole fraction of D-phenylalanine predicted by the model versus the known values.

Table 2
Absolute and percent relative errors obtained for the mole fraction ϕ of D-phenylalanine in 15 mM BCD and deionized water

Actual ϕ D	Method I ^a			Method II ^b			Method IIIA ^c			Method IIIB ^d		
	Predicted ϕ D	Absolute error	Relative error (%)	Predicted ϕ D	Absolute error	Relative error (%)	Predicted ϕ D	Absolute error	Relative error (%)	Predicted ϕ D	Absolute error	Relative error (%)
0.490	0.511	0.021	4.29	0.528	0.038	7.76	0.524	0.034	6.94	0.499	0.009	1.84
0.590	0.591	0.001	0.169	0.552	-0.038	-6.44	0.587	-0.003	-0.508	0.577	-0.013	-2.20
0.690	0.660	-0.030	-4.35	0.732	0.042	6.09	0.749	0.059	8.55	0.758	0.068	9.85
0.715	0.689	-0.026	-3.64	0.680	-0.035	-4.90	0.695	-0.020	-2.80	0.708	-0.007	-0.979
1.000	1.036	0.036	3.60	0.983	-0.017	-1.70	0.964	-0.036	-3.60	0.978	-0.022	-2.20
0.050	0.023	-0.027	-54.4	0.079	0.029	57.1	0.039	-0.011	-22.2	0.0349	-0.015	-30.2
0.600	0.583	-0.017	-2.83	0.579	-0.021	-3.50	0.588	-0.012	-2.00	0.588	-0.012	-2.00
0.650	0.617	-0.033	-5.08	0.595	-0.055	-8.46	0.598	-0.052	-8.00	0.605	-0.045	-6.92
0.700	0.663	-0.037	-5.29	0.674	-0.026	-3.71	0.665	-0.035	-5.00	0.702	0.002	0.286
0.221	0.277	0.056	25.3	0.216	-0.005	-2.26	0.230	0.009	4.07	0.196	-0.025	-11.3
0.293	0.325	0.032	10.9	0.280	-0.013	-4.44	0.276	-0.017	-5.80	0.245	-0.048	-16.4
0.705	0.561	-0.144	-20.4	0.637	-0.068	-9.65	0.647	-0.058	-8.23	0.584	-0.121	-17.2
0.080	0.128	0.048	60.0	0.112	0.032	40.0	0.080	0.000	-0.175	0.0821	0.002	2.68
0.230	0.154	-0.076	-33.0	0.206	-0.024	-10.4	0.232	0.002	-0.870	0.212	-0.018	-7.83
0.380	0.362	-0.018	-4.74	0.393	0.013	3.42	0.421	0.041	10.8	0.378	-0.002	-0.526
0.430	0.513	0.038	19.3	0.461	0.031	7.20	0.461	0.031	7.21	0.456	0.026	6.05
0.530	0.556	0.026	4.91	0.513	-0.017	-3.21	0.564	0.034	6.42	0.549	0.019	3.58
0.580	0.535	-0.045	-7.76	0.481	-0.099	-17.1	0.588	0.008	1.38	0.544	-0.036	-6.21
0.930	1.005	0.075	8.07	0.928	-0.002	-0.215	0.928	-0.002	-0.215	0.902	-0.028	-3.01
1.000	0.980	-0.020	-2.00	0.930	-0.070	-7.00	1.042	0.042	4.20	0.940	-0.060	-6.00
RMS value		0.0528	21.8		0.0410	17.0		0.0316	7.34		0.0403	9.92

^a Spectral data used without adjustment for concentration.

^b Concentration included as an explicit variable.

^c Spectral data normalized using laboratory-determined concentrations.

^d Spectral data normalized using program-determined concentrations.

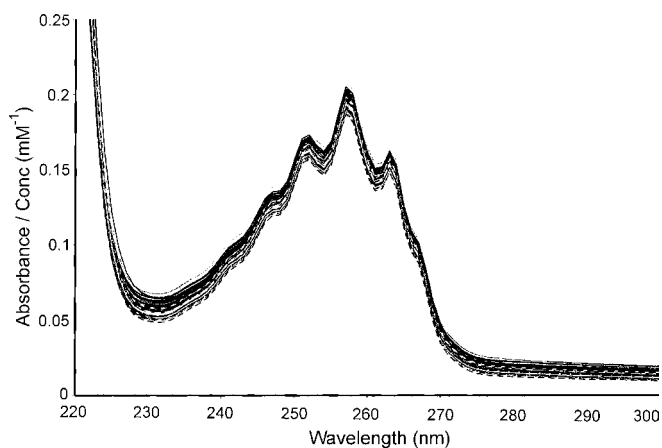


Fig. 5. Normalized UV-vis spectra of 90 solutions of phenylalanine and 15 mM BCD in deionized water with varying enantiomeric compositions and concentrations; 220–300 nm; without mean-centering. Total phenylalanine concentration: 6.01–9.13 mM.

Fig. 4 shows the regression results for the 70 samples used in the calibration phase.

Again, the scores plot (Fig. 4a) shows five separate distributions of points along the horizontal axis, corresponding to the five different concentration levels. In this case, the combined total of the first eight of the PLS components explains 97% of the variance in enantiomeric composition (Fig. 4c). In the plot of the regression coefficients versus wavelength (Fig. 4b), the last variable on the *x*-axis represents the explicitly entered concentration, which is clearly a modest contributor to the model. The figures of merit for the regression model (Fig. 4d) are given in Table 1.

In the validation phase, the same 20 validation samples were used as in Method I in order to make a more consistent comparison. The results of the validation studies for Method II, where millimolar concentration is entered as a variable, are shown in Table 2 (phenylalanine, Method II). These results appear the same or perhaps slightly better than those obtained from Method I in which no concentration data were entered in the analysis.

3.2.3. Method III: normalized data analysis

In Method III, the same 70 calibration spectra were normalized with respect to total known analyte concentration prior to mean centering and statistical analysis. Each absorbance value was divided by the total, known phenylalanine concentration in millimolar units. The normalized spectra, shown in Fig. 5, still show some spectral variation, but not as much as when the data are not normalized (Fig. 2).

Fig. 6 shows a summary of the regression results for this analysis. The scores plot (Fig. 6a) no longer shows a distribution by concentration level, and the samples are now randomly scattered along the first two PLS components. Fig. 6c demonstrates that only seven PLS components are needed to explain 98% of the data, and the regression coefficients in Fig. 6b appear smoother. (The sharp dip in Fig. 6b is due to the disconnect in the wavelength range used in the model.) Figures of merit in Fig. 6d are also better, as shown in Table 1 (phenylalanine, Method IIIA).

Validation results for the same 20 samples used in Methods I and II are shown in Table 2 (Method IIIA). It seems clear that normalizing the spectra according to concentration provides the best predictive ability in determining enantiomeric composition. This suggests that the normalization process has eliminated many differences due to concentration, leaving primarily the diastereomeric spectral differences in the D- and L-phenylalanine BCD complexes.

Although normalization of spectral data results in the best predictive ability, even this step has a limitation. The total concentration must be known in order to normalize the data. Since these solutions appear to obey Beer's Law, it should be possible to calculate the total analyte concentration from the spectra themselves. Although multivariate analysis is not strictly necessary to determine the total analyte concentration (a univariate calibration curve from the standard solutions should be sufficient), multivariate regression is required in the second step, so the Unscrambler statistical program was used first to determine the concentration and then to determine the enantiomeric composition. Multivariate regression predicted the concentration of all 20 solutions with excellent accuracy (RMS percent relative error 0.507%). These predicted concentrations were then used to normalize the spectra. The new normalized spectra were used in the validation step, and the results are shown in Table 2 (Method IIIB). These results do not appear to be significantly different from those found using laboratory calculated concentrations to normalize the spectra (Method IIIA).

3.3. Studies with norephedrine

Norephedrine has been used as a test pharmaceutical in studies determining enantiomeric composition employing both native and modified cyclodextrins [69–74]. Studies indicate that norephedrine forms an inclusion complex with β -cyclodextrin, although the complex is not fully characterized [75]. To determine whether the results obtained in this study with phenylalanine could be applied to other chiral molecules, the concentration study was repeated with norephedrine. Norephedrine was also of interest because the molecule has two centers of optical activity, whereas phenylalanine has only one.

3.3.1. Method I: no correction for variation in concentration

As was the case with phenylalanine (see Fig. 2), the 89 unmodified norephedrine spectra showed clear groupings, indicating the five different concentration levels of the stock solutions. All 89 samples of norephedrine were first modeled without any data treatment other than mean-centering. The statistical program identified two of the 9.02 mM (X-Hi) samples as outliers.

Practical application of statistical methods often have one or more observations showing outliers, i.e., a departure from the bulk of the data. These may occur for many different reasons and need not indicate a mistake has been made [54]. Because there was no obvious experimental reason to exclude the two outlier values, other than the results of the statistical treatment, we chose to retain both in the calibration and validation steps.

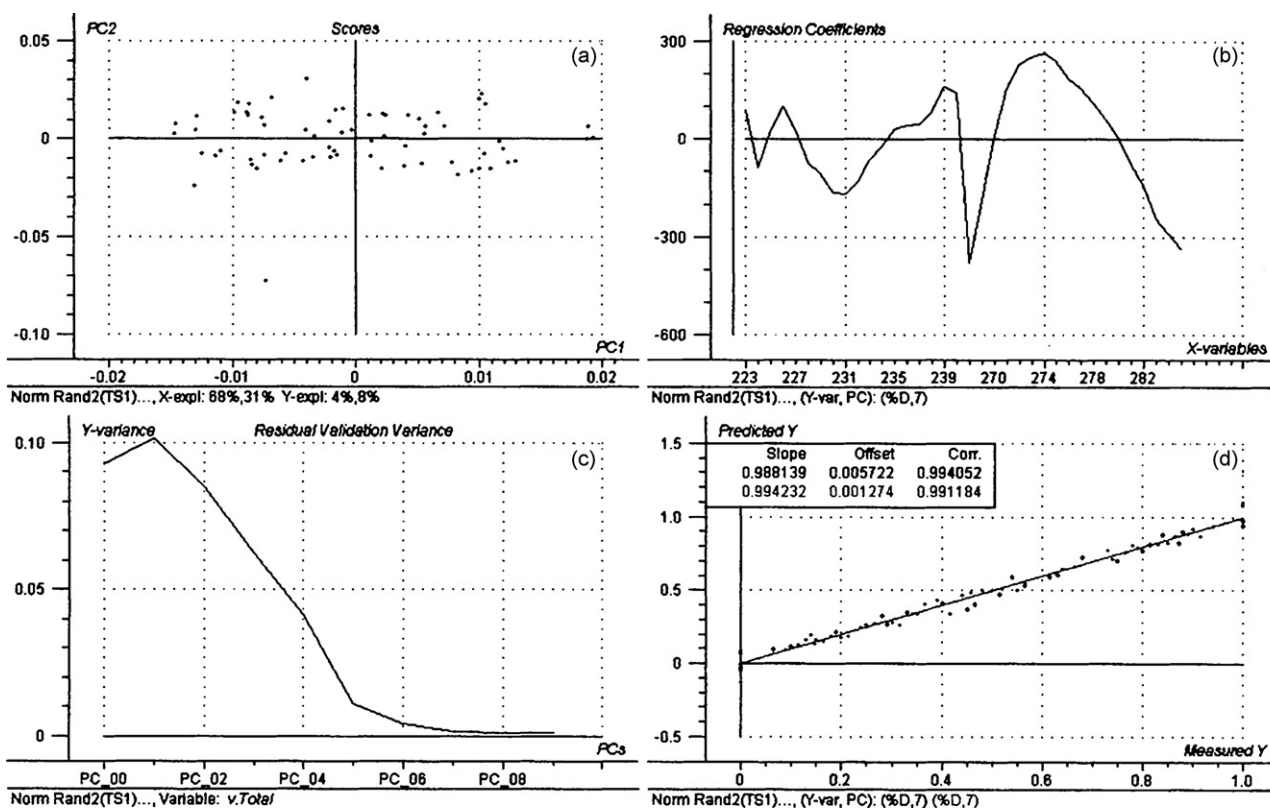


Fig. 6. Summary of regression results for 70 calibration samples of phenylalanine and 15 mM BCD in deionized water (223–240, 268–285 nm); data normalized with respect to total phenylalanine concentration in millimolar units: (a) scores plot; (b) regression coefficients as a function of wavelength; (c) residual variance as a function of the number of PLS components (PC); (d) plot of the mole fraction of D-phenylalanine predicted by the model versus the known values.

A random number generator next selected 20 samples to make up an independent validation set, which, by chance, included one of the outliers. A separate PLS-1 regression model was then calculated on the remaining 69 samples, which served as the calibration set for the analysis. This calculation required the statistical program to sort out differences in enantiomeric composition in the presence of differences in total concentration. The regression results obtained for the calibration set appear qualitatively similar to those obtained for phenylalanine using Method I (see Fig. 3 for a comparison). The figures of merit for the regression model for norephedrine are given in Table 1 (norephedrine, Method I).

The regression model developed in the calibration phase was used to predict the 20 samples in the validation set, and the results of the prediction are shown in Table 3 (Method I).

The one validation sample statistically identified as an outlier is marked with an asterisk. While the predicted results for this sample are included in Table 3, they are not included in the error calculations. Table 3 (Method I) shows that even with no data manipulation, this technique can accommodate a wide range of analyte concentrations with reasonable error.

3.3.2. Method II: concentration treated as an explicit variable

Method II includes concentration as a variable when computing the model. The x -variables in this case consisted of

mean-centered spectral data and the total analyte concentration of the sample entered in millimolar units. For this analysis, the same 69 calibration and 20 validation samples were used as in Method I in order to make the comparison more meaningful. The regression results appear qualitatively similar to those obtained for phenylalanine using Method II. (See Fig. 4 for a comparison.) The figures of merit for the regression model are given in Table 1 (norephedrine, Method II).

The regression model, developed with concentration included, was used to predict the 20 samples in the validation set, and the results are shown in Table 3 (Method II). Again, the sample identified as an outlier is marked with an asterisk. Although the predicted value for the outlier is listed in Table 3, its value was not included in the error calculations. For Method II, the root mean square absolute error and the root mean square percent relative error appear slightly worse, but are probably not significantly different from the errors found for Method I. It appears, then, that for this analyte and chiral auxiliary pair, there is no significant advantage to including concentration as a variable in the calculation.

3.3.3. Method III: normalized data analysis

In this method, each individual spectrum was normalized with respect to its calculated concentration, and the normalized, mean-centered spectra were used in the regression analysis. The same 69 calibration and 20 validation samples were used as in Methods I and II to make the comparisons more meaningful.

Table 3
Absolute and relative errors obtained for the mole fraction ϕ of (–)-norephedrine in 15 mM BCD and deionized water

Concentration level ^a	Actual ϕ	Method I ^b			Method II ^c			Method IIIA ^d			Method IIIB ^e		
		Predicted ϕ	Absolute error	Relative error (%)	Predicted ϕ	Absolute error	Relative error (%)	Predicted ϕ	Absolute error	Relative error (%)	Predicted ϕ	Absolute error	Relative error (%)
X-Low	0.190	0.278	0.088	46.3	0.298	0.108	56.8	0.214	0.024	12.6	0.201	0.011	5.80
X-Low	0.390	0.421	0.031	7.95	0.425	0.035	8.97	0.384	–0.006	–1.54	0.375	–0.015	–3.85
X-Low	0.540	0.574	0.034	6.30	0.583	0.043	7.96	0.556	0.016	2.96	0.544	0.004	0.741
X-Low	0.740	0.698	–0.042	–5.68	0.697	–0.043	–5.81	0.689	–0.051	–6.89	0.680	–0.060	–8.11
Low	0.165	0.150	–0.015	–9.09	0.115	–0.050	–30.3	0.112	–0.053	–32.1	0.109	–0.056	–33.9
Low	0.265	0.237	–0.028	–10.6	0.237	–0.028	–10.6	0.224	–0.041	–15.5	0.220	–0.045	–17.0
Low	0.465	0.478	0.013	2.80	0.467	0.002	0.430	0.478	0.013	2.80	0.470	0.005	1.08
Low	0.765	0.743	–0.022	–2.88	0.754	–0.011	–1.44	0.787	0.022	2.88	0.778	0.013	1.70
Low	0.915	0.904	–0.011	–1.20	0.931	0.016	1.75	0.967	0.052	5.68	0.959	0.044	4.81
Medium	0.100	0.150	0.050	50.0	0.146	0.046	46.0	0.140	0.040	40.0	0.136	0.036	36.0
Medium	0.400	0.376	–0.024	–6.00	0.362	–0.038	–9.50	0.370	–0.030	–7.50	0.383	–0.017	–4.25
Medium	0.650	0.678	0.028	4.31	0.648	–0.002	–0.308	0.660	0.010	1.54	0.682	0.032	4.92
Medium	0.800	0.770	–0.030	–3.75	0.750	–0.050	–6.25	0.761	–0.039	–4.88	0.789	–0.011	–1.38
High	0.146	0.159	0.013	8.90	0.170	0.024	16.4	0.241	0.095	65.1	0.237	0.091	62.3
High	0.457	0.493	0.036	7.88	0.491	0.034	7.44	0.523	0.066	14.4	0.528	0.071	15.5
X-High	0.080*	–0.197	–0.277	–346	–0.156	–0.236	–295	–0.04883	–0.12883	–161	–0.0575	–0.1375	–172
X-High	0.230	0.156	–0.074	–32.2	0.149	–0.081	–35.2	0.200	–0.030	–13.0	0.183	–0.047	–20.4
X-High	0.480	0.476	–0.004	–0.833	0.498	0.018	3.75	0.479	–0.001	–0.208	0.468	–0.012	–2.5
X-High	0.730	0.750	0.020	2.74	0.764	0.034	4.66	0.695	–0.035	–4.79	0.689	–0.041	–5.62
X-High	0.880	0.883	0.003	0.341	0.893	0.013	1.48	0.826	–0.054	–6.14	0.826	–0.054	–6.14
RMS value			0.0367	18.1		0.0437	20.9		0.0422	20.4		0.0425	19.9

^a X-Low: 6.03 mM total norephedrine; Low: 6.76 mM total norephedrine; Medium: 7.49 mM total norephedrine; High: 8.41 mM total norephedrine; X-High: 9.01 mM total norephedrine. All solutions in 15 mM BCD and deionized water.

^b Spectral data used without adjustment for concentration.

^c Concentration included as an explicit variable.

^d Spectral data normalized using laboratory-determined concentrations.

^e Spectral data normalized using programmed-determined concentrations.

* Outlier; see text.

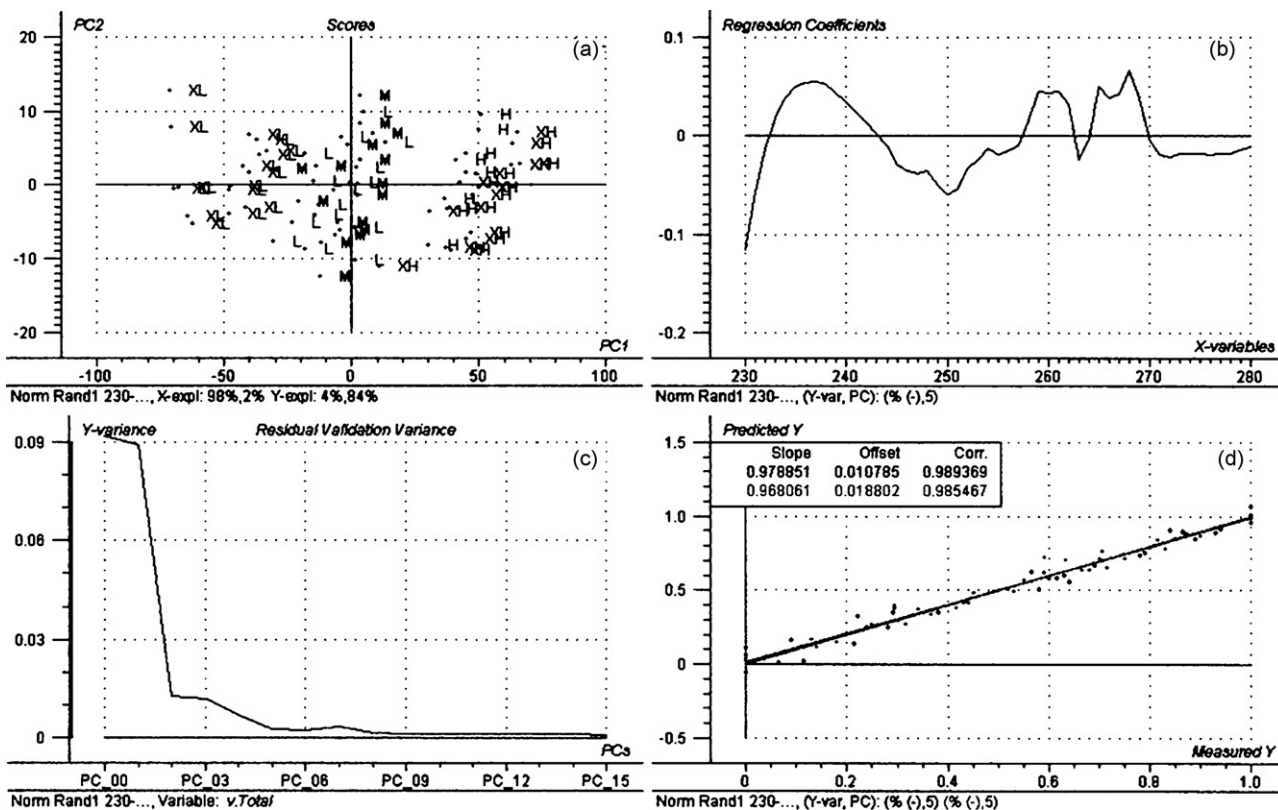


Fig. 7. Summary of regression results for 69 calibration samples of norephedrine and 15 mM BCD in deionized water, (230–280 nm); data normalized with respect to total norephedrine concentration in millimolar units: (a) scores plot; (b) regression coefficients as a function of wavelength; (c) residual variance as a function of the number of PLS components (PC); (d) plot of the mole fraction of (–)-norephedrine predicted by the model versus the known value.

The regression results for the calibration set are summarized in Fig. 7.

The scores plot (Fig. 7a) shows that the samples still retain some general pattern along the x -axis, indicating that groupings by concentration are reduced, but not completely eliminated. Some concentration dependence is also reflected in the first PLS component (Fig. 7a) which explains 4% of the variation in enantiomeric composition. The second PLS component explains 84% of the variation in the y -variable, and the third, fourth and fifth PLS components explain an additional 10%. The figures of merit for this regression model are given in Table 1 (norephedrine, Method IIIA, five total analyte concentrations).

The results of the validation phase for the 20 samples in the validation set are shown in Table 3 (Method IIIA). The outlier sample is reported, but not used in the calculation of the root mean square errors. It was expected that normalization of the spectra would simplify the data for norephedrine, making it easier to discern differences in enantiomeric composition. However, as shown in Table 3, normalization did not make a significant difference in the predictability of the model.

As a variation in the normalization method, the statistical program was used to calculate the concentrations of the validation samples from known concentrations in the calibration set using Beer's Law. The prediction of total concentration was straightforward (RMS percent relative error 0.296%), and only two PLS components were needed to explain 100% of the variation in concentration.

The spectra of the 20 samples in the validation set were normalized using the concentration predicted from Beer's Law, mean centered, and then analyzed. The results are summarized in Table 3 (Method IIIB). The root mean square absolute error and the root mean square percent relative error are nearly identical to the results from the Method IIIA analysis, indicating that predicting the concentration using the UV–vis spectra is a viable alternative if the total concentration of both optical isomers is not known. This implies that even in the absence of clear concentration data, the total concentration of both enantiomers can be successfully predicted from the UV–vis spectra, the predicted concentration can be used to normalize the data, and the normalized data can be used to predict the enantiomeric composition with accuracy better than 0.05 mole fraction units.

3.3.4. Additional methods

Examination of Table 3 suggests that in the case of norephedrine, there is little difference between the results obtained using any of the three methods of adjusting for total concentration differences. As an independent measure of the effectiveness of the technique, samples within each total concentration level were analyzed separately. This gave five different sets of predictions. Within each set, the total concentration of norephedrine was held constant, and only ϕ was varied.

A random number generator selected five samples from each of the five total concentration levels to serve as a validation

Table 4

Absolute and relative errors obtained using fixed concentrations of norephedrine in 15 mM BCD in deionized water using an independently prepared calibration set

Actual ϕ of (–)-norephedrine	Predicted ϕ of (–)-norephedrine	Absolute error	Relative error (%)
0.190	0.143	–0.047	–24.7
0.290	0.332	0.042	14.5
0.440	0.406	–0.034	–7.73
0.590	0.612	0.022	3.73
0.740	0.701	–0.039	–5.27
RMS value ^a		0.0378	13.6
0.165	0.187	0.022	13.3
0.265	0.255	–0.010	–3.77
0.315	0.320	0.005	1.59
0.415	0.399	–0.016	–3.86
0.465	0.456	–0.009	–1.94
RMS value ^b		0.013	6.53
0.150	0.160	0.010	6.67
0.400	0.404	0.004	1.00
0.500	0.488	–0.012	–2.40
0.550	0.549	–0.001	–0.182
0.800	0.822	0.022	2.75
RMS value ^c		0.0122	3.43
0.146	0.142	–0.004	–2.74
0.457	0.445	–0.012	–2.63
0.632	0.612	–0.020	–3.16
0.872	0.886	0.014	1.61
RMS value ^d		0.0137	2.60
0.380	0.358	–0.022	–5.79
0.480	0.465	–0.015	–3.13
0.630	0.603	–0.027	–4.29
0.730	0.711	–0.019	–2.60
0.880	0.879	–0.001	–0.114
RMS value ^e		0.0190	3.70

^a 6.03 mM (X-Low) total norephedrine concentration and 15 mM BCD in deionized water.

^b 6.76 mM (Low) total norephedrine concentration and 15 mM BCD in deionized water.

^c 7.49 mM (Medium) total norephedrine concentration and 15 mM BCD in deionized water.

^d 8.41 mM (High) total norephedrine concentration and 15 mM BCD in deionized water.

^e 9.01 mM (X-High) total norephedrine concentration and 15 mM BCD in deionized water.

set, and a partial-least squares regression model was built with the remaining samples at that concentration level. In the X-Low concentration set, four PLS components were required to explain 99% of the variation in enantiomeric composition. In all remaining concentration sets, only two PLS components were required. The figures of merit for each of the five regression models are given in Table 1 (norephedrine, single concentrations), and the prediction results using each of these models are shown in Table 4.

While all five concentration levels performed adequately, the 6.03 mM (X-Low) concentration has an absolute error that appears significantly higher than the other levels (Table 4). Table 4 also shows that in the case of the 9.01 mM (X-Hi) con-

Table 5

Absolute and relative errors obtained from middle three concentration levels of norephedrine in 15 mM BCD and deionized water with an independently prepared calibration set; normalized data analysis; 230–280 nm

Concentration level ^a	Actual ϕ of (–)-norephedrine	Predicted ϕ of (–)-norephedrine	Absolute error	Relative error (%)
Low	0.065	0.0818	0.0168	25.8
Low	0.215	0.229	0.014	6.51
Low	0.315	0.317	0.002	0.635
Low	0.415	0.412	–0.003	–0.723
Low	0.465	0.468	0.003	0.645
Low	0.565	0.524	–0.041	–7.26
Low	0.715	0.674	–0.041	–5.73
Low	0.815	0.801	–0.014	–1.72
Medium	0.150	0.133	–0.017	–11.3
Medium	0.300	0.289	–0.011	–3.67
Medium	0.500	0.480	–0.020	–4.00
Medium	0.700	0.691	–0.009	–1.29
Medium	0.850	0.862	0.012	1.41
High	0.221	0.245	0.024	10.9
High	0.632	0.637	0.005	0.791
RMS value			0.0195	8.48

^a 6.76 mM (Low) total norephedrine concentration; 7.49 mM (Medium) total norephedrine concentration; 8.41 mM (High) total norephedrine concentration.

centration, all of the absolute errors are negative, meaning that the model predicted a low value of ϕ for each sample. Two of the samples in the 9.01 mM set had been identified as outliers by the statistical program, and inclusion of these samples undoubtedly influenced the prediction.

Assuming the results of both the 6.03 mM (X-Low) and 9.01 mM (X-Hi) might be compromised in some way, the analysis was repeated using only the middle three concentration levels (6.76, 7.49 and 8.41 mM) consisting of 49 samples. A validation set consisting of 15 samples was randomly selected, the remaining 34 spectra were normalized using laboratory-calculated values, mean-centered, and finally subjected to a partial-least squares regression analysis. The regression results appeared very similar to those shown in Fig. 7 with the X-Hi and X-Low points removed.

In the scores plot, the Med and Low concentration levels (6.76 and 7.49 mM) appeared relatively well mixed, but the High level (8.41 mM) was well removed from the others. This indicates that the 8.41 mM samples were distinctly different from the other samples. The figures of merit for this calibration model are shown in Table 1 (norephedrine, Method IIIA, three total analyte concentrations).

A prediction analysis was performed on the 15 samples in the validation set using the model developed above. The results are shown in Table 5.

These results are an improvement over those found using any of the three methods employing all five concentration levels (Table 3).

4. Conclusions

In this study, three methods of compensating for variations in total analyte concentration were studied and compared. Method

I allowed total analyte concentration to vary and relied on the statistical analysis to sort out variations due to enantiomeric composition in the presence of variations due to total concentration differences. Method II included the total analyte concentration as an explicit variable in the statistical analysis. Method III normalized the spectra with respect to total analyte concentration prior to statistical analysis. Total analyte concentration could be calculated either from the known laboratory-prepared stock solutions (Method IIIA), or by incorporating Beer's Law into the statistical program in a separate PLS-1 regression (Method IIIB). The RMS percent relative errors for determination of concentration were small and on the order of 0.3–0.5%

Phenylalanine and norephedrine were used as analytes with total concentrations centered around $7.5 \text{ mM} \pm 20\%$, and β -cyclodextrin was used as the chiral auxiliary at a fixed concentration of 15 mM. Since both phenylalanine and norephedrine solutions gave absorbances at selected wavelengths that adhered to Beer's Law over the concentration ranges studied, spectral normalization was expected to eliminate variations in spectra due to concentration differences, leaving only variations due to differences in enantiomeric composition.

In the case of phenylalanine, a molecule with only one chiral center, normalizing the data (Method III) using either laboratory- or statistically determined values for total analyte concentration proved most successful. In the case of norephedrine, a molecule with two chiral centers, all three methods gave comparable results. The levels of accuracy for norephedrine were comparable to Method I (raw data analysis) for phenylalanine. In all methods, it proved possible to make a determination of enantiomeric composition of either analyte with an accuracy of 0.05 mole fraction units or better.

It appears that for norephedrine, total analyte concentration may be a more important factor than in the case of phenylalanine. Since all of the norephedrine samples were dissolved in 15 mM BCD, the ratio of analyte to cyclodextrin varies among the levels. Phenylalanine has been reported to form a 1:1 complex with BCD [66–68]. The nature of the interaction of BCD with norephedrine is not definitively known [75]. Given that the norephedrine molecule has two optically active sites, we suggest that more than one kind of interaction might be involved. If these interactions are concentration dependent, the effect could accentuate spectral variations at different total norephedrine concentrations. Other factors, including unknown experimental errors that contribute to apparent deviations from Beer's Law during the procedure, cannot be ruled out at this point.

This study has demonstrated that a major limitation of our previous work, i.e., the need to maintain a constant analyte concentration, has been successfully overcome for two specific compounds. Concentration can be allowed to vary within a given range and, depending on the accuracy required, still give acceptable results. The choice of method depends on the analyte, and even raw data analysis without adjustment for concentration may be sufficient in some cases. Structural differences in the analyte and chiral auxiliary may contribute to the degree of success for each of the three methods.

Acknowledgment

We thank CAMO Inc. for the donation of chemometric software and the Baylor University Sabbatical Committee for support of this project (M. Busch).

References

- [1] F. Crick, *Life Itself*, Simon and Schuster, New York, 1981.
- [2] D. Kondepudi, K. Asakura, in: K.W. Busch, M.A. Busch (Eds.), *Chiral Analysis*, Elsevier, Amsterdam, 2006, pp. 25–45 (Chapter 1).
- [3] H.Y. Aboul-Enein, I.W. Wainer, *The Impacts of Stereochemistry on Drug Development and Use*, John Wiley, New York, 1997.
- [4] Y.S. Ding, J.S. Fowler, N.D. Volkow, S.L. Dewey, G.J. Wang, J. Logan, J. Gatley, N. Pappas, *Psychopharmacology* 131 (1997) 71.
- [5] K.D. Tripathi, *Indian J. Pharmacol.* 25 (1993) 73.
- [6] J. Hudson, *The History of Chemistry*, Macmillan, London, 1992, pp. 257–260.
- [7] P. Knightly, E. Potter, *Suffer the Children: The Story of Thalidomide*, Viking Press, New York, 1979, pp. 5–95.
- [8] I. Agranat, H. Caner, J. Caldwell, *Nat. Rev. Drug Discov.* 1 (2002) 753.
- [9] G.T. Tucker, *Lancet* 355 (2000) 1085.
- [10] I. Ali, V.K. Gupta, H.Y. Aboul-Enein, *Curr. Sci.* 84 (2003) 152.
- [11] I. Ali, H.Y. Aboul-Enein, *Chiral Pollutants: Distribution, Toxicity and Analysis by Chromatography and Capillary Electrophoresis*, Wiley, New York, 2004, pp. 75–144 (Chapter 3).
- [12] I. Ali, H.Y. Aboul-Enein, *Chiral Pollutants: Distribution, Toxicity and Analysis by Chromatography and Capillary Electrophoresis*, Wiley, New York, 2004, pp. 7–8.
- [13] D. Mangelings, Y.V. Heyden, *Combinatorial Chemistry and High Throughput Screening* 10 (2007) 317.
- [14] M. Reetz, *Angew. Chem. Int. Ed.* 40 (2001) 284.
- [15] M.G. Finn, in: K.W. Busch, M.A. Busch (Eds.), *Chiral Analysis*, Elsevier, Amsterdam, 2006, pp. 79–94 (Chapter 4).
- [16] M. Finn, *Chirality* 14 (2002) 534.
- [17] K.W. Busch, I.M. Swamidoss, S.O. Fakayode, M.A. Busch, *J. Am. Chem. Soc.* 125 (2003) 1690.
- [18] Y. Wang, F. Zhang, J. Liang, H. Li, J. Kong, *Mol. Biomol. Spectrosc.* 68A (2007) 279.
- [19] Y. Wang, F. Zhang, J. Liang, H. Li, J. Kong, *Chin. Chem. Lett.* 12 (2006) 1599.
- [20] L. Zhou, Z. Lin, C.J. Welch, Z. Ge, D. Ellison, *Chirality* 18 (2006) 306.
- [21] C.D. Tran, V.I. Grishko, D. Oliveira, *Anal. Chem.* 75 (2003) 6455; Erratum C.D. Tran, V.I. Grishko, D. Oliveira, *Anal. Chem.* 76 (2004) 2157.
- [22] C.D. Tran, D. Oliveira, V.I. Grishko, *Anal. Biochem.* 325 (2004) 206.
- [23] K.W. Busch, M.A. Busch, in: K.W. Busch, M.A. Busch (Eds.), *Chiral Analysis*, Elsevier, Amsterdam, 2006, pp. 363–395 (Chapter 12).
- [24] S.O. Fakayode, A.A. Williams, M.A. Busch, K.W. Busch, I.M. Warner, *J. Fluoresc.* 16 (2006) 659.
- [25] S.O. Fakayode, M.A. Busch, K.W. Busch, *Talanta* 68 (2006) 1574.
- [26] S.O. Fakayode, I.M. Swamidoss, M.A. Busch, K.W. Busch, *Talanta* 65 (2005) 838.
- [27] S.O. Fakayode, M.A. Busch, D. Bellert, K.W. Busch, *Analyst* (Cambridge, U.K.) 130 (2005) 233.
- [28] K.W. Busch, I.M. Swamidoss, S.O. Fakayode, M.A. Busch, *Anal. Chim. Acta* 525 (2004) 53.
- [29] S.O. Fakayode, *Dissertation*, Baylor University, 2004.
- [30] T. Kowalska, J. Sherma, *Thin Layer Chromatography in Chiral Separations and Analysis*, John Wiley, New York, 2007.
- [31] C. Garcia-Ruiz, M.L. Marina, *Electrophoresis* 27 (2006) 195.
- [32] G. Guebitz, M.G. Schmid, *Mol. Biotechnol.* 32 (2006) 159.
- [33] A. Van Eeckhaut, Y. Michotte, *Electrophoresis* 27 (2006) 2880.
- [34] G.L. Erny, A. Cifuentes, *J. Pharm. Biomed. Anal.* 40 (2006) 509.
- [35] H.Y. Aboul-Enein, I. Ali, *Chiral Separations by Liquid Chromatography: Theory and Applications*, Marcel Dekker, New York, 2003.

- [36] G. Subramanian, *Chiral Separation Techniques: A Practical Approach*, Wiley–VCH, Weinheim, 2001.
- [37] W. Vetter, K. Bester, in: K.W. Busch, M.A. Busch (Eds.), *Chiral Analysis*, Elsevier, Amsterdam, 2006, pp. 131–214 (Chapter 6).
- [38] S.M. Khopkar, *Analytical Chemistry of Macrocyclic and Supramolecular Compounds*, Marcel Dekker, Narosa Publishing House, New Delhi, 2005.
- [39] D.J. Bornhop, S. Dotson, in: K.W. Busch, M.A. Busch (Eds.), *Chiral Analysis*, Elsevier, Amsterdam, 2006, pp. 343–362 (Chapter 11).
- [40] E.W. Blanch, L. Hecht, L.D. Barron, in: K.W. Busch, M.A. Busch (Eds.), *Chiral Analysis*, Elsevier, Amsterdam, 2006, pp. 545–594 (Chapter 16).
- [41] L.D. Barron, F. Zhu, L. Hecht, *Vibrational Spectroscopy* 42 (2006) 15.
- [42] N. Berova, K. Nakanishi, R.W. Woody (Eds.), *Circular Dichroism: Principles and Applications*, Wiley–VCH, New York, 2000.
- [43] J. Gawronski, P. Skowronek, in: K.W. Busch, M.A. Busch (Eds.), *Chiral Analysis*, Elsevier, Amsterdam, 2006, pp. 343–362 (Chapter 13).
- [44] P.L. Polavarapu, *Chem. Record* 7 (2007) 125.
- [45] D.J. Minick, R.D. Rutkowske, L.A.D. Miller, *Am. Pharm. Rev.* 10 (2007) 118.
- [46] B. Chavali, K. Drishnamurthy, J. Dage, *Am. Pharm. Rev.* 10 (2007) 94.
- [47] L.A. Nafie, R.K. Dukor, in: K.W. Busch, M.A. Busch (Eds.), *Chiral Analysis*, Elsevier, Amsterdam, 2006, pp. 505–544 (Chapter 13).
- [48] P. Polavarapu, J. He, *Anal. Chem.* 76 (2004) 61A.
- [49] K.W. Busch, I.M. Swamidoss, S.O. Fakayode, M.A. Busch, U.S. Patent 7,191,070 (2007).
- [50] L. Stryer, *Biochemistry*, fourth ed., W.H. Freeman and Company, New York, 1995, pp. 19–21.
- [51] W.N. Kernan, C.M. Viscoli, L.M. Brass, J.P. Broderick, T. Brott, E. Feldmann, L.B. Morgenstern, J.L. Wilterdink, R.I. Horwitz, *N. Engl. J. Med.* 343 (2000) 1826.
- [52] M. Otto, *Chemometrics: Statistics and Computer Application in Analytical Chemistry*, Wiley–VCH, Weinheim, 1999 (Chapter 1).
- [53] M.J. Adams, *Chemometrics in Analytical Spectroscopy*, Royal Society of Chemistry, Cambridge, 1995.
- [54] H. Martens, T. Naes, *Multivariate Calibration*, John Wiley, New York, 1989.
- [55] E.R. Malinowski, *Factor Analysis in Chemistry*, John Wiley, New York, 1991.
- [56] K.H. Esbensen, *Multivariate Data Analysis—In Practice*, fourth ed., Camo, Woodbridge, NJ, 2000.
- [57] K.R. Beebe, R.J. Pell, M.B. Seasholtz, *Chemometrics: A Practical Guide*, John Wiley, New York, 1998.
- [58] F. Chau, Y. Liang, J. Gao, X. Shao, *Chemometrics: From Basics to Wavelet Transform*, John Wiley, Hoboken, NJ, 2004.
- [59] S.J. Haswell (Ed.), *Practical Guide to Chemometrics*, Marcel Dekker, New York, 1992.
- [60] H. Mark, J. Workman Jr., *Statistics in Spectroscopy*, second ed., Elsevier, Boston, 2003.
- [61] G. Grigorean, S. Gronert, C.B. Lebrilla, *Int. J. Mass Spectrom.* 219 (2002) 79.
- [62] R. Wimmer, F.L. Aachmann, K.L. Larsen, S.B. Peterson, *Carbohydr. Res.* 337 (2002) 841.
- [63] G. Grigorean, J. Ramirez, S.H. Ahn, C.B. Lebrilla, *Anal. Chem.* 72 (2000) 4275.
- [64] J. Ramirez, F. He, C.B. Lebrilla, *J. Am. Chem. Soc.* 120 (1998) 7387.
- [65] J. Mrozek, B. Banecki, J. Karolczak, W. Wiczak, *Biophys. Chem.* 116 (2005) 237.
- [66] I.V. Terekhova, O.V. Kulikov, R.S. Kumeev, M.Y. Nikiforov, G.A. Al'per, *Russ. J. Coord. Chem.* 31 (2005) 218.
- [67] P. Sompornpisut, N. Deechalao, J. Vongsvivut, *ScienceAsia* 28 (2002) 263.
- [68] J. Lehmann, E. Kleinpeter, J. Krechl, *Inclusion Phenom. Macrocyclic Chem.* 10 (1991) 233.
- [69] M. Thunhorst, U. Holzgrabe, *Magn. Reson. Chem.* 26 (1998) 211.
- [70] B. Lin, X. Zhu, S. Wuerthner, U. Epperlein, B. Koppenhoefer, *Talanta* 46 (1998) 743.
- [71] E. Szoko, J. Gyimesi, L. Barcza, L.K. Magyar, *J. Chromatogr. A* 745 (1996) 181.
- [72] M.W.F. Nielen, *Anal. Chem.* 65 (1993) 885.
- [73] C.L. Flurer, L.A. Lin, R.D. Satzger, K.A. Wolnik, *J. Chromatogr. A* 669 (1995) 133.
- [74] K. Pihlainen, R.J. Kostianen, *J. Chromatogr. A* 1033 (2004) 91.
- [75] B. Chankvetadze, N. Burjanadze, D. Maynard, K. Bergander, D. Bergenthal, G. Blaschke, *Electrophoresis* 23 (2002) 3027.

Simultaneous determination of one nonionic and two anionic surfactants using Fourier transform infrared spectrometry and multivariate analysis

K. Kargosha^{a,*}, S.H. Ahmadi^a, M. Mansourian^a, J. Azad^b

^a Chemistry and Chemical Engineering Research of Iran, P.O. Box 14335-186, Tehran, Iran

^b Chemistry Department, Alzahra University, Vanak, Tehran, Iran

Received 1 August 2007; received in revised form 24 November 2007; accepted 26 November 2007

Available online 15 December 2007

Abstract

A direct and reagent free procedure for simultaneous determination of sodium lauryl ether sulfate (SLES), coconut diethanol amide (CDEA) and linear alkylbenzene sulfonate (LABS) in undiluted samples of hand dishwashing liquids has been developed. This determination was carried out by using attenuated total reflectance Fourier transform infrared spectrometry (ATR-FTIR) and multivariate analysis.

An implementation of the PLS statistical approach to quantitative analysis of one nonionic and two anionic surfactants was applied to a set of mid-infrared spectra (1305–990 cm^{-1}) recorded for commercial detergent samples and ternary standard solutions. An orthogonal calibration design for three components and five levels for standards were employed. Number of factors and scans and also the resolution were optimized.

The statistical parameters such as the root mean square error of calibration (RMSEC), root mean square error of cross-validation (RMSECV), standard error of prediction (SEP) and relative standard deviation (R.S.D.) were evaluated. These parameters were obtained as: RMSEC 0.13, 0.20 and 0.14, RMSEV 0.09, 0.17 and 0.04 and SEP 0.12, 0.39 and 0.18 (g per 100 g) for SLES, CDEA and LABS, respectively. R.S.D. for five independent analyses were 1.69 for SLES, 3.76 for CDEA and 1.76 for LABS. The component linear correlation coefficients comparing actual and predicted concentrations of SLES, CDEA and LABS in some real samples were 0.9995, 0.9915 and 0.9974, respectively.

© 2007 Elsevier B.V. All rights reserved.

Keywords: Nonionic and anionic surfactants; Fourier transform infrared spectrometry; Multivariate analysis

1. Introduction

Surfactants are the primary cleaning ingredients in hand dishwashing detergents to provide cleaning performance. They are also the primary drivers for suds or foams, which are important sensory signals for consumers on the cleaning power of hand dishwashing detergents. Beyond cleaning and suds performance, mildness to human skin is another key requirement. Three main classes of surfactants that have found widespread applications in hand dishwashing detergents are anionic, non-ionic and amphoteric [1].

Anionic surfactants are the workhorses for grease cleaning performance of these detergents. They help to reduce the interfacial tension (IFT) between greasy soils and wash water to achieve

effective cleaning. In most dishwashing detergents, anionic surfactants are often used in combination with nonionic surfactants such as fatty alkanol amides. These mixed surfactant systems help to achieve very low IFT between greasy soils and wash water and thus significantly improve the detergent's cleaning efficiency [2]. These fatty amides are also good foam booster with unique values to hand dishwashing detergents. These amide surfactants are typically used in conjunction with linear alkylbenzene sulfonate (LABS)-based formulations, likely due to the unique foaming properties of this surfactant combination [1]. The most commonly fatty amide used in dishwashing detergents is coconut diethanol amide (CDEA).

The recent tendency has been to move from the traditional workhorse surfactant of all detergent products, LABS, to other anionic surfactants such as sodium lauryl ether sulfate (SLES). SLES has a lower sensitivity than LABS to water hardness and exhibits Kraft temperatures that are significantly lower than the one of LABS [3]. In particular, SLES shows increased skin mildness versus LABS [4]. With these favourable characteristics, in

* Corresponding author at: Chemistry and Chemical Engineering Research of Iran, Analytical Chemistry & Instrumentation, P.O. Box 14335-186, Tehran, Iran. Fax: +98 21 44580762.

E-mail address: K.Kargosha@ccerci.ac.ir (K. Kargosha).

today's dishwashing detergents formulations, LABS is at least partially replaced by SLES.

However, formulated hand dishwashing detergents have become increasingly complex, which has raised an increasingly need for very rapid quality control analysis requiring no separation.

Conventionally, methylene blue, ethyl violet and Co(III)-5-Cl PADP were proposed as suitable ion association reagents for the spectrophotometric determination of anionic surfactants [5,6].

Zhang and Chen reported a chemiluminescence method for determination of the anionic surfactants [7]. Chan et al. employed an optode for the quantitation of LABS [8]. In the finished formulations, SLES was the only surfactant that has been determined by potentiometric method using an ion-selective electrode [9,10]. Martinez-Barrachina et al. presented a potentiometric flow-injection method for the determination of nonionic surfactants [11]. Borrego et al. described mixed aggregate-based methodology to the quantification of nonionic surfactants [12]. Scullion et al. employed liquid chromatography–mass spectrometry for the determination of nonionic surfactants [13]. Another liquid chromatographic method is also reported for determination of CDEA and coconut monoethanol amide [14]. Most of these methods are developed for and restricted to a specific class of anionic or nonionic surfactants. In marked contrast, only a few methods have also been developed for the determination of more than one specific class of surfactants. For example Cao et al. reported a chemiluminescence method for the determination of an anionic surfactant (sodium dodecyl sulfate, SDS) and a nonionic surfactant (Triton X 100) [15]. Park and Rhee presented a liquid chromatographic method for the determination of anionic (sodium lauryl sulfate, SLS) and nonionic (CDEA) surfactants [16]. Most recently an attenuated total reflectance Fourier transform infrared (ATR-FTIR) spectrometric method is described for the simultaneous determination of an anionic (SLES), a nonionic (CDEA) and an amphoteric cocoamidopropyl betaine (CAPB) surfactant in shampoo and liquid soap [17]. It seems that this is the first appearance of the quantitative applications of ATR-FTIR to surfactants in the literature [17].

However, the growing desire for acceptance of finished products with minimal delay has made the development of direct and reagent free analytical methods for surfactant analysis a coveted goal. In this work, we tried to fulfill these requirements by using ATR-FTIR method. Our aim was analysis of ternary mixtures of LABS, SLES and CDEA, with no separation and dilution, in formulated hand dishwashing liquids.

2. Experimental

2.1. Equipments

A Magna 550 FTIR spectrometer (Nicolet, Madison, WI, USA) equipped with a DTGS detector, an ever-glow source and a Ge/KBr beam splitter, was employed for spectral measurements with a nominal resolution of 8 cm^{-1} . Omnic 1.2 and Quant IR 1.2 software packages (Nicolet) were used for acquisition of the spectra, statistical treatment of data and performing the PLS

Table 1

Concentration data for ternary standard solutions used as calibration (1–25) and validation (26–28) sets

Samples	Concentration (%w/w)		
	SLES	CDEA	LABS
1	3.00	2.00	13.00
2	3.00	1.00	11.00
3	1.00	1.00	15.00
4	1.00	3.00	12.00
5	5.00	1.50	15.00
6	2.00	3.00	13.00
7	5.00	2.0	12.00
8	3.00	1.50	12.00
9	2.00	1.50	14.00
10	2.00	2.50	15.00
11	4.00	3.00	14.00
12	5.00	2.50	13.00
13	4.00	2.00	15.00
14	3.00	3.00	15.00
15	5.00	3.00	11.00
16	5.00	1.00	14.00
17	1.00	2.50	11.00
18	4.00	1.00	13.00
19	1.00	2.00	14.00
20	3.00	2.50	14.00
21	4.00	2.50	12.00
22	4.00	1.50	11.00
23	2.00	1.00	12.00
24	1.00	1.50	13.00
25	2.00	2.00	11.00
26	4.73	2.63	13.26
27	3.56	1.94	12.31
28	1.50	1.75	11.50

method. All measurements were carried out using a cylindrical Spectra-Tech ATR cell with a ZnSe crystal rod.

2.2. Reagents and samples

Surfactants used for the preparation of sample solutions were the commercial surfactant materials used in the mass production of hand dishwashing liquids without further purification. These were obtained from Chemical and Petrochemical Industries of Iran. The results of the analysis for the surfactant content (in w/w) of these commercial products, as reported by the company, were: 70.60% SLES ($MW = 384\text{ g mol}^{-1}$), 96.60% LABS ($MW = 322\text{ g mol}^{-1}$) and 86.00% CDEA ($MW = 285\text{ g mol}^{-1}$). Industrial urea and other chemical reagents were supplied by Merck (Darmstadt, Germany).

An orthogonal design with a training set of standards containing SLES, CDEA and LABS at five concentration levels covering a total of 25 solutions, based on the model 5^2 standards was taken. In Table 1, the compositions of these ternary mixtures used in the calibration matrix design are summarized. Three more ternary standard solutions were prepared for evaluation of this calibration matrix design by mixing different weights of two calibration samples. The composition of these three validation set is also shown in Table 1. Each sample in calibration set was prepared by dissolution of different weight of SLES, LABS and CDEA in warm distilled water. To make the matrix

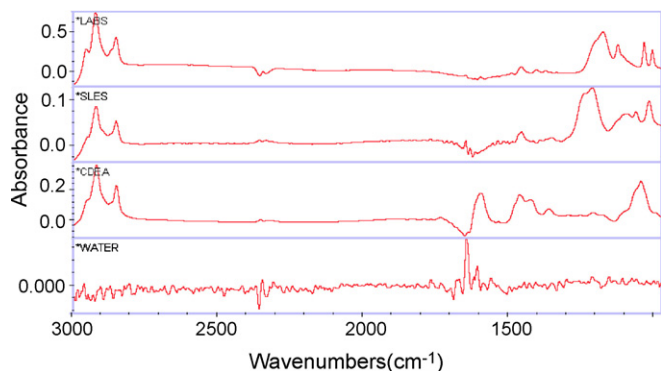


Fig. 1. The FTIR absorbance spectra of aqueous solutions of LABS (12%, w/w), SLES (5%, w/w), CDEA (2%, w/w) and water, using water as reference.

of these samples more similar to real samples, one gram of 2% (w/w) urea solution was added to each sample. Final weight of each sample was kept equal to 50 g.

3. Results and discussion

3.1. Spectral region and PLS calibration

Sample solutions were added into the ATR cell and spectra were recorded at a nominal resolution of 8 cm^{-1} with 32 co-added scans. A triangle function was used to apodize each infrared spectrum of the samples. Fig. 1 shows the absorbance spectra of monocomponent aqueous solutions of LABS, SLES and CDEA in wavenumber range $3000\text{--}990\text{ cm}^{-1}$, using water as reference. These spectra shows one main doublet peak at $1220\text{--}1100\text{ cm}^{-1}$ for LABS, one broad band at $1305\text{--}1160\text{ cm}^{-1}$ for SLES and one broad band at $1150\text{--}990\text{ cm}^{-1}$ for CDEA. These absorbance bands can be correlated to the stretching of --SO_3^- in LABS, the symmetric bending of R--O--SO_3^- in SLES and the stretching of C--O in CDEA, respectively [12]. The partially overlapping of these surfactants characteristic peaks with each other are also shown in Figs. 1 and 2 shows the spectrum of three ternary standard solutions of SLES, CDEA and LABS containing different amounts of these components in the spectral region of $1305\text{--}990\text{ cm}^{-1}$. As can be seen, the resulting difference spectra shows that the relative changes in absorbance appear to be linearly spaced in this wavenumber range for these ternary solutions.

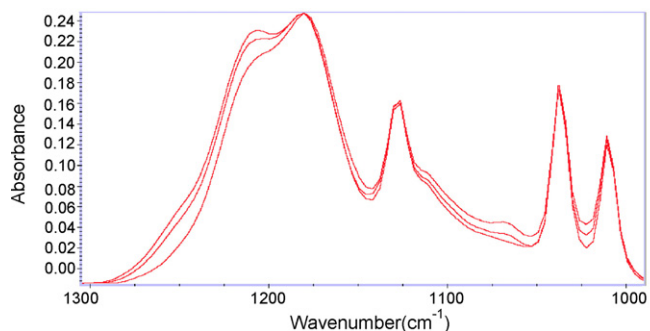


Fig. 2. Absorbance spectra of ternary standard solutions containing different amounts of SLES, CDEA and LABS (sample nos. 26, 27 and 28 of Table 1).

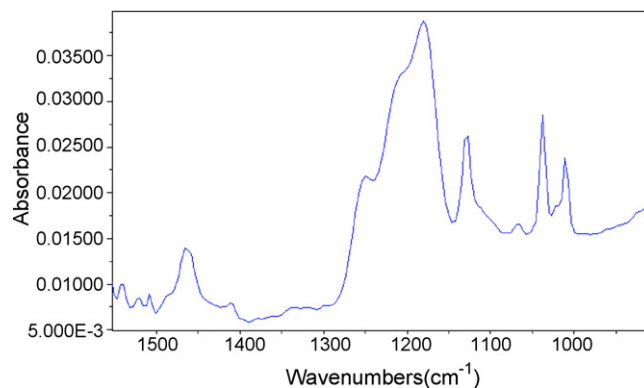


Fig. 3. The variance spectrum obtained by calculating the square of the standard deviation about the mean absorbance values for the calibration samples.

Multivariate calibrations are useful tools to be used in spectral analysis in order to overcome the spectral overlapping and to improve the precision and predictive abilities [18]. With the aim of simultaneous determination of SLES, CDEA and LABS in liquid hand dishwashing formulations, the PLS multivariate model was applied with the absorbance spectra data obtained for each ternary solution of calibration and validation sets.

To select the best spectral region for simultaneous determination of these surfactants, the variance plot was employed. Fig. 3 shows the variance display for the calibration data in wave number range $1550\text{--}900\text{ cm}^{-1}$. The variance plot was generated by calculating the average absorbance at each wavenumber position over the entire spectral range root of the variance about that mean for the entire calibration data set by using Quant IR 1.2 software [19]. In this software package this display has been named standard deviation plot. This standard deviation plot can be very useful for identification of active versus inactive spectral regions. The selected spectral region used for the model should be restricted to those regions showing the highest spectral response. As suggested by this standard deviation plot, three wavenumber ranges of $1305\text{--}990$, $1305\text{--}1115$ and $1305\text{--}1140\text{ cm}^{-1}$ were selected as most convenient spectral ranges.

Three sets of absorption spectra were obtained at these three spectral regions for all of the calibration ternary standard samples (Table 1). Baseline correction was applied for all these three sets of spectra. For each set of spectra, by using PLS algorithm a calibration model was constructed. The viability of these model were tested by comparing the optimal number of PLS factor, root mean square error of calibration (RMSEC), root mean square error of cross-validation (RMSECV), standard error of prediction (SEP) and square correlation coefficient (R^2) obtained for each component of ternary standard samples in each model.

To select the optimum number of factors in PLS algorithm, for each component of ternary calibration standards, the cross-validation method was used [20]. RMSECV was calculated each time a new factor was added giving rise to different PLS models. One reasonable choice for the optimum number of factors would be that number which yields the minimum RMSECV. Each sample of calibration set was predicted at each of these spectra range and then RMSEC and the R^2 for each component of the sample

Table 2
Statistical comparison of results obtained in analyzing samples of calibration and validation sets at three spectral ranges of 1305–990, 1305–1115 and 1305–1140 cm⁻¹

Statistical parameters	Spectral regions								
	1305–990 cm ⁻¹			1305–1115 cm ⁻¹			1305–1140 cm ⁻¹		
	SLES	CDEA	LABS	SLES	CDEA	LABS	SLES	CDEA	LABS
Number of factors	6	8	9	5	9	8	6	1	7
RMSECV (%w/w)	0.20	0.17	0.39	0.21	0.43	0.47	0.22	0.79	0.50
RMSEC (%w/w)	0.13	0.09	0.12	0.15	0.13	0.22	0.14	0.73	0.26
SEP (%w/w)	0.14	0.04	0.16	0.21	0.56	0.32	0.22	0.38	0.12
R ²	0.9989	0.9993	0.9983	0.9885	0.9639	0.9759	0.9925	0.9000	0.9660

in each model were also calculated [20]. SEP which is an indication of the average error in the analysis of validation ternary samples was calculated using expression

$$SEP = \sqrt{\frac{E^m(C_i - \hat{C}_i)^2}{m}}$$

where m is the number of ternary mixtures in validation set, C_i is the actual concentration of each component in the sample i and \hat{C}_i represents the predicted concentration of that component in the sample.

The optimal number of factor, RMSECV, RMSEC, SEP and R^2 values obtained for SLES, CDEA and LABS in each wavenumber region are summarized in Table 2. As it can be seen, the statistical parameters obtained in 1305–990 cm⁻¹ spectra ranges are the most favourite parameters. Hence, this wavenumber region was selected as most valuable spectra range.

3.2. Evaluation of selected model

Plots of the actual concentrations versus the values predicted by selected PLS model for each component of the 25 calibration ternary standard mixtures (Table 1) revealed a good correlation. The square correlation coefficient of these regression lines (R^2) were 0.9989 for SLES, 0.9993 for CDEA and 0.9983 for LABS. For validation set of ternary samples R^2 , were also calculated and found to be 0.9999 for SLES, 0.9998 for CDEA and 0.9983 for LABS.

To evaluate the precision of the selected model, the concentration of each component of sample number 6 of the calibration set was predicted ($n=9$) by performing the selected model and calculating relative standard deviation (R.S.D.). The R.S.D. were found to be 1.69 for SLES, 3.76 for CDEA and 1.76 for LABS.

All chemometric methods were found to be influenced by the method for data preprocessing (data scaling) or preparing information prior to application of mathematic algorithms [20]. Data scaling is usually used to remove or reduce irrelevant sources of variation (either random or systematic) for which the primary modeling tool may not account. Mean centering and auto scaling are two most common methods for data scaling [20]. By applying these two data scaling methods on analytical results, the effect of data preprocessing on the quality of the results was evaluated. Data obtained from baseline corrected absorption spectra at wavenumber range 1305–990 cm⁻¹ for calibration ternary standard mixtures were subjected to mean centering and auto

scaling prior to any other treatment by using Quant IR 1.2 software. Then the PLS calculations were performed on these two sets of treated data and the RMSEC and the RMSECV were calculated. The RMSEC and RMSECV for these two sets of the results and a set of the results obtained without applying mean centering or auto scaling (non-preprocessing) are given in Table 3. As we can see in Table 3, by applying auto-scaling method the errors were reduced and better results were obtained.

3.3. Real samples analysis

The proposed method was applied for the determination of SLES, CDEA and LABS in five hand dishwashing preparations. Two commercially available hand dishwashing liquids, A and B, were obtained from Pakshoo company and three other formulated samples, C, D and E, were supplied by Taj and Glan companies. Three latter samples were formulated from the commercial raw materials used in the mass production of dishwashing liquids, after standardization but without further purification. These samples were prepared using analytical balance and a strirrer, mixing all the components of formulation for 30 min. These five samples were analysed and the results obtained are summarized in Table 4. As can be seen, for all five hand dishwashing liquids, the assay results are in good agreement with the declared contents.

Table 3
Validation (RMSECV) and calibration (RMSEC) error results obtained by applying the different preprocessing methods in the determination of SLES and CDEA of the calibration samples

Preprocessing methods	Component	Errors (%w/w)	
		RMSECV ^a	RMSEC
Auto scaling	SLES	0.19	0.12
	CDEA	0.17	0.08
	LABS	0.37	0.11
Mean centering	SLES	0.20	0.12
	CDEA	0.17	0.08
	LABS	0.42	0.13
Non-preprocessing ^b	SLES	0.20	0.13
	CDEA	0.17	0.09
	LABS	0.39	0.12

^a Number of factors: six for SLES, eight for CDEA and nine for LABS.

^b Only baseline correction was applied.

Table 4
Determination of SLES, CDEA and LABS in commercial available formulation and laboratory formulated hand dishwashing liquids

Samples	Source	Declared value (%w/w)			Found (%w/w)		
		LABS	CDEA	SLES	LABS	CDEA	SLES
A	Pakshoo	4.12	0.64	12.78	4.13 ± (0.07)	0.65 ± (0.03)	12.78 ± (0.22)
B	Pakshoo	4.00	2.40	15.60	4.38 ± (0.08)	2.33 ± (0.08)	15.45 ± (0.28)
C	Taj	3.00	2.00	15.00	3.10 ± (0.05)	2.10 ± (0.08)	14.95 ± (0.27)
D	Glan	3.50	1.20	11.80	3.45 ± (0.06)	1.22 ± (0.05)	11.90 ± (0.22)
E	Glan	3.50	1.00	11.80	3.49 ± (0.06)	1.10 ± (0.04)	11.80 ± (0.20)

^a Average of three determinations. S.D. values are given in parentheses.

4. Conclusions

The proposed system of ATR-FTIR combined with PLS regression shows considerable appropriations for the simultaneous determination of three surfactants in hand dishwashing liquids. Undiluted and minute amounts of samples without any treatment are employed and spectra are recorded rapidly. The relative errors in simultaneous determination of these three surfactants can be similar and possibly better than those obtained by conventional methods, e.g. classical, potentiometric and extraction methods which are capable of determining a single component at a time.

References

- [1] R.F. Modler, R. Gubler, A. Kishi, *Surfactants, Household Detergents and Their Raw Materials*, CEH Marketing Research Report, 503. 8000A, SRI International, 2002.
- [2] K. Holmberg, B. Jonsson, B. Kronberg, B. Lindman, *Surfactant and Polymers in Aqueous Solutions*, 2nd ed., John-Wiley and Sons, Hoboken, NJ, 2003 (Chapter 18).
- [3] G. Jakobi, A. Lohr, *Detergents and Textile Washing*, VCH Verlagsgesellschaft, Weinheim, Germany, 1987.
- [4] O. Ranery, in: K.R. Lange (Ed.), *Surfactants*, Carl Hanser Verlag, Munich, 1999, pp. 191–203.
- [5] S. Motomizu, S. Fujiwara, A. Fujiwa, K. Toei, *Anal. Chem.* 54 (1982) 392.
- [6] S. Taguchi, I. Kasahara, Y. Fukushima, K. Goto, *Anal. Chim. Acta* 219 (1989) 239.
- [7] G.F. Zhang, H.Y. Chen, *Anal. Chim. Acta* 409 (2000) 75.
- [8] W.H. Chan, A.W.M. Lee, J.-Z. Lu, *Anal. Chim. Acta* 361 (1995) 55.
- [9] T. Masadome, T. Imato, *Fresen. J. Anal. Chem.* 363 (1999) 241.
- [10] M.T. Fielden, P.M. Claesson, *J. Colloid Interf. Sci.* 198 (1998) 261.
- [11] S. Martinez-Barrachia, M. Delvalle, L. Matia, R. Prats, J. Alonso, *Anal. Chim. Acta* 454 (2002) 217.
- [12] E. Borrego, D. Sicilia, S. Rubio, D. Perez-Bendito, *Analyst* 125 (2000) 1507.
- [13] S.D. Scullion, M.K. Clench, M. Cooks, A.E. Ashcroft, *J. Chromatogr.* 733 (1996) 207.
- [14] A. Nakae, K. Kunihire, *J. Chromatogr.* 156 (1978) 167.
- [15] Z. Cao, C. Lau, J. Lu, *Analyst* 129 (2004) 1262.
- [16] H.S. Park, C.K. Rhee, *J. Chromatogr. A* 1046 (2004) 289.
- [17] L. Carolei, I.G.R. Gutz, *Talanta* 66 (2005) 118.
- [18] M. Khanmohammadi, K. Kargosha, *Talanta* 65 (2005) 824.
- [19] M.P. Fuller, G.L. Ritter, C.S. Draper, *Appl. Spectrosc.* 42 (1988) 228.
- [20] R.G. Bereton, *Chemometrics*, in: *Data Analysis for the Laboratory and Chemical Plant*, John Wiley and Sons Ltd., Chichester, England, 2003.

ITO pattern fabrication of glass platforms for electropolymerization of light sensitive polymer for its conjugation to bioreceptors on a micro-array

T. Konry^a, B. Hadad^c, Y. Shemer-Avni^d, S. Cosnier^e, R.S. Marks^{a,b,*}

^a Department of Biotechnology Engineering, Faculty of Engineering Science, P.O. Box 653, Beer Sheva 84105, Israel

^b National Institute for Biotechnology in the Negev and ILSE Kats center for Meso and Nanoscale Science and technology, P.O. Box 653, Beer Sheva 84105, Israel

^c The Weiss Family Laboratory for Nano-scale Systems, P.O. Box 653, Beer Sheva 84105, Israel

^d Department of Virology and Molecular Development, Faculty of Health Science, Ben Gurion University of the Negev, P.O. Box 653, Beer Sheva 84105, Israel

^e Département de Chimie Moléculaire, UMR-5250, ICMG FR-2607, CNRS, Université Joseph Fourier BP 53, 38041 Grenoble Cédex 9, France

Received 11 November 2007; received in revised form 19 November 2007; accepted 20 November 2007

Available online 31 January 2008

Abstract

We present herein an effective and versatile method to fabricate a micro-patterned structure of conductive polymer, poly(pyrrole-benzophenone), on Indium Tin Oxide (ITO) glass chips for the subsequent photo-immobilization of various bioreceptor, antigens. Such methodologies are based on photolithography of ITO pattern fabrication on non-conductive surfaces, glass slides, and on a photo-active electrogenerated polymer films. The photo-active polymer serves as a substrate platform for the photo-immobilization of the bioreceptor reagents used for subsequent immunoreactions. We were able to show the resolution of electropolymerization on an ITO pattern as well as immobilization of more than one bioreceptor for the simultaneous detection of several analytes. The antigen micro-arrays were tested for sensitivity, specificity, and overall practicality for the simultaneous detection of analyte anti-Cholera Toxin B, anti-Hepatitis B virus surface and core protein antibodies. In addition we used our pattern ITO-poly(pyrrole-benzophenone) micro-array for the detection of serum samples of Hepatitis B virus patients previously screened by a standard hospital detection method.

© 2007 Elsevier B.V. All rights reserved.

Keywords: Cholera Toxin B; Hepatitis B virus; Antigen micro-array; Indium Tin Oxide; Polypyrrole; Photolithography

1. Introduction

Rapid detection and monitoring in clinical diagnostics has paved the way for the elaboration of alternative, state-of-the-art analytical devices, known as biosensors, micro-arrays or biochips [1–3]. Micro-arrays have features attractive in a detection platform such as portability, low rate of false positives, short time for analysis and flexibility with respect to analytes that can be studied as well as potential for facile application in clinical and field ready diagnostic devices. Moreover miniaturized and parallelized immunoassays are of general interest for all diagnostic applications, where several parameters in an individual

sample have to be determined simultaneously from a limited amount of material.

The preparation of micro-array platforms requires immobilization of bioreceptors on surfaces for future analyte capture. Established protein assays such as ELISA or Western blot use non-covalent surface interaction with hydrophobic (nitro-cellulose, polystyrene) or positively charged (poly-lysine, aminosilane) surfaces [4] in order to allow bioreceptor immobilization. Those methods may suffer from loss of capture molecules during the assay procedure since non-covalent attachment of bioreceptors might be too weak. In addition, though membranes possess a large surface area and have high protein binding capacity, they also suffer from background problems due to auto-fluorescence and non-specific protein binding. One way to counteract this problem is to use glass slides that can be prepared as ultraflat devices with a minimal degree of fluorescence. However, glass shows poor protein binding capability

* Corresponding author at: Department of Biotechnology Engineering, Faculty of Engineering Science, P.O. Box 653, Beer Sheva 84105, Israel. Tel.: +972 8 6477182; fax: +972 8 6472857.

E-mail address: rsmarks@bgu.ac.il (R.S. Marks).

and therefore surface modifications are required to facilitate protein binding. Established surface treatments for glass surfaces are covalent attachment performed using a variety of chemically activated surfaces (e.g. aldehyde, epoxy, active esters) [5–7], specific bimolecular interactions (e.g. avidin–biotin [8,9], His-tag–nickel–chelates [10]) or non-covalent attachment (self-assembling monolayers and hydrogel modification [11]).

In a previous work we reported that it is possible to create surface-conductive fiber-optics or glass slides by depositing a thin layer of Indium Tin Oxide (ITO) upon which a poly(pyrrole-benzophenone) thin film may be electropolymerized [12–14]. This surface is then used to affinity coat the biosensor platform with recognition probes. Using this immobilization method we were able to overcome one of the biggest challenges met by biosensors devices, which is the immobilization strategy used to conjugate intimately the bio-specific entity onto the transducer [15]. However the limitation of previously presented optic fiber and glass slides biosensors lays in the inability of simultaneous detection of several analytes using one biosensor platform.

Herein we extended our previous study and created a platform for the immobilization of bioreceptors for a two-analyte detection system distributed over separate micro-localities for the detection of antibodies to Hepatitis B virus (HBV). In particular we created separated patterns of light sensitive polymer, poly(pyrrole-benzophenone) surfaces and introduced different antigens to each separated pattern while exposing it to UV light. This allowed us to immobilize different bioreceptors reagents on the same array for the subsequent capture of different analytes.

Techniques for patterning of conducting polymers have been recently reviewed in the literature [16]. For the formation of micro-patterns of conducting polymers, photolithography [17], electron-beam (e-beam) writing [18], laser writing [19], screen printing [20], and ink-jet printing [21] have been conventionally employed. However, these methods may either cause damage to the conducting polymer layer or involve high costs, while new opportunities in micro-fabrication require new types of patterning technology [22]. Polypyrrole (Ppy) is an attractive material owing to its high electrical conductivity upon doping and good thermal and environmental stability in both doped and undoped states. Because of their insolubility, Ppy films are typically formed by electrochemical [23–26], or frequently by plasma deposition [27] techniques. In particular, the electrogeneration of polymer films that is compatible with bulk manufacturing procedures provides an easy control over the properties of the polymeric coating such as morphology and thickness. In order to create a patterned surface of light sensitive Ppy film by electrochemical polymerization a pattern of ITO was first applied to the glass slide surface.

To fabricate an ITO conductive pattern surface with high density arrays we used a photolithography method, “Lift-off process”. It is a simple, easy method for patterning deposited films over an entire surface simultaneously which affords exact control over the shape and size of the objects it creates. In addition patterns can be defined with extremely high fidelity and for very fine geometries.

We report on a procedure for the fabrication of a conductive pattern of ITO coated platforms for electropolymerization. In addition we were able to show the resolution of electropolymerization over decreasing sizes of created ITO patterns of micro-locations as well as immobilization of more than one bioreceptor for the putative simultaneous detection of several analytes. The micro-arrays were tested for sensitivity, specificity, and overall practicality for the simultaneous detection of anti-Cholera Toxin B (CTB), anti-HBV surface and core protein antibody analytes. In addition we used our pattern ITO-poly(pyrrole-benzophenone) micro-array for the detection of serum samples of HBV patients previously screened by standard hospital detection methods.

2. Experimental part

2.1. Materials

LOR 7b, Poly-methyl methacrylate (PMMA) resist, SU8 resist and Methoxy-2-Propanol (PM) acetate were purchased from MicroChem while SPR220 came from ROHM & HAAS. The pyrrole monomer, functionalized with a photo-reactive benzophenone group was prepared as previously described by the esterification of the 3-benzoylbenzoic acid with 1-(3-hydroxypropyl) pyrrole using the carbodiimide method [28]. BSA (A4503, fraction V), CTB (C 1655, used at a concentration of $4 \mu\text{g mL}^{-1}$), anti-Rabbit IgG-FITC conjugate (F 9887, used at a concentration of $0.08 \mu\text{g mL}^{-1}$), and anti-CTB (S 9008) were all purchased from Sigma.

HBV surface (8930) and core (8927) antigens used at concentrations of $4 \mu\text{g mL}^{-1}$, and monoclonal anti-HBV surface (1861, from Mouse) and anti-HBV core (1841, from Mouse) antibodies were purchased from ViroStar. Anti-Mouse IgG-FITC (72992) and anti-human IgG-FITC were purchased from Jackson ImmunoResearch. HBV sera samples, previously screened by AxSYM Abbott (Architect), were obtained from Soroka University Medical Center.

2.2. Fabrication of micro-array

2.2.1. Optical lithography

Fig. 1 shows a scheme of the photo-masks used in the lithographical laying of the ITO pattern over the glass slide platforms in the fabrication of micro-arrays. Two types photo-masks were used, one for fabrication of two antigen arrays with four lines on each side of the glass slide, each with six square patterns of 100 and $50 \mu\text{m}$ (Fig. 1, right side), and one for the fabrication of one antigen arrays with one line containing four square patterns with different sizes (100, 50, 10, $1 \mu\text{m}$, Fig. 1 left side).

LOR 7b is a resist based on polydimethylglutarimide. Its unique properties enable LOR products to perform exceptionally well when used either as a sacrificial layer or as an undercut layer in bi-layer lift-off processing. Herein, LOR 7b was used with the conventional positive resist, SPR, as an inert, non-UV-sensitive polymer, one that can be etched with most standard developers. A positive resist is a type of photoresist in which the portion of the photoresist that is exposed to light becomes

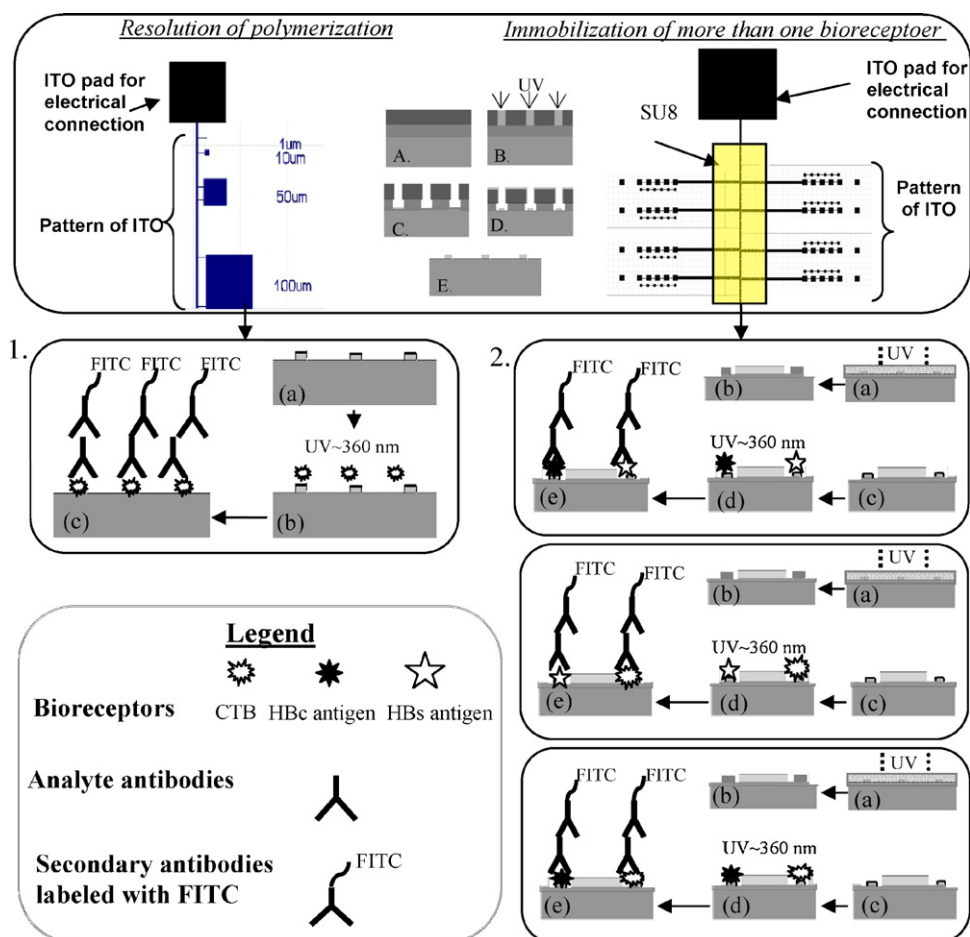


Fig. 1. Scheme of the photo-masks used in the lithographic fabrication of the ITO pattern over the glass slide platforms and the fabrication process used to generate micro-arrays. (Left) The PhotoMask pattern generated for the bio-chip evaluation process, employing a $1\ \mu\text{m}$ to $100\ \mu\text{m}$ square patterns. (Right) The PhotoMask pattern for the fabrication of antigen arrays for the simultaneous detection of more than one analyte. The fabrication process for creating a microelectrode array involves: (A) substrate with an underlying LOR (gray) and an overlying SPR layer (dark gray); (B) an area of SPR resist exposed to UV radiation (light gray); (C) an underlying LOR etched by developer; (D) directional sputter of ITO film; (E) lift-off processing and cleaning. (1) A CTB micro-array for determination of the immobilization resolution attained following (a) electropolymerization of poly(pyrrole-benzophenone) on the ITO-created pattern (b) pattern photo-immobilization of bioreceptors-CTB, (c) analyte conjugation and labeling with secondary fluorescent antibodies. (2) Generation of a two antigen micro-array involved (a) SU-8 was added to the system as a separator between pattern areas, (b) development of samples with PM acetate, leaving a separation layer of SU8 between patterns, (c) electropolymerization of poly(pyrrole-benzophenone) on the created pattern ITO, (d) pattern photo-immobilization of bioreceptors (HBV core and surface protein, CTB), and (e) analyte conjugation and labeling with secondary fluorescent antibodies.

soluble to the photoresist developer and the portion of the photoresist that is unexposed remains insoluble to the photoresist developer.

To obtain maximum reliability in the process, a substrate should be clean and dry prior to LOR application. Therefore, the glass slides were rinsed with acetone, followed by methanol and isopropanol (IPA) and dehydrated at $250\ ^\circ\text{C}$ for 1 h, and cooled down to room temperature. Thereafter, LOR 7b was spun at 2500 rpm on the wafer and baked for 3 min, and then the standard positive photoresist, SPR, was spun at 3000 rpm on the substrate and baked for 90 s. The SPR was exposed and the substrate developed (Fig. 1(B)). The standard developer, Az 400 K, diluted with double distilled (dd) H_2O (1:4, v/v) cleared the exposed SPR areas, and also “etched” away the LOR, leading to undercutting of the photoresist (Fig. 1(C)) for subsequent directional sputter of the ITO film (Fig. 1(D)). The resist was

then lifted-off using acetone or a resist removal solvent (such as *N*-methyl pyrrolidone (NMP)) (Fig. 1(E)).

Generally, SU8 was designed as a negative photoresist for micro-machining and other micro-electronic applications, whenever a thick, chemically and thermally stable pattern was desired. A negative resist is a type of photoresist in which the portion of the photoresist that is exposed to light becomes relatively insoluble to the photoresist developer. The unexposed portion of the photoresist is dissolved by the photoresist developer. To create a distinct pattern of ITO for the construction of a two antigen-array system, SU-8 was added as a separator between the two sides of the patterned areas (Fig. 1(2), in the middle area of the chip surface). SU8 was deposited on the patterned ITO surface by a spin-coating process and then baked for 3 min at $65\ ^\circ\text{C}$, followed by a 9 min bake at $90\ ^\circ\text{C}$. The samples were then cooled for 10 min. Thereafter, the samples were

exposed by a MJB4 aligner after performing an alignment process for 8 s. After that, the samples were baked for 1 min at 65 °C, followed by a 5 min bake at 95 °C and cooling for 10 min. Then, after the samples were developed with PM acetate, a thick layer of SU8 was left between the two sides of the ITO pattern on the masked slide. This prevented the bioreceptor solutions from crossing from one side to the other, where the solution drop was added, so that the second bioreceptor drop could be added without causing cross-contamination.

2.2.2. Indium Tin Oxide sputtering

The depositions were carried out in an r.f.—sputtering system. The sputtering target was a 2 in. diameter circular disk of hot pressed powder 99.9% purity ITO. The sputtering chamber was evacuated to a pressure lower than 1.33×10^{-4} Pa.

Argon gas was introduced into the sputtering chamber with partial pressures of 10^{-2} Pa. The glass slides were exposed to the sputter beam for 1–1½ h.

2.2.3. Deposition of pyrrole-benzophenone onto the chip surface by electropolymerization

All electrochemical experiments were performed with a Princeton Applied Research model 173 equipped with a model 179 digital coulometer and a model 175 universal programmer in conjunction with a Kipp and Zonen BD 91 XY/t recorder. The electropolymerization of pyrrole-benzophenone and the characterization of the resulting modified electrode were run at room temperature in a conventional three-electrode cell (Metrohm). A 10 mM Ag/Ag⁺ in CH₃CN electrode was used as a reference electrode in acetonitrile electrolyte. The working electrodes were the ITO-modified glass slides, an electrical contact being established with a platinum wire (diameter 50 µm) connected to an ITO pad for electrical connection (Fig. 1) above the acetonitrile solution. The poly(pyrrole-benzophenone) films were prepared by controlled potential oxidation (0.85 V) of the monomer (2 mM) in CH₃CN + 0.1 M LiClO₄.

2.3. Photo-immobilization of the antigens on the solid phase pattern polymer surface of micro-array platform

The immobilization of target antigens was performed by photo-activation of the previously electrogenerated polymer. To produce the desired activation radiation we used a MJB4 aligner with a light source near UV400 (350–450 nm). The MJB4 exposure system was manufactured from Herasil and suitable for processes using near UV (UV400) or mid-UV (UV300) radiation. The MJB4 achieves its performance with the unfiltered spectrum of a 200 W high pressure mercury arc lamp and its associated exposure system with a diffraction-reduced light path. The filter elements provide the different spectral ranges of the *g*-, *h*- and *i*-line of the mercury spectrum. The 200 W lamp provides an intensity of around 40 mW/cm² at broadband and 25 mW/cm² using the *i*-line filter, conditions used here.

2.4. Construction of antigen arrays

After electrogeneration of a polymer pattern, an antigen array, consisting of HBV core protein and HBV surface protein, HBV core protein and CTB, and HBV surface protein and CTB, were immobilized onto 2 cm × 1.5 cm coated glass slides by introducing different antigens to the two sides of the pattern separated by SU8, while exposing it to UV light. A single analyte detection array for anti-CTB antibodies was created in the same manner without SU8. Antigen solutions of 4 µg mL⁻¹ of each antigen, i.e. the CTB, HBV surface and core antigens, in phosphate buffer saline (PBS) were added to the pattern array element. The surface was then irradiated with the 365 nm emission line of a Near-UV, UV400 (350–450 nm), 200 W Hg lamp, with an intensity of 25 mW/cm² in the *i*-line filter, for 30 min.

Subsequently, the surfaces of the micro-arrays patterned with immobilized antigens, CTB and HBV core protein and HBV surface protein, were profusely rinsed with PBS 3× (pH 7.4) and air-dried.

2.5. Immunoassay

The blocking treatment was carried out on a glass surface, coated with polymer and antigen with 5% (w/v) BSA for 1 h in a Petri dish to block putative free spaces on the chip surface where the monomer did not polymerize. After incubation with BSA, the slides were rinsed with PBS × 3 (pH 7.4). Thereafter, the CTB, HBV core and surface antigen-conjugated micro-arrays were incubated for 20 min with 15 µL of diluted antibody solutions of anti-HBV surface antibody (anti-HBs) at various concentrations (0.01, 0.02, 0.04, 1.6, 160, 320, 640, 1280 µg mL⁻¹) and anti-CTB, anti-HBV core antibodies (anti-HBc and anti-CTB) at concentration of 320 µg mL⁻¹. Subsequently, the chip surfaces were rinsed and washed once with PBS × 3 (pH 7.4) and ddH₂O. Next, the chips exposed to the analyte were introduced to a solution containing FITC-labeled secondary immunoglobulin for 20 min, and finally, rinsed with PBS × 3 and ddH₂O. To check the specificity of the system, sets of series of glass-chips coated with polymer and antigens were set aside for use as blanks. The analyte solution was substituted by sera negative for anti-CTB, anti-HBc, anti-HBs antibodies, previously screened with the Abbott test.

The fluorescence from the bound FITC-labeled antibodies was visualized by capturing the image formed on a CCD camera. The intensity of the fluorescence emission of the FITC-labeled antibodies was measured using WinView32 software from the CCD-modified microscope.

2.6. Fluorescence microscopy

Fluorescence microscopy was performed using a Fluorescent inverted microscope (model IX-70, Olympus), using 20× and 10× objectives for observation of fluorescent images above 515 nm through the excitation band between 470 and 490 nm. Images were acquired using a CCD camera (Micromax, Roper scientific, USA).

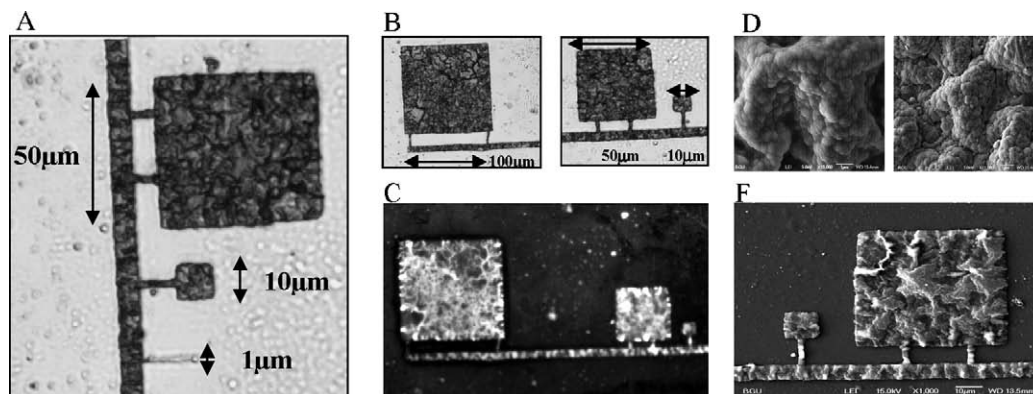


Fig. 2. The surface analysis of the conjugated biochip platform. (A and B) The pattern of polymerized ITO onto glass slide with square-like pattern of 1, 10, 50, 100 μm . (C) Fluorescence images of the immuno-array designed for detection of anti-CTB antibodies ($320 \mu\text{g mL}^{-1}$). (F and D) SEM analysis of the array film.

2.7. Scanning electron microscope

Micrographs of ITO-glass-chip surfaces were made with a Scanning Electron Microscope (SEM) (JEOL JSM—7400F). Micrographs were taken at 129 eV resolution of detector (Si) with an exposure time of 100 s. Cathodoluminescence images were made by a MiniCL imaging system (185–850 nm) attached to the SEM.

3. Results and discussion

3.1. Photo-immobilization of the antigen onto the polymerized biochip surface

The pattern ITO-glass slides coated with poly(pyrrole-benzophenone) were introduced to the antigen solution and then irradiated with UV light. Benzophenone and most of its derivatives absorb a photon at around 345 nm resulting in the promotion of one electron from a nonbonding sp^2 -like n-orbital on oxygen to an antibonding π^* -orbital of the carbonyl group. The actual electron-deficient oxygen n-orbital becomes electrophilic and therefore interacts with weak C–H σ -bonds, resulting in a hydrogen abstraction to complete the half-filled n-orbital. When amines or similar heteroatoms are in the vicinity of the excited carbonyl, an electron transfer step may occur, followed by proton abstraction from an adjacent group. In biological systems, the most effective H-donors include backbone C–H bonds in amino acids, thus, methylene groups of amino acid side chains, are good candidates providing abstractable hydrogens through the general mechanism shown in Ref. [13].

3.2. The surface studies of the conjugated biochip platform

Resolution of the possible polymerization onto the ITO pattern was studied. The prepared electrodes with different sizes of the ITO pattern were immersed in the monomer solution and a constant voltage of 0.85 V was applied for 5, 6 and 7 min. The films prepared during 6 and 7 min showed low adhesion to the ITO surface, due to formation of the thicker films. These films were partially mechanically removed after polymerization following immunosensor construction steps. Therefore the polymer

films used in the construction of immunosensors in this study were prepared using a constant voltage of 0.85 V applied for 5 min.

The ITO patterned glass slides (ITO squares 1, 10, 50, 100 μm in width) were polymerized once for 5 min and then examined microscopically (Fig. 2(A and B)). The polymer homogeneously covers the pattern of ITO surface of 10, 50, 100 μm in width. The polymerization occurred both on the ITO coated squares as well as on the ITO connecting lines, 1 μm in width. However, for the 1 μm square pattern, the ITO connection lines to the square pattern were less than 1 μm in width. Therefore, due to a low density of radicals and hence, poor polymerization, the obtained film was extremely thin and transparent, if occurred at all (Fig. 2(A)). The fluorescence images of the immuno-array for the detection of anti-CTB antibodies ($320 \mu\text{g mL}^{-1}$) are shown in Fig. 2(C).

SEM analysis of the array film showed homogeneous and compact structures of the polymer. The surface was characterized by a cauliflower-like arrangement of the poly(pyrrole) films constituted by microspherical grains (Fig. 2(D and F)). The quality of the polymer was illustrated by the absence of cracks or detachment of the film.

3.3. Immuno-array behavior

The detection of anti-CTB, anti-HBc and anti-HBs antibodies was achieved using a sandwich immunoassay (Fig. 1). As shown in Fig. 1, three antigen array platforms for simultaneous determination of (1) anti-CTB and anti-HBc antibodies, (2) anti-CTB and anti-HBs antibodies, and (3) anti-HBs and anti-HBc antibodies were constructed.

3.3.1. Immuno-array behavior for simultaneous detection of anti-HBs and anti-HBc antibodies

The anti-HBs antibody test is the most common one used for detection of immunity to HBV. The presence of such antibodies indicates previous exposure to HBV and protection from future HBV infection. In addition, this test is performed to determine the need for vaccination (if anti-HBs is absent), or following the completion of vaccination against the disease. Therefore, the quantitation potential of this test is crucial. Hence, eight

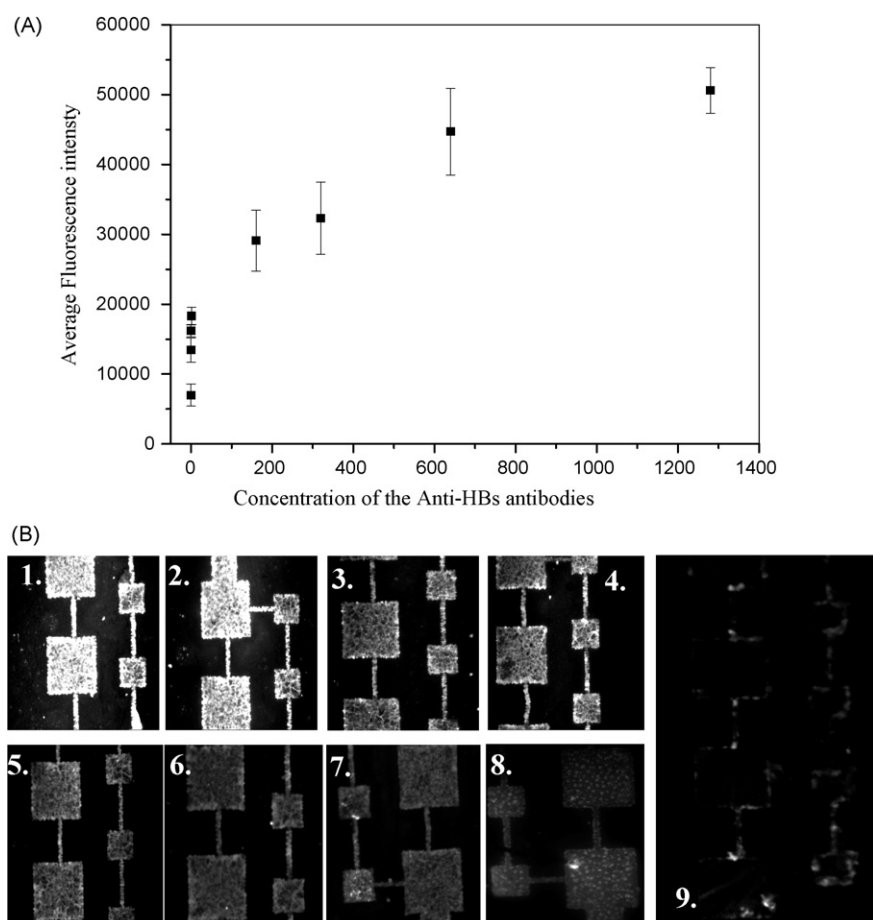


Fig. 3. Immuno-array behavior of the detection of anti-HBs antibodies. (A) Calibration curve obtained for the detection of anti-HBs antibodies. (B) Fluorescent images of the chip surface, each panel representing a different concentration of the analyte ((1) 1280 $\mu\text{g mL}^{-1}$, (2) 640 $\mu\text{g mL}^{-1}$, (3) 320 $\mu\text{g mL}^{-1}$, (4) 160 $\mu\text{g mL}^{-1}$, (5) 1.6 $\mu\text{g mL}^{-1}$, (6) 0.04 $\mu\text{g mL}^{-1}$, (7) 0.02 $\mu\text{g mL}^{-1}$, (8) 0.01 $\mu\text{g mL}^{-1}$, and (9) the fluorescence image of the negative sera sample (anti-HBc-/anti-HBs-) on two antigen micro-array previously conjugated with antigens (HBc antigen+/HBs antigen+).

different concentrations of the anti-HBs antibodies were used to test the sensitivity and quantifying potential of the antigen-array. Fig. 3(A and B) shows the standard curve and fluorescence images for the anti-HBs antibodies sandwich immunoassay obtained by collecting the average fluorescence intensity level through pixel counts of two bigger squares with a typical size of 100 μm and two smaller squares with a typical size of 50 μm , at antibody concentrations of 0.01, 0.02, 0.04, 1.6, 160, 320, 640 and 1280 $\mu\text{g mL}^{-1}$.

Furthermore, we received positive sera samples which were screened for post-vaccination for the presents of an adequate (i.e. protective) antibody response. Those samples were detected as positive for anti-HBs antibodies by the antigen micro-array (Table 1, line 5).

The core antigen is found in virus particles but disappears early in the course of infection, while anti-HBc antibodies are produced during and after an acute HBV infection. These antibodies are usually found in chronic HBV carriers, as well as those who have cleared the virus, and usually persist for life. Anti-HBc testing is either specific for IgM anti-HBc antibodies, the present of which indicates acute infection, or alternatively measures the ratio of total antibody to anti-HBc antibodies, indicating of past infection, either acute or chronic. Various reports

have concluded that virtually all commercially available anti-HBc procedures have poor specificity for HBV. We therefore propose herein a new procedure for screening anti-HBc antibodies.

In addition, micro-arrays constructed for the simultaneous detection of anti-HBs and anti-HBc antibodies can be used to determine recovery from prior HBV past infection (anti-

Table 1
Applicability of the proposed micro-array

Analyte	Immobilized antigen		
	CTB	HBV core	HBV surface
(1) Anti-HBc+/anti-HBs-/anti-CTB-	-	+	-
(2) Anti-HBc-/anti-HBs+/anti-CTB-	-	-	+
(3) Anti-HBc-/anti-HBs-/anti-CTB+	+	-	-
(4) Serum anti-HBc+/anti-HBs-	-	+	-
(5) Serum anti-HBc-/anti-HBs+	-	-	+
(6) Serum anti-HBc+/anti-HBs+	-	+	-
(7) Serum anti-HBc-/anti-HBs-	-	-	-

Different analyte solutions were introduced to the array surfaces previously immobilized with the two different antigens (array platforms are shown in Fig. 1). (+) Indicates positive fluorescence reaction on the pattern micro-array. (-) Indicates negative fluorescence reaction on the pattern micro-array.

Table 2
Reference experiments carried out to determine the possible influence of non-specific effects on the obtained response

Exp.	Step					
	ITO sputtering	UV radiation on poly(pyrrole-benzophenone)	Bioreceptor	Analyte	Secondary antibody labeled FITC	Visualize fluorescent response in CCD
1	+	+	+	+	+	+
2	+	+	+	+	–	–
3	+	+	+	–	+	–
4	+	+	–	+	+	–
5	+	–	+	+	+	–

The (+) and (–) signs indicate those steps conducted or omitted, respectively, for each experiment. Responses were recorded in all experiments using analyte antibodies at the highest concentration of $1280 \mu\text{g mL}^{-1}$.

HBs+/anti-HBc+) or if the patient was not infected by HBV but responded successfully to the hepatitis B vaccine shots (anti-HBs+/anti-HBc–).

The practicality of the proposed micro-array approach was tested on human sera samples. The sera samples used in this study (anti-HBs+/anti-HBc+, anti-HBs–/anti-HBc+, anti-HBs+/anti-HBc–, and anti-HBs–/anti-HBc–) were previously screened by the standard single analyte detection system used by hospitals (i.e. AxSYM, Abbott). We were able to confirm all positive samples as positive, and negative samples as negative (Table 1).

3.3.2. Specificity and cross-reactivity of antigen micro-array

In addition, the cross-reactivity of the two antigen array was determined (Table 1). No specific fluorescence was detected from the antigen array when non-specific antibodies were introduced to the immobilized antigen, reflecting the absence of cross-reactivity between the three IgG analytes (Table 1). The negative sera for HBV (anti-HBs–/anti-HBc–) showed no fluorescence, indicative of no attachment to the antigen-conjugated surface. Fluorescent contamination could however, be seen on the glass around the pattern.

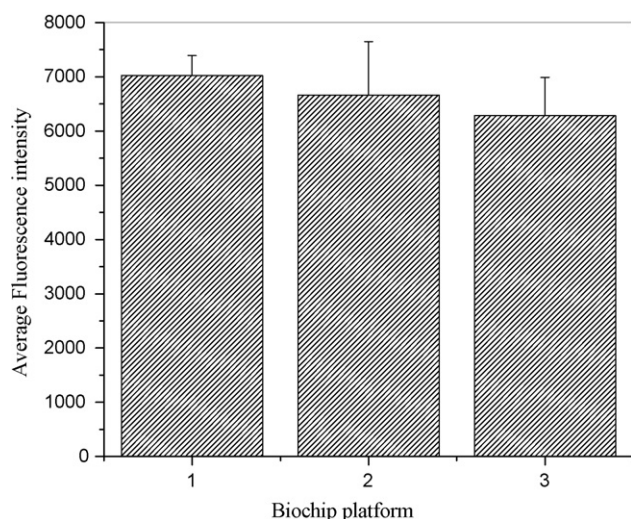


Fig. 4. The reproducibility of the biochip platforms, using $0.01 \mu\text{g mL}^{-1}$ of the anti-HBs antibodies.

To assess the influence of possible non-specific interactions on overall FITC responses, a set of reference experiments was carried out. Table 2 shows the conditions used for the set of different experiments that were carried out. The steps shown in the table correspond to those illustrated in Fig. 1. The results in Table 2 show that the responses from experiments 2–5 (obtained in the absence of UV illumination, antigen, analyte antibodies and secondary antibodies labeled with FITC, respectively, showed no fluorescence indicating the absence of non-specific attachment.

In addition, the reproducibility of the system was verified by measuring the fluorescence signal for three biochips (i.e. average of three lines in each biochip platform, Fig. 4). As can be seen, comparable behavior was obtained from all three biochips, using the same analyte concentration ($0.01 \mu\text{g mL}^{-1}$).

4. Conclusions

We were able to show the fabrication of conductive patterns of ITO coated platforms for the electropolymerization of functional monomers. In addition we were able to show the resolution of $1 \mu\text{m}$ electropolymerization over the created ITO pattern. We were able to immobilize more than one bioreceptor for the simultaneous detection of several analytes. The micro-arrays were tested for sensitivity, specificity, and overall practicality for the simultaneous analyte detection of anti-CTB, anti-HBV surface and anti-HBV core antibodies. We were able to show the quantitation potential of HBV micro-array detecting anti-HBs antibodies at a concentration of 10 ng mL^{-1} . In addition we were able to show the practicality of our pattern ITO-poly(pyrrole-benzophenone) micro-array for the detection of serum samples of HBV patients previously screened by standard hospital detection methods. The micro-array was shown to be as sensitive and selective as standard hospital detection methods.

Acknowledgments

We thank R. Nof, M. Sharabi and M. Shani Sekler for their technical assistance, as well as, the team at the Ben-Gurion University fabrication facility at the Weiss family Laboratory for Nano-Scale Systems, for the manufacture of the Bio-Chips used in this work. We further thank the Yeshaya Horowitz Asso-

ciation (project BioPen) and the EC6th Framework under the DENFRAME program #517711 for their financial assistance.

References

- [1] T. Vo-Dinh, B. Cullum, *Fresen. J. Anal. Chem.* 366 (2000) 540.
- [2] R.S. Marks, E. Bassis, A. Bychenko, M.M. Levine, *Opt. Eng.* 36 (1997) 3258.
- [3] F.S. Ligler, C.R. Taitt, L.C. Shriver-Lake, K.E. Sapsford, Y. Shubin, J.P. Golden, *Anal. Bioanal. Chem.* 377 (2003) 469.
- [4] G. MacBeath, S.L. Schreiber, *Science* 289 (2000) 1760.
- [5] D.M. Disley, P.R. Morri, K. Sproule, C.R. Lowe, *Biosens. Bioelectron.* 14 (1999) 481.
- [6] G.H.W. Sanders, A. Manz, *TRAC* 19 (2000) 364.
- [7] B.A.S. lawas, W.M. Reichert, *Biomaterials* 19 (1998) 595.
- [8] K. Nakanishi, H. Muguruma, I. Karude, *Anal. Chem.* 68 (1996) 1695.
- [9] L.C. Shriver-Lake, B. Donner, R. Edelstein, K. Breslin, S. KBhaia, F.S. Ligler, *Biosens. Bioelectron.* 12 (1997) 1101.
- [10] D.J. Pritchard, H. Morgan, J.M. Cooper, *Anal. Chem.* 67 (1995) 3605.
- [11] P. Arenkov, A. Kukhtin, A. Gemmell, S. Voloshchuk, V. Chupeeva, A. Mirzabekov, *Anal. Biochem.* 278 (2000) 123.
- [12] T. Konry, R.S. Marks, *Thin Solid Films* 492 (2005) 313.
- [13] T. Konry, A. Novoa, Y. Shemer-Avni, N. Hanuka, S. Cosnier, A. Lepellec, R.S. Marks, *Anal. Chem.* 77 (2005) 1771.
- [14] T. Konry, M. Bouhirfd, M. Whelan, F. Rossi, R.S. Marks, *Biosens. Bioelectron.* 22 (2007) 2230.
- [15] W.H. Scouten, J.H.T. Luong, R.S. Brown, *Trends Biotechnol.* 13 (1995) 178.
- [16] S. Holdcroft, *Adv. Mater.* 13 (2001) 1753.
- [17] J. Bargon, W. Behnck, T. Weidenbrueck, T. Ueno, *Synth. Met.* 41 (1991) 1111.
- [18] S.H. Magnus Persson, P. Kyreklev, O. Inganas, *Adv. Mater.* 8 (1996) 405.
- [19] M.S.A. Abdou, Z.W. Xie, A.M. Leung, *Synth. Met.* 7 (1992) 526.
- [20] F. Garnier, F. Hadjlaoui, A. Yasser, P. Srivastave, *Science* 265 (1994) 1684.
- [21] T.R. Hebner, J.C. Sturm, *Appl. Phys. Lett.* 73 (1998) 1775.
- [22] H.O. Jacobs, G.M. Whitesides, *Science* 291 (2001) 1763.
- [23] G.S. Akundy, J.O. Iroh, *Polymer* 42 (2001) 9665.
- [24] S. Sadki, P. Schottland, N. Brodie, G. Sabouraud, *Chem. Soc. Rev.* 29 (2000) 283.
- [25] M. Zhou, J. Heinze, *J. Phys. Chem. B* 103 (1999) 8443.
- [26] S. Cosnier, *Anal. Lett.* 22 (2007) 1612.
- [27] G.J. Cruz, J. Morales, R. Olayo, *Thin Solid Films* 342 (1999) 119.
- [28] S. Cosnier, A. Senillou, *Chem. Commun.* 3 (2003) 414.

Efficient separation of acetate and formate by ion chromatography: Application to air samples in a cultural heritage environment

Velichka Kontozova-Deutsch^a, Agnieszka Krata^{a,*}, Felix Deutsch^{a,b},
László Bencs^{a,c}, René Van Grieken^a

^a *Micro and Trace Analysis Centre, Department of Chemistry, University of Antwerp, Universiteitsplein 1,
B-2610 Antwerp, Belgium*

^b *Centre for Integrated Environmental Studies, Flemish Institute for Technological Research (VITO),
Boeretang 200, B-2400 Mol, Belgium*

^c *Research Institute for Solid State Physics and Optics, Hungarian Academy of Sciences,
P.O. Box 49, H-1525 Budapest, Hungary*

Received 31 July 2007; received in revised form 3 November 2007; accepted 8 November 2007

Available online 17 November 2007

Abstract

A method for the separation of acetate and formate anions by ion chromatography has been optimized under various measurement conditions (e.g. the composition of the mobile phase, and the flow rate of the eluent). For this purpose, two different analytical columns were examined: the IonPac AS14 (250 mm × 4 mm i.d.; designed mostly for the separation of inorganic anions) and the Allsep A-2 (150 mm × 4.6 mm i.d.; designed for the separation of low-molecular mass organic acids). However, nearly baseline separation of acetate and formate has been found on each column using the following conditions: (i) IonPac AS14 column and 2.0 mM Na₂B₄O₇ solution as an eluent with a flow rate of 1.0 ml/min, or (ii) Allsep A-2 column and an eluent containing a mixture of 1.2 mM Na₂CO₃ plus 1.5 mM NaHCO₃ with a flow rate of 1.3 ml/min. Additionally, the separation of fluoride from acetate and formate on both columns was studied. On the IonPac AS14 column it was possible to separate all three investigated anions. However, on the Allsep A-2 column, when the concentration of fluoride was comparable to, or higher than acetate, it was impossible to achieve good separation of these two anions, even using the optimized elution procedure. Therefore, the measurements of real samples were carried out with the use of IonPac AS14 column. The concentrations of acetate and formate have been determined in the air samples of the Cathedral of Cologne (Germany), after sampling the corresponding acids by passive diffusion tubes. Average concentrations of 122 and 9 μg/m³ for acetic and formic acids were found, respectively, inside the Cathedral and in a depot with medieval stained glass panels.

© 2007 Elsevier B.V. All rights reserved.

Keywords: Acetate; Formate; Passive diffusive sampling; Ion chromatography; Fluoride; Cultural heritage; Indoor air-quality

1. Introduction

For cultural heritage (CH) environment, it is important to keep concentrations of indoor air pollutants as low as possible from the point of view of the preservation of cultural property. Acetic acid and formic acid have been assumed to be dangerous for certain objects of art and can cause a major problem for curators and conservators of collections. Inorganic materials including lead, bronze, copper, shells, limestone, and ceramics can suffer

irreversible damages by the attack of organic acids. The sources of these acids have been well established; they mostly include wood and wooden products [1–5]. As wood is often used as an interior material, it is necessary to monitor concentrations of acetic and formic acids in the indoor air of buildings displaying CH items [5].

Ion chromatography (IC) is a very convenient and effective analytical method for the determination of various ionic species in aqueous solutions. As it is well known, this technique is based on the affinity of ions in the mobile phase for oppositely charged ions on the stationary phase. The availability of stationary phases of different selectivity has provided a range of options for the separation of various ions. The stationary phases

* Corresponding author. Tel.: +32 3 820 23 81; fax: +32 3 820 23 76.
E-mail address: agnieszka.krata@ua.ac.be (A. Krata).

adapted to IC have been polystyrene–divinylbenzene (PS–DVB) resins surrounded by a monolayer of charged latex particles. The use of substrates based on ethylene–vinylbenzene (EVB) cross-linked with 55% divinylbenzene resulted in solvent-compatible materials. Methacrylate-based latex anion resins, consisting of glycidylmethacrylate (GMA) monomers cross-linked with ethylene glycol dimethacrylate (EDM), are also utilized for IC analyses. Several approaches to a proper stationary phase design for the separation and determination of inorganic and organic acids in various matrices by IC were studied over recent years [6–10].

The most widely applied, commercially available columns for IC measurements are designed for the analysis of inorganic anions under isocratic [11,12] or gradient elution [13]. As manufacturers state, some of them can also be adapted for the separation of low-molecular mass organic anions, even along with common inorganic anions. Although for ionic species having very close affinity, as fluoride and acetate, acetate and formate, a baseline separation is difficult to achieve [14]. Isocratic elution conditions could not separate completely above-mentioned pairs of anions and gradient elution seems to be a better choice, but in many laboratories such a procedure is inadvisable for routine analysis.

One of the analytical columns used in described subject was the IonPac AS4A-SC (250 mm × 4 mm i.d., Dionex, Sunnyvale, CA, USA). This column is composed of 13 μm diameter, highly cross-linked (55%) EVB–DVB substrate agglomerated with permeable latex particles, which are completely aminated. The ion exchange capacity is 20 μequiv./column. In the case of the separation of acetate and formate, different eluents were used, i.e. disodium tetraborate ($\text{Na}_2\text{B}_4\text{O}_7$) solutions with a flow rate of 1.5 ml/min [15], carbonate-based buffers ($\text{NaHCO}_3 + \text{Na}_2\text{CO}_3$) with a flow rate of 1.7 ml/min [6], or sodium hydroxide (NaOH) solutions with a flow rate of 1.7 ml/min [10]. In all cases, the separation of both anions was obtained in a fairly short time (less than 5 min). It should be mentioned, that even using gradient elution it was rather difficult to achieve a complete baseline separation on this column for acetate and fluoride, as was found by Lee et al. [16] in the case of snow and ice samples.

The column IonPac AS11 (250 mm × 4 mm i.d., Dionex) was also studied for the separation of acetate and formate. The resin of this column is composed of 13 μm diameter, highly cross-linked (55%) EVB–DVB substrate particles, aminated with latex containing hydroxyl groups. The IonPac AS11 column has a higher percentage of latex cross-linking (6%), and consequently, a much lower uptake of water, when compared to the AS4A-SC column with only 0.5% latex cross-linking. The ion exchange capacity of this column is 45 μequiv./column. For this type of column, either NaOH solutions with a flow rate of 1.0 ml/min [17,18], or $\text{Na}_2\text{B}_4\text{O}_7$ solutions with a flow rate of 1.5 ml/min [19] have typically been used as an eluent. The separation of acetate and formate was achieved shorter than in 8 min. However, poor reproducibility for acetate on this column has been observed by Morales et al. [18] under the presence of fluoride in rainwater samples.

The IonPac AS10 column (250 mm × 4 mm i.d., Dionex), another type of cross-linked (55%) EVB–DVB substrate

(8.5 μm particle diameter), with an exchange layer functionalized with quaternary ammonium groups has also been used for the separation of acetate and formate. This column has 5% of latex cross-linking and a very high ion exchange capacity of 170 μequiv./column. For this column, either NaOH solutions [20,21], or $\text{Na}_2\text{B}_4\text{O}_7$ solutions [8,20] have been used as eluents. The flow rate in all cases was set to 1.0 ml/min. With the use of the former eluent the separation was completed within 4 min, but in the case of the latter eluent the separation time was very long—approximately 20 min.

A much known column, widely applied for the analysis of inorganic anions is the IonPac AS14 (250 mm × 4 mm i.d., Dionex) [22,23]. This column is packed with 9 μm diameter, highly cross-linked (55%) EVB–DVB substrate particles and the anion-exchange layer is functionalized with quaternary ammonium groups grafted to the surface. Its ion exchange capacity is 65 μequiv./column. Vanatta and Coleman studied this column for the separation of fluoride and acetate using isocratic elution [14]. The separation of anions was investigated for two mobile phases: (i) 2.5 mM $\text{Na}_2\text{CO}_3 + 3.4$ mM NaHCO_3 and (ii) 0.1 mM $\text{Na}_2\text{CO}_3 + 0.1$ mM NaHCO_3 . With the application of the former eluent, the two peaks were retained out of the void volume, but did not show baseline separation. However, nearly complete resolution was achieved with the eluent of weaker ionic strength after 12 min and it was possible to quantify both acetate and fluoride.

A newly available column, Allsep A-2 (150 mm × 4.6 mm i.d., 7 μm particle diameter) is produced by Alltech (Deerfield, IL, USA), to resolve acetate and formate signals. In order to improve the chromatographic separation between these organic anions, the traditional 100 mm Allsep A-2 column has been adapted to a custom-type 150 mm stainless steel column. This column is packed with a high capacity, methacrylate-based anion exchanger with quaternary amine functional groups. This material is hydrophilic and stable within the pH range of 2–11. As it is suggested by vendor, the separation of these anions can be completed in less than 4 min.

To the authors' knowledge, neither the recently introduced Allsep A-2 column, nor the IonPac AS14 column being available for a long time, has so far been systematically investigated for the separation of acetate and formate.

The aim of this work was to optimize conditions for the best separation of acetate and formate by IC. Two different analytical anion-exchange columns, not yet studied in the relevant literature, were chosen: IonPac AS14 (Dionex) and Allsep A-2 (Alltech). The retention behaviour of analytes depends mainly on the eluent concentration. Therefore, for optimizing the elution of anions, solutions of $\text{Na}_2\text{B}_4\text{O}_7$, or mixtures of NaHCO_3 and Na_2CO_3 at varying concentrations and flow rates were studied. The analytical performance of both columns for the separation of acetate and formate was compared. Also, much attention was paid to the presence of fluoride, since it has a very similar retention time to acetate and could have influence on its signal [16,18]. The optimized conditions were subsequently applied to the determination of the levels of both ions in air samples from a CH environment.

2. Experimental

2.1. Air sampling

Sampling of acetic and formic acids were carried out by means of Radiello[®] diffusion tubes (Fondazione Salvatore Maugeri, Padova, Italy) on polyester microfiber cartridges coated with triethanolamine (TEA). Both acids were adsorbed by TEA and subsequently extracted with 5 ml high purity Milli-Q water (Millipore). The exposure time of the cartridges was 1 week inside and outside the Cathedral of Cologne (Germany).

By means of one type of diffusion tube, four important gaseous pollutants can be sampled simultaneously, i.e. NO₂, SO₂, acetic and formic acids. For NO₂ and SO₂, the experimentally determined sampling rates of the diffusion tubes were adapted. For acetic and formic acids the sampling rates were calculated from the diffusion coefficients of these compounds and the experimentally determined effective geometric constant of the Radiello[®] diffusion tubes [3].

Levels of acetic and formic acids were investigated inside of a depot for stained glass panels in the Cathedral of Cologne. As it is well known, acids play an important role in the glass deterioration processes. The valuable glass panels were stored on wooden shelves, which are possible emission sources of acetic and formic acids.

2.2. Apparatus

All the measurements were carried out on a Dionex model DX-120 (Sunnyvale, CA, USA) ion chromatograph equipped with an AS-50 (Dionex) autosampler. A 20 µl aliquot of the sample/standard solution was loaded into the eluent-stream. The ions were detected by suppressed conductivity of the eluent using an ASRS-ULTRA self-regenerating suppressor column (Dionex). Data acquisition, construction of calibration curves and peak integration were achieved with the aid of the Peaknet[®] Dionex software package, Version 6.11.

For the separation of the concerned ions, two columns were examined: (i) an IonPac AS14 (250 mm × 4 mm i.d.) analytical column with an AG14 (50 mm × 4 mm i.d.) guard column produced by Dionex, and (ii) an Allsep A-2 column

(150 mm × 4.6 mm i.d.) with a GA-1 (7.5 mm × 4.6 mm i.d.) guard column, produced by Alltech.

2.3. Reagents

All the reagents were of analytical grade. Standard solutions of acetate and formate were prepared by appropriate dilution of their stock solutions (each 1000 µg/ml, Merck, Darmstadt, Germany) in Milli-Q water. The limits of detection (LODs) for acetate and formate correspond to 3σ confidence of the blank solutions. Standard solutions of fluoride were prepared by appropriate dilution of the stock solution (20 µg/ml, Dionex) in Milli-Q water.

The eluents, solutions of Na₂B₄O₇, were prepared by dissolving appropriate amounts of Na₂B₄O₇·10H₂O (Merck) in Milli-Q water. Eluents containing mixtures of Na₂CO₃–NaHCO₃ at various concentrations were prepared by dissolving appropriate amounts of Na₂CO₃ (Merck) and NaHCO₃ (Merck) powders in Milli-Q water. Accurate weighing of chemicals was performed on Chyo JL-180 model (Japan) analytical balance.

The calibration curves were constructed with five standard solutions. Each standard/sample solution was measured three times, from which the average concentration and standard deviation (SD) were calculated.

2.4. Optimization of the separation procedure

The conditions recommended by Dionex for the separation of acetate from formate are 2 mM Na₂B₄O₇ as an eluent with a flow rate of 1.5 ml/min under gradient elution. The recommended isocratic elution conditions by Alltech for the separation of acetate from formate are a flow rate set to 2.0 ml/min and an eluent containing a mixture of 2.1 mM NaHCO₃ and 1.6 mM Na₂CO₃. As it follows, both types of columns assured the signal of fluoride should be resolved from acetate and formate ions.

In the case of the IonPac AS14 column, solutions of Na₂B₄O₇ with various concentrations were tested as an eluent: (i) 1.0 mM; (ii) 2.0 mM; (iii) 3.5 mM; or (iv) 5.0 mM. The eluent flow rate was studied in the range of 0.7–1.5 ml/min.

For the Allsep A-2 column, the following eluents were tested: (i) 2.1 mM NaHCO₃/1.6 mM Na₂CO₃; (ii) 1.5 mM

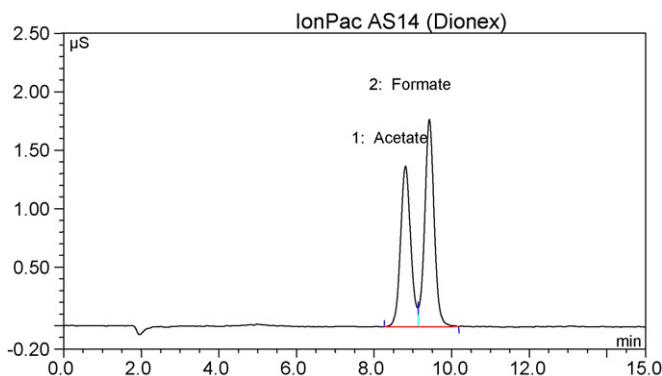


Fig. 1. Separation of 10 mg/l acetate and 5 mg/l formate on an IonPac AS14 (standard solution).

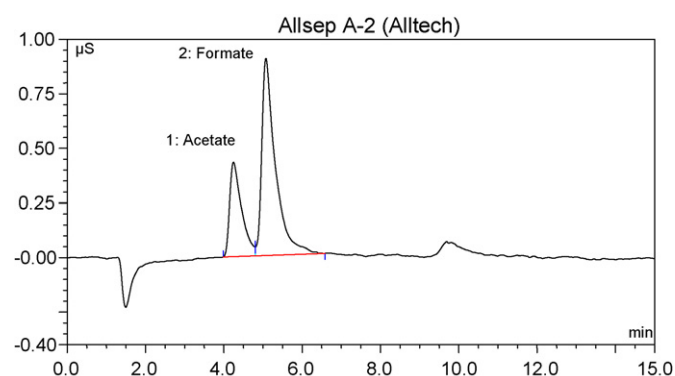


Fig. 2. Separation of 10 mg/l acetate and 5 mg/l formate on an Allsep A-2 (standard solution).

Table 1
Comparison of the analytical performance of columns: IonPac AS14 and Allsep A-2

Parameter	IonPac AS14		Allsep A-2	
	Acetate	Formate	Acetate	Formate
Limit of detection (mg/l)	0.61	0.46	0.68	0.51
Precision (RSD) (%)	4.0	5.0	3.5	4.7
Correlation coefficient (r^2)	0.9989	0.9982	0.9993	0.9992
Retention time (min)	8.8	9.4	4.1	5.1
Upper limit of dynamic range (mg/l)	200	100	300	100

NaHCO₃/1.2 mM Na₂CO₃; (iii) 1.0 mM NaHCO₃/0.8 mM Na₂CO₃; (iv) 1.6 mM NaHCO₃/2.1 mM Na₂CO₃; (v) 1.2 mM NaHCO₃/1.5 mM Na₂CO₃; (vi) 0.8 mM NaHCO₃/1.0 mM Na₂CO₃. The eluent flow rate in the range of 0.7–1.5 ml/min was investigated. It should be mentioned that the separation was provided under isocratic conditions on both columns.

3. Results and discussion

3.1. Conditions for the separation of acetate and formate

In the case of the IonPac AS14 column, the best separation, nearly a baseline resolution of both anions was obtained when using a solution of 2.0 mM Na₂B₄O₇, as suggested by the manufacturer for gradient elution, and a flow rate of 1.0 ml/min was found to be optimal. Under these conditions, retention times of 8.8 min for acetate and 9.4 min for formate were received and peak shapes were not skewed (Fig. 1). The resolution could depend on the amount of one analyte, which could affect the response of the second, i.e. the peak area for a given level of fluoride could depend on the level of acetate. Therefore, a series of standard solutions were prepared and analyzed. Their acetate and formate contents were in mg/l: 1 + 1, 10 + 5, 100 + 50, 200 + 100, 400 + 50, and 500 + 100, respectively. A good separation of the two chromatographic signals was achieved up to 100 and 50 mg/l acetate and formate concentrations, respectively. At concentrations higher than these, the resolution of peaks decreased.

For the Allsep A-2 column, it was possible to use the eluent recommended by Alltech for the separation of organic acids: a mixture of 2.1 mM NaHCO₃ and 1.6 mM Na₂CO₃. However, using a flow rate of 1.3, or 1.5 ml/min has been found to be more optimal for the separation of acetate and formate. At a flow rate of 2.0 ml/min, the column pressure quickly rises above the maximum permissible level for the IC system. Nearly baseline separation between acetate and formate was achieved when using a mixture of 1.5 mM NaHCO₃ and 1.2 mM Na₂CO₃ buffer solution as an eluent, at a flow rate of 1.3 ml/min. Under these conditions, retention times of 4.1 and 5.1 min were observed for acetate and formate, respectively (Fig. 2). Also, in the case of this column, a series of standard solutions were prepared and analyzed at the same concentrations as for the IonPac AS14 column. A good resolution of the peaks was obtained even up to 500 and 100 mg/l concentrations of acetate and formate, respectively. It was also noticed that when a flow rate lower than

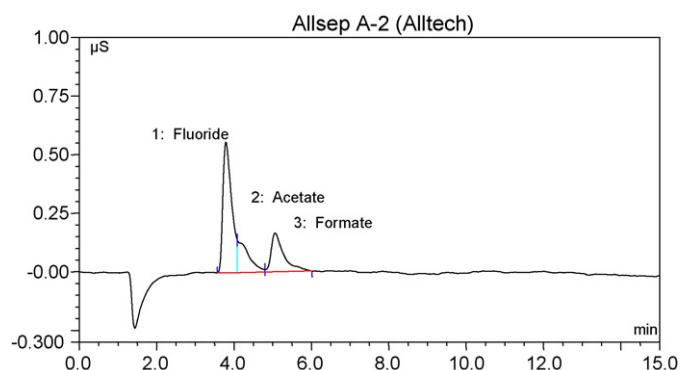


Fig. 3. Separation of 1 mg/l fluoride, 1 mg/l acetate and 5 mg/l formate on an Allsep A-2 (standard solution).

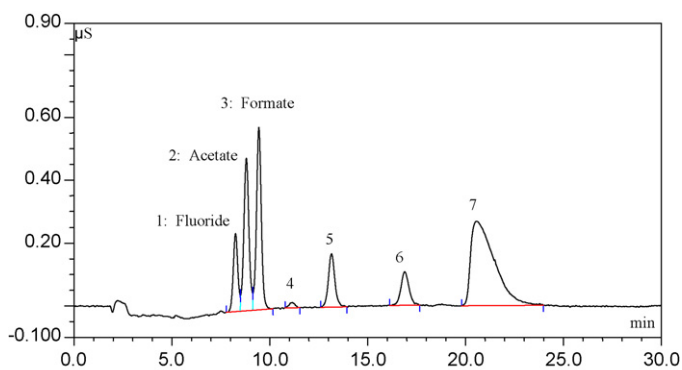
1.1 ml/min was used, tailing of the chromatographic signals of acetate and formate occurred and they become rather broad.

3.2. Analytical performance data

The analytical performance data for both columns are listed in Table 1. Lower LODs for acetate and formate were received with the use of the IonPac AS14 column: 0.61 and 0.46 mg/l, respectively. The obtained precision, expressed as the relative standard deviation (RSD), was similar for both columns, below 4% for acetate and below 5% for formate. In the case of the Allsep A-2 column, retention times were only half of those obtained on AS14. However, the sensitivity was found to be two times higher, when applying the IonPac AS14 column in comparison to the Allsep A-2 (see Figs. 1 and 2).

3.3. Separation of fluoride from acetate and formate

With the use of Radiello[®] diffusion tubes, hydrogen fluoride is also sampled simultaneously in addition to acetic and formic acids. As a consequence, fluoride is also present in the sample solutions and could have influence on the signals of acetate and formate. Therefore, the separation of fluoride from acetate and



Peaks: 4, 5, 6 and 7 – not identified

Fig. 4. Separation of fluoride, acetate and formate on an IonPac AS14 in a real sample taken at the Cathedral of Cologne.

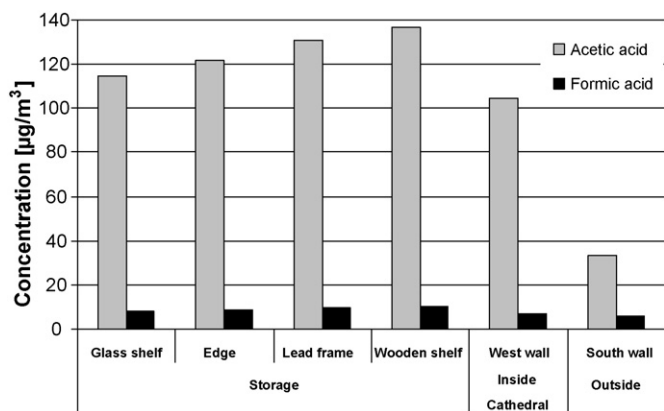


Fig. 5. Concentrations of acetic acid and formic acid in samples taken at various locations inside and outside the Cathedral of Cologne.

formate on both columns was studied with a variety of mixed standard solutions of the analytes. The concentrations of acetate and formate in these solutions were always the same 10 and 5 mg/l, respectively. However, the concentration of fluoride was as follows in mg/l: 1, 2.5, 5, 7.5, 10, 12.5, or 15. The analyses on the IonPac AS14 revealed very good separation of fluoride, acetate and formate peaks in all cases and also showed no dependence on the amount of fluoride present in the samples. However, the situation was opposite when using the Allsep A-2 column. It was not possible to resolve the peaks of these anions in the case of fluoride concentrations comparable to, or higher than acetate, even using the optimized elution procedure. The influence of fluoride was proven to be significant, as appears on Fig. 3.

3.4. Application of the method to ambient air samples

Taking into account the influence of fluoride in the case of air samples, collected in the Cathedral of Cologne, the IonPac AS14 column was used for the separation of acetate and formate. The analysis showed nearly baseline separation of all investigated anions (Fig. 4). The concentrations of acetic acid ranged from 33 to 137 µg/m³ with an average value of 122 µg/m³ inside the depot. The concentration obtained for the sample taken outdoors was much lower. The concentrations of formic acid ranged from 6 to 10 µg/m³ with an average value of 9 µg/m³ inside the depot. The obtained results are shown in Fig. 5. It can be clearly seen that relatively high concentrations of both acids were found in the indoor environment, especially for acetic acid.

4. Conclusions

In this work, results are presented for the optimization of the separation of acetate and formate on two types of analytical columns, i.e. an IonPac AS14 and an Allsep A-2. As optimum conditions for resolution of the peaks of these anions, the following parameters were found under isocratic conditions: 2.0 mM Na₂B₄O₇ solution as an eluent with a flow rate of 1.0 ml/min for the IonPac AS14 column (in contrast to vendor, which suggested gradient elution), and an eluent containing a mixture of 1.2 mM Na₂CO₃ plus 1.5 mM NaHCO₃ with a flow rate of 1.3 ml/min for

the Allsep A-2 column (in contrast to vendor, which suggested a stronger eluent,—a mixture of 2.1 mM NaHCO₃ and 1.6 mM Na₂CO₃). Nearly baseline separation of acetate and formate was achieved on both columns. The chromatograms obtained by the Allsep A-2, the specifically designed column for the separation of low-molecular mass organic anions, were as good as the ones received on the IonPac AS14 column. Lower LODs for acetate and formate were achieved with the use of the IonPac AS14 column: 0.61 and 0.46 mg/l, respectively. The sensitivity was found to be two times higher on this column, but the analysis time was two times longer than on the former one. Also, no influence of the amount of fluoride present in the solutions was noticed on the IonPac AS14. For the Allsep A-2, a higher tolerance of the increasing analyte concentration in the sample solution can be acquired compared to the IonPac AS14, i.e. a higher dynamic range for the efficient separation of the anions concerned. On the other hand, it should be stressed that on the Allsep A-2 column, even when using the optimized elution conditions, it was not possible to separate fluoride and acetate with acceptable resolution. The separation of these anions strongly depended on the concentration of fluoride present in the samples. With the application of the proposed method, and using the IonPac AS14 column, it was possible to quantify the levels of acetic and formic acids in the ambient air of monuments displaying CH items.

Acknowledgement

One of the authors (László Bencs) gratefully acknowledges the support from the Hungarian Scientific Research Fund (OTKA) under the project of F67647.

References

- [1] L.T. Gibson, B.G. Cooksey, D. Littlejohn, N.H. Tennent, *Anal. Chim. Acta* 341 (1997) 11.
- [2] J. Tetreault, E. Stamatopoulou, *Stud. Conserv.* 42 (1997) 141.
- [3] V. Kontozova, Z. Spolnik, A. Worobiec, R. Godoi, R. van Grieken, F. Deutsch, L. Bencs, in: R. Van Grieken, K. Janssens (Eds.), *Cultural Heritage Conservation and Environmental Impact Assessment by Non-Destructive Testing and Micro-Analysis*, Taylor and Francis Group, London, 2005, pp. 245–264.
- [4] T. Oikawa, T. Matsui, Y. Matsuda, T. Takayama, H. Niinuma, Y. Nishida, K. Hoshi, M. Yatagai, *J. Wood Sci.* 51 (2005) 363.
- [5] J. Tetreault, E. Cano, M. van Bommel, D. Scott, M. Dennis, M.-G. Barthes-Labrousse, L. Minel, L. Robbiola, *Stud. Conserv.* 48 (2003) 237.
- [6] M.C. Bruzzoniti, E. Mentasti, C. Sarzanini, P. Hajós, *J. Chromatogr. A* 770 (1997) 13.
- [7] C. Sarzanini, M.C. Bruzzoniti, P. Hajós, *J. Chromatogr. A* 867 (2000) 131.
- [8] M. Madera, W. Hoflinger, R. Kadnar, *J. Chromatogr. A* 997 (2003) 279.
- [9] Y. Chen, L. Jing, X. Li, Y. Zhu, *J. Chromatogr. A* 1118 (2006) 3.
- [10] K. Horváth, P. Hajós, *J. Chromatogr. A* 1104 (2006) 75.
- [11] P. Hatsis, C.A. Lucy, *J. Chromatogr. A* 920 (2001) 3.
- [12] Application Note 135, Dionex Corporation, Sunnyvale, CA, 2001.
- [13] M.A.J. Curran, A.S. Palmer, *J. Chromatogr. A* 919 (2001) 107.
- [14] L.E. Vanatta, D.E. Coleman, *J. Chromatogr. A* 804 (1998) 123.
- [15] R. Edwards, W. Bordass, D. Farrell, *Analyst* 112 (1997) 1517.
- [16] X. Lee, D. Qin, G. Jiang, H. Zhou, *Cold Reg. Sci. Technol.* 34 (2002) 127.

- [17] J.E. Madden, N. Avdalovic, P.E. Jackson, P.R. Haddad, J. Chromatogr. A 837 (1999) 65.
- [18] J.A. Morales, L.S. de Graterol, H. Velasquez, M.G. de Nava, B.S. de Borrego, J. Chromatogr. A 804 (1998) 289.
- [19] Y. Suzuki, J. Chromatogr. A 773 (1997) 123.
- [20] R. Kadnar, J. Rieder, J. Chromatogr. A 706 (1995) 339.
- [21] M. Toofan, J.R. Stillian, C.A. Pohl, P.E. Jackson, J. Chromatogr. A 761 (1997) 163.
- [22] P.E. Jackson, D.H. Thomas, B. Donovan, C.A. Pohl, R.E. Kiser, J. Chromatogr. A 920 (2001) 51.
- [23] R. Kadnar, M. Madera, R. Schlifke, J. Chromatogr. A 997 (2003) 285.

Calculation of equilibrium constants by matrix method for complexes of gold(III)

A.G. Kudrev

Institute of Chemistry, St.-Petersburg State University, University pr. 26, 198504 St.-Petersburg, Russia

Received 31 July 2007; received in revised form 16 October 2007; accepted 7 November 2007

Available online 21 November 2007

Abstract

A new matrix approach is proposed to calculate the equilibrium constants of ligands substitution in a metal ion inner coordination sphere with fixed binding sites positions. The proposed method allows to reduce the number of independent variables, necessary for the titration curves fitting without deterioration in the description accuracy. The square planar complexes $[MY_{4-n}X_n]$ $n=0-4$ formation in solution model includes three independent variables \bar{K} , ω_{cis} and ω_{trans} (\bar{K} —equilibrium constant of replacement of first ligand, ω_{cis} , ω_{trans} —parameters of mutual influence) as an alternative to four stepwise equilibrium constants and two microconstants. In the present investigation experimental spectrophotometric data published in the literature for system $\{Au^{3+}-Cl^- - Br^-\}$ were analysed. With the help of the proposed method the equilibrium constants of chloride by bromide ion substitution in internal coordination sphere of Au(III) are calculated $\bar{K} = 50$; $\omega_{cis} = 1.3$; $\omega_{trans} = 0.7$.
© 2007 Elsevier B.V. All rights reserved.

Keywords: Equilibrium constants; Matrix model

1. Introduction

Numerous examples are well known, when in a solution containing some metal ion and a ligand, formation of mononuclear complexes have been observed [1,2]. For such systems changes in spectral and potentiometrically measured characteristics as function of a ligand concentration commonly interprets as due to the successive formation of complexes ML_n [3]. The parameters of the model are independent from each other, stepwise stability constants. Number of independent variables equal to number of formed complexes. To determine this number unequivocally from experimental data is rather difficult, that leads to model uncertainty. If we deal with the mixed ligands complexes formation process when stepwise substitutions take place via direct ligand displacement then the case is similar to the solvent replacement in internal coordination sphere of a metal ion in the successive complexes formation process and the constants of replacement are similar to stepwise equilibrium constants [3]. Let us assume binding sites in internal coordination sphere of the central ion are fixed and that the affinity to binds a ligand of a given binding site depend on the presence of other same sort of bound ligands in this sphere. Such assumption

permits to reduce the number of independent variables, necessary for the equilibrium system description [4]. In this approach a ligand binds to an isolated site with intrinsic association (substitution) constant \bar{K} which is similar to the constant of first ligand binding by a central ion. The constants of ligand–ligand interaction between bound ligands ω_{cis} and ω_{trans} as a matter of fact, are similar to parameters of cooperativity of a ligand binding which were proposed for the polyelectrolyte effect description for oligomers [5]. The calculation of the intrinsic constants in the present work was carried out based on the matrix approach.

The aim of the present study is to get an alternative view on solving problem of description of successive ligands substitution in equilibrium complex formation and to check up adequacy of use the matrix method for the description of such equilibria. In this paper, a system Au^{3+} –chloride ion–bromide ion in aqueous solution is selected as an experimental example.

2. Computational details

2.1. Calculation of the equilibrium constants by the matrix method

The background of physical model applied for a titration curves description in the present work is the account of mutual

E-mail address: kudrevandrei@mail.ru.

influence between the neighbours in the compound containing a fixed binding sites. Let ion of metal be capable to reversible binds two kinds of ligands X and Y. Consider experimental conditions when a metal ion inner coordination sphere is completely filled by ligand Y. In this case mixed ligands complexes formation will occur as a result of replacement of ligand Y on X in various combinations. Assuming the square planar complexes $[MY_{m-n}X_n]$ ($m=4; n=0, 1, 2, 3, 4$) to be present in a solution. Permutation and simple combinations of two ligands among four binding sites leads to 16 possible configurations of complexes. The formation constant for a complex in each from 16 possible configurations can be written as:

$$\lg B_k = \sum_i^N \lg(\beta_{ki}) \quad (1)$$

where β_{ki} is the constants of replacement a ligand Y by X on separate site. For calculation β_{ki} we shall enter a configurations matrix \mathbf{M} ($2^N, N$). The matrix of configurations \mathbf{M} is defined as a set from 2^N of binary numbers. The line of matrix \mathbf{M} displays a complex configuration by a sequence of zeroes in sites where metal is bound to ligand Y and with a sequence of ones in sites where metal is bound to ligand X. The equilibrium constant of any ligand replacement appears as product of an element \mathbf{M} , intrinsic equilibrium constants (\bar{K}) of the reaction of a first ligand Y replacement by X, and interaction correction parameter (ω):

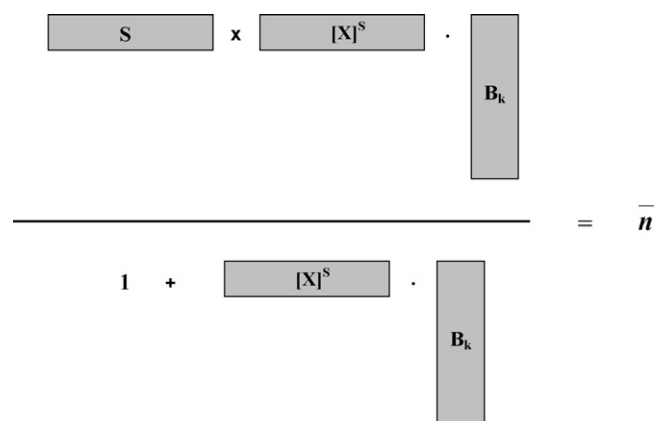
$$\beta_{ki} = (M_{ki} \bar{K} \omega_{ki})_{M_{ki} \neq 0} \quad (2)$$

Here ω_{ki} is the parameter of interaction correction (or mutual influence), which generally was taken into account, depending on geometry of coordination polyhedron. In particular case, for square planar D_{4h} geometry as follows: for i from 1 up to N , if $M_{ki} \equiv 1$ and $M_{ki+1} \equiv 1$, then $\omega_i = \omega_{cis}$ and $\omega_{i+1} = \omega_{cis}$, if $M_{ki} \equiv 1$ and $M_{ki+2} \equiv 1$ then $\omega_i = \omega_{trans}$ and $\omega_{i+2} = \omega_{trans}$. The formation function for each total concentration C_X , C_Y and C_M can be expressed as (see also Scheme 1)

$$\bar{n} = \frac{C_R - [R]}{C_M} = \frac{S \times [R]^S \cdot \mathbf{B}_k}{1 + [R]^S \cdot \mathbf{B}_k}$$

$$= \frac{[S_1 \ S_2 \ \dots \ S_{16}] \times [[R]^{S_1} \ [R]^{S_2} \ \dots \ [R]^{S_{16}}] \cdot \begin{bmatrix} B_1 \\ B_2 \\ \dots \\ B_{16} \end{bmatrix}}{1 + [[R]^{S_1} \ [R]^{S_2} \ \dots \ [R]^{S_{16}}] \cdot \begin{bmatrix} B_1 \\ B_2 \\ \dots \\ B_{16} \end{bmatrix}} \quad (3)$$

where \mathbf{S} is a row vector with the sum over each column of \mathbf{M} ; \times, \cdot are signs of array and matrix multiplication; $C_R = C_X/C_Y$; $[R] = [X]/[Y]$; \mathbf{B}_k is the vector of stability constants defined by Eq. (1). As follows from Eq. (3), \bar{n} depends on the ratio of ligand equilibrium concentrations, and independent variables \bar{K} , ω_{cis} and ω_{trans} . This model has the advantage that the number of fitting variables, which have to be evaluated via Eq. (3) is reduced, relative to the successive complex formation model. If



Scheme 1.

we introduce a matrix $\mathbf{P}(2^N, 5)$ intended for summation concentrations of complexes with equal ligand X number through all configurations, than we can calculate a matrix \mathbf{C}_{form} of species equilibrium concentration at a definite ligands concentration ratio (the superscript T means the transpose of a matrix) (see also Scheme 2)

$$\mathbf{C}_{form} = \left[C_M \times \left[\mathbf{B}_k \times [[R]^{S_i}]^T / (1 + [R]^S \cdot \mathbf{B}_k) \right]^T \cdot \mathbf{P} \right]$$

$$= \left[\frac{C_M \times \begin{bmatrix} B_1 \\ B_2 \\ \dots \\ B_{16} \end{bmatrix} \times \begin{bmatrix} [R]^{S_1} \\ [R]^{S_2} \\ \dots \\ [R]^{S_{16}} \end{bmatrix}}{1 + \begin{bmatrix} [R]^{S_1} & [R]^{S_2} & \dots & [R]^{S_{16}} \end{bmatrix} \cdot \begin{bmatrix} B_1 \\ B_2 \\ \dots \\ B_{16} \end{bmatrix}} \right]^T \cdot \mathbf{P}$$

$$= [B_1[R]^{S_1}[M] \ B_2[R]^{S_2}[M] \ \dots \ B_{16}[R]^{S_{16}}[M]] \cdot$$

$$\begin{bmatrix} 1 & 0 & 0 & 0 & 0 \\ 0 & 1 & 0 & 0 & 0 \\ \dots & \dots & \dots & \dots & \dots \\ 0 & 0 & 1 & 0 & 0 \\ \dots & \dots & \dots & \dots & \dots \\ 0 & 0 & 0 & 1 & 0 \\ 0 & 0 & 0 & 0 & 1 \end{bmatrix}$$

$$= [[MY_4] \ [MY_3X] \ [MY_2X_2] \ [MYX_3] \ [MX_4]] \quad (4)$$

For instance, for the system under investigation $Au^{3+}-Cl^- - Br^-$, application of Eq. (4) gives a matrix of equilibrium concentrations of following species $AuCl_4^-$, $AuCl_3Br^-$, $AuCl_2Br_2^-$, $AuClBr_3^-$, $AuBr_4^-$. Finally with using of Eq. (4) we can compute augmented matrix \mathbf{C}_f for full set of concentrations.

$$\begin{aligned}
 & \left[\begin{array}{c} C_M \times B_k \times [X]^s \\ \hline 1 + [X]^s \cdot B_k \end{array} \right] \cdot P = \\
 & = B_i [X]^{s_i} [M] \cdot P = \\
 & = [MY_{m-n} X_n] = C_{form}
 \end{aligned}$$

Scheme 2.

2.2. The procedure of fitting

In the present study least-squares fitting of multivariate absorption data has been done for two models. For an ordinary model of successive formation of complexes and a matrix model described above. In order to evaluate linear as well as non-linear parameters for both models a decomposition of the experimental absorbance data matrix A_{exp} is performed under non-negativity constraint. According to Lambert-Beer's law, A_{exp} can be decomposed into the product of a concentration C matrix and a matrix E of molar absorptivities. Corresponding matrix equation having general form is given as

$$A_{exp} = C \cdot E + R \quad (5)$$

where the dimensions of the matrices are: $A_{exp}(NR,NC)$, $C(NR,NS)$, $E(NS,NC)$; $R(NR,NC)$; NR is the number of rows in data matrix A_{exp} equal to the number of studied solutions with different concentrations of components, NC is the number of columns in data matrix A_{exp} equal to the number of wavelengths and NS is the number of chemical species absorbing the light; R is the residual matrix with the data variance unexplained by $C \cdot E$. Multiplication of both side of Eq. (5) on pseudoinverse matrix

[6] of C computed with initial guess of required parameters gives current estimation E^* of true matrix of molar absorptivities E . Finding of E^* for systems under investigation can be expressed by

$$E^* = A_{exp} / C_f^* \quad (6)$$

here slash '/' is the sign of a operator of matrix division (multiplication on pseudoinverse matrix); C_f^* is the current concentration matrix of the spectral forms calculated by using Eq. (4) or using stepwise equilibrium constants for full set of concentrations. To minimise the ambiguity of the solution, the iterative calculation of C and E is always subject to constraints [7]. Constraint applicable to UV/vis titration data is non-negativity. Product of E^* and C_f^* gives A_{calc} at the current values of non-linear parameters. Consequently iteration formula for computation of required non-linear parameters \bar{K} , ω_{cis} and ω_{trans} as well as stepwise equilibrium constants can be written as

$$A_{calc} = \left[\frac{A_{exp}}{C_f^*} \right]_{>0} \cdot C_f^* \quad (7)$$

Here $[\cdot \cdot \cdot]_{>0}$ is the operator cutting negative values which have not physical meaning. For refinement of non-linear parameters Levenberg–Marquard algorithm [8] of non-linear least square fitting is used. This algorithm has been proven is successful in calculations of equilibrium constants from data of spectrophotometric titrations [9]. Iterative procedure described above is used to find minimum of the objective function PE.

$$PE(A_{exp}, A_{calc})$$

$$= \sqrt{\frac{\text{Trace}[(A_{exp} - A_{calc}) \cdot (A_{exp} - A_{calc})^T]}{\text{Trace}[A_{exp} \cdot A_{exp}^T]}} \times 100 \quad (8)$$

here Trace is the sum of the diagonal elements. The optimization is stopped when the relative difference in PE between consecutive iterations is below a threshold value. In using weighting scheme setting the weights as $W_k = (1/A_{exp_k})^2$ and minimizing the sum of squared residuals is equivalent to minimizing the sum of squared relative residuals with unit weight [10]. The assumption of equal population variances were checked using standard F -test [11].

3. Results and discussion

3.1. Calculations of substitution constants from experimental data

Spectrophotometric data on halide substitution processes in chloro complex of gold(III) previously published in [12] were used as an experimental example. The equilibrium constants in the cited work were determined from kinetics. The changes in UV/vis absorbance spectra as function of concentrations of an chloride and bromide ions $C_R = C_{Br^-} / C_{Cl^-}$ ratios were recorded for equilibrated solutions. But these data were not used directly for calculations of equilibrium constants. Therefore for comparison in the present work the stepwise constants was decided to calculate also with use of traditional model

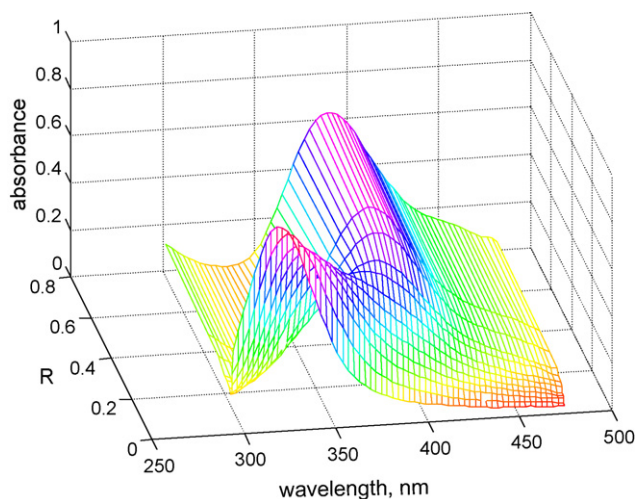


Fig. 1. Absorption spectra of solutions with constant C_{Au} and variable C_{Br^-}/C_{Cl^-} ; $C_{Au} = 1.71 \times 10^{-4}$ M; 1 M NaClO₄; 25 °C.

of independent successive complex formation. The absorbance data matrix A_{exp} (see Fig. 1) was obtained from the spectra image published in [12], with the help of the home-made computer program. Singular value decomposition [6] of matrix A_{exp} has shown, that five contributions or components better reproduce the original data matrix within usual (2%) noise level without problem of rank deficiency. From chemical reasons and previous investigations results it seems possible to use five complexes which are included in equilibrium interactions: $AuCl_4^-$, $AuCl_3Br^-$, $AuCl_2Br_2^-$, $AuClBr_3^-$, $AuBr_4^-$ as spectral forms for explanation the results of mathematical decomposition of initial data matrix. The equilibrium constants calculated by least squares fitting of data matrix A_{exp} in accordance to the orthodox model of successive complex formation for the system $Au^{3+}-Cl^- - Br^-$ in a solution, are given in Table 1. Worth to note that the ratios of successive constants remarkably differs from statistical expected values at the absence of mutual influence between coordinated ligands ($K_0/K_1:K_1/K_2:K_2/K_3 = 2.67:2.25:2.67$ [3]). Such behaviour

Table 1

The ordinary equilibrium constants of stepwise halide substitution and substitution constants calculated with help of the matrix method for the system $Au^{3+}-Cl^- - Br^-$

	$AuCl_{4-n}Br_n^- + Br^- = AuCl_{3-n}Br_{n+1}^- + Cl^-$	
$K_{n=0}$	186	243 ± 40 [12] (288) [13]
$K_{n=1}$	91	98 ± 20 [12] (135) [13]
$K_{n=2}$	34	49 ± 10 [12] (65) [13]
$K_{n=3}$	9	17 ± 5 [12] (23) [13]
	PE = 1.0	–
K_0/K_1	2.0	2.5 (2.1)
K_1/K_2	2.7	2.0 (2.1)
K_2/K_3	3.8	2.9 (2.8)
\bar{K}	50	–
ω_{cis}	1.3 (0.78)	–
ω_{trans}	0.7 (1.34)	–
	PE = 1.0	–

$C_{Au} = 1.71 \times 10^{-4}$ M; 1 M NaClO₄; 25 °C.

indicates on the presence of specific interactions between coordinated ligands. Complexes of gold(III) nearly always have square planar structure. The binding sites in square planar compound are not equivalent to each other and therefore according to matrix model, the formation function will be defined by three equilibrium binding constants \bar{K} , ω_{cis} and ω_{trans} . Those constants evaluated by least squares fitting of data matrix A_{exp} according to matrix model (Eqs. (1)–(4)) are given in Table 1. In accordance with statistical test, lack of fit of reproducing original data set with matrix model does not exceed the limit of tolerance and lack of fit of reproducing original data with help of the model based on four stepwise complex formation constants. Hence we can conclude that both models adequately describes

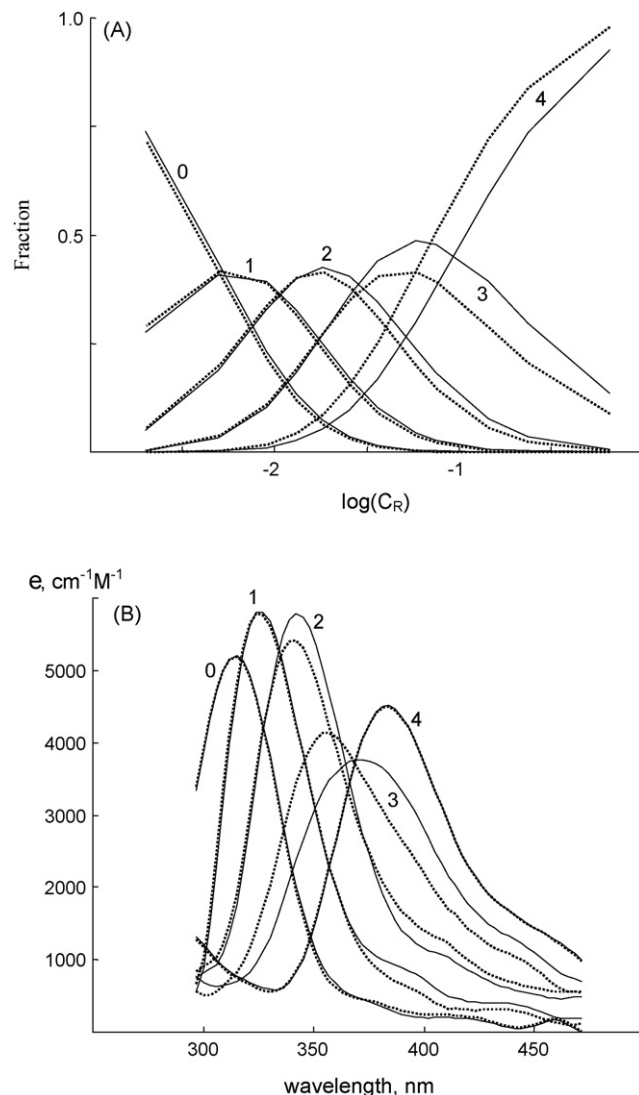
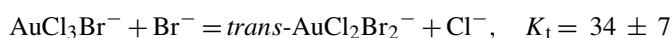


Fig. 2. (A) The distribution plots of gold(III) between species 0— $AuCl_4^-$, 1— $AuCl_3Br^-$, 2— $AuCl_2Br_2^-$, 3— $AuClBr_3^-$, 4— $AuBr_4^-$ calculated from the equilibrium constants $K_0 = 186$, $K_1 = 91$, $K_2 = 34$, $K_3 = 9$; as a function of logarithm of concentrations ratios $C_R = C_{Br^-}/C_{Cl^-}$; the dotted lines is distribution calculated with help of the matrix method (Eq. (4)) $\bar{K} = 50$; $\omega_{cis} = 1.3$; $\omega_{trans} = 0.7$; $C_{Au} = 1.71 \times 10^{-4}$ M; 1 M NaClO₄; 25 °C. (B) Molar absorptivities corresponding for the species $AuCl_{4-n}Br_n^-$ calculated from data matrix A_{exp} and the concentration profiles in (A); the dotted lines is calculated with using of the matrix model.

changes of absorbance spectra due to variations of the components concentrations in system $\text{Au}^{3+}\text{-Cl}^-\text{-Br}^-$ in a solution. The plots of gold(III) distribution between species AuCl_4^- , AuBrCl_3^- , $\text{AuBr}_2\text{Cl}_2^-$, AuBr_3Cl^- , AuBr_4^- calculated from the stepwise equilibrium constants in the same conditions as with use of matrix model are presented in Fig. 2A. The resolved spectra for all 5 complexes shown in Fig. 2B were calculated using data matrix A_{exp} and the equilibrium constants in Table 1. It is possible to note that both models gives very similar concentration profiles as well as profiles of spectra are also alike. We can see some difference just in the shapes and λ_{max} of species AuBr_3Cl^- . But the approach considered above gives two equivalent solutions with different values of parameters *trans* and *cis* influence see Table 1. It is impossible unequivocally define proper pair of values ω_{cis} and ω_{trans} directly from the spectral data measured in the equilibrium conditions. The decision requires additional information for instance quantum chemical calculations. Fortunately the particular feature of the $\text{Au}^{3+}\text{-Cl}^-\text{-Br}^-$ system is the formation of *cis*- and *trans*-isomers with different speeds. The microconstants for the isomers formation reactions have been determined using stop-flow spectrophotometry [12].



We can see that the formation of the *cis* isomer is thermodynamically more favourable, than *trans* form. Parameters of mutual influence appropriate to the ratio $\omega_{\text{cis}}(\text{Br}^-) > \omega_{\text{trans}}(\text{Br}^-)$ obviously should be accepted. As it have been mentioned in Section 1 the parameters of mutual influence are similar to parameters of cooperativity used earlier at the description of adsorption of ligands with polymers and oligomers. In accordance with tentatively found changes in UV/vis absorbance spectra and matrix model, the replacement of chloride ion by bromide ion in *cis*-position is analogous to so-called co-operative process, and the

replacement in *trans*-position is analogous to anticooperative process.

4. Conclusions

The focus of this paper is on developing computational tool which allows not only to describe titration curves but also can help systematically gain insight into the mechanism underlying mixed ligand complex formation. We have shown that when using a matrix model, one can reduce the constants set which is necessary for the descriptions of equilibrium. Our ability to reduce dimensionality of space of independent variables with simple model changes highlights the fact that complexity is not inherent to the mixed ligand complex formation process and we can reformulate the problem in a simpler form.

References

- [1] A.E. Martell, R.M. Smith, Critical Stability Constants, Plenum Press, New York, vols. 1–6, 1974, 1975, 1977, 1976, 1982, 1989.
- [2] NIST Standard Reference Database 46. Critically Selected Stability Constants of Metal Complexes Database. Compiled by R.M. Smith, A.E. Martell, R.J. Motekaitis, Version 7.0 for Windows, 2003. US National Institute of Standards and Technology Standard Reference Data Program, Gaithersburg, MD 20899.
- [3] M. Beck, I. Nagypal, Chemistry of Complex Equilibria, Akad. Kiado., Budapest, 1989, p. 411.
- [4] A.G. Kudrev, Rus. J. Coord. Chem. 34 (2008) 1.
- [5] A.G. Kudrev, Polym. Sci. Ser. A 42 (2000) 527.
- [6] G.H. Golub, Ch.F. Van Loan, Matrix Computations, The Johns Hopkins University Press, London, 1989, p. 476.
- [7] R. Tauler, A. Smilde, B. Kowalski, J. Chemom. 9 (1995) 31.
- [8] D.W. Marquardt, J. Soc. Ind. Appl. Math. 11 (1963) 431.
- [9] R.M. Dyson, S. Kaderli, G.A. Lawrance, M. Maeder, A.D. Zuberbühler, Anal. Chim. Acta 353 (1997) 381.
- [10] P. Gans, A. Sabatini, A. Vacca, Talanta 43 (1996) 1739.
- [11] I.N. Bronshtain, K.A. Semendyaev, Spravochnik po Matematike (Reference Book for Mathematics), Nauka, Moscow, 1986.
- [12] L.I. Elding, A.-B. Groning, Acta Chem. Scand. A32 (1978) 867.
- [13] E. Almgren, Acta Chem. Scand. 25 (1971) 3713.

Analysis of 17 polar to semi-polar pesticides in the Ebro river delta during the main growing season of rice by automated on-line solid-phase extraction-liquid chromatography–tandem mass spectrometry

Marina Kuster^{a,*}, Maria José López de Alda^a, Carlos Barata^a,
Demetrio Raldúa^b, Damià Barceló^a

^a *Institute of Chemical and Environmental Research of Barcelona (IIQAB), Spanish Council for Scientific Research (CSIC),
Jordi Girona 18-26, 08034 Barcelona, Spain*

^b *Technical University of Catalonia, Laboratory of Environmental Toxicology, CN 150 Km 14-5, Terrassa 08220, Spain*

Received 27 August 2007; received in revised form 26 October 2007; accepted 7 November 2007

Available online 17 November 2007

Abstract

This work describes the optimization of a fully automated method based on on-line solid-phase extraction-liquid chromatography–electrospray–tandem mass spectrometry (SPE-LC–ESI-MS/MS) for the simultaneous determination of 17 medium to polar pesticides in water. The list of target analytes included organophosphates, triazines, phenylureas, anilides, chloroacetanilides, acidic herbicides and thiocarbamates. Detection limits achieved were below 5 ng/L for all compounds except metolachlor (12 ng/L), alachlor (17 ng/L), malathion (36 ng/L) and fenitrothion (50 ng/L). The method developed was used to investigate the occurrence of the target pesticides in a total of 52 water samples collected monthly (from May to August 2005) at 14 selected locations in the rice cultivation area of the Ebro river delta. The study showed high levels, in the µg/L range, of bentazone, MCPA, propanil, molinate and atrazine, in basically all the samples investigated. The remaining pesticides were present at lower levels (<0.1 µg/L) or only detected sporadically (*e.g.* fenitrothion and malathion). The sampling campaign performed in July showed comparatively higher levels than the other three campaigns.

© 2007 Elsevier B.V. All rights reserved.

Keywords: Pesticides analysis; On-line solid-phase extraction; Liquid chromatography–tandem mass spectrometry; Ebro river delta

1. Introduction

Rice cultivation requires the use of high amounts of pesticides which pose an elevated risk of contamination of surface waters near rice cropping areas [1,2] and cause adverse effects on aquatic organisms [3]. Studies report that high levels at µg/L of several pesticides (*e.g.* molinate, propanil and some organophosphate insecticides) are frequently detected in the drainage channels of the main rice cultivating countries in Europe [4–7].

The Ebro river delta is among the three biggest rice growing areas in Spain. It has an approximate area of 20,600 ha of rice cropping and a production of 113,500 Tm. This area receives a high load of pesticides as a consequence of the intensive agri-

cultural activities that are carried out both upstream and in the Delta itself. The rice growing areas are situated in the Delta del Ebro Natural Park where other activities, such as mussel farming, also take place. The main pesticides used for weed control in the studied area are the frequently used in rice crops in Europe [5] propanil, bentazone, MCPA and molinate [8]. The insecticides fenitrothion and malathion are employed occasionally if necessary. Recently, the seafood farmers have complained about a loss of production in the periods of rice cultivation which has raised public concern about the toxicity of the water in this area.

The objective of this work was to develop a fully automated multi-residue analytical method, based on on-line solid-phase extraction-liquid chromatography–tandem mass spectrometry (SPE-LC–MS/MS), for the simultaneous determination (in a single run) of 17 selected pesticides in water and to apply this method in the Ebro river delta in the frame of a project aiming to investigate the potential toxicity effects of pesticides in this area and to assess whether the high mortality of bivalves observed in

* Corresponding author. Tel.: +34 934 006 100; fax: +34 932 045 904.
E-mail address: makqam@iiqab.csic.es (M. Kuster).

the delta in the period of rice cultivation is due to the occurrence of these chemicals.

The target analytes selected for the present work included organophosphates (fenitrothion, malathion, and diazinon), triazines (simazine, atrazine, and cyanazine), phenylureas (chlortoluron, isoproturon, and diuron), anilides (propanil), chloroacetanilides (alachlor and metolachlor), acidic herbicides (bentazone, MCPA, 2,4-D, mecoprop) and thiocarbamates (molinate). This list comprises not only rice cropping pesticides but also pesticides included in the list of priority substances in the field of water (Decision no. 2455/2001/EC), namely, atrazine, simazine, diuron, isoproturon, and alachlor, among others.

The analysis of pesticides in environmental waters has been largely confined to the investigation of apolar, persistent compounds, whose analysis has been traditionally performed by GC–MS after previous liquid–liquid or solid-phase extraction (SPE). However, most modern pesticides are polar, low volatile and/or thermo/labile compounds, not amenable to GC–MS analysis. For the analysis of these polar pesticides LC–MS/MS is considered the technique of choice because it does not need derivatization and provides great sensitivity, selectivity and reliability of results when acquiring two SRM transitions per compound [9–11]. The analytical method developed combines the use of this technique with on-line SPE, which can be considered one of the most advantageous sample preparation techniques available [12–16]. The main advantages of this technique are minimum sample manipulation, automation, time and labor savings, and improved throughput [11]. All these features make the analytical method developed one of the most valuable described in the literature in terms of performance.

2. Experimental

2.1. Reagents and chemicals

High purity (98–99.9%) standards of the 17 selected pesticides bentazone, MCPA, 2,4-D, mecoprop, simazine, cyanazine, atrazine, chlortoluron, isoproturon, diuron, metolachlor, alachlor, fenitrothion, malathion, diazinon, molinate and propanil were purchased as powders from Sigma (St Louis, MO, USA). Stock standard solutions for each of the analytes were prepared in methanol at 1 mg/mL and stored in the dark at 4 °C. Standard solutions of the mixtures of all compounds at concentrations ranging between 1 ng/mL and 500 µg/mL were prepared by appropriate dilution of the stock solutions in methanol. The standard mixtures were used as spiking solutions for preparation of the aqueous calibration standards and in the recovery studies. Aqueous standard solutions did not contain more than 0.1% of methanol.

Pesticide-grade solvents methanol and acetonitrile, and LC-grade water were supplied by Merck (Darmstadt, Germany).

2.2. On-line solid-phase extraction

Fully automated on-line trace enrichment and analysis of samples, aqueous standards and blanks was performed with an automated on-line SPE sample processor Prospekt-2 (Spark

Holland, Emmen, The Netherlands) configured for high sample volumes and connected in series with the LC–MS/MS instrument. The Prospekt-2 system consists of an automated cartridge exchange (ACE) module and a high-pressure dispenser module (HPD) for handling of solvents and samples by way of a 2 mL high-pressure syringe. This system allows performing the extraction of one sample in a sequence while the elution and analysis of the previously extracted one is simultaneously carried out.

Extraction of the pesticides from the water samples, previously filtered through 0.45 µm Nylon filters (Whatman, Maidstone, UK), was performed with disposable trace enrichment polymeric cartridges Hysphere Resin GP (polydivinylbenzene, 10 mm × 2 mm i.d., 10–12 µm particle size) from Spark Holland.

The samples (10 mL) were loaded at a flow rate of 8 mL/min onto the cartridges previously conditioned with 1 mL acetonitrile and 1 mL water at a flow rate of 5 mL/min. Subsequent washing of the cartridges was carried out with 1 mL of water at a flow rate of 5 mL/min. Elution of the target analytes directly onto the chromatographic column was performed with the chromatographic mobile phase. All steps of the sample preparation procedure were programmed on and automatically controlled by means of SparkLink Version T2.20-01 software (Spark Holland).

2.3. Liquid chromatographic separation

LC–MS/MS analyses were carried out in a system consisting of a Waters Alliance 2690 LC pump equipped with an auto-sampler with the volume injection set to 20 µL (Waters, Milford, MA, USA) and connected in series with the MS/MS detector. The auto-sampler was only used in the optimization procedure to assess the recovery of the method developed by comparing the peak areas obtained in the on-line analysis of spiked water samples with those obtained from the injection of standard mixtures of the analytes in methanol at equivalent concentrations.

Chromatographic separation was performed using a reversed-phase Purospher STAR-RP-18e analytical column (125 mm × 2 mm, 5 µm particle diameter) preceded by a guard column (4 mm × 4 mm, 5 µm) of the same packing material from Merck (Darmstadt, Germany).

Elution of the trapped compounds onto the chromatographic column was performed at 0.2 mL/min with a 45 min gradient starting from 10% acetonitrile in water, increasing to 50% acetonitrile in 5 min and continuing to 80% in 20 min. During the following 5 min the column was cleaned with 100% acetonitrile, readjusted to the initial conditions in 2 min, and equilibrated for further 13 min.

2.4. Tandem mass spectrometric detection

Detection was performed using a Quattro triple-quadrupole mass spectrometer from Micromass (Manchester, UK), equipped with an orthogonal electrospray (ESI) ionization source. Two different selected reaction monitoring (SRM) transitions were monitored per compound: the first and more abundant transition was used for quantitation and the second transition for confirmation (see Table 1). To maximize sensi-

Table 1
Mass spectrometric conditions for the simultaneous analysis of 17 pesticides

Pesticide	Time	Mode of ionization	SRM transition (m/z) Precursor ion → product ion	Cone (V)	Coll. (eV)
Bentazone	00.0–13.25	NI	239 → 132	35	25
			239 → 197	35	20
MCPA			199 → 141	20	15
			201 → 143	15	15
2,4-D			219 → 161	15	10
			219 → 125	15	30
Mecoprop			213 → 141	15	15
			215 → 143	15	15
Simazine	13.25–16.85	PI	202 → 132	30	20
Cyanazine			202 → 124	30	20
			241 → 214	30	15
Chlortoluron			241 → 174	30	20
			213 → 72	25	15
Isoproturon			213 → 140	25	25
			207 → 72	25	15
Atrazine			207 → 165	25	25
			216 → 174	30	15
Diuron			216 → 132	30	20
			233 → 72	15	15
Propanil	16.85–19.55	NI	235 → 72	15	30
			216 → 160	30	15
Molinate	19.55–24.70	PI	218 → 162	30	15
			188 → 126	25	10
Metolachlor			188 → 83	25	20
			284 → 252	25	15
Alachlor			284 → 176	25	25
			270 → 238	15	10
Malathion			270 → 162	15	25
			353 → 195	25	15
Fenitrothion	20.90–24.70	NI	353 → 227	25	15
			262 → 122	25	30
Diazinon	24.70–35.00	PI	262 → 152	25	20
			305 → 169	25	20
			305 → 153	25	20

tivity, data acquisition was performed under time-scheduled conditions. Due to the different preferential ionization of the target compounds, the electrospray interface was operated in both negative and positive modes, either sequentially or simultaneously, along the chromatographic run.

Other MS/MS experimental conditions were as follows: capillary voltage, 3.5 kV; source temperature, 150 °C; desolvation temperature, 450 °C; extractor voltage, 2 V; and RF lens, 0.4 V. Nitrogen was used as both the nebulizing and the desolvation gas. The flow-rate of the nebulizing gas was set at 60 L h⁻¹, and that of the desolvation gas at 550 L h⁻¹. Argon was used as collision gas with a pressure of 2.58 × 10⁻³ mbar.

Instrument control, data acquisition and evaluation were performed by Masslynx 4.0 software (Micromass, Manchester, UK).

2.5. Site description and sample collection

The delta of the Ebro river (NE Spain) is a network of irrigation and drainage channels that occupies an area of 20,600 ha of rice crop cultivation (Fig. 1). The distribution and operation of

the channels and its connection with the Mediterranean Sea is described in more detail elsewhere [17]. Previous studies have reported the occurrence of pesticides at high concentrations, in many cases in the µg/L range, in this area [18–20] and others, e.g., in rice paddies of Japan [21], and Greece [5].

To obtain a picture of the occurrence and distribution of pesticides in this area 52 samples were collected during a monitoring program consisting of four sampling campaigns performed monthly during the main growing season of rice (from May to August 2005). Each campaign a total of 12–14 water samples were collected at the selected locations marked in Fig. 1 as ERT, Ebro river upstream of the Delta; CD1–CD4, various sites along one of the main drainage channels; CD5–CD8, different drainage channels closer to the sea; BA and EL, Alfacs Bay and Encanyada Lagoon, respectively; and CE1–CE3, irrigation channels; CE2 and CE3, which are channels used only when there is very little water going through the irrigation channels to re-pump water from the drainage channels to the fields, were only sampled in June and July.

Water samples were collected in amber polyethylene terephthalate (PET) bottles and transported to the laboratory under

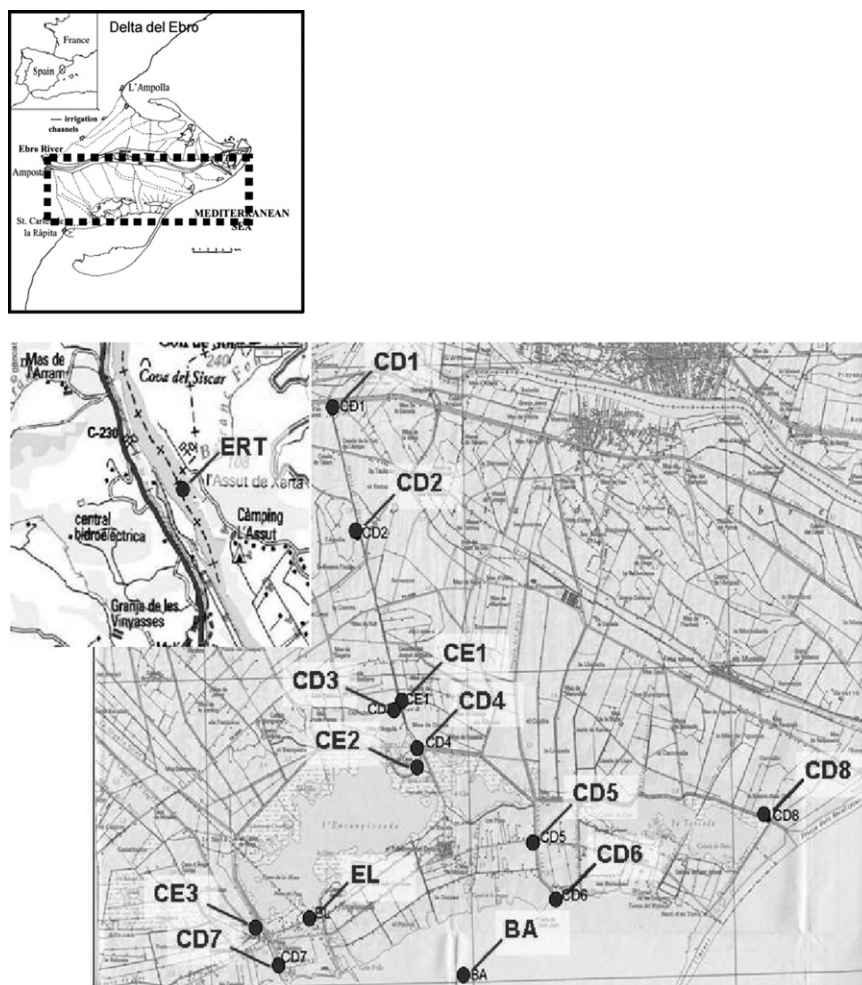


Fig. 1. Map of the studied area in the Ebro river delta: ERT, Ebro river; CD, drainage channels; CE, entrance channels; BA, Alfacs Bay; EL, Encanyada Lagoon.

cooled conditions (4 °C). Upon reception, samples were filtered through 0.45 µm Nylon filters (Whatman, Maidstone, UK) to eliminate particulate matter and other suspended solid matter and then stored at 4 °C in the dark until analysis which was always carried out within 48 h of collection to keep microbial degradation to a minimum.

3. Results and discussion

The analytical method developed is based on a method previously described by the authors for the analysis of 20 pesticides, in two chromatographic runs, in natural and treated waters [22,23]. The multi-analyte determination of acidic and neutral pesticides is usually accomplished in two separate analyses [24–26]; however, this doubles the analysis time. In this work, one single procedure has been optimized for the simultaneous analysis of the 17 selected pesticides in water.

3.1. MS/MS optimization

Optimization of the MS/MS conditions, *i.e.*, choice of the ionization mode, identification of the parent and product ions, and selection of the cone and collision voltages, most favorable for analysis of the target analytes was performed with on-column

injection of their individual standard solutions by recording in both modes of ionization, NI and PI, full scan and product ion mass spectra at different values of cone and collision energies, respectively. As shown in Table 1, six of the 17 selected pesticides, namely, bentazone, MCPA, 2,4-D, mecoprop, propanil and fenitrothion, showed more efficient ionization in the NI mode, whereas the remaining eleven pesticides showed preferential ionization in the PI mode. To carry out the analysis of all compounds in a single run, the electrospray interface was programmed to change the mode of operation, between NI and PI, along the chromatographic analysis. As previously indicated, acquisition was performed under time-scheduled conditions, *i.e.*, the various selected transitions were programmed into different time acquisition windows in order to avoid a decrease in sensitivity. The maximum number of transitions recorded simultaneously was 12 (corresponding to the analysis of six pesticides), which is close to the limit from which the sensitivity starts to decrease. The time-schedule program was optimized in such a way that the electrospray interface worked in either NI mode or PI mode, except when fenitrothion (NI mode, fifth time window) is measured at the same time as metolachlor, alachlor and malathion (PI mode, fourth window), because of the closeness of their retention times. Fig. 2 shows for illustration an SRM chromatogram obtained from the analysis of a standard

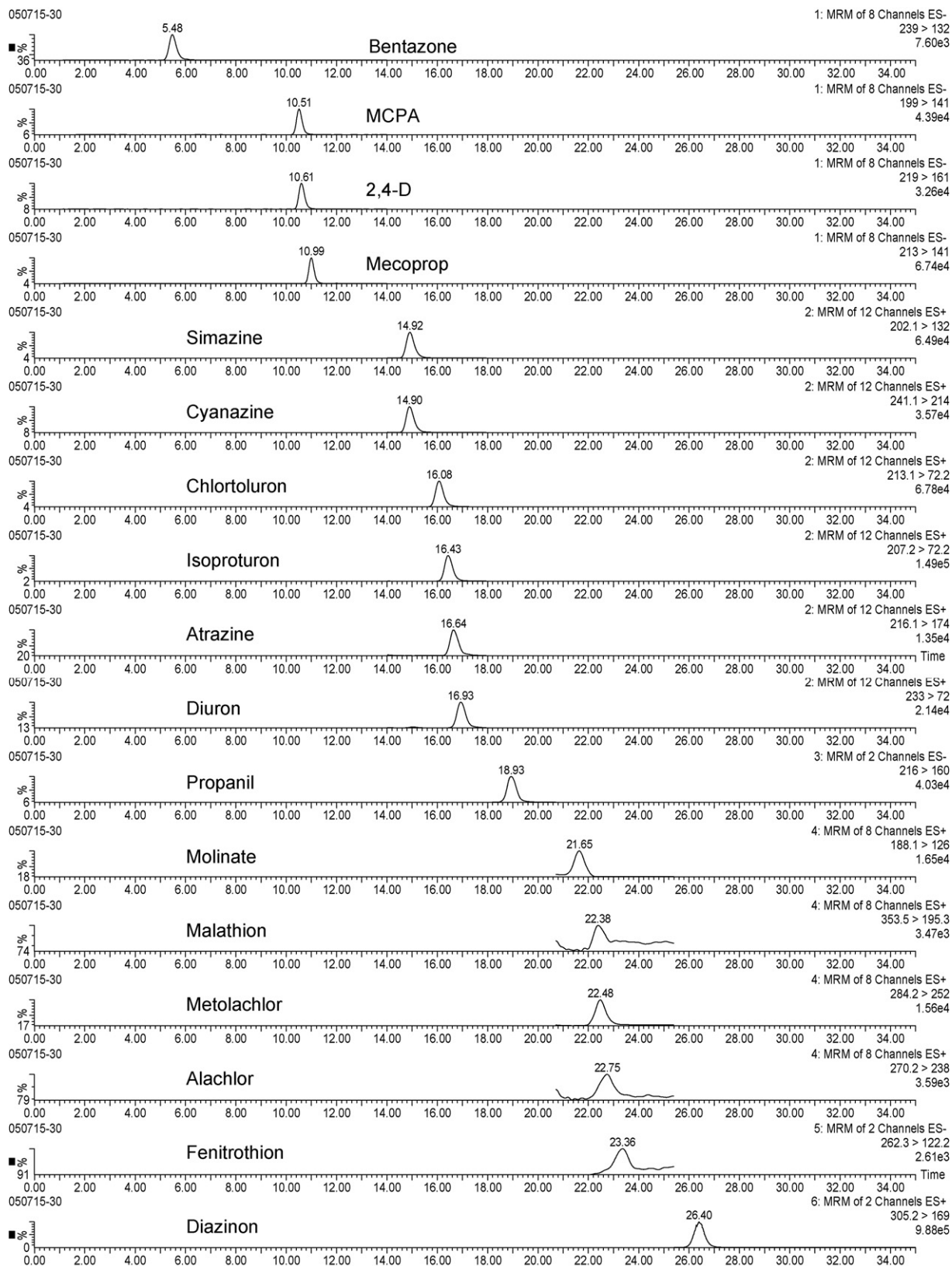


Fig. 2. Chromatogram showing the quantitation transition of all target analytes in an LC-grade aqueous standard solution at 100 ng/L (fenitrothion at 500 ng/L).

Table 2
Performance parameters of the method

Pesticide	SRM1/SRM2 ratio	Linear range (ng/L)	r^2	R.S.D. ($n=4$)	LOD ng/L	LOQ ng/L	% R ^a ($n=4$)
Bentazone	1.85	5–500,000	0.9950	21.6	1.9	4.9	66
MCPA	3.23	1–10,000	0.9989	13.8	0.3	0.8	75
2,4-D	8.20	5–1,000	0.9986	12.2	0.7	1.8	66
Mecoprop	3.07	5–1,000	0.9990	5.9	0.6	1.6	93
Simazine	0.97	5–1,000	0.9960	12.0	0.8	2.0	66
Cyanazine	12.6	5–1,000	0.9979	11.8	1.9	5.1	130
Chlortoluron	13.5	5–1,000	0.9944	8.9	0.9	2.3	53
Isoproturon	137	5–1,000	0.9936	12.5	1.5	3.9	73
Atrazine	3.51	10–5,000	0.9967	17.7	3.6	9.5	180
Diuron	2.09	5–1,000	0.9987	13.4	1.6	4.1	59
Propanil	1.51	1–1,000	0.9991	5.7	0.4	0.9	59
Molinate	3.19	10–1,000	0.9970	4.2	2.7	7.2	63
Metolachlor	2.61	50–1,000	0.9689	14.5	12	33	157
Alachlor	12.5	50–1,000	0.9972	9.0	18	47	55
Malathion	1.55	100–1,000	0.9961	10.3	37	98	77
Fenitrothion	1.01	250–1,000	0.9949	16.0	50	130	120
Diazinon	1.70	1–1,000	0.9970	5.2	0.1	0.2	95

^a % Recovery obtained by spiking 0.1 $\mu\text{g/L}$.

mixture of the pesticides at 100 ng/L (500 ng/L for fenitrothion).

3.2. Optimization of the SPE procedure

The two most important parameters influencing the efficiency of a SPE procedure are the cartridge and the sample volume.

The selection of the cartridge, HySphere Resin GP, was based on the recovery data reported by Kampioti et al. [22], according to which this cartridge is the only one, out of five different tested (HySphere C₁₈ EC, HySphere C₁₈ HD, HySphere C2, HySphere Resin GP and PLRP-s), capable of extracting the pesticides of interest, which comprise both acidic and neutral compounds, with fairly satisfactory recoveries (above 60% for all compounds except for simazine (29%), cyanazine (43%) and chlortoluron (47%), for a 20 mL sample volume). These low recovery values, which correspond to the most polar compounds, have been somewhat improved in the present work (from 29% to 66%, from 43% to 130%, and from 47% to 53%) by reducing the sample volume from 20 to 10 mL (see Table 2).

The selection of 10 mL as sample volume responded also to the need of minimizing potential matrix effects. LC–MS is known to be a technique particularly prone to matrix effects [9,27] and experience has shown that these effects tend to be notoriously variable and unpredictable in occurrence and intensity. Some authors suggest the use of standard addition or isotopically labelled internal standards [24,28] to overcome this problem; however, these techniques are rather expensive or time consuming making their implementation difficult in practice for routine analysis. The presence or absence of such effects, which may be observed as increased or decreased detector responses, may be demonstrated by comparing the response produced from the analyte in a simple solvent solution with that obtained from the same quantity of analyte in the presence of the sample matrix [29].

In a study conducted to evaluate the susceptibility of the target pesticides to matrix interferences when extracting different

sample volumes (20, 10 and 5 mL), variable behaviors were observed. A so-called “interference factor” (f_i) was estimated for each pesticide from the real (RC) and the calculated (C) concentrations obtained in the analysis of the river water sample collected in the first sampling campaign (river), the same sample spiked with a standard mixture of the analytes at 500 ng/L (river₅₀₀), and an aqueous standard solution of 500 ng/L (std₅₀₀), in accordance with the following equations.

$$C_{\text{river}} = \text{RC}_{\text{river}} f_i \quad (1)$$

$$C_{\text{river500}} = \text{RC}_{\text{river}} f_i + \text{RC}_{\text{std500}} f_i \quad (2)$$

$$C_{\text{river500}} = C_{\text{river}} + \text{RC}_{\text{std500}} f_i \quad (3)$$

$$f_i = \frac{C_{\text{river500}} - C_{\text{river}}}{\text{RC}_{\text{std500}}} \quad (4)$$

According to Eq. (1), the concentration of pesticide calculated in the river sample (C_{river}) can be regarded as the real pesticide concentration present in the sample (RC_{river}) multiplied by the interference factor (f_i). Thus, a f_i equal to 1 means no matrix interferences, whereas $f_i > 1$ and $f_i < 1$ indicate enhanced and decreased responses, respectively.

Assuming that both the concentration in the river sample (RC_{river}) and the concentration in the spiked river sample (C_{river500}) are affected to the same extent by the interference factor f_i , the concentration calculated in the spiked river sample can be regarded (Eq. (2)) as the sum of the concentration naturally present in the river (non-spiked) sample (RC_{river}) plus the concentration in the aqueous standard ($\text{RC}_{\text{std500}}$) multiplied by f_i .

The first term of Eq. (2) can then be replaced by the concentration calculated in the river (C_{river} , Eq. (1)) giving Eq. (3). Further simplification of the latter gives the formula to calculate the interference factor f_i (Eq. (4)).

Fig. 3 shows the interference factors calculated for various pesticides representative of the different classes investigated at the three sample volumes tested. As shown in this figure, the matrix effects observed varied considerably in intensity and

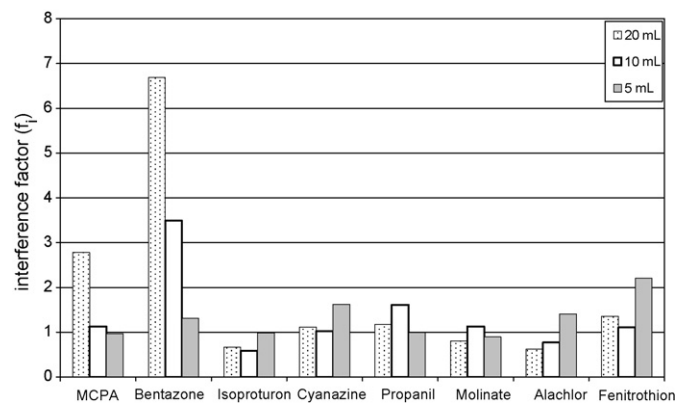


Fig. 3. Interference factors obtained for different pesticides, representative of each class, at different sample volumes in a study of matrix effects.

nature depending on the compound. An increase of the detector response with increasing sample volumes (signal enhancement) was observed in the case of the acidic pesticides (MCPA, mecoprop, 2,4-D and, especially, bentazone), which are the most affected by matrix effects. The opposite effect, a decrease in the detector response with increasing sample volumes (most likely due to ionization suppression) was observed in the case of phenylureas (as shown in the figure for isoproturon). The remaining pesticides showed an irregular pattern which in the case of triazines, anilines and organophosphates was characterized by an increase of the signal obtained ($f_i > 1$) at 5 mL.

The average absolute deviation of f_i from 1 (where 1 means the absence of matrix effects) calculated for all compounds at each sample volume was considerably high for 20 mL (0.80) and lower, with very close values, for 10 mL (0.45) and 5 mL (0.42) indicating that no overall significant improvement is achieved by working with only 5 mL, which would be critical for the compounds with the highest limits of detection malathion and fenitrothion. The choice of 10 mL was thus found to be an acceptable compromise between matrix effects and sensitivity for the analysis of the 17 selected pesticides in one single chromatographic run.

3.3. Analytical quality control parameters

The analytical method developed showed satisfactory performance characteristics in terms of linearity, repeatability, accuracy, selectivity and sensitivity, aside from other advantages, such as fast analysis, minimum sample manipulation, full automation, cost efficiency, and robustness.

Quantitation was performed by external standard calibration. Five-to-nine point calibration curves, based on peak areas, were calculated for each of the two SRM transitions selected per compound from the on-line SPE-LC-MS/MS analysis of aqueous standard solutions at concentration ranges between approximately the limit of quantitation and 1 $\mu\text{g/L}$ (5, 10 and 500 $\mu\text{g/L}$ for atrazine, MCPA and bentazone, respectively). Calibration curves were shown to be linear, with correlation coefficients (r^2) higher than 0.99, for all compounds except metolachlor (see Table 2). In the case of bentazone, the wide range of concentra-

tions found in the samples investigated (from 0.01 to 127 $\mu\text{g/L}$) obliged to expand the working concentration range of the calibration curve over four orders of magnitude where the detector response followed a second order (quadratic), rather than a first order (linear), regression.

The accuracy and precision of the method were estimated from the replicate ($n = 4$) analysis of 10 mL aliquots of Milli-Q water spiked with the standard mixture of the analytes at two different concentrations (0.1 and 0.5 $\mu\text{g/L}$, which correspond to the maximum admissible concentrations set in Directive 98/83/EC on the quality of water intended for human consumption for individual and total pesticides, respectively [30]). Method extraction recoveries, which are automatically corrected by processing both the samples and the aqueous standards in the same way along the whole analytical procedure, were above 50% for all compounds. Unexpectedly high percentages were obtained for cyanazine (130%), metolachlor (157%), and atrazine (180%) (also in spiked river water as deduced from the calculated interference factor f_i) without any plausible explanation, since memory effects, which could account for such results, were tested but found not to exist.

As is typical of automated methods with minimum sample preparation requirements and minimum manipulation by the analyst, the repeatability of the procedure was satisfactory, with relative standard deviations always below 22% (see Table 2).

The limits of detection (LODs) and quantitation (LOQs) of the method were experimentally estimated from the on-line analysis of spiked LC-grade water samples as the minimum concentration of analyte giving a signal-to-noise ratio of 3 and 8, respectively. As shown in Table 2, LODs were below 5 ng/L for all compounds except those analyzed in the fourth and fifth time windows: metolachlor (12 ng/L), alachlor (18 ng/L), malathion (37 ng/L) and fenitrothion (50 ng/L). Thus, it appears that when the electrospray interface is operated simultaneously in both ionization modes the ionization of the compounds is negatively affected, especially in the case of fenitrothion. Limits of quantitation were within the range 0.8–130 ng/L.

The method developed is also highly selective and with the monitoring of two SRM transitions per compound, which is essential to reduce the risk of false positive results [9,31], the minimum number of identification points (3) required by the European Commission (2002/657/CE) for reliable identification and quantification of organic residues in animals and fresh meat, a guideline that is increasingly being adopted in the environmental field [11], is achieved.

For the positive confirmation of analytes in the samples, strict criteria had to be met: the chromatographic retention time of the analyte in the sample could not vary more than 2%, and the relative abundance of the two SRM transitions monitored had to lie within the 20% margin, compared to the calibration standards. The ratio between the two SRM transitions recorded per compound is shown in Table 2. These ratios correspond to the average of those determined for the various aqueous standard solutions used to construct the calibration curves employed in each of the four monitoring campaigns and had an associated relative standard deviation (R.S.D.) lower than 22% in all cases (see Table 2).

Further advantages of the method developed are full automation (up to 22 solutions distributed as required into samples, calibration solutions and blanks can be analyzed unattended), autonomy (which makes possible the performance of up to 192 analyses), fairly high throughput (analysis time per sample is approximately 45 min), robustness and low maintenance (according to our experience it can be left running for months without any problems), and cost efficiency in terms of both reagents (no use of nitrogen for evaporation, or solvents for elution, as in off-line procedures) and personnel (instrument programming is very simple and data processing, including construction of calibration curves, quantification, and calculation of detection and quantification limits, is performed automatically by means of the software Masslynx, which means that analyses can be performed by trained, but not necessarily highly qualified, staff).

3.4. Occurrence of pesticides

The cumulative pesticide levels detected at each location in the various sampling campaigns, carried out from May to August 2005, are presented in Fig. 4. Bentazone, MCPA, propanil, molinate, atrazine and fenitrothion were the compounds found at the highest concentrations. In general strong differences were observed in the levels and the profile of the pesticides detected among sampling periods. All the results are presented in Appendix A (Tables A1 and A2).

As expected taking into account the agricultural practices in the area, the highest concentrations were found in June and July, showing a profile dominated by high concentrations of bentazone and MCPA.

Table 3

Highest and average concentrations (in $\mu\text{g/L}$) and percentage of samples found to be positive for the various pesticides investigated

Pesticide	Highest concentration detected	Average concentration (positive samples)
Cyanazine	–	– (0%)
Chlortoluron	0.003	0.003 (2%)
Isoproturon	0.007	0.006 (14%)
Mecoprop	0.026	0.008 (90%)
Metolachlor	0.027	0.027 (2%)
Diuron	0.036	0.015 (85%)
Diazinon	0.044	0.006 (78%)
2,4 D	0.172	0.024 (89%)
Malathion	0.218	0.218 (2%)
Simazine	0.376	0.045 (94%)
Fenitrothion	0.681	0.336 (21%)
Molinate	0.849	0.222 (83%)
Atrazine	0.901	0.314 (98%)
MCPA	13.90	1.877 (98%)
Propanil	16.82	0.969 (87%)
Alachlor	62.90	15.80 (15%)
Bentazone	126.8	30.51 (100%)

The highest and the average concentrations of each pesticide are presented in Table 3. Its detection frequency is reflected by the percentage of positive samples. Cyanazine was the only pesticide not detected. All other pesticides were found in more than 78% of the samples, except for chlortoluron, isoproturon, metolachlor, alachlor, malathion and fenitrothion, which were detected in less than 21% of the samples.

To provide a closer look into pesticide concentration fluctuations individual profiles of selected compounds are shown in Fig. 5. This figure shows an irregular pattern for MCPA

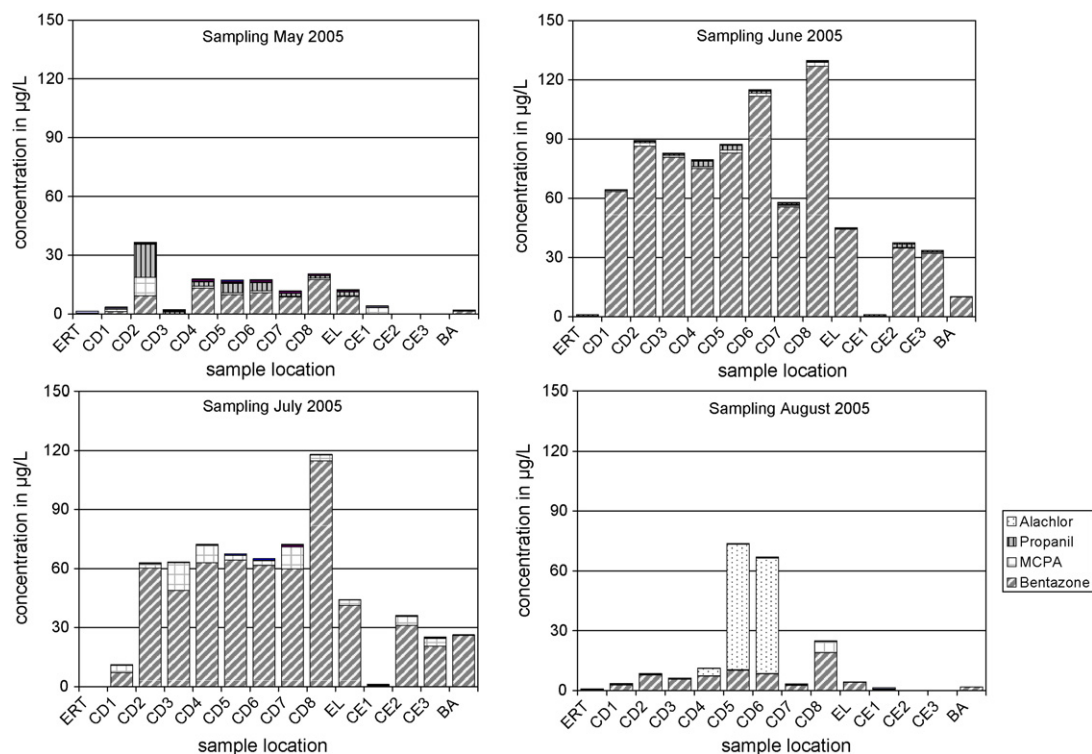


Fig. 4. Cumulative levels of all pesticides in each of the sampling campaigns performed in the Ebro river delta. Only the most abundant pesticides appear in the legend.

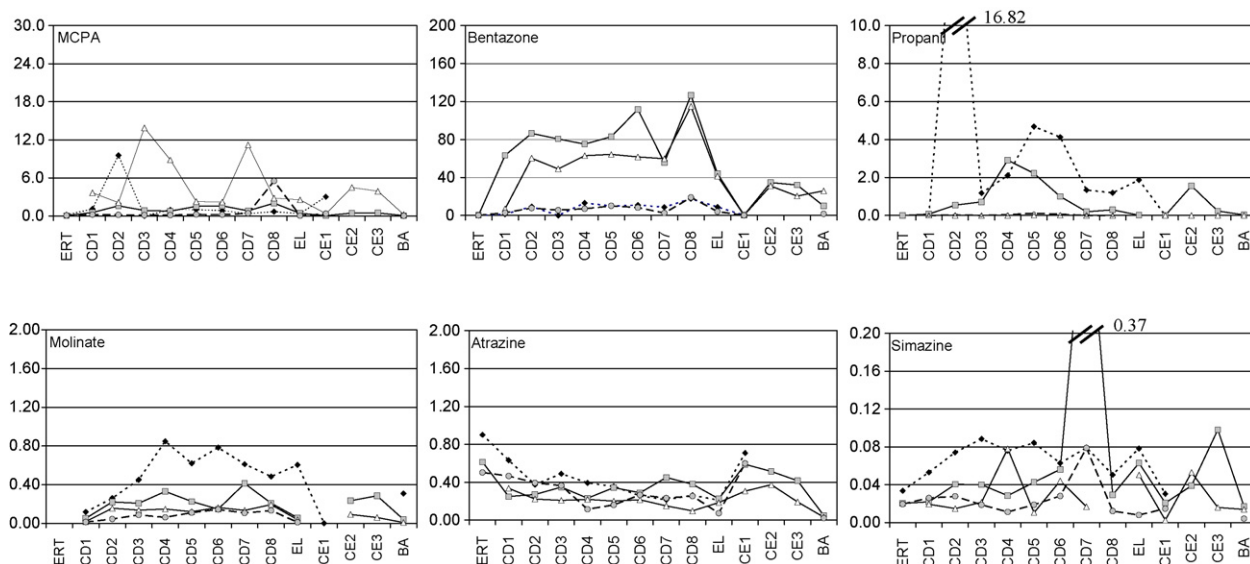


Fig. 5. Individual profiles of MCPA, bentazone, propanil, molinate, atrazine and simazine in all samples. Campaigns: (◆) May; (□) June; (△) July; (○) August concentrations in ng L^{-1} .

with occasionally very high concentrations in July. Bentazone showed clearly higher concentrations in the months of June and July. Propanil was found at distinctly higher concentrations in May and June with a peak of concentration in May in one of the drainage channels (CD2). Molinate showed its highest levels in May. Simazine and atrazine did not show significant differences between the sampling campaigns although simazine concentrations were somewhat higher in May.

In general, the highest levels were detected in the drainage channels (CD) and the lowest levels in the Ebro river upstream of the delta (ERT), in the Alfacs Bay (BA) and in the Encanyada Lagoon (EL). An in-depth analysis by chemometric and geostatistical methods of the data generated in the present work to assess both temporal and spatial variations of main pollution patterns by pesticides in this area has been performed by Terrado et al. [17].

The resulting data set of pesticides concentrations has been integrated with results obtained in the study of different biomarkers and the histopathology of aquatic organisms (clams and mussels) collected in the same area to elucidate possible cause–effect relationship. So far, investigations carried out with *Daphnia magna* revealed a significant, negative correlation between the dominant pesticide residues and some biological markers (severe effects on grazing rates, a strong inhibition of cholinesterases and carboxylesterases, which are specific biomarkers of organophosphorous and carbamate pesticides; among others) [3].

4. Conclusion

A multi-residue analytical method based on on-line SPE-LC–MS/MS has been developed for the fast and simultaneous analysis of 17 selected pesticides in surface waters. The main advantages of the developed method are as follows: (1) full automation, (2) high sensitivity with limits of detection below 50 ng/L for all compounds, (3) good reproducibility with relative

standard deviations below 22%, (4) improved accuracy because aqueous calibration standards are processed in the same way as samples, (5) high selectivity, inherent to the MS/MS detection technique, (6) reliability of results, derived from the acquisition of two SRM transitions per compound, attaining four identification points as required by the EU for confirmatory analysis [32]), (7) high-throughput, 45 min/sample and hence 32 samples/day, (8) low sample volume requirements (10 mL), (9) cost efficiency, and (10) robustness.

Application of the method developed in a monitoring program carried out in the Ebro river delta showed the presence of several pesticides (bentazone, MCPA, propanil, molinate) at high levels, in the $\mu\text{g/L}$ range, and in most samples. The pesticides used for rice crop were, as expected, the most relevant in this study (concentrations up to $127 \mu\text{g/L}$ were found for bentazone). Other pesticides, such as atrazine, simazine and 2,4-D, were also frequently detected but at concentrations below $1 \mu\text{g/L}$. The remaining pesticides were present at lower levels, usually below $0.1 \mu\text{g/L}$. Comparatively higher levels of pesticides were found in June and July with unexpectedly high concentrations of MCPA and bentazone.

Acknowledgements

This work is supported by the European Union in “Integrate modelling of the river-sediments–soil–groundwater system; advanced tools for the management of catchment areas and river basins in the context of global change” [AQUATERRA, GOCE 505428] and the Spanish Ministry of Education and Science [CTM2005-25168-E] and reflects the author’s view. The EU is not liable for any use that may be made of the information contained in it. Marina Kuster gratefully acknowledges the I3P Program (Itinerario integrado de inserción profesional; co-financed by CSIC and European Social Funds) for a pre-doctoral grant. Merck is acknowledged for the gift of LC columns and Spark Holland for the gift of SPE cartridges.

Appendix A

References

See Tables A1 and A2.

[1] D.G. Karpouzias, E. Capri, Paddy Water Environ. 4 (2006) 29.

Table A1
Levels (in ng L⁻¹) of malathion, fenitrothion, molinate, atrazine, MCPA, propanil, alachlor and bentazone found in all four campaigns

Sampling	Sample	Malathion	Fenitrothion	Molinate	Atrazine	MCPA	Propanil	Alachlor	Bentazone
Sampling May	ERT	n.d.	n.d.	n.d.	901.5	183.4	1.5	285.7	177.0
	CD1	n.d.	202.7	118.8	631.7	1103.4	56.9	n.d.	1370.0
	CD2	217.9	n.d.	261.2	376.2	9558.3	16826.6	n.d.	9330.0
	CD3	n.d.	<LOQ	452.2	489.3	5.6	1181.4	n.d.	10.0
	CD4	n.d.	209.7	848.7	393.9	978.4	2107.9	n.d.	13240.0
	CD5	n.d.	588.6	621.9	356.4	998.2	4680.3	n.d.	9980.0
	CD6	n.d.	372.5	783.6	255.8	855.1	4123.2	n.d.	10990.0
	CD7	n.d.	398.1	613.3	215.1	381.4	1344.6	n.d.	8760.0
	CD8	n.d.	207.5	485.2	262.3	682.8	1195.2	n.d.	17630.0
	EL	n.d.	401.6	605.5	211.1	379.1	1869.8	n.d.	8970.0
	CE1	n.d.	n.d.	<LOQ	708.5	3024.8	7.6	130.0	180.0
	CE2	n.s.	n.s.	n.s.	n.s.	n.s.	n.s.	n.s.	n.s.
	CE3	n.s.	n.s.	n.s.	n.s.	n.s.	n.s.	n.s.	n.s.
	BA	n.d.	n.d.	308.5	42.6	156.5	21.5	n.d.	1490.0
Sampling June	ERT	n.d.	n.d.	n.d.	613.3	54.1	1.0	n.d.	360.0
	CD1	n.d.	n.d.	53.8	249.0	558.9	77.8	n.d.	63330.0
	CD2	n.d.	n.d.	222.8	271.1	1608.2	547.6	n.d.	86470.0
	CD3	n.d.	n.d.	209.0	349.3	883.7	717.0	n.d.	80710.0
	CD4	n.d.	n.d.	330.9	232.1	763.3	2915.0	n.d.	75140.0
	CD5	n.d.	n.d.	227.7	344.1	1524.4	2220.1	n.d.	82970.0
	CD6	n.d.	n.d.	147.9	288.5	1605.8	1000.9	127.4	111690.0
	CD7	n.d.	n.d.	413.3	450.2	821.3	197.4	n.d.	55610.0
	CD8	n.d.	n.d.	210.3	379.4	2026.8	300.6	n.d.	126790.0
	EL	n.d.	n.d.	59.1	224.8	435.1	14.4	n.d.	44260.0
	CE1	n.d.	n.d.	n.d.	588.5	60.0	12.5	n.d.	360.0
	CE2	n.d.	n.d.	235.2	513.9	448.2	1555.0	n.d.	34710.0
	CE3	n.d.	n.d.	286.2	416.2	474.1	235.1	n.d.	32100.0
	BA	n.d.	n.d.	42.1	49.2	49.1	34.9	n.d.	10080.0
Sampling July	ERT	n.a.	n.a.	n.a.	n.a.	n.a.	n.a.	n.a.	n.a.
	CD1	n.d.	n.d.	20.1	336.4	3644.0	12.4	n.d.	7080.0
	CD2	n.d.	n.d.	158.2	223.3	2115.5	6.0	n.d.	60390.0
	CD3	n.d.	n.d.	137.7	208.8	13903.4	3.5	n.d.	49020.0
	CD4	n.d.	n.d.	149.9	219.4	8832.8	<LOQ	n.d.	63010.0
	CD5	n.d.	470.7	121.9	200.9	2285.1	13.0	n.d.	64330.0
	CD6	n.d.	680.6	165.2	215.8	2205.4	12.3	n.d.	61690.0
	CD7	n.d.	130.5	136.4	150.3	11203.4	6.2	870.7	59780.0
	CD8	n.d.	n.d.	194.6	97.8	2814.1	2.7	n.d.	114900.0
	EL	n.d.	n.d.	40.0	185.2	2556.6	n.d.	n.d.	41410.0
	CE1	n.d.	n.d.	n.d.	307.6	366.0	1.0	n.d.	310.0
	CE2	n.d.	27.8	94.3	374.1	4481.2	1.2	n.d.	31110.0
	CE3	n.d.	n.d.	62.9	192.3	3912.3	8.7	476.7	20510.0
	BA	n.d.	n.d.	10.7	31.4	224.0	1.2	n.d.	26110.0
Sampling August	ERT	n.d.	n.d.	n.d.	503.1	87.3	n.d.	n.d.	250.0
	CD1	n.d.	n.d.	15.8	466.1	220.1	1.8	n.d.	2850.0
	CD2	n.d.	n.d.	46.4	393.5	172.2	37.0	n.d.	7820.0
	CD3	n.d.	n.d.	88.6	365.4	138.8	5.3	n.d.	5680.0
	CD4	n.d.	n.d.	63.4	115.2	139.3	45.5	3759.3	7150.0
	CD5	n.d.	n.d.	113.3	160.6	239.6	113.8	62900.5	10150.0
	CD6	n.d.	n.d.	145.6	266.7	211.8	69.1	57835.8	8350.0
	CD7	n.d.	n.d.	108.7	233.9	419.6	1.8	n.d.	2580.0
	CD8	n.d.	n.d.	134.1	254.0	5511.8	2.5	n.d.	19070.0
	n.d.	n.d.	13.0	73.5	38.7	n.d.	n.d.	4180.0	
	n.d.	n.d.	n.d.	598.9	367.8	n.d.	n.d.	220.0	
	CE2	n.s.	n.s.	n.s.	n.s.	n.s.	n.s.	n.s.	n.s.
	CE3	n.s.	n.s.	n.s.	n.s.	n.s.	n.s.	n.s.	n.s.
	BA	n.d.	n.d.	n.d.	21.7	25.4	n.d.	n.d.	1710.0

n.d., not detected; n.s., not sampled; n.a., not analysed; <LOQ, below limit of quantitation.

Table A2

Levels (in ng L⁻¹) of cyanazine, chlortoluron, isoproturon, mecoprop, metolachlor, diuron, diazinon, 2,4-D and simazine found in all four campaigns.

Sampling	Sample	Cyanazine	Chlortoluron	Isoproturon	Mecoprop	Metolachlor	Diuron	Diazinon	2,4-D	Simazine
Sampling May	ERT	n.d.	<LOQ	6.2	11.8	27.4	14.5	0.6	36.1	33.6
	CD1	n.d.	<LOQ	5.3	8.6	<LOQ	24.8	0.9	36.8	53.1
	CD2	n.d.	2.7	4.4	6.5	n.d.	26.5	0.2	17.8	74.1
	CD3	n.d.	n.d.	<LOQ	n.d.	<LOQ	24.8	0.3	n.d.	88.4
	CD4	n.d.	n.d.	<LOQ	6.7	n.d.	36.1	0.2	14.8	76.1
	CD5	n.d.	n.d.	<LOQ	6.1	n.d.	27.3	0.4	18.6	84.2
	CD6	n.d.	n.d.	<LOQ	4.8	n.d.	26.9	<LOQ	15.7	62.8
	CD7	n.d.	n.d.	<LOQ	4.3	n.d.	20.3	0.2	13.0	79.2
	CD8	n.d.	n.d.	<LOQ	4.3	n.d.	19.1	<LOQ	13.9	50.5
	EL	n.d.	n.d.	<LOQ	5.3	n.d.	20.3	0.2	13.5	78.3
	CE1	n.d.	n.d.	6.0	12.1	<LOQ	12.8	<LOQ	35.2	30.4
	CE2	n.s.	n.s.	n.s.	n.s.	n.s.	n.s.	n.s.	n.s.	n.s.
	CE3	n.s.	n.s.	n.s.	n.s.	n.s.	n.s.	n.s.	n.s.	n.s.
BA	n.d.	n.d.	<LOQ	1.7	n.d.	4.2	<LOQ	5.0	15.3	
Sampling June	ERT	n.d.	n.d.	7.5	9.7	n.d.	12.6	0.3	15.4	20.3
	CD1	n.d.	n.d.	<LOQ	5.0	n.d.	17.8	<LOQ	6.9	22.0
	CD2	n.d.	<LOQ	<LOQ	5.4	n.d.	22.3	<LOQ	13.1	40.4
	CD3	n.d.	n.d.	<LOQ	5.1	n.d.	16.4	<LOQ	8.3	40.0
	CD4	n.d.	n.d.	<LOQ	5.6	n.d.	22.4	n.d.	7.6	28.5
	CD5	n.d.	n.d.	<LOQ	4.6	n.d.	19.1	0.4	4.6	42.6
	CD6	n.d.	n.d.	<LOQ	5.0	n.d.	19.9	<LOQ	5.1	56.3
	CD7	n.d.	n.d.	<LOQ	4.8	n.d.	23.5	0.3	16.0	376.6
	CD8	n.d.	n.d.	<LOQ	3.6	n.d.	n.d.	n.d.	4.4	29.4
	EL	n.d.	n.d.	<LOQ	2.3	n.d.	12.9	0.7	3.4	62.9
	CE1	n.d.	n.d.	5.8	9.9	n.d.	14.2	0.3	12.7	20.7
	CE2	n.d.	n.d.	4.3	8.2	n.d.	23.1	0.3	11.4	39.0
	CE3	n.d.	n.d.	<LOQ	6.5	n.d.	19.2	0.9	9.6	98.1
BA	n.d.	n.d.	n.d.	n.d.	n.d.	4.8	1.2	n.d.	17.1	
Sampling July	ERT	n.a.	n.a.	n.a.	n.a.	n.a.	n.a.	n.a.	n.a.	n.a.
	CD1	n.d.	n.d.	<LOQ	19.8	n.d.	10.9	12.1	37.8	19.4
	CD2	n.d.	n.d.	<LOQ	13.7	n.d.	14.1	11.5	35.2	14.8
	CD3	n.d.	n.d.	<LOQ	24.5	n.d.	10.2	10.6	35.4	21.5
	CD4	n.d.	n.d.	<LOQ	15.4	n.d.	13.9	38.4	41.8	78.1
	CD5	n.d.	n.d.	n.d.	14.0	n.d.	7.9	11.1	15.6	10.5
	CD6	n.d.	n.d.	<LOQ	13.8	n.d.	13.1	11.6	16.0	44.1
	CD7	n.d.	n.d.	<LOQ	11.5	n.d.	8.5	43.7	40.4	16.8
	CD8	n.d.	n.d.	<LOQ	10.0	n.d.	4.6	4.2	16.8	n.d.
	EL	n.d.	n.d.	<LOQ	11.7	n.d.	5.3	8.3	21.5	50.3
	CE1	n.d.	n.d.	<LOQ	26.1	n.d.	4.3	16.9	79.3	2.5
	CE2	n.d.	n.d.	<LOQ	18.0	n.d.	12.5	33.1	50.4	53.1
	CE3	n.d.	n.d.	<LOQ	19.7	n.d.	8.8	22.2	57.4	16.0
BA	n.d.	n.d.	<LOQ	3.6	n.d.	n.d.	1.1	n.d.	13.9	
Sampling August	ERT	n.d.	n.d.	<LOQ	6.6	n.d.	5.5	0.8	20.2	19.6
	CD1	n.d.	n.d.	<LOQ	3.8	n.d.	5.0	0.7	46.3	26.0
	CD2	n.d.	n.d.	<LOQ	3.2	n.d.	5.0	0.6	15.2	27.8
	CD3	n.d.	n.d.	<LOQ	2.8	n.d.	5.0	0.6	10.4	18.7
	CD4	n.d.	n.d.	<LOQ	2.9	n.d.	9.0	0.3	19.2	11.2
	CD5	n.d.	n.d.	<LOQ	2.5	n.d.	n.d.	0.3	9.6	18.8
	CD6	n.d.	n.d.	<LOQ	3.1	n.d.	7.9	0.6	9.7	28.1
	CD7	n.d.	n.d.	<LOQ	2.3	n.d.	5.6	0.7	7.9	78.9
	CD8	n.d.	n.d.	<LOQ	2.7	n.d.	<LOQ	0.6	9.1	12.1
	EL	n.d.	n.d.	n.d.	n.d.	n.d.	<LOQ	0.6	n.d.	8.0
	CE1	n.d.	n.d.	<LOQ	7.2	n.d.	<LOQ	0.6	172.7	14.7
	CE2	n.s.	n.s.	n.s.	n.s.	n.s.	n.s.	n.s.	n.s.	n.s.
	CE3	n.s.	n.s.	n.s.	n.s.	n.s.	n.s.	n.s.	n.s.	n.s.
BA	n.d.	n.d.	n.d.	n.d.	n.d.	n.d.	0.5	n.d.	4.2	

n.d., not detected; n.s., not sampled; n.a., not analysed; <LOQ, below limit of quantitation.

- [2] L. Padovani, E. Capri, C. Padovani, E. Puglisi, M. Trevisan, *Chemosphere* 62 (2006) 303.
- [3] C. Barata, J. Damasio, M.A. López, M. Kuster, M.J. López de Alda, D. Barceló, M.C. Riva, D. Raldúa, *Environ. Toxicol. Chem.* 26 (2007) 370.
- [4] I.K. Konstantinou, D.G. Hela, T.A. Albanis, *Environ. Pollut.* 141 (2006) 555.
- [5] MED-Rice, EC Document Reference SANCO/1090/2000-rev. 1 (2003) 108.
- [6] T.C.R. Santos, J.C. Rocha, D. Barcelo, *J. Chromatogr. A* 879 (2000) 3.
- [7] C. Tarazona, J.M. Carrasco, C. Sabater, in: A.A.M. Del Re, E. Capri, C. Padovani, M. Trevisan (Eds.), *Proceedings of the XII Symposium Pesticide Chemistry*, Piacenza, Italy, 2003, pp. 727–735.
- [8] D. Barceló, M.-C. Hennion, *Trace Determination of Pesticides and Their Degradation Products in Water*, Elsevier, Amsterdam, 1997.
- [9] T. Reemtsma, *Trends Anal. Chem.* 20 (2001) 533.
- [10] Y. Picó, C. Blasco, G. Font, *Mass Spectrom. Rev.* 23 (2004) 45.
- [11] M. Kuster, M.J. López de Alda, D. Barceló, *Mass Spectrom. Rev.* 25 (2006) 900.
- [12] A. Asperger, J. Efer, T. Koal, W. Engewald, *J. Chromatogr. A* 960 (2002) 109.
- [13] F. Hernández, M. Ibáñez, J.V. Sancho, O.J. Pozo, *Anal. Chem.* 76 (2004) 4349.
- [14] F. Hernandez, J.V. Sancho, O. Pozo, A. Lara, E. Pitarch, *J. Chromatogr. A* 939 (2001) 1.
- [15] A.C. Hogenboom, P. Speksnijder, R.J. Vreeken, W.M.A. Niessen, U.A.T. Brinkman, *J. Chromatogr. A* 777 (1997) 81.
- [16] J.M. Marin, J.V. Sancho, O.J. Pozo, F.J. Lopez, F. Hernandez, *J. Chromatogr. A* 1133 (2006) 204.
- [17] M. Terrado, M. Kuster, D. Raldúa, M. López de Alda, D. Barceló, R. Tauler, *Anal. Bioanal. Chem.* 387 (2007) 1479.
- [18] A. Claver, P. Ormad, L. Rodriguez, J.L. Ovelleiro, *Chemosphere* 64 (2006) 1437.
- [19] C. Aguilar, I. Ferrer, F. Borrull, R.M. Marce, D. Barcelo, *Anal. Chim. Acta* 386 (1999) 237.
- [20] L. Brossa, R.M. Marce, F. Borrull, E. Pocurull, *Environ. Toxicol. Chem.* 24 (2005) 261.
- [21] T. Iwakuma, H. Shiraiishi, S. Nohara, K. Takamura, *Chemosphere* 27 (1993) 677.
- [22] A.A. Kampioti, A.C. Borba da Cunha, M.J. López de Alda, D. Barceló, *Anal. Bioanal. Chem.* 382 (2005) 1815.
- [23] A.C. Borba da Cunha, M.J. López de Alda, D. Barceló, T.M. Pizzolato, J.H.Z. dos Santos, *Anal. Bioanal. Chem.* 378 (2004) 940.
- [24] L.G. Freitas, C.W. Gotz, M. Ruff, H.P. Singer, S.R. Muller, *J. Chromatogr. A* 1028 (2004) 277.
- [25] F. Hernandez, O.J. Pozo, J.V. Sancho, F.J. Lopez, J.M. Marin, M. Ibanez, *Trends Anal. Chem.* 24 (2005) 596.
- [26] K. Stoob, H.P. Singer, C.W. Goetz, M. Ruff, S.R. Mueller, *J. Chromatogr. A* 1097 (2005) 138.
- [27] E. Dijkman, D. Mooibroek, R. Hoogerbrugge, E. Hogendoorn, J.-V. Sancho, O. Pozo, F. Hernandez, *J. Chromatogr. A* 926 (2001) 113.
- [28] B.A. Ingelse, R.C.J. van Dam, R.J. Vreeken, H.G.J. Mol, O.M. Steijger, *J. Chromatogr. A* 918 (2001) 67.
- [29] EU, EC Document Reference SANCO/10232/2006 (2006) 10.
- [30] Council of the European Communities, *Off. J. Eur. Commun. L.* 330 (1998) 32.
- [31] O.J. Pozo, J.V. Sancho, M. Ibanez, F. Hernandez, W.M.A. Niessen, *Trends Anal. Chem.* 25 (2006) 1030.
- [32] F. Andre, K.K.G. De Wasch, H.F. De Brabander, S.R. Impens, L.A.M. Stolker, L. van Ginkel, R.W. Stephany, R. Schilt, D. Courtheyn, Y. Bonnaire, P. Furst, P. Gowik, G. Kennedy, T. Kuhn, J.-P. Moretain, M. Sauer, *Trends Anal. Chem.* 20 (2001) 435.

Crosslinked and quaternized poly(4-vinylpyridine)/polypyrrole composite as a potential candidate for the detection of low humidity

Yang Li*, Lijie Hong, Mujie Yang

Department of Polymer Science and Engineering, Zhejiang University, Hangzhou 310027, China

Received 26 July 2007; received in revised form 4 November 2007; accepted 8 November 2007

Available online 19 November 2007

Abstract

Poly(4-vinylpyridine) was crosslinked and quaternized with 1,4-bromobutane to form a polyelectrolyte humidity sensitive film on an interdigitated gold electrode, which was further coated with a layer of polypyrrole by a facile method of vapor phase polymerization. The composite so prepared was characterized by UV–vis spectroscopy and scanning electron microscopy. The investigations on the humidity sensitive properties of the composite revealed that it exhibited an impedance as low as $10^5 \Omega$ even at 0%RH due to the existence of intrinsic conducting polypyrrole, thus conquering the difficulties in measuring low humidity with resistive-type humidity sensors. The impedance of the composite changed linearly with humidity in the range of 0–60%RH with good sensitivity. In addition, its response time ($t_{90\%}$) for adsorption and desorption between 33% and 97%RH was estimated to be 33 s and 110 s, respectively, and a hysteresis of 5%RH was observed. All these suggest it is promising as a sensitive material for low humidity detection. The effect of concentration and ratio of oxidizing agent to doping agent, polymerization temperature of pyrrole on the humidity sensitive properties of the composite have been investigated. A sensitive mechanism of the composite was proposed by taking into account the contribution of both the intrinsic electronic conduction and ionic conduction.

© 2007 Elsevier B.V. All rights reserved.

Keywords: Polypyrrole; Poly(4-vinylpyridine); Composite; Humidity detection

1. Introduction

Humidity is ever-existing in our environment, and its monitoring and control have been of great concern in industrial and agricultural production, environmental protection, meteorology, etc. [1–3], which greatly promoted the development of various types of humidity sensors. Among them, resistive-type polymeric humidity sensors became popular in recent years. Compared with capacitive-type humidity sensors, they exhibited higher sensitivity, easier fabrication and thus lower cost [4–6]. In addition, their stability is better than that of ceramic-based humidity sensors, which exhibited a serious drifting in the electrical response and needed to be cleaned by heating for maintaining the humidity sensing characteristics [7]. However, they also suffered from the problems of poor durability at humid envi-

ronment and the limitation in the detection of environment where humidity was low, especially when it was lower than 20%RH. The first problem obviously originated from the water solubility of the sensitive materials, which are mainly polyelectrolyte. Great attention has been paid to address the shortcoming, and methods including reducing the water solubility of the sensing film by copolymerizing with hydrophobic monomers, preparing sensitive films with crosslinking structures or even interpenetrating networks, applying protection films, etc. have been adopted to effectively improve the water-resistance of the polymeric humidity sensors [8–11]. In contrast, the efforts to solve the other problem, which results from the limited ionic conductivity of polyelectrolyte at low humidity, are rarely reported [12–14], in spite of the strong needs for measurement and control of very low humidity in the production of lithium ion batteries, cables and transformers, supercapacitors, low temperature drying of some medicines, etc.

Polypyrrole (PPy) is a typical intrinsic conducting polymer. It bears a conjugated backbone in which π -electrons can be delocalized, and its electronic conduction in doped state makes it conductive even in the absence of humidity. Geng

* Corresponding author at: Department of Polymer Science and Engineering, Zhejiang University, Institute of Polymer Science, 38 Zhe Da Road, Hangzhou 310027, China. Tel.: +86 571 87952444; fax: +86 571 87952444.

E-mail address: liyang@zju.edu.cn (Y. Li).

and coworkers investigated the humidity sensitive properties of chemically prepared PPy. They reported that PPy covered with a protective film of cellulose showed high sensitivity to humidity, but only in the medium to high humidity range (>54%RH). In addition its impedance was quite high at low humidity [15]. Su and Huang prepared a composite of PPy and TiO₂ for the detection of humidity, but the impedance at low humidity was still very high [16]. Obviously, they are not suitable for detection of low humidity.

In this paper, we tried to prepare a composite of quaternized and crosslinked poly(4-vinylpyridine) (QC-PVP) and organic acid doped PPy as a sensitive material of resistive-type humidity sensors. It is expected that the QC-PVP may exhibit high sensitivity, which is characteristic of polyelectrolyte humidity sensitive material, and good stability due to its crosslinking structure [13,17,18]. While the doped PPy could confer the composite with high conductivity at low humidity by taking advantage of its high intrinsic electronic conductivity. In addition, the deposition of PPy on QC-PVP film by vapor phase polymerization may lead to uniform distribution of PPy and better adhesion between the two sensitive films, thus enhances their stability and sensitivity. The humidity sensitive properties of the composite, especially in the low humidity range, were investigated. The effects of preparation conditions of PPy on the sensitive properties of the composite were studied, and the sensing mechanism was explored.

2. Experimental

2.1. Materials

All the reagents used were of analytic grade. 4-Vinylpyridine was distilled under reduced pressure before use. Benzoylperoxide (BPO) was purified by recrystallization. 4-Hydroxy-2,2,6,6-tetramethyl piperidinoxyl (TEMPO) (Beijing Yang Cun Chemical Reagent Co., Ltd.) and pyrrole (Zhejiang Qingquan Medical and Chemical Reagent Co., Ltd.) were used as received.

2.2. Preparation of poly(4-vinylpyridine)

The preparation of poly(4-vinylpyridine) (PVP) has been described in previous work [12]. Briefly, 4-vinylpyridine was polymerized in the presence of BPO and TEMPO at 125 °C for 29 h. The resultant was dissolved with methanol, precipitated in ether, filtered and dried under vacuum to obtain a light-red solid. FT-IR (KBr pellet) (cm⁻¹) (3067, 3024, 1598, 1556, 1416, 995 (pyridine ring); 2927, 2855 (–CH₂–)). ¹H NMR (CDCl₃) (ppm) 8.76–7.97 (CH–N–CH), 7.23–6.09 (–CH–C–CH), 1.75–1.18 (–CH₂–CH(C₅H₅N)).

2.3. Preparation of humidity sensors

Appropriate amount of PVP and 1,4-dibromobutane were added into *N,N*-dimethylformamide (DMF) and aged at 30 °C for 12 h with magnetic stirring. After that, it was deposited onto a clean glass ceramic substrate (4 mm × 6 mm × 0.5 mm), where an interdigitated array of gold electrodes had been previously

evaporated and photolithographically defined (the distance and width of tracks were both 40 μm), by the method of dip-coating with an automatic dip-coating machine (concentration of PVP: 24 g dL⁻¹, dipping rate: 2.5 mm s⁻¹). The electrode was then dried in air, heated at 110 °C for 10 h for the quaternization and crosslinking of PVP, washed with ethanol for three times and dried at 80 °C for 30 min to obtain a humidity sensor based on QC-PVP.

The QC-PVP-based sensor was further dipped into an aqueous solution of ammonium persulfate (APS) and *p*-toluenesulfonic acid (TSA), taken out and dried in air. Afterwards, it was put in a closed vessel containing a certain amount of pyrrole, where the vapor phase polymerization of pyrrole proceeded at different temperatures for 4 h. Finally it was washed with ethanol for three times and dried at 110 °C for 30 min to obtain a humidity sensor based on the composite of QC-PVP and PPy.

2.4. Measurement

FT-IR spectra were recorded on a Bruker Vector 22 R spectrometer (KBr pellets). ¹H NMR measurements were carried out on a 500 MHz Varian Mercury Plus NMR spectrometer (solvent: CDCl₃; internal standard: tetramethylsilane). UV–vis spectra were obtained on a Varian Cary 100 Bio UV–vis spectrophotometer. The morphologies of the composites were observed on a field emission scanning electron microscopy (SEM) instrument (Sirion, FEI company). The molecular weight and its distributions of PVP were determined by gel permeation chromatography (GPC) on a Waters 1525/2414 chromatography calibrated with polystyrene standards at 35 °C in DMF.

The humidity sensitive properties of the sensor were investigated by recording its electrical response at different humidities at room temperature using a homemade setup. The applied voltage was 1 V and frequency was 1 kHz. The sensor was placed in a chamber where humidity was controlled by adjusting the mixed ratio of dry to wet gases. The response time measurement was performed by recording online the electrical response of the sensor over different saturated salt solutions in their equilibrium state (MgCl₂ for 33%RH and K₂SO₄ for 97%RH) [18]. The time to reach 90% of the impedance change was denoted as the response time (*t*_{90%}).

3. Results and discussion

3.1. Characterization of the composite

In this paper, a composite of crosslinked and quaternized PVP (QC-PVP) and PPy synthesized by vapor phase polymerization was prepared and used as a sensitive material for the detection of low humidity. QC-PVP is a typical polyelectrolyte humidity sensitive material with good sensitive properties [13,17,18]. The formation of crosslinking structure provided it with enough durability in humid environment. In particular, PVP used in the research was prepared by nitroxide-mediated living polymerization, and featured with a narrow molecular weight distribution.

The molecular weight M_n , M_w and its distribution was found to be 3.56×10^4 , 3.79×10^4 and 1.06, respectively.

In addition, different from the normally adopted methods of electrochemical polymerization and solution chemical polymerization, PPy was prepared by vapor phase polymerization and deposited on QC-PVP film. Once the vapor of volatile pyrrole contacted the film already impregnated with the oxidizing agent (APS) and doping agent (TSA), chemical oxidative polymerization proceeded to obtain a layer of PPy. Obviously the facile method of vapor phase polymerization enjoyed the advantages of simplicity (without the need to use sophisticated electrochemical device for electropolymerization, economy and slighter impact to environment by circumventing the problem of producing greatly excessive PPy in the form of precipitated waste during solution chemical polymerization), uniformity of PPy layer on any substrate and better adhesion of PPy with QC-PVP and the underlying electrode. The UV–vis spectra of QC-PVP and QC-PVP/PPy composite are shown in Fig. 1. The peak at 256 nm in the spectra of QC-PVP is attributed to the π – π^* transition of pyridine ring. In the spectrum of the composite, apart from the peak at 256 nm resulting from QC-PVP, another adsorption peak at 470 nm is observed, which is characteristic of π – π^* transition in doped PPy [19]. The UV–vis spectrum of the composite, which is just the superposition of the spectra of QC-PVP and PPy, suggested the preparation of the composite of QC-PVP and doped PPy.

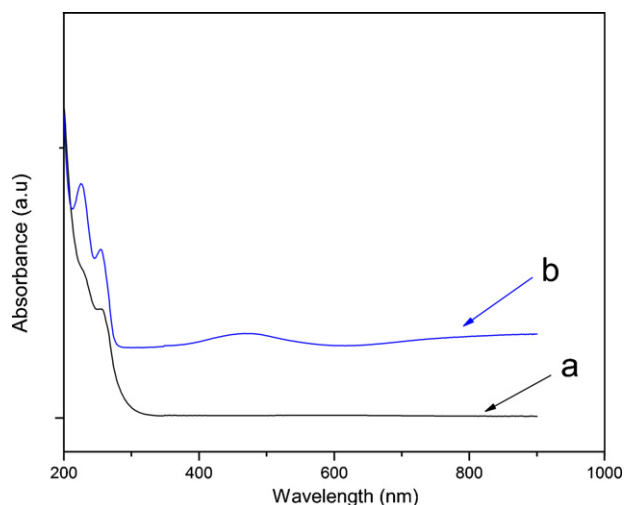


Fig. 1. UV–vis spectra of films of (a) QC-PVP and (b) QC-PVP/PPy composite.

Fig. 2 shows the SEM micrographs of sensing films of QC-PVP and its composite with PPy prepared at different temperatures. It can be seen clearly that the film of QC-PVP is quite smooth and uniform with few defects (Fig. 2a). After the deposition of a layer of PPy, some cracks are observed in the composite film prepared by vapor phase polymerization at a low temperature (3°C) (Fig. 2b and c). In contrast, the film seems

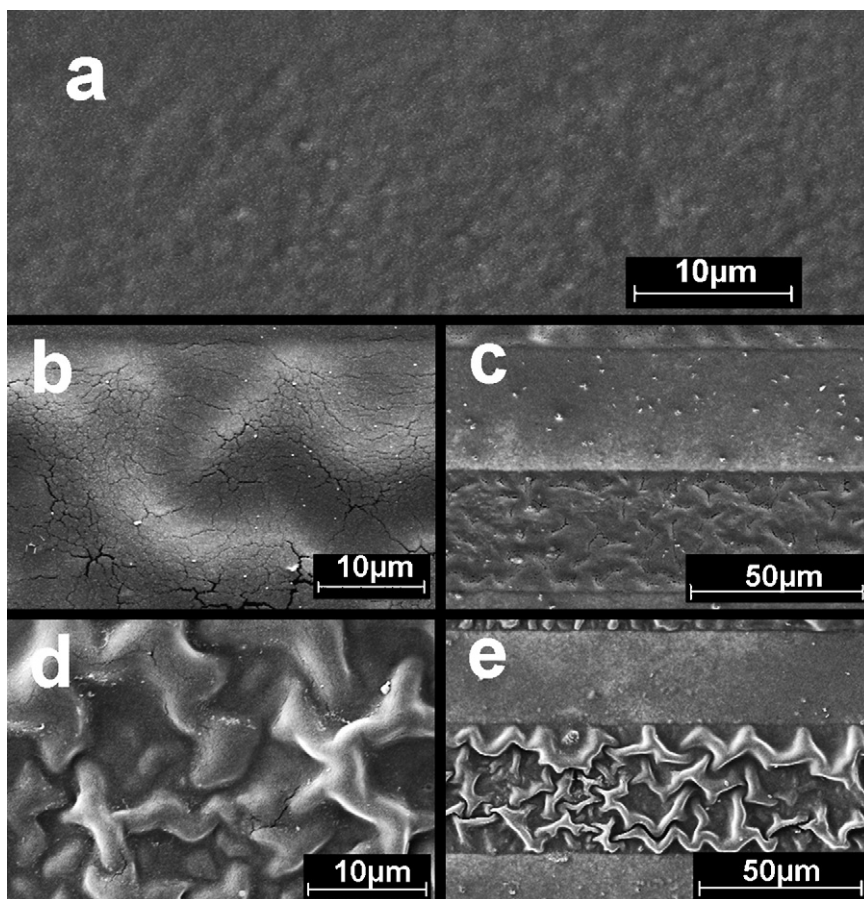


Fig. 2. SEM micrographs of (a) QC-PVP and QC-PVP/PPy composite prepared by vapor phase polymerization at (b and c) 3°C and (d and e) 25°C .

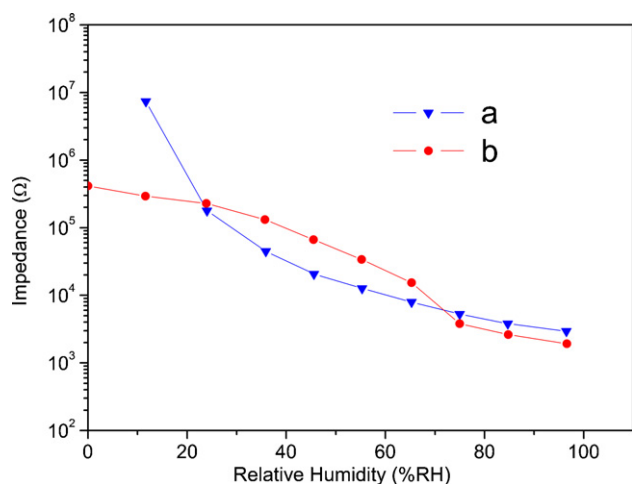


Fig. 3. The response calibration curves of (a) QC-PVP and (b) QC-PVP/PPy composite prepared by vapor phase polymerization at 25 °C.

to be twisted and full of folds and cracks when the polymerization temperature was raised to 25 °C (Fig. 2d and e). More cracks are observed in the composite film prepared at an even higher polymerization temperature (40 °C) (figure not shown). The results suggest that polymerization temperature can greatly affect the morphology of the composite film. As reported by Matsuguchi et al. [20], the morphology of sensitive films has a great effect on their sensing behavior, together with the nature of the sensing material. Therefore, it is expected that the composite in which pyrrole polymerized at different temperatures may exhibit different sensing behaviors, as will be discussed later.

3.2. Humidity sensitive properties of the composite

As a typical polyelectrolyte humidity sensitive material, QC-PVP exhibited an impedance decrease of nearly four orders of magnitude when humidity was increased from 12% to 96%RH as depicted in Fig. 3, showing high sensitivity and moderate linearity on a semi-logarithmic scale. However, its impedance was quite high in dry atmosphere, reaching $7.4 \times 10^6 \Omega$ at 12%RH. At even lower humidity, the impedance was too high to be measured. The fact indicated that such kind of sensitive material alone could not be used for the detection of low humidity. In contrast, when it formed a composite with PPy by the method of vapor phase polymerization, the impedance at low humidity was greatly decreased to only $4 \times 10^5 \Omega$ even at 0%RH. The results suggest that the composite can be used for the detection of humidity even in very dry atmosphere. Obviously, the decreased impedance was related to the electronic conduction inherent to the doped PPy.

It is known that the concentration and ratio of oxidizing agents to doping agents can affect the conductivity of PPy, and their effect on the humidity sensitive properties of QC-PVP/PPy composite has been investigated and shown in Figs. 4 and 5. As illustrated in Fig. 4, the impedance of the composite at 12%RH decreased by two orders of magnitude when the concentration of APS was increased from 0.5 g dL^{-1} to 1.5 g dL^{-1} . The impedance at low humidity was further decreased, but to a

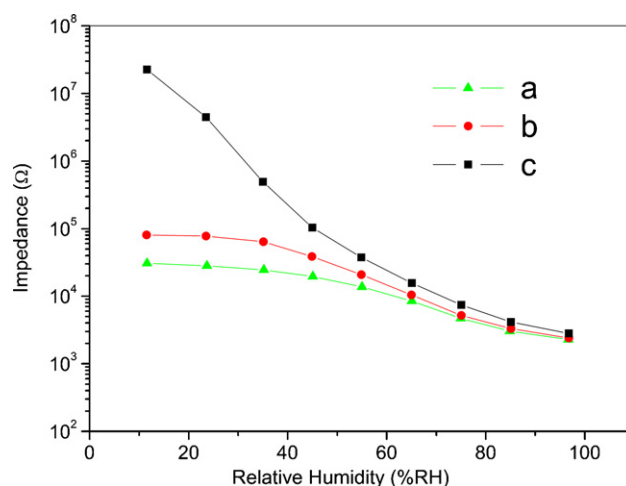


Fig. 4. The response calibration curves of QC-PVP/PPy composite prepared with APS of different concentrations: (a) 3.0 g dL^{-1} , (b) 1.5 g dL^{-1} , (c) 0.5 g dL^{-1} (APS/TSA = 1/1.4, mole ratio).

much lesser extent, when the concentration reached 3.0 g dL^{-1} . From Fig. 5, it can be seen that the impedance of the composite decreased with the increase in the ratio of TSA to APS. In addition, it is noticeable that the composite with lower impedance at low humidity also exhibited a greatly depressed sensitivity. When TSA/APS = 2.8/1 (mole ratio), the composite with the lowest impedance became almost insensitive to humidity change. By considering the sensitivity and the impedance at low humidity, the concentration of APS and the mole ratio of TSA to APS was set at 1.5 g dL^{-1} and 1/1.4, respectively, in the preparation of the composite in the following discussion.

As mentioned above, polymerization temperature has a great effect on the morphology of the composite films, which may affect their humidity sensitive characteristics. Fig. 6 presents the impedance as a function of relative humidity of the composites in which pyrrole was polymerized at different temperatures. At a polymerization temperature of 40 °C, the composite obtained exhibited very high impedance, presumably due to the fact that

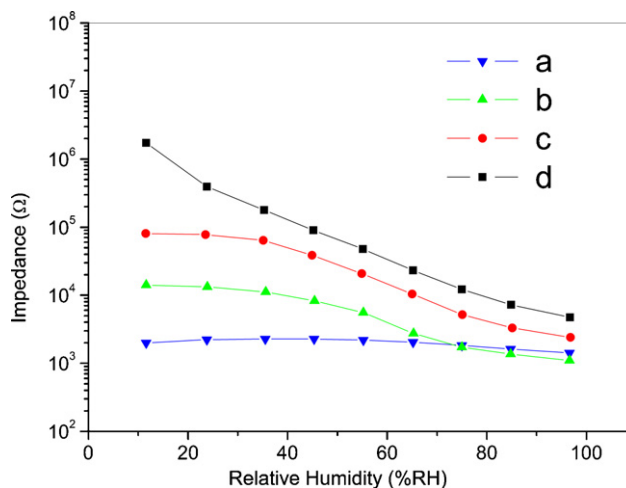


Fig. 5. The response calibration curves of QC-PVP/PPy composites prepared with different mole ratios of APS to TSA: (a) 1:2.8, (b) 1:2.1, (c) 1:1.4, (d) 1:0.7 ([APS] = 1.5 g dL^{-1}).

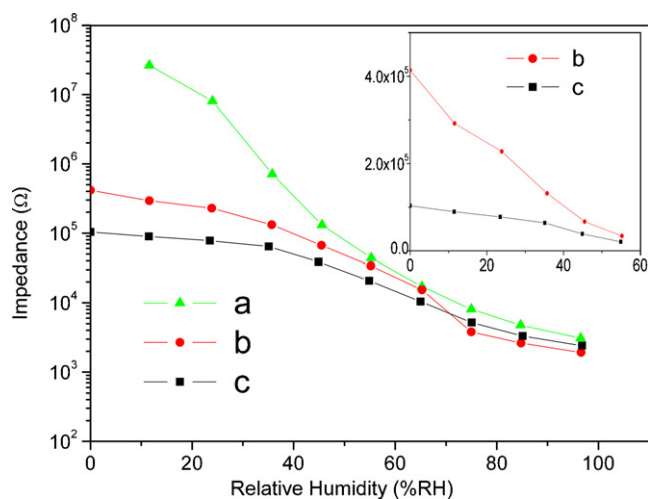


Fig. 6. The response calibration curves of QC-PVP/PPy composite prepared by vapor phase polymerization at various temperatures: (a) 40 °C, (b) 25 °C, (c) 3 °C.

the conductivity of PPy prepared was much lower at higher polymerization temperature [21]. The sensitivity was still high since QC-PVP might easily contact with adsorbed water molecules through the large number of cracks on the composite films and exhibited great impedance change. By decreasing the temperature to 25 °C and 3 °C, the impedance of the composites at 0%RH was reduced to only $4.1 \times 10^5 \Omega$ and $1.0 \times 10^5 \Omega$, respectively. However, the sensitivity was also much depressed. This could be explained as follows. At lower polymerization temperature, PPy exhibited a higher conductivity, and a lower impedance was observed at dry atmosphere. In addition, the QC-PVP film was better covered by the PPy film. Therefore its contact with adsorbing water molecules at increasing humidities was hindered, which resulted in smaller impedance changes and a lower sensitivity.

The inset of the figure presents the plot of impedance versus relative humidity of the composites in the range of 0–60%RH on a linear scale. It clearly shows that the impedance of the composite in which PPy prepared at 25 °C changed almost linearly for one order of magnitude with variation of relative humidity, suggesting its potential of working as a sensitive material for low humidity detection. The results indicate that only at a suitable polymerization temperature, can the inclusion of PPy effectively decrease the impedance of the composite at dry atmosphere while maintain its good sensitivity for the humidity detection at the same time.

In addition to the calibration curves of the impedance response to relative humidity, response time and hysteresis are two important parameters for humidity sensors. It was found that QC-PVP showed a faster response in the humidification process than in the desiccation process, with a $t_{90\%}$ of 25 s and 76 s for adsorption and desorption between 33% and 97%RH, respectively (figures not shown). After the deposition of PPy layer, the response of the composite was slower, and $t_{90\%}$ for adsorption and desorption between 33% and 97%RH was prolonged to 33 s and 110 s, respectively. In addition, the hysteresis is estimated to be 6% and 5%RH for QC-PVP and the composite, respectively.

However, it is found that the maximum hysteresis for the composite was observed at higher than 50%RH, and the hysteresis is only 2–3%RH when humidity was lower than 40%RH (figures not shown). This indicates that the composite may exhibit a smaller hysteresis when used in the detection of low humidity.

3.3. Sensing mechanism

The present research indicates that the composite of PPy and QC-PVP exhibited decreased impedance with the humidity increasing, which is in agreement with the humidity sensitive characteristics of PPy covered by cellulose film [15], PPy/TiO₂ [16] and PPy/Fe₃O₄ composites [22]. In contrast, Cho et al. investigated the effect of humidity on the methanol vapor sensing properties of PPy, and reported its resistance increased during the humidification process, which was attributed to the reduction in the number of charge carrier holes in PPy layer by absorbed water vapor [23]. It is therefore necessary to explore the sensing mechanism of our composite.

It is known that the conduction of polymeric humidity sensor is composed of both electric and ionic conduction. At low humidity, due to the high intrinsic electronic conduction in relation with the conjugated main chain of the doped PPy, the impedance of the composite was only in the order of $10^5 \Omega$ even at 0%RH. While the contribution of ionic conduction in dry atmosphere became negligible since the ions in the composite could not move freely without the assistance of water molecules. With the humidity increase, the conductivity of PPy changed little, as revealed by the slight change in resistance of PPy deposited on an insulating substrate by vapor phase polymerization process [20]. On the other hand, water adsorbed on the sensitive film promoted the dissociation of ions in the composite, thus ionic conductivity at higher humidity was greatly promoted, and its contributions to the overall conductivity was enhanced. At high humidity, the ionic conductivity played a dominant role, thus QC-PVP and the composite exhibited similar impedance as illustrated in Fig. 3. As a result, the composite, which exhibited a much higher conductivity than that of QC-PVP alone at low humidity due to the contribution of electronic conduction of PPy, could not exhibit an impedance change as large as that of the polyelectrolyte alone. Thus its sensitivity is good, but lower than that of QC-PVP alone.

4. Conclusions

Polypyrrole can be deposited on the surface of quaternized and crosslinked PVP film to prepare a composite by vapor phase polymerization. The composite is featured with low impedance even at 0%RH, good sensitivity and fast response. The polymerization conditions of pyrrole have great effect on the humidity response of the composite. QC-PVP/PPy can be a promising candidate for the detection of low humidity.

Acknowledgements

This work is financially supported by the National Natural Science Foundation of China (contract no. 50403020), Zhejiang

Provincial Natural Science Foundation of China (Grant no. M203093) and National “863” program of China (contract no. 2006AA10Z215).

References

- [1] J. Barkauskas, *Talanta* 44 (1997) 1107.
- [2] I. Fratoddi, P. Altamura, A. Bearzotti, A. Furlani, M.V. Russo, *Thin Solid Films* 458 (2004) 292.
- [3] C.Y. Lee, G.B. Lee, *Sens. Lett.* 3 (2005) 1.
- [4] P.G. Su, C.L. Uen, *Talanta* 66 (2005) 1247.
- [5] R. Nohria, R.K. Khillan, Y. Su, R. Dikshit, Y. Lvov, K. Varahramyan, *Sens. Actuators B* 114 (2006) 218.
- [6] G. Casalbore-Miceli, M.J. Yang, Y. Li, A. Zanelli, A. Martelli, Y.S. Chen, Y. She, N. Camaioni, *Sens. Actuators B* 114 (2006) 584.
- [7] B.M. Kulwicki, *J. Am. Ceram. Soc.* 74 (1991) 697–708.
- [8] C.W. Lee, B.K. Choi, M.S. Gong, *Analyst* 129 (2004) 651.
- [9] P.G. Su, C.L. Uen, *Sens. Actuators B* 107 (2005) 317.
- [10] Y. Li, Y.S. Chen, C. Zhang, T.X. Xue, M.J. Yang, *Sens. Actuators B* 125 (2007) 131.
- [11] C.W. Lee, S.W. Joo, M.S. Gong, *Sens. Actuators B* 105 (2005) 150.
- [12] H.W. Chen, R.J. Wu, K.H. Chan, Y.L. Sun, P.G. Su, *Sens. Actuators B* 104 (2005) 80.
- [13] C. Caliendo, I. Fratoddi, M.V. Russo, *Appl. Phys. Lett.* 80 (2002) 4849.
- [14] Y. Li, L.J. Hong, Y.S. Chen, H.C. Wang, X. Lv, M.J. Yang, *Sens. Actuators B* 123 (2007) 554.
- [15] W.C. Geng, N. Li, X.T. Li, R. Wang, J.C. Tu, T. Zhang, *Sens. Actuators B* 125 (2007) 114.
- [16] P.G. Su, L.N. Huang, *Sens. Actuators B* 123 (2007) 501.
- [17] Y. Sakai, Y. Sadaoka, M. Matsuguchi, *J. Electrochem. Soc.* 136 (1989) 171.
- [18] Y. Li, M.J. Yang, Y. She, *Sens. Actuators B* 107 (2005) 252.
- [19] K.G. Neoh, H.W. Teo, E.T. Kang, *Langmuir* 14 (1998) 2820.
- [20] M. Matsuguchi, A. Okamoto, Y. Sakai, *Sens. Actuators B* 94 (2003) 46.
- [21] Y. Li, X.Y. Cheng, M.Y. Leung, J. Tsang, X.M. Tao, M.C.W. Yuen, *Synth. Met.* 155 (2005) 89.
- [22] R.P. Tandon, M.R. Tripathy, A.K. Arora, S. Hotchandani, *Sens. Actuators B* 114 (2006) 768.
- [23] J.H. Cho, J.B. Yu, J.S. Kim, S.O. Sohn, D.D. Lee, J.S. Huh, *Sens. Actuators B* 108 (2005) 389.

Chemiluminescence of tryptophan and histidine in $\text{Ru}(\text{bpy})_3^{2+}$ - KMnO_4 aqueous solution

Zhijie Lin^a, Xiaomei Chen^a, Zhimin Cai^a, Peiwei Li^a,
Xi Chen^{a,b,*}, Xiaoru Wang^a

^a Department of Chemistry and Key Laboratory of Analytical Sciences of the Ministry of Education College of Chemistry and Chemical Engineering, Xiamen University, Xiamen 361005, China

^b State Key Laboratory of Marine Environmental Science, Xiamen University, Xiamen 361005, China

Received 14 August 2007; received in revised form 13 November 2007; accepted 16 November 2007

Available online 11 January 2008

Abstract

Amino acids with different chemical structures have different abilities in terms of increasing the intensity of chemiluminescence (CL) of tris(2,2'-bipyridine)ruthenium(II) [$\text{Ru}(\text{bpy})_3^{2+}$]. In a flow system, CL caused by the reaction between $\text{Ru}(\text{bpy})_3^{3+}$ and 15 amino acids was observed, but only tryptophan (Trp) and histidine (His) enhanced the intensity obviously, and so the CL of Trp and His and their molecular groups was studied. A calculation of the ionization potentials (IPs) of their N atom indicated that the CL intensities of these compounds depended on their IPs. In addition, the flow system was used for the determination of Trp and His, and the detection limits were $3 \times 10^{-8} \text{ mol L}^{-1}$ for His and $2.5 \times 10^{-9} \text{ mol L}^{-1}$ for Trp. The calibration curves for the two amino acids were 1.0×10^{-7} to $5.0 \times 10^{-3} \text{ mol L}^{-1}$ for His and 1.0×10^{-8} to $1.0 \times 10^{-4} \text{ mol L}^{-1}$ for Trp. The proposed approach was applied to the determination of His in *Ganoderma*.

© 2007 Elsevier B.V. All rights reserved.

Keywords: Chemiluminescence; Amino acids; Tris(2,2'-bipyridine)ruthenium; FIA; *Ganoderma*

1. Introduction

Amino acids are important components in numerous samples, in particular in biological tissues and fluids, foods and industrial products. Recently, there have been several reports dealing with the detection of chemiluminescence (CL) in amino acids [1–5]. Since the first report of tris(2,2'-bipyridine)ruthenium(II) [$\text{Ru}(\text{bpy})_3^{2+}$] CL in an acidic solution [6], $\text{Ru}(\text{bpy})_3^{2+}$ has become both an extremely versatile base CL and electrogenerated chemiluminescence (ECL) reagent [7–10]. Common to all analytical applications of $\text{Ru}(\text{bpy})_3^{2+}$, the relative oxidant, $\text{Ru}(\text{bpy})_3^{3+}$, is generated by an oxidation process, during which luminescence results from the reduction of $\text{Ru}(\text{bpy})_3^{3+}$ to the excited state [$\text{Ru}(\text{bpy})_3^{2+*}$]. Although a wide variety of compounds can reduce $\text{Ru}(\text{bpy})_3^{3+}$, only those with amine groups

or oxalates cause CL with this reagent [11–17]. Amino acids are therefore likely to produce a reasonably intense emission when oxidized by $\text{Ru}(\text{bpy})_3^{3+}$. Generally, the amine group of amino acids produces a secondary amine following by a dealkylation process in the presence of water. The intermediate neutral amine radicals have sufficient energy to react with $\text{Ru}(\text{bpy})_3^{2+}$ or $\text{Ru}(\text{bpy})_3^{3+}$ to yield the excited state $\text{Ru}(\text{bpy})_3^{2+*}$ and hence light emission.

A variety of methods including chemical/photochemical and in situ electrochemical oxidation ECL have been used for the transformation of $\text{Ru}(\text{bpy})_3^{2+}$ to $\text{Ru}(\text{bpy})_3^{3+}$. Common oxidants such as cerium (IV) [18], hydrogen peroxide [1], and acidic KMnO_4 [19] have been used to efficiently produce $\text{Ru}(\text{bpy})_3^{3+}$ from $\text{Ru}(\text{bpy})_3^{2+}$. To date, research based on the CL reaction of drugs, such as enalapril maleate [20], metoclopramide hydrochloride [15], pyrrolizidine alkaloids [21] and tetracycline [22], with $\text{Ru}(\text{bpy})_3^{2+}$ and acidic KMnO_4 have been reported. Cosin et al. [23] report that tryptophan and its biological derivatives, which contain an indole moiety, produce bright CL in orthophosphoric acid at pH 2.0. Clear CL emissions of tyrosine were obtained in both acidic and neutral

* Corresponding author at: Department of Chemistry and Key Laboratory of Analytical Sciences of the Ministry of Education College of Chemistry and Chemical Engineering, Xiamen University, Xiamen 361005, China.
Tel.: +86 592 2184530; fax: +86 592 218 6401.

E-mail address: xichen@xmu.edu.cn (X. Chen).

conditions, and the detection limit was $5 \times 10^{-8} \text{ mol L}^{-1}$ at pH 2.0 and $1 \times 10^{-8} \text{ mol L}^{-1}$ at pH 6.75. Generally, column separation including high performance liquid chromatography (HPLC) [24,25], electrophoresis [26,27] or even HPLC-MS [28] is necessary for the determination of amino acids in Chinese medicine samples, but this involves a complex procedure and a high test cost. The development of a simpler and lower cost approach for the instant determination of amino acids became an attractive research field. Recently, a flow injection method for the determination of histidine (His) in a pharmaceutical injection by the ECL of luminol is proposed [29]. In addition, Liang and his collaborators [30] present their results on the CL of Trp in hydrogen peroxide-nitrite-sulfuric acid medium, and apply the proposed method to the analysis of Trp in pharmaceutical preparations and human serum.

In this study, the CL phenomena of 15 amino acids in $\text{Ru}(\text{bpy})_3^{2+} \text{KMnO}_4$ acidic solution were investigated. The aim of this work was to investigate the relationship between the structural attributes of His and Trp, as well as their residue model compounds. Either a Trp residue model, such as tryptamine, indole, pyrrole, and alanine, or a His residue model such as histamine, imidazole, and alanine, were selected to reveal their possible CL mechanisms. His and Trp presented bright CL in acidic $\text{Ru}(\text{bpy})_3^{2+} \text{-KMnO}_4$ solution with determination limits of $3 \times 10^{-8} \text{ mol L}^{-1}$ for His and $2.5 \times 10^{-9} \text{ mol L}^{-1}$ for Trp. Since His emitted a bright CL in the selected medium, it was applied to the determination of His in *Ganoderma*.

2. Materials and methods

2.1. Chemicals and standard solutions

All amino acids were purchased from Wako Pure Chemical Industries LTD (Osaka, Japan). Tryptamine, indole, histamine, pyrrole, imidazole and $\text{Ru}(\text{bpy})_3\text{Cl}_2 \cdot 6\text{H}_2\text{O}$ were obtained from Sigma Chemical Company (St. Louis, MO, USA) and used without further purification. All other chemicals were of guaranteed grade. The water used throughout was purified with a Millipore system (Millipore Co., USA). The stock solution (1.0 mmol L^{-1}) of each amino acid was prepared using the carrier solution, and the working solutions were diluted in the same carrier solution.

2.2. Apparatus and procedures for determination of chemiluminescence

The CL intensity was observed using CL instrumentation designed in our laboratory. The main body of the thin layer flow cell was constructed from two pieces of Diflon block separated by a $200 \mu\text{m}$ thick Teflon spacer. The volume of the thin layer cell was about $6.0 \mu\text{L}$. The experimental setup, composed of the flow system equipped with a Rheodyne 7125 sample injector (Cototi, CA, USA, $20 \mu\text{L}$) and an injection loop of $20 \mu\text{L}$, is shown in Fig. 1. Light emission was detected using a photomultiplier tube (R464, Hamamatsu, Japan) and the signal was amplified and recorded using a Chromatographic Processor (Echro 98, Yilite

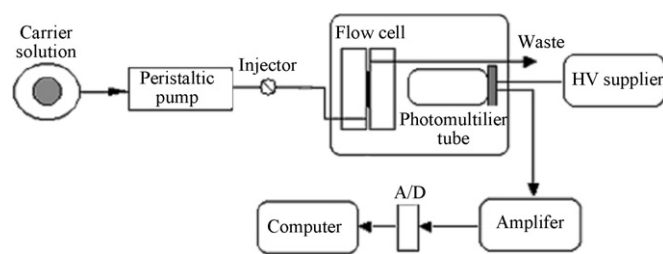


Fig. 1. Experimental set up for measurement of chemiluminescence.

Co. Ltd., Dalian, China). All pH measurements were made using a Delta 320A pH-meter (Mettler Toledo Instruments-Shanghai Co., Shanghai, China).

To calculate the ionization potentials (IPs) of these compounds, we used the hybrid B3LYP density functional method [31,32] as implemented in the Gaussian98 package [33], and the standard 6-31G* basis set for all atoms. Geometrical optimization of both the neutral and ionized compounds was performed using analytical gradients and the Berny algorithm with no constrained degrees of freedom. The theoretical IP was defined as the difference in the total energies of the cationic and neutral compounds, i.e., $\text{IP} = E_{\text{total}}(\text{cation}) - E_{\text{total}}(\text{neutral})$.

2.3. Sample preparation and data processing

In a nitrogen atmosphere, 5.0 mg of pulverized dried *Ganoderma* was immersed in 1.0 mL 6.0 mol L^{-1} HCl at a temperature of 110°C for 24 h. The samples were ultrasonically mixed for 20 min (1.0 MHz, AS-2060B, Autoscience Co. Ltd., Tianjing, China), and the same procedure was repeated twice. The extracts were combined and centrifuged at 3500 rpm for 10 min, filtered using a $0.45 \mu\text{m}$ cellulose acetate membrane filter, and then diluted to 50.0 mL with pure water as the stored sample solution. The stored sample solution was further diluted 100 times using the mobile solution ($0.5 \text{ mmol L}^{-1} \text{ Ru}(\text{bpy})_3^{2+}$, $0.5 \text{ mmol L}^{-1} \text{ KMnO}_4$ and $0.1 \text{ mol L}^{-1} \text{ H}_2\text{SO}_4$) and then used for flow analysis.

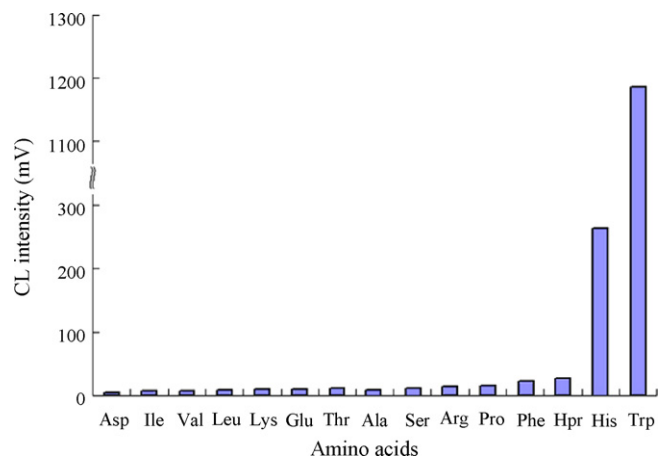


Fig. 2. Comparison of CL intensity for 15 amino acids. Conditions: $0.5 \text{ mmol L}^{-1} \text{ Ru}(\text{bpy})_3^{2+}$ - $0.5 \text{ mmol L}^{-1} \text{ KMnO}_4$ - $0.1 \text{ mol L}^{-1} \text{ H}_2\text{SO}_4$, flow rate: 0.5 mL min^{-1} . Concentration for each amino acid: $5.0 \times 10^{-6} \text{ mol L}^{-1}$.

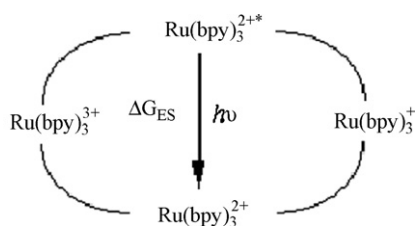
Calibration curves in the concentration range 1.0×10^{-7} to $5.0 \times 10^{-3} \text{ mol L}^{-1}$ for His, and 1.0×10^{-8} to $1.0 \times 10^{-4} \text{ mol L}^{-1}$ for Trp were constructed by plotting the peak-height of analyte standards of His and Trp concentration. Least squares linear regression analysis was used to determine the slope, intercept and correlation coefficient. The concentration of His or Trp samples was determined from the ECL peak height by using the equations of linear regression obtained from the calibration curve.

For the recovery studies, His or Trp standard solution with a final concentration of 0.5, 1.0 and 1.5 mg g^{-1} was added to samples, and the mixture was extracted or diluted and analyzed using the procedure described previously.

3. Results and discussion

3.1. Investigation of amino acid chemiluminescence

The majority of compounds containing an amine group, including amino acids, elicit CL with $\text{Ru}(\text{bpy})_3^{3+}$. Chemiluminescence of amino acids in the presence of $\text{Ru}(\text{bpy})_3^{2+}$, leading to the production of light, is type- and pH-dependent. Investigations by He et al. [13] show that secondary amino acids such as proline or hydroxyproline generate the greatest CL response amongst 18 kinds of amino acids in an alkaline solution (pH 11.0). Uchikura et al. report that the suitable pH for the determination of tryptophan is pH 3, but pH 8 is good for primary amine after derivatization with divinylsulfone [34]. A comparison of CL intensities associated with the oxidation of different amino acids in a $\text{Ru}(\text{bpy})_3^{2+} \text{ KMnO}_4$ acidic solution was performed (Fig. 2). Preliminary screening within an acidic region (pH 1–6) revealed that Trp and His exhibited substantially greater CL response than the other amino acids at a concentration of $2.0 \mu\text{mol L}^{-1}$. A 5.2 fold increase of CL intensity for Trp than for His was obtained in the solution of $0.5 \text{ mmol L}^{-1} \text{ Ru}(\text{bpy})_3^{2+} - 0.5 \text{ mmol L}^{-1} \text{ KMnO}_4 - 0.1 \text{ mol L}^{-1} \text{ H}_2\text{SO}_4$. However, investigation in the alkaline range pH 7 to 12 showed negligible CL response for all the amino acids. As mentioned in the introduction, the CL of $\text{Ru}(\text{bpy})_3^{2+}$ was caused by the generation of its excited form, $\text{Ru}(\text{bpy})_3^{2+*}$, and its intensity was enhanced in the presence of amine radicals, which were yielded from the oxidation of amines or amino acids in the medium. Based on the report of Bock et al. [35] as shown in Scheme 1, the oxidation potential for $\text{Ru}(\text{bpy})_3^{2+}$ to $\text{Ru}(\text{bpy})_3^{3+}$ is +1.29 V. Lin et al. [36] indicate that the CL intensity of $\text{Ru}(\text{bpy})_3^{2+}$ in KMnO_4 solution is greatly affected by the acidity of the carrier solution and increases with the addition of H_2SO_4 solution. In



Scheme 1. Redox processes of $\text{Ru}(\text{bpy})_3^{2+}$ and the corresponding potentials.

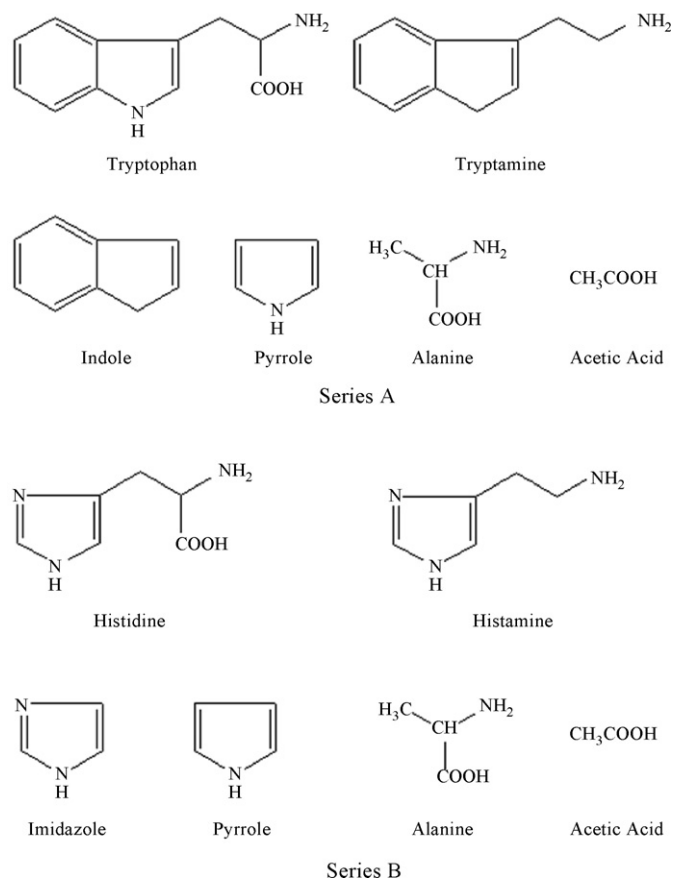


Fig. 3. Chemical structures for Trp (series A) and His (series B) groups.

an acidic medium, a 1.51 V standard potential of $\text{MnO}_4^-/\text{Mn}^{2+}$ is high enough to oxidize $\text{Ru}(\text{bpy})_3^{2+}$ to its $\text{Ru}(\text{bpy})_3^{3+}$ oxidized form, but the oxidation potential of MnO_4^- decreases to 0.34 V in an alkaline solution, which predicts that it is essentially impossible to transfer $\text{Ru}(\text{bpy})_3^{2+}$ by MnO_4^- .

According to the screening result, as in Fig. 2, we note that many amino acids did not noticeably increase the CL of $\text{Ru}(\text{bpy})_3^{2+}$ in acidic KMnO_4 solution. Only Trp and His together with the pyrrole or imidazole moiety produced brighter CL. In order to assess whether this observation was caused by the existence of a pyrrole moiety, the CLs of the two groups of compounds, including Trp, tryptamine, indole, pyrrole and alanine for the Trp residue model, and His, histamine, imidazole and alanine for the His residue model, were selected and compared (Fig. 3). As can be seen from Fig. 4, the related pyrrole compounds such as tryptamine, Trp and indole gave brighter CL signals (Fig. 4a), but weaker CL emissions for imidazole, histamine or His were also found for the His group (Fig. 4b). Interestingly, a weak CL of acetic acid is obtained in $\text{Ru}(\text{bpy})_3^{2+} \text{ KMnO}_4$ acidic solution, caused by a radical-mediated oxidation between $\text{Ru}(\text{bpy})_3^{2+}$ and the carboxyl intermediate of acetic acid [37]. The CL of Trp and His without $\text{Ru}(\text{bpy})_3^{2+}$ in acidic KMnO_4 medium are reported by Cosin et al. [23]. In our study, the addition of $\text{Ru}(\text{bpy})_3^{2+}$ greatly enhanced the CL intensity, and the intensity was slightly increased when the concentration of $\text{Ru}(\text{bpy})_3^{2+}$ was above 0.40 mmol L^{-1} . Zhang et al. [38] sug-

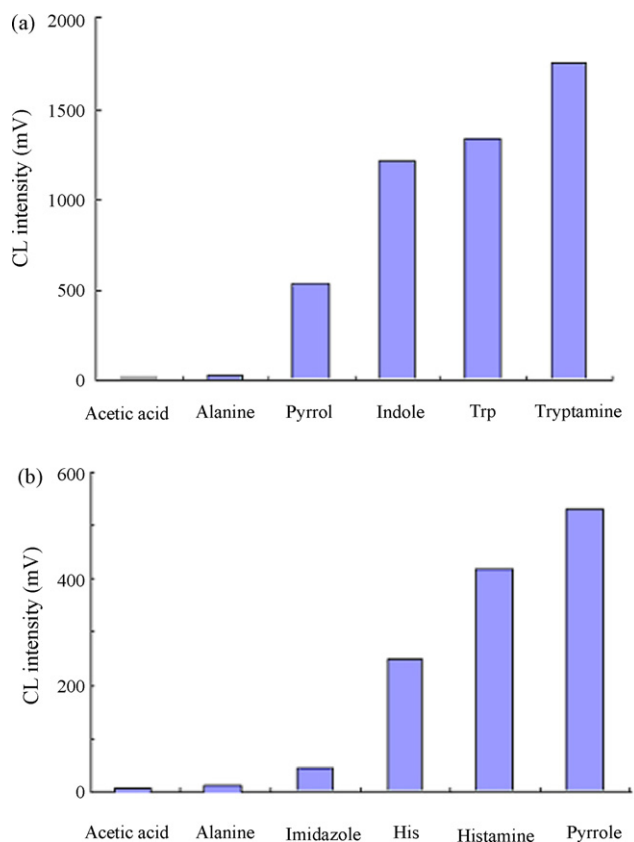


Fig. 4. Comparison of CL intensities for the Trp group (a) and His group (b). Experimental conditions are the same as shown in Fig. 2. Concentration for each compound: $2.0 \times 10^{-6} \text{ mol L}^{-1}$.

gest that the aromatic amino group is the key functionality for the production of CL with *p*-aminobenzoate-type compounds. As can be seen in Fig. 4a, pyrrole contributed an observable CL emission, and the CL intensity was greatly increased if the compound contained an aromatic group in the pyrrole, such as tryptamine, Trp or indole. It is suggested that aromatic amino acid residues in the proteins mediate the electron transfer reaction as pathway molecules [39,40]. Zhang et al. [8] report that 3-methylindole and a model of Trp residue could increase the electroactivity of the $\text{Ru}(\text{bpy})_3^{2+}$ in a polymer film, which reveals that the aromatic group combined with indole enhances the CL activities of compounds in the Trp group. These results suggest that the aromatic group increases the amine group activity of pyrrole, and furthermore, improves the reaction rate with $\text{Ru}(\text{bpy})_3^{2+}$, and hence yields a brighter CL for indole or Trp.

3.2. Ionization potential calculation and luminescence intensity

In our previous studies, the IP value of a compound could be successfully applied to estimate the general trend of luminescence intensity [16,41]. In general, as in Noffsinger and Danielson's [11] suggestion, the CL reaction mechanism of $\text{Ru}(\text{bpy})_3^{2+}$ and amines involves a charge-transfer process, the first IP for the alkyl amines generally decreasing in the order primary > secondary > tertiary. Based on the B3LYP/6-31 G(d)

calculation results (Table 1), a lower IP value of the N atom in the amine group corresponded to a higher CL intensity. CL intensities of tryptamine, Trp or indole with IPs of 6.710, 6.771 and 7.064 eV were 1752, 1337 and 1211 mV, respectively. Obviously, after combining an aromatic ring of pyrrole, the IP of pyrrole with 7.297 eV was changed to 7.064 eV of indole. The CL intensity of indole increased about 5-fold over that of pyrrole. In addition, although the above results had already confirmed that the CL associated with the free Trp reaction could have been caused by initial electrophilic attack on the indole moiety, more attacks on the alanine or ammonium group should be taken into account. After comparing the CL intensities of Trp, Lys, *n*-butylamine, 3-methylindol and Ala, Aspée and Lissi [3] postulate that the independent contribution of the ammonium group and the indole moiety is 0.43 and 0.40, respectively. Actually, the contribution of indole reached over 0.90 based on comparison of the CL intensities of indole and Trp (Table 1). Additionally, in terms of the contribution of alanine or ammonium, the effect of the substituent group should be considered. Generally, the electron-donating substituent attaches to the alpha- or beta-carbon atom and stabilizes positive or electron-deficient radical ions of amine, and hence, tends to decrease its IP and further increase the CL activity of the compound. A comparable IP decrease could be found when hydrogen was replaced by alanine, resulting in a lower IP value (6.771 eV) and brighter CL emission of Trp. The same conclusion can be obtained by a comparison of the CLs of imidazole, His and histamine. The CL activity of the amine group in imidazole was much lower than that in pyrrole. Because of its higher IP, a lower CL intensity was obtained.

3.3. Measurement of absorptive and luminescent spectra

In order to evaluate the characteristics of the CL process associated with Trp and His oxidation in acidic $\text{Ru}(\text{bpy})_3^{2+}$ - KMnO_4 solution, the UV-vis spectral change of Trp and His were measured in the solution. The maximum absorbance wavelength of $\text{Ru}(\text{bpy})_3^{2+}$ showed at 454 nm, which indicated that a typical MLCT with a transition of the t_{2g} metal orbital to the π^* ligand orbital occurs (Fig. 5a and b). With the addition of KMnO_4 , new absorptive peaks appeared at wavelengths of 515,

Table 1
Chemical structures and corresponding ionic potentials

Compound	IP (eV)	CL (mV)	Compound	IP (eV)	CL (mV)
Tryptophan	6.771	1337	Acetic acid	8.367	15
Tryptamine	6.710	1752	Histidine	7.388	296
Indole	7.064	1211	Histamine	7.378	152
Pyrrol	7.297	267	Imidazole	8.083	22
Valine	8.253	7.3	Leucine	8.388	9.0
Isoleucine	8.208	6.9	Threonine	9.324	13.1
Phenylalanine	7.795	23.0	Proline	7.854	16.0
Serine	8.223	9.2	Hydroproline	7.658	27.2
Aspartic acid	8.510	3.9	Glutamic acid	8.426	6.1
Lysine	8.402	7.2	Arginine	7.427	14.3

*B3LYP/6-31 G(d) calculation method was applied to obtain IP values. Concentration for each compound was kept at $2.0 \times 10^{-6} \text{ mol L}^{-1}$.

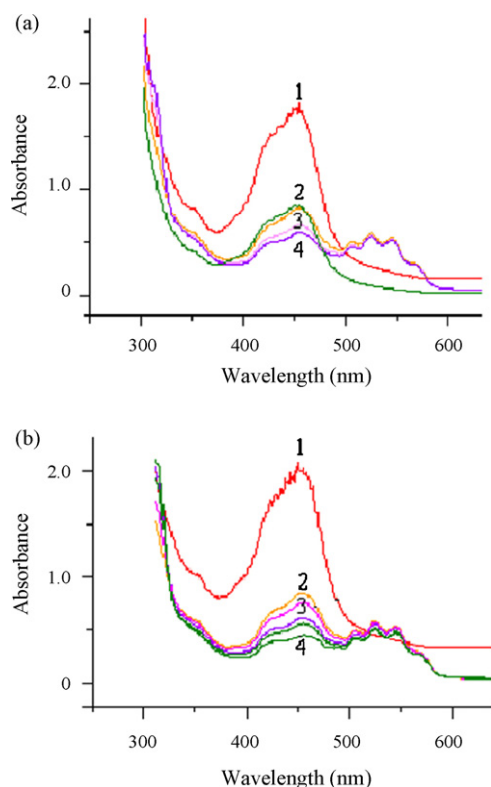


Fig. 5. UV-vis absorption spectral changes of $\text{Ru}(\text{bpy})_3^{2+}$ in KMnO_4 with the addition of Trp (a) and His (b). Solution condition: 0.5 mmol L^{-1} $\text{Ru}(\text{bpy})_3^{2+}$, 0.5 mmol L^{-1} KMnO_4 and 0.1 mol L^{-1} H_2SO_4 , Concentration of amino acid: 0.5 mmol L^{-1} .

530 and 545 nm and, synchronously, the absorptive intensity at 454 nm obviously decreased due to the reaction of $\text{Ru}(\text{bpy})_3^{2+}$ and KMnO_4 . The intensity at 454 nm was further reduced with the addition of His or Trp. Absorptions of KMnO_4 at 515, 530 and 545 nm rapidly decreased, and finally disappeared when Trp was added into the solution (Fig. 5a), but only slight decrease occurred for His addition (Fig. 5b). These results further confirmed that Trp presented more CL activity than His.

It is clear that luminescence of $\text{Ru}(\text{bpy})_3^{2+}$ is caused by the reaction between the radical intermediate and $\text{Ru}(\text{bpy})_3^{3+}$, which produces the excited state [42]. In the CL reaction of $\text{Ru}(\text{bpy})_3^{2+}$ and Trp or His in acidic KMnO_4 solution, a reduced intermediate of the radical cation was generated from the oxidation of Trp or His by $\text{Ru}(\text{bpy})_3^{3+}$, and yielded the excited state $\text{Ru}(\text{bpy})_3^{2+*}$. The CL emission spectra at 610 nm in both $\text{Ru}(\text{bpy})_3^{2+}$ and a mixture of $\text{Ru}(\text{bpy})_3^{2+}$ with Trp or His solution, could further confirm that the emission at 610 nm resulted from transition of the excited state $\text{Ru}(\text{bpy})_3^{2+*}$ to the ground state by means of an electron transfer reaction.

3.4. Chemiluminescence response performance

Chemiluminescence intensities of amino acids are known to greatly depend on the concentrations of $\text{Ru}(\text{bpy})_3^{2+}$, H_2SO_4 and KMnO_4 [4]. To establish the parameters which gave the greatest CL signal with Trp and His, a series of univariate searches were performed. The variables investigated included

the concentrations of $\text{Ru}(\text{bpy})_3^{2+}$, H_2SO_4 , KMnO_4 , as well as the flow rate. A concentration of Trp at $1.0 \times 10^{-6} \text{ mol L}^{-1}$ or His at $5.0 \times 10^{-6} \text{ mol L}^{-1}$ was selected for all investigations. The concentration of $\text{Ru}(\text{bpy})_3^{2+}$ which gave the best emission intensity was $5.0 \times 10^{-4} \text{ mol L}^{-1}$. Although a higher concentration of $\text{Ru}(\text{bpy})_3^{2+}$ slightly increased the CL intensity, this implied higher cost and pollution. The oxidation of $\text{Ru}(\text{bpy})_3^{2+}$ to $\text{Ru}(\text{bpy})_3^{3+}$ was the key step for Trp and His CL, and this was obviously affected by the solution pH and concentration of KMnO_4 . According to the experimental results, an acidic medium was suitable for Trp or His CL. Thus, the addition of H_2SO_4 into the carrier solution greatly increased CL emission, but the background noise increased greatly when the H_2SO_4 concentration exceeded 0.2 mol L^{-1} . In addition, the effect of varying the KMnO_4 concentration on the CL response was studied. The CL signal was greatly increased with the increase of KMnO_4 concentration. CL intensity remained constant when the KMnO_4 concentration was above $4.5 \times 10^{-4} \text{ mol L}^{-1}$ due to the reaction of KMnO_4 and $\text{Ru}(\text{bpy})_3^{2+}$. For analytical application, therefore, a KMnO_4 concentration of $5.0 \times 10^{-4} \text{ mol L}^{-1}$ was used. Since the CL intensity was significantly affected by the reaction pH, the effect of H_2SO_4 concentration on CL intensity was investigated. Finally, 0.1 mol L^{-1} H_2SO_4 was applied. A lower flow rate of reagent caused a larger background signal, and the optimal flow rate of 0.5 mL min^{-1} was recommended.

Under these optimum experimental conditions, the carrier stream was selected as $5.0 \times 10^{-4} \text{ mol L}^{-1}$ KMnO_4 , 0.1 mol L^{-1} H_2SO_4 and $5.0 \times 10^{-4} \text{ mol L}^{-1}$ $\text{Ru}(\text{bpy})_3^{2+}$. The CL intensity increased linearly with the concentrations of His and Trp over the concentration range 1.0×10^{-7} to $5.0 \times 10^{-3} \text{ mol L}^{-1}$ for His, and 1.0×10^{-8} to $1.0 \times 10^{-4} \text{ mol L}^{-1}$ for Trp. The detection limit was $3 \times 10^{-8} \text{ mol L}^{-1}$ and $2.5 \times 10^{-9} \text{ mol L}^{-1}$ for His and Trp, respectively, at an S/N of 3. CL intensities displayed good reproducibility and were precise to within 3% for 10 replicate injections for all samples at a concentration of $2.0 \times 10^{-6} \text{ mol L}^{-1}$.

3.5. Effects of co-existing substances

The effects of co-existing substances commonly found in *Ganoderma* were investigated. When the tolerated limit for a foreign substance was taken as the largest amount yielding a relative error of less than 10% for the determination of $2.0 \times 10^{-6} \text{ mol L}^{-1}$ His, no obvious effects could be found in the presence of $5.0 \times 10^{-2} \text{ mol L}^{-1}$ K^+ , Na^+ , or NH_4^+ ; $5.0 \times 10^{-3} \text{ mol L}^{-1}$ Ca^{2+} , Zn^{2+} , Mg^{2+} , Mn^{2+} , Cl^- , SO_4^{2-} , PO_4^{3-} , or NO_3^- ; $1.0 \times 10^{-4} \text{ mol L}^{-1}$ Ni^{2+} , Cu^{2+} , Co^{2+} , Al^{3+} , or Fe^{3+} ; and $2.0 \times 10^{-5} \text{ mol L}^{-1}$ Fe^{2+} , Pb^{2+} , or Cd^{2+} . As shown in Table 2, weaker CL of carbohydrates and acids containing $-\text{OH}$ groups (such as mannose, fructose, ascorbic acid, saccharic acid, malic acid and tartaric acid) were noted. A stronger light emission was generated by compounds such as sodium oxalate but the lower concentration of sodium oxalate in *Ganoderma* samples limits its effect. When considering the effects of co-

Table 2
Chemiluminescence intensities for co-existing substances^a

Compound	CL intensity (mV)	Compound	CL intensity (mV)
Fructose	2.4	Retinoic acid (Vitamin A)	–
Glucose	0.8	Thiamine HCl (Vitamin B ₁)	0.5
Mannose	11.2	Riboflavin (Vitamin B ₂)	0.4
Sucrose	1.2	Pyridoxine HCl (Vitamin B ₆)	0.6
Ethanol	1.5	Calciferol (Vitamin D ₂)	–
Glycerol	0.6	Tocopherol (Vitamin E)	–
Mannitol	0.2	Folic acid (Vitamin B _c)	–
Glucitol	1.5	Starch (soluble 2%)	1.6
Saccharic acid	2.3	Sodium oxalate	1386
Benzoic	–	Caramel	0.2
Maleic acid	–	Human serum albumin	–
Malic acid	0.6	Choline	–
Citric acid	8.8	Indole-3-acetic acid	166.8
Ascorbic acid	23.8	Benzoic acid	–
Tartaric acid	3.5	Tannic acid	3.8
Sorbitol	1.4	Urea	6.5
Betains	–	Uric acid	0.3

^a Concentration for each compound was kept at 2.0×10^{-6} mol L⁻¹.

Table 3
Determination of histidine in *Ganoderma* samples

<i>Ganoderma</i> sample	GB/T18246-2000	Proposed method ^a (mg g ⁻¹)	Added (mg g ⁻¹)	Found ^a (mg g ⁻¹)	Average recovery (%)
<i>G. lucidum</i> (Wild)	0.65	0.72 ± 0.07	0.50	0.44 ± 0.08	88
			1.00	0.92 ± 0.07	92
<i>G. lucidum</i> (Log-cultivated)	1.10	1.28 ± 0.12	1.00	0.97 ± 0.07	97
<i>G. curtisii</i>	0.84	0.87 ± 0.08	1.00	1.08 ± 0.06	108
<i>G. calidophilum</i>	1.44	1.67 ± 0.12	1.00	0.93 ± 0.10	93
			1.50	1.32 ± 0.12	88
<i>G. sinense</i> (Wild)	1.42	1.48 ± 0.16	1.00	1.02 ± 0.05	102
			1.50	1.47 ± 0.14	98
<i>G. sinense</i> (Log-cultivated)	1.13	0.93 ± 0.07	1.00	0.85 ± 0.04	85
<i>G. duropora</i>	1.12	1.15 ± 0.10	1.00	1.07 ± 0.07	107
<i>G. cochlear</i>	1.19	1.37 ± 0.15	1.00	0.92 ± 0.09	92
			1.50	1.47 ± 0.12	98

^a Mean value ± S.D. (n = 6).

existing amino acids, based on their CL characteristics in the acidic KMnO₄-Ru(bpy)₃²⁺ medium and their normal contents in *Ganoderma* samples [43,44], their CL contributions were estimated to be 12% less for His.

3.6. Sample analysis

The method proposed was applied to the determination of His in *Ganoderma* samples obtained from Fujian province. A content of His ranging from 0.72 to 1.67 mg g⁻¹ was found in the different types of *Ganoderma* samples (Table 3), which agreed well with those obtained by the National Standard Method (GB/T18246-2000). The relative standard deviation (R.S.D.) for the determination ranged from 7.5 to 12.6%. The recovery of the CL method, measured as the percentage difference between the mean concentrations found and the amounts added, ranged from 88 to 108%. The determination results indicated that the content of His in wild *Ganoderma* samples was not obviously

higher than that in the log-cultivated samples. The content of His greatly depended on the type of *Ganoderma* used.

4. Conclusions

Chemiluminescence of His or Trp with Ru(bpy)₃²⁺ was attributed to the oxidation of Ru(bpy)₃²⁺ by reaction with KMnO₄ to form Ru(bpy)₃³⁺. In the CL reaction, the acidic medium plays a key role in the oxidation of Ru(bpy)₃²⁺, since KMnO₄ does not have the ability to oxidize Ru(bpy)₃²⁺ in an alkaline or neutral solution. Based on analysis of the CL of Trp and His, one electron of the amine group of His or Trp is known to yield a radical cation by the oxidation of Ru(bpy)₃³⁺. The IP calculation of the amino group reveals a changing trend of CL intensity as a whole. Additionally, the CL conditions for the determination of Trp and His has been optimized. The results indicated that the method presented is suitable for the CL determination of His in biological fluids such as *Ganoderma* extracts,

or in Chinese medicine, because only His and Trp produced distinct CL signals among the amino acids tested. Furthermore, the approach presented provides a relatively sensitive route for the analysis of His and Trp.

Acknowledgement

This research work was financially supported by the Program for New Century Excellent Talents in Chinese Universities (NCET), the National Nature Scientific Foundations of China (No. 20775064, 20735002) and NFFTBBS (No. J0630429), which are gratefully acknowledged. Furthermore, we would like to extend our thanks to Professor John Hodgkiss of The University of Hong Kong for his assistance with English.

References

- [1] M.C. Sanfeliu Alonso, L. Lahuerta Zamora, J. Martínez Calatayud, *Talanta* 60 (2003) 369.
- [2] A. Aspée, E.A. Lissi, *Luminescence* 15 (2000) 273.
- [3] A. Aspée, E.A. Lissi, *Luminescence* 17 (2002) 158.
- [4] W. Yang, Z. Zhang, W. Deng, *Talanta* 59 (2003) 951.
- [5] R. King, G.M. Miskelly, *Talanta* 67 (2005) 345.
- [6] D.M. Hercules, F.E. Lytle, *J. Am. Chem. Soc.* 88 (1966) 4745.
- [7] S.N. Brune, D.R. Bobbitt, *Talanta* 38 (1991) 419.
- [8] J. Zhang, M. Yagi, M. Kaneko, *J. Electroanal. Chem.* 445 (1998) 109.
- [9] M.E. Bolden, N.D. Danielson, *J. Chromatogr. A* 828 (1998) 421.
- [10] A. Townshend, W. Ruengsitagoon, C. Thongpoon, S. Liawruangrath, *Anal. Chim. Acta* 541 (2005) 105.
- [11] J.B. Noffsinger, N.D. Danielson, *Anal. Chem.* 59 (1987) 865.
- [12] K. Uchikura, M. Kirisawa, *Anal. Sci.* 7 (1991) 971.
- [13] L. He, K.A. Cox, N.D. Danielson, *Anal. Lett.* 232 (1990) 195.
- [14] I. Rubinsteln, C.R. Martin, A.J. Bard, *Anal. Chem.* 55 (1983) 1580.
- [15] N.A. Al-Arfaj, *Talanta* 62 (2004) 255.
- [16] X. Chen, C. Yi, M. Li, X. Lu, Z. Li, P. Li, X. Wang, *Anal. Chim. Acta* 466 (2002) 79.
- [17] F.A. Aly, S.A. Al-Tamimi, A.A. Alwarthan, *Talanta* 53 (2001) 885.
- [18] L. Guo, Z. Xie, X. Lin, X. Liu, W. Zhang, G. Chen, *Luminescence* 19 (2004) 64.
- [19] N.A. Alarfaj, S.A.A. El-Razeq, *J. Pharm. Biomed. Method* 41 (2006) 1423.
- [20] N.A. Alarfaj, *Anal. Sci.* 19 (2003) 1145.
- [21] B.A. Gorman, N.W. Barnett, R. Bos, *Anal. Chim. Acta* 541 (2005) 119.
- [22] M.M. Abdel-Khalek, M.S. Mahrous, *Talanta* 30 (1983) 792.
- [23] J.W. Cosin, P.S. Francis, S.W. Lewis, *Anal. Chim. Acta* 480 (2003) 67.
- [24] Y. Shi, Y. Ming, C. Wang, X. Zhao, R. Zhang, J. You, *Chin. J. Anal. Chem.* 34 (2006) 503.
- [25] V.P. Hanko, J.S. Rohrer, *Anal. Biochem.* 308 (2002) 204.
- [26] C. Wang, S. Zhao, H. Yuan, D. Xiao, *J. Chromatogr. B* 833 (2006) 129.
- [27] M. Jaworska, Z. Szuliska, M. Wilk, *J. Chromatogr. A* 993 (2003) 165.
- [28] Y.G. Chi, Y.L. Feng, S. Wen, H.X. Lu, Z.Q. Yu, W.B. Zhang, G.Y. Sheng, J.M. Fu, *Talanta* 72 (2007) 539.
- [29] L. Zhu, Y. Li, G. Zhu, *Chin. Chem. Lett.* 13 (2002) 1093.
- [30] Y. Liang, J. Song, *J. Pharm. Biomed. Anal.* 38 (2005) 100.
- [31] A.D. Becke, *J. Chem. Phys.* 98 (1993) 5648.
- [32] C. Lee, W. Yang, R.G. Parr, *Phys. Rev. B* 37 (1989) 785.
- [33] M.J. Frisch, G.W. Trucks, B.H. Schlegel, et al., *Gaussian 98, Revision A.10*, Gaussian, Inc., Pittsburgh, PA, 1998.
- [34] K. Uchikura, M. Kirasawa, A. Sugh, *Anal. Sci.* 9 (1993) 121.
- [35] C.R. Bock, J.A. Connor, A.R. Guierrez, T.J. Meyer, D.G. Whitten, B.P. Sullivan, J.K. Nagle, *J. Am. Chem. Soc.* 101 (1979) 4815.
- [36] J. Lin, F. Qu, M. Yamada, *Anal. Bioanal. Chem.* 374 (2002) 1159.
- [37] X. Chen, W. Chen, Y. Jiang, L. Jia, X. Wang, *Microchem. J.* 59 (1998) 427.
- [38] X.R. Zhang, W.R.G. Baeyens, G. Van der Weken, A.G. Calokerinos, K. Imai, *Anal. Chim. Acta* 303 (1995) 137.
- [39] D.N. Beratan, J.N. Onuchie, J.N. Betts, B.E. Bowler, H.B. Gray, *J. Am. Chem. Soc.* 112 (1990) 7915.
- [40] O. Farver, I. Pecht, *J. Am. Chem. Soc.* 114 (1992) 5764.
- [41] X. Chen, Y. Tao, Z. Xie, G. Chen, *Luminescence* 20 (2005) 109.
- [42] N.E. Tokel, A.J. Bard, *J. Am. Chem. Soc.* 94 (1972) 2862.
- [43] T. Chen, J. Xu, J. Wu, *Strait Pharm. J.* 16 (2004) 1.
- [44] Z. Shen, L. Wu, *Chin. J. Med. Lab. Sci.* 21 (1998) 151.

Enhancement of the response of poly(dimethylsiloxane) hollow prisms through air mirrors for absorbance-based sensing

A. Llobera^{a,b,*}, R. Wilke^a, S. Büttgenbach^a

^a *Institut für Mikrotechnik, Technische Universität Braunschweig, Alte Salzdhahmer Straße 203, 38124 Braunschweig, Germany*

^b *Centre Nacional de Microelectrònica, Campus UAB, 08193 Bellaterra, Spain*

Received 9 July 2007; received in revised form 12 November 2007; accepted 14 November 2007

Available online 22 November 2007

Abstract

The hollow prisms are photonic lab-on-a-chip systems with a high degree of monolithic integration that consist of micro-optical (prism and microlenses), microfluidics and structural elements (self-alignment systems) obtained in PDMS by soft lithography. Despite their interesting optical and sensing properties, their working principle, based on the absorption of the working wavelength ($\lambda = 460$ nm) by the different substances that can fill the hollow prisms, always involves at least one reflection at the walls of the hollow prism. Due to the low refractive index contrast between the PDMS and the phosphate buffer that fills the hollow prism, the reflectivity at this interface is very low, requiring long integration times. In this paper, we tackle this severe limitation with the definition of an air mirror, which solves the low reflectivity problems: with the appropriate design, the working wavelength matches with the condition of total internal reflection (TIR) only at the air mirror and is reflected back to the hollow prism. Experimental results have shown that the use of air mirrors enhances the sensing properties of the hollow prisms due to several reasons: first, the integration time is strongly reduced, from 2.5 s to 80 ms. Second, although the integration time is reduced, the signal-to-noise ratio (SNR) is increased from 12 dB to 19.5 dB. Third, an important improvement of the LOD (with values close to 1 μ M and 400 nM for fluorescein and methylorange diluted in phosphate buffer, respectively) has been experimentally measured. Finally, as compared to the system without the air mirror, the sensitivity is increased by a factor between 1.32 and 2.49 (depending on the geometry used), respectively when this simple, however effective element is included into the system.

© 2007 Elsevier B.V. All rights reserved.

Keywords: u-TAS; Absorbance sensors; Photonic lab-on-a-chip; Poly(dimethylsiloxane)

1. Introduction

Recently, there has been a major interest in the miniaturization of microreactors for analytical and chemical synthesis applications. Due to this effort, a true “lab-on-a-chip” system, which may be understood as the integration of sample handling, pre-treatment, reaction, separation (whenever required), analyte detection readout and product isolation on the same substrate, is expected to be obtained in the following years. Portability and disposability, together with a reduction of the analysis time, the reactants consumption and the size of the sample are only some of the major advantages that lab-on-a-chip systems can offer to a

large variety of fields, as could be molecular biology, chemistry and medicine.

Reduction of the cost per device is also a major issue due to the expectable high demand of such systems, therefore, although there has been some interesting results, both in silicon [1] and glass technology [2], there is a clear tendency towards the use of low-cost materials such as polyimide [3], SU-8 [4] or more commonly used, poly(dimethylsiloxane) (PDMS) [5]. Due to its unique properties, this material has been used for a large variety of systems, as could be laser-induced fluorescence (LIF) [6], cytometry [7], chromatography [8] and genomics [9].

Interestingly, most of the previous examples make use of light as interrogation mechanism. As a rule, optical techniques play a crucial role in (bio)chemical analysis and therefore, a large effort has been invested by several research groups for its implementation on a lab-on-a-chip system. Nowadays, two configurations have been used: integrated optics and micro-optics. In the first case, the system comprises one or several waveguides, an

* Corresponding author at: Institut für Mikrotechnik, Technische Universität Braunschweig, Alte Salzdhahmer Straße 203, 38124 Braunschweig, Germany. Tel.: +49 531 391 9752; fax: +49 531 391 9751.

E-mail address: andreu.llobera@cnm.es (A. Llobera).

interrogation region and finally, the readout [10,11]. Nevertheless, since end-fire coupling is commonly the method used both for in- and out-coupling the light on the device, the insertion losses and the robustness of the device is a challenging issue. Although some very interesting advances towards the full integration of light source and photodetector with a lab-on-a-chip system has already been presented [4], the use of SU-8 waveguides (which generally present higher attenuation than its silicon-based counterparts), together with the necessity of an external light source for pumping the dye is a challenge to the handling of the system in real experiments.

Micro-optic systems primarily take advantage of the excellent optical properties of the PDMS to define microlenses in or in the vicinity of the interrogation region [12]. With such configuration the alignment of the fiber optic is solved by defining microchannels into which the fiber can be inserted and clamped. Other additional optical components, as could be pinholes, can also be easily included in the system.

It has to be noted, that in these applications where multiplexing properties are required (for example, to distinguish between excitation and emitted light), filtering generally has to be done outside the system, which is a severe limitation for the full integration of readout electronics. In a previous paper, a photonic lab-on-a-chip system comprised of a hollow prism, two biconvex lenses and a self-alignment system for detection based on absorption and refractive index (RI) and with multiplexing capabilities was presented [13]. Such configuration was optimized [14], obtaining experimental limits of detection (LOD) in the μM range for absorbance measurements with fluorescein and methyloange diluted in buffer solution. Nevertheless, the device required a long integration time that prevented a high throughput.

Hence, when comparing hollow structures with an equivalent microchannel lab-on-a-chip configuration, several advantages can be outlined: firstly, as it has been previously mentioned, they have demultiplexing capabilities, that is, they are capable to discriminate between excitation and emission wavelengths. This makes them especially attractive for fluorescence measurements, since this feature cannot be obtained with the microchannel systems. Secondly, as it will be discussed afterwards, it is possible to increase the optical path length and simultaneously reducing the fluidic path, which allows obtaining more compact and miniaturized lab-on-a-chip systems. Finally, a microchannel configuration would either need a very wide or a very long channel so as to have the same sensitivity as the proposed hollow structures. In the first case, to correct the beam divergence, an accurate lens design would be required so as to collect the maximum light at the output (and filtering would then be required). In the second case, light would have to remain confined in a material with RI lower than the surrounding media, which makes the design of the microchannel tricky and complex, in opposition to the single-mask hollow prisms.

In the present work we demonstrate that defining an air mirror on the vicinity of hollow prisms substantially improves their performance, resulting in a reduction of the integration time and at the same time an increasing of the signal-to-noise ratio (SNR), which leads to a higher sensitivity and a lower

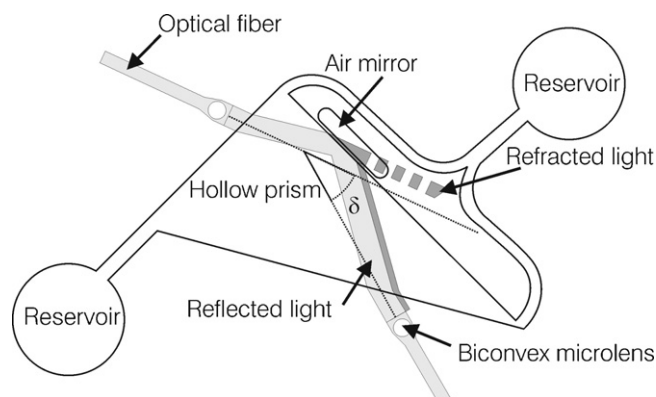


Fig. 1. Schematic representation of the microfluidic system comprising the hollow prism, the microlenses, the reservoirs, the microchannels and the air mirror (not to scale). The optical path with and without the air mirror is also shown. δ stands for the total deviation angle.

LOD of the hollow prisms. It has to be noted that although this air mirror has been implemented in the hollow prisms, it can also be implemented in a large variety of photonic lab-on-a-chip systems where reflections at the interface take place.

2. Structures

2.1. Design

The working principles of the hollow prisms have already been presented in Ref. [13]. Nevertheless, for clarification, some basic principles are recapitulated in this work. A drawing of one of the optical systems (Abbe) under study is shown in Fig. 1: the main structure is a hollow prism connected to two fluidic ports. An auxiliary microchannel is also defined on the system to avoid air entrapment at the unstable upper meniscus. From an optical point of view, the system comprises two microchannels for fiber optics positioning, which directly heads-on the fiber optics to two biconvex cylindrical microlenses. Accurate positioning of the fiber optic is achieved by defining a constriction at the microchannels, which allows having the end of the fiber at the focus of the lens and therefore, having parallel beams at the surface of the prism. Considering the RIs of the PDMS ($n = 1.41$), the buffer solution (phosphate buffer, pH 7.4, 10 mM, $n = 1.334$) and air ($n = 1.00$), together with the working wavelength ($\lambda = 460$ nm), the relative angle between the input fiber optics and the hollow prism is defined in such a way this wavelength propagates through the prism with the so-called minimum deviation condition [15] and emerges from the prism at a concrete deviation, exhibiting a total angle δ . Any other wavelength propagating through the prism does not fulfil the minimum deviation condition and emerges at a higher angle, being not collected by the output fiber optics. A variation of the RI inside the prism will result in a modification of the minimum deviation conditions, and therefore the working wavelength will not emerge at the angle where the collecting fiber optics is located. The total angle depends on the geometry and the RI of the prism, but it always involves at least one reflection at the wall of the hollow

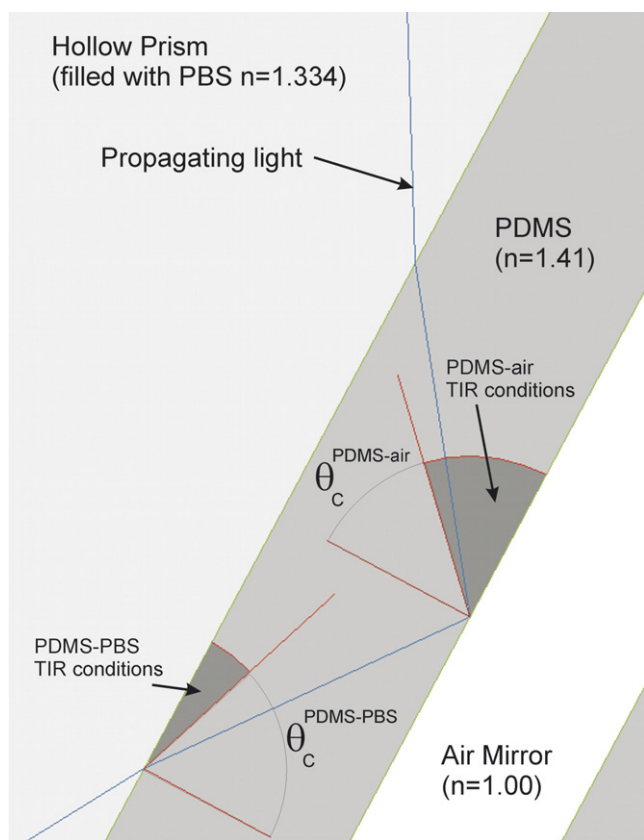


Fig. 2. Ray tracing of the propagating light at the air mirror vicinity. The angles where the condition of TIR is hold are marked in dark grey.

prism. Despite the interesting optical and sensing properties, the small RI step between the buffer solution and the PDMS causes that most of the light is transmitted to the PDMS and only a small amount of light reflects back towards the collecting fiber optics. As an example, using the Fresnel's coefficients, the reflection coefficients of this interface at the Abbe prism can be calculated to be 0.029 for TE-polarization and 0.062 for its TM counterpart. Hence, long integration times are required to obtain a clear signal, resulting in a low throughput of the hollow prisms.

This drawback, which limits the application of the hollow prisms, is tackled in this paper. An air mirror is designed to reflect back the light outcoming from the hollow prism and thus achieve its collection by the output fiber optics. A ray tracing simulation considering the light propagating through the proposed system is presented in Fig. 2, where a detailed view of the reflection region can be observed. At the first boundary region, light is propagating from a media with low RI ($n = 1.334$) to the PDMS, which has a higher RI ($n = 1.41$). Therefore, from the previous calculation of the reflection coefficients, most of the light is coupled to the PDMS and does not reach the collecting fiber optics (not shown in Fig. 2). Conversely, if an air mirror is included, the light coupled at the PDMS reaches a region with lower RI (air, $n = 1.00$) and total internal reflection (TIR) at the PDMS–air layer can be obtained (with the appropriate incidence angle), resulting in a complete back reflection of the light towards the PDMS. Considering the RIs of the media

involved (PDMS and air) and using the Snell's law, the critical propagation angle is $\theta_c^{\text{PDMS-air}} = 45.17^\circ$. All the propagation angles $\theta > \theta_c^{\text{PDMS-air}}$ (marked in dark grey in Fig. 2) causes the light to be under TIR conditions and is reflected back to the PDMS, reaching the hollow prism. Considering again the RI of the materials involved (PDMS and phosphate buffer), in this boundary region the critical angle is $\theta_c^{\text{PDMS-PBS}} = 70.60^\circ$ (the angles where TIR regime happens are also marked in dark grey). As it can be observed in Fig. 2, the propagation angles match with the TIR regime at the PDMS–air region, but do not at the PDMS–PBS interface. This is the optimal situation since then light does not remain confined at the PDMS and is coupled back to the hollow prism. Hence, the readout signal obtained is highly enhanced, allowing the reduction of the integration time, as it will be presented in Section 4. The effectiveness of the air mirrors related of the RI of the analyte inside the hollow prism can also be evaluated: for liquids with RI higher than that of PDMS, the incidence angle can be tailored so as to match the conditions of TIR at the PDMS–liquid interface, being then unnecessary to implement the air mirrors (or used as secondary reflector). Conversely, as the RI of the analyte decreases below the RI of PDMS, the angle in which TIR condition holds at the PDMS–analyte progressively increases. Then, if no accurate design of the facets is done, light reflected at the air mirror could remain confined at the PDMS, obtaining a “PDMS waveguide”, which will cause that light not to reach the collecting fiber optics.

3. Fabrication

The optical system's production process is based on standard soft lithography. The fabrication of a master of SU-8 (MicroChem Corporation, Newton, MA, USA) is followed by casting of PDMS (Sylgard 184 elastomer kit, Dow Corning, Midland, MI, USA). Focused on the reduction of the cost per device, the substrate is a low-cost 700- μm -thick soda-lime glass. After its cleaning and dehydration, a Cr layer is sputtered and dehydrated again. Then, a 4 μm -thick SU-8 layer is spun at 3000 rpm for 60 s. After 10 min drying at 95°C , it is exposed without mask for 10 s and then a post-exposure bake (PEB) of 5 min at 95°C is made. The subsequent SU-8 layers adhere to this initial seed SU-8 film, resulting in a better mechanical stability, robustness and durability of the master. A single spin-on process using SU-8 50 (400 rpm for 30 s), is done. After 3 h drying at 95°C , an exposure of 100 s is done and the wafers are then placed for 20 min at 95°C . After developing in propylene glycol methyl ether acetate (PGMEA, MicroChem Corporation, Newton, MA, USA), the structures show a thickness of 250 μm , which will allow the hassle-free insertion of the optical fibres (which have a diameter of 230 μm).

The PDMS pre-polymer was prepared by mixing the curing agent with the elastomer base in a 1:10 ratio (v/v). The subsequent mixture was poured over the master and cured for 20 min at 80°C . Afterwards, the cured PDMS was peeled off from the master and the fluidic ports were opened. An oxygen plasma treatment [16] allowed irreversible sealing of PDMS to a soda-lime wafer and finishes the fabrication of the systems.



4. Characterization

Light emitted from an SLED working at $\lambda = 460$ nm, is coupled into a multimode fiber optics with a diameter of $230 \mu\text{m}$. This fiber is inserted into the channel until it reaches the constriction. The readout consists of an identical fiber optics also inserted into a microchannel which carries the signal to a spectrometer (P.117, STEAG MicroParts, Dortmund, Germany) with a spectral resolution of 12 nm. Measurements have been done at room temperature in a temperature-controlled lab.

The following experimental procedure has been done: firstly, the prisms have been filled with buffer solution and the readout obtained has been considered as a reference. Dilutions with progressively higher concentrations of the analyte have been successively injected. After reaching the highest concentration, the buffer solution is injected again to check possible fluctuations of the reference signal and reversibility of the system.

Previous work in which hollow prisms were combined with microlenses and microfluidics demonstrated that such systems had a dual response: for high analyte concentrations, it was possible to detect variations of the RI [13], causing a deviation of the Beer–Lambert law [17], whereas for low concentrations, its absorbance was proportional to the analyte concentration and no measurable RI shift was observed. According to the optimization presented in Ref. [14], the hollow prisms that exhibit higher performance in terms of LOD and sensitivity are presented in Table 1, together with their most significant features. In the Abbe prism, the light exhibits a total deviation of $\delta = 60^\circ$, whereas in the Pr₉₀, this deviation increases until 90° . These two configurations exhibit the lowest LOD for two main reasons: in the Abbe configuration, the fluidic path length (distance between the input and output fluidic ports) was the highest, which results in the largest optical path length and straightforwardly the highest sensitivity. Clearly, as the fluidic path length increases, the optical path length will also increase. Nevertheless, this situation leads to each time bigger systems which are unattractive for lab-on-a-chip applications. The optimal situation would be to reduce the fluidic path length while increasing the optical path length. This can be accomplished if, instead of having the total deviation at 60° , the geometry is varied, having the output at 90° . Concretely, for a fixed volume, the change from the Abbe to the Pr₉₀ configuration results in a reduction of

Table 1
Features of hollow prisms with higher performance, after [14]

Label	Scheme	
	Abbe	Pr ₉₀
		
Volume (μL)	1.777	0.790
Optical path length (μm)	3581	2766
Fluidic path length (μm)	6102	2790
Total deviation ($^\circ$)	60	90

31% in the fluidic path length while increasing 12% the optical path length. In addition, due to the relative position of the input/output fiber optics in the Pr₉₀ configuration, the amount of noise at the detector is reduced, resulting in a decrease of the LOD.

The results obtained in Ref. [14] have been taken as reference for this work. For an adequate comparison between the results, fluorescein (Sigma–Aldrich Chemie GmbH, Steinheim, Germany) and methylorange (Sigma–Aldrich Chemie GmbH, Steinheim, Germany) diluted in phosphate buffer have also been used as analytes and the absorbance as a function of the concentration has been measured, being then possible to determine the LOD and the sensitivity. Concretely, for determining the LOD the three-sigma IUPAC definition has been used [18,19].

The first expected result obtained is a drastic reduction of the required integration time. The experimental results presented in Ref. [14] required an integration time of 2.5 s, which is perhaps the most severe limitation of the hollow prism. Conversely, with the air mirror, this integration time can be reduced more than 30 times. Measurements done with an integration time of only 80 ms show a SNR between 18.5 dB and 19 dB, which is much higher than those previously reported, in which this magnitude was between 12 dB and 14 dB after an integration time of 2.5 s.

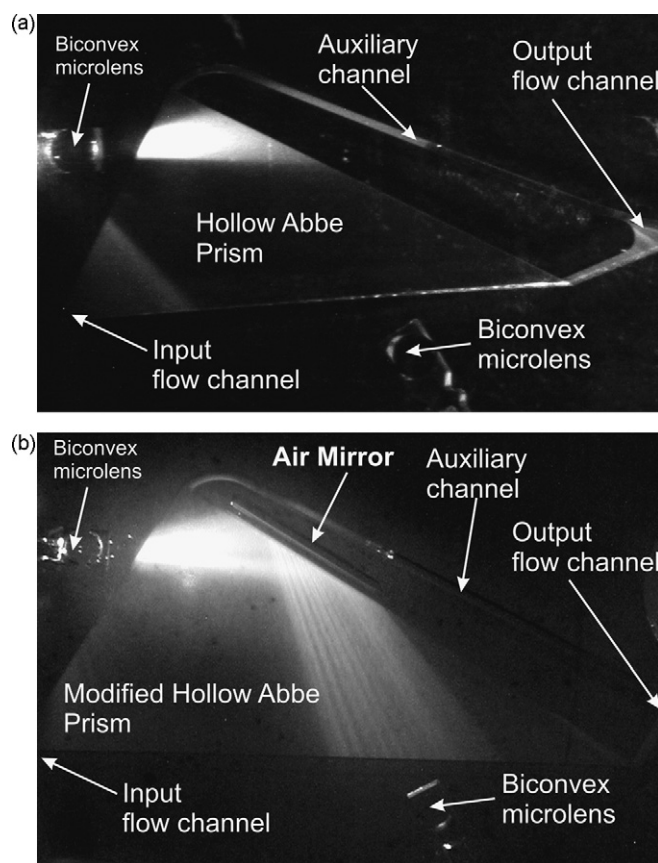


Fig. 3. Photograph of two identical hollow Abbe prisms filled with buffer solution + $50 \mu\text{M}$ of fluorescein, which shows the input/output PDMS biconvex lenses and the optical fibres can be seen: (a) system without the air mirror; (b) system with air mirror, the enhancement of the reflectivity when this element is added to the system can be clearly seen.

The enhancement of the sensing abilities of the hollow prisms can be clearly seen in Fig. 3, where pictures of one of the previously mentioned Abbe configuration are shown. Fig. 3a corresponds to the configuration without air mirror, in which it can be observed how light is mostly refracted at the prism–PDMS interface, causing the emission of the fluorescein diluted in phosphate buffer located at the output microchannels (a concentration of 50 μM was used). Conversely, in Fig. 3b, the same configuration is presented, but in this case, the air mirror has been implemented. As it can be seen, light is mostly reflected and reaches the output fiber optics, as it was predicted with the ray-tracing model presented in Fig. 2. The high reflection at the air mirror explains the experimental enhancement of the SNR as compared to the previous results. It can also be observed in Fig. 3b how an interference pattern is obtained from the light back reflected from the air mirror. Although it may seem that this is a drawback for the data readout, since the system is self-aligned and the collecting fiber optics is clamped at a fixed position, it always collect the same interference pattern and hence no alignment errors occur. Additionally, this interference pattern can be taken in advantage, as it could be used for measuring the speed of a fluorescent particle, which will confer to the hollow structures an additional feature. This point is currently under investigation.

Once it has been shown that the air mirrors are suitable elements to be integrated with photonic lab-on-a-chip systems, the sensitivity and the LOD of the hollow prisms with the air mirror implemented were determined and compared with the same results without this micro-optic element. To this effect, concentrations of fluorescein ranging between 0 μM and 37.5 μM have progressively been injected. The results of the Abbe and the Pr₉₀ prism with air mirror are presented in Fig. 4 together with these reported in Ref. [14]. It can be observed how there is a good agreement with the Beer–Lambert law, since there is a linear behavior of the absorbance as a function of the fluorescein concentration, but with the air mirror, the hollow prisms have a much higher sensitivity. This can be better observed in Table 2, where the linear fit, the values of R^2 and the LOD are presented. As it was mentioned before, the LOD has been calculated using the three-sigma IUPAC definition, which takes into account both the error and the slope of the lineal fit. From these results, it can be seen that there is a remarkable enhancement of the sensing properties of the hollow prisms when the air mirror is integrated into the structure. Concretely, for the Abbe configuration, the sensitivity is increased by a factor of 1.56 and the LOD has

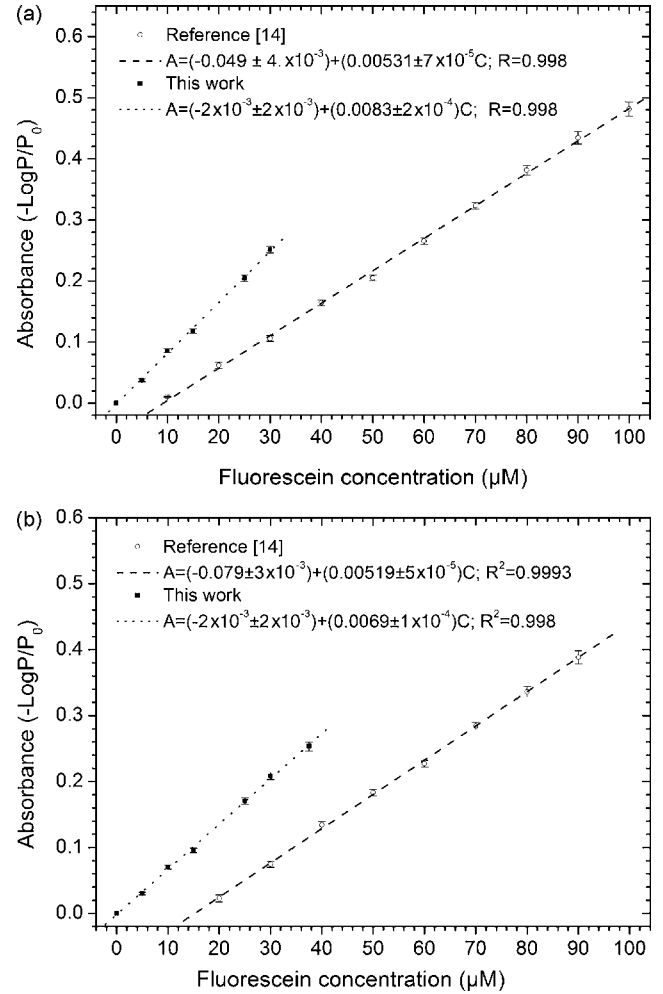


Fig. 4. Absorbance vs. fluorescein concentration for the Abbe prism (a) and the Pr₉₀ prism (b) with and without air mirror, together with their respective linear fit.

improved, being now 0.44 times the value without air mirror. For the Pr₉₀ hollow prism, the enhancement factors are 1.32 and 0.59 for the sensibility and the LOD, respectively. In both structures, it has been possible to reach values in the μM range. Therefore, a clear enhancement of the performance of the hollow prisms can be observed with the definition of air mirrors on the system, which allow both an increase of the sensitivity and the SNR, while reducing the LOD and the required integration time.

Table 2

Linear fit, values of R^2 and LOD of the fluorescein measurements performed with hollow prisms with and without air mirror

	Linear fit	R^2	N	LOD [μM]
Without air mirror				
Abbe	$A = (-0.049 \pm 4 \times 10^{-3}) + (0.00531 \pm 7 \times 10^{-5})C$	0.998	10	2.34 ± 0.03
Pr ₉₀	$A = (-0.079 \pm 3 \times 10^{-3}) + (0.00519 \pm 5 \times 10^{-5})C$	0.9993	8	1.83 ± 0.02
With air mirror				
Abbe	$A = (2.10^{-3} \pm 3 \times 10^{-3}) + (0.0083 \pm 2 \times 10^{-4})C$	0.998	6	1.03 ± 0.02
Pr ₉₀	$A = (-2.10^{-3} \pm 2 \times 10^{-3}) + (0.0069 \pm 1 \times 10^{-4})C$	0.998	7	1.08 ± 0.02

N is the number of experiments. A and C stand for the absorbance and the fluorescein concentration, respectively.

Table 3
Linear fit, values of R^2 and LOD of the methylorange measurements performed with hollow prisms with and without air mirror

	Linear fit	R^2	N	LOD [μM]
Without air mirror				
Abbe	$A = (2 \times 10^{-5} \pm 0.001) + (0.00408 \pm 1 \times 10^{-5})C$	0.99993	6	0.757 ± 0.003
Pr.90	$A = (-0.0047 \pm 0.0008) + (0.00341 \pm 1 \times 10^{-5})C$	0.9997	6	0.683 ± 0.003
With air mirror				
Abbe	$A = (2 \times 10^{-3} \pm 1 \times 10^{-3}) + (0.01018 \pm 3 \times 10^{-5})C$	0.99994	8	0.398 ± 0.001
Pr.90	$A = (1 \times 10^{-3} \pm 1 \times 10^{-3}) + (0.00803 \pm 2 \times 10^{-5})C$	0.99994	8	0.396 ± 0.001

N is the number of experiments. A and C stand for the absorbance and the fluorescein concentration, respectively.

Methylorange, diluted in phosphate buffer (pH 7.4, 10 mM) ranging between 0 μM and 100 μM was also used to test the properties of the hollow prisms with air mirror in the case of absorption of the working wavelength without photonic re-emission. Results of the absorbance as a function of the methylorange concentration for the two types of hollow prisms, together with those presented in Ref. [14] are presented in Fig. 5. Again, an increase of the sensitivity for both systems can be observed. Details concerning the linear fit using methylorange are shown in Table 3.

Using methylorange, it can be seen that the sensitivity and the LOD of the Abbe prism could be improved by a factor 2.49 and 0.52, respectively. With the Pr_90, these parameters have changed by a factor of 2.35 and 0.57, respectively. With both configurations, it is possible to obtain LOD far below the μM range. Again, as it was mentioned in Ref. [14], since there is no photonic re-emission of the light absorbed by methylorange, a better linear fit can be obtained (as it can be observed in the R^2 parameter) and therefore, the LOD is significantly lower in the case of methylorange than in the case of fluorescein. Comparing the values of the LOD obtained in this work with those previously reported in the literature that does not use hollow prism configuration, it can be concluded that only by using a complex system comprising high photon flux excitation and microavalanche photodiodes (μAPD), the LOD can be decreased to 25 nM [20], which is only one order of magnitude lower than the results presented in this work and that require a larger number of photolithographic steps and a more complex readout. Definition of hollow prisms with air mirrors is a cheap single-mask process that allows obtaining highly sensitive optical lab-on-a-chip systems with a high degree of integration (mirror, lenses, microfluidics, self-alignment channels for positioning the fiber optics. . .) with LOD below the μM level.

5. Conclusions

The drawbacks of the hollow prism configuration have been tackled in this paper. Enhancement of the reflectivity has been assured by using an air mirror, which is defined in the same photolithographic step as the rest of the hollow prism. This air mirror has been designed in such a way that the light refracted at the hollow prism wall matches the conditions of TIR at this mirror and is reflected back into the prism. With this extremely simple modification, the integration times can be reduced more than 30 times and the SNR is enhanced to values close to 19 dB. Direct comparison with the experiments previously reported has been done, using exactly the same configurations and analytes but with the air mirror defined on the structures. Using fluorescein and methylorange diluted in phosphate buffer, the experimental results show an improvement of the sensitivity by a factor of between 1.32 and 2.49, while the LOD is lowered to values close to 1 μM in the case of fluorescein and around 400 nM when using methylorange as analyte.

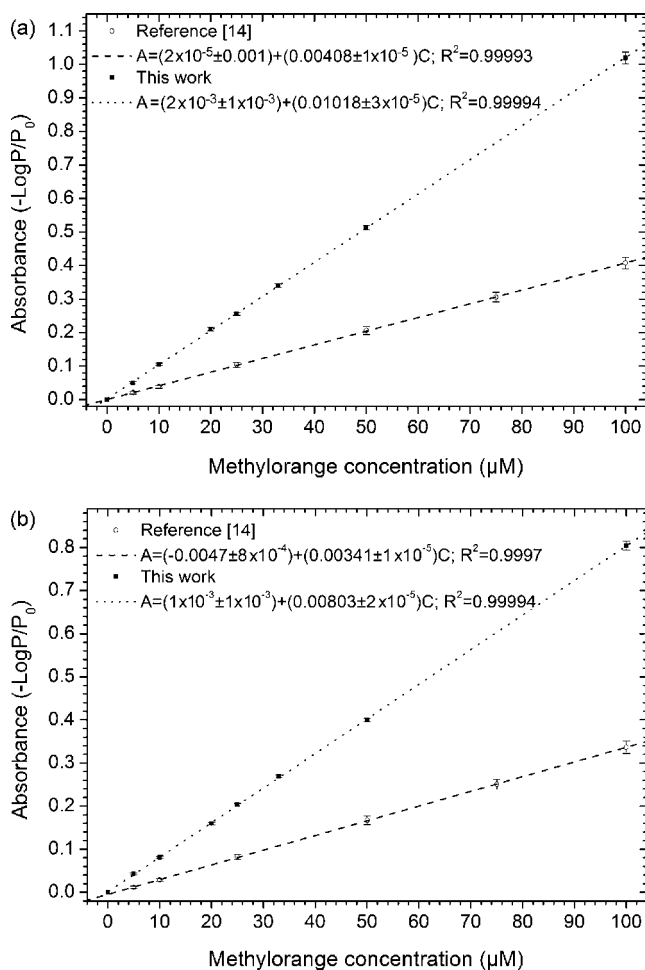


Fig. 5. Absorbance vs. methylorange concentration for the Abbe prism (a) and the Pr.90 prism (b) with and without air mirror, together with their respective linear fit.

Acknowledgement

The authors thank the German Research Foundation (DFG) for support of this work.

References

- [1] B. Sepúlveda, J. Sánchez del Río, M. Moreno, F.J. Blanco, K. Mayora, C. Domínguez, L.M. Lechuga, *J. Opt. A: Pure Appl. Opt.* 8 (2006) 561.
- [2] R. Su, J.-M. Lin, K. Uchiyama, M. Yamada, *Talanta* 64 (2004) 1024.
- [3] R.W. Applegate, J. Squier, T. Vestad, J. Oakey, D.W.M. Marr, P. Bado, M.A. Dugan, A.A. Said, *Lab Chip* 6 (2006) 422.
- [4] S. Balslev, A.M. Jorgensen, B. Bilenberg, K.B. Mogensen, D. Snakenborg, O. Geschke, J.P. Kutter, A. Kristensen, *Lab. Chip.* 6 (2006) 213.
- [5] H.-L. Zeng, H.-F. Li, X. Wang, J.-M. Lin, *Talanta* 69 (2006) 226.
- [6] D.C. Duffy, J.C. McDonald, O.J.A. Schueller, G.M. Whitesides, *Anal. Chem.* 65 (1998) 2637.
- [7] C.H. Lin, G.B. Lee, *J. Micromech. Microeng.* 13 (2003) 447.
- [8] P.G. Vahey, S.H. Park, B.J. Marquardt, Y. Xia, L.W. Burgess, R.E. Synovec, *Talanta* 51 (2000) 1205.
- [9] L.M. Shamansky, C.B. Davis, J.K. Stuart, W.G. Kuhr, *Talanta* 55 (2001) 909.
- [10] M. Puyol, I. Salinas, I. Garcés, F. Villuendas, A. Llobera, C. Domínguez, J. Alonso, *Anal. Chem.* 74 (2002) 3354.
- [11] J.M. Ruano, A. Glidle, A. Cleary, A. Walmsley, J.S. Aitchison, J.M. Cooper, *Biosens. Bioelectron.* 18 (2003) 175.
- [12] S. Camou, H. Fujita, T. Fujii, *Lab Chip* 3 (2003) 40.
- [13] A. Llobera, R. Wilke, S. Büttgenbach, *Lab Chip* 4 (2004) 24.
- [14] A. Llobera, R. Wilke, S. Büttgenbach, *Lab Chip* 5 (5) (2005) 506.
- [15] E. Hecht, A. Zajac, *Optics*, Addison-Wesley, 1986, p. 139.
- [16] B.H. Jo, L.M. Van Lerberghe, K.M. Motsegood, D.J. Beebe, *J. Microelectromech. S* 9 (2000) 76.
- [17] W. Göpel, J. Hesse, J.N. Zemel, E. Wagner, R. Dändliker, K. Spenner, *Sensors: a Comprehensive Survey*, VCH, 1991.
- [18] IUPAC Compendium of Chemical Terminology, Electronic version, <http://goldbook.iupac.org/L03540.html>, 2007.
- [19] V. Thomsen, D. Schatzke, D. Mercurio, *Limits of Detection in Spectroscopy, Spectroscopy.* 18 (12) (2003) 112.
- [20] M.L. Chabiny, D.T. Chiu, J.C. McDonald, A.D. Stroock, J.F. Christian, A.M. Karger, G.M. Whitesides, *Anal. Chem.* 73 (2001) 4491.

Generation of time-dependent concentration profiles using a reduced-size continuous-flow manifold

Ignacio López-García^a, Jesús Arroyo-Cortez^b, Manuel Hernández-Córdoba^{a,*}

^a Department of Analytical Chemistry, Faculty of Chemistry, University of Murcia, E-30071 Murcia, Spain

^b University Lisandro Alvarado, UCLA, Barquisimeto, Venezuela

Received 16 July 2007; received in revised form 12 November 2007; accepted 14 November 2007

Available online 22 November 2007

Abstract

A computer-controlled manifold allowing the automatic generation of concentration profiles is described. For this purpose, the sample or standard solution is placed inside a semi-closed loop to which diluent is incorporated at a given flow rate, while the solution is removed at the same flow rate and directed towards the detector. The flow manifold, which works in a similar way to the tank model, includes a membrane micropump to recirculate the solution in the semi-closed loop. For simplicity purposes in the assessment of the system, a flame atomic absorption spectrometer is used for both withdrawing liquid and detection, although the basic idea can easily be extended to other detectors. The experimental data, verified by measuring the calcium, magnesium, sodium and potassium contents of some soft drinks demonstrate that the approach is reliable and may be a basis for developing portable instruments of reduced-size.

© 2007 Elsevier B.V. All rights reserved.

Keywords: Calibration; Automation; On-line dilution; Micropumps; MPFS

1. Introduction

As pointed out few years ago [1], after almost three decades of basic developments and applications of flow analysis, it seems difficult to find new uses for continuous flow systems other than the simple adaptation of well-known manual procedures. However, interesting ideas such as multicommutation [2] or multipumping [3–5] have shown that miniaturization of the propelling devices and the intensive use of computers may open up new developments that will take us one step further than the simple replacement of a routine procedure. Of particular interest is the possibility of generating on-line concentration gradients useful for analytical purposes. The subject is not new and has received attention from a number of authors almost since the beginning of continuous flow studies, the approaches used being of very different natures, as reflected in some earlier works [6,7], reviews [8–10] and books [11].

Obtaining a concentration gradient is the key step in the calibration process and in the subsequent quantification stage,

irrespectively of whether the process is carried out manually or automatically [12–16]. It is evident that the use of low-cost reduced-size membrane-based micropumps as propelling devices [17,18] represents an excellent way of devise new alternatives, allowing concentration gradients to be obtained on-line and then to be used for developing compact, portable analytical systems [4].

This work deals with the possibility of using a semi-closed loop to obtain on-line time-dependent concentration profiles, and could be the basis of portable analytical instruments.

2. Experimental

2.1. Instrumentation and reagents

All the measurements were obtained using a Perkin-Elmer Model 1100B (Norwalk, CT, USA) atomic absorption spectrometer. Air-acetylene flames were used exclusively. Measurements were carried out at 285.2, 324.8, 422.7, 589.0 and 766.6 nm for magnesium, copper, calcium, sodium and potassium, respectively, using ordinary cathode lamps as the radiation sources. Stock standard solutions of these elements ($1000 \mu\text{g ml}^{-1}$) were obtained from Panreac (Barcelona, Spain). To study solutions

* Corresponding author. Fax: +34 968364148.

E-mail address: hcordoba@um.es (M. Hernández-Córdoba).

with very high concentrations, a stock standard solution of copper ($10000 \mu\text{g ml}^{-1}$) was prepared by dissolving metallic copper in nitric acid. Appropriate dilutions of the above stock solutions were made to obtain working standard solutions.

Commercial micro-pumps (Bio-Chem Valve Inc., Boston, USA) that dispense nominal volumes of 8, 20, 40 and $50 \mu\text{l}$ (references 090SP12-8, 120SP12-20, 120SP12-40 and 120SP12-50, respectively) were used. These micropumps are membrane-based devices that operate by means of square wave signals (12 V for the amplitude). The frequency of operation can be adjusted up to 250 strokes (pulses) per minute, which means maximum flow rates of 2, 5, 10 and 12.5 ml min^{-1} , respectively. Details for the operation of these membrane pumps are given elsewhere [21]. A 3-way valve obtained from NResearch (Caldwell, NJ, USA) operated by 12 V strokes and with a $27 \mu\text{l}$ internal volume was used. The flow lines were made of 0.5 mm i.d. PTFE tubing and gradient tubes of 3 mm i.d. silicone tubing. Mixing points and end-fittings were obtained from Omnifit (Cambridge, UK).

To maintain a complete control over the system, Windows[®]-based software was developed specifically in collaboration with the Central Unit for Supporting Research of the University of Murcia. This software together with a home-made data acquisition card and an analogical-digital interface entirely developed at the Department of Analytical Chemistry of the University of Murcia allowed the easy remote control of different devices, including pumps and valves. The software controlled the frequency of operation of the MP, the number of consecutive experiments (n) and the time required for refilling the system with a given solution (t_0). The analytical signal was obtained directly from the motherboard of the instrument before digitalization. The software allowed direct, real-time plotting on the computer screen of the analytical signal, and saved the data in ASCII format, permitting its later treatment.

2.2. Manifold and general procedure

The fully computer-controlled manifold studied is shown in Fig. 1. To introduce the sample (or standard) solution, a $50 \mu\text{l}$ internal volume micropump (MP) was used for most of the

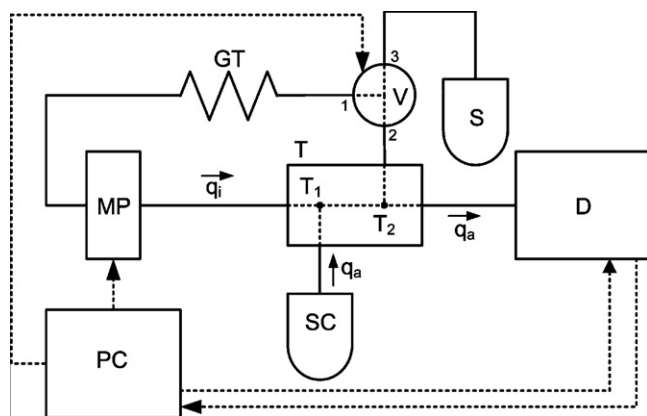


Fig. 1. Manifold studied. MP, micropump; GT, gradient tube; V, three-way electrovalve; SC, solvent channel; S, sample or standard solution; D, flame atomic absorption spectrometer; T, connecting piece; PC, personal computer.

experiments. Other MPs with different internal volumes were also assayed. Preliminary experiments were carried out using a peristaltic pump but, for obtaining a more compact, small-size manifold, it was finally replaced by the MP.

At the beginning of the experiment the MP is switched on, thus moving liquid at flow rates which are dependent on its frequency of operation, while the 3-way valve, V, connects ports 1 and 3. In this way, the sample or standard solution refills the system. Once a constant signal is obtained, which lasts a few seconds (t_0), the valve switches to the 1-2 position and the passage of diluent through the solvent channel, SC, gradually decreases the concentration of the solution inside the loop, as indicated by the gradual decrease in the analytical signal provided by the detector. Once the analytical signal has decreased to a prefixed value, the software makes a mark in the signal-time profile to indicate that the experiment has finished, and valve V is switched to the 1-3 position again to prepare the system for the following experiment.

3. Results and discussion

3.1. Foundations of the approach

The essential point about the way in which the manifold functions is the fact that, once the system is filled with a given solution and valve V is switched to the 1-2 position, the suction caused by the nebulizer uptake rate, q_a , causes the liquid to enter the solvent channel, SC, at the same flow rate as a result of the liquid moved by MP towards the double T-piece being withdrawn from the open part of the semi-closed circuit. In this way, the concentration of the solution reaching the detector changes continuously due to the solvent entering through T₁ and the continuous withdrawal of solution through T₂. The dilution effect and, consequently, the versatility of the system to automatically obtain on-line concentration gradients can be increased if a gradient tube, GT, is included in the manifold, as shown in Fig. 1. Two points should be noted to better understand this basic idea. Firstly, there is no need to use a micropump, and an ordinary peristaltic pump may be used instead. In fact, preliminary experiments were made using this latter type of propelling device. However, the reduced-size of MPs makes them more suitable for the purpose of obtaining a compact, reduced-size system. Secondly, the idea may be adapted to other detectors. The advantage of using FAAS to verify the foundations of the approach lies in the simplicity of the manifold required, since this technique, in addition to act as the detection system with no need to add reagents, represents an easy way of withdrawing liquid from the system. If any other technique is used for detection, in order to take on the suction effect caused by the nebuliser, an additional pump is required after the detector.

The dilution process here discussed is similar to the tank dispersion model, since liquid is added and removed continuously from a "vessel" (the semi-closed system obtained when valve V is in the 1-2 position) and so it should obey similar equations. The application of a mass-balance to this model means that the rate of variation in the analyte concentration, C , is given by the difference between the amount that is entering during the

($n - 1$) stage and that withdrawn from the system during the n stage, which is expressed by the following equation:

$$V_i \frac{dC}{dt} = q_a C_{n-1} - q_a C_n$$

where V_i is the inner volume of the system and q_a is the flow rate at which liquid is supplied and removed from the system.

The extension of the process until a time, t , has elapsed provides:

$$\int_{C_0}^{C_t} \frac{dC}{C} = -\frac{q_a}{V_i} \int_0^t dt$$

and so the equations relating the concentration of the solution leaving the control volume (the volume between points T_1 and T_2) and time are:

$$C_t = C_0 e^{-(q_a/V_i)t}$$

$$\ln C_0 = \ln C_t + \frac{q_a}{V_i} t$$

These equations mean that, in the above described system, once the time required to completely refill the system (t_0) has elapsed and the 3-way valve is switched to the 1-2 position, a concentration profile which varies logarithmically with time should be obtained. An increase in the internal volume of the system, or a decrease in the flow rate at which liquid is being added to (and removed from) the system, should lead to an increase in the time required to achieve a given degree of dilution.

Fig. 2 presents four consecutive absorbance-time profiles obtained when a $25 \mu\text{g ml}^{-1}$ copper solution was used as the analyte. The profiles are shown exactly as they were seen on the computer screen, with no additional filtering. For practical purposes, the experiments were considered as finished once the analyte concentration had decreased to reach a given value. For the experiments here discussed, the end of the concentration profile was considered to be the time, t_e , necessary to decrease

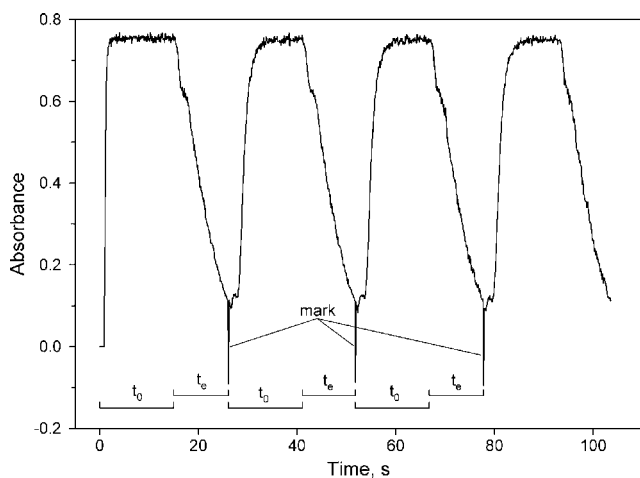


Fig. 2. Four consecutive time-dependent concentration profiles obtained for a $25 \mu\text{g ml}^{-1}$ copper solution. A $20 \mu\text{l}$ MP and a $250 \mu\text{l}$ GT were used. The t_0 value was adjusted to 15 s. The marks are signals made by the software to show the end of each experiment.

the analytical signal (absorbance value) to 0.1 and this end-point was implemented in the software and reported on the computer screen.

3.2. Effect of the experimental variables

For the equations depicted above to be strictly obeyed, the model requires the complete and instantaneous mixing of solution and diluent, a condition that is not fulfilled in practice. For this reason, the way in which both the inner volume of the loop and the flow rate delivered by the propelling device affect the process and, especially, the time required to reach the pre-set absorbance value was experimentally studied. In all experiments the nebulizer uptake rate, q_a , was maintained constant in order to obtain the same response factor of the spectrometer.

Fig. 3 shows the results obtained when the inner volume of the system was varied by including different gradient tubes. The insert shows that, as expected, the higher the inner volume of the system the higher the time, t_e , required to reach the end of the experiment. It was verified that, once the analytical signal was within the linear response range of the instrument, the absorbance-time profiles obtained follow exponential functions as predicted by the theoretical model. The gradient tube that is to be used should be selected on the basis of a compromise between sampling frequency and reproducibility of the measurements, as is discussed below.

It should be noted that although the flow rate, q_i , delivered by the propelling device does not appear in the equations, it affects the dilution process, since the mixing of diluent and solution in the volume between points T_1 and T_2 is far from being complete. Fig. 4 shows some of the experiments that were carried out using different q_i values. These data were obtained by using three MPs with different internal volumes and running at the optimal frequency. Similar experiments were also carried out using a single pump operated at different frequencies, in which case the absorbance-time profiles were slightly distorted

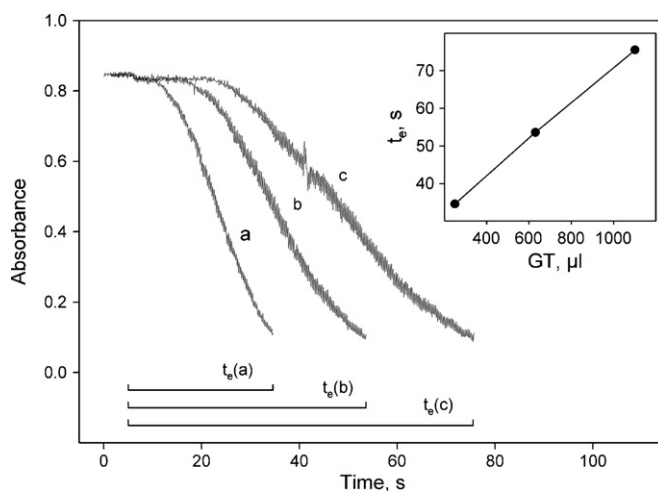


Fig. 3. Concentration-time profiles obtained for a $100 \mu\text{g ml}^{-1}$ copper solution using GTs of different volume. Curves a, b, and c, correspond to GTs of 250, 630 and $1100 \mu\text{l}$, respectively. The $20 \mu\text{l}$ MP was used. The insert shows the effect of the GT volume on the time required to finish the experiment, t_e .

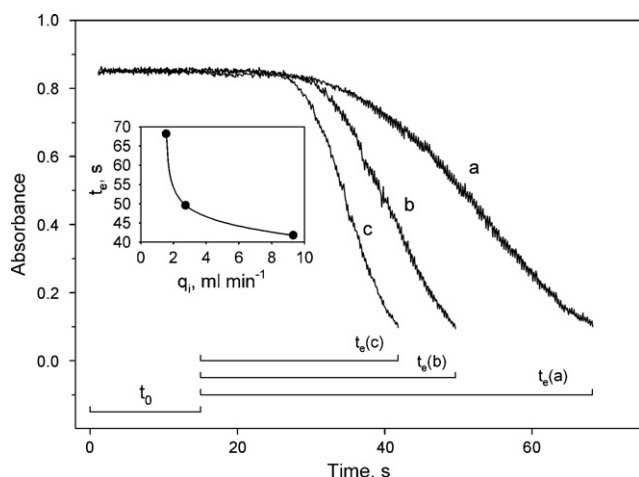


Fig. 4. Concentration–time profiles obtained for a $300 \mu\text{g ml}^{-1}$ copper solution using different MPs. Curves a, b, and c correspond to MPs with 8, 20 and $50 \mu\text{l}$ internal volume, respectively. The insert shows the effect of the MP flow rate on t_e .

by the oscillations in the flow rate when the MP runs at low frequencies. As Fig. 4 demonstrates, the higher the value of q_i , the faster the analytical signal decreased, while for even higher flow rates (not shown in the Figure) the time elapsing until the end of the experiment, t_e , was constant. It is interesting to note that this behaviour, which is a consequence of the incomplete homogenization of the liquids, is not a drawback from an analytical point of view, since for each q_i value the time required to decrease the absorbance until the pre-set value remains proportional to the initial analyte concentration. On the contrary, advantage can be taken of this effect to increase the versatility of the procedure, since different concentration profiles can be obtained by varying q_i for a given combination of V_i and q_a .

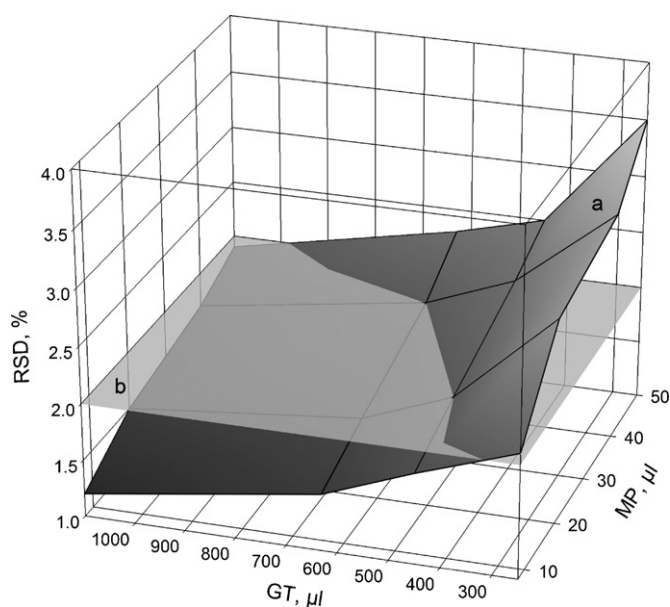


Fig. 5. Plane a shows the influence of the volume of the gradient tube, GT, and the internal volume of the MP used on the reproducibility. Plane b, which corresponds to a 2% RSD is shown for better visualisation.

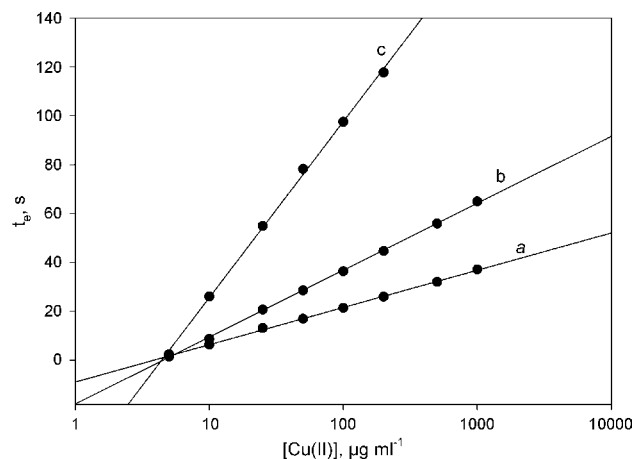


Fig. 6. Calibration graphs obtained in different experimental conditions. Line a, MP of $50 \mu\text{l}$ and GT of $250 \mu\text{l}$; line b, 50 and $550 \mu\text{l}$; line c, 20 and $550 \mu\text{l}$, respectively.

3.3. Reproducibility and validation of the procedure

Special attention was paid to carefully checking the reproducibility of the procedure, for which purpose the relative standard deviations (RSDs) were calculated for sixteen different experimental conditions obtained by using each one of the four MPs available and including four gradient tubes. Ten consecutive measurements were obtained for each experimental condition and the RSDs obtained for each one of these experiments are given in Fig. 5. As expected, high RSDs were obtained when the MP with a higher pumping capacity ($50 \mu\text{l}$) was used together with a minimum internal volume although in no case was the RSD higher than 3.5%, most of the values being close to 2%. To obtain good sampling frequency, the $50 \mu\text{l}$ MP together with gradient tubes with volumes above $500 \mu\text{l}$ are recommended. The use of the $20 \mu\text{l}$ MP in combination with a $630 \mu\text{l}$ gradient tube allowed a sampling frequency of $51 \text{ samples h}^{-1}$ to be obtained, this value increasing to $70 \text{ samples h}^{-1}$ when the $50 \mu\text{l}$ MP pump was used together with a $1100 \mu\text{l}$ gradient tube. All these data were obtained by running the MPs at 200 pulses per minute.

Fig. 6 shows some of the graphs obtained when the concentration of the solution being used to obtain the on-line time-concentration profile was plotted against the time required for the analytical signal to decrease to a pre-set value. These lines, which were obtained using different experimental con-

Table 1
Results obtained using the procedure indicated in the text^a

[Cu] taken ($\mu\text{g/ml}$)	[Cu] found ^b ($\mu\text{g/ml}$)	Difference (%)
20	19.7 ± 0.4	-1.3
80	80.5 ± 0.5	+0.6
150	150.6 ± 0.5	+0.4
300	299.3 ± 0.4	-0.2
700	698.7 ± 0.6	-0.2

^a Calibration graph was obtained by using 5, 10, 25, 50, 100, 200, 500 and $1000 \mu\text{g/ml}$ copper standard solution injected in triplicate.

^b Mean value \pm confidence interval (at 95% confidence level, $n = 3$).

Table 2
Results for the analysis of soft drinks

Sample	Analyte	Content ^a ± CI (µg/ml)		
		Proposed procedure	Proposed procedure with standard addition	Conventional procedure ^b
Cola soft drink	Calcium	14.3 ± 0.3	14.5 ± 0.5	14.5 ± 0.4
	Magnesium	8.71 ± 0.10	8.65 ± 0.16	8.51 ± 0.12
	Sodium	19.5 ± 0.3	19.6 ± 0.7	19.7 ± 0.5
	Potassium	29.6 ± 0.4	29.3 ± 0.5	29.3 ± 0.6
Orange soft drink	Calcium	20.5 ± 0.5	20.6 ± 0.5	21.1 ± 0.5
	Magnesium	14.3 ± 0.5	14.5 ± 0.6	14.1 ± 0.4
	Sodium	35.7 ± 0.6	35.8 ± 0.6	35.3 ± 0.6
	Potassium	110 ± 2	112 ± 1	113 ± 1
Lemon soft drink	Calcium	24.3 ± 0.6	24.1 ± 0.5	23.9 ± 0.7
	Magnesium	13.5 ± 0.5	13.8 ± 0.7	13.1 ± 0.5
	Sodium	44.1 ± 0.6	44.3 ± 0.5	44.7 ± 0.5
	Potassium	57.2 ± 0.5	57.9 ± 0.6	58.5 ± 0.6

^a Mean value ± confidence interval (at 95% confidence level, $n = 3$).

^b See text for details.

ditions, can be used for calibration and, consequently for the quantification of unknown solutions. Table 1 shows some of the results of experiments made to verify the reliability of these calibration graphs that cover a wide range of concentrations. A calibration graph for copper was obtained and then five “unknown” copper solutions were measured in triplicate, the results agreeing with the expected values.

In addition, an experimental verification using real samples was made by determining calcium, magnesium, sodium and potassium in soft drinks. The level of these analytes in the samples is above the linear response range of the spectrometer, so that a previous dilution is required in the case of conventional measurement. However, the approach here described allows the dilution to be made automatically. For this specific purpose, a 20 µl MP was used together with a 250 µl GT, the prefixed absorbance value at which the dilution process is considered finished being adjusted to 0.05 to achieve a high degree of dilution. This extreme dilution minimized interferences so that the measurements were made directly without the need for added releasing agents. The results obtained using the proposed procedure directly, the proposed procedure with standard additions and the conventional procedure based on complete mineralization with acids followed by manual dilution and aspiration into FAAS in the usual way are given in Table 2. The application to these data of a common ANOVA-test for repetitive measurements [22] shows the absence of significant differences (95% confidence level).

4. Conclusion

The use of a semi-closed circuit to which a diluent is continuously incorporated and from which a liquid is being simultaneously withdrawn at the same flow rate represents a reliable way to obtain a time-variable concentration profile of the solution filling the semi-closed system. This task is easily carried out in a reduced-size, compact and fully computer-controlled continuous manifold. It should be noted that the manifold here

discussed works in a similar way to the tank model, which is far from being a novelty (e.g. see an earlier work of Koscielniak [19] and the recent paper of Paredes et al. [20]) but, as far as we know, the arrangement used and the focus of the approach developed here has not been reported, and show advantages over similar procedures. Thus, the sampling frequency is higher than that obtained for tank-dilution based procedures [23]. With respect to the methodology based in using on-line dilution, by means of programmed flow rates, the advantages are both a saving in the volume of sample required for measurement and the application to a wide range of concentrations. In our opinion the main interest of the approach here discussed is that it can be applied to analytical measurements using reduced-size, low-cost detectors. This extension could result in portable analytical devices of practical interest. A research line on this subject with the purpose of developing water-analyzers for use in the field and for the purpose of enzymatic analysis has just been started in our group.

Acknowledgements

The authors are grateful to the Spanish MEC (Project CTQ2006-08037/BQU) for financial support. J. Arroyo-Cortez also acknowledges financial support of the UCLA, Venezuela

References

- [1] M. Valcárcel, S. Cárdenas, M. Gallego, Trends Anal. Chem. 21 (2002) 251.
- [2] B.F. Reis, M.F. Giné, E.A.G. Zagatto, J.L.F.C. Lima, R.A.S. Lapa, Anal. Chim. Acta 293 (1994) 129.
- [3] J.L.F.C. Lima, J.L.M. Santos, A.C.B. Dias, M.F.T. Ribeiro, E.A.G. Zagatto, Talanta 64 (2004) 1091.
- [4] A.F. Lavorante, A. Morales-Rubio, M. De la Guardia, B.F. Reis, Anal. Bioanal. Chem. 381 (2005) 381.
- [5] F.R.P. Rocha, E. Ródenas-Torrallba, B.F. Reis, A. Morales-Rubio, M. De la Guardia, Talanta 67 (2005) 673.
- [6] A. Ríos, M.D. Luque de Castro, M. Valcárcel, Talanta 32 (1985) 845.
- [7] A. Ríos, M. Valcárcel, Talanta 38 (1991) 1359.

- [8] J.L. Burguera, M. Burguera, *J. Anal. At. Spectrom.* 12 (1997) 643.
- [9] P. Koscielniak, J. Kozak, *CRC Crit. Rev. Anal. Chem.* 34 (2004) 25.
- [10] J.L.M. Santos, M.F.T. Ribeiro, J.L.F.C. Lima, A.C.B. Dias, E.A.G. Zagatto, *Spectrosc. Lett.* 40 (2007) 41.
- [11] M. de la Guardia, in: A. Sanz-Medel (Ed.), *Flow Analysis with Atomic Spectrometric Detectors*, Elsevier, Amsterdam, 1999 (Chapter 4).
- [12] I. López-García, P. Viñas, M. Hernández-Córdoba, *J. Anal. At. Spectrom.* 9 (1994) 553.
- [13] I. López-García, P. Viñas, J. González, M. Hernández-Córdoba, *Spectrochim. Acta Part B* 55 (2000) 849.
- [14] P. Koscielniak, *Anal. Chim. Acta* 438 (2001) 323.
- [15] I. López-García, P. Viñas, J. González, M. Hernández-Córdoba, *Talanta* 56 (2002) 787.
- [16] L. Ferrer, G. de Armas, M. Miró, J.M. Estela, V. Cerdá, *Talanta* 64 (2004) 1119.
- [17] D.A. Weeks, K.S. Johnson, *Anal. Chem.* 68 (1996) 2717.
- [18] R.C. Prados-Rosales, J.L. Luque-García, M.D. Luque de Castro, *Anal. Chim. Acta* 461 (2002) 169.
- [19] P. Koscielniak, *J. Anal. At. Spectrom.* 3 (1987) 329.
- [20] E. Paredes, S.E. Maestre, J.L. Todolí, *Anal. Bioanal. Chem.* 384 (2006) 531.
- [21] I. López-García, J. Kozak, M. Hernández-Córdoba, *Talanta* 71 (2007) 1369.
- [22] J.C. Miller, J.N. Miller, *Statistics and Chemometrics for Analytical Chemistry*, fifth ed., Prentice Hall, Harlow, Essex, UK, 2005.
- [23] I. López-García, J. Arroyo-Cortez, M. Hernández-Córdoba, *J. Anal. At. Spectrom.* 79 (1992) 1291.

Thermodynamic and Raman spectroscopic speciation to define the operating conditions of an innovative cleaning treatment for carbonated stones based on the use of ion exchangers—A case study

I. Martínez-Arkarazo*, A. Sarmiento, A. Usobiaga,
M. Angulo, N. Etxebarria, J.M. Madariaga

Kimika Analitikoaren Saila-Department of Analytical Chemistry, Faculty of Science and Technology, University of the Basque Country (EHU/UPV), P.O. Box 644, E-48080, Bilbao, Basque Country, Spain

Received 15 May 2007; received in revised form 13 November 2007; accepted 15 November 2007

Available online 4 January 2008

Abstract

Thermodynamic and Raman spectroscopic speciation was used to define the operating conditions for an innovative cleaning treatment of the decayed carbonate-based stones using ion exchange technology. The conditioning process of the Lewatit OC1071 anion exchanger with EDTA (Y) was monitored by ionic chromatography. Characterisation of the initial (R–Cl) and the final (R₂–H₂Y) forms of the ion exchanger was carried out by dispersive Raman microprobe spectroscopy. The subtraction spectrum obtained between the chloride and the EDTA forms of the ion exchanger shows Raman bands at 1403, 1324, 1223, 1122, 932, 908, 591, 431 and 350 cm⁻¹, which agree with bands showed in the spectrum of the standard solution of the H₂Y²⁻ species. Therefore, this seems to be the EDTA species which takes part in the cleaning treatment performed by using resin poultices on black crusted limestone samples from an historical building.

© 2007 Elsevier B.V. All rights reserved.

Keywords: Cleaning; Carbonated stones; Anion exchange; EDTA; Dispersive Raman microprobe spectroscopy; Speciation

1. Introduction

Cleaning is one of the first steps considered in the restoration of stone materials used in artworks or buildings of Cultural Heritage. The main reason to carry out this type of treatment is usually the change of appearance of the work from its initial view. In an urban environment, acid gasses (NO_x, SO_x and CO₂) and carbonaceous particles are mainly responsible for the damage suffered by stone materials, especially those of carbonaceous type [1]. In surfaces exposed to rain wash, the visual effects seem not to be significant, but in surfaces protected from the rain wash the typical black crust are easily encountered. Soot particles trapped in gypsum [2–5], and in some cases nitrates [6], are the common composition of black crusts affecting the carbonaceous materials of buildings, monuments and open door artworks.

Traditional cleaning treatments applied on such surfaces are usually based on pressure water application or sand and steam blasting, both producing abrasion of the treated surface. Several detergents, which formulation is under patent, can be found as well [7,8]. The use of additives such as EDTA, NaHCO₃, (NH₄)HCO₃, (NH₄)₂CO₃, hydrogen peroxide or sepiolite poultices is another choice used most of the time with mechanical cleaning [9].

Nowadays, laser cleaning is an excellent alternative to the physical abrasion [10,11], but this methodology is expensive and requires to take a high number of safety precautions to avoid possible decaying after treatments.

At the end of 20th century, strong basic anion exchangers were claimed to be a safe alternative for removal of sulphates composing the black crusts [12] and have been applied, since then, to clean even high sensitive artworks [13]. The technological development of ion exchange technology in the last years has been so high that now it is possible to find commercially available exchangers for multiple applications, both in the inor-

* Corresponding author. Tel.: +34 94 601 32 91; fax: +34 94 601 35 00.
E-mail address: irantzu.martinez@ehu.es (I. Martínez-Arkarazo).

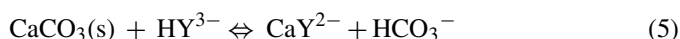
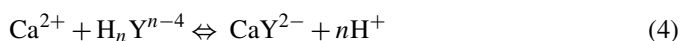
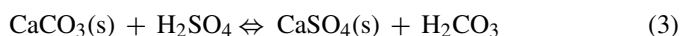
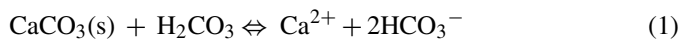
ganic and organic chemical world, most of them developed from the knowledge of the chemical interactions occurred in the system under study [14–18]. Surprisingly, this new knowledge has resulted in few applications in the field of Cultural Heritage preservation. In this work, a new cleaning procedure for carbonated-based stones has been developed based on the application of a commercial exchanger (Lewatit® VP OC1071, Bayer AG, Germany). The exchanger has been modified in such a way to promote some chemical reactions, previously defined through thermodynamic speciation modelling, to remove the black crusts.

On the other hand, the monitoring of the cleaning actions has been studied with several analytical techniques, but all of them analyse the surface to be cleaned, not the “cleaner”. Since few years, vibrational spectroscopic techniques have been used in the characterisation of ion exchangers, providing direct information about their chemical form [19–22]. As Raman spectroscopy can be used to analyse the bulk and degradation products of the surface [6,23] as well as the bulk of the ion exchanger [22], we have selected a portable Raman equipment to use as the monitoring device for both the surface and the cleaner. Moreover, as the different species involved in the cleaning reactions will have different Raman responses, the use of this analytical technique should allow us to confirm the presence/absence of those species.

1.1. Reaction hypothesis

The calcium carbonate of the decayed calcite stone becomes (a) calcium hydrogen carbonate as a result of the CO₂ acidic attack according to reaction (1), where the calcium cation and the bicarbonate anion are written separately because calcium bicarbonate is a soluble salt without any ion pair formation, (b) calcium nitrate (in fact the tetrahydrate form) as a result of the NO_x acidic attack according to reaction (2) or (c) calcium sulphate (in fact gypsum, the dihydrate form) if the attack comes from the SO_x acid gases (see reaction (3)). These are three examples of the decayed products reported in the literature for degradation of carbonated stones [6].

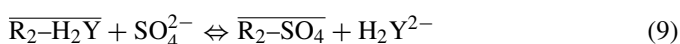
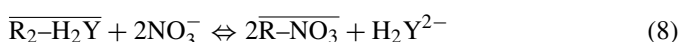
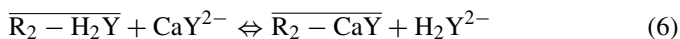
If an EDTA solution is set in contact with that surface of the decayed stone, depending on the pH of the solution, reaction (4) could take place. But the ligand itself can react with the most external calcium carbonate layers at the microscopic level, especially if the EDTA is in an acidic form, as for example the monoprotonated form, leading to reaction (5):



Reaction (5) is valid also for other salts like calcium nitrate or calcium sulphate, leaving dissolved nitrates or sulphates, respectively while the calcium is as an anionic complex with the EDTA (CaY²⁻).

After completion of equation (4) type reactions and/or reactions (5) on carbonate, nitrate or sulphate, the added acid–base species of EDTA became as the calcium–EDTA complex of anionic nature, CaY²⁻. Thus, the total EDTA consumption is equivalent to the decayed calcium of the original carbonaceous stone, independently on the chemical form of that degraded calcium on the stone surface.

Let us assume that an ion exchanger, of the basic type in an EDTA form, is set together with the solution carrying the dissolved EDTA. As the anionic species of EDTA are four, one or several anionic EDTA species could be in the resin phase. If the ion exchanger is the proper one, all the dissolved anionic species (HCO₃⁻, NO₃⁻, HSO₄⁻ or SO₄²⁻, CaY²⁻, etc.) will be exchanged by the resin, according to reactions like (6)–(9).



Thus, all the dissolved anionic species, appearing on the stone surface as a consequence of the degradation processes, could be exchanged by the H₂Y²⁻ species, regenerating its concentration in continuing the “cleaning process” through reactions (4) and (5).

2. Experimental

2.1. Instruments and operation conditions

A portable Raman microprobe Renishaw RA 100 spectrometer, with an excitation wavelength of 785 nm (diode laser), 500 mW laser power and CCD detector (Peltier cooled) was used to analyse the anion exchanger. This system was calibrated with 520.5 cm⁻¹ silicon line.

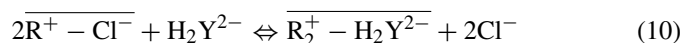
The spectra were taken with a resolution of 2 cm⁻¹ in the range 2200–200 cm⁻¹, accumulating several scans from each spectrum to improve the signal-to-noise ratio. A microscope lens of 20× built-in the microprobe was used to analyse the solid surfaces. The motorised probe has a colour TV microcamera for a perfect focusing of the laser beam’s spot (approximately 40–60 μm). Lewatit® VP OC1071 strong base ion exchanger is of 0.4–1.6 mm bead-size and it retains 55–61% of water [24]. Hence, Raman spectroscopic mappings were carried out (at least eight measurements) in order to get the typical Raman spectrum for each chemical form. Characterisation of aqueous samples is possible as well thanks to a liquid probe model RP2785/12-5 by InPhotonics. A higher number of scans were necessary in the measurements performed by the liquid probe in order to get Raman intensities similar to those obtained during the measurements performed on the ion exchanger.

Data acquisition was carried out with the Spectralcalc software package GRAMS (Galactic Industries, Salem, NH, USA) and the analysis of the results was performed with the Omnic software (Thermo-Nicolet) by comparing with a home made data base [25].

A Dionex ICS 2500 suppressed ionic chromatograph with a conductivity detector model ED60 was used to quantify the anions involved in the charge process of the ion exchanger. An IonPac AS11-HC (4 mm × 250 mm) 9 μm particle size column and IonPac GS11-HC (4 mm × 50 mm) anion precolumn were used for the separation. 1.5 ml min⁻¹ flow of 30 mM NaOH (Suprapur Baker) and a 112 mA suppression current were used as operation conditions.

2.2. Resin conditioning method and charge/regeneration protocol

The ion exchanger based on acryl-divinilbenzene copolymer is sold by the manufacturer in the chloride form [24]. If the diprotonated EDTA form (H₂Y²⁻) must be introduced in the resin, the following conditioning reaction is required:



The high number of anionic EDTA species requires a careful control of reaction [10] to quantitatively condition the resin in the H₂Y²⁻ form. This can be done by combining the thermodynamic speciation of EDTA as a function of pH and the spectroscopic differentiation of the four anionic EDTA species, H₃Y⁻, H₂Y²⁻, HY³⁻ and Y⁴⁻. The thermodynamic speciation of EDTA was simulated using the MEDUSA software [26]. The spectroscopic characterisation of the dissolved anionic species of EDTA was performed by Raman spectroscopy.

Fig. 1 shows the distribution diagram of a nearly saturated, 34.0 μM, solution of ethylenediaminetetraacetic acid (H₄Y). As the concentration is so low, the first deprotonation occurs immediately after dissolution of the solid added to water, reaching a pH ≈ 2.4. The diagram shows the distribution of the acidic species (after addition of HCl for instance) and basic species H₃EDTA⁻ (H₃Y⁻), H₂EDTA²⁻ (H₂Y²⁻), HEDTA³⁻ (HY³⁻) and EDTA⁴⁻ (Y⁴⁻) (after addition of NaOH without diluting the solution).

As seen, it is not possible to find a pH where the H₃Y⁻ species is the only one present in solution. On the contrary, H₂Y²⁻ is present over 95% at pH ≈ 4.6, the HY³⁻ species is the only one

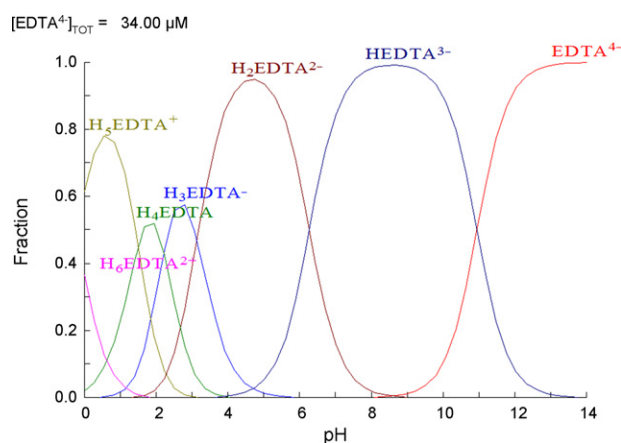


Fig. 1. Distribution diagram of the EDTA species ($C_{TOT}(\text{EDTA}) = 34 \mu\text{M}$) as a function of pH.

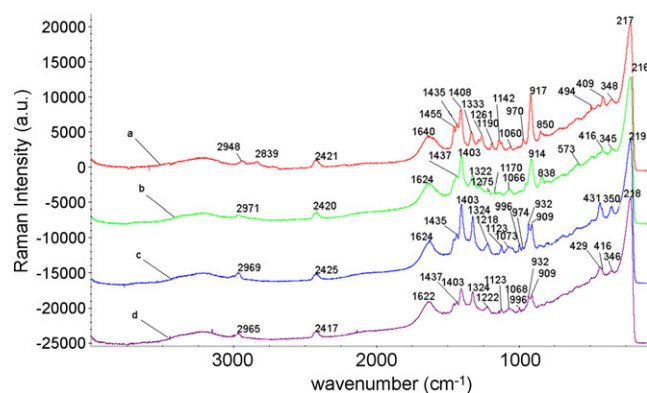


Fig. 2. Raman spectra of EDTA species' standards; (a) Y⁴⁻ (pH ≈ 13); (b) HY³⁻ (pH 8.6); (c) H₂Y²⁻ (pH 4.6); (d) H₂Y²⁻ + H₃Y⁻ (pH 3.2).

at pH ≈ 8.6, and Y⁴⁻ is at pH > 13. Fig. 2 shows the Raman spectra obtained from four EDTA solutions: (a) Y⁴⁻ (pH ≈ 13); (b) HY³⁻ (pH 8.6); (c) H₂Y²⁻ (pH 4.6); (d) H₂Y²⁻ + H₃Y⁻ (pH 3.2), obtained by a 13.6 mM solution of Na₂H₂Y·2H₂O (solution c), mixed with concentrated NaOH to obtain solution (a) and (b) or with HCl to obtain solution (d). At lower pH values, the EDTA precipitates quantitatively.

The four Raman spectra show the signals of the fibre optic parts of the probe (bands at 416, 1062 and 2420 cm⁻¹) as well as some water bands (218, 1632 and 3180–3240 cm⁻¹). Fortunately, all these bands are of the weak type in comparison with those of compounds with a medium to high Raman scattering, like the EDTA has.

Apart from those bands that all the spectra have in common, several bands are shown as belonging to each EDTA species like those in the 838–996 cm⁻¹ and the 1123–1408 cm⁻¹ wavenumber ranges. The only noticeable difference between the H₂Y²⁻ species and the H₃Y⁻ one is in the 345–431 cm⁻¹ range; this may be due to the low presence (c.a. 40%) of H₃Y⁻ at pH 3.2. From comparison between the spectrum obtained in the resin phase with those of standard solutions, the EDTA species trapped in the resin could be identified.

The conditioning of the resin was carried out in two steps:

- (i) Treatment with a 13.4 mM of the disodium salt (Na₂H₂Y·2H₂O) solution to displace chloride anion. This process was monitored by ion chromatography till the disappearance of the chloride anion signal in the chromatogram.
- (ii) Treatment with a 0.034 mM solution of the most acidic form, the tetraprotonated one (H₄Y), for conditioning till the pH values required for a cleaning experiment. This process was monitored by measuring the Raman spectrum of the resin phase.

The EDTA content of the Lewatit[®] VP OC1071 will change during the cleaning process because other anions will be exchanged by the EDTA species, conducting to a more or less degree of exhaustion in the ion exchanger. Thus, a regeneration procedure for the ion exchanger is required in order to recover and reuse the ion exchanger used in a cleaning experience.



Fig. 3. Location of a black crusted limestone sample in the facade of the historical building.

The discharge process was monitored by ionic chromatography till the disappearance of any other anion than chloride. The Raman spectrum obtained once the regeneration process was finished fitted in all bands wavenumbers with the one obtained for the ion exchanger in its chloride form (see Fig. 4b below).

These experiments also reveal that the EDTA conditioning is reversible; that is, in a real situation of a cleaning treatment at massive scale, the ion exchanger can be regenerated and reutilised, saving the corresponding costs.

2.3. Application of the cleaning product on black crusted limestones of an historical building

Limestone samples were extracted from an historical building located in the metropolitan Bilbao. These samples were covered by a black crust composed mainly by gypsum, nitrates and soot, as revealed by the diagnosis made on the conservation state of stone materials (two sandstone types and a grey limestone) composing the facades of the historical building [6]. Fig. 3 shows the location of one of the treated samples, where two different affections of the stone are visible, a zone with a black crust and another where the stone has a whitish appearance in comparison with the original colour of the limestone in the photograph.

A step-by-step cleaning protocol, from less harmful solvents till the use of more hard chemicals, was designed as the most adequate treatment [27]. Water was used as the first step and then a saturated solution of the most acidic EDTA species was applied to the surface. Then, poultices consisting on a mixture of the ion exchanger, in a given EDTA form, and an agglutinant which gives the consistence necessary but without changing the pH of the mixture, were applied. The poultices were covered with a plastic film in order to avoid the evaporation and/or dilution of the mixture. One of the principal advantages of this step-by-step cleaning method is that the use of poultices allows a local application of the cleaning treatment on the black crust when part of the dirtiness has been already removed.

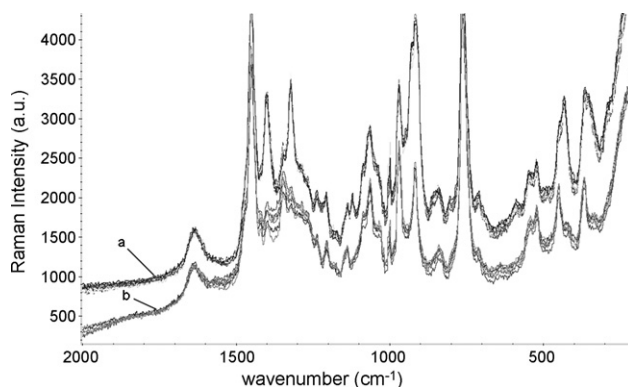


Fig. 4. Comparison between the Raman spectra of (a) Lewatit® VP OC1071 in the EDTA form and (b) in the chloride form of the ion exchanger.

3. Results and discussion

3.1. Identification of the EDTA species in the resin phase involved in the cleaning process

At the end of any conditioning process, the Raman spectrum of the EDTA form of Lewatit® VP OC1071 was obtained. This spectrum is different to that of the original resin in the chloride form as it can be seen in Fig. 4.

The bands appearing in common in spectra (a) and (b) in Fig. 4 are those belonging to the ion exchanger itself. As chloride has not a Raman signal, Fig. 4b could be considered as the Raman spectrum of Lewatit® VP OC1071. Thus, the subtraction of the Raman spectrum of the ion exchanger in the chloride form from the spectrum of the resin in the EDTA form will give us the Raman spectrum of the EDTA species that has been trapped by the ion exchanger. This can be seen in Fig. 5, where bands at 1403, 1324, 1223, 1122, 932, 908, 591, 431 and 350 cm^{-1} are clearly shown for several subtraction spectra of the ion exchanger in the EDTA form and in the chloride form of the ion exchanger. The subtraction spectrum is the same independently of the pH value, ranging from 3.6 till 6.8, used in the final conditioning of the resin to perform the different cleaning experiments.

The experimental evidence shown in Fig. 5 allows us to confirm that only one EDTA species, that is H_2Y^{2-} , is trapped in the

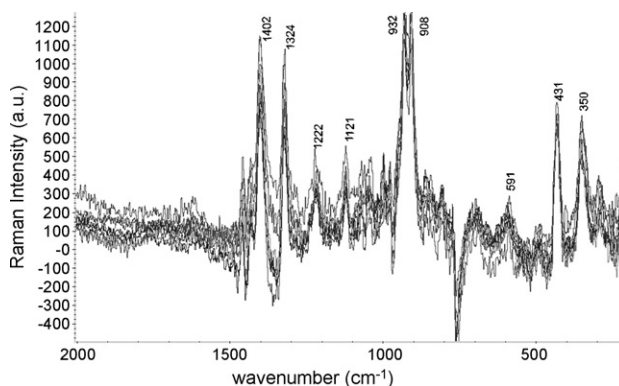


Fig. 5. Result of spectra subtraction between the R–Y (3.6 < pH < 6.8) and R–Cl forms of the ion exchanger.

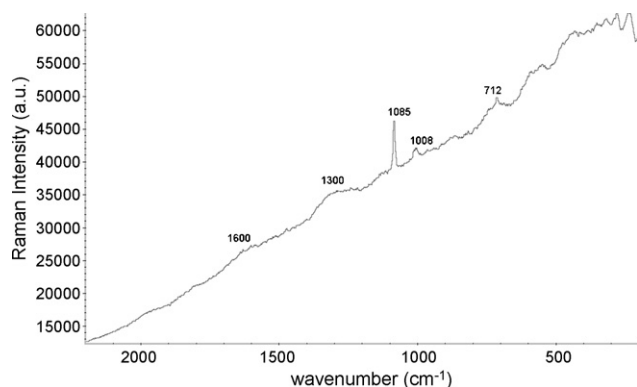


Fig. 6. Raman spectrum of a limestone sample with a black crust before the cleaning treatment.

resin phase as it can be concluded by comparing the subtraction spectra of Fig. 5 with the standards of the different acid–base species of EDTA, shown in Fig. 2. Moreover, this species seems to be the responsible of the ion exchange process during the cleaning.

3.2. Results of the cleaning process

Previous to the cleaning of the detached limestone samples, taken from the ground floor of the civil building, a chemical characterisation of the black crust, including Raman measurements, was carried out. According to the Raman measurements alone, the black crust is composed mainly by soot and gypsum. However, as cited in a previous work performed on the diagnosis of the building [6], nitrates were also present in a substantial quantity in this black crust (determined by ion chromatography after a soluble salt extraction by an ultrasound-based method). Nitrates are hardly detectable by Raman spectroscopy unless pure crystals of nitrate salts are focused by the Raman microprobe or microscope.

Fig. 6 shows a Raman spectrum taken on the surface of one of the limestone samples. Apart from calcite bands, related to the original composition of the stone, the strongest Raman band of gypsum at 1008 cm^{-1} and the characteristic wide bands of amorphous carbon (soot) centred on ~ 1600 and $\sim 1300\text{ cm}^{-1}$ can be seen.

After application of the described step-by-step cleaning procedure (three poultices of the cleaning product were finally applied), the black crusts of the samples were removed satisfactorily. Fig. 7 shows the appearance of two of the samples, one having the initial black crust on the surface and the other after finishing the cleaning treatment. The cleaned samples had at the end a colour similar to the characteristic of a rain washed grey limestone, without any presence of whitish patinas.

As the black crusts affecting this building are composed by gypsum and nitrates, the reactions in expressions (8) and (9) took place during the cleaning process. Calcium ions composing the gypsum and nitrocalcite have been probably exchanged according to expression (6) and probably part of the carbonate following reaction (7). This fact was confirmed by ion chromatography analyses performed on the eluate resulting from the



Fig. 7. Appearance of a sample after the cleaning treatment in comparison with a sample having the initial black crust on the surface.

regeneration of the exhausted Lewatit® VPOC1071 resin, where calcium, sulphate, nitrate and bicarbonate were measured.

As a consequence, all the decaying products are exchanged by the resin, while H_2Y^{2-} comes out from the ion exchanger to react again with the calcium composing sulphate or nitrate salts still present on the stone surface or with calcium bicarbonate resulted from the decaying of the bulk material.

4. Conclusions

Ionic chromatography allows monitoring the anions involved in the conditioning process (Cl^- , and EDTA) of the ion exchanger. Furthermore, each of the conditioned forms of the anion exchanger has a singular Raman spectrum, which helps in the identification of the EDTA species captured by the ion exchanger.

The Raman bands of the subtraction spectra, obtained from several pair of spectra of the resin in EDTA and chloride form ((R–Y)-(R–Cl)), fit with the bands of the diprotonated (H_2Y^{2-}) species. This EDTA species makes possible the reactions from (6)–(9), which are necessary to occur during the cleaning of a carbonate-based stone surface suffering from the most common degradation products of this kind of stones in polluted areas.

Raman spectroscopy measurements confirmed that the charge process of the ion exchanger with the EDTA species is reversible; therefore, the ion exchanger can be reused in consecutive cleaning treatments. Moreover, Raman spectroscopy proved to be an effective tool to determine the bulk composition and the degradation products of carbonaceous stones prior to their cleaning.

Finally, the consecutive application of ion exchanger poultices in the EDTA form (the diprotonated species) was effective on the elimination of the degradation products appearing as black crusts (mainly composed by soot, nitrates and gypsum) in limestone samples from the historical building case of study.

Acknowledgements

This work was supported by project INGAPROX (ref.: DIPE06-12), funded by the Diputación Foral de Bizkaia and the

University of the Basque Country. I. Martínez-Arkarazo and A. Sarmiento gratefully acknowledge their predoctoral fellowships from the University of the Basque Country and the Spanish MEC (FPU Programme), respectively.

References

- [1] L. Bityukova, *Water, Air Soil Pollut.* 172 (2006) 239–271.
- [2] A. Moropoulou, K. Bisbikou, K. Torfs, R. Van Grieken, F. Zezza, F. Macri, *Atmos. Environ.* 32 (1998) 967–982.
- [3] P. Maravelaki-Kalaitzaki, D. Anglos, V. Kilikoglou, V. Zafirooulos, *Spectrochim. Acta, Part B* 56 (2001) 887–903.
- [4] Y. Bai, G.E. Thompson, S. Martínez-Ramírez, S. Brüeggerhoff, *Sci. Total Environ.* 302 (2003) 247–251.
- [5] N. Bakaoukas, J. Kaposos, A. Koliadima, G. Karaiskakis, *J. Chromatogr. A* 1087 (2005) 169–176.
- [6] I. Martínez-Arkarazo, M. Angulo, L. Bartolomé, N. Etxebarria, M.A. Olazábal, J.M. Madariaga, *Anal. Chim. Acta* 584 (2007) 350–359.
- [7] T. Hosokawa, M. Ito, H. Osawa, Y. Ito, *Jpn. Kokai Tokkyo Koho* (2004), pp. 31.
- [8] G.V. Yakovlev, L.A. Yakovleva, *Russ.* (2006) pp. 5.
- [9] R. Fort, M.C. Azcona, *Materiales de Construcción* 50 (2000) 37–50.
- [10] G. Lanterna, M. Matteini, *J. Cult. Herit.* (2000) S29–S35.
- [11] E. Armani, G. Calcagno, C. Menichelli, M. Rosseti, *J. Cult. Herit.* (2000) S99–S104.
- [12] G. Pizzigoni, P. Parrini, Patent EP 263,486 (1988), Patent US 5,069,811 (1991), Patent CA 1,295,781 (1992).
- [13] A. Castellano, G. Buccolieri, S. Quarta, M. Donativo, *X-ray Spectrosc.* 35 (2006) 276–279.
- [14] F. Gode, E. Pehlivan, J. Hazard. Mater. 100 (2003) 231–243.
- [15] B. Bolto, D. Dixon, R. Eldridge, *React. Funct. Polym.* 60 (2004) 171–182.
- [16] K. Vaaramaa, J. Lehto, *Desalination* 155 (2003) 157–170.
- [17] V.A. Leão, G.C. Lukey, J.S.J. Van Deventer, V.S.T. Ciminelli, *Hydrometallurgy* 61 (2001) 105–119.
- [18] B. Lee, L.L. Bao, H.J. Im, S. Dai, E.W. Hagaman, J.S. Lin, *Langmuir* 19 (2003) 4246–4252.
- [19] C.T. Buscher, R.J. Donohoe, S.L. Mecklenburg, J.M. Berg, C.D. Tait, K.M. Huchton, D.E. Morris, *Soc. Appl. Spectrosc.* 53 (1999) 943–953.
- [20] V.F. Selemenev, A.A. Zagorodni, *React. Funct. Polym.* 39 (1999) 53–62.
- [21] A.A. Zagorodni, D.L. Kotova, V.F. Selemenev, *React. Funct. Polym.* 53 (2002) 157–171.
- [22] A. De Santis, *Polymer* 46 (2005) 5001–5004.
- [23] M. Pérez-Alonso, K. Castro, I. Martínez-Arkarazo, M. Angulo, M.A. Olazábal, J.M. Madariaga, *Anal. Bioanal. Chem.* 379 (2004) 42–50.
- [24] <http://ion-exchange.com/products/anions/vpoc1071.pdf>.
- [25] K. Castro, M. Pérez-Alonso, M.D. Rodríguez-Laso, L.A. Fernández, J.M. Madariaga, *Anal. Bioanal. Chem.* 382 (2005) 248–258.
- [26] I. Puigdomenech, *Make Equilibrium Diagrams Using Sophisticated Algorithms (MEDUSA)*, Inorganic Chemistry Department, The Royal Institute of Technology, Stockholm, 2001.
- [27] I. Martínez-Arkarazo, M. Angulo, J.M. Madariaga, J. Les, in: J.J. Durán, P.A. Robledo, J. Vázquez (Eds.), *Cuevas turísticas: aportación al desarrollo sostenible. Part IV*, Instituto Geológico y minero de España, Madrid, 2007, pp. 265–276.

Target label-free, reagentless electrochemical DNA biosensor based on sub-optimum displacement

Mònica Mir¹, Ioanis Katakis*

Bioengineering and Bioelectrochemistry Group, Departament d'Enginyeria Química, Escola Tècnica Superior d'Enginyeria Química, Universitat Rovira i Virgili, Avd. Països Catalans 26, 43007 Tarragona, Spain

Received 2 August 2007; received in revised form 5 November 2007; accepted 8 November 2007

Available online 21 November 2007

Abstract

One of the most time consuming and complex steps in the detection of DNA target with a biosensor is the previous labeling of the target. In this paper, a novel target label-free, reagentless and easy to use DNA biosensor is reported. Electrochemical transduction (cyclic voltammetry, differential pulse voltammetry and impedance spectroscopy) and optical red out by surface plasmon resonance were chosen for the platform optimization.

This target label-free DNA detection method is based on displacement of sub-optimum labeled oligonucleotide. This strategy requires the pre-hybridization of the capture probe immobilized on the electrode surface with a sub-optimum mutated oligonucleotide pre-labeled with an electrochemically active ferrocene moiety. Due to the higher affinity of the target that is fully complementary to the capture probe, the sub-optimum ferrocene-labeled sequence is displaced when the fully complementary target is introduced into the system. The decrease of the electrochemical signal from the ferrocene verifies the presence of the target, which is proportional to the target concentration. A variation of this strategy was employed to enhance the ferrocene signal. A diffusional mediator, ferrocyanide, was introduced in the system to help in this purpose. This platform attains a stable, specific and reproducible response (5–15%), with a detection limit in the range of μM .

This electrochemical sensor is the first example of this kind of sensor to detect cystic fibrosis, however, this configuration could be generically applied to any application where the detection of a DNA target is involved.

© 2007 Elsevier B.V. All rights reserved.

Keywords: Label-free electrochemical biosensor; e-SPR; Impedance; Cystic fibrosis gene

1. Introduction

DNA arrays have attracted the attention of medical diagnostic and analytical chemists. The broad range of applications that has been found for DNA arrays makes them an important analytical tool. DNA arrays are relevant for the diagnosis of genetic diseases [1], detection of infectious agents [2], study of genetic predisposition [3], development of personalized medicine, detection of differential genetic expression, forensic science [4], drug screening [5], food safety [6] and environmental monitoring [7].

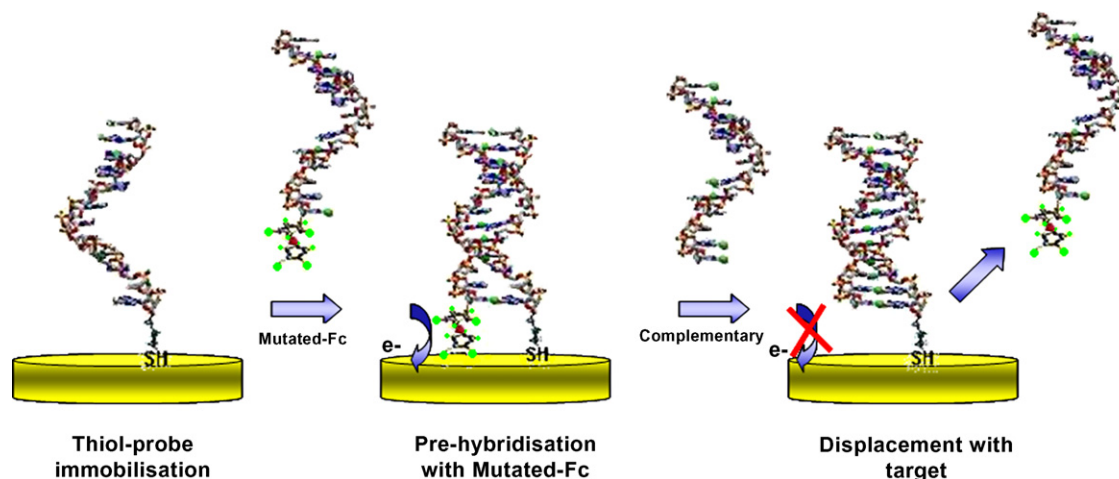
Despite the great promise of DNA arrays in health care and their success in medical and biological research, the technology is still not employed in everyday use in the clinic and is even further from implementation in home-diagnosis [8]. The principal challenges to their more wide spread use include high cost and complexity. Expensive laboratory instrumentation and biological knowledge for the labeling of the DNA prior to the sample injection into the array are both required. Moreover, false positives from non-specific adsorption are more likely. Development of target label-free methods for DNA sensors can potentially address these challenges.

Some examples of electrochemical label-free DNA sensors have already been commercialized. The eSensorTM fabricated by Motorola Life Science Inc. [9], proceeds via a sandwich hybridization assay. Thiol-capture probe is self-assembled on gold electrode, where it is hybridized to the DNA target. A third ssDNA ferrocene labeled is required to readout the target hybridization. Other examples of electrochemical sandwich

* Corresponding author: Universitat Rovira i Virgili, Avd. Països Catalans, 26, 43007 Tarragona, Spain. Tel.: +34 977559655; fax: +34 977558721.

E-mail address: ioanis.katakis@urv.cat (I. Katakis).

¹ Present address: Max-Planck-Institute of Polymer Research, Ackermannweg, 10, 55128 Mainz, Germany.



Scheme 1. Conceptual schematic of sub-optimum ferrocene-labeled mutated oligonucleotide displacement detection.

DNA sensors using dimethylcarbonyl ferrocene [10], or colloidal gold nanoparticles as labels [11] were reported.

Friz Biochem commercialized the EDDATM (Electrically Detected Displacement Assay) for single nucleotide polymorphism (SNP) detection. The sensor was based on displacement of the target hybridized with the capture probe. The SNP that contains the target produces instability in the duplex with the capture probe, which allows the displacement of the target by a labeled oligonucleotide complementary to the capture probe [12]. A similar approach was reported by Mir and Katakis [13] but in this case the mismatched sequence was labeled and pre-hybridized with the capture probe. In this system is the target, which displaces the pre-hybridized labeled sequence. Thus, in this platform is not required a step after the addition of the target, which make it reagentless and more easy to used, increasing its applicability.

Toshiba developed the GenalyzerTM. This DNA sensor is based on the electrochemical detection of the Hoechst 33258 molecule intercalated into the dsDNA [14]. When an intercalator such as Hoechst33258 or daunomycin [15] was inserted between the double-helix structures of the dsDNA which is facilitated by its planar aromatic ring, an enhancement in the intercalator's redox signal was observed. In contrast, some intercalators such as methylene blue have an affinity towards ssDNA, and a decrease of electrochemical signal was observed after hybridization [16]. Several metal complexes such as cobalt phenanthroline [17], cobalt bipyridine [18] ruthenium bipyridine [19], and anti-cancer agents such as echinomycin [20] and epirubicin [21], were used as labels for the detection of hybridization.

Fan et al. [22] reported the realization of an electrochemical sensor involving a molecular beacon strategy. The molecular beacon was a ferrocene-labeled DNA stem-loop structure that self-assembles onto gold. Hybridization with the target sequence induced the opening of the stem-loop, which in turn significantly altered the electron-transfer tunneling distance between the electrode and the ferrocene label. The resulting change in electron transfer efficiency was readily measured by cyclic voltammetry.

The label-free detection of DNA hybridization was also achieved using a ferrocyanide solution. This negatively charged

molecule is repelled by the negative charges of the ssDNA capture probe on the surface, but this repulsion is more evident when the negative charges were duplicated after hybridization with the oligonucleotide target, which changes the electron-transfer resistance that can be measured by impedance spectroscopy [23,24].

Here we report novel strategy to develop a target label-free easy to use electrochemical DNA sensor. This sensor is based on the displacement of a pre-labeled sub-optimum oligonucleotide by a label-free target (Scheme 1). The detection strategy requires the pre-hybridization of the capture probe immobilized on the electrode surface with a sub-optimum mutated oligonucleotide labeled with a ferrocene molecule. Due to the higher affinity of the target that is fully complementary to the capture probe, the sub-optimum label can be displaced when the complementary target is introduced in the system. The decrease of the signal from the redox label verifies the presence of the target that is proportional to its concentration.

An improvement to the system's sensitivity was introduced by the inclusion of a diffusional mediator to help in the transfer of electrons produced by the ferrocene moiety. Both strategies were tested with a variety of electrochemical detection techniques (cyclic voltamperometry (CV), differential pulse voltammetry (DPV) and electrochemical impedance spectroscopy (EIS)) in order to decide on the one that could confer the highest sensitivity and also surface plasmon resonance (SPR) to obtain more information about the surface modification. The cystic fibrosis gene is the target described here but the strategy could be generically applied to any DNA sequence.

2. Experimental

2.1. Reagents

The 15-mer oligonucleotide sequences specific for detection of the cystic fibrosis gene were purchased from VBC Biotech Service GmbH (Austria) and Eurogentec (Belgium). The oligonucleotide sequences involved in cystic fibrosis gene detection by sub-optimum displacement are listed below:

- 15-mer amine-labeled mutated oligonucleotide, for its bioconjugation with ferrocene (ferrocene-sub-optimum): amine-C₆-5'-AATATCAITGGTGTT-3'.
- 15-mer thiol-labeled capture probe oligonucleotide (thiol-capture probe): 5'-ACACCAAAGATGATA-C₆-thiol-3'.
- 15-mer complementary oligonucleotide (target): 5'-TATCATCTTTGGTGT-3'.
- 22-mer non-complementary oligonucleotide (non-complementary) used for controls: 5'-GAGGCGATCACACCGCAGACGT-3'.

All stock oligonucleotide solutions were made at 1 mg mL⁻¹ with autoclaved Milli-Q water and stored at -20 °C.

N, N'-Dicyclohexylcarbodiimide (EDC), sodium tetraborate, tris(hydroxymethyl)aminomethane-hydrochloride acid (Tris-HCl), polyethylene glycol sorbitan monolaurate (Tween), ethylenedinitril tetraacetic acid (EDTA), Denhard's solution, diammonium citrate, saline sodium citrate buffer (SSC), ferrocyanide, ferricyanide and 2-mercaptoethanol were purchased from Sigma. Sodium tetraborate, dimethylformamide, ferrocene acetic acid, dithiothreitol (DTT), and *N*-hydroxysuccinimide (NHS) were from Aldrich and 3-hydroxypicolinic acid (HPA) from Fluka. The Sephadex G-25 DNA grade resin was purchased from Amersham Pharmacia Biotech.

2.2. Instrumentation

For characterization of ferrocene-labeled oligonucleotide, matrix assisted laser desorption ionization-time-of-flight mass spectrometry (MALDI-TOF) detection was carried out in a stainless steel plate with a Voyager DE-STR from Applied Biosystems.

The electrochemical surface plasmon resonance (e-SPR) measurements were performed with double channel Autolab ESPRITTM equipment from Eco Chemie. The e-SPR electrochemical cell is a two-electrode system, with a 4.8 mm² gold layer sensor disk working electrode that is defined by a gasket when the cell is assembled. The 35 μL cell has platinum reference and counter electrode. The instrument can be programmed for automatic injection and washing steps. Electrochemical measurements were carried out in a CH Instruments Inc. potentiostat. The impedance curve fitting was performed with ZView 2 software.

2.3. Ferrocene DNA labeling

A freshly prepared solution of 125 nmol of NHS and 250 nmol of EDC in anhydrous dimethylformamide were added to a solution of 100 nmol of ferrocene acetic acid in the same solvent. The final volume was 300 μL. The reaction mixture was stirred at room temperature under argon until appearance of a precipitate. EDC forms an active ester functional group with carboxylate group using NHS. In this reaction a precipitate of *o*-acylurea is formed that was removed by centrifugation and the supernatant was added to 90 μL of 0.1 M sodium tetraborate buffer at pH 8.5 containing 10 nmol of the amino modified oligonucleotide and it was left to react for 6 h at room

temperature. The active ester group in the presence of amine nucleophiles is attacked; the NHS group leaves as a precipitate, creating a stable amide linkage with the amine. The white precipitate was separated by centrifugation. The supernatant contained a ferrocene-labeled oligonucleotide. The modified oligonucleotide was purified with G-25 Sephadex column. UV spectrophotometry was used to collect the appropriate fraction from the column. The product was characterized by UV spectrometry, cyclic voltammetry and MALDI-TOF.

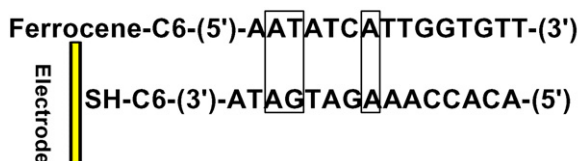
Cyclic voltammetry of ferrocene-aptamer was performed in 10 mM Tris-HCl buffer, 150 mM NaCl, pH 7.5 at 0.025 V s⁻¹ with an 18 mm² gold working electrode and a reference and counter Ag/AgCl electrode. MALDI-TOF characterization was carried out using a HPA matrix. A 50 g L⁻¹ solution of HPA in Milli-Q water and 50 g L⁻¹ solution of diammonium citrate were prepared and both reagents were combined in a ratio of HPA:NH₄ citrate (9:1). The mixture was stirred for 1 min and centrifuged to separate the white precipitate. The same volume of supernatant was mixed with ferrocene-aptamer, in a final concentration of 12 pmol μL⁻¹. Two microliters of the mixture was allowed to air-dry on a stainless steel plate. Twenty thousand volts of accelerating voltage, 92% of grid voltage, 400 ns of extraction delay time, 1715 of laser intensity and 50 of shots were applied in a linear mode for the measurement.

2.4. Immobilization and hybridization of thiol-capture probe

Twelve micrograms per milliliter of thiol-capture probe in 1 M KH₂PO₄ was immobilized for 1 h at room temperature on the gold e-SPR chips. One millimolar of mercaptoethanol was used for 1 h at room temperature to block the remaining gold surface non-occupied by the capture probe. Pre-hybridization of ferrocene-modified oligonucleotide was performed by incubating 48 μg mL⁻¹ of this oligonucleotide in 10 mM Tris-HCl, 1 mM EDTA, 0.3 × SSC and 2 × Denhard's solution at pH 7.5 (hybridization buffer) for 60 min at room temperature. After pre-hybridization CV, DPV and EIS were carried out in buffer and in ferrocyanide/ferricyanide. Afterwards 30 μg mL⁻¹ of target in hybridization buffer was incubated for 30 min at room temperature. After displacement CV, DPV and EIS were recorded in the same manner. After each step the cell was washed with a solution of 100 mM Tris-HCl pH 7.5, 150 mM NaCl and 1% Tween.

2.5. Electrochemical monitoring of direct displacement

The e-SPR cell was used to detect the pre-hybridization of the ferrocene-modified oligonucleotide and the subsequent displacement by CV, DPV and EIS. The conditions used for the electrochemical measurements were; for CV a scan rate of 0.1 V s⁻¹, between -0.5 and 0.5 V was applied, in the case of DPV scanning between -0.2 and 0.2 V, with an increment of potential of 0.005 V, amplitude of 0.05 V, pulse width of 0.05 s and a pulse period of 0.5 s was used and for EIS initial potential of 0.005 V, frequencies from 0.1 MHz to 0.1 Hz and amplitude of 0.005 V was applied. All experiments were carried out in 35 μL of 10 mM PBS, 150 mM NaCl pH 7.5.



Scheme 2. Representations of capture probe sequence and mutated oligonucleotide ferrocene labeled. The three mutations that contain the sub-optimum oligonucleotide are inside the rectangle.

2.6. Electrochemical monitoring of mediated displacement

The same measurements CV, DPV and EIS were carried out with an equimolar mixture of ferrocyanide and ferricyanide at a concentration of 1 mM in 10 mM PBS, 150 mM NaCl pH 7.5. Afterwards the cell was cleaned with wash buffer and cleanliness was verified by CV. The same CV shape as before the detection of ferrocyanide/ferricyanide should be obtained to assure the cleanliness of the surface.

3. Results and discussion

The sequence of the ferrocene-labeled sub-optimum oligonucleotide used in the displacement assay is offset from the capture probe by 1 bp and contains three mutations. The 1 bp offset might enhance the unzipping and zipping by the complementary oligonucleotide (target) contributing to easier displacement. Two of the mutations in the sub-optimum are separated from the first base by one base to facilitate the displacement. Thus, initiation only requires breaking 1 bp to start the sub-optimum displacement by the target (Scheme 2).

The following four parameters that impact both detections and surface architecture were examined with the goal of optimizing sensor performance.

- The position of the ferrocene label position for impacting hybridization as well as in the electrochemical detection.
- The concentration of the capture probe in solution during electrode modification for controlling the surface coverage.
- The concentration of ferrocene-sub-optimum for reducing the change in the zero current and increasing the efficiency of displacement.
- The NaCl concentration in the hybridization buffer for improving the pre-hybridization stability of the duplex.

The criteria that was used for optimization was the efficiency of displacement as percentage of the initial signal (pre-hybridization of labeled sub-optimum oligonucleotide) after 30 min of displacement when incubated with $30 \mu\text{g mL}^{-1}$ concentration of target. At a second level the inferred (as explained below) non-specific or “zero” displacement by buffer was used as a criterion (such “zero” displacement was minimized).

Optical and electrochemical techniques were used to investigate this system. SPR provided information on surface processes without the need for labeling. SPR detection can monitor in real time the immobilization of the thiol-capture probe on gold chips, the pre-hybridization of ferrocene-sub-optimum

oligonucleotide, and displacement of this pre-hybridized by the complementary target. Electrochemical methods were primarily used to record the difference in electrochemical response before and after displacement. Various electrochemical techniques (CV, DPV and EIS) were used to record the system response. Since each technique is based on different principles, advantages of sensitivity signal/ratio etc. can be discovered by a survey of techniques.

Two different strategies were followed to detect ferrocene-sub-optimum displacement by the target. The first was the direct detection of the ferrocene label, and the second was the indirect detection of this label through the mediation of a ferrocyanide solution.

3.1. SPR detection

The non-specific or “zero” displacement due to the presence of buffer can be obtained from SPR. A general rule of thumb used for the calculation of surface coverage in Autolab SPR is that 120 m° of change corresponds to 1 ng mm^{-2} . The coverage of a monolayer ($3.7 \times 10^{-13} \text{ mol mm}^{-2}$, [25]) of target ($\text{MW} = 4564 \text{ g mol}^{-1}$) should yield about 200 m° of response. Loss of the base structure in buffer occurs and it can be readily detected. However, when the ferrocene-sub-optimum oligonucleotide ($\text{MW} = 5003 \text{ g mol}^{-1}$) is displaced by another oligonucleotide with similar molecular weight, a very small difference in refractive index results. The typical response for the hybridization of the sub-optimum is in the range of 220 m° . We consider any SPR results that show an angle change much higher than 20 m° after displacement are the result of non-specific displacement by buffer. Obviously, the higher this delta, the higher the non-specific displacement is, and the less reliable the architecture. Thus, an additional criterion (displacement value over 20 m°) was used for the qualitative exclusion of configurations if other criteria were similar.

The first parameter investigated was the position of the label. Ferrocene labeled at the 5'-end of the mutated oligonucleotide (close to the surface) should offer higher electrochemical signal due to its proximity to the electrode surface. However, steric impediment of the label might cause problems in the hybridization event. The pre-hybridization of the ferrocene-sub-optimum with the immobilized capture probe was tested with two different ferrocene-sub-optimum oligonucleotides, one labeled in the 5' and another labeled in the 3'-end. The SPR result shows that the labeling at 3' produced slightly more hybridization (79 m°), than the 5' labeled (70 m°), indicating some impact to hybridization due to the position of the label.

However, a large difference was observed for the electrochemical detection of the ferrocene. CV in buffer carried out after the hybridization of ferrocene-sub-optimum with the capture probe showed ferrocene peaks in the case of ferrocene label at 5'. No peaks were detected in the case of ferrocene label at 3'. All subsequent experiments were performed with the ferrocene label at the 5' end.

Using the previous approach procedure the concentration of capture probe immobilized on the gold surface was optimized.

The optimal density of capture probe on the surface is a balance between maintaining sufficient distance between strands to allow for high hybridization efficiencies while at the same time maintaining the highest density of capture probes to provide the greatest number of hybridization events. The trade-off is that maximum hybridization signal and maximum hybridization efficiency are not obtained at the same probe density [26]. DNA probes that are too closely packed cannot participate in the hybridization reaction due to steric hindrance or electrostatic interactions [27,28].

As shown in Fig. 1, the increase of capture probe concentration in solution increases the amount of immobilized probe on the surface and results in a greater amount of hybridization with ferrocene-sub-optimum oligonucleotide. At a concentration of $24 \mu\text{g mL}^{-1}$ the capture probe was close to the hybridization saturation. However, at the $24 \mu\text{g mL}^{-1}$ concentration a higher non-specific or “zero” displacement was also observed. Probably higher repulsion from the closer neighboring strands is obtained in a more packed capture probe configuration, destabilizing the duplex. We subsequently selected $12 \mu\text{g mL}^{-1}$ of capture probe for further experimentation.

The next variable optimized was the concentration of ferrocene-sub-optimum oligonucleotide that was used for pre-hybridization with the capture probe. An increase of the pre-hybridization of the ferrocene-sub-optimum contributes to a system with higher signal, being easier to detect the displacement at lower target concentrations.

It appears that with a concentration of $48 \mu\text{g mL}^{-1}$ ferrocene-sub-optimum system arrives to the hybridization saturation and a higher non-specific displacement was observed at lower concentrations of ferrocene-sub-optimum, therefore $48 \mu\text{g mL}^{-1}$ of ferrocene-sub-optimum was chosen as the optimum concentration by this technique.

The last variable to be optimized was the concentration of sodium chloride in the hybridization buffer. An increase of cations in the hybridization environment might stabilize the duplex because both strands in the duplex are negatively charged and suffer mutual repulsion.

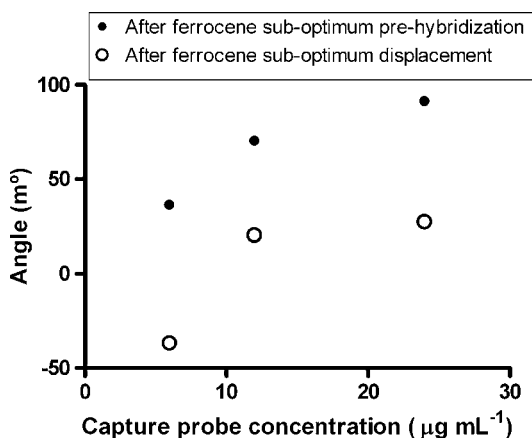


Fig. 1. Results obtained by SPR from the pre-hybridization of $12 \mu\text{g mL}^{-1}$ ferrocene-sub-optimum oligonucleotide and the subsequent displacement with $30 \mu\text{g mL}^{-1}$ complementary target oligonucleotide at different concentrations of capture probe (6, 12 and $24 \mu\text{g mL}^{-1}$) in $1 \text{ M KH}_2\text{PO}_4$.

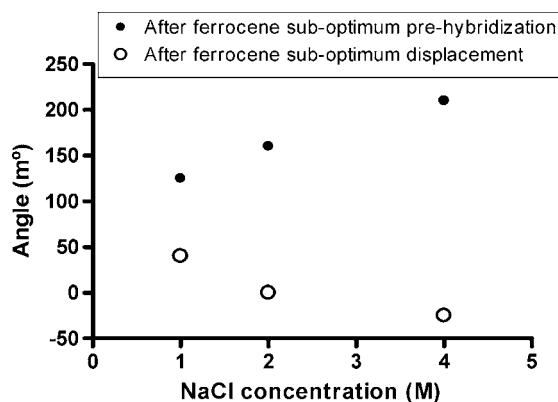


Fig. 2. Results obtained by SPR from the pre-hybridization of ferrocene-sub-optimum oligonucleotide and the subsequent displacement with complementary target oligonucleotide at different concentrations of NaCl (1, 2 and 4 M) in hybridization buffer during the pre-hybridization of ferrocene-sub-optimum oligonucleotide. Electrodes modified with $12 \mu\text{g mL}^{-1}$ of capture probe and $48 \mu\text{g mL}^{-1}$ of ferrocene-sub-optimum.

Fig. 2 shows a high enhancement of hybridization of ferrocene-sub-optimum oligonucleotide with the capture probe when the concentration of NaCl in hybridization buffer increased. So it seems correct the hypothesis that higher concentrations of salt during hybridization stabilize the duplex, however, at the same time, it appears that extreme non-specific displacement also is enhanced when the target appear in 1 M NaCl hybridization buffer, because higher destabilization of the duplex is obtained when more drastic change of the ionic strength is applied.

For this reason, 1 M of NaCl in pre-hybridization and displacement was chosen as optimum.

3.2. Direct ferrocene-sub-optimum displacement electrochemical detection

Ferrocene label is direct detected in this strategy after and before displacement in buffer 10 mM PBS , 150 mM NaCl pH 7.5.

The results observed with the three electrochemical techniques for detection of direct displacement event is described. First CV in buffer was used, after pre-hybridization of ferrocene-sub-optimum this technique detected the redox peak of the ferrocene molecule at -0.26 and 0.06 V versus Pt. When complementary oligonucleotide displaced ferrocene-sub-optimum oligonucleotide, the height of the peak decreases depending on the amount of ferrocene molecules that are removed close to the electrode

Since CV results in small changes, DPV in buffer was used as an alternative. As in CV, the height of the peak is directly related with the amount of ferrocene molecules immobilized, so after displacement the peak decreases in comparison to the peak before displacement. Current DPV allows for a very effective correction of the charging background current, which should allow better sensitivity. Fig. 3, shows a typical DPV.

Finally impedance spectroscopy in buffer was also used to try to discern differences of the spectrum before and after

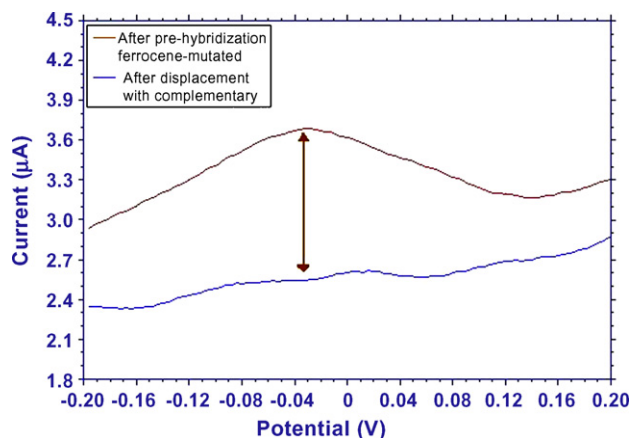


Fig. 3. Typical DPV before and after displacement of ferrocene-sub-optimum oligonucleotide. DPV was performed between -0.2 and 0.2 V, with an increment of potential of 0.005 V, an amplitude of 0.05 V, a pulse width of 0.05 s and a pulse period of 0.5 s in the presence of 10 mM PBS, 150 mM NaCl, pH 7.5 . The highlighted signal difference is indicative of displacement.

displacement. The change of ferrocene concentration close to the electrode surface affects mostly the electron-transfer resistance.

Laviron [29] related the parameters of electron-transfer resistance (R_{et}) and capacitance of the immobilized layer (C_{ads}) with the heterogeneous electron-transfer rate constant (k_f) through the following equation:

$$k_f = (2R_{et}C_{ads})^{-1}$$

When the amount of ferrocene molecule increases enhancement of electron transfer between the label and the electrode was observed ($k_f = 30,800$ for a pre-hybridization of $48 \mu\text{g mL}^{-1}$ sub-optimum oligonucleotide). After displacement the amount of ferrocene molecules decreases with the subsequent decrease of k_f ($k_f = 22,000$ for a displacement with $30 \mu\text{g mL}^{-1}$ complementary target oligonucleotide).

Impedance data was analyzed by fitting it to an equivalent electrical circuit model, which is required to obtain the values of R_{et} and C_{ads} . Impedance values detected in displacement of ferrocene-sub-optimum system in buffer were fitted to the next circuit (Fig. 4).

In this circuit, R_s is the solution resistance, C_{dl} is the double-layer capacitance, R_{et} is the electron-transfer resistance and CPE_{ads} is a constant phase element of immobilized molecules. CPE is capacitor that does not behave ideally, due to surface roughness and/or different ion adsorption/desorption kinetics.

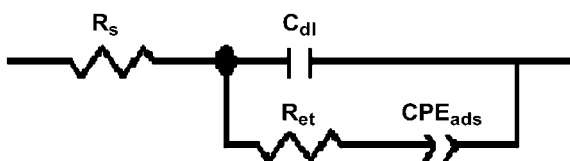


Fig. 4. Equivalent circuit for displacement of ferrocene-sub-optimum oligonucleotide system in buffer.

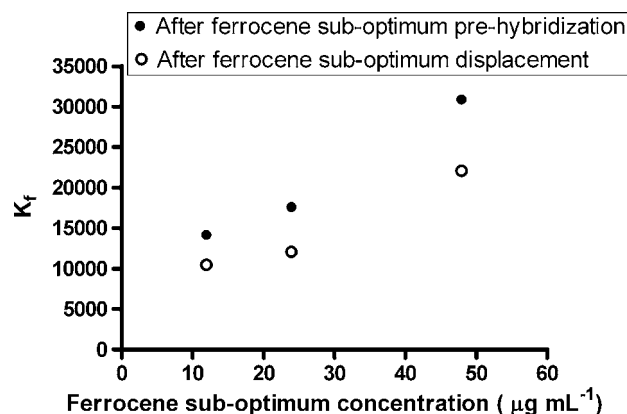


Fig. 5. Results obtained by EIS from the immobilization of $24 \mu\text{g mL}^{-1}$ capture probe oligonucleotide and displacement with $30 \mu\text{g mL}^{-1}$ complementary target oligonucleotide at different concentrations of ferrocene-sub-optimum (12 , 24 and $48 \mu\text{g mL}^{-1}$).

Additionally optimization of all the variables were made as mentioned by means of the different electrochemistry techniques.

The results obtained by CV in buffer showed an increase of peak height at higher concentrations of capture probe, which was also corroborated with SPR results. It is assumed that this increase corresponds to higher amount of ferrocene-sub-optimum hybridized. After displacement of ferrocene-sub-optimum by the target a decrease of peak height was obtained, which demonstrate the functionality of the system. Best signal displacement was obtained with $24 \mu\text{g mL}^{-1}$ of capture probe. Similar results were obtained with DPV and in impedance.

In ferrocene-sub-optimum oligonucleotide concentration optimization similar trends but higher signals were obtained as with the capture probe concentration optimization. In this case also an increase of concentration of ferrocene-sub-optimum oligonucleotide showed an increase of electrochemical signal and a decrease of signal after displacement As with SPR better displacement was obtained with $48 \mu\text{g mL}^{-1}$ of ferrocene-sub-optimum (Fig. 5).

NaCl concentration in hybridization buffer was also optimized. By SPR an increasing hybridization of ferrocene-sub-optimum was obtained with increasing concentration of NaCl, whereas by CV, DPV (Fig. 6) and impedance in buffer a decrease of electrochemical signal was detected at increasing concentration of salt. A similar behavior was already reported by Liu et al. [30] and Hartwich et al. [31]. They assume that at low ionic strength the duplex are oriented perpendiculars to the surface, because of the electrostatic repulsion between strands, facilitating the electron transfer. In contrast, high ionic strength produces a shield of the DNA charge, resulting in a collapsed configuration of the duplex, forming an obstacle for the electron transfer. Another reason for this behavior might be the formation of chloride film on the electrode surface due to the high concentration of NaCl during the pre-hybridization incubation, which might affect electron transfer

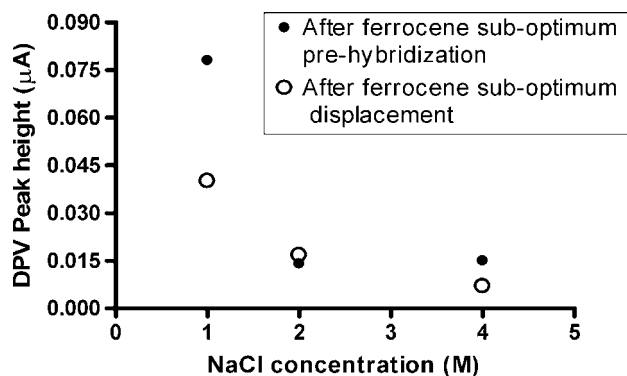


Fig. 6. Results obtained by DPV from the pre-hybridization of ferrocene-sub-optimum oligonucleotide and the subsequent displacement with complementary target oligonucleotide at different concentrations of NaCl (1, 2 and 4 M) in hybridization buffer during the pre-hybridization of ferrocene-sub-optimum oligonucleotide. Electrodes modified with $12 \mu\text{g mL}^{-1}$ of capture probe and $48 \mu\text{g mL}^{-1}$ of ferrocene-sub-optimum.

Thus as also demonstrated SPR 1 M NaCl is the optimum concentration for pre-hybridization of the sub-optimum oligonucleotide with the capture probe.

3.3. Mediated ferrocene-sub-optimum displacement electrochemical detection

In order to improve the sensitivity of the ferrocene-sub-optimum detection a mediator was added in solution. Ferrocyanide/ferricyanide can help to transfer the electrons produced in the redox reaction of ferrocene label to the electrode surface enhancing the signal. As well the ferrocyanide/ferricyanide solution has a catalytic effect that improves the ferrocene detection. However, this modification renders to a system no longer reagentless.

Steel et al. [32] and Choi et al. [33] used ferricyanide in solution and CV to detect changes in the surface charge of gold electrodes and the consequent electrochemical interaction between $\text{Fe}(\text{CN})_6^{3-}$ and the electrode when a dsDNA was hybridized on the electrode surface. Because when hybridization was done the reduction/oxidation of negative charges on the sugar-phosphate backbone of dsDNA cover the electrode surface, which prevents $\text{Fe}(\text{CN})_6^{3-}$ from approaching the surface, decreasing current signal. So a similar decrease of current might be obtained in the displacement system. However, this system can not be directly compared with the Steel and Choi experiments because a ferrocene label was attached to the 5'-end of the hybridized species. The positively charged ferrocene molecule linked to the negatively charged oligonucleotide, produced an opposite effect of $\text{Fe}(\text{CN})_6^{4-}/\text{Fe}(\text{CN})_6^{3-}$ attraction, hence increasing the current signal.

The effect of the attraction of ferricyanide to a positively charged molecule attached to DNA was already reported by Park and Hahn [34]. A dsDNA-modified electrode was treated with an intercalating agent, proflavine, then the negative charges on the duplex strands were compensated with the positive charges of intercalator molecules, which provides a surface-charge condition that facilitates the approach of $\text{Fe}(\text{CN})_6^{3-}$ to the electrode

surface, detecting an increase of signal when proflavine was intercalated in the dsDNA.

Furthermore an effect of enhancement of ferricyanide signal with a ferrocene label was reported by Heeger et al. [35]. Their approach worked by the addition of an electrochemical mediator, ferricyanide, that was reduced by the ferrocene label, thus in the presence of ferricyanide the electrode repeatedly reduced each ferrocene increasing the peak currents. A similar system was reported by Ostatna et al. [36] and Boon et al. [37], in this case the reduction of methylene blue was considerably improved in the presence of an electron acceptor, $\text{Fe}(\text{CN})_6^{3-}$.

So a double effect of attraction and enhancement of the signal is produced by the ferrocene label to ferrocyanide/ferricyanide, which allows more sensitive detection of the pre-hybridization of ferrocene-sub-optimum and the subsequent displacement.

The redox reaction produced between ferrocene label and ferricyanide is shown Scheme 3.

As the scheme shows, this system is based on transfer of the electrons from the reduced form of ferrocene to $\text{Fe}(\text{CN})_6^{3-}$ resulting in the conversion of $\text{Fe}(\text{CN})_6^{3-}$ to $\text{Fe}(\text{CN})_6^{4-}$ and the oxidation of ferrocene, which is reduced on the electrode surface. So in the presence of ferricyanide the electrode repeatedly reduces each ferrocene molecules immobilized on the electrode surface increasing the current signal.

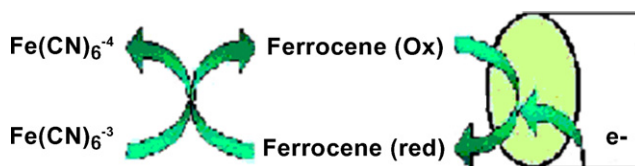
To demonstrate this hypothesis chronoamperometry of a modified electrode with complementary oligonucleotide hybridized with capture probe immobilized on the surface and other electrodes with ferrocene-sub-optimum oligonucleotide hybridized with immobilized capture probe was carried out.

Each electrode was immersed in $15 \mu\text{L}$ of 10 mM PBS, 150 mM NaCl pH 7.5 in a two-electrode cell set up with platinum as reference and counter electrode. A potential of -0.2 V was applied to record reduction of ferrocene. When the current arrived at the base line (after 100 s) $5 \mu\text{L}$ 4 mM of $\text{Fe}(\text{CN})_6^{3-}$ in 10 mM PBS, 150 mM NaCl pH 7.5 was injected into the cell to record the effect of ferrocyanide in the reduction of ferrocene.

Fig. 7 shows the results obtained in the chronoamperometry. Red and blue lines show a sustained reduction current of about $0.47 \mu\text{A}$ due to the cycle between ferrocene and ferrocyanide shown in Scheme 3. This cycle was not produced in the absence of ferrocyanide (black line) or of ferrocene (green line)

These experiments demonstrate an electrocatalytic cycle that results in signal amplification when ferrocyanide was present in the system with a ferrocene label.

The CVs and DPV scans of the capture probe ferrocene-sub-optimum duplex showed an enhancement in signal in the presence of ferrocyanide/ferricyanide in solution.



Scheme 3. Redox catalytic reaction produced between ferrocene label and ferricyanide.

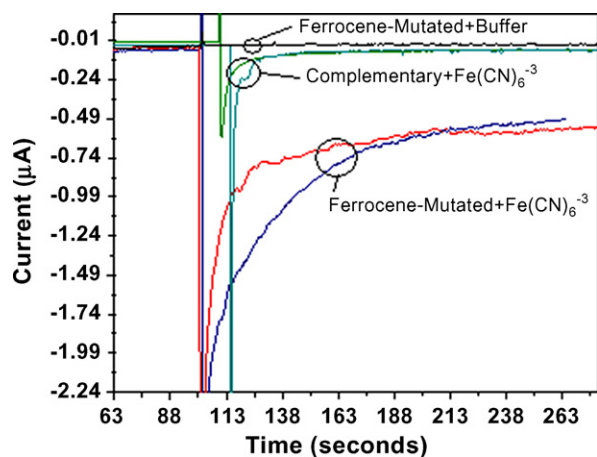


Fig. 7. Chronoamperometry of ferrocene-sub-optimum oligonucleotide hybridized with immobilized capture probe (red and blue line) and complementary oligonucleotide hybridized with immobilized capture probe (sky-blue and green line) with 1 mM ferrocyanide in solution. Ferrocene-sub-optimum hybridized electrodes were also detected in buffer without ferrocyanide as control (black line).

Pre-hybridization of ferrocene-sub-optimum oligonucleotide resulted to a higher reduction current comparing with the signal after displacement or with the bare gold electrode. It is believed that the ferrocene electron transfer is catalyzed by ferrocyanide/ferricyanide increasing the current and after displacement this effect is reduced due to the relative absence of ferrocene molecules. It also should be noted that this effect is more pronounced for the reduction reaction of ferrocene as explained before.

The use of ferrocyanide/ferricyanide in impedance spectroscopy has been widely used for the detection of biomolecules interactions. The change on the electrode surface due to the hybridization event reveals an increase in the electron-transfer resistance at the electrode surface upon the construction of the double-stranded assembly. This is attributed to the electrostatic repulsion of ferrocyanide upon formation of the negatively charged double-stranded superstructure [38]. However, in this case the ferrocene molecule immobilized on the surface has to be taken into account in the system. Thus, when ferrocene-sub-optimum was hybridized on the surface, $\text{Fe}(\text{CN})_6^{4-}/\text{Fe}(\text{CN})_6^{3-}$ ions suffered two electrostatic effects, the repulsion by the negative charged phosphate backbone of the DNA and an attraction by the positive charged ferrocene molecule, to this effect was added the electron transfer produced by the ferrocene molecules on the electrode surface. Whereas after displacement only the repulsion produced by the double-stranded DNA to the $\text{Fe}(\text{CN})_6^{4-}/\text{Fe}(\text{CN})_6^{3-}$ ions increased the electron-transfer resistance value.

The results obtained with ferrocene-sub-optimum displacement with ferrocyanide/ferricyanide in solution were fitted to the next circuit (Fig. 8).

R_s is the solution resistance, CPE_{dl} is the double-layer pseudo-capacitance, R_{et} is the electron-transfer resistance and W is the Warburg element, which is related with the diffusion of the $\text{Fe}(\text{CN})_6^{4-}$ and $\text{Fe}(\text{CN})_6^{3-}$ ions.

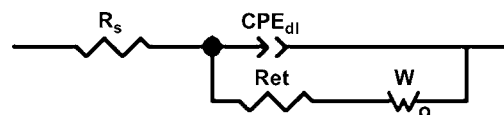


Fig. 8. Equivalent circuit for displacement of ferrocene-sub-optimum oligonucleotide system in ferrocyanide/ferricyanide.

The previous variables were also optimized with this strategy using the same electrochemical techniques.

CV and DPV in the presence of ferrocyanide/ferricyanide showed in general also an increase of signal with an increase of capture probe concentration. Impedance in ferrocyanide/ferricyanide detected a decrease of R_{et} when the concentration of ferrocene on the surface increases, so after displacement an increase of R_{et} was detected as expected. In this case, the most pronounced displacement effect was detected at $24 \mu\text{g mL}^{-1}$ of capture probe. Although most of the cases $24 \mu\text{g mL}^{-1}$ appeared to be the optimum concentration, taking into account the possible non-specific adsorption detected by SPR, $12 \mu\text{g mL}^{-1}$ of capture probe was chosen as optimum concentration to enhance specific displacement.

In the optimization of ferrocene-sub-optimum concentration CV and DPV in ferrocyanide/ferricyanide showed an increase of peak height at higher concentrations of the oligonucleotide (Fig. 9), due to the higher amount of ferrocene immobilized on the surface. For the same reason a decrease of R_{et} response was obtained by impedance when the ferrocene-sub-optimum concentration increased and an increase after displacement. As demonstrate previous techniques, the optimum concentration of ferrocene-sub-optimum concentration was $48 \mu\text{g mL}^{-1}$.

Opposite results comparing with the direct electrochemical detection was obtained in the optimization of NaCl concentration. CV and DPV in ferrocyanide/ferricyanide show the same trend as SPR, probably because mixture of ferrocyanide/ferricyanide competed with the metal-chloride in the surface compensating the effect that this film produced in the electrochemically active surface area. It is

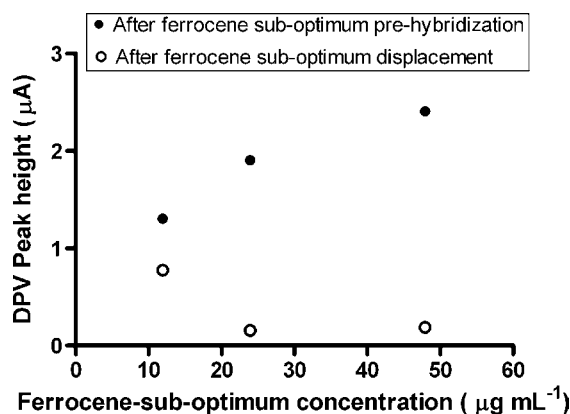


Fig. 9. Results obtained by DPV from the pre-hybridization of ferrocene-mutated oligonucleotide and the subsequent displacement with complementary oligonucleotide at different concentrations of ferrocene-sub-optimum (12, 24 and $48 \mu\text{g mL}^{-1}$) in the presence of 1 mM of ferrocyanide/ferricyanide in 10 mM PBS, 150 mM NaCl, pH 7.5. $12 \mu\text{g mL}^{-1}$ of capture probe and $30 \mu\text{g mL}^{-1}$ of target was used in these experiments.

also significant the low values of R_{et} were obtained in impedance with ferrocyanide/ferricyanide in solution compared to previous optimizations. At higher concentrations of NaCl, high concentrations of ions were free in the solution, so the increase in the concentration of electrolyte enhances the electron transfer, decreasing the electron-transfer resistance.

After optimization, the best conditions for pre-hybridization of ferrocene-sub-optimum oligonucleotide and subsequent displacement with complementary target oligonucleotide were: incubation of $12 \mu\text{g mL}^{-1}$ capture probe, pre-hybridization with of $48 \mu\text{g mL}^{-1}$ ferrocene-sub-optimum and 1 M of NaCl in hybridization buffer. DPV was the electrochemical technique that provides maximum advantages for detection because offered higher sensitivity and shorter detection times. The addition of the ferrocyanide mediator in the system offered higher signals currents, however, the use of a mediator leads to a sensor that is no longer reagentless.

3.4. Reproducibility, background and specificity evaluation

The reproducibility of the detection of ferrocene-sub-optimum displacement was evaluated in a home made $20 \mu\text{L}$ two electrode thin layer cell with a 18 mm^2 square gold sheet as a working electrode opposite to a solid state platinum reference and counter electrode by DPV with ferrocyanide/ferricyanide in solution. Peak height of DPV was measured before and after displacement obtaining $9.9 \pm 0.5 \mu\text{A}$ ($n=5$) after the pre-hybridization of ferrocene-sub-optimum and $4.5 \pm 0.7 \mu\text{A}$ ($n=5$) after displacement with complementary target.

Non-specific displacement signal was show in Fig. 10. Displacement of pre-hybridized ferrocene-sub-optimum oligonucleotide was detected by DPV in ferrocyanide/ferricyanide. Displacement was carried out with a complementary oligonucleotide as target, with buffer as control and another control was performed with a 22-mer non-complementary oligonucleotide.

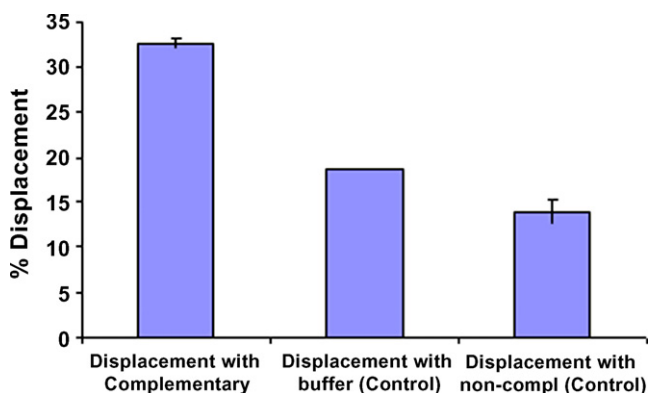


Fig. 10. Percentage of electrochemical displacement detection of pre-hybridized ferrocene-sub-optimum by complementary oligonucleotide target. The controls were carried out displacing with buffer or with a non-complementary oligonucleotide instead of complementary. These results were obtained with DPV in ferrocyanide/ferricyanide. The electrode was modified with $12 \mu\text{g mL}^{-1}$ of capture probe, $48 \mu\text{g mL}^{-1}$ of ferrocene-sub-optimum and the signal was displaced with $16 \mu\text{g mL}^{-1}$ of complementary target.

32.6% of ferrocene-sub-optimum displacement with complementary oligonucleotide was achieved while 18.7% was obtained with buffer and 13.9% with a non-complementary oligonucleotide. Thus the specific displacement was equal to 14% (Fig. 10). More studies about stringency of pre-hybridization and displacement of ferrocene-sub-optimum should be carried out to decrease the background due to the non-specific displacement, which could improve the sensitivity of the system.

Proportionality of signal displaced with the concentration of the target was tested. Higher percentage of displaced signal was detected at higher concentrations of target, a fact that demonstrates the functionality of the system to detect label-free oligonucleotide hybridization. However, below $1.2 \mu\text{M}$ of target the displacement cannot be differentiated from the non-specific displacement by the buffer.

4. Conclusions

Ferrocene-sub-optimum displacement assay was demonstrated to be a useful platform towards a label-free reagentless and easy to use electrochemical DNA biosensors.

Different techniques were used to demonstrate this system (SPR, CV, DPV and EIS), obtaining a faster and higher response with DPV.

Two different strategies were followed to perform displacement assay. First the direct detection of the ferrocene label and then to increase the signal response an indirect detection of ferrocene labeled was performed by means of a ferrocyanide solution. This mediator helps in the electron transfer and produces an electrocatalytic cycle that results in signal amplification. However, the addition of this mediator solution leads this approach not longer reagentless.

33% of the signal produced by the pre-hybridization of the ferrocene-sub-optimum oligonucleotide was displaced by the target and this percentage was demonstrated to be proportional to the target concentration. The specificity of the system was tested with a non-complementary oligonucleotide that non-specifically displaced 14% of the signal. A good reproducibility was obtained with this approach that was 5–15% of the signal.

However, this approach is still far from a commercial biosensor. Further studies should be carried out to improve the sensitivity of the system. A decrease of the non-specific displacement by the buffer or other molecules should be carried out. With this aim, stringency conditions of pre-hybridization and displacement of ferrocene-sub-optimum need to be tested and optimized. Moreover stability of the biomolecules on the surface and large quantities fabrication reproducibility should be tested.

This label-free electrochemical sensor was designed to detect cystic fibrosis, however, this system can be applied in any application where the detection of a DNA targets are involved.

Acknowledgements

This work has been partially supported by the Commission of the European Communities, project SAFER; Isolation of fetal cells from maternal blood (NEST-ADVENTURE 04977).

References

- [1] A. Fushan, G. Monastyrskaya, I. Abaev, *Res. Microbiol.* 157 (2006) 684.
- [2] Y.M. Liu, Z.L. Gong, N. Morin, *Anal. Chim. Acta* 578 (2006) 75.
- [3] A. Barzilai, G. Rotman, Y. Shiloh, *DNA Repair* 1 (2002) 3.
- [4] B. Jiang, Y. Li, H. Wu, *Forensic Sci. Int.* 162 (2006) 66.
- [5] R.P. Huang, *Comb. Chem. High T. Scr.* 6 (2003) 769.
- [6] S. Brul, F. Schuren, R. Montijn, *Int. J. Food Microbiol.* 112 (2006) 195.
- [7] S. Rodriguez-Mozaz, M.J.L. de Alda, D. Barcelo, *Anal. Bioanal. Chem.* 386 (2006) 1025.
- [8] D.R. Walt, In *Chemistry World*, Royal Society Of Chemistry, August, (2006).
- [9] D.H. Farkas, *Clin. Chem.* 47 (2001) 1871.
- [10] C.J. Yu, Y. Wan, H. Yowanto, J. Li, C. Tao, M.D. James, C.L. Tan, T.J. Meade, *J. Am. Chem. Soc.* 123 (2001) 11155.
- [11] M. Ozsoz, A. Erdem, K. Kerman, D. Ozkan, B. Tugrul, N. Topcuoglu, H. Ekren, M. Taylan, *Anal. Chem.* 75 (2003) 2181.
- [12] P. Liepold, H. Wieder, H. Hillebrandt, A. Friebe, G. Hartwich, *Bioelectrochemistry* 67 (2005) 143.
- [13] M. Mir, I. Katakis, *Anal. Bioanal. Chem.* 381 (2005) 1033.
- [14] K. Hashimoto, K. Ito, Y. Ishimori, *Anal. Chem.* 66 (1994) 3830.
- [15] J. Wang, M. Jiang, *J. Am. Chem. Soc.* 120 (1998) 8281.
- [16] B. Meric, K. Kerman, D. Ozkan, P. Kara, S. Erensoy, U.S. Akarca, M. Mascini, M. Ozsoz, *Talanta* 56 (2002) 837.
- [17] A. Erdem, K. Kerman, B. Meric, U.S. Akarca, M. Ozsoz, *Electroanalysis* 11 (1999) 586.
- [18] K.M. Millan, S.R. Mikkelsen, *Anal. Chem.* 65 (1993) 2317.
- [19] D.F. Yang, C.P. Wilde, M. Morin, *Langmuir* 12 (1996) 6570.
- [20] F. Jelen, A. Erdem, E. Palecek, *Bioelectrochemistry* 55 (2002) 165.
- [21] A. Erdem, M. Ozsoz, *Anal. Chim. Acta* 437 (2001) 107.
- [22] C. Fan, K.W. Plaxco, A.J. Heeger, *Proc. Natl. Acad. Sci. U.S.A* 100 (2003) 9134.
- [23] S. Hason, J. Dvorak, F. Jelen, V. Vetterl, *Talanta* 56 (2002) 905.
- [24] E. Katz, I. Willner, *Electroanalysis* 15 (2003) 913.
- [25] J. Li, X. Chu, Y. Liu, J. Jiang, Z. He, Z. Zhang, G. Shen, R. Yu, *Nucleic Acids Res.* 33 (2005) 168.
- [26] F. Fixe, M. Dufva, P. Telleman, C.B. Christensen, *Nucleic Acids Res.* 32 (2004) e9.
- [27] A. Vainrub, B.M. Pettitt, *Biopolymers* 68 (2003) 265.
- [28] M.S. Shchepinov, S.C. Case-Green, E.M. Southern, *Nucleic Acids Res.* 25 (1997) 1155.
- [29] E. Laviron, *J. Electroanal. Chem.* 97 (1979) 135.
- [30] J. Liu, L. Tiefenauer, S. Tian, P.E. Nielsen, W. Knoll, *Anal. Chem.* 78 (2005) 470.
- [31] G. Hartwich, J.D. Caruana, T. Lumley-Woodyear, Y. Wu, C.N. Campbell, A. Heller, *J. Am. Chem. Soc.* 121 (1999) 10803.
- [32] A.B. Steel, T.M. Herne, M.J. Tarlov, *Anal. Chem.* 70 (1998) 4670.
- [33] Y.S. Choi, K.S. Lee, D.H. Park, *Bull. Kor. Chem. Soc.* 26 (2005) 379.
- [34] N.K. Park, J.H. Hahn, *Anal. Chem.* 76 (2004) 900.
- [35] A.J. Heeger, C. Fan, K. Plaxcon, US Patent, 435,006,000 2004.
- [36] V. Ostatná, N. Dolinnaya, S. Andreev, T. Oretskaya, J. Wang, T. Hianik, *Bioelectrochemistry* 67 (2005) 205.
- [37] E.M. Boon, D.M. Ceres, T.G. Drummond, M.G. Hill, J.K. Barton, *Nat. Biotechnol.* 18 (2000) 1096.
- [38] M. Venkataramanan, T. Pradeep, *Anal. Chem.* 72 (2000) 5852.

Determination of mercury in table salt samples by on-line medium exchange anodic stripping voltammetry

Füsün Okçu*, Hasan Ertaş, F. Nil Ertaş

Ege University, Faculty of Science, Department of Chemistry, 35100 Bornova, İzmir, Turkey

Received 3 August 2007; received in revised form 3 November 2007; accepted 8 November 2007

Available online 22 November 2007

Abstract

A new method for the determination of traces of total mercury by using a gold film electrode in salt samples was developed. Table salts are known to contain mercury at ultra-trace level as well as a high quantity of chloride ions that cause severe disturbance during the stripping step when gold is used as the electrode material in voltammetric measurements. The interference of high chloride content in the determination of mercury was eliminated by reducing its concentration down to $3 \times 10^{-3} \text{ mol L}^{-1}$ level which is optimum for the determination by using on-line medium exchange procedure immediately after the deposition step. The deposition potential applied to the electrode was maintained at 0.2 V (vs. Ag/AgCl double junction electrode) while the cell content was sucked by a pump and replaced with fresh electrolyte simultaneously. The analyte loss resulted from the air contact of the electrode was prevented by this means. The mercury ions present in the salt samples were collected at +0.2 V for 60 s, the electrolyte was replaced by $0.1 \text{ mol L}^{-1} \text{ HClO}_4$ and the potential was scanned, attaining a detection limit of $0.17 \mu\text{g L}^{-1}$, with R.S.D. of 1.2% (S/N = 3).

The recovery of the method was 94.6%. The performance and accuracy of the method was compared with that of atomic fluorescence spectrometry (AFS). Consequently, this developed method can offer a wide range of application in saline samples.

© 2007 Elsevier B.V. All rights reserved.

Keywords: Anodic stripping voltammetry; On-line medium exchange; Mercury; Table salt

1. Introduction

Mercury is one of the most toxic elements. Its very small amounts can cause severe effects to human [1]. Different species of mercury changing from metallic form to organometallic compounds are released into the environment by natural and anthropogenic processes. The marine sediments serve as a sink for mercury, which may be mobilized through bio-methylation. The spectrometric methods developed for the determination of mercury and other heavy metals in sea water samples are rather complicated since high saline content of the matrix can cause a variety of interferences [2,3]. A matrix separation, preconcentration or sample pretreatment steps are, therefore, needed in accordance with the method chosen. For this purpose several techniques have been undertaken including co-precipitation [4], solid phase extraction on a microcolumn [5] or electrochemical

preconcentration onto a gold electrode [2] prior to the spectroscopic detection. However, high mobility of the element leads to analyte loss in the analysis steps in some degree via volatilization or adsorption.

Salt industry utilizes sea water or water from some lakes in their process. Heavy metal content of table salt should be rigorously controlled, considering the wide participation of salt in food preparations. Although many methods including stripping techniques have been reported for the determination of mercury in sea water [2–10], no data are available in the literature for table salts. In fact, the studies on heavy metal content of table salt are rather limited probably due to the severe matrix effect. Recently, a flame atomic absorption spectrophotometric (FAAS) method for the determination of cadmium and lead contents of table salt samples was reported [11]. The method is based on the liquid–liquid extraction of metal ions as dithizone complexes followed by a direct aspiration of the organic phase into the nebulizer for the spectrometer.

Differential pulse anodic stripping analysis (DP ASV) employing gold electrode is one of the instrumental techniques

* Corresponding author. Tel.: +90 232 3884000x2356; fax: +90 232 3888264.
E-mail address: fusun.okcu@ege.edu.tr (F. Okçu).

applicable in the determination of very low concentrations of mercury, alleviating the detection limit even at sub-ppb level [12–18]. Mercury has so far been preconcentrated by employing glassy carbon [12], gold disc [12–15], gold fiber [16] and gold film on different substrates [12,15,18]. However, in spite of having a short preconcentration time and high sensitivity, the use of gold electrodes suffers from chloride interference in saline samples. High concentration of chloride ion irreversibly damage the electrode surface and results in the dissolution of gold at potentials more positive than +0.7 V versus the Ag/AgCl reference electrode [19]. On the other hand, a small amount of HCl is added to the cell to shift the mercury stripping peak to more negative potentials where the residual current is lower and the peak distortion is smaller [12]. This shift in the peak potential was attributed to the involvement of chloride in the stripping step of mercury stabilizing the Hg_2Cl_2 species on the electrode surface [18].

It has been verified experimentally that the optimal HCl concentration is in the range of $1 \times 10^{-3} \text{ mol L}^{-1}$ to $5 \times 10^{-3} \text{ mol L}^{-1}$ and mostly $3 \times 10^{-3} \text{ mol L}^{-1}$ was used to ensure a sufficient shift in the peak potential without hampering the gold film electrode [12,18]. Hence, it is essential to maintain the chloride concentration at this level when working with saline samples. To reduce the concentration down to this level, dilution is not a proper solution since it will result in the analyte concentration far below the sensitivity limits.

Recently, a gold microwire electrode modified using mercapto compounds was utilized to eliminate calomel formation in mercury determination by square wave ASV [10]. In KNO_3 solutions the sensitivity for mercury was found to be improved by surface modifications. However, the effect of abundant chloride was noted for sea water samples as it complexes with mercury.

Similar matrix effect was observed for sea water samples and was eliminated by using a procedure of medium exchange to a de-aerated stripping solution prior to the ASV measurement [9,12]. However, the analyte would be lost in some degree since the electrode contacts with air during the transfer step. To avoid this kind of hindrance, Mikkelsen and Schroder have introduced a new procedure called on-line medium exchange where the deposition potential is maintained while the electrolyte is replaced [20].

Present study describes an on-line medium exchange procedure for the determination of mercury in table salt samples by DP ASV at a gold film electrode. Here, the concentration of interfering ion, chloride, is reduced to a suitable level by sucking the sample solution while the stripping solution was introduced through Teflon tubing. By this means the electrode is ensured not to come in to contact with air. The performance and accuracy of the method was compared with that of atomic fluorescence spectrometry (AFS).

2. Experimental

2.1. Chemicals

A stock solution of Hg(II) (1000 mg L^{-1}) was prepared by adding concentrated HNO_3 solution into pure mercury in a mole

ratio of 1:4. The mixture was carefully heated near dryness and dissolved in few mL of HClO_4 before diluting with ultra-pure water up to 1.0 L. This stock solution was standardized by titrating with standard thiocyanate (0.053 mol L^{-1} KSCN) solution. Standard solutions were daily prepared from the stock solution.

A stock solution of Au(III) (500 mg L^{-1}) was prepared by dissolving pure metallic gold in 1 mL HNO_3 + 4 mL HCl mixture till the NO_x gases was observed to be removed. The solution was then diluted into 500 mL with ultra-pure water. In AFS studies, the reducing agent was standard Sn(II) solution prepared from its chloride salt to be 3.0 g in 100 mL.

2.2. Sample preparation

Table salt samples were obtained commercially and 1.0000 g of the samples was weighed precisely and dissolved in ultra-pure water. The solution was made up several volumes and a few drops of concentrated HClO_4 were added to the sample solution. All glasswares were soaked in 10% nitric acid for at least 24 h before use and then rinsed with ultra-pure water. The measurements were made at ambient temperature.

2.3. Instrumentation

The DP ASV measurements were made with Metrohm 693 VA Processor with a 694 VA Stand Voltammetric Analyzer. The working electrode was a gold film electrode (GFE) that was prepared by electrochemical deposition of Au(III) on a rotating glassy carbon electrode (GCE) support supplied from Metrohm. The active surface area of the electrode was 3.14 mm^2 . The counter electrode was a platinum wire and an Ag/AgCl (3 mol L^{-1} KCl) electrode was mostly used as the reference electrode. For the experiments carried out in the absence of chloride ions, a double junction Ag/AgCl/KCl/ KNO_3 was employed.

The parameters used for all the measurements were as follows: the pulse amplitude and frequency were 50 mV and 0.3 s, respectively. The potential scan rate was 20 mV s^{-1} , pre-electrolysis time was usually 60 s and the equilibration time of 5 s was used. The test solutions were de-aerated with nitrogen for 300 s before each measurement.

Cold vapor atomic fluorescence (CV AFS) measurements were made with PSA 10.004 (PS Analytical, Sevenoaks, Kent, UK), which consisted of a PSA 20.099 random access model auto-sampler, continuous-flow vapor generation system and a fluorescence detector. Automated continuous-flow generation system (PSA 10.003) was used to generate gaseous mercury. The generated mercury was, then, detected by utilizing a 254 nm interference filter to achieve wavelength isolation and reduction of background scatter (Merlin, PSA 10.023). Wet gas from the gas–liquid separator was continuously dried by using a semi-permeable Nafion membrane dryer tube (Perma Pure Products, USA).

2.4. Preparation of gold film electrode

The GCE surface was polished with Al_2O_3 on a piece of velvet and rinsed with pure water. Following the sonication in

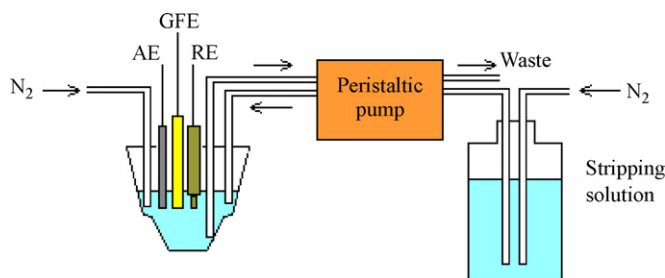


Fig. 1. Schematic representation of on-line medium exchange (OLME) procedure.

water for 5 min, the electrode was placed in the cell containing 20 mL of electrolysis solution ($1 \times 10^{-5} \text{ mol L}^{-1} \text{ HAuCl}_4$ in $0.1 \text{ mol L}^{-1} \text{ HCl}$). Then electrochemical cleaning process was initiated by cycling the potential 100 times at the potential range of 0.2–0.8 V at a rate of 1000 mV s^{-1} . The gold film was prepared by depositing the gold from Au(III) ions in the solution by three successive electrolysis steps performed at -0.5 V for 300 s while the GCE was rotating at a rate of 1600 rpm. The conditioning step was repeated between deposition periods to remove any deposited metallic impurities. A relatively large positive potential (0.6 V) is applied to remove adsorbed species and deposited metals from the gold film before a single determination.

For avoiding the chloride interference, voltammograms were recorded by using double-junction electrode as the reference electrode. Factors affecting the sensitivity of the method were studied by using $0.1 \text{ mol L}^{-1} \text{ HClO}_4$ solution to create a non-interfering medium for mercury determination. The deposition was made at 0.2 V for 60 s in stirred solutions (1600 rpm) and the quantification of mercuric ions was carried out by standard addition method with three spikes for each determination.

2.5. On-line medium exchange procedure

The electrode was immersed in the cell containing 20 mL of standard or sample solution in $0.1 \text{ mol L}^{-1} \text{ HClO}_4$ to perform the electrochemical deposition of mercury. After deposition step, the cell content was sucked by a peristaltic pump at a flow rate of 10 mL min^{-1} through Teflon tubing, placed near the bottom of the cell, till half of the solution remains to keep the electrode in contact with solution. Then, the cell was refilled with de-aerated stripping solution containing $0.1 \text{ mol L}^{-1} \text{ HClO}_4$ through upper tubing while the bottom tubing was working simultaneously as can be seen from Fig. 1. Since the time passed in this step determines the dilution ratio of the sample solution, it was optimized by checking the chloride concentration left over in the cell by Argentometric titration. This technique takes few minutes (90 s)

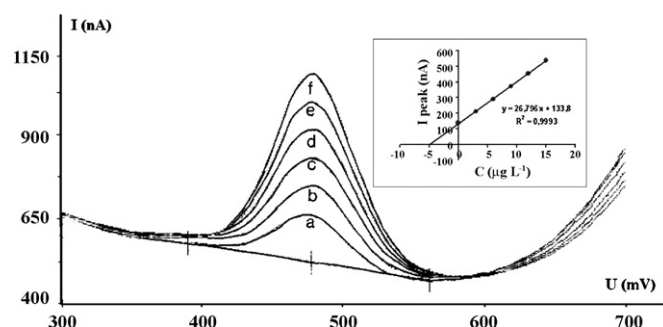


Fig. 2. DP ASV peaks obtained for a solution containing (a) $0.1 \text{ mol L}^{-1} \text{ HClO}_4$ and 20 mL of salt sample ($1.0000 \text{ g in } 100 \text{ mL}^{-1}$) after addition of Hg(II) solution to be (b) $3.0 \mu\text{g L}^{-1}$, (c) $6.0 \mu\text{g L}^{-1}$, (d) $9.0 \mu\text{g L}^{-1}$, (e) $12.0 \mu\text{g L}^{-1}$ and (f) $15.0 \mu\text{g L}^{-1}$ by using in situ ASV measurement method.

to reach optimum chloride level and then, the stripping procedure was executed.

3. Results and discussion

Initial studies were designed to construct a calibration curve with standard solutions in a cell containing $3 \times 10^{-3} \text{ mol L}^{-1} \text{ HCl}$ in $0.1 \text{ mol L}^{-1} \text{ HClO}_4$ solution as pointed out to be optimum in former studies [12,17]. The potential of the GFE electrode was fixed at 0.2 V for 60 s for deposition of mercuric ions as amalgam. Upon scanning the potential towards positive direction, a stripping peak at 0.58 V, well separated from the large peak of gold oxidation, was observed, and these peaks have displayed a linear change with Hg(II) concentration as tabulated in Table 1.

Nevertheless, it is not accordingly straightforward to work with saline samples as the determination of mercury in saline samples at a GFE has some constrains. The main problem working with a saline sample is the difficulty in the establishing a stable background current for blank as the peak alters in the absence of chloride ion. On the other hand, even high purity form of chloride salts might contain small amounts of mercury. In fact, the baseline signal was obtained as $41.918 \pm 35.076 \text{ nA}$ ($n=7$) from the measurements performed in $0.1 \text{ mol L}^{-1} \text{ HClO}_4$ containing $3 \times 10^{-3} \text{ mol L}^{-1}$ chloride ion. This high uncertainty in the baseline reflects in high LOD levels (Table 1).

Another drawback of in situ method is the alteration of peak characteristics in the voltammograms depending on the chloride content [18]. Dilution is not a proper solution since it can yield an analyte concentration far below the sensitivity limits.

Fig. 2 illustrates the voltammograms obtained with salt samples, in 1.0000 g portions dissolved in 100 mL of pure water, by standard addition manner. The stripping peak of mercury

Table 1
Calibration characteristics and limit of detection values calculated for ASV by in situ deposition and on-line medium exchange procedure and AFS methods for mercury determination

Method	Concentration range ($\mu\text{g L}^{-1}$)	Calibration equation	LOD ($\mu\text{g L}^{-1}$)
In situ	2.0–6.0	$y = 32.6 (\pm 13.0)x + 36.9 (\pm 21.6)$	2.04
OLME	1.0–3.0	$y = 272.7 (\pm 14.7)x + 160.34 (\pm 12.9)$	0.17
AFS	0.5–2.0	$y = 4.25 (\pm 1.5)x - 0.02 (\pm 0.5)$	0.14

appeared at 0.48 V was proportionally built up upon addition of standard Hg(II) solution in a range of 3.0–15 $\mu\text{g L}^{-1}$.

The considerable change in the slope has indicated that replicated measurements have failed to give reproducible results for salt samples (Table 1). At higher concentrations (mostly $>50 \mu\text{g L}^{-1}$), symmetrical shape of mercury peak was deteriorated and an additional peak at more negative potentials has appeared as a shoulder. This irregularity was attributed to a chemical reaction between the Hg(II) ions in the solution and the elemental mercury on the electrode surface resulting in a calomel formation in the presence of chloride.

A former study carried out in this lab revealed that the addition of the acetone into the voltammetric cell after the deposition step results in a chemical reaction with the calomel molecule at the electrode surface liberating metallic mercury [21]. In fact, upon addition of 1 mL of acetone into the cell after deposition step, the anodic peak has gained its shape after the solution reached an optimal concentration of mercury. On the other hand, the surface-active property of acetone limits its use in this technique and requires freshly prepared stripping solutions prior to each scan.

In the literature, medium exchange technique is recommended for eliminating the matrix effect encountered in deposition of the sample solution [12]. Accordingly, at the end of the electrochemical deposition process, the system was switched off and the reference and counter electrodes were rinsed with distilled water. The cell solution was replaced with equal volume of pure base electrolyte that was formerly de-aerated. Subsequently, the stripping procedure was executed. Nevertheless, much lower anodic currents were observed with lower precision most probably due to the lose in deposited mercury during the transfer step.

For preventing the air contact, the electrode was kept in its position in touch with the solution while the cell content was exchanged by means of a peristaltic pump as depicted in Fig. 1. This technique is in fact another version of on-line medium exchange (OLME) procedure as reported by Mikkelsen and Schroder [20]. By this means, the interference of saline content was reduced by simply diluting the cell content with an electrolyte suitable for stripping step by means of a peristaltic pump till the chloride content is reduced to $3 \times 10^{-3} \text{ mol L}^{-1}$ level. The flow rate was kept constant and the medium exchange time was optimized on checking the chloride concentration of the cell solution by argentometric titration till the optimum level is reached. Among the medium exchange times studied (60, 90 and 120 s), 90 s was found to be optimum for OLME studies. The stripping procedure was then executed.

This technique provides a faster and safer transfer of the electrode from the sample to the stripping solution; therefore more reproducible results were obtained. The calibration curve plot parameters obtained by this means can be seen in Table 1 with an improved sensitivity.

The method was also applied to the determination of mercury content of table salt samples and the resulting voltammograms and related standard addition curve can be seen in Fig. 3. The reproducibility of the slope of curves obtained for subsequent analysis reflects on the results (R.S.D. 1.2%). However, as the

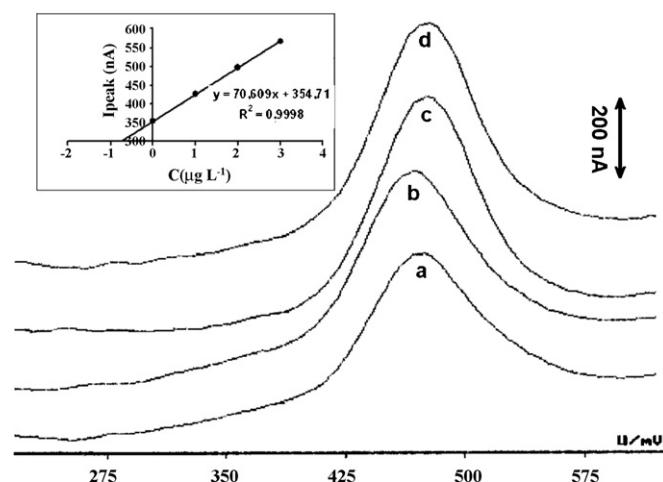


Fig. 3. Anodic stripping voltammograms of (a) the salt sample solution (1.0000 g in 100 mL) containing $0.1 \text{ mol L}^{-1} \text{ HClO}_4$ after addition of Hg(II) solution to be (b) $1.0 \mu\text{g L}^{-1}$, (c) $2.0 \mu\text{g L}^{-1}$ and (d) $3.0 \mu\text{g L}^{-1}$ by using OLME procedure and standard addition graph.

dilution factor is too high, background correction is needed for accurate measurements. For establishing a reliable baseline current in OLME procedure, the deposition was exchanged with $0.1 \text{ mol L}^{-1} \text{ HClO}_4$ and then the medium was exchanged with stripping solution prior to the stripping step. The mean mercury content of the blank was established as $0.59 \pm 0.05 \mu\text{g L}^{-1}$.

The developed method, on the other hand, was proved to be reliable as the recovery figures maintain the satisfactory results (94.6%). The generally accepted procedure for the verification of the accuracy of a method is to measure the same sample with a reference method. Table 2 lists the results obtained for the salt samples to compare the performance of in situ deposition, medium exchange (ME), on-line medium exchange (OLME) and atomic fluorescence spectrometric (AFS) methods.

Total mercury level determined by AFS ($0.25 \mu\text{g g}^{-1}$) was found lower than those of ASV analysis. This can be attributed to the interaction of mercury ions with high levels of chloride during the reducing step. Similarly, the interferences of bromide and iodide in the determination of mercury by CV AFS have been reported [22].

On comparison of the stripping methods, it can be clearly said that total mercury determination by in situ deposition is strongly affected by chloride content. Conventional medium exchange procedure yielded the lowest results probably due to the analyte loss.

In addition, random errors in the value of the slope and intercept ($s_{y/x}$) can give an indication about the precision [23].

Table 2
Mercury content of the salt sample analyzed by in situ, medium exchange (ME), on-line medium exchange (OLME) ASV methods and standard AFS procedure

Method	Total mercury concentration ($\mu\text{g/g}$) ($n=3$)
In situ	0.32 ± 0.14
Ex situ ME	0.22 ± 0.09
Ex situ OLME	0.44 ± 0.05
AFS	0.25 ± 0.03

Calibration curves with similar slopes can be attained by OLME procedure and relatively low $s_{y/x}$ value (1.64) is obtained in comparison to that of in situ analysis (6.08) which is also reflected in high LOD levels.

4. Conclusions

Anodic stripping voltammetry was applied to total mercury determination in table salt samples. The chloride content of saline samples was adjusted to an optimum level by on-line medium exchange procedure. This step provides a justification of chloride concentration as the high levels create the interference while its controlled amounts are required to improve the peak characteristics. Mercury content of the sample was electrochemically collected at a gold film electrode, and on-line medium exchange procedure was then performed to reduce the chloride concentration to an optimum level. Well developed and reproducible peaks were obtained by this means. Consequently, this method can offer wide range of application in saline samples.

References

- [1] S.E. Manahan, Environmental Science and Technology, Lewis Publ., Boca Raton, 1997.
- [2] E.L. Seibert, V.L. Dressler, D. Pozebon, A. Curtius, J. Spectrochim. Acta, Part B 56 (2001) 1963–1971.
- [3] L. Elçi, U. Şahin, S. Öztaş, Talanta 44 (1997) 1017–1023.
- [4] L. Elçi, S. Saraçoğlu, Talanta 46 (1998) 1305–1310.
- [5] H. Bagheri, A. Gholami, Talanta 55 (2001) 1141–1150.
- [6] I. Gustavsson, J. Electroanal. Chem. 214 (1986) 31–36.
- [7] R. Di Roso, M. Waeles, P. Monbet, C.J. Chaumery, Anal. Chim. Acta 410 (2000) 97–105.
- [8] R.P. Mason, K.R. Rolffhus, W.F. Fitzgerald, Mar. Chem. 61 (1998) 37–53.
- [9] E.M. Richter, M.A. Augelli, G.H. Kume, R.N. Mioshi, L. Angnes, Fresenius J. Anal. Chem. 366 (2000) 444–448.
- [10] A. Widmann, C.M.G. van den Berg, Electroanalysis 17 (10) (2005).
- [11] F.A.C. Amorim, S.L.C. Ferreira, Talanta 65 (2005) 960–964.
- [12] M. Hatle, Talanta 34 (1987) 1001–1007.
- [13] Y. Bonfil, M. Brand, E. Kirowa-Eisner, Anal. Chim. Acta 424 (2000) 65–76.
- [14] Y. Bonfil, M. Brand, E. Kirowa-Eisner, Rev. Anal. Chem. 19 (2000) 201–216.
- [15] P. Ugo, S. Zampieri, L. Moretto, D. Paolucci, Anal. Chim. Acta 434 (2001) 291–300.
- [16] H. Huiliang, D. Jagner, L. Renman, Anal. Chim. Acta 202 (1987) 117–122.
- [17] I. Svancara, M. Matousek, E. Sikora, K. Schachl, K. Kalcher, K. Vytras, Electroanalysis 9 (1997) 827–833.
- [18] F. Okçu, F.N. Ertaş, H.İ. Gökçel, H. Tural, Turk. J. Chem. 29 (2005) 355–366.
- [19] J. Wang, Stripping Analysis, VCH Publishers, 1985.
- [20] O. Mikkelsen, K.H. Schroder, Anal. Chim. Acta 458 (2002) 249–256.
- [21] F.N. Ertaş, H.İ. Gökçel, H. Tural, Turk. J. Chem. 24 (2000) 261–267.
- [22] G. Lindstedt, Analyst (London) 95 (1970) 264–271.
- [23] J.C. Miller, J.N. Miller, Statistics for Analytical Chemistry, Ellis Harwood PTR Prentice Hall, 1993.

Towards minimization of chlorinated solvents consume in Fourier transform infrared spectroscopy determination of Propamocarb in pesticide formulations

Guillermo Quintás, Sergio Armenta, Salvador Garrigues*, Miguel de la Guardia

Department of Analytical Chemistry, University of Valencia, Edifici Jeroni Muñoz, 50th Dr. Moliner, 46100 Burjassot, Valencia, Spain

Received 11 June 2007; received in revised form 24 October 2007; accepted 7 November 2007

Available online 17 November 2007

Abstract

A method has been developed for Fourier transform infrared (FTIR) spectroscopy determination of Propamocarb in emulsifiable pesticide concentrate formulations. Five microliter sample was directly injected without any pretreatment in a CHCl_3 stream at 2 mL min^{-1} into a closed system and the FTIR spectra of sample and standard solutions were obtained using a nominal resolution of 4 cm^{-1} from 4000 to 900 cm^{-1} spectral region and accumulating 2 scans per spectrum. Propamocarb determination was based on the measurement of flow injection analysis (FIA) recording height established from FTIR peak area measurements from 1713 to 1703 cm^{-1} corrected using a baseline defined at 2000 cm^{-1} . The concentration of Propamocarb in samples was calculated by interpolation in an external calibration line obtained from several injections of $2 \mu\text{L}$ of a 47% (w/v) standard solution into the CHCl_3 closed system. This procedure provided a limit of detection of 0.8% (w/v) in the original sample, a sensitivity of 0.3190 absorbance units mL mg^{-1} for a pathlength of 0.11 mm and a relative standard deviation of 0.2% for five independent measurements at 0.74 mg mL^{-1} concentration level. The maximum sampling frequency of the whole procedure was 34 h^{-1} and the waste generation was reduced to only 2 mL of CHCl_3 solution per sample and additional 2 mL for the whole calibration line.

© 2007 Elsevier B.V. All rights reserved.

Keywords: Propamocarb; Pesticide formulations; Flow injection analysis; Fourier transform infrared spectrometry; Green methods

1. Introduction

Propamocarb, propyl-3-(dimethylamino) propylcarbamate, is a carbamate fungicide used to control *Pythium* species and *Phytophthora* spp. on turf, outdoor woody and herbaceous ornamentals. Propamocarb is relatively non-toxic [1]. This fungicide is formulated as soluble concentrate with concentrations from 60 to 72% (w/v) [2]. Since Propamocarb was first registered as a pesticide in 1984 in the U.S. this fungicide has been widely used. Only in the United States the amount of Propamocarb employed varies approximately from 100,000 to 200,000 pounds of active ingredient per year [3].

The Collaborative International Pesticides Analytical Council (CIPAC) recommended procedure for the determination of Propamocarb in formulated pesticides uses high performance liquid chromatography with UV detection [4], other methods

which have been also reported for its determination at trace levels in environmental samples are based on gas chromatography with either nitrogen–phosphorous [5] or mass-spectrometry [6] detection.

Fourier transform infrared (FTIR) spectrometry is a scarcely used technique in pesticide analysis, despite of that pesticides generally present absorption bands in the mid-IR region (from 4000 to 400 cm^{-1}) due to the presence of specific functional groups in the active principle molecules.

Several methods for the determination of dithiocarbamate pesticides by FTIR transmittance [7] or carbamate pesticides like carbofuran and metalocarb by HPLC-FTIR [8] in either commercial formulations or environmental samples have been proposed showing the suitability of this technique for this type of determinations.

In recent years our research group has developed a series of methodologies for the FTIR determination of different analytes in pesticide formulations [9]. However, the need of using chlorinated solvents for the complete dissolution of many active principles and their determination by IR measurements

* Corresponding author. Tel.: +34 354 3158; fax: +34 354 4838.

E-mail address: salvador.garrigues@uv.es (S. Garrigues).

is a general drawback of the aforementioned methodologies taking into consideration the negative environmental impact of this type of solvents.

The object of this study has been the development of a FTIR spectrometric procedure for fast, accurate and direct determination of Propamocarb in commercial pesticides which can be used in the quality control of this type of products, also reducing as much as possible the waste generation of chlorinated solvents through the use of flow injection analysis (FIA) methodology, in a closed system, following the purposes to establish environmentally friendly analytical methods [10].

2. Experimental

2.1. Apparatus and reagents

A Nicolet (Madison, WI, USA) Magna 750 FTIR spectrometer, equipped with a temperature-stabilized deuterated tryglycine sulphate (DGTS) detector, was employed for spectral measurements, using a 0.11 mm pathlength microflow through cell with a ZnSe and a CaF₂ windows.

The manifold employed for the FIA-FTIR Propamocarb determination has been described earlier for the determination of malathion in pesticide formulations [11]. It was built up by employing a six-way Rheodyne 5041 injection valve (Cotati, CA, USA), a directional three-way valve and a Gilson Minipuls 2 peristaltic pump (Villiers-le-Bel, France) furnished with Viton® (iso-versinic) tubes (1 mm i.d. and 3 mm o.d.) placed after the measurement cell, in order to do the Propamocarb extraction with CHCl₃ and sample transport and carrier aspiration through the system while avoiding bubble formation. The connecting tubes employed in the setup were made on PTFE of 0.8 and 1.5 mm i.d. Hamilton (Bonoluz, Switzerland) 7000 series syringes (dead-volume free) of 2.0 and 5.0 μL were used for standard and sample injection in flow-FTIR determination of Propamocarb.

Propamocarb standard (95%, w/v) was supplied by Fluka (Buchs, Switzerland). Analytical grade chloroform stabilized with ethanol supplied by Scharlau (Barcelona, Spain), was employed for the preparation of samples and standards.

Propamocarb 60.5% (w/v) emulsifiable concentrate commercial formulations were obtained from the local market. Synthetic samples were prepared in the laboratory by the dilution of commercial ones with chloroform.

2.2. FTIR procedure

2.2.1. Stopped-flow procedure

Twenty milligram of sample was accurately weighted and diluted with 4 g of CHCl₃. The solution was introduced in the FTIR measurement cell by using a peristaltic pump and spectra were obtained from 4000 to 900 cm⁻¹ in the stopped-flow mode at 4 cm⁻¹ resolution and accumulating 25 scans per spectrum versus a background of the cell filled with the solvent.

A calibration line was established from Propamocarb external standards obtained by successive dilutions of 2 μL of a 47% (w/v) standard of Propamocarb dissolved in CHCl₃ injected in

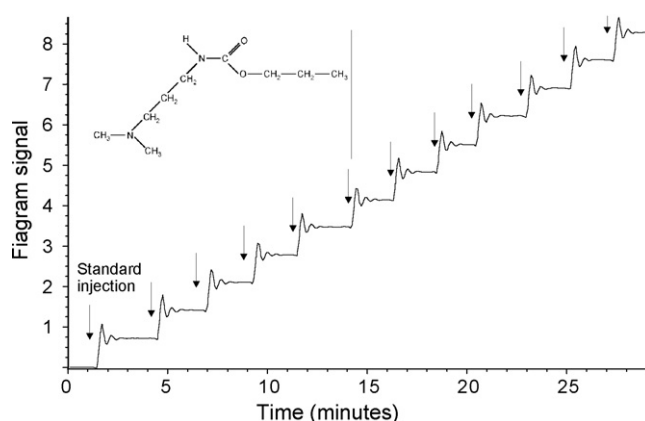


Fig. 1. Figram established from peak area measurements between 1713 and 1703 cm⁻¹ using a baseline correction at 2000 cm⁻¹ for the measurement of 12 successive injections of a 47% (w/v) Propamocarb standard. Resolution: 4 cm⁻¹; number of cumulated scans: 2; CHCl₃ volume: 2 mL; injection volume (standard): 2 μL.

a closed flow CHCl₃ system, thus provides a final concentration range from 0.47 to 38.73 mg mL⁻¹. Peak area values were measured between 1713 and 1703 cm⁻¹ being corrected by a baseline defined at 2000 cm⁻¹. Sample absorbance spectra, measured in the same conditions as standards, were interpolated in the calibration line.

2.2.2. Flow injection procedure

Five-microliter sample was injected in the FIA manifold in which 2 mL CHCl₃ was recirculating at a 2 mL min⁻¹ flow rate in a 4 mL closed system. The FTIR spectrum, between 4000 and 900 cm⁻¹, was recorded every 2.06 s as a function of time, by using a nominal resolution of 4 cm⁻¹ and accumulating 2 scans per point. A chemigram was established from peak area measurements from 1713 to 1703 cm⁻¹ using a baseline correction at 2000 cm⁻¹.

The concentration of Propamocarb in samples was calculated by interpolation in an external calibration line obtained by measuring the height to zero figram values measured after the steady-state was reached in the closed flow of CHCl₃ after every successive injection of 2 μL of a 47% (w/v) Propamocarb standard (see Fig. 1).

3. Results and discussion

3.1. FTIR spectrum of Propamocarb

Fig. 2 shows the FTIR spectra in the wavenumber region from 2000 to 1100 cm⁻¹ of a Propamocarb standard solution of 2.6 mg mL⁻¹ in CHCl₃ and a sample solution containing 2.5 mg mL⁻¹ Propamocarb. Sample and standard spectra present the same absorption bands all those corresponding to Propamocarb, except that at 1602 cm⁻¹ due to the presence of water in the pesticide formulation.

The most intense FTIR band of Propamocarb is the carbonyl stretching one at 1708 cm⁻¹. The band at 1516 cm⁻¹ is produced by the stretching of the N–H bond. The band at 1466 cm⁻¹ is

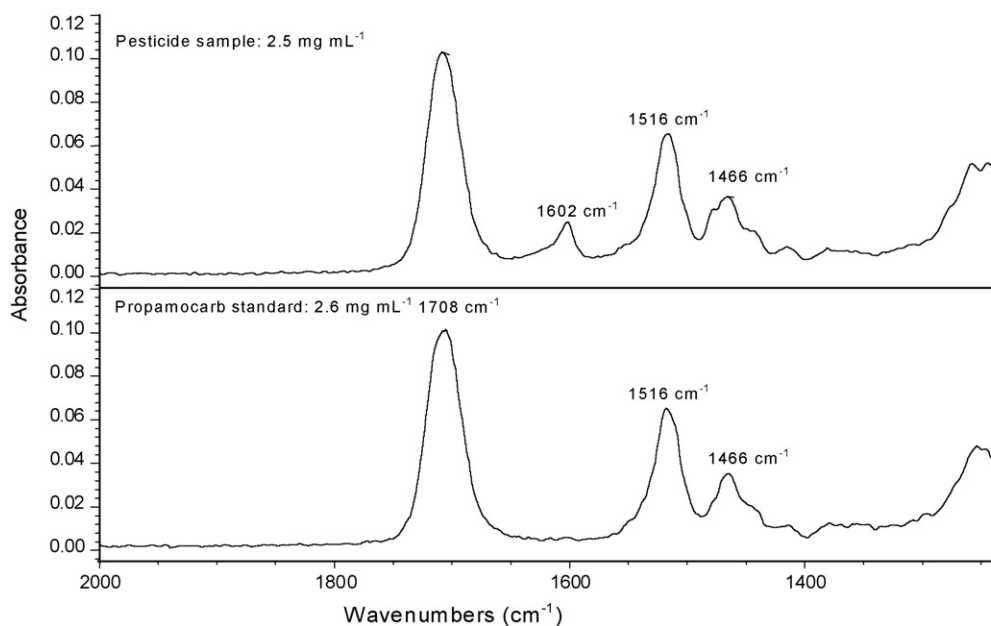


Fig. 2. Absorbance spectra of both a Propamocarb standard and a sample solution in CHCl_3 with concentrations of 2.6 and 2.5 mg mL^{-1} , respectively. Number of accumulated scans: 25, resolution: 4 cm^{-1} .

due to CH_3 and also to the CH_2 , CH and O-CH_2 deformation bands [12].

3.2. Effect of measurement conditions

In order to select the most appropriate conditions to carry out the determination of Propamocarb in emulsifiable pesticide formulations, the effect of different measurement conditions was studied. For the determination in the stopped flow mode, it was used a nominal resolution of 4 cm^{-1} and a number of accumulated scans of 25, as in previous studies [13,14].

In the case of FIA-FTIR measurements, the effect of the number of accumulated scans per spectrum on the signal intensity was evaluated using a 4 cm^{-1} nominal resolution. As can be seen in Fig. 3, the signal obtained from the diagram decreases when the number of scans increases. Two scans were selected in order

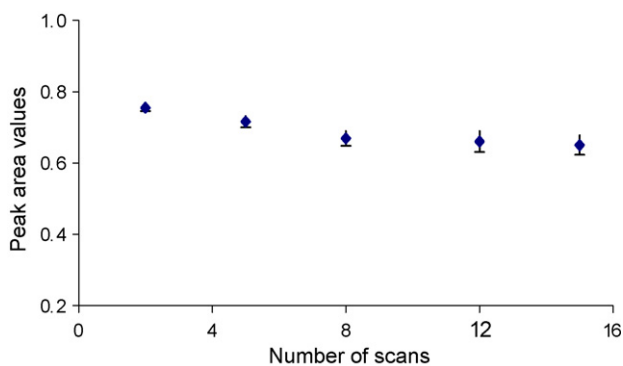


Fig. 3. Effect on the peak area values of a 2.6 mg mL^{-1} Propamocarb concentration of the increasing number of accumulated scans in the FIA-FTIR procedure using a nominal resolution of 4 cm^{-1} . See the text for details about other measurement conditions.

to increase the number of points of each signal by reducing the data acquisition time.

The effect of flow rate on the sample analysis frequency was evaluated by using values from 1 to 2.6 mL min^{-1} . As depicted in Fig. 4, for an injection volume of 5 μL , flow rates higher than 2 mL min^{-1} did not reduce the time needed to reach the steady-state, providing a sample injection frequency of 34 h^{-1} .

3.3. Selection of the appropriate bands for the FTIR measurement of Propamocarb

Table 1 summarizes the regression lines obtained for peak height and peak area measurements of the most intense absorption band for Propamocarb using different baseline criteria. In every case good linear fittings were obtained with R^2 values higher than 0.999. It can be observed that for a same band

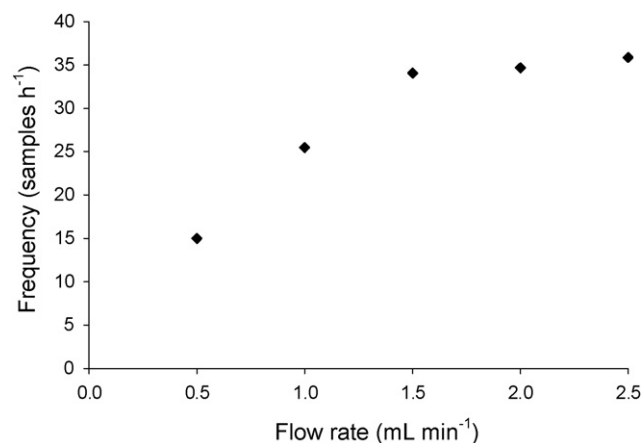


Fig. 4. Study of the effect of different flow rates on the sample injection frequency.

Table 1
Analytical characteristics of FIA-FTIR Propamocarb determination using different measurement modes and baseline criteria

Measurement mode	Wavenumber (cm ⁻¹)	Baseline correction	Calibration curve ($y = a + bC$ (mg mL ⁻¹))				
			$a \pm s_a$	$b \pm s_b$	R^2	%R.S.D.	LOD (% w/v)
Height	1708	2000	-0.0016 ± 0.0004	0.03357 ± 0.00008	0.99998	0.3	0.6
		1749–1674	-0.0006 ± 0.0007	0.0303 ± 0.0001	0.99993	0.4	1.2
Area	1713–1703	2000	-0.013 ± 0.005	0.3190 ± 0.0009	0.99997	0.2	0.8
		1749–1674	-0.007 ± 0.002	0.2861 ± 0.0003	0.999996	0.3	1.4

Nominal resolution: 4 cm⁻¹. Number of accumulated scans: 2.

Table 2
Determination of Propamocarb in emulsifiable pesticide commercially available formulations

	FTIR batch	Precision %R.S.D.	Accuracy %E _r	FIA-FTIR	Precision %R.S.D.	Accuracy %E _r	Reported value
1	60.5 ± 0.3 ^a	0.5	0.0	60.4 ± 0.3	0.5	0.2	60.5
2	60.3 ± 0.2	0.3	0.3	60.5 ± 0.3	0.5	0.0	
3	60.4 ± 0.4	0.7	0.2	60.5 ± 0.2	0.3	0.0	
4	–	–	–	6.34 ± 0.12	1.9	-1.2	6.42
5	–	–	–	12.68 ± 0.16	1.3	-1.2	12.83
6	–	–	–	19.2 ± 0.2	1.0	-0.16	19.23
7	–	–	–	25.6 ± 0.2	0.8	-0.04	25.61
8	–	–	–	31.3 ± 0.3	0.9	-2.1	31.98

Samples 1–3 correspond to commercially available agrochemicals and samples 4–8 were synthetic samples prepared in the laboratory.

^a Concentration values (% w/v) are the average of three independent analysis ± standard deviation.

the sensitivity was in all the cases approximately one order of magnitude lower for peak height values than for peak area ones.

The precision, as relative standard deviation of five measurements of 0.74 mg mL⁻¹ concentration level, ranged between 0.2 and 0.4% independently on the use of peak height or peak area values. The limit of detection values obtained, for a sample volume of 5 µL, varied between 0.6 and 1.4% (w/v). So, the aforementioned figures of merit are appropriate for Propamocarb determination in commercial pesticide formulations.

The band located at 1708 cm⁻¹ was chosen because in this region the carbonyl band is not overlapped with any other band in the sample matrix. Another reason is that this band is intense enough to achieve a high signal to noise ratio when compared with the bands at 1516 or 1466 cm⁻¹.

The use of a baseline correction at 2000 cm⁻¹ provides lower relative errors than those found when using a two points baseline. Results with the lowest relative accuracy error (results not shown) were found when peak area measurements were employed to build the fiagrams for both, samples and standards.

3.4. On-line FTIR Propamocarb determination analytical characteristics

The sensitivity of the FIA-FTIR analysis of Propamocarb corresponds to 0.3190 ± 0.0009 absorbance units mg⁻¹ mL. Using the recommended procedure, the limit of detection was 0.8% (w/v), for a 5 µL sampling volume and provided a repeatability of 0.2% as relative standard deviation for five independent measurements of a 0.74 mg mL⁻¹ concentration level.

To assure the accuracy of the procedure matrix effect was also studied. The calibration line calculated by standard addi-

tion method was $y = (0.464 \pm 0.004) + (0.3179 \pm 0.0007)C$ with a regression coefficient $R^2 = 0.99998$, where y is the fiagram signal and C the concentration of Propamocarb in mg mL⁻¹. It can be shown that there is no matrix effect on Propamocarb FTIR determination when the measurement of FIA recording height was established from FTIR peak area values between 1713 and 1703 cm⁻¹ corrected with a horizontal baseline at 2000 cm⁻¹.

3.5. Determination of Propamocarb in agrochemicals

A set of commercially formulated pesticides, obtained from the Spanish market, was analyzed by FTIR using both, batch and FIA, measurements. Results provided by both procedures (see Table 2) were statistically comparable for a probability level of 95% with those reported by the manufacturer. Additionally, a set of synthetic samples prepared in the laboratory was also analyzed by the FIA-FTIR procedure in order to assess the accuracy of the methodology. As it can be seen, the relative accuracy errors obtained for the analysis of these synthetic samples were lower than 2.1%.

4. Conclusions

In this paper, a fully mechanized FIA-FTIR procedure has been developed, in which the contact of the operator with toxic solvents is avoided. The proposed FTIR procedure can be used for the quality control of Propamocarb in emulsifiable pesticide commercial formulations providing a fast, simple and environmentally friendly alternative to classical chromatographic methods in which a high dilution of the sample with appropriate solvents are required.

Acknowledgements

Authors acknowledge the financial support of the Ministerio de Educación y Ciencia (Project CTQ2005-05604, FEDER) and Direcció General d'Investigació i Tràsferència Tecnològica de la Generalitat Valenciana (Project ACOMP/2007/131) and Universitat de València (Convocatòria d'Accions Especials, Project UV-AE-20070213). S. Armenta the FPU Grant of the Ministerio de Educación, Cultura y Deporte (Ref. AP2002-1874).

References

- [1] USDA/Extension Service/National Agricultural Pesticide Impact Assessment Program. Extension Toxicology Network.
- [2] C. de Liñan, *Vademecum de productos fitosanitarios y nutricionales*, Ediciones Agrotécnicas S. L., Madrid, 2000.
- [3] Environmental Protection Agency, USA. Prevention, Pesticides and Toxic Substances, 1995, EPA-783-F-95-031.
- [4] Collaborative International Pesticides Analytical Council (CIPAC) Handbook, vol. E, CIPAC Ltd., 1994, pp. 184–186.
- [5] T. Nagayama, M. Kobayashi, H. Shioda, T. Tomomatsu, J. AOAC Int. 79 (1996) 769.
- [6] S. Nemoto, K. Sasaki, M. Toyoda, Y. Saito, J. Chromatogr. Sci. 35 (1997) 467.
- [7] A. Cassella, R.J. Cassella, S. Garrigues, R.E. Santelli, R.C. de Campos, M. de la Guardia, *Analyst* 125 (2000) 1829.
- [8] J.C. Jones, D. Littlejohn, P.R. Griffiths, *Appl. Spectrosc.* 53 (1999) 792.
- [9] S. Armenta, G. Quintas, S. Garrigues, M. de la Guardia, *TrAC Trends Anal. Chem.* 24 (2005) 772.
- [10] M. de la Guardia, J. Ruzicka, *Analyst* 120 (1995) 17N.
- [11] G. Quintas, S. Armenta, A. Morales-Noe, S. Garrigues, M. de la Guardia, *Anal. Chim. Acta* 502 (2004) 213.
- [12] D. Lin-Vien, N.B. Colthup, W.G. Fateley, J.G. Grasselli, *Infrared and Raman Characteristic Frequencies of Organic Molecules*, Academic Press, London, 1991.
- [13] S. Armenta, G. Quintas, J. Moros, S. Garrigues, M. de la Guardia, *Anal. Chim. Acta* 468 (2002) 81.
- [14] G. Quintas, S. Armenta, A. Morales-Noe, S. Garrigues, M. de la Guardia, *Anal. Chim. Acta* 480 (2003) 11.

Determination of boron at sub-ppm levels in uranium oxide and aluminum by hyphenated system of complex formation reaction and high-performance liquid chromatography (HPLC)

Radhika M. Rao¹, Suresh K. Aggarwal*

Fuel Chemistry Division, Bhabha Atomic Research Centre, Mumbai 400085, India

Received 29 August 2007; received in revised form 20 November 2007; accepted 22 November 2007

Available online 15 January 2008

Abstract

Boron, at sub-ppm levels, in U_3O_8 powder and aluminum metal, was determined using complex formation and dynamically modified reversed-phase high-performance liquid chromatography (RP-HPLC). Curcumin was used for complexing boron extracted with 2-ethyl-1,3-hexane diol (EHD). Separation of complex from excess reagent and thereafter its determination using the online diode array detector (DAD) was carried out by HPLC. Calibration curve was found to be linear for boron amounts in the sample ranging from 0.02 μg to 0.5 μg . Precision of about 10% was achieved for B determination in samples containing less than 1 ppmw of boron. The values obtained by HPLC were in good agreement with the data available from other analytical techniques. The precision in the data obtained by HPLC was much better compared to that reported by other techniques. The present hyphenated methodology of HPLC and complex formation reaction is interesting because of cost performance, simplicity, versatility and availability when compared to other spectroscopic techniques like ICP-MS and ICP-AES.

© 2008 Published by Elsevier B.V.

Keywords: Boron; Curcumin; Boron–curcumin complex; RP-HPLC; Spectrophotometry; Tetra butyl ammonium bromide; EHD; Uranium; Aluminum

1. Introduction

Determination of boron at sub-ppm levels is an important requirement in nuclear technology in materials such as uranium metal, uranium oxide and aluminum. It is well-known to researchers working with boron that it is a difficult element to determine especially when present in sub-ppm amounts. This can be attributed to several reasons such as (i) loss of boron during dissolution of sample, (ii) contamination of sample with boron present in the environment, (iii) non-availability of suitable and well-characterized reference materials and (iv) matrix/spectral interferences. Different methods using colorimetry [1–6], fluorimetry [7,8], atomic emission spectrometry [9–11], mass spectrometry [12–14], non-destructive methods (e.g. nuclear track detection, prompt gamma neutron activation analysis) [15] have been reported for the determination of boron.

All these methods, except for the non-destructive ones, require an initial separation of boron from matrix and a preconcentration step.

Amongst the different methods reported in literature, spectrophotometry is the most commonly used method as the instrumentation is simple and cost effective. Derivatives of anthraquinone such as dianthrime, quinalizarin, carminic acid, HTPA have been used for preparing complexes of boron but these complexes are formed only in concentrated sulphuric acid medium and in some cases, the concentration of sulphuric acid is critical. Chromogenic reagents such as curcumin, chromotropic acid, azomethine H [1–6] have been used more frequently. The boron–azomethine H complex has an absorptivity lower by a factor of 10 compared to that of boron complex with curcumin and was, therefore, not used in view of the relatively poor sensitivity. The determination of boron at sub-ppm levels in aluminum and uranium using chromotropic acid was not pursued since it was observed that the peak response for the boron chromotropic complex was less than expected in presence of the matrix in spite of using masking agents. The curcumin method is a very sensitive method where boron is determined spectrophotometrically after separation of boron by distillation as methylborate [1,4]

* Corresponding author. Tel.: +91 22 2559 3740; fax: +91 22 2550 5151/5345.

E-mail addresses: skaggr@barc.gov.in,

skaggr2002@rediffmail.com (S.K. Aggarwal).

¹ Tel.: +91 22 2559 0637; fax: +91 22 2550 5151.

or by solvent extraction using 2-ethyl-1,3-hexane diol (EHD) [2,3] or by pyrohydrolysis or fusion techniques. Extraction of boron with EHD is fast and offers the advantage of boron being present in non-aqueous medium, which eliminates the interference in color development with curcumin at aqueous volumes more than 0.2 mL. Quantitative extraction of boron from different dissolution media, 1 M sulphuric acid (for steel) [2], dilute sulphuric acid (for uranium oxide) [3] using 10% (0.65 M) EHD in chloroform have been reported. However, in most of the spectrophotometric approaches, limitations in the determination arise due to two reasons: (i) absorption at the same wavelength by the chromogenic reagent and the boron complex and (ii) absorbance due to interfering species present in the solution.

HPLC with online absorbance detectors has been used for the determination of boron in steel and water samples. Ion-pair liquid chromatography and ion exchange chromatography have been used for the separation of boron chromotropic acid complex from excess of reagent [16,17]. Trace amounts of boron in water were determined by ion-exclusion chromatography with post-column method using azomethine H as a chromogenic reagent [18]. The aim of the present work was to develop an HPLC method using curcumin as a complexing agent for the determination of boron present at sub-ppm levels in uranium and aluminum samples. As mentioned earlier, the merit of HPLC technique versus that of spectrophotometry is mainly the possibility to remove interferences thereby allowing reliable and sensitive determination. In spite of the well-known limitations of curcumin, like its inability to react with boron in aqueous medium and requirement of a strong acid medium for the complex formation reaction, it has been used widely for boron determination due to its high sensitivity. Since, both the boron complex and the protonated curcumin absorb at the same wavelength (i.e. at 550 nm), parameters in HPLC were optimized in the present work to resolve these two peaks. This paper presents details of the methodology developed and its validation using uranium and aluminum samples containing known amounts of boron.

2. Experimental

2.1. Instrumentation

The HPLC (Merck Hitachi) system used in the present work consisted of a low pressure quaternary gradient pump (L-7100), a Rheodyne sampling valve (7725i) with 20 μ L sample loop, a guard column C₁₈ type (1 cm), a Chrompack C₁₈ analytical column (15 cm \times 4.6 mm) with 5 μ m particle size, a column oven (Model L-7350) and a 512 Diode Array Detector (DAD) (L-7450A). The eluted species flowing through the 8 μ L flow cell were monitored at 550 nm. The signal from the detector was processed by HSM D-7000 software package and the chromatograms were recorded using PC.

2.2. Reagents and materials

EHD 98% (Merck), Curcumin (Ferak, Germany), Analpure sulphuric acid 94% (Scharlau), Suprapur hydrochloric acid 30% (Merck), tetra butyl ammonium bromide, i.e. TBABr 99%

(Fluka), sodium 1-octane sulphonate 97% (Fluka), HPLC grade methanol 99.7% (Merck), GR acetic acid 99.8% (Merck), boron standard SRM 951 (NIST) were used. Freshly deionized water (18.2 M Ω cm) purified with a Milli Q system (Gradient, Millipore) was used for all the dilutions and dissolutions.

Quartz wares were used for dissolving the samples. All apparatus and flasks were thoroughly leached in 3 M nitric acid, washed with Milli Q water and methanol, and dried before use.

2.3. Procedure

2.3.1. Dissolution of U and Al samples

Five samples of uranium oxide, synthetically prepared, containing boron in the range of 0.25–1.6 ppmw and two aluminum samples from Indal (Cochin, Kerala, India) and Aviatube (France) containing less than 10 ppmw of boron were used for validation of the HPLC methodology. 100 mg to 500 mg of uranium oxide sample was dissolved in 15 mL of 3 M nitric acid, evaporated to nearly dryness and was subsequently re-dissolved in 10 mL of 1 M HCl. This was essential to prevent the interference from nitrate in boron complex formation. This conversion from nitrate to chloride medium was carried out under an IR lamp so as to avoid any loss of boron due to volatilization [19]. For aluminum, 80 mg to 120 mg of the sample was dissolved in 10 mL of 2 M HCl. Boron was extracted from 1 M HCl solution by EHD, complexed with curcumin and subjected to HPLC separation. The absence of any boron loss during the dissolution and evaporation of the sample was confirmed by spiking a small amount of sample (5 mg of uranium from which boron was extracted) with known amount of boron and subjecting this sample to the above procedure. The amount of boron determined was in agreement with the added boron amount indicating that boron is not lost during the dissolution step. It appears that in presence of matrix, boron does not volatilize so easily.

2.3.2. Extraction procedure

Extraction of boron was carried out from 10 mL of 1 M HCl solution by 10% (0.65 M) EHD in chloroform, in two steps of 2 and 1 mL of extractant with an equilibration period of 3 min. All the extracts were combined in a quartz beaker. Chloroform in the boron extract was evaporated by heating the extract under an IR lamp. This method gave 100% extraction for boron. When the third extract was tested for boron, absorption values similar to those for blank sample were obtained which confirmed that all boron was extracted completely in the first two extractions.

2.3.3. Complex formation

The boron curcumin complex (rosocyanin) was formed by reaction of protonated curcumin with boron [1–4]. The procedure involved the addition of 1 mL of 0.01 M curcumin in acetic acid and 0.25 mL of 18 M sulphuric acid to the extract. After 30 min, the solution was diluted with methanol to 10 mL. To 0.5 mL of this solution, 0.3 mL of 0.05 M TBABr was added and the solution was further diluted to 5 mL with methanol. This dilution step lowered the acidity to less than 0.1 M and reduced the fraction of protonated curcumin. 20 μ L of this solution was injected onto the HPLC column.

It may be mentioned that other metal ions, e.g. Fe may interfere when the complex formation with curcumin is carried out without separation of boron with EHD. In the present work, since boron was present at sub-ppm levels, the separation of boron with EHD serves the purpose of purification as well as preconcentration of boron. Thus the interference from other metal ions during the formation of rosocyanin was not observed.

2.3.4. HPLC conditions

Separation was carried out in a column oven maintained at 35 °C. Isocratic mode of elution was used for all the experiments. The mobile phase used was 0.003 M TBABr in 85% methanol. The flow rate was 0.8 mL/min and the chromatogram was monitored at 550 nm.

3. Results and discussion

3.1. Mobile phase studies

During the initial stages of the present work, when 85% methanol was used as the mobile phase, chromatographic peaks for curcumin and its protonated species were observed. The boron complex was retained on the column. It appeared that though the complex is ionic, its large hydrophobic group is strongly held on the non-polar C₁₈ column and thus is not eluted by methanol. Hence ions having hydrophobic component viz. sodium *n*-octane sulphonate and TBABr were introduced into the mobile phase (0.003 M in 85% methanol). A broad peak of the complex was obtained at 4 min for a flow rate of 1 mL/min for *n*-octane sulphonate. The adsorption of *n*-octane sulphonate on the column reduces the hydrophobic sites available for the boron complex and it also displaces the boron complex (rosocyanin) adsorbed onto the column. This results in elution of the complex.

When octyl group in the mobile phase was replaced with a bulkier tetra-butyl group by using 0.003 M TBABr as an additive in 85% methanol a much sharper peak at 2.96 min was obtained for the boron complex. The Fig. 1 shows the chromatogram obtained when the column temperature was raised to 35 °C. As expected, the faster mass transfer resulted in a narrow and sharper elution peak. The retention time of boron-complex was 3.25 min instead of 2.96 min since the flow rate was reduced to 0.8 mL/min instead of 1 mL/min. Different eluting species at the monitored wavelength of 550 nm are shown. As can be seen, both the protonated curcumin and un-protonated curcumin show the absorbance at 550 nm along with the boron–curcumin complex.

3.2. Effect of moisture and EHD on the absorbance

Hayes and Metcalfe [1] reported that presence of moisture in excess of 0.25 mL during direct complexation of boron with curcumin has an effect on formation of rosocyanin due to reduction in the acidity. In colorimetric determination of boron, Donaldson [2] used only a small portion of extract containing 0.1 mL of 0.65 M EHD for color development to avoid interference from EHD. It was considered worthwhile to see

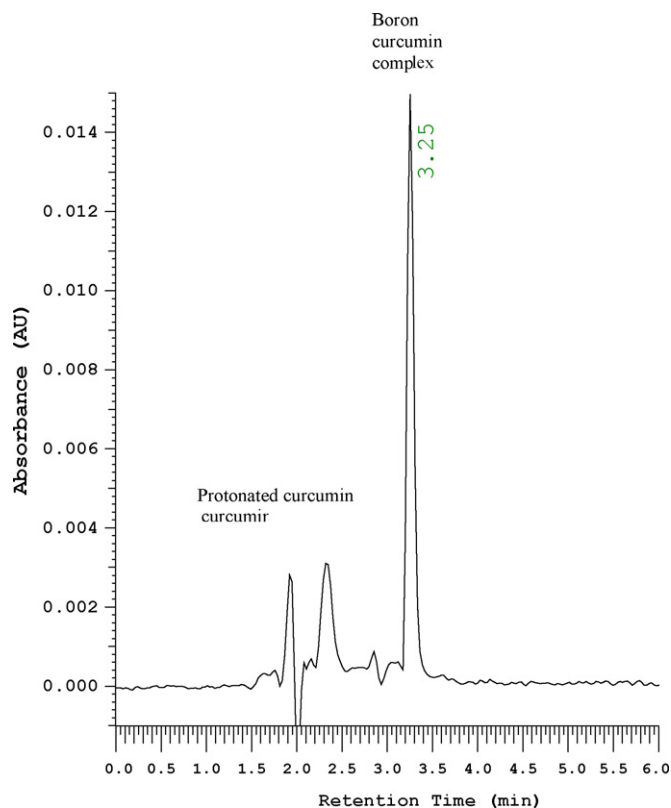


Fig. 1. Chromatogram under optimized conditions (mobile phase 0.003 M TBABr in 85% methanol, isocratic mode of elution; flow rate 0.8 mL/min, column oven temperature 35 °C, monitoring wavelength 550 nm, boron solution loaded on column 20 μ L of 5×10^{-7} M).

the effect on sensitivity by increasing the amount of extract as this would be applicable for samples with low boron content. Therefore, preliminary spectrophotometric studies were carried out to investigate the change in absorptivity, if any, due to interference from moisture and EHD. It was observed that presence of moisture above 0.25 mL and use of 3 mL of 0.65 M EHD in chloroform containing boron reduced the absorbance drastically from 1.6×10^5 L mole⁻¹ cm⁻¹. However, on heating the solution under IR to remove chloroform and moisture, the absorptivity increases to original value. The EHD and boron–EHD complex formed have low volatility (bp 244 °C) which prevents the loss of boron even if heated under an IR lamp for a period of 1 h.

3.3. Calibration curve

Aliquots with boron in the range of 0.02–0.5 μ g were used for developing the calibration curve. In view of the extraction being quantitative, direct complexation of boron standard was followed. Complexation and HPLC separation were carried out according to the procedure described above. Reagent blank was also determined under identical conditions. Peak height was used for quantification in view of the low concentration. For simplifying the calculation procedure during analysis of unknown samples, the boron amount (μ g) initially taken for complexing was used in the calibration curve instead of the amount injected

Table 1
Determination of boron in uranium oxide and aluminum samples

Sl. no.	Sample	B (ppmw)		Expected value ^a (ppmw)
		I analysis	II analysis	
1	ILCE-I (U ₃ O ₈)	0.104 ± 0.007 ^b	0.111 ± 0.005 ^b	0.21 ± 0.06
2	ILCE-II (U ₃ O ₈)	0.211 ± 0.006	0.206 ± 0.006	0.32 ± 0.14
3	ILCE-III (U ₃ O ₈)	0.566 ± 0.008	0.554 ± 0.009	0.73 ± 0.23
4	CRM-1 (U ₃ O ₈)	1.02 ± 0.02	1.09 ± 0.02	1.0 ± 0.3
5	CRM-2 (U ₃ O ₈)	1.60 ± 0.03	1.70 ± 0.02	1.6 ± 0.3
6	Al (Indal)	8.32 ± 0.08	8.40 ± 0.06	<10
7	Al (French)	6.65 ± 0.06	6.72 ± 0.08	<10

^a ILCE samples were prepared in 1982 and different methods such as emission spectroscopy, spark source mass spectrometry, atomic absorption spectrophotometry and spectrophotometry were employed for boron determination. Certified reference material, CRMs, were prepared in 1999 and characterized employing ICP-AES, DC-arc-AES and ICP-MS techniques.

^b S.D. from three independent injections.

into the column. The actual amount of boron injected and thus loaded on the column varied from 4 pg to 100 pg.

3.4. Method validation

The reagent blank was determined following exactly the same procedure as that for samples. Since, heating the acid alone could result in loss of boron [19] and thus lead to erroneous value for blank, about 5 mg of boron-free uranium/aluminum was added to the dissolving acids during the evaporation step. This helped to give accurate values for reagent blank. The reagent blank determined included boron in the dissolution acids and extraction medium. It was observed that the total amount of boron blanks varied from 0.014 µg to 0.069 µg, depending upon the quality and volume of water and acids used. These blank values can further be reduced by using ultra pure reagents obtained by sub-boiling and by improving the laboratory environment.

Table 1 gives the data on boron determination in the different samples of uranium oxide and aluminum. Columns 3 & 4 of the Table give the boron values obtained from two independent experiments. These values have been corrected for boron blank contribution. The Table also includes the expected boron concentration values in different samples. The expected values for the five uranium oxide samples are the mean of mean values obtained by different methodologies like atomic emission spectroscopy, spark source mass spectrometry and ICP-AES during inter-laboratory inter-comparison experiments (ILCE) conducted among different laboratories of the Atomic Energy Department in India during 1982 and 1999. Since, no commercially available reference materials were accessible to us, hence these ILCE samples were used for validating the HPLC methodology. As can be seen, the data obtained using HPLC are in good agreement for all the uranium oxide samples, except for the first sample, which has large uncertainty (30%) on the expected value. For the two aluminum samples, the expected values are not certified but are only indicated for information purpose. The duplicate values of boron for each sample obtained are in good agreement. Hence the above studies demonstrate the applicability of HPLC method with curcumin complex formation for the determination of boron at sub-ppm levels in uranium and aluminum samples.

4. Conclusion

Determination of boron by HPLC using curcumin as a chromogenic agent is a useful analytical technique. This hyphenated technique of HPLC and complex formation reaction is interesting because of cost performance, simplicity, versatility and availability compared to other spectroscopic techniques like ICP-MS and ICP-AES. Boron, at sub-ppm levels, can be determined by the developed methodology with a reproducibility of better than 10% in uranium and aluminum.

Acknowledgement

The authors are thankful to Dr V. Venugopal, Director, RC & I Group for his interest in the activities of Mass Spectrometry Section.

References

- [1] M.R. Hayes, J. Metcalfe, *Analyst* 87 (1962) 956.
- [2] E.M. Donaldson, *Talanta* 28 (1981) 825.
- [3] K.R. Betty, G.T. Day, *Analyst* 111 (1986) 455.
- [4] K. Takada, M. Ishikuro, K. Tozawa, M. Hosoya, K. Abiko, *Phys. Status Solidi A: Appl. Res.* 167 (2) (1998) 399.
- [5] T. Korenaga, S. Motomizu, K. Toel, *Analyst* 103 (1978) 745.
- [6] L. Zaijun, Z. Zhu, T. Jan, C.G. Hsu, P. Jiaomai, *Anal. Chim. Acta* 402 (1999) 253.
- [7] J. Lapid, S. Farhi, Y. Koresh, *Anal. Lett.* 9 (4) (1976) 355.
- [8] S. Motomizu, M. Oshima, Z. Jun, *Anal. Chim. Acta* 251 (1991) 269.
- [9] K. Satyanarayana, G.V. Ramanaih, G. Srinivasan, R.K. Malhotra, *Atom. Spectrosc. (USA)* 16 (1995) 235.
- [10] P. Fuxing, T. Dezhi, R. Ming, M. Heying, *Talanta* 40 (1993) 1107.
- [11] S. Marin, S. Cornejo, C. Jara, N. Duran, *Fres. Z. Anal. Chem.* 355 (1996) 680.
- [12] N. Demuth, K.G. Heumann, *J. Anal. Atom. Spectrom.* 14 (1999) 1449.
- [13] K. Fujimoto, M. Shimura, S. Satoh, *Mater. Trans. (Jpn.)* 43 (2) (2002) 101.
- [14] Millipore, Technical Publications, RD003 (1999).
- [15] P. Vittoz, R.A. Oliver, G. Vivier, S.A. Kerr, F. Hoyler, *Geostandard Newslett.* 11 (1987) 43.
- [16] S. Motomizu, I. Sawatani, M. Oshima, K. Toel, *Anal. Chem.* 55 (1983) 1629.
- [17] Z. Jun, M. Oshima, S. Motomizu, *Analyst* 113 (1988) 1631.
- [18] Y. Inoue, Y. Data, *Kogyo Yosui* 433 (1994) 45.
- [19] Y.K. Xiao, R.D. Voike Jr., G.H. Swihart, Y. Xiao, *Anal. Chem.* 69 (1997) 5203.

In situ electrochemical solid-phase extraction of anions and cations using polypyrrole and overoxidized sulfonated polypyrrole

Yücel Şahin*, Betül Ercan, Mutlu Şahin

Anadolu University, Faculty of Science, Department of Chemistry, 26470 Eskişehir, Turkey

Received 27 July 2007; received in revised form 22 October 2007; accepted 7 November 2007

Available online 17 November 2007

Abstract

A new method for the extraction of both anions and cations is proposed using electro-synthesized polypyrrole (PPy) and overoxidized sulfonated polypyrrole film (OSPPy). In situ anion (chloride, nitrate, sulfate) and cation (calcium, magnesium) uptake and release were examined under controlled potential conditions for prospective applications in electrochemically controlled solid-phase extraction (EC-SPE). The PPy film was used as an anode (anion-exchanger) and OSPPy film was used as a cathode (cation-exchanger) material and reverse order of the electrodes were investigated in EC-SPE. This new cell arrangement containing two ion exchanger polymer electrodes was developed to provide in situ removal of both anions and cations from aqueous solution. Simple preparation of the film coatings on a platinum plate was possible using a constant potential method. Applied positive and negative potentials facilitated the in situ extraction and desorption of ions, respectively. Both anions and cations were desorbed into sample aliquot and were determined by ion chromatography (IC). The method was validated using a standard reference material and tested for the determination of the ions in real water samples.

© 2007 Elsevier B.V. All rights reserved.

Keywords: Polypyrrole; Overoxidized sulfonated polypyrrole; Ion chromatography; Solid-phase extraction

1. Introduction

Solid-phase extraction (SPE) is based on the partitioning of the analyte between the extracting phase and the analyte matrix (water, air, etc.). In applying this method steps are often necessary in analysis of complex matrix samples to reduce the influence of interferences [1]. SPE has advantages of simplicity, low cost, ease of use and rapid pre-concentration and extraction of analytes that exist in low concentrations.

The electrochemical doping/undoping features of certain conducting organic polymer electrodes could be advantageous as SPE films for pre-concentration and matrix separation of anionic [2,3], cationic [3–5] and neutral analytes [6,7]. Polypyrrole (PPy) and its derivatives, have attracted great interest in the development of electrochemically controlled solid-phase extraction (EC-SPE) as ion exchange material for charged species [3,4,8]. The main advantage of using conducting polymers in

SPE is that the charge of the coatings can readily be controlled by oxidation and reduction of the polymers. PPy with small counterions, e.g. Cl^- , ClO_4^- , NO_3^- mainly exhibits anion-exchanger behavior due to the high mobility of these ions in the polymer matrix. Cation-exchanger behavior can be achieved by incorporating large polyanionic counter-ions, such as polystyrene sulfonate (PSS), because of their immobility in the polymer matrix [9].

Recent studies have proposed the use of overoxidized polypyrrole (OPPy) films for enhancing the selectivity towards cationics [10,11]. The overoxidized film works as a porous electrode coating, which has cation-exchange and molecular sieve properties. It has been reported that, during overoxidation, polypyrrole loses most of its electroactivity due to ejection of dopant, and oxygen-containing groups such as carbonyl and carboxylate are introduced into the pyrrole unit [12–15]. Preparation and characterization of the overoxidized sulfonated polypyrrole film as solid-phase microextraction device was extensively described in a recent work from our laboratory [16–18]. Sulfonation and overoxidation in the pyrrole ring lead to effective rejection of the anionic species and preferential collection of the cationic species.

* Corresponding author. Tel.: +90 222 3350580; fax: +90 222 3204910.
E-mail address: ysahin@anadolu.edu.tr (Y. Şahin).

A number of studies were reported on the modification of conducting polymers, especially PPy, for water purification process. Weidlich et al. developed an electrochemically switchable ion exchanger based on conducting polymers for water softening (i.e. removal of Ca^{2+} and Mg^{2+} ions). For that reason, they employed PPy modified with PSS^- counter-ions [9,19,20]. However there is no any report about using of PPy and OSPPy electrode for in situ removal of both anions and cations from water sample in the literature.

This work describes a new electrodes configuration for the use of electrochemical control of anion-exchange properties of polypyrrole and cation-exchange properties of overoxidized sulfonated polypyrrole film to obtain rapid extraction and selective determination of trace levels of chloride, nitrate, sulfate, calcium and magnesium ions by ion chromatographic system. The developed method is straightforward and suitable for the in situ extraction and analysis of anionic and cationic species in aqueous samples.

2. Experimental

2.1. Chemicals and reagents

Pyrrole (99%) was obtained from Aldrich (Milwaukee, WI, USA) and distilled before use and kept under nitrogen atmosphere. Anhydrous fluorosulfonic acid (FSO_3H , triple-distilled, Aldrich) was used as both sulfonation reagent and electrolyte in the same solution. Hydrochloric acid, acetonitrile (anhydrous), LiClO_4 , NaNO_3 , Na_2SO_4 , NaCl , $\text{Ca}(\text{NO}_3)_2$, $\text{Mg}(\text{NO}_3)_2$ were obtained from Aldrich and used without further purification. NaOH was purchased from Fluka. All solutions were prepared by appropriate dilution from stock solutions using pre-distilled $18\text{ M}\Omega\text{ cm}^{-1}$ deionized water.

2.2. Instrumentation and analytical conditions

Chromatographic measurements were carried out using a Dionex DX100 Model ion chromatography (Dionex, Sunnyvale, CA, USA), with $25\ \mu\text{L}$ sample loop, consisting of an isocratic pump, an anion separator column (Dionex IonPac AS9-SC, 4 mm) coupled with an anion self-regenerating suppressor (ASRS), for anion analysis, a cation-separation column (Dionex IonPac CS12) coupled with a cation self-regenerating suppressor (CSRS), for cation analysis, a conductivity detector and computer. The eluent used was 20 mM HCl for cation and 1.8 mM Na_2CO_3 –1.7 mM NaHCO_3 for anion separations at a flow rate of $1.0\ \text{mL min}^{-1}$.

The electrochemical instrumentation consisted of an Autolab PGSTAT-100 Potentiostat/Galvanostat with GPES software (EcoChemie, The Netherlands). A three-electrode single-compartment cell and an Ag/AgCl reference electrode were used for voltammetric measurements.

2.3. Preparation of the PPy anion-exchanger electrodes

Polymer film formation was achieved in a conventional one-compartment three-electrode cell. Ag/AgCl and a Pt were used

as a reference and counter electrode, respectively. PPy was electrochemically prepared from aqueous solutions of 0.1 M monomer (distilled pyrrole) and 0.2 M LiClO_4 as supporting electrolyte under nitrogen atmosphere on $1.0\ \text{cm} \times 0.5\ \text{cm}$ platinum foil at a constant potential of +0.80 V (vs. Ag/AgCl) during 8 min. The growth of the films was controlled based on the amount of charge passed. Prior to each electrochemical measurement, the Pt electrode was polished with an aqueous suspension of $0.05\ \mu\text{m}$ Gamma Alumina Powder (CH Instruments Inc.), washed with deionized water and alcohol to eliminate the alumina after that dried.

2.4. Preparation of the OSPPy cation-exchanger electrodes

The incorporation of sulfonate groups into polypyrrole backbone has been successfully carried out, using FSO_3H as a sulfonation reagent in the electropolymerization solution and it was extensively described in a recent work from our laboratory [16]. Electrodeposition of sulfonated polypyrrole (SPPy) was performed in acetonitrile solution of 0.1 M monomer (distilled pyrrole) and 0.01 M FSO_3H , at constant potential (+1.0 V). Our previous investigations showed that overoxidation of the SPPy films was carried out in aq. 0.1 M NaOH by cycling the potential between +0.80 and +1.200 V at a scan rate of $20\ \text{mV s}^{-1}$ [17,18]. The overoxidation process was monitored by the following current decay and continued until the current was approximately leveled off. All experiments were run at room temperature.

2.5. In situ EC-SPE of anions and cations

The PPy and OSPPy films were washed with water to remove excess electrolyte and pyrrole before the experiments. Then, both PPy and OSPPy electrodes were immersed the same target solution as an anode and as a cathode for in situ anion and cation extraction, respectively. The optimum potentials for uptake (+0.75 V) and release (−0.50 V) of the ions were found, respectively, in our previous work and summarized in Table 1 [17,18,21]. After extraction, each electrode was washed with water, and then transferred to different 10 mL cells containing 0.01 M LiClO_4 solutions.

3. Results and discussion

3.1. Electrochemical behavior of PPy, SPPy and OSPPy films

Cyclic voltammetric behavior of PPy, SPPy and OSPPy are compared in monomer free solution in Fig. 1 where quite dif-

Table 1
Optimized experimental conditions for in situ EC-SPE for Cl^- , NO_3^- , SO_4^{2-} , Ca^{2+} and Mg^{2+} determination

Uptake potential (V)	+0.75
Release potential (V)	−0.50
Uptake time (min)	3
Release time (min)	4

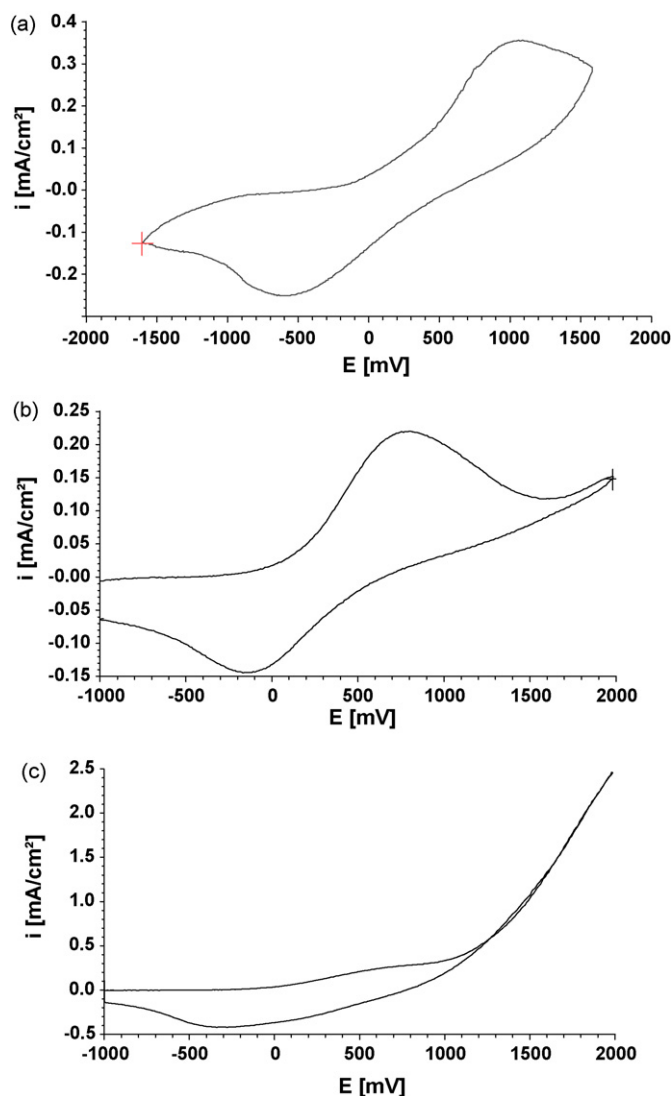


Fig. 1. Cyclic voltammetric behavior of (a) polypyrrole, (b) sulfonated polypyrrole, and (c) overoxidized sulfonated polypyrrole in 0.1 M LiClO_4 aqueous solution of LiClO_4 (monomer free solution) with a scan rate at 100 mV s^{-1} .

ferent behavior is seen. Fig. 1(a) shows the electrochemical behavior of polypyrrole in 0.1 M LiClO_4 solution. A broad oxidation peak was observed at the peak potential of +0.90 V. A responsible reverse cathodic peak was seen at a peak potential of -0.60 V (vs. Ag/AgCl). In contrast for sulfonated polypyrrole, the oxidation peak was shifted to more cathodic and the reduction peak was shifted to more anodic potentials (Fig. 1(b)) due to insertion of the SO_3^- groups into the polypyrrole chains. The sulfonic acid groups are covalently bonded to the polypyrrole structure in the SPPy (self-doped) [16–18]. These acidic anionic groups act as counter anions as well. So there is no need to use an external doping anion in the polymer structure. Therefore, the counter-ion change during reduction and oxidation occurred between pyrrole units and covalently bonded sulfonic acid groups. This interaction involves the fast transfer of charge in the SPPy chain and causes a shift of the oxidation and reduction peaks according to PPy. Briefly, the electron transfer reaction is easier in SPPy than PPy. Because of the

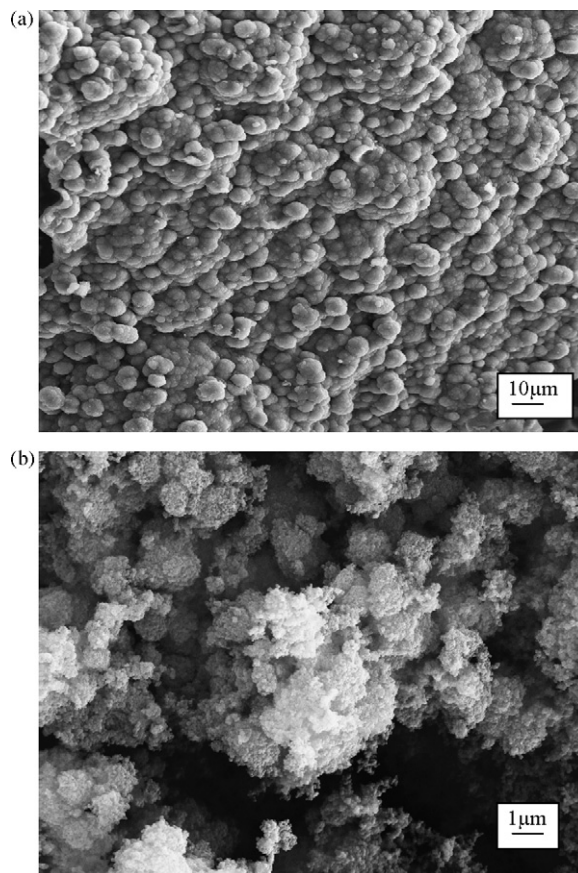


Fig. 2. Scanning electron micrographs of the (a) PPy and (b) OSPPy films at 5000 magnification.

overoxidation process, the OSPPy film lost its conductivity and electroactivity. Fig. 1(c) shows the decrease of electroactivity of OSPPy film.

3.2. Surface morphology

The morphologies of both PPy and OSPPy film were investigated by scanning electron microscopy (SEM). The pictures (Fig. 2) clearly show that sulfonation and overoxidation affect the morphological properties of the polymer films. The OSPPy film has more porous structure with smaller particle diameter (<200 nm). The PPy film shows typical “cauliflower” morphology that has approximately $5 \mu\text{m}$ particle diameters. Decreasing the conductivity and electroactivity of the film by overoxidation process led to an important difference in anion and cation uptake selectivity. The stability and robustness of the OSPPy film was better than the PPy film.

The extraction capacity of a device for an anion and/or cation will be limited by the concentration of analyte in matrix and volume of the polymer film. When the polymer films are coated onto a solid electrode material, as is the case in our study (Pt), it would indeed be difficult to describe the diffusion of ions from one side of the film to the other. The accumulation of the analyte ions can occur at the outer part and in the inner part of the film because of its porosity. The dopant ions (ClO_4^-) used in the electropolymerization of pyrrole could be acted as

a molecular template, and it was removed from the electrode surface during the extraction process. The pores can be used for extraction of the analyte ions. The polymer film thickness influences the extraction efficiency due to the increased surface area. Thickness is effective on the surface area up to a certain value due to porous structure of the film. It does not mean that the extraction capacity and sensitivity increased with increasing the thickness of the coating up to limitless. After certain thickness value diffusion limitation starts to limit the extraction amount. The thickness of the polymer film was measured by the charge passed through the electropolymerization process according to the literature data [22]. The polymer coatings used in this study are about 122 μm .

3.3. EC-SPE of both anions and cations with new cell arrangement

The optimum conditions for electrochemically solid-phase extraction of cations [17,18] and anions [21] on the extracted amounts of ions was extensively described in our recent works. In the present work, we used those parameters which were given in Table 1 for in situ anion and cation extraction.

The polymer films (PPy and OSPPy) were washed with water for in situ solid-phase extraction of anions and cations. The films were then transferred to 10 mL sample of aqueous target solutions for extraction, by applying +0.75 V potential (Figs. 3(a) and 4(a)). After completion of the in situ extrac-

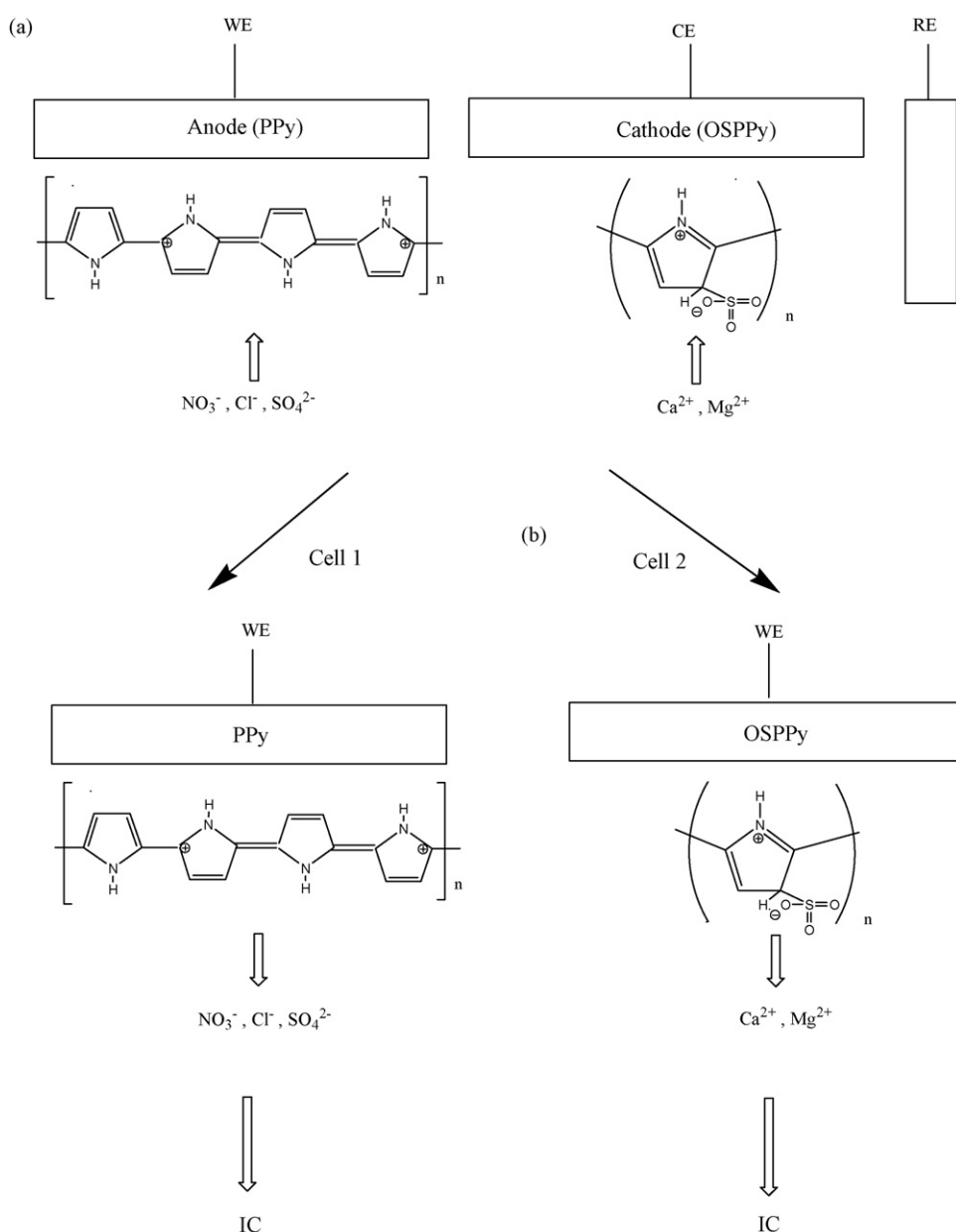


Fig. 3. Scheme of the in situ electrochemically controlled solid-phase extraction process with PPy and OSPPy film electrodes: (a) extraction and (b) desorption of ions.

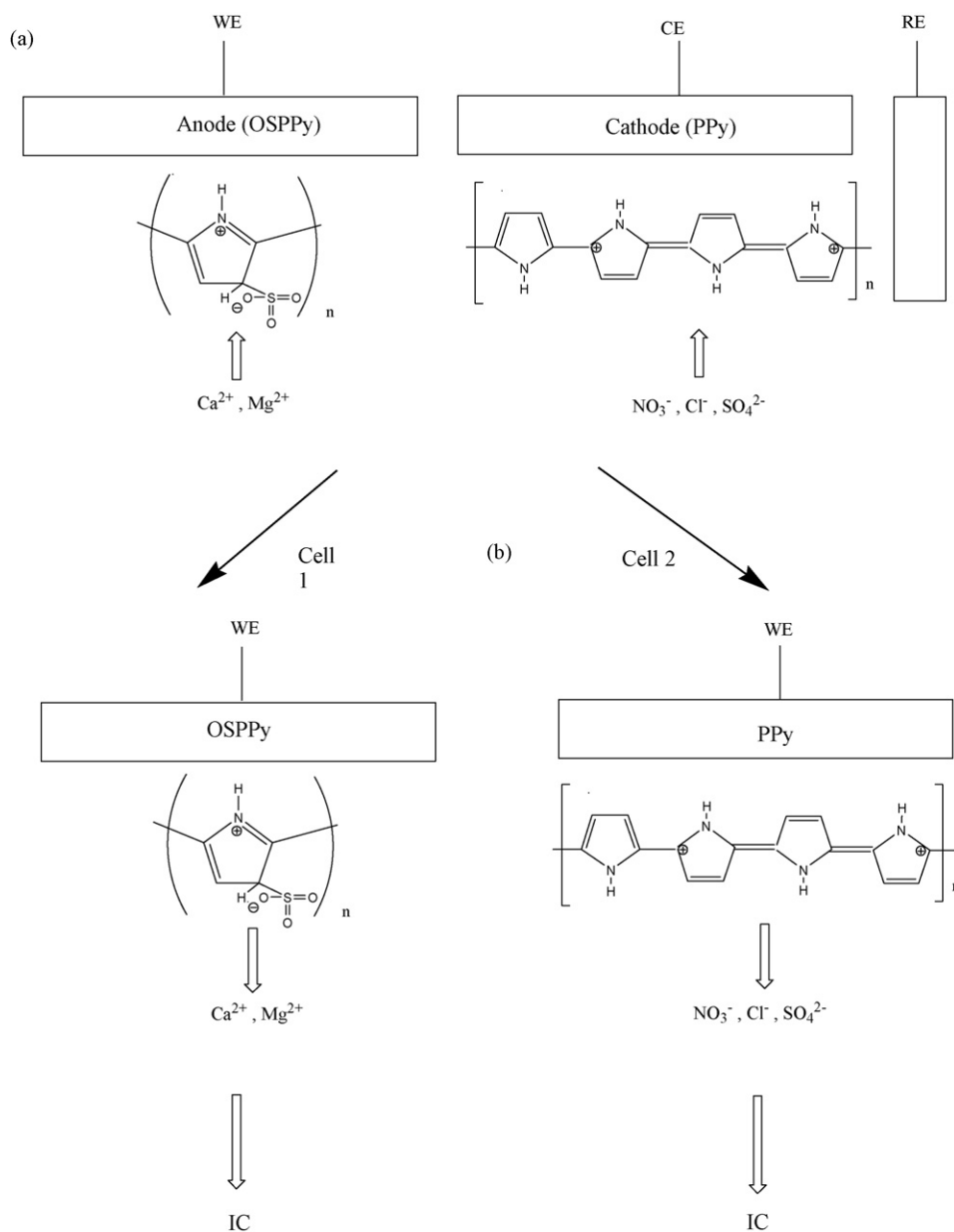


Fig. 4. Scheme of the in situ electrochemically controlled solid-phase extraction process with PPy and OSPPy film electrodes: (a) extraction and (b) desorption of ions.

tion process, the electrodes were washed with water, and then transferred to two different cells (Cell 1 and Cell 2 in Figs. 3(b) and 4(b)) for desorption process of the extracted anions and cations at -0.50 V potential. These processes were summarized in Figs. 3 and 4. The amount of extracted ions was determined by ion chromatography system.

Conducting polymers, especially PPy, were used for water purification process in a few papers in the literature. Weidlich et al. developed an electrochemically switchable ion exchanger based on PPy modified with PSS^- counter-ions [9,19,20] for water softening (i.e. removal of Ca^{2+} and Mg^{2+} ions). In the reduced state of PPy the negative charges of the anionic sulfonyl groups of PSS are compensated by the absorption of cations from the surrounding solution. During oxidation of polypyrrole, the positive charges on the PPy chain are compensated by the

anionic sulfonyl groups and the cations are desorbed back into the solution. However, removal of anions was not worked in those studies. There is also no report about using of PPy and OSPPy electrodes for in situ removal of both anions and cations from water samples in the literature. In this configuration, not only the electrode configuration is new but also using of OSPPy electrode in situ electrochemical solid-phase extraction process is new and reported for the first time. It is also superior to the others in that any membrane was not used to divide the ion-exchanger electrodes in the cell. This configuration provides the low cost, economic advantages compared to conventional ion-exchangers, ease of modification, renewal, and miniaturization. In situ EC-SPE of anions and cations process can be achieved by an anion-exchanger (PPy) and a cation-exchanger (OSPPy) electrode. PPy film was used as an anode and OSPPy film was

used as a cathode material in this work (Fig. 3(a)). We did not use any membrane to divide the ion-exchanger electrodes in the electrochemical cell. For in situ EC-SPE, the anion-exchanger PPy electrode was oxidized and positive charged were formed on the PPy chain and thus takes up Cl^- , NO_3^- , SO_4^{2-} ions from the solution. The cation-exchanger OSPPy electrode was reduced simultaneously and negative charged were formed on the OSPPy chain and takes up Ca^{2+} and Mg^{2+} ions from the same solution. The PPy has been used to control release a variety of anions. The anions and cations are firstly electrochemically entrapped into PPy and OSPPy films, respectively, during oxidation (Fig. 3(a)) and then released during electroreduction (Fig. 3(b)). This process is based on the electrochemical oxidation and reduction of the PPy and OSPPy, respectively. The cation-exchanger behavior of OSPPy can be achieved by incorporating oxygen-containing groups such as hydroxyl, carbonyl and carboxylate into the pyrrole unit with the loss of cationic charge on the pyrrole nitrogen [12–15]. The attachment of negatively charged groups to the pyrrole ring induces the cation-exchange and anion-exclusion properties of the polymer film. Ionic exchangeability feature of the film plays an important role in the uptake and release processes.

To determine the effect of overoxidation and sulfonation of the polymer on the extraction efficiency for Ca^{2+} and Mg^{2+} ions, the PPy was first overoxidized (OPPy) and sulfonated (SPPy). Then SPPy was overoxidized (OSPPy) as explained in the experimental section. It was found that the cation uptake capacity increased with increasing the negative charge on the polymer chain. The polymers with a higher effective negative charge will tend to be absorbed quickly by electrochemically extraction within the pores of the polymers. The results showed that the highest cation uptake capacity was obtained by OSPPy (Table 2). The cation uptake capacity order of $\text{PPy} < \text{OPPy} < \text{SPPy} < \text{OSPPy}$ as observed in this work is well

Table 2

The effect of overoxidation and sulfonation of the PPy on the extraction efficiency for Ca^{2+} and Mg^{2+} ions

Polymer	Extraction efficiency (%) for Ca^{2+} and Mg^{2+} ions
PPy	5–10
OPPy	10–22
SPPy	14–30
OSPPy	22–45

justified. The results clearly show that sulfonation and overoxidation greatly influence the cation uptake capacity for OSPPy film.

After this part of the work, we changed the sequence of the polymer electrodes, PPy was used as a cathode and OSPPy was used as an anode, to compare the extraction efficiency of the electrode materials was shown in Fig. 4(a). In this configuration, only the charge of the polymers was changed by controlling the electrode potential. Considering the cation uptake efficiency of the polymers, the OSPPy film electrode exhibits higher efficiency for Ca^{2+} and Mg^{2+} ions (Fig. 3) compared to those of OSPPy film electrode (Fig. 4). According to the extraction performance of PPy film towards the anions, the extracted amount of the anions on PPy anode (Fig. 3(a)) was higher than that of PPy cathode (Fig. 4(a)). From these results we decided to use the PPy as an anode and OSPPy as a cathode material for in situ EC-SPE process of anions and cations in the analysis of real water samples.

Calibration curves of anions (Cl^- , NO_3^- and SO_4^{2-}) and cations (Mg^{2+} and Ca^{2+}) (constructed by spiking of the ions to be extraction matrices) for PPy and OSPPy films and their corresponding data are listed in Tables 3 and 4, respectively. These values were obtained from IC by using aqueous samples of analytes. From these results we concluded that PPy and OSPPy

Table 3

Calibration curves for ion chromatographic measurements of chloride, nitrate and sulfate ions after EC-SPME process for PPy^a

Anions	Linear range ^b ($\mu\text{g mL}^{-1}$)	R^2	% R.S.D. ^c	Extraction efficiency (%)	Limit of detection ^d (ng mL^{-1})
Cl^-	1–100	0.983	5.43	26.6	1
NO_3^-	3–70	0.995	4.41	40.2	3
SO_4^{2-}	5–60	0.999	4.11	14.4	4

All data points represent the average of five replicate. Uptake and release volumes are 10 mL.

^a PPy film was used as an anode.

^b Based on linear plot of concentration vs. IC signal.

^c % R.S.D. calculated from five separate experiments.

^d Three times of the standard deviation of blank measurements.

Table 4

Calibration curves for ion chromatographic measurements of magnesium and calcium ions after EC-SPME process for OSPPy^a

Cations	Linear range ^b ($\mu\text{g mL}^{-1}$)	R^2	% R.S.D. ^c	Extraction efficiency (%)	Limit of detection ^d (ng mL^{-1})
Mg^{2+}	2–80	0.999	5.10	22.5	2.0
Ca^{2+}	2–90	0.995	4.40	38.7	2.0

All data points represent the average of five replicate. Uptake and release volumes are 10 mL.

^a OSPPy film was used as a cathode.

^b Based on linear plot of concentration vs. IC signal.

^c % R.S.D. calculated from five separate experiments.

^d Three times of the standard deviation of blank measurements.

Table 5

Amount of anions and cations extracted from Porsuk River (Eskişehir) using the PPy and OSPPy electrodes

Ions	Amount of extracted ion ($\mu\text{g mL}^{-1}$) ^a	% R.S.D. ^b
Cl ⁻	0.79	6.50
NO ₃ ⁻	2.42	7.31
SO ₄ ²⁻	3.50	5.76
Mg ²⁺	0.55	6.10
Ca ²⁺	2.12	6.80

^a Obtained by ion chromatographic measurements.

^b % R.S.D. calculated from three separate experiments.

Table 6

Amount of anions and cations extracted from Eskişehir tap water using the PPy and OSPPy electrodes

Ions	Amount of extracted ion ($\mu\text{g mL}^{-1}$) ^a	% R.S.D. ^b
Cl ⁻	0.63	6.50
NO ₃ ⁻	2.25	6.31
SO ₄ ²⁻	0.42	7.76
Mg ²⁺	0.24	6.10
Ca ²⁺	0.78	6.80

^a Obtained by ion chromatographic measurements.

^b % R.S.D. calculated from three separate experiments.

films could reliably be used as EC-SPE electrode materials for anions and cations, respectively.

3.4. Real water samples

In situ electrochemically controlled solid-phase extraction of anions and cations was applied to two real water samples, Porsuk River (Eskişehir, Turkey) and tap water of Eskişehir, using IC method according to procedure given in the experimental section and obtained data were given in Tables 5 and 6. Electrochemical measurements were carried out in a one-compartment electrochemical cell. The real water samples were only filtered before analysis and no other purification process was applied to the water samples. After the EC-SPE step, an aliquot of final extraction were injected into the IC system to test the new cell arrangement for removal of both anions and cations.

4. Conclusions

The electroactivity and reversible redox properties of conducting polymers, especially PPy, have attracted great interest in the development of electrochemically controlled separation systems for charged species. The results of the present study clearly show that in situ EC-SPE of anions and cations process can be achieved by using of two type of conducting polymers as an anion-exchanger (PPy) and as a cation-exchanger (OSPPy). For in situ EC-SPE, the anions and cations are firstly electrochemically entrapped into PPy and OSPPy films, respectively, during oxidation and then released during electroreduction. This process is based on the electrochemical oxidation and reduction of the polymer films. As the present technique allows poten-

tial controlled steps from the extraction step to the release step the described approach offers increased control over the whole extraction procedure. Sulfonation and overoxidation in the pyrrole ring lead to effective rejection of the anionic species and preferential collection of the cationic species. The method can be more developed by using larger electrode size and different polymer films. Further studies on the variations of polymer synthesis conditions, film thickness, linearity of response and quantitative kinetics of uptake and release, etc. are underway. The developed method is straightforward and suitable for the in situ extraction and analysis of both anionic and cationic species in aqueous samples. The anion-exchange properties of PPy and cation-exchange properties of OSPPy provides an alternative way for future designing of water purification system.

Acknowledgements

Financial support of Anadolu University Research Found (project no: 031064) is gratefully acknowledged. Y. Şahin would like to thank to Servet Turan and Hilmi Yurdakul for taking the SEM picture of the polymer films.

References

- [1] J. Pawliszyn, Solid Phase Microextraction: Theory and Practice, Wiley-VCH, New York, 1997.
- [2] T.P. Gbatu, Ö. Ceylan, K.L. Sutton, J.F. Rubinson, A. Galal, J. Caruso, H.B. Mark Jr., Anal. Commun. 36 (1999) 203.
- [3] J. Wu, W.M. Mullet, J. Pawliszyn, Anal. Chem. 74 (2002) 4855.
- [4] J. Wu, X. Yu, H. Lord, J. Pawliszyn, Analyst 125 (2000) 391.
- [5] K.R. Tamsamani, Ö. Ceylan, S. Öztemiz, T.P. Gbatu, B.J. Yates, A.M. Stalcup, H.B. Mark Jr., W.J. Kutner, Solid State Electrochem. 6 (2002) 494.
- [6] B.J. Yates, K.R. Tamsamani, Ö. Ceylan, S. Öztemiz, T.P. Gbatu, R. LaRue, U. Tamer, H.B. Mark Jr., Talanta 58 (4) (2002) 739.
- [7] U. Tamer, B. Yates, A. Galal, T. Gbuta, R. LaRue, C. Schmiesing, K. Tamsamani, Ö. Ceylan, H.B. Mark Jr., Microchim. Acta 143 (2003) 205.
- [8] G. Liljegren, J. Petersson, E.K. Markides, L. Nyholm, Analyst 127 (2002) 591.
- [9] C. Weidlich, K.-M. Mangold, K. Jüttner, Electrochim. Acta 50 (2005) 5247.
- [10] A. Jaramillo, L.D. Spurlock, V. Young, A. Brajter-Toth, Analyst 124 (1999) 1215.
- [11] Z. Gao, M. Zi, B. Chen, J. Electroanal. Chem. 373 (1994) 141.
- [12] F. Beck, P. Braun, M. Oberst, Ber. Buns. Phys. Chem. 91 (1987) 967.
- [13] A. Witkowsky, M.S. Freund, A. Brajter-Toth, Anal. Chem. 63 (1991) 622.
- [14] T.-F. Kang, G.-L. Shen, R.-Q. Yu, Talanta 43 (1996) 2007.
- [15] C. Hsueh, A. Brajter-Toth, Anal. Chem. 66 (1994) 2458.
- [16] Y. Şahin, A. Aydın, Y.A. Udum, K. Pekmez, A. Yıldız, J. Appl. Polym. Sci. 93 (2004) 526.
- [17] U. Tamer, Y. Şahin, N. Ertaş, Y.A. Udum, K. Pekmez, A. Yıldız, J. Electroanal. Chem. 570 (2004) 6.
- [18] U. Tamer, N. Ertaş, Y. Udum, Y. Şahin, K. Pekmez, A. Yıldız, Talanta 67 (2005) 245.
- [19] C. Weidlich, K.-M. Mangold, K. Jüttner, Electrochim. Acta 47 (2001) 741–745.
- [20] C. Weidlich, K.-M. Mangold, K. Jüttner, Synth. Met. 119 (2001) 263–264.
- [21] Y. Şahin, B. Ercan, M. Şahin, J. Appl. Polym. Sci., in press.
- [22] M. Hepel, J. Electrochem. Soc. 145 (1998) 124.

Study on acetate ion recognition and sensing in aqueous media using a novel and simple colorimetric sensor and its analytical application

Jie Shao^a, Hai Lin^b, Ming Yu^a, Zunsheng Cai^a, Huakuan Lin^{a,*}

^a Department of Chemistry, Nankai University, Weijin Road 94#, Tianjin 300071, PR China

^b Key Laboratory of Functional Polymer Materials of Ministry of Education, Nankai University, Tianjin 300071, PR China

Received 27 August 2007; received in revised form 13 November 2007; accepted 16 November 2007

Available online 3 January 2008

Abstract

A new and simple phenylhydrazone-based sensor 1 for acetate has been investigated in DMSO and even in the 95:5 DMSO/H₂O (v/v) mixtures. Binding of anions such as AcO⁻, F⁻ and H₂PO₄⁻ results in a noteworthy change in the visible region of spectrum (approximately 100 nm red shift), which can be detected by the ‘naked-eye’. The further insights to the nature of interactions between the sensor 1 and AcO⁻ were investigated by ¹H NMR titration experiments in DMSO-*d*₆. In particular, analytical application and detection of acetate ion have been also studied in the aqueous. © 2007 Elsevier B.V. All rights reserved.

Keywords: Colorimetric; Acetate sensor; Aqueous solution

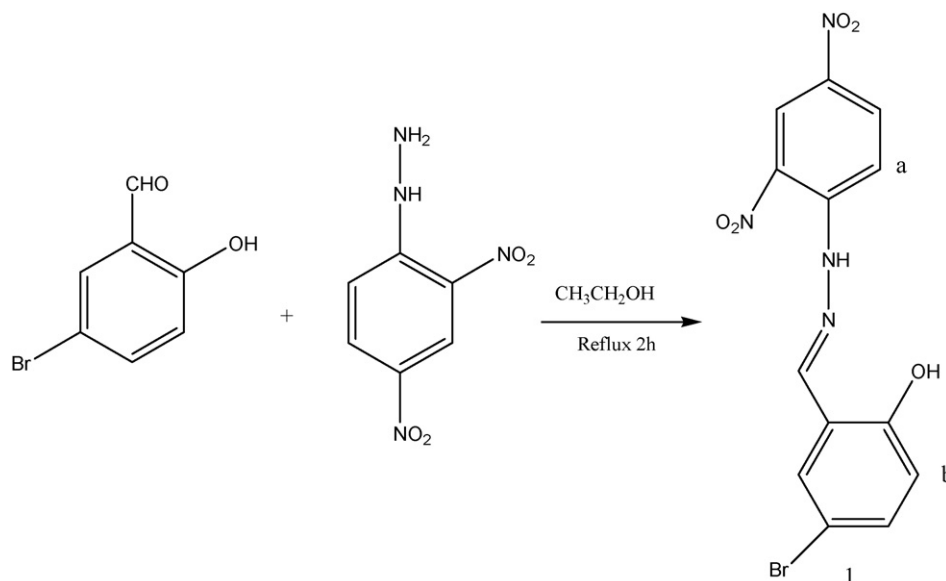
1. Introduction

Over the past few years, the recognition and sensing of inorganic and biotic anions have been a key research area of supramolecular chemistry [1,2] owing to anions’ fundamental role in the environment, biological systems, and the clinic and so on. In particular, the carboxylate anions [3] exhibit specific biochemical behaviors in the enzymes and antibodies and are also critical components of numerous metabolic processes. So the recognition and sensing of acetate ion is considered to be more important than the other biologically functional anions. In this connection, we [4] found recently that the phenylhydrazone-based indole receptor was an effective sensor for acetate ion in dry DMSO. Cheng et al. [5] showed that the pyrrole- and cysteine-based cyclopeptido-mimetics were able to bind fluoride and acetate ions well in CH₃CN. Besides, BF₂ complexes of fluorinated dipyrrolyldiketone derivatives were also proven to be efficient receptors for acetate anions by Maeda and Ito [6].

Despite these remarkable achievements, there are still many disadvantages in large numbers of examples throughout the literature. For example, the recognition or/and sensing of anions only ever occurred in the noncompetitive organic solvents [4–7] (e.g. DMSO, CH₃CN, etc.) but not in the competitive protic solvents such as H₂O, CH₃CH₂OH. Or there were no color changes [5] in the titration experiments at all. Consequently, there is a need to develop receptors capable of anion binding within competitive media, which is simultaneously accompanied with the ‘naked-eye’ color changes [8]. The sensors based on anion-induced changes in color in aqueous media appear particularly attractive because they offer the potential in many biological and analytical applications. A common approach to obtain such anions receptors is that functional groups such as amine [9], urea/thiourea [10], –OH [7,11] as well as pyrrole [12] are covalently [13] or noncovalently [14] linked to chromophoric groups.

In this paper, we designed and synthesized a new and simple phenylhydrazone-based receptor which was a charge-neutral colorimetric chemosensor. The sensing of the biologically important AcO⁻, H₂PO₄⁻ and F⁻ anions was achieved in aqueous solution by virtue of forming the hydrogen bonding at charge-neutral sites. In addition, the anion binding was

* Corresponding author. Tel.: +86 22 23502624; fax: +86 22 23502458.
E-mail address: hklin@nankai.edu.cn (H. Lin).

Scheme 1. General synthetic routes to the target compound **1**.

accompanied by a visually notable color change, giving ‘naked-eye’ anion sensing.

2. Experimental

2.1. Apparatus

^1H NMR spectra were obtained on a Varian UNITY Plus-400 MHz Spectrometer using tetramethylsilane (TMS) as an internal standard. ESI-MS was performed with a MARINER apparatus. C, H, N elemental analyses were made on an elemental vario EL. UV–vis spectra were recorded on a Shimadzu UV2450 Spectrophotometer with a quartz cuvette (path length = 1 cm).

2.2. Reagents

Unless otherwise specified, all reagents for synthesis were obtained commercially and were used without further purification. In the titration experiments, all the anions were added in the form of tetra-*n*-butylammonium (TBA) salts, which were purchased from Sigma–Aldrich Chemical, stored in a vacuum desiccator containing self-indicating silica and fully dried before using. DMSO was dried with CaH_2 and then distilled in reduced pressure.

2.3. General method

All experiments were carried out at 298 K, unless otherwise mentioned. UV–vis spectra were measured using an UV–vis spectrophotometer, UV2450 (Shimadzu Corp., Kyoto, Japan). A 2.0×10^{-4} M solution of the compound **1** in DMSO was prepared and stored in the dry atmosphere. This solution was used for all spectroscopic studies after appropriate dilution. Solutions of 1.0×10^{-2} M tetrabutylammonium (TBA) salts of the respective anions were prepared in dried and distilled DMSO and were

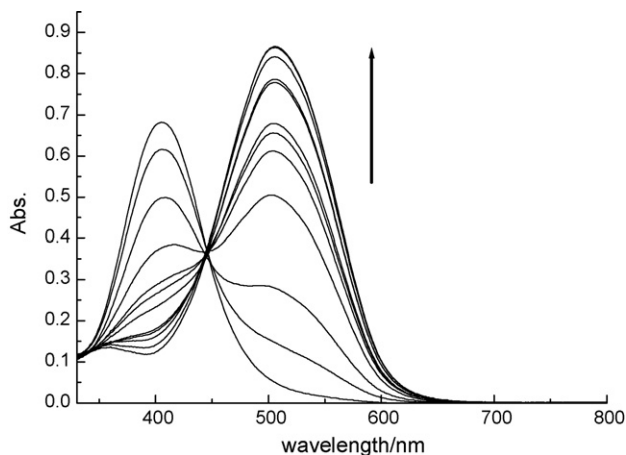


Fig. 1. UV–vis spectrum changes of receptor **1** (2×10^{-5} M) upon addition of fluoride ion in DMSO:H₂O mixtures at 298.2 ± 0.1 K.

stored under a dry atmosphere. Then, the mixture of 0.2 ml solution of the receptor **1**, given amount of anions and 0.25 ml H₂O (H₂O would be not added when titrations were carried out in dry DMSO) was diluted with DMSO to 5 ml, whose absorbance was tested immediately. Then affinity constants of receptor **1** for



Fig. 2. Color changes of **1** (2×10^{-5} M) upon addition of 8 equiv. of different anions in DMSO:H₂O (95:5, v/v) mixtures at 298.2 ± 0.1 K (from left to right: **1** only, **1** + AcO^- , **1** + F^- , **1** + H_2PO_4^- , **1** + Cl^- , Br^- , I^-). (For interpretation of color in this artwork, the reader is referred to the web version of the article).

Table 1
Association constants for various anions toward receptor 1 in DMSO and 95:5 DMSO/H₂O (v/v) at 298.2 ± 0.1 K, respectively

Anions ^a	AcO ⁻	H ₂ PO ₄ ⁻	F ⁻	Cl ⁻	Br ⁻	I ⁻
$K_{\text{ass}}(\text{M}^{-1})^{\text{b}}$	$5.97 (\pm 0.83) \times 10^4$	$5.38 (\pm 0.72) \times 10^3$	$9.57 (\pm 1.07) \times 10^3$	ND ^d	ND	ND
$K_{\text{ass}}(\text{M}^{-1})^{\text{c}}$	$5.31 (\pm 0.57) \times 10^3$	$1.03 (\pm 0.11) \times 10^3$	$3.16 (\pm 0.55) \times 10^3$	ND	ND	ND

^a The anions were added as their tetrabutylammonium salts.

^b K_{ass} was determined in dry DMSO.

^c K_{ass} was determined in 95:5 DMSO:H₂O solution.

^d ND indicated that the spectra showed little or no change with the addition of anion so that the association constants cannot be determined using the spectra.

anionic species were determined by non-linear fitting analyses of the titration curves according to the equation described by Valeur [15].

¹H NMR titration experiments were carried out in the DMSO-*d*₆ solution (TMS as an internal standard). A 1.0×10^{-2} M solution of the compound **1** in DMSO-*d*₆ was prepared. Then, the increased amount of acetate anion (1.0 M in DMSO-*d*₆) was added to the solution above-mentioned and ¹H NMR of the host–guest system was tested.

2.4. Synthesis of

5-bromosalicylaldehyde-2,4-dinitrophenyl-hydrazone (**1**)

The receptor **1** was synthesized according to Scheme 1. 0.198 g (1 mmol) 2,4-dinitrophenyl-hydrazine, 0.201 g (1 mmol) 5-bromosalicylaldehyde and three drops of acetic acid were dissolved in 40 ml CH₃CH₂OH and then the resulting solution was heated and refluxed for 2 h. The mixture solution was cooled to room temperature after reaction. Precipitate formed was filtered, washed twice with ethanol (2 × 5 ml) and obtained 0.30 g in 78% yield. ¹H NMR (DMSO-*d*₆) δH 11.749 (s 1H), 10.510 (s 1H), 8.90 (t 2H), 8.394 (m 1H), 8.12 (d 1H), 7.974 (d 1H), 7.445 (m 1H), 6.90 (d 1H). ESI-mass: *m/z* 381.1 (*M* + H)⁺. Elemental analysis calcd. for C₁₃H₉BrN₄O₅ (*M* = 381.14): C, 40.97; H, 2.38; N, 14.70. Found: C, 40.86; H, 2.41; N, 14.58.

3. Results and discussion

3.1. UV–vis spectral responses of **1**

First, the binding ability of receptor **1** with different anions such as CH₃CO₂⁻, H₂PO₄⁻, and halide anions (as the tetrabutylammonium salts) was investigated by UV–vis spectroscopy in dry DMSO solution. Fig. S1 (in the supplementary data) shows the UV–vis spectral changes of **1** during the titration with acetate ion. With the addition of gradual amount of acetate ions, the absorbance peak at the λ_{max} of 406 nm resulting from the π–π* transition [16] of the chromophore (2,4-dinitrophenyl-hydrazine), disappeared gradually accompanying with the formation of a new band centred at 507 nm, which was ascribed to the intramolecular charge transfer (ICT) between the anion-bond –NH or –OH units and the electron-deficient –NO₂ moiety. And the color of the sensor solution changed from yellow to red at the same time (see Fig. S3 in the supplementary data). Obviously, there was one well-defined isosbestic points at 445 nm, which indicated that there existed only one type of host–AcO⁻ complex. The spectral responses of **1** toward vari-

ety of anions such as H₂PO₄⁻, F⁻, Cl⁻, Br⁻ and I⁻ were also investigated in DMSO. H₂PO₄⁻ and F⁻ ions induced similar spectral changes with AcO⁻ ion, but Cl⁻, Br⁻ and I⁻ did not result in any spectra response (see supplementary data).

Secondly, to explore potential and analytical application of the sensor **1** for acetate, the UV–vis titrations were carried out in the 95:5 DMSO/H₂O mixtures. As we all know, the protic solvent such as H₂O and CH₃CH₂OH would compete with anions for binding sites of the host and, therefore, could disturb the interaction between host and guest. However, the surprising results from the current study were that upon addition of competitive hydrogen-bonding solvents (e.g. H₂O), the color changes were observed still. Consequently, identical titration results of **1** were obtained in aqueous (5% water) solution, where **1** showed a strong absorption band at 406 nm. Upon addition of AcO⁻, F⁻, and H₂PO₄⁻, this solution immediately gave rise to distinctive color changes, which were shown in Fig. 2 (from yellow to red), suggesting that the receptor **1** acted as a real-time, sensitive and visible colorimetric sensor. Just as Fig. 1 shows, there was a new ICT band at 507 nm and a well-defined isosbestic point at 445 nm. As for other anions tested, there were spectral responses only to H₂PO₄⁻ and F⁻ anions but not to Cl⁻, Br⁻ and I⁻ ions. This behavior clearly demonstrated that **1** was capable of sensing AcO⁻, H₂PO₄⁻ and F⁻ in highly competitive media, where the recognition was through hydrogen bonding. Recently, Peng et al. [17] reported the thiourea-based receptor in the less protic, 3% MeOH solution. And their results showed that the saturated spectroscopic absorptions could hardly be reached while 1000 equiv. of F⁻ ions was introduced and that the binding constant was determined as $K_{\text{ass}} = 3235 \text{ M}^{-1}$, which was smaller than that of the sensor **1** (5310 M^{-1}) in 5% H₂O solution. Therefore, the receptor **1** was a more effective chemosensor for these anions in aqueous solution (Fig. 2).

The stoichiometry of the host–guest interaction was confirmed to be 1:1 from the Job plot (particular, as for the acetate ion, see Fig. 3). Affinity constants of receptor **1** for anionic species (in DMSO or 95:5 DMSO/H₂O), which were shown in Table 1, were determined by non-linear fitting analyses of the titration curves according to the equation derived from the 1:1 host–guest complexation. Obviously shown in Table 1, the selectivity trend of binding affinity of anions for **1** was determined to be AcO⁻ > H₂PO₄⁻ ~ F⁻ > ~ Cl⁻ ~ Br⁻ ~ I⁻, not only in DMSO but also in the aqueous solution. Although a full understanding of the principles that govern anion recognition has not yet been achieved, it already becomes clear early on that the selectivity for special anions can be rationalized on the basis of the guest basicity and the shape complementarity between

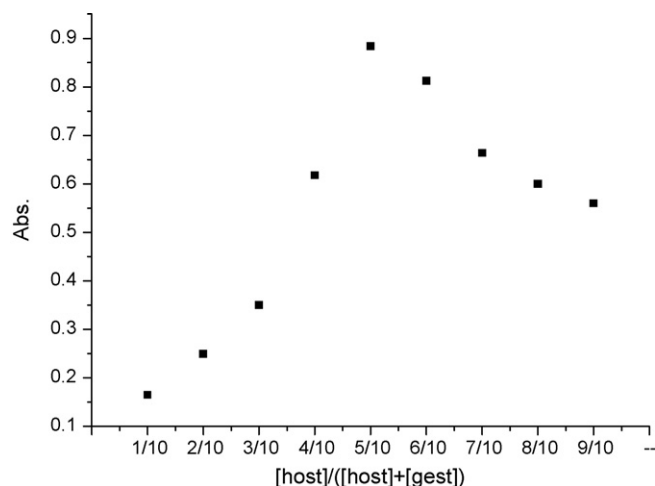


Fig. 3. The stoichiometry analysis of complex $1 \cdot \text{AcO}^-$ by Job plot analysis.

the host and the anionic guests [18]. In particular, multiple hydrogen-bonding interactions are necessary in high-affinity anion binding sites. As expected from the basicity of anions, H_2PO_4^- , F^- and AcO^- gave stronger complexation than other anions. Moreover, the acetate anion with an O–C–O angle of ca. 120° is a triangular anion and might be the fittest for the two hydrogen atoms on the binding sites of the receptor 1 among the anions tested, to form multiple hydrogen-bonding interaction (see Scheme 2). That might be the reason for why AcO^- could be recognized selectively from the other anions.

3.2. ^1H NMR titration

To further look into the nature of host–guest interactions, ^1H NMR titration experiments were conducted in $\text{DMSO}-d_6$ because of the limited solubility of 1 in $\text{DMSO}:\text{H}_2\text{O}$ (95:5, v/v) mixtures. Before discussing the spectroscopic features in detail, two effects, which were responsible for ^1H NMR changes

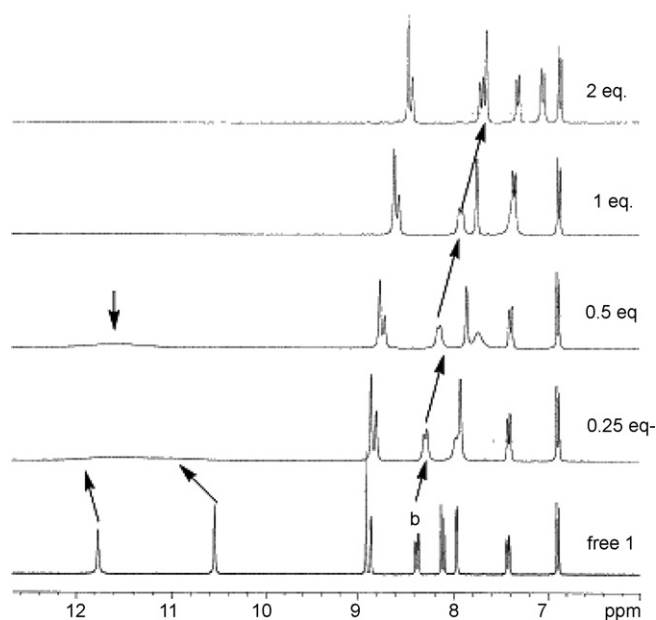
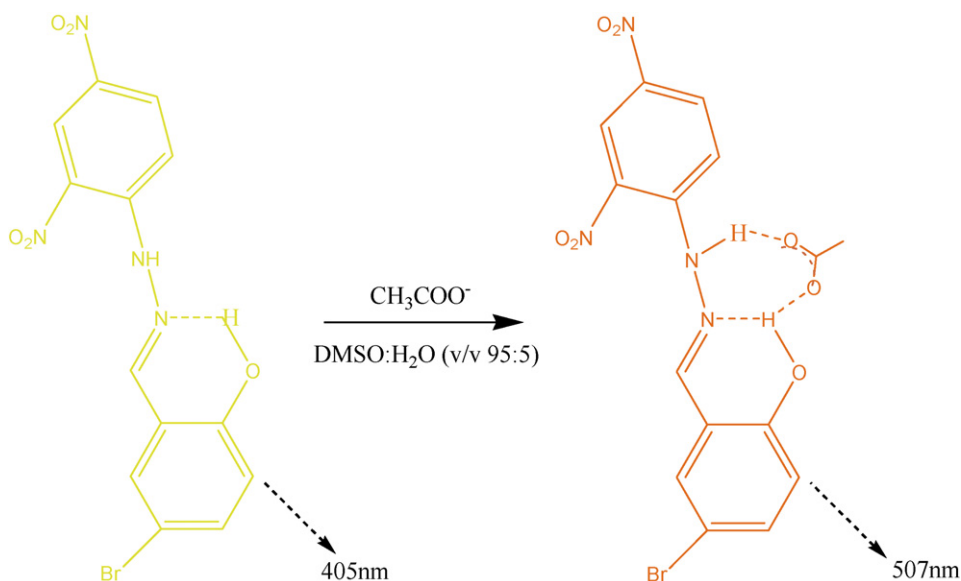


Fig. 4. ^1H NMR titration of a 1×10^{-2} M solution of 1 in $\text{DMSO}-d_6$ with $[\text{Bu}_4\text{N}]\text{AcO}$.

upon hydrogen-bond formation, should be considered [19]: (1) through-bond effects, which increase the electron density of the phenyl ring and promote an upfield shifts in NMR spectrum, and (2) through-space effects, which polarize C–H bond in proximity to hydrogen bond, create the partial positive charge on the proton and cause a downfield shifts. ^1H NMR acetate titration spectra of the sensor 1 was shown in Fig. 4. Upon addition of 0.25 equiv. of acetate ions, the peaks at 10.510 ppm and 11.749 ppm, which were assigned to –NH and –OH, respectively, shifted downfield and the signals on the phenyl rings changed slightly. This indicated the formation of a hydrogen-bonding complex at this stage. With further addition of acetate ions, the phenyl protons especially for the protons H_b shifted upfield significantly, which



Scheme 2. The proposed host–guest binding mode in solution.

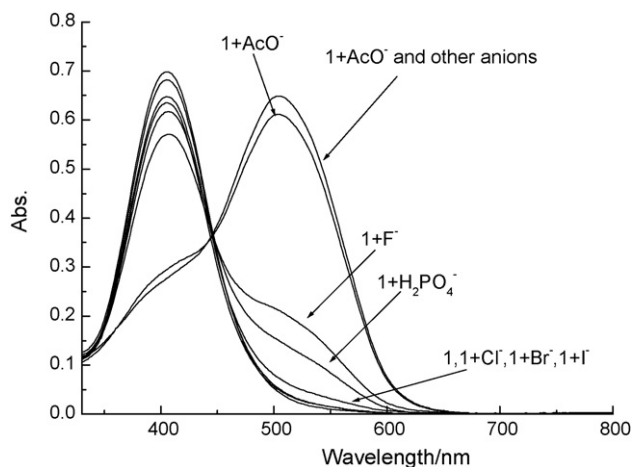


Fig. 5. UV-vis spectra of **1** (2×10^{-5} M) in 95:5 DMSO/H₂O (v/v) in the presence of 8 equiv. of AcO[−] ion and miscellaneous anions including F[−], H₂PO₄[−], Cl[−], Br[−] and I[−].

indicated the increase of the electron density on the phenyl ring owing to the through-bond effects. Simultaneously, the signals derived from the binding sites had a downshift and disappeared finally and this indicated the complete deprotonation of the receptor **1**. All the results observed indicated that there were two steps in the anions recognition process: (1) in the first step, the acetate ion exhibited a hydrogen-bonding interaction with **1**, and (2) in the second step, the deprotonation of the sensor **1** took place. Thus, the results of ¹H NMR titration also corroborated the above supposition of the interactions between the host and acetate ion.

4. Analytical application

In order to examine the potential application of the sensor for analytical chemistry, the receptor **1** has been applied in detection of biologically important anions such as acetate ion in aqueous solution. On the one hand, the color of the sensor solution is changed from yellow to red upon addition of 8 equiv. of AcO[−], H₂PO₄[−] and F[−]. However, the color induced by acetate was deep red and by H₂PO₄[−] or F[−] ions was light red, which could be easily distinguished by ‘naked-eye’ (see Fig. 2). Therefore, acetate could easily be identified among anions tested according to color changes of the sensor **1** solution. On the other hand, the analyses were performed by UV-vis titration using the method of non-linear least square fitting and the results were summarized in Table 1. Obviously, seen in Table 1, acetate could give the stronger complex than the other anions. Thus, affinity constants also provided us with another indication that AcO[−] could be detected selectively from various anions. In particular, the miscellaneous competitive anions did not lead to any significant changes in absorption spectra. Moreover, in the presence of miscellaneous competitive anions, the presence of AcO[−] ion still resulted in the similar absorption (see Fig. 5). Further, the increases of absorbance resulting from the addition of the AcO[−] ion would not be influenced by the subsequent addition of miscellaneous anions. All these indicated that the selectivity of **1** for

the AcO[−] ion over other competitive anions in aqueous medium was remarkably high and the sensor **1** would be convenient and quick application in the practical detection of anions.

5. Conclusion

In summary, we have succeeded in presenting a new kind of colorimetric chemosensor, which showed strong binding affinity as well as a good sensing ability and selectivity for acetate ion in aqueous (5% water) solution. Significantly, its sensing ability was not significantly affected by the co-presence of other biologically anions such as F[−], H₂PO₄[−], Cl[−], Br[−] and I[−]. Considering its convenience in preparation and high sensing ability for AcO[−], it is expected to be useful for detection of AcO[−].

Acknowledgement

This project was supported by the National Natural Science Foundation of China (20371028 and 20671052).

Appendix A. Supplementary data

Supplementary data associated with this article can be found, in the online version, at doi:10.1016/j.talanta.2007.11.048.

References

- [1] T. Gunnlaugsson, M. Glynn, G.M. Tocci, P.E. Kruger, F.M. Pfeffer, *Coord. Chem. Rev.* 250 (2006) 3094–3117.
- [2] E.A. Katayev, Y.A. Ustynyuk, J.L. Sessler, *Coord. Chem. Rev.* 250 (2006) 3004–3037.
- [3] T. Gunnlaugsson, A.P. Davis, J.E. O’Brien, M. Glynn, *Org. Lett.* 4 (2002) 2449–2452.
- [4] Y.H. Wang, H. Lin, J. Shao, Z.Sh. Cai, H.K. Lin, *Talanta* 74 (2008) 1122–1125.
- [5] Y.H. Zhang, Zh.M. Yin, J.Q. He, J.P. Cheng, *Tetrahedron Lett.* 48 (2007) 6039–6043.
- [6] H. Maeda, Y. Ito, *Inorg. Chem.* 45 (2006) 8205–8210.
- [7] M. Yu, H. Lin, G.H. Zhao, H.K. Lin, *J. Mol. Recogn.* 20 (2007) 69–73.
- [8] T. Gunnlaugsson, P.E. Kruger, P. Jensen, J. Tierney, H.D.P. Ali, G.M. Hussey, *J. Org. Chem.* 70 (2005) 10875–10878.
- [9] X.F. Shang, H. Lin, Z.Sh. Cai, H.K. Lin, *Talanta* 73 (2007) 296–303.
- [10] J. Shao, H. Lin, X.F. Shang, H.M. Chen, H.K. Lin, *J. Incl. Phenom. Macrocycl. Chem.* 59 (2007) 371–375.
- [11] D.A. Jose, P. Kar, D. Koley, B. Ganguly, W. Thiel, H.N. Ghosh, A. Das, *Inorg. Chem.* 46 (2007) 5576–5584.
- [12] P. Anzenbacher Jr., M.A. Palacios, K. Jursiková, M. Marquez, *Org. Lett.* 7 (2005) 5027–5030.
- [13] T.D. Thangadural, N.J. Singh, I.C. Hwang, J.W. Lee, R.P. Chandran, K.S. Kim, *J. Org. Chem.* 72 (2007) 5461–5464.
- [14] M.M. Linn, D.C. Poncio, V.G. Machado, *Tetrahedron Lett.* 48 (2007) 4547–4551.
- [15] J. Bourson, J. Pouget, B. Valeur, *J. Phys. Chem.* 97 (1993) 4552–4557.
- [16] Zh.H. Lin, Sh.J. Qu, Ch.Y. Duan, B.G. Zhang, Zh.P. Bai, *Chem. Commun.* (2006) 624–626.
- [17] F. Han, Y.H. Bao, Zh.G. Yang, T.M. Fyles, J.Zh. Zhao, X.J. Peng, J.L. Fan, Y.K. Wu, Sh.G. Sun, *Chem. Eur. J.* 13 (2007) 2880–2892.
- [18] I.V. Korendovych, M. Cho, P.L. Butler, R.J. Staples, E.V. Rybak-Akimova, *Org. Lett.* 8 (2006) 3171–3174.
- [19] M. Bonizzoni, L. Fabbrizzi, A. Taglietti, F. Tiengo, *Eur. J. Org. Chem.* (2006) 3567–3574.

Amperometric sensor for nitrite based on copper tetrasulphonated phthalocyanine immobilized with poly-L-lysine film

Aline L. Sousa^a, Wilney J.R. Santos^b, Rita C.S. Luz^b, Flavio S. Damos^b,
Lauro T. Kubota^b, Auro A. Tanaka^a, Sônia M.C.N. Tanaka^{a,*}

^a Center of Sciences and Technology, UFMA, Avenida dos Portugueses s/n, 65085-580 São Luís, MA, Brazil

^b Institute of Chemistry, UNICAMP, P.O. Box 6154, 13084-971 Campinas-SP, Brazil

Received 12 July 2007; received in revised form 5 October 2007; accepted 9 October 2007

Available online 16 October 2007

Abstract

In this work, an amperometric sensor for nitrite detection based on a glassy carbon electrode modified with copper tetrasulphonated phthalocyanine immobilized by polycationic poly-L-lysine film is presented. The modified electrode showed an excellent catalytic activity toward nitrite oxidation. A linear response range from 0.12 up to 12.20 $\mu\text{mol L}^{-1}$ was obtained with a sensitivity of 0.83 $\mu\text{A L } \mu\text{mol}^{-1}$. The detection limit for nitrite was 36 nmol L^{-1} . The repeatability of the proposed sensor, evaluated in terms of relative standard deviation, was 1% for 10 measurements of 10 $\mu\text{mol L}^{-1}$ nitrite solution. Finally, the developed sensor was applied for nitrite determination in water samples and the results were in agreement to the comparative method. The average recovery for the samples was 101 (± 4)%.

© 2008 Published by Elsevier B.V.

Keywords: Nitrite; Copper tetrasulphophthalocyanine; Poly-L-lysine; Amperometric sensor; Electrocatalytic oxidation

1. Introduction

Nitrite is commonly used as an additive in some foods, is present in soils, water and in physiological systems, playing an important role. However, it is a precursor of *N*-nitrosamines, which has been proved to be carcinogenic [1,2]. The potential toxicity of nitrite has intrigued many specialists [3]. Considering its use as fertilizer, the environmental impact caused by the contamination of water sources is nowadays under investigation [4].

Since its determination is important for environmental and public health, many methods have been developed in recent years [4–7], which some of them involves laborious and time-consuming procedures [8,9]. In contrast, owing to the rapid response and simple use, electrochemical detection techniques might be favorable for the nitrite determination [5,10].

Although nitrite is electroactive at carbon electrodes, its redox process occur with low sensitivity. In addition, the electrochemical nitrite determination is susceptible to the interference from

other readily reducible or oxidizable compounds, depending on the electrochemical route. Recently, the anodic nitrite determination has attracted great attention because it offers several advantages, namely no interference from nitrate and molecular oxygen, which are usually the major limitations in the cathodic determination of nitrite. Also, the electrochemical reduction of nitrite yield several products depending on the electrode conditions and nature of the catalyst employed, while its oxidation is a straight forward reaction, with nitrate being the final product [11].

In this context, the development of new methods to modify the surface of low-cost electrodes with suitable electrocatalysts for nitrite oxidation is highly important to improve the electrode's sensitivity and selectivity. In an attempt to stabilize the modifiers on the electrode surfaces, poly-L-lysine has received particular attention as a simple, efficient and rapid supporting material for attaching charged catalysts [12–14]. This polyelectrolyte is able to immobilize catalysts by electrostatic attractions [15] and has opened a field of modified electrode with high stability. This phenomenon has been attributed to the electrostatic potential energy bringing the counterion close to the polymer backbone. In this way, the present work reports the development of a sensor for nitrite determination based on copper tetrasulphonated

* Corresponding author. Tel.: +55 98 21098244; fax: +55 98 21098229.
E-mail address: sonia@ufma.br (S.M.C.N. Tanaka).

phthalocyanine immobilized in a poly-L-lysine film onto glassy carbon (GC) electrode.

2. Experimental

2.1. Chemical and solutions

All used chemicals were of analytical grade. Copper (II) tetrasulfophthalocyanine (CuTSPc) was synthesized and purified according to the Weber and Busch procedure [16]. Sodium nitrite (NaNO_2) was acquired from Isifar, Rio de Janeiro, Brazil. Monobasic potassium phosphate (KH_2PO_4), sodium hydroxide (NaOH), monosodium phosphate (NaH_2PO_4), disodium phosphate (Na_2HPO_4), citric acid ($\text{C}_6\text{H}_8\text{O}_7$) and hydrochloric acid (HCl) were acquired from Merck, Rio de Janeiro, Brazil. Poly-L-lysine hydrochloride (PLL) and Sulfanilamide ($\text{C}_6\text{H}_8\text{N}_2\text{O}_2\text{S}$) were acquired from Sigma, St. Louis, USA. *N*-(1-naphthyl)ethylenediamine dihydrochloride was acquired from Furlab, São Paulo, Brazil. All solutions were prepared with water purified in a Milli-Q Millipore system and the actual pH of the buffer solutions were determined with a Corning pH/Ion Analyser model 350.

2.2. Electrochemical measurements

The voltammetric and amperometric measurements were carried out with a potentiostat PGSTAT 30 from Echo Chemie (Utrecht, Netherlands) coupled to a PC microcomputer. An electrochemical cell containing 10.0 mL of buffer solution with a saturated calomel electrode (SCE) as reference, a Pt wire as auxiliary and a modified GC with 4 mm diameter were used for all measurements. In the NO_2^- determination aliquots of 75 μL of the sample were added into the measurement cell and several additions of 20 $\mu\text{mol L}^{-1}$ standard solution were performed to the electrochemical cell. The current density for each addition was recorded.

2.3. Spectrophotometric measurements

The obtained results for the NO_2^- determination with the sensor were compared to the Griess method (spectrophotometric) [17]. The spectrophotometric measurements were performed with a HP 8425 spectrophotometer using a cell with 1 cm path length. Next, sulphanilamide and *N*-(1-naphthyl)-ethylenediamine solutions were added into 200 μL of the samples and the absorbance of the resulting solutions were measured at 540 nm.

2.4. Electrode preparation

A glassy carbon (GC) electrode acquired from Metrohm-Switzerland, with geometrical area of 0.126 cm^2 was used for the sensor preparation. Prior to the modification, the electrode surface was treated, according to the procedure described by Rocha et al. [18]. After cleaning the electrode, the layers were prepared on the electrode surface by drop-casting transferring 15 μL of a CuTSPc solution with concentrations of 0.3, 0.5, 0.8, 1.0 and 1.5 mmol L^{-1} and PLL solution with concentrations of

Table 1

Influence of [CuTSPc] used in the film preparation on the peak current obtained with the sensor in phosphate buffer solution (pH 7.0) containing 10 $\mu\text{mol L}^{-1}$ NO_2^-

[CuTSPc] (mmol L^{-1})	I_p (μA)
0.3	11.19
0.5	11.53
0.8	12.24
1.0	13.07
1.5	12.98

[PLL] = 0.02 mmol L^{-1} . Scan rate: 0.015 V s^{-1} .

0.02, 0.04, 0.12, 0.16 and 0.32 mmol L^{-1} , to the electrode surface and let to dry at 80 °C temperature for 8 min. The solutions of CuTSPc and PLL were prepared with deionized water.

3. Results and discussion

3.1. Influence of CuTSPc and PLL amounts on the sensor response

Initially, the influence of the amount of CuTSPc and PLL on the electrode response for nitrite was investigated by using cyclic voltammetry (CV). Table 1 presents the dependence of the CuTSPc amount on the peak current obtained with the sensor for nitrite. The amount of CuTSPc was investigated by modifying the electrode with a solution containing different concentrations of CuTSPc (0.3, 0.5, 0.8, 1.0 and 1.5 mmol L^{-1}) and a fixed concentration of PLL (0.02 mmol L^{-1}). The best responses were obtained with 1.0 mmol L^{-1} CuTSPc solution and, therefore, such concentration was chosen for membrane preparations. In the next step, the influence of PLL concentration on the sensor response was investigated with 0.02, 0.04, 0.12, 0.16 and 0.32 mmol L^{-1} solutions and CuTSPc concentration fixed at 1.0 mmol L^{-1} . The results presented in Table 2 shows a better response of the sensor with a PLL concentration of 0.12 mmol L^{-1} . Lower PLL concentrations produced smaller and unstable responses, which was attributed to CuTSPc leaching out from the PLL film, since the amount of PLL was insufficient for CuTSPc immobilization. On the other hand, PLL concentrations higher than 0.12 mmol L^{-1} produced a slight decrease in the sensor's response, suggesting that high amounts of PLL may form a barrier to the interactions between the analyte and CuTSPc sites as well as to the thickness effect of the formed film. Thus, glassy carbon surfaces modified with a mixture of

Table 2

Influence of [PLL] used in the film preparation on the peak current obtained with the sensor in phosphate buffer solution (pH 7.0) containing 10 $\mu\text{mol L}^{-1}$ NO_2^-

[PLL] (mmol L^{-1})	I_p (μA)
0.02	13.08
0.04	13.36
0.12	14.08
0.16	13.81
0.32	13.38

[CuTSPc] = 1.0 mmol L^{-1} . Scan rate: 0.015 V s^{-1} .

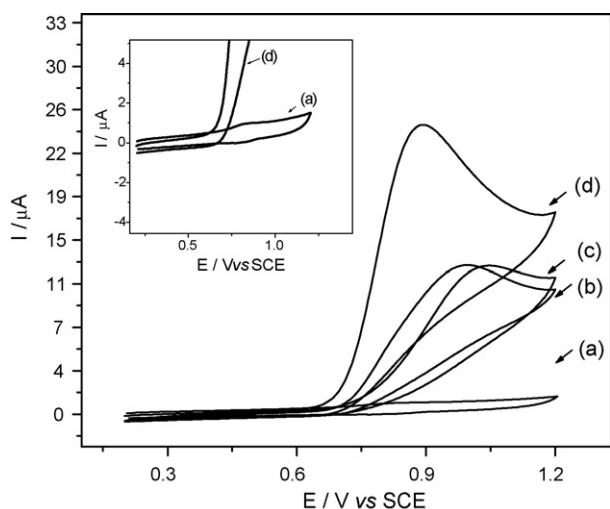


Fig. 1. Cyclic voltammograms for CuTSPc/PLL modified electrode in the absence (a) and presence (d) of $0.25 \text{ mmol L}^{-1} \text{ NO}_2^-$; for a bare GC electrode (b) and for an electrode with PLL only (c), both in presence of $0.25 \text{ mmol L}^{-1} \text{ NO}_2^-$, in 0.1 mol L^{-1} phosphate buffer solution (pH 7.0). Scan rate: 0.05 V s^{-1} . Inset: large-scale cyclic voltammograms for CuTSPc/PLL modified electrode in absence (a) and presence (d) of $0.25 \text{ mmol L}^{-1} \text{ NO}_2^-$.

1 mmol L^{-1} CuTSPc and 0.12 mmol L^{-1} PLL solutions allowed the attainment of highly stable chemically modified electrodes, with good sensitivity.

3.2. Electrocatalytic oxidation of nitrite on CuTSPc/PLL film modified electrode

Fig. 1 shows the cyclic voltammograms for the GC modified with CuTSPc immobilized on PLL in phosphate buffer (pH 7.0) solutions in absence (a) and presence of $0.01 \text{ mmol L}^{-1} \text{ NO}_2^-$ (d). For comparison, this figure also presents the behavior of bare GC electrode (b) and GC modified with PLL only (c), both in presence of nitrite. As can be seen, the best response was obtained with the GC modified with CuTSPc/PLL film (Fig. 1d). This modified electrode presented higher peak current and lower oxidation potential for NO_2^- than the bare GC and PLL modified electrodes as well as a shift of 150 mV in the peak potential toward a less positive value. This behavior suggests that the CuTSPc complex is working as catalyst for NO_2^- oxidation on the sensor surface. Indeed, the high activity of the modified GC electrode for NO_2^- oxidation in aqueous solutions can also be associated with the low-charge transfer resistance of the CuTSPc/PLL film. In order to corroborate this supposition a measurement using an electrode modified with PLL only was performed for NO_2^- oxidation. As expected, the use of this film promoted no catalyzed NO_2^- oxidation (Fig. 1c).

3.3. Influences of pH, buffer and its concentration

The influence of the solution pH in the electrochemical response for NO_2^- using 0.1 mol L^{-1} phosphate buffer at pH 5.0, 6.0, 7.0 and 8.0 was investigated. The peak current reached a maximum value at pH 7.0 as can be seen in Fig. 2a. On the other hand, the peak potential was independent on the solution

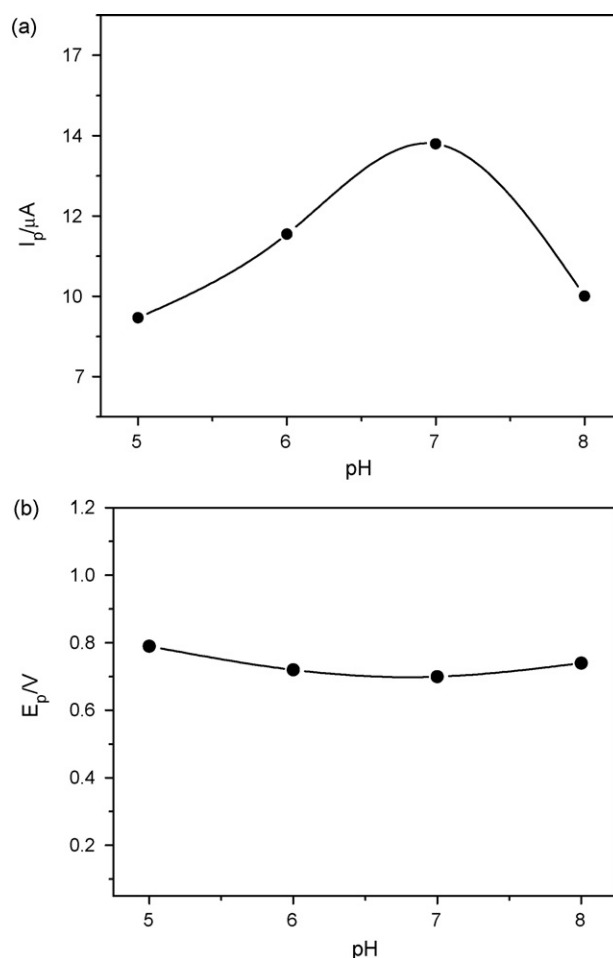


Fig. 2. Influences of pH on the peak current (a) and on the peak potential (b) obtained by CV in 0.1 mol L^{-1} phosphate buffer containing $0.01 \text{ mmol L}^{-1} \text{ NO}_2^-$. Scan rate: 0.015 V s^{-1} .

pH (Fig. 2b). Similar behavior was verified by Pournaghi-Azar et al. [19]. This can also be attributed to the kinetic of the nitrite oxidation, indicating that the catalytic step is proton independent. Similar observations were also noticed on Prussian Blue modified electrodes for nitrite and hydrazine oxidation [20].

Table 3 presents the influence of the buffer solution on the peak current obtained with the sensor for nitrite. The sensor response was verified in three different buffer solutions (MacIlvaine, phosphate, and Sørensen,) with concentrations of 0.1 mol L^{-1} and indicated that phosphate buffer solution gives the best responses. In this sense, the phosphate buffer solution was chosen for further experiments.

Table 3

Influence of the 0.1 mol L^{-1} buffer solution containing $10 \mu\text{mol L}^{-1} \text{ NO}_2^-$ on the sensor current obtained by CV

Buffer solution	I_p (μA)
MacIlvaine	10.88
Phosphate	14.04
Sørensen	7.17

Scan rate: 0.015 V s^{-1} .

Table 4

Influence of the phosphate buffer concentration on the peak current obtained by CV with the sensor in a solution containing $10 \mu\text{mol L}^{-1} \text{NO}_2^-$

[Buffer] (mol L^{-1})	I_p (μA)
0.025	6.07
0.05	8.89
0.10	14.00
0.25	13.00
0.50	12.80

Scan rate: 0.015 V s^{-1} .

Table 4 shows the peak current obtained by cyclic voltammetry for the measurements carried out in different concentrations of phosphate (0.025, 0.050, 0.10, 0.25 and 0.50 mol L^{-1}). Phosphate buffer concentrations from 0.1 up to 0.50 mol L^{-1} presented almost constant current. In this sense, the concentration of 0.1 mol L^{-1} was chosen for the further experiments because, in this concentration, a slightly higher response was observed.

3.4. Electrochemical studies of the nitrite oxidation on the modified electrode

Additional information about NO_2^- oxidation on the modified electrode surface was obtained by using the catalytic current from cyclic voltammograms. According to the theoretical model of Andrieux and Savéant [21], the catalytic current I_p depends on the potential scan rates v as follows Eq. (1):

$$I_p = 0.496 F A C_0 D_0^{1/2} \left(\frac{Fv}{RT} \right)^{1/2} \quad (1)$$

where, C_0 is the analyte concentration, D_0 represents the diffusion coefficient of the analyte, F the Faraday constant, R the gas constant and T is the temperature. Furthermore, a catalytic system can behave as a totally irreversible system controlled by diffusion for large values of kinetic parameters (*i.e.* high values of the rate constant, k) [21,22]. Therefore, a plot of the catalytic current density versus square root of the potential scan rate was plotted and resulted in a straight line (Fig. 3a), suggesting that the process is controlled by diffusion as expected for a catalytic system with high-rate constant.

Considering that a catalytic system behaves as a totally irreversible process [21,22], the number of electrons, n , involved in the overall reaction can be obtained from the slope of I_p versus $v^{1/2}$ plot according to Eq. (2) for a totally irreversible process controlled by diffusion [21,22]:

$$I_p = (2.99 \times 10^5) n [(1 - \alpha) n_a]^{1/2} C_0^* A D_0^{1/2} v^{1/2} \quad (2)$$

where α is the electron transfer coefficient, n_a represents the number of electrons involved in the rate-determining step, D_0 ($\text{cm}^2 \text{ s}^{-1}$) the diffusion coefficient of the electroactive species and C_0^* (mol cm^{-3}) is the concentration of the electroactive species. The other terms with their meanings as mentioned before. In the present study, the values of the concentration and diffusion coefficient used for NO_2^- in aqueous solution were 0.25 mmol L^{-1} and $3.7 \times 10^{-5} \text{ cm}^2 \text{ s}^{-1}$ [23], respectively.

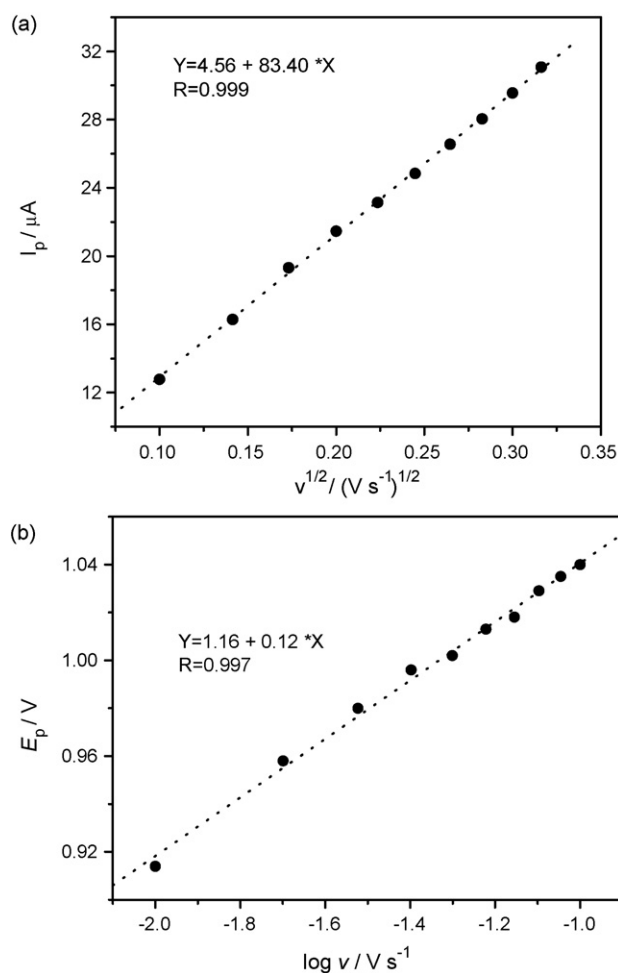


Fig. 3. Plots of I_p vs. $v^{1/2}$ (a) and E_p vs. $\log v$ (b) for CuTSPc/PLL modified electrode in 0.1 mol L^{-1} phosphate buffer (pH 7.0) containing $0.25 \text{ mmol L}^{-1} \text{NO}_2^-$. Scan rate: 0.010 – 0.100 V s^{-1} .

In addition, considering that the $(1 - \alpha) n_a$ value has to be known, one approach was employed for the NO_2^- oxidation reaction based on its dependence with the difference between the peak potential E_p and the potential of the half peak current $E_{p/2}$ given by Eq. (3) [21,22]:

$$(1 - \alpha) n_a = \frac{47.7 \text{ mV}}{E_p - E_{p/2}} \quad (3)$$

The estimated value of $(1 - \alpha) n_a$ was 0.26. Thus, using this value in Eq. (2) and the slope of the plot $91.70 \mu\text{A}/(\text{V s}^{-1})^{1/2}$ extracted from Fig. 3a, the value of $n = 2$ electrons was estimated to NO_2^- oxidation. When NO_3^- is the main product of the reaction the number of electrons should be 2, in agreement with other works also based on the catalytic oxidation of nitrite [24–26]. As can be seen, the values of $(1 - \alpha n_a)$ obtained from this approach indicates that the nitrite oxidation occur involving two electrons, in agreement with the literature, where the NO_3^- is the product [27–29]:



Table 5
Influence of applied potential on the sensor response

Potential (V) vs. SCE	Sensitivity ($\mu\text{A L } \mu\text{mol}^{-1}$)
0.74	0.75
0.80	0.79
0.84	0.83
0.90	0.81
0.94	0.78

Measurements carried out in 0.1 mol L^{-1} phosphate buffer solution (pH 7.0) containing $10 \mu\text{mol L}^{-1} \text{NO}_2^-$.

3.5. Analytical characterization

The sensor characteristics were verified by chronoamperometry. In the chronoamperometric measurements, an initial study was performed in order to determine the best potential to be applied on the electrode. The applied potential was chosen based on measurements of the catalytic current intensities in the optimized conditions and the highest current was verified at an applied potential of 0.84 V versus SCE. Table 5 shows the effects of the applied potential on the nitrite sensor response. In order to obtain an analytical curve for the developed sensor, experiments were carried out with additions of NO_2^- into 10 mL of 0.1 mol L^{-1} phosphate buffer at pH 7.0, under an applied potential of 0.84 V versus SCE (Fig. 4). Under optimized conditions the proposed sensor showed a linear response range from 0.12 up to $12.2 \mu\text{mol L}^{-1}$, which can be expressed according to the following equation (4):

$$\Delta I (\mu\text{A}) = 0.05 (\pm 0.01) + 0.83 (\pm 0.05) [\text{NO}_2^-] (\text{mmol L}^{-1}) \quad (4)$$

with a correlation coefficient of 0.999 ($n = 15$) with better sensitivity than those reported in the literature [5,10,18–20,27–29]. Such good sensitivity can be attributed to the efficiency of the

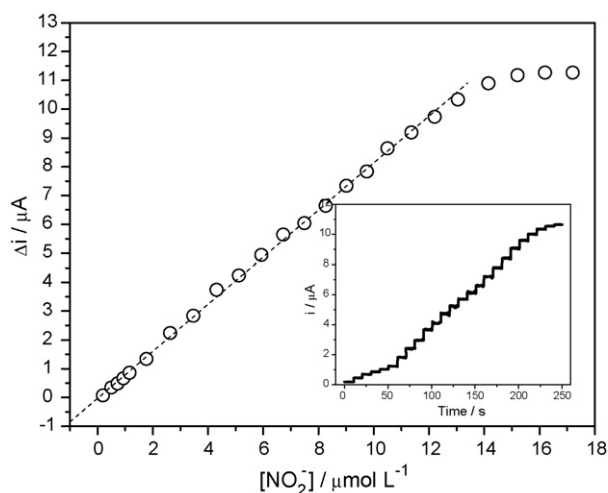


Fig. 4. Analytical curve for nitrite oxidation on CuTSPc/PLL modified electrode under optimized conditions in 0.1 mol L^{-1} phosphate buffer (pH 7.0) solutions containing 0.12 ; 0.42 ; 0.64 ; 0.86 ; 1.08 ; 1.69 ; 2.55 ; 3.39 ; 4.23 ; 5.04 ; 5.85 ; 6.64 ; 7.41 ; 8.18 ; 8.93 ; 9.67 ; 10.42 ; 11.28 ; 12.20 ; 12.96 ; 14.07 ; 15.12 ; 16.11 and $17.12 \text{ mmol L}^{-1} \text{NO}_2^-$. (Inset: amperogram of the analytical curve.) Applied potential of 0.84 V vs. SCE.

electron transfer between the modified electrode and nitrite, which can be favored by a high-reaction rate and low-charge transfer resistance of the film, as a consequence of a highly dispersed phthalocyanine in the PLL film.

A detection limit of 36 nmol L^{-1} was determined using a $3\sigma/\text{slope}$ ratio and quantification limit was 120 nmol L^{-1} using $10\sigma/\text{slope}$, where σ is the standard deviation of the mean value for ten amperograms of the blank, determined according to the IUPAC recommendations [30], which were lower than those reported in the literature.

The modified electrode presented a good repeatability for NO_2^- determinations. The relative standard deviation (R.S.D.) of the peak current for 10 determinations in phosphate buffer (pH 7.0) $10 \mu\text{mol L}^{-1} \text{NO}_2^-$ (stock solution) was 1% . Additionally, a series of ten sensors prepared in the same manner and tested at phosphate buffer (pH 7.0) containing $10 \mu\text{mol L}^{-1} \text{NO}_2^-$ gave responses with a relative standard deviation lower than 5.0% . The stability of the CoTSPc/PLL film modified electrode was checked with successive nitrite additions equivalents to $10 \mu\text{mol L}^{-1}$ in the electrochemical cell and recording the current associated to the analyte oxidation by amperometric measurements in 0.1 mol L^{-1} phosphate buffer solution at pH 7.0. After 200 measurements no significant change of the sensor response was observed for the modified electrode. Indeed, when the modified electrode was stored at room temperature no significant change in the response was observed for 1 month. These experiments indicate that the GC electrodes modified with CuTSPc/PLL films have good stability and repeatability, probably associated with the PLL's ability for fixing and protecting the CuTSPc on the electrode surface by a strong electrostatic interaction.

The effects of foreign ions on the determination of nitrite ion were investigated and the results are summarized in Table 6. The sensor response was evaluated in presence of NO_3^- , H_2PO_4^- , Cl^- , SO_3^{2-} , SO_4^{2-} , K^+ , NH_4^+ and Na^+ . As can be verified, this study reveal that the developed sensor can tolerate a high concentration of interfering ions and, therefore, can be stated as selective over the commonly present interfering ions.

3.6. Application in samples

This sensor was applied for NO_2^- determination in two natural water samples (1 and 2) in triplicate. The samples pre-

Table 6
Effect of foreign ions on the nitrite determination ($10 \mu\text{mol L}^{-1}$)

Ion added	Mole ratio 1:0.5	Mole ratio 1:1	Mole ratio 1:2
NO_3^-	98 ± 2	99 ± 3	101 ± 4
H_2PO_4^-	98 ± 2	99 ± 3	100 ± 3
Cl^-	99 ± 3	100 ± 4	101 ± 4
SO_3^{2-}	98 ± 2	100 ± 3	102 ± 3
SO_4^{2-}	99 ± 2	99 ± 4	101 ± 3
K^+	99 ± 2	98 ± 2	99 ± 3
NH_4^+	99 ± 3	100 ± 3	102 ± 4
Na^+	98 ± 3	99 ± 4	101 ± 4

Mole ratio = $[\text{NO}_2^-] : [\text{interfering ion}]$. Values \pm S.D. for six measurements. Relative response (%) obtained with the sensor.

Table 7
Nitrite determination in two samples of river water ($n=3$)

Sample	Proposed method ($\mu\text{mol L}^{-1}$)	Spectrophotometric method [17] ($\mu\text{mol L}^{-1}$)
A	0.51 (± 0.09)	0.48 (± 0.12)
B	0.55 (± 0.07)	0.52 (± 0.17)

Table 8
Recovery data of nitrite in two samples of natural water ($n=3$) obtained with the modified electrode

Samples	NO_2^- added ($\mu\text{mol L}^{-1}$)	NO_2^- expected ($\mu\text{mol L}^{-1}$)	NO_2^- found ($\mu\text{mol L}^{-1}$)	Recovery (%)
A	0.0	–	0.51 (± 0.09)	–
	0.15	0.66	0.65 (± 0.08)	99 (± 1)
B	0.0	–	0.55 (± 0.07)	–
	0.15	0.70	0.73 (± 0.06)	104 (± 4)

sented nitrite concentrations of (0.51 ± 0.09) and (0.55 ± 0.07) $\mu\text{mol L}^{-1}$, respectively. The nitrite concentration was determined using the standard addition method and the results were compared with those obtained by spectrophotometric method [17] (Table 7). The relative standard deviation of the proposed method was lower than those obtained by comparative method. In addition, applying a paired *t*-Student's test to compare such methods, it was possible to observe that, at 95% confidence level, there is no significant statistical difference between the results obtained by the comparative and the proposed method.

3.7. Recovery tests

For an additional check on the accuracy of the developed method, analytical recovery experiments were performed by adding known amounts of NO_2^- in three samples of natural water. The percentage of the recovery values were determined by comparing the concentration obtained from the samples with actual and added concentrations. The recoveries found for the samples are shown in Table 8. It can be clearly observed that a good recovery was obtained assuring accuracy with the proposed method.

4. Conclusions

The glassy carbon electrode modified with CuTSPc/PLL film exhibits a high-electrocatalytic activity to nitrite oxidation and become a feasible alternative for its analytical determination. Optimization of the experimental conditions for amperometry yielded a detection limit and sensitivity for NO_2^- , much better than those described in the literature. Indeed, this sensor showed good repeatability for the measurements and electrode preparation evaluated in terms of relative standard deviation. The proposed sensor was applied in water samples and the results were in agreement with those obtained by comparative method,

as well a good recovery average was obtained for these samples. In this sense, this work demonstrated that the glassy carbon electrode modified with CuTSPc/PLL is a sensitive, robust and stable sensor, presenting great potential for NO_2^- determination.

Acknowledgements

The authors acknowledge financial support from Fundação de Amparo à Pesquisa do Estado de São Paulo (FAPESP), Conselho Nacional de Desenvolvimento Científico e Tecnológico (CNPq) and Coordenação de Aperfeiçoamento de Pessoal de Nível Superior (CAPES). W.J.R.S., R.C.S.L and F.S.D are indebted to FAPESP for fellowships.

References

- [1] Y.G. Huang, J.D. Ji, Q.N. Hou, *Mutat. Res. Fund. Mol. Mech. Mutagen.* 358 (1996) 7.
- [2] K.K. Choi, K.W. Fung, *Analyst* 105 (1980) 241.
- [3] C.S. Bruning-Fann, J.B. Kaneene, *Vet. Hum. Toxicol.* 35 (1993) 521.
- [4] A. Aydın, O. Ercan, S. Tascioglu, *Talanta* 66 (2005) 1181.
- [5] Z.H. Wen, T.F. Kang, *Talanta* 62 (2004) 351.
- [6] A. Afkhami, M. Bahram, S. Gholami, Z. Zand, *Anal. Biochem.* 336 (2005) 295.
- [7] R. Burakham, M. Oshima, K. Grudpan, S. Motomizu, *Talanta* 64 (2004) 1259.
- [8] T. Chen, A. Tong, Y. Zhou, *Spectrochim. Acta A* 66 (2007) 586.
- [9] T. Cherian, B. Narayana, *J. Braz. Chem. Soc.* 17 (2006) 577.
- [10] L. Jiang, R. Wang, X. Li, L. Jiang, G. Lu, *Electrochem. Commun.* 7 (2005) 597.
- [11] C.A. Caro, F. Bedioui, J.H. Zagal, *Electrochim. Acta* 47 (2002) 1489.
- [12] X.E. Jiang, L.P. Guo, X.G. Du, *Talanta* 61 (2003) 247.
- [13] R.C.S. Luz, F.S. Damos, A.A. Tanaka, L.T. Kubota, *Sens. Actuators B: Chem.* 114 (2006) 1019.
- [14] R.C.S. Luz, F.S. Damos, A.B. Oliveira, J. Beck, L.T. Kubota, *Talanta* 64 (2004) 935.
- [15] M. Muthukuma, *J. Chem. Phys.* 120 (2004) 9343.
- [16] J.H. Weber, D.H. Busch, *Inorg. Chem.* 4 (1965) 469.
- [17] I. Guevara, J. Iwanejko, A. Dembiń-Kieć, J. Pankiewicz, A. Wanat, P. Anna, I. Gołbek, S. Bartuś, M. Malczewska-Malec, A. Szczudlik, *Clin. Chim. Acta* 274 (1998) 177.
- [18] J.R.C. Rocha, L. Angnes, M. Bertotti, K. Araki, H.E. Toma, *Anal. Chim. Acta* 452 (2002) 23.
- [19] M.H. Pournaghi-Azar, H. Dastangoo, *J. Electroanal. Chem.* 567 (2004) 211.
- [20] J.M. Zen, A. Senthil Kumar, H.-W. Chen, *Electroanalysis* 13 (2001) 1171.
- [21] C.P. Andrieux, J.M. Savéant, *J. Electroanal. Chem.* 93 (1978) 163.
- [22] A.J. Bard, L.R. Faulkner, *Electrochemical Methods, Fundamentals and Applications*, Wiley, New York, 1980.
- [23] A.P. Doherty, M.A. Stanley, D. Leech, J.G. Vos, *Anal. Chim. Acta* 319 (1996) 111.
- [24] A. Doménech, F.J. Torres, J. Alarcón, *Electrochim. Acta* 49 (2004) 4623.
- [25] W.S. Cardoso, Y. Gushikem, *J. Electroanal. Chem.* 583 (2005) 300.
- [26] X. Ren, P.J. Puckup, *J. Electroanal. Chem.* 420 (1997) 251.
- [27] N. Chebotareva, T. Nyokong, *J. Coord. Chem.* 46 (1999) 433.
- [28] M. Bertotti, D. Pletcher, *Anal. Chim. Acta* 337 (1997) 49.
- [29] W.J.R. Santos, A.L. Sousa, R.C.S. Luz, F.S. Damos, L.T. Kubota, A.A. Tanaka, S.M.C.N. Tanaka, *Talanta* 70 (2006) 588.
- [30] Analytical Methods Committee, *Analyst* 112 (1987) 199.

Sensitized chemiluminescence of CdTe quantum-dots on Ce(IV)-sulfite and its analytical applications

Chunyan Sun, Bin Liu, Jinghong Li*

Department of Chemistry, Key Laboratory of Bioorganic Phosphorus Chemistry & Chemical Biology, Tsinghua University, Beijing 100084, China

Received 4 August 2007; received in revised form 8 November 2007; accepted 8 November 2007

Available online 17 November 2007

Abstract

Water-soluble CdTe quantum-dots (QDs) of different sizes capped with thioglycolic acid (TGA) were synthesized via a microwave-assisted method. It was found that CdTe QDs, as a kind of sensitizer, could enhance the chemiluminescence (CL) emission from the redox reaction of SO_3^{2-} with Ce(IV) in acidic medium. In combination with the flow injection technique, the effects of reactant concentrations, the sizes of CdTe QDs, some organic compounds, and several electron transfer proteins on the CL emission were investigated in detail. The sensitized CL displayed the size-dependent effect and increased along with increasing the QDs sizes. Organic compounds containing OH, NH_2 , or SH groups, and some electron transfer proteins such as cytochrome *c*, hemoglobin and myoglobin, which readily interact with CdTe QDs, were observed to inhibit the CL signal of the Ce(IV)– SO_3^{2-} –CdTe QDs system, which made it applicable for the determination of such compounds and proteins. The CL enhancement mechanism was also discussed briefly on the basis of the photoluminescence (PL) and CL spectra. This work is not only of importance for gaining a better understanding of the unique optical and physical chemistry properties of semiconductor nanocrystals but also of great potential to find applications in many fields such as luminescence devices, bioanalysis, and multicolor labeling probes.

© 2007 Elsevier B.V. All rights reserved.

Keywords: Sensitized chemiluminescence; CdTe quantum-dots; Ce(IV)-sulfite

1. Introduction

Chemiluminescence (CL) analysis has the advantages of high sensitivity, wide linear range, simple instrumentation and no background scattering light interference, and has been extensively utilized in various fields, such as chip technique [1], drug analysis [2], environmental monitoring [3], clinical diagnose [4]. Traditionally, the study of CL was limited to molecular systems. In recent years, much attention has been paid to the CL of nano-material systems, to improve the sensitivity and the stability, mainly resulting from the high surface area and special structure of nanomaterials. Metallic and semiconducting nanoparticles represent increasingly intensively explored materials that bridge bulk material and molecular behavior and offer novel chemical properties. Many investigations have indicated that use of metal nanoparticles in CL reactions has provided new avenues to enhance the inherent sensitivity and expand new applications of

this mode of detection [5–9]. For example, Cui et al. have found that gold nanoparticles of different sizes can enhance the CL of the luminol– H_2O_2 system, originating from the catalysis of gold nanoparticles [5]. This system has been exploited to determine a range of compounds that readily react with gold nanoparticles at the nanomole per liter level with the inhibited CL. Subsequently, our group has found that specially shaped, irregular gold nanoparticles (IGNPs) display much stronger catalytic activity on luminol CL than spherical gold nanoparticles, and developed a simple and sensitive method for in situ amplified chemiluminescence detection of sequence-specific DNA and immunoassay of IgG using highly active IGNPs as labels [6].

Colloidal semiconductor nanocrystals (NCs), also called quantum dots (QDs), have attracted extensive interest in the past two decades due to their remarkable size-dependent optical and electronic properties [10]. Compared with conventional organic fluorophores, QDs offer attractive advantages including high emission quantum yields, good chemical and photo stability, size-tunable emission profiles and narrow spectral bands. They have been widely used as fluorescence biological probes [11], as donors or acceptors of fluorescence

* Corresponding author. Tel.: +86 10 62795290; fax: +86 10 62795290.
E-mail address: jhli@mail.tsinghua.edu.cn (J. Li).

resonance energy transfer [12], and in bio-imaging [13]. The reduced and oxidized NCs, generated at a certain electrochemical potential, can react through the annihilation process or react with some co-reactants to produce electrochemiluminescence (ECL) [14–20]. To the best of our knowledge, there are only a few reports involving in chemiluminescence of semiconductor nanocrystals. Talapin et al. described the CL property of CdSe/CdS core/shell nanostructure dealing with the emitting state related to the quantum-confined orbitals [21]. Our group also reported the CL of CdTe NCs directly oxidized by some oxidants, such as H_2O_2 and KMnO_4 , and its size-dependent and surfactant-sensitized effects [22]. Ren et al. have demonstrated an efficient chemiluminescence resonance energy transfer between luminol donors and CdTe QDs acceptors based on horseradish peroxidase (HRP)-QD conjugates and the immuno-reaction of the QD-BSA (bovine serum albumin) and anti-BSA-HRP in the luminol- H_2O_2 CL reaction catalyzed by HRP [23]. Recently, it has been found that H_2O_2 can directly oxidize CdS NCs to produce CL emission, and the first analytical applications of QDs CL in liquid-phase systems has been developed based on the inhibited CL by some biological molecules and metal ions [24]. Thus, it would be of great significance to explore the novel CL behavior of semiconductor QDs for developing novel CL sensors.

Most CL reactions have low quantum efficiencies and thus show weak luminescence. The weak emission can be greatly enhanced by sensitizers, normally fluorescent compounds with high quantum efficiency. Energy is transferred from the excited species to the sensitizer, emitting the characteristic radiation of the sensitizer. The oxidation of sulfite in acidic solutions using cerium(IV) or KMnO_4 is an important CL reaction, but the CL emission is quite weak. Some fluorescent compounds, such as fluoroquinolone [25], and Tb^{3+} -fluoroquinolone complexes [26], via energy transfer from the redox reaction, could enhance the CL intensity of the Ce(IV)-sulfite reaction.

In the present work, we explored the effect of CdTe QDs on the CL emitted from the cerium(IV)-sulfite reaction in combination with flow-injection analysis (FIA) technique. It was found that the addition of CdTe QDs into cerium(IV)-sulfite system could induce a great of enhancement on CL signals. The possible enhancement mechanism of CdTe QDs on cerium(IV)-sulfite CL was further investigated based on the photoluminescence and CL spectra. Organic compounds containing OH, NH_2 , and SH groups, and some electron transfer proteins such as cytochrome *c*, hemoglobin and myoglobin, were observed to inhibit the CL signal of the Ce(IV)- SO_3^{2-} -CdTe QDs system, which made it applicable for the determination of such compounds and proteins.

2. Experimental

2.1. Reagents and materials

Te powder and thioglycolic acid (TGA) were purchased from Acros Organics (Geel, Belgium). CdCl_2 , NaHB_4 , $\text{Ce}(\text{SO}_4)_2$,

Na_2SO_3 and H_2SO_4 were obtained from Beijing Chemical Reagent Company (Beijing, China). A stock solution of $1.0 \times 10^{-2} \text{ mol L}^{-1}$ Na_2SO_3 was prepared daily in water and diluted as required. The solution of $5.0 \times 10^{-4} \text{ mol L}^{-1}$ $\text{Ce}(\text{SO}_4)_2$ was prepared daily in 0.02 mol L^{-1} H_2SO_4 solution. All the reagents were of analytical grade, and double distilled water was used throughout.

2.2. Synthesis of CdTe QDs

TGA-capped CdTe QDs were synthesized as the procedure described in Refs. [27] and [28] with little modification. Briefly, N_2 -saturated CdCl_2 solution was added to NaHTe solution which was prepared by the reaction between NaHB_4 and Te powder in the presence of TGA. The concentration of Cd^{2+} was 2.0 mM, and the molar ratio of $\text{Cd}^{2+}:\text{Te}^{2-}:\text{TGA}$ was fixed at 1:0.5:2.5. After mixing, the solution was heated with microwaves for different time. The sizes of the CdTe QDs could be tuned by simply varying the heating time.

For the purified CdTe QDs samples, the free CdCl_2 and TGA were removed via dialysis for 2 days in 0.01 M NaOH solution according to the procedure in Ref. [22]. A dialysis membrane with a molecular weight of cutoff 7000 was used for the purification of CdTe QDs.

2.3. Apparatus

Chemiluminescence detection was conducted on the MPI-B type flow-injection ultraweak luminescence analyzer (Remax Electronic Science and Technology Co. Ltd., Xi'an, China). The photoluminescence spectra and UV-vis absorption spectra of CdTe QDs were measured by a LS-550 fluorophotometer (PE Elmer, UK) and a model UV-2100s spectrophotometer (Shimadzu, Japan), respectively. The CL spectra of the proposed systems were measured by inserting a series of high-energy cut-off optical filters (460, 490, 535, 555, 575, 620, 640 nm) between the flow CL cell and the PMT.

2.4. Chemiluminescence measurements

Fig. 1(A) depicts the schematic diagram for the flow injection chemiluminescence detection system used in this work. Two peristaltic pumps, P1 and P2, were respectively used to deliver CdTe QDs sample and the other reactant solutions. Polytetrafluoroethylene (PTFE) tubing (0.8 mm i.d.) was used to connect all components in the flow system. CdTe QDs sample injection (50 μL) was operated using a six-way injection valve, allowing 20 s for sampling step and 30 s for sample injection step, which was automatically operated by the microcomputer. In order to decrease consumption of CdTe QDs, the rotate speed of P1 was set at 20 r/min at the sampling step and 2 r/min at the sample injection step. The carrier, cerium(IV) and sulfite solutions were introduced into the manifold at equal flow rate with the rotate speed of P2 fixed at 90 r/min to carry out the fast Ce(IV)- SO_3^{2-} -CdTe QDs CL reaction. By keeping the valve in the sampling position, water as the carrier, cerium(IV) and sulfite solutions were continuously pumped, mixed, and the weak CL

radiation emitted from this reaction was continuously recorded as the baseline. Then in the sample injection procedure, CdTe QDs colloid solution was injected into the stream of carrier, and mixed with Na_2SO_3 and then with Ce(IV), finally reached the flow cell to produce CL emission. The distance between the mixing position and the flow cell was about 9 cm. The flow cell was made by organic glass with microchannels of about 1 mm and located directly facing the window of the CR-105 photomultiplier tube (PMT, Hamamatsu, Japan) which monitored the CL signals. Static CL detection for the CL reactions was carried out using a colorless glass beaker (10 mL) as the detection cell. CdTe QDs and sulfite solutions were placed into the glass beaker, then Ce(IV) solution was injected into the beaker using an injector through the rubber plug in the lid of detector of the luminescence analyzer. Data acquisition and treatment were performed with MPI-B software running under Windows XP.

The schematic diagram for the investigation of effects of organic compounds or proteins on the Ce(IV)– SO_3^{2-} –CdTe QDs system is shown in Fig. 1(B). The values of $\Delta I = (I_0 - I)$ show their effects on the CL intensity, where I_0 and I stand for the signals without and with organic compounds or proteins, respectively.

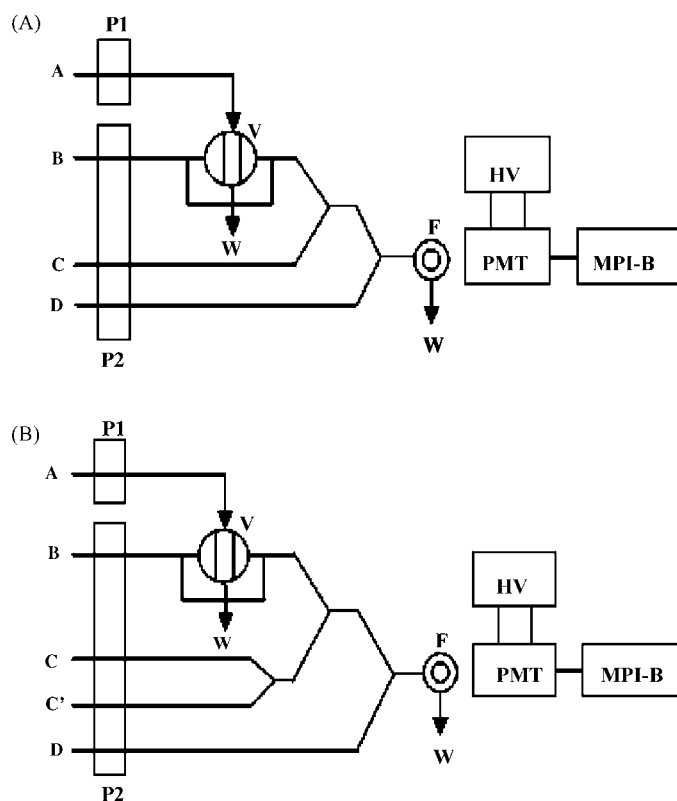


Fig. 1. Schematic diagram of flow-injection chemiluminescence detection systems for (A) the investigation of CL mechanism and (B) the investigation of effects of organic compounds or proteins. Key: A, CdTe QDs solution; B, H_2O ; C, SO_3^{2-} solution; C', organic compound solution; D, Ce(IV) solution; P1, P2, peristaltic pump; V, injection valve; F, flow cell; W, waste; HV, negative high voltage; PMT, photomultiplier tube; MPI-B, luminescence analyzer controlled by personal computer.

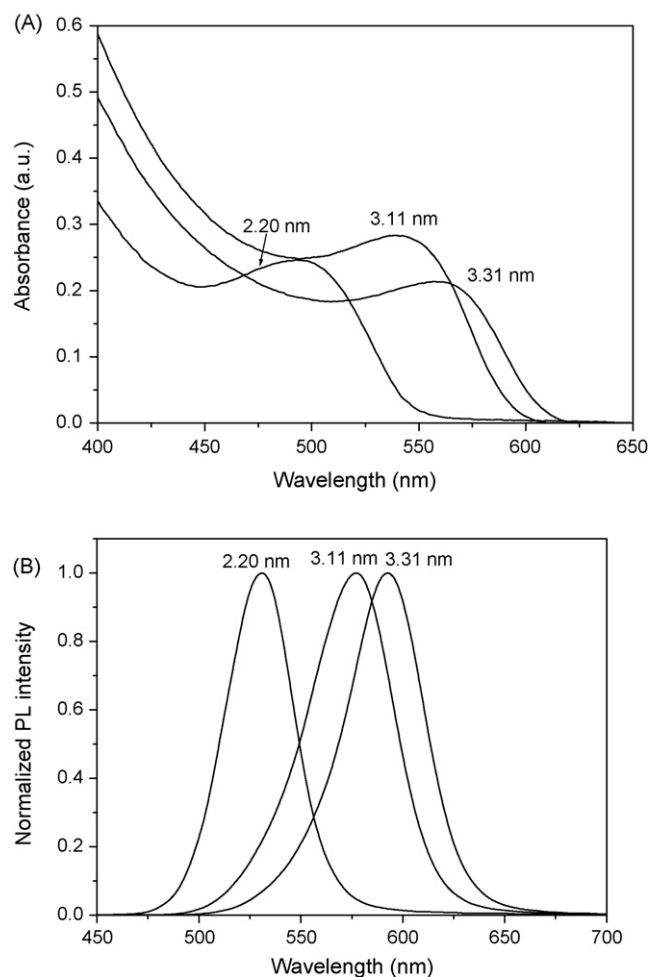


Fig. 2. Absorption spectra (A) and photoluminescence spectra (B) of CdTe QDs with different sizes. The excitation wavelength is 400 nm.

3. Results and discussion

3.1. Absorption and photoluminescence spectra of CdTe QDs

Using a microwave-assisted synthetic process, we prepared different sized, water-soluble, TGA-stabilized CdTe QDs, and their absorption and photoluminescence (PL) spectra are shown in Fig. 2(A) and (B), respectively. These CdTe QDs possessed a relative well-resolved absorption maximum of the first electronic transition. According to the literature calculation method [29], the particle sizes of the as-prepared CdTe QDs are calculated in virtue of the following expression: $D = (9.8127 \times 10^{-7})\lambda^3 - (1.7147 \times 10^{-3})\lambda^2 + (1.0064)\lambda - 194.84$. In the above equation, D (nm) is the size of a given nanocrystal sample, and λ (nm) is the wavelength of the first excitonic absorption peak of the corresponding sample. The results show that the particle diameters of the prepared CdTe QDs are around 2.20, 3.11 and 3.31 nm, respectively, corresponding to the first excitonic absorption peaks of 495, 539 and 557 nm. The PL spectra of these CdTe QDs exhibited the peaks at 531, 577 and 593 nm, respectively. The absorption maximum and photoluminescence peak shifted to longer wavelengths with

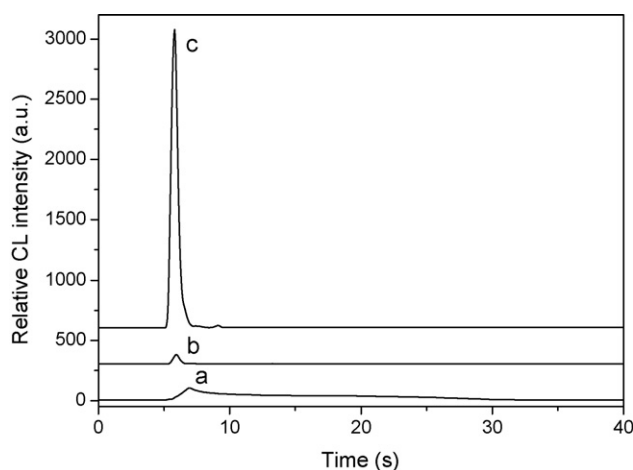


Fig. 3. Dynamic CL intensity–time profiles of Ce(IV)–SO₃²⁻ (a), Ce(IV)–CdTe QDs (b) and Ce(IV)–SO₃²⁻–CdTe QDs (c) CL reactions in static-injection mode. Conditions: 2.0 mL 2.0 × 10⁻⁴ M Ce(IV) in 0.001 M H₂SO₄ was injected into a mixture of 1.0 mL SO₃²⁻ (or water) and 0.1 mL 0.2 mM 3.11 nm CdTe QDs solution (or water). High voltage, –600 V.

increasing QDs sizes as a consequence of quantum confinement effects.

3.2. Chemiluminescence of Ce(IV)–SO₃²⁻–CdTe QDs

The effects of CdTe QDs on the Ce(IV)–SO₃²⁻ CL system were firstly investigated with 3.11 nm CdTe QDs in static-injection mode, and the obtained CL kinetic curves are shown in Fig. 3. The results indicated that Ce(IV) could directly oxidize sulfite or CdTe QDs to generate weak CL emission (Fig. 3, curves a and b), but the CL signal of Ce(IV)–SO₃²⁻ system could be remarkably enhanced in the presence of CdTe QDs (Fig. 3, curve c). Control experiments, including free CdCl₂, TGA, and Cd(TGA) complex solutions with the same concentrations as those used in the synthesis of CdTe QDs, were also carried out to explore the origins of the enhancement. The obtained results demonstrated that these coexisting substances had no contribution to the enhancement effect, and the purified CdTe QDs sample via a dialysis procedure had greater CL enhancement effects on Ce(IV)–SO₃²⁻ system than the unpurified sample. Therefore, the CL enhancement for Ce(IV)–SO₃²⁻ system was ascribed to CdTe QDs, and all the CdTe QDs used throughout were purified via dialysis. Moreover, the CL intensity-time profiles (Fig. 3) confirmed that the CL reactions were very quick and the maximum emission intensity was attained within 0.9 s for Ce(IV)–SO₃²⁻ system and 0.6 s for Ce(IV)–SO₃²⁻–CdTe QDs system after initiating the reactions. The presence of CdTe QDs not only enhanced the CL intensity but also increased the rate of light emission.

3.3. Optimization of the reaction conditions

A series of experiments were conducted to establish the optimum reaction conditions for the Ce(IV)–SO₃²⁻–CdTe QDs CL system in a FIA-CL mode using 1.0 mM 3.11 nm CdTe QDs. The parameters optimized included reagent concentrations and

some physical variables such as flow rate and the mixing tube length.

The flow injection configuration can be designed to provide three different reaction sequences for examining the CL signal generated by the sensitizing effect of CdTe QDs on the oxidation of sulfite by Ce(IV). Optimal CL emission profile was obtained only when the CdTe QDs sample was injected into water, mixed with sodium sulfite and then with Ce(IV) in H₂SO₄ medium prior to the detector, as shown in Fig. 1(A). The CL emission from Ce(IV)–SO₃²⁻–CdTe QDs was a flash-type emission, and therefore it was apparently controlled by the mixing speed, namely the rotate speed of pump P2 in the present experiment. The effect of rotate speed of pump P2 on the CL intensity is shown in Fig. 4(A). The CL intensity increased sharply with increasing rotate speed from 20 to 90 r/min, and only slightly increased at higher speed. So the rotate speed of P2 was selected as 90 r/min for the subsequent assays. For the purpose of obtaining the maximum CL signal in the flow cell, a mixing tube (0.8 mm i.d.) connected between the mixing position and the flow cell. The length of the mixing tube was examined in the range 5–30 cm, and the optimal length of the mixing tube was about 9 cm.

In sulfuric acid solution, cerium(IV) is highly stable and does not require any special precaution to prevent the decomposition. Therefore, sulfuric acid was used in the present work. The influence of H₂SO₄ concentration in Ce(IV) solution on the CL intensity was tested in the range of 0.005–1.0 mol L⁻¹, as shown in Fig. 4(B). The most suitable H₂SO₄ concentration for Ce(IV)–SO₃²⁻–CdTe QDs CL system was 0.02 mol L⁻¹. When the H₂SO₄ concentration exceeded the 0.02 mol L⁻¹ level, a simultaneous decrease of CL intensity was observed.

The effect of sulfite concentration on CL emission was investigated over the range of 0–2.0 × 10⁻² mol L⁻¹ (Fig. 4(C)), and the CL intensity increased as the sulfite concentration increased from 0 up to 1.0 × 10⁻³ mol L⁻¹, after which the intensity started to decrease. Therefore, the optimum sulfite concentration was chosen to be 1.0 × 10⁻³ mol L⁻¹. The effect of Ce(IV) concentration upon the CL intensity was examined in the range of 0.01–1.0 mmol L⁻¹ in 0.02 mol L⁻¹ H₂SO₄ (Fig. 4(D)). The CL intensity increased with the increasing Ce(IV) concentration below 5.0 × 10⁻⁴ mol L⁻¹, and then decreased with further increases of Ce(IV) concentration, which may be explained that the excess of Ce(IV) might absorb a significant amount of the emitted light. Therefore, 5.0 × 10⁻⁴ mol L⁻¹ Ce(IV) concentration was used for subsequent work.

Size effect is a basic characteristic of semiconductor nanocrystals. A mass of reports have demonstrated the size-dependent property of semiconductor nanocrystals [29–33], and an experiment investigating the size effect on CL response was conducted in the present work. Under the optimized conditions for the FIA-CL mode, the response of above-mentioned different sized CdTe QDs to the Ce(IV)–SO₃²⁻–CdTe QDs CL system was investigated, as shown in Fig. 5. It was found that the CL intensity gradually increased as the particle size of CdTe QDs increased, indicating that CL of CdTe QDs had size-dependent effect in the present CL system. The size-dependent character of QDs CL has been reported in the direct oxidation chemilu-

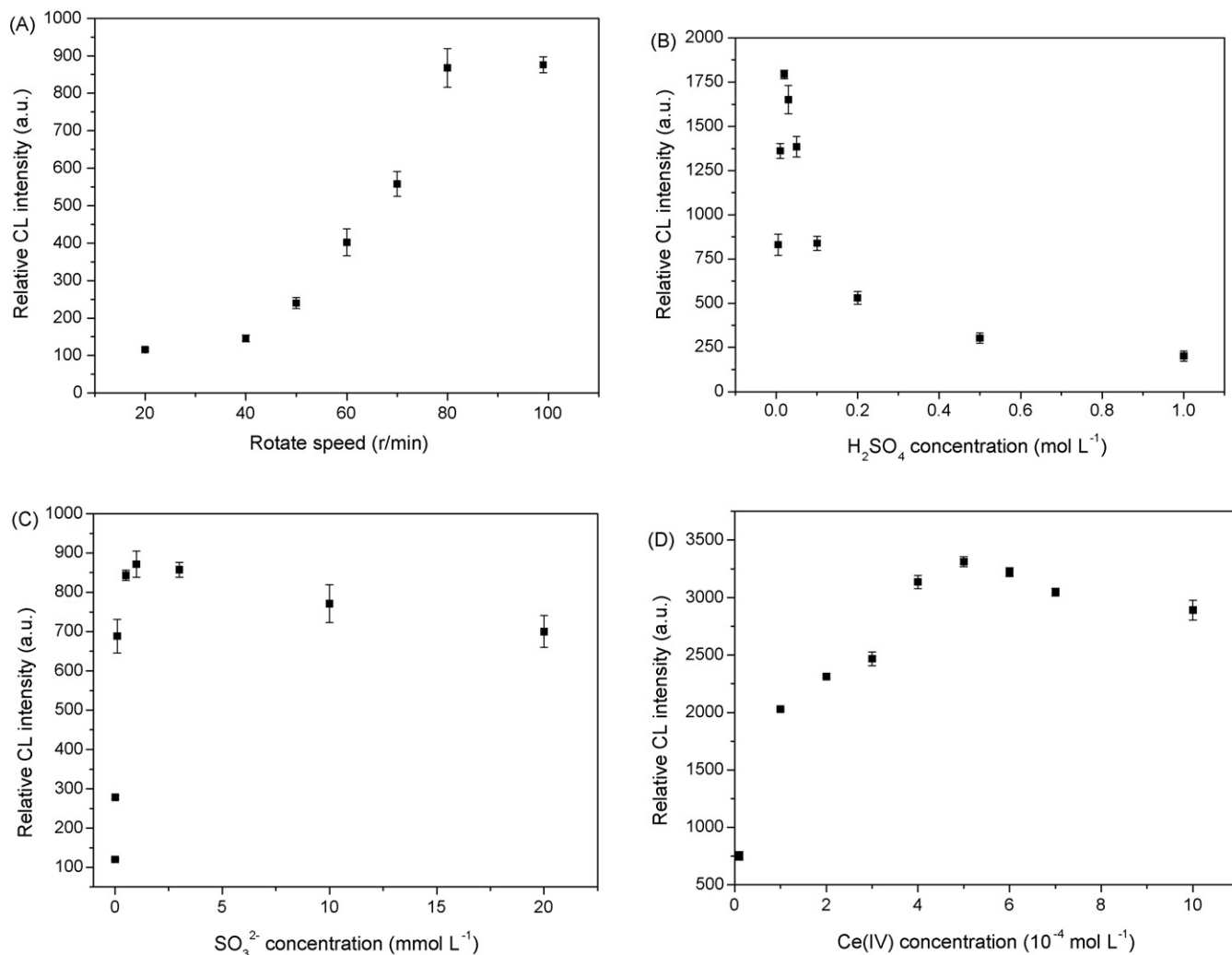


Fig. 4. Effects of the experimental conditions on the Ce(IV)–SO₃²⁻–3.11 nm CdTe QDs (1.0 mM) CL system at –800 V high voltage. (A) Effects of rotate speed of pump P2: 2.0×10^{-4} M Ce(IV) in 0.1 M H₂SO₄, 1.0×10^{-3} M SO₃²⁻; (B) effects of H₂SO₄ concentration in Ce(IV) solution: 2.0×10^{-4} M Ce(IV), 1.0×10^{-3} M SO₃²⁻; (C) effects of sulfite concentration: 2.0×10^{-4} M Ce(IV) in 0.02 M H₂SO₄; (D) effects of Ce(IV) concentration in 0.02 M H₂SO₄: 1.0×10^{-3} M SO₃²⁻.

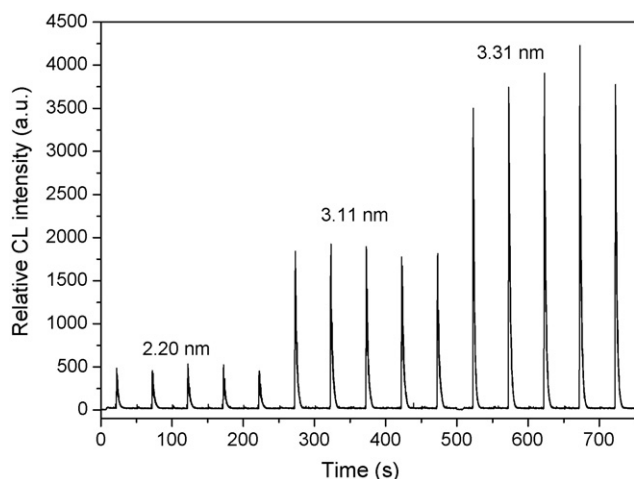


Fig. 5. Profiles of CL intensity via the particle sizes of CdTe QDs. High voltage, –800 V.

minescence [22,24]. The response of different concentration of 3.11 nm CdTe QDs to the Ce(IV)–SO₃²⁻–CdTe QDs CL system was investigated under the optimal reaction conditions. The CL intensity increased linearly with increasing CdTe QDs concentration from 1.0×10^{-6} M to 5.0×10^{-5} M. Meanwhile, it was found that the CL intensity was also linear with the concentration of the other sized CdTe QDs.

3.4. Mechanism

The CL emission during the oxidation of sulfite by KMnO₄ or Ce(IV) in acidic solutions has been attributed to the formation of excited sulfur dioxide molecules (SO₂^{*}) which radiate during deexcitation [34,35]. SO₂^{*} could act as the chemiluminescence emitter or transfer the energy to fluorescent compounds which acted as sensitizers in enhanced chemiluminescence reaction system. In order to investigate the reaction mechanism of CL enhancement and confirm the emission species, we measured the CL spectra of the Ce(IV)–SO₃²⁻–CdTe QDs systems with the three different sized CdTe QDs, using a series of high-energy

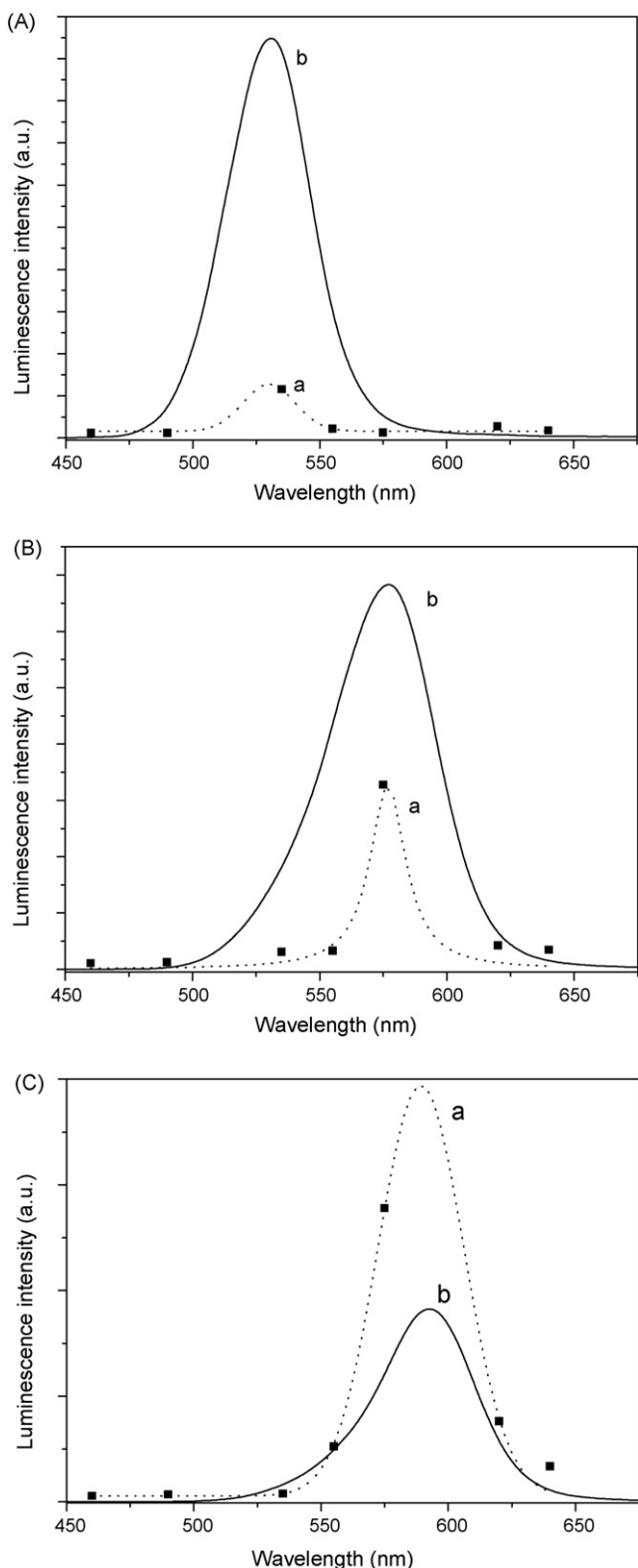
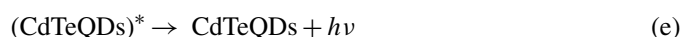
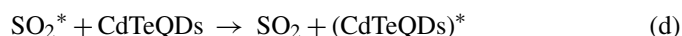
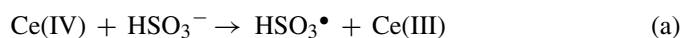


Fig. 6. CL spectra of the Ce(IV)–SO₃²⁻–CdTe QDs system (a) and PL spectra (b) of different sized CdTe QDs: (A) 2.20 nm CdTe QDs; (B) 3.11 nm CdTe QDs; (C) 3.31 nm CdTe QDs.

cutoff filters of various wavelengths, as shown in Fig. 6 (curve a). It could be clearly seen that there was only one emission band over the range of 460–640 nm for the CL reaction and the emission peak was around 530, 576 and 588 nm, respec-

tively, corresponding to 2.20 nm (Fig. 6A), 3.11 nm (Fig. 6B) and 3.31 nm (Fig. 6C) CdTe QDs. Fig. 6 also gives the PL spectra of CdTe QDs with a maximum emission around 531, 577 and 593 nm for 2.20, 3.11 and 3.31 nm CdTe QDs, respectively (curve b), which displayed an emission band similar to the CL spectrum of the Ce(IV)–SO₃²⁻–CdTe QDs reaction system. It is well known that the PL spectrum of the stable emitting species should be identical with the CL spectra for common CL reaction. Moreover, the results from control experiments have indicated that the other coexisting substrates in the CdTe QDs could not enhance the CL of Ce(IV)–SO₃²⁻. Therefore, the emissive species for the observed CL are rather possibly the excited state of CdTe QDs generated in situ during the reaction. It has been reported that the CL spectrum of SO₂^{*}, the emitter of the Ce(IV)–SO₃²⁻ CL reaction, is within the range of 450–600 nm [36]. The CL emission spectrum of SO₂^{*} overlaps well with the broad absorption band (Fig. 2A) of these CdTe QDs with narrow emission band. Theoretically, there is a possibility that CdTe QDs as sensitizers, via energy transfer from the redox reaction, enhance the CL intensity of the cerium(IV)–sulfite reaction. Therefore, the possible mechanism of the sensitized CL reaction induced by CdTe QDs can be simply concluded as the following expressions. In the acid environment, the oxidation product of HSO₃⁻ by Ce(IV) should be HSO₃[•] radical ((a)). Two HSO₃[•] radicals then combined to produce S₂O₆²⁻, which gave the excited intermediate product SO₂^{*} ((b) and (c)). A CL resonance energy transfer between SO₂^{*} as donors and QDs as acceptors occurred, and CdTe QDs were excited and gave the CL emission when it returned to its ground state ((d) and (e)).



According to the CL energy match theory [37], the size-dependent CL character of CdTe QDs in this CL system is probably attributed to the energy matching degree between the chemical energy generated during CL redox reaction and the required excitation energy for the formation of excited state of luminophor. The more the chemical energy matches the excitation energy needed, the stronger the CL intensity and efficiency will be. It is known that the energy band gap of QDs decreases with the increment of particle size [38]. In this case, the energy of SO₂^{*} generated during redox reaction between Ce(IV) and sulfite possibly more matches the smaller energy band gap of the studied QDs with different sizes, resulting in increased CL intensity and emission efficiency with increasing particle size.

3.5. Analytical application

Organic compounds containing hydroxyl (OH), amino (NH₂), or mercapto (SH) groups such as catechol or dopamine [39], electron transfer proteins such as cytochrome *c*,

Table 1

Inhibition effects of organic compounds and electron transfer proteins on the Ce(IV)–SO₃²⁻–CdTe QDs CL system

Compounds	Concentration (mol L ⁻¹)	<i>I</i>	Quenching (%)	Concentration (mol L ⁻¹)	<i>I</i>	Quenching (%)
Blank		2090				
Catechol	5.0 × 10 ⁻⁴	1151	44.9	5.0 × 10 ⁻³	456	78.2
Resorcinol	5.0 × 10 ⁻⁴	1527	26.9	5.0 × 10 ⁻³	805	61.5
Hydroquinone	5.0 × 10 ⁻⁴	954	54.3	5.0 × 10 ⁻³	125	94.0
Dopamine	1.0 × 10 ⁻⁴	1578	24.5	1.0 × 10 ⁻³	691	66.9
Ascorbic acid	5.0 × 10 ⁻⁴	670	67.9	5.0 × 10 ⁻³	71	96.6
L-Cysteine	5.0 × 10 ⁻⁴	1002	52.1	5.0 × 10 ⁻³	207	90.1
Uric acid	2.0 × 10 ⁻⁴	1356	35.1			
Hemoglobin	1.0 × 10 ⁻⁶	1082	48.2	1.0 × 10 ⁻⁵	766	63.3
Myoglobin	1.0 × 10 ⁻⁶	1138	45.5	1.0 × 10 ⁻⁵	689	67.0
Cytochrome <i>c</i>	1.0 × 10 ⁻⁶	1191	43.0			

The percentage of quenching was calculated as $1 - I/I_0$. The blank CL signal I_0 (2090) was obtained by Ce(IV)–SO₃²⁻–CdTe QDs (3.11 nm) without organic compounds or proteins.

hemoglobin or myoglobin [40] have been reported to interact readily with semiconductor quantum dots and quench their fluorescence. It is possible that these compounds or proteins interact with CdTe QDs in the proposed CL reaction resulting in changes in CL emission responses. Herein, the effects of such organic compounds or proteins on the Ce(IV)–SO₃²⁻–CdTe QDs CL system were investigated in the flow-injection mode as shown in Fig. 1(B) and the results are listed in Table 1. These organic compounds and proteins had no effect on the CL emission of Ce(IV)–SO₃²⁻. As expected, all the tested compounds and proteins inhibited the CL signal of Ce(IV)–SO₃²⁻–CdTe QDs system. Taking hemoglobin (Hb) as an example, the analytical potential of the inhibition effects of these compounds on the proposed Ce(IV)–SO₃²⁻–CdTe QDs CL system was explored using 3.31 nm CdTe QDs. The obtained calibration curve for Hb ($\log \Delta I = 6.29582 + 0.42413 \log C(\text{mol L}^{-1})$; $R^2 = 0.9957$) shows good correlation, demonstrating the linear response over the tested concentrations of 4.0×10^{-9} to 1.0×10^{-5} mol L⁻¹, and the detection limit is 3.8×10^{-10} mol L⁻¹ with a signal-to-noise ratio of 3. The results demonstrate that the Ce(IV)–SO₃²⁻–CdTe QDs CL system is capable of responding to a number of substances and detecting them. Moreover, the proposed CL system may be used to achieve the simultaneous detection of numerous compounds or proteins in combination with separation techniques such as high performance liquid chromatography and capillary electrophoresis.

4. Conclusions

In summary, CdTe luminescent quantum-dots were found to enhance the cerium(IV)–sulfite CL signals in this work. The preliminary investigations demonstrated that there existed an efficient CL resonance energy transfer between an chemiluminescence donors (SO₂^{*}) obtained in the Ce(IV)–SO₃²⁻–CL reaction and luminescent quantum-dots as acceptors. Some organic compounds containing hydroxyl, amino, or mercapto groups and electron transfer proteins such as cytochrome *c*, hemoglobin and myoglobin interacting with CdTe QDs were observed to inhibit the CL signals of the Ce(IV)–SO₃²⁻–CdTe QDs system at the experimental conditions. This work is impor-

tant for the investigation of new and efficient catalysts for chemiluminescent reactions. Moreover, there exists the potential application for multiple QDs acceptors with different emission wavelengths to multiplex analysis. Further work can be done to broaden the CL of QDs to various analytical applications such as bioanalysis, cell and tissue imaging.

Acknowledgments

This work was supported financially by the National Natural Science Foundation of China (No. 20675044 and 20575032) and National Basic Research Program of China (No. 2007CB310501)

References

- [1] K. Tsukagoshi, N. Jinno, R. Nakajima, *Anal. Chem.* 77 (2005) 1684.
- [2] A. Roda, M. Guardigli, P. Pasini, M. Mirasoli, *Anal. Bioanal. Chem.* 377 (2003) 826.
- [3] Z. Zhang, S. Zhang, X. Zhang, *Anal. Chim. Acta* 541 (2005) 37.
- [4] C. Dodeigne, L. Thunus, R. Lejeune, *Talanta* 51 (2000) 415.
- [5] Z. Zhang, H. Cui, C. Lai, L. Liu, *Anal. Chem.* 77 (2005) 3324.
- [6] Z. Wang, J. Hu, Y. Jin, X. Yao, J. Li, *Clin. Chem.* 52 (2006) 1958.
- [7] Z. Zhang, H. Cui, M. Shi, *Phys. Chem. Chem. Phys.* 8 (2006) 1017.
- [8] H. Cui, Z. Zhang, M. Shi, *J. Phys. Chem. B* 109 (2005) 3099.
- [9] H. Cui, Z. Zhang, M. Shi, Y. Xu, Y. Wu, *Anal. Chem.* 77 (2005) 6402.
- [10] C. Burda, X. Chen, R. Narayanan, M.A. El-Sayed, *Chem. Rev.* 105 (2005) 1025.
- [11] A. Wolcott, D. Gerion, M. Visconte, J. Sun, A. Schwartzberg, S. Chen, J.Z. Zhang, *J. Phys. Chem. B* 110 (2006) 5779.
- [12] A.R. Clapp, I.L. Medintz, H. Mattoussi, *ChemPhysChem* 7 (2006) 47.
- [13] J.K. Jaiswal, S.M. Simon, *Trends Cell Biol.* 14 (2004) 497.
- [14] Y. Bae, N. Myung, A.J. Bard, *Nano Lett.* 4 (2004) 1153.
- [15] N. Myung, Y. Bae, A.J. Bard, *Nano Lett.* 3 (2003) 1053.
- [16] N. Myung, Z.F. Ding, A.J. Bard, *Nano Lett.* 2 (2002) 1315.
- [17] Z.F. Ding, B.M. Quinn, S.K. Haram, L.E. Pell, B.A. Korgel, A.J. Bard, *Science* 296 (2002) 1293.
- [18] G. Zou, H. Ju, *Anal. Chem.* 76 (2004) 6871.
- [19] S. Ding, J. Xu, H. Chen, *Chem. Commun.* (2006) 3631.
- [20] H. Jiang, H. Ju, *Chem. Commun.* (2007) 404.
- [21] S.K. Poznyak, D.V. Talapin, E.V. Shevchenko, H. Weller, *Nano Lett.* 4 (2004) 693.
- [22] Z. Zhang, J. Li, B. Liu, J. Hu, X. Yao, J.H. Li, *J. Phys. Chem. B* 109 (2005) 23304.
- [23] X. Huang, L. Li, H. Qian, C. Dong, *J. Ren. Angew. Chem.* 118 (2006) 5264.

- [24] Y. Li, P. Yang, P. Wang, X. Huang, L. Wang, *Nanotechnology* 18 (2007), 225602 (8 pp.).
- [25] Y. Rao, Y. Tong, X. Zhang, G. Luo, W.R.G. Baeyens, *Anal. Lett.* 33 (2000) 1117.
- [26] N. Lian, H. Zhao, C. Sun, S. Chen, Y. Lu, L. Jin, *Microchem. J.* 74 (2003) 223.
- [27] J. Li, X. Hong, Y. Liu, D. Li, Y. Wang, J. Li, Y. Bai, T. Li, *Adv. Mater.* 17 (2005) 163.
- [28] J. Li, X. Hong, D. Li, K. Zhao, L. Wang, H. Wang, Z. Du, J. Li, Y. Bai, T. Li, *Chem. Commun.* 2004 (1740).
- [29] W. Yu, L. Qu, W. Guo, X. Peng, *Chem. Mater.* 15 (2003) 2854.
- [30] A.P. Alivisatos, *Science* 271 (1996) 933.
- [31] Y. Wang, N.J. Herron, *Phys. Chem.* 95 (1991) 525.
- [32] L. Brus, *J. Phys. Chem.* 90 (1986) 2555.
- [33] S.K. Poznyak, N.P. Osipovich, A. Shavel, D.V. Talapin, M. Gao, A. Eychmuller, N. Gaponik, *J. Phys. Chem. B* 109 (2005) 1094.
- [34] M. Kato, M. Yamada, S. Suzuki, *Anal. Chem.* 56 (1984) 2529.
- [35] I.M. Psarellis, N.T. Deftereos, E.G. Sarantonis, A.C. Calokerinos, *Anal. Chim. Acta* 294 (1994) 27.
- [36] J. Lin, T. Hobo, *Anal. Chim. Acta* 323 (1996) 69.
- [37] A.M. Garc-Campa, W.R.G. Baeyens, *Chemiluminescence in Analytical Chemistry*, Marcel Dekker, New York, 2001.
- [38] L. Spanhel, M. Haase, H. Weller, A. Henglein, *J. Am. Chem. Soc.* 109 (1987) 5649.
- [39] Y. Ma, C. Yang, N. Li, X. Yang, *Talanta* 67 (2005) 979.
- [40] Y. Ma, H. Bai, C. Yang, X. Yang, *Analyst* 130 (2005) 283.

Polysiloxane–poly(propylene oxide) hybrid discs as solid phase in anti-HCV detection using a recombinant core protein

S.A. Tagliavini^{a,b,*}, A.Y. Mikawa^b, H. Yamanaka^a,
F. Henrique-Silva^c, P.I. Costa^b

^a Unesp-Universidade Estadual Paulista, Instituto de Química, R. Prof. Francisco Degni s/n, 14800-900 Araraquara, Brazil

^b Unesp-Universidade Estadual Paulista, Faculdade de Ciências Farmacêuticas, R. Expedicionários do Brasil n 1621, 14801-902 Araraquara, Brazil

^c UFSCar-Universidade Federal de São Carlos, Rodovia Washington Luís, km 235, 13565-905 São Carlos, SP, Brazil

Received 27 August 2007; received in revised form 13 November 2007; accepted 13 November 2007

Available online 21 November 2007

Abstract

In this work, siloxane–poly(propylene oxide) discs (PPO disc) prepared using the sol–gel process were used as solid phase in enzyme-linked immunosorbent assays (ELISA) for the detection of anti-hepatitis C virus (HCV) antibodies. The HCV RNA from serum (genotype 1b) was submitted to the RT-PCR technique and subsequent amplification of the HCV core 408 pb. This fragment was cloned into expression vector pET42a and expressed in *Escherichia coli* as recombinant protein with glutathione S-transferase (GST). Cell cultures were grown and induced having a final concentration of $0.4 \times 10^{-3} \text{ mol L}^{-1}$ of IPTG. After induction, the cells were harvested and the soluble fraction was analyzed using polyacrilamide gel 15% showing a band with an approximate molecular weight of 44 kDa, the expected size for this GST-fused recombinant protein. The recombinant protein was purified and confirmed by immunological detection using HCV-positive serum and showed no cross-reactivity with positive samples for other infectious diseases. An ELISA was established using 1.25 ng of recombinant protein per PPO disc, a dilution of 1:10,000 and 1:40 for a peroxidase conjugate and serum, respectively, and solutions of hydrogen peroxide and 3,3',5,5'-tetra-methylbenzidine in a ratio of 1:1. The proposed methodology was compared with the ELISA conventional polystyrene-plate procedure and the performance of the PPO discs as a matrix for immunodetection gave an easy synthesis, good performance and reproducibility for commercial application.

© 2007 Elsevier B.V. All rights reserved.

Keywords: Hepatitis C virus; Core protein; Recombinant antigen; Siloxane–poly(propylene oxide) discs

1. Introduction

The hepatitis C virus (HCV) infection affects approximately 170 million individuals worldwide and leads to severe liver diseases (steatosis, liver cirrhosis and hepatocellular carcinoma). The disease constitutes the main cause of liver transplantation in the world [1]. This virus is a member of the genus Hepacivirus within the Flaviridae family and possesses a viral genome consisting of a single, positive-strand RNA with a nucleotide length of about 9.4 kb [2]. Its genome carries a single open reading frame (ORF) encoding a large precursor polypeptide of approx-

imately 3000 amino acids [3] which is processed by a host and viral proteases at the endoplasmic reticulum membrane and yields the following viral proteins: core (C), envelope (E1 and E2), p7 as structural protein and NS2, NS3, NS4A, NS4B, NS5A and NS5B as nonstructural protein [4,5]. Among the structural and nonstructural proteins, the core or the nucleocapsid region (amino acids 1–191) has been shown to have a high degree of homology between different strains of the virus [6]. This protein is highly immunogenic and it induces the production of antibodies quickly after the infection [7].

A variety of tests have been developed for the diagnosis and management of HCV infection, which include (i) serologic tests to detect HCV antibodies, (ii) molecular tests to detect and quantify HCV RNA, and (iii) genotyping techniques. enzyme-linked immunosorbent assays (ELISA) using the direct adsorption of proteins into polystyrene microplates or immunoblot assays for the detection of HCV antibodies have been used in the screening

* Corresponding author at: Unesp-Universidade Estadual Paulista, Instituto de Química, R. Prof. Francisco Degni s/n, 14800-900 Araraquara, São Paulo Brazil. Tel.: +55 16 3301 6622; fax: +55 16 3301 6692.

E-mail addresses: tagliavinisa@yahoo.com.br (S.A. Tagliavini), hidekoy@iq.unesp.br (H. Yamanaka).

out of infectious blood donations and the diagnosis of hepatitis C. However, the use of new material as a support for protein immobilization could increase the sensitivity, diminish costs and could be an alternative for screening and diagnostic of hepatitis C.

In this study, a fragment of the HCV core protein was recombinantly expressed fused to glutathione S-transferase using a prokaryotic expression system and the recombinant protein was immobilized onto siloxane–polypropyleneglycol discs in an immunoassay for the detection of anti-HCV antibodies. The results were compared to conventional ELISA.

2. Experimental

2.1. Samples and solutions

Sera samples were obtained from individuals infected with HCV and donated by the Hepatitis Health Service at the faculty of pharmaceutical sciences, UNESP. Sequences amplified from the core region of a type 1b HCV virus were used for the synthesis of the antigen for antibody screening. The primers were supplied by Life Technology (Gaithersburg, MD, USA). All oligonucleotide stock solutions ($200 \mu\text{g mL}^{-1}$) were prepared in deionized water and kept frozen. Dilute solutions of the oligonucleotides were prepared daily in phosphate buffer solution (0.1 mol L^{-1} , pH 7.0). Buffer solutions were prepared from analytical grade DNase- and RNase-free reagents and deionized water.

2.2. HCV RNA detection and genotyping (HCV 1, 2a/c, 2b and 3)

HCV RNA detection screened in serum was RT-PCR using the AMPLICOR Hepatitis C Virus Test, version 2.0 (Roche Molecular Systems, Branchburg, NJ, USA) and both the genotypes and subtypes were determined by the line probe reverse hybridization assay (INNO-LIPA HCV-Innogenetics, Belgium). The assays were performed according to the manufacturer's instructions.

2.3. Cloning of the HCV core region

HCV RNA was extracted and reverse-transcribed using the AMPLICOR Hepatitis C Virus Test. cDNA was amplified by nested PCR using primers derived from the core region based on the published nucleotide sequences 968R [8] that belongs to HCV-1b. The nucleotide positions (nt) are numbered according to hepatitis C virus type 1b polyprotein mRNA (GenBank accession no. [AF333324](#)). Primers were designated for the 408 bp amplification product (nt 1–408) covering part of the HCV core region. The primers for the first-stage PCR were 5'-ATGAGCACAAATCCTAACCTC, and 5'-AGCGGAAGCTGGGATGGTCAAA. The inner primers for the second-stage PCR were 5'-ATGAGCACAAATCCTAACCTC and 5'-GTACCCCATGAGGTCGGCGAAG. Amplification of the PCR product representing a part of the core protein coding region (amino acids 1–136) of HCV-1b genotype was carried

out using a polymerase chain reaction (PCR) using primers corresponding to the 5'- and 3'-end of the core 408 gene plus BamHI and NcoI sites respectively. PCR products were cloned into the expression plasmids pET42a (Novagen, UK) cut with the enzymes BamHI and NcoI. The resulting plasmid, named pET42-136core, encodes the HCV core protein fused to a glutathione S-transferase protein. Recombinant clones were sequenced by the dideoxy chain termination method [9], using the ETDyynamic terminator in an ABI Prism 377 DNA sequencer.

2.4. Expression and purification of recombinant protein

Plasmid pET42-136core was used to transform *Escherichia coli* Rosetta (Novagen, UK) calcium chloride competent. Cells were grown overnight at 37°C , and 5 mL of this culture was diluted 1:100 in 0.5 l of fresh medium and cultured at 37°C , 200 rpm, until reach an optical density of 0.4–0.6 nm. The recombinant protein expression was then induced by adding isopropyl- β -D-thiogalactopyranoside (IPTG) (Sigma, St. Louis, MO, USA) to a final concentration of $0.4 \times 10^{-3} \text{ mol L}^{-1}$. The culture was incubated for an additional 4 h and the bacteria were harvested by centrifugation at $10,000 \times g$ for 10 min. The resulting pellet was resuspended in PBS (0.140 mol L^{-1} NaCl, $0.0027 \text{ mol L}^{-1}$ KCl, 0.01 mol L^{-1} Na_2HPO_4 , $0.0018 \text{ mol L}^{-1}$ KH_2PO_4 , pH 7.4) and sonicated three times for 30 s in the cold with 1 min intervals. The sonicated cell lysate was centrifugated at $10,000 \times g$ for 15 min and the soluble recombinant protein, dubbed GST–HCV–core, was purified from supernatant using an affinity GST–agarose column (GSTrap FF-Amersham Biosciences) previously equilibrated with PBS. The proteins bound to column were eluted with 15 mL of PBS containing $5 \times 10^{-3} \text{ mol L}^{-1}$ reduced glutathione, in fractions of 3 mL. Two milliliters of each fraction were analyzed on 15% SDS polyacrylamide gel electrophoresis gels, as described [10]. The purified protein was kept at -20°C until use.

2.5. Polyacrylamide gel electrophoresis and immunoblotting analysis

Proteins were separated in 15% SDS polyacrylamide gel electrophoresis (SDS-PAGE) and transferred to a nitrocellulose filter [11] using Mini V8 Blot Module apparatus set (BRL-Life Technologies, Gaithersburg, MD, USA) at 100 V for 2 h. The membranes were blocked with 5% non-fat dry milk in PBS-T (0.140 mol L^{-1} NaCl, $0.0027 \text{ mol L}^{-1}$ KCl, 0.01 mol L^{-1} Na_2HPO_4 , $0.0018 \text{ mol L}^{-1}$ KH_2PO_4 , pH 7.4) overnight at 4°C . The membranes were cut in 5 cm strips, which were incubated for 1 h at room temperature with human serum from HCV patients and non-infected individuals diluted 1:40 in dilution buffer (5% non-fat dry milk in PBS-T). The strips were washed in PBS-T, and incubated for 1 h at room temperature with anti-human IgG–peroxidase conjugate (Sigma, St. Louis, MO, USA) diluted to 1:10,000 in dilution buffer (5% non-fat dry milk in PBS-T). Finally, the strips were washed with PBS-T and the reaction developed with 3,3'-diaminobenzidine tetrahydrochloride–TMB (Sigma, St. Louis, MO, USA) as sub-

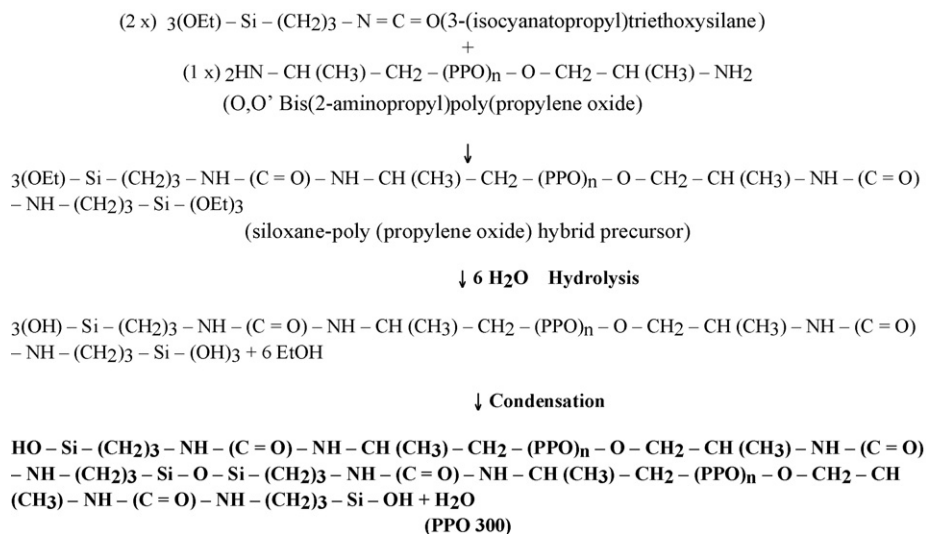


Fig. 1. Synthesis of PPO 300 by hydrolysis and polycondensation reactions of the hybrid precursor.

strate. The recombinant protein was also tested against positive sera for the hepatitis B virus (HBV), human immunodeficiency virus (HIV), human T-lymphotropic virus (HTLV), Chagas' disease and rheumatoid factor to test cross-reactivity.

2.6. Synthesis of the siloxane-poly(propylene oxide) hybrid discs

Siloxane-poly(propylene oxide) nanocomposites (PPO) were prepared using the sol-gel method as described [12]. 3-(Isocyanatopropyl)triethoxysilane (IsoTrEOS) and polypropylene glycol bis(2-amino-propyl-ether) with a molecular weight of 300 g mol^{-1} (Aldrich Chemical Co., USA) in the molar ratio of 2:1 were mixed and stirred with tetrahydrofuran (THF) (Aldrich Chemical Co., USA) under reflux at 80°C for 24 h. The THF was evaporated and the stable hybrid precursor $3(\text{EtO})\text{Si}-(\text{PPO})-\text{Si}(\text{OEt})_3$ was obtained. At a temperature of 25°C , 1.0 g of the precursor was mixed with 2.0 mL of ethanol containing NH_4F ($[\text{NH}_4\text{F}]/[\text{Si}] = 0.001$), which was used as a neutral catalyst. The mixture was agitated until a homogeneous solution was obtained and after this, 0.2 mL of water was added under stirring to promote the hydrolysis and polycondensation of the hybrid precursor forming the sol (PPO 300). The hydrolysis and polycondensation reactions of the hybrid precursor are shown in Fig. 1. The homogeneous sol ($10 \mu\text{L}$) was then transferred to molds and allowed to solidify for 7 days at 25°C and then kept in 0.067 mol L^{-1} sodium phosphate buffer at pH 7.2 at 4°C until use. Such a polymer has already been used to immobilize oligonucleotides on an electrode surface [13].

2.7. GST-HCV-core immobilization

The PPO 300 molded discs were placed in 96-well cell culture microplates (Corning Incorporation Life Sciences, USA) and were incubated overnight at 4°C with $100 \mu\text{L}$ of recombinant antigen core (1.25 ng), prepared in phosphate-buffered saline (PBS at pH 7.4). The discs containing the immobilized

protein were then washed twice with PBS containing 0.05% (w/v) Tween 20 (PBS-T) and incubated with skimmed milk blocking buffer in PBST solution (4%, w/v) at 37°C for 1 h and washed twice with PBS-T. Sequentially, the construction of the PPO-ELISA was developed, as illustrated in Fig. 2.

2.8. ELISA for HCV antibodies detection

The discs were incubated with $100 \mu\text{L}$ of infected human HCV serum, diluted to 1:40 in blocking buffer at 37°C for 1 h, washed three times with PBST and then incubated in $100 \mu\text{L}$ of an anti-human IgG-peroxidase conjugate (Sigma) diluted to 1:10,000 in blocking buffer at 37°C for 1 h. After washing, $100 \mu\text{L}$ of solutions of TMB (3,3',5,5'-tetra-methylbenzidine) and hydrogen peroxide in the ratio of 1:1 were added and incubated for 10 min at room temperature in the dark. The reaction was interrupted by the addition of $100 \mu\text{L}$ of H_2SO_4 (1 mol L^{-1}) and was read spectrophotometrically in an ELISA Microplate Reader at a wavelength of 450 nm (reference wavelength 540 nm). The optimal conditions for the procedure described above were established as follows. The concentration of antigen and serum was fixed and the conjugate was diluted (1:1000, 1:2000, 1:5000, 1:10,000, 1:20,000) and the serum titration (1:10, 1:20, 1:40, 1:80, 1:160) was established using fixed values of antigen concentration and conjugate dilution. At last, the antigen concentration (0.16, 0.31, 0.62, 1.25, 2.5 ng) was determined using the most convenient fixed values of conjugate (1:10,000) and serum titration (1:40). A conventional ELISA was carried out simultaneously in 96-well ELISA polystyrene microplates using the same parameters defined for the nanocomposites prepared using the sol-gel method, replacing the bicarbonate buffer at pH 9.6 for PBS and not using the PPO discs during antigen immobilization. All samples were positive for HCV antibodies verified by third-generation HCV enzyme-linked immunosorbent assay (ORTHO HCV version 3.0 enzyme-linked immunosorbent assay) and the quality control of the proposed methodology was at least duplicated using

both ORTHO HCV version 3.0 negative and positive controls. The cut-off values were obtained by average of absorbance value of 20 individual negative controls plus two standard deviations.

3. Results and discussion

3.1. Expression of the truncated GST–HCV–core (1–136) fusion protein

Since the identification and molecular characterization of the hepatitis C virus in 1989 [3], a variety of diagnostic tests based on the detection of hepatitis virus antibodies or HCV RNA in serum have been developed and refined. The recombinant core protein has been commonly used for serologic tests to detect HCV antibodies [14]. In the present work, the pET42a-136core plasmid was constructed by cloning the Bam HI–Nco I fragment of the HCV core gene encoding 136 amino acids fused to the gene for glutathione S-transferase. Expression of the soluble GST–HCV–core was efficiently done in *E. coli* Rosetta (DE3), with a yield of about 1.2 mg of protein per liter of culture. The recombinant protein was confirmed by immunological detection using HCV positive serum. This protein reacted specifically with HCV positive serum and did not exhibit any cross-reactivity with non-infected serum and other diseases, such as HBV, HIV, HTLV, Chagas' disease and rheumatoid factor (data not shown). In addition, only GST protein did not react with serum from either HCV or normal patients, indicating that the interaction between the GST–HCV–core (136) fusion protein and a patient's serum is generated only from the core protein. These results demonstrated that this protein could play a potential key role in the development of HCV diagnostic tests.

3.2. Protein immobilization and the ELISA test

The bioimmobilization process on sol–gel biomaterials has been designed for applications in affinity chromatography, biosensors and the solid phase used in immunodiagnosics [15]. There are few studies about the immobilization of biological molecules on organic–inorganic hybrid prepared using the sol–gel method [16], regards to ELISA immunoassay the litera-

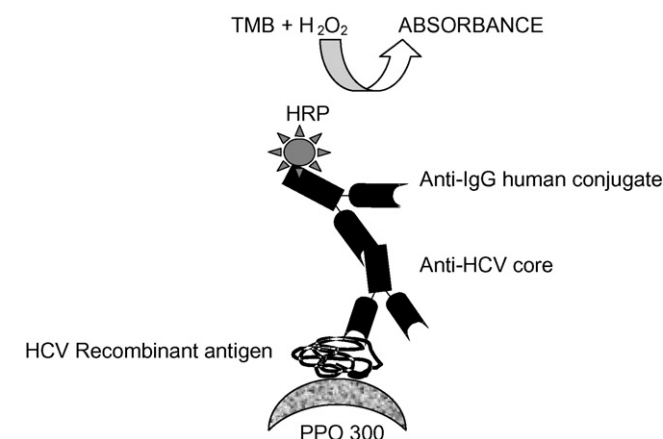


Fig. 2. Scheme of PPO–ELISA for HCV antibody detection.

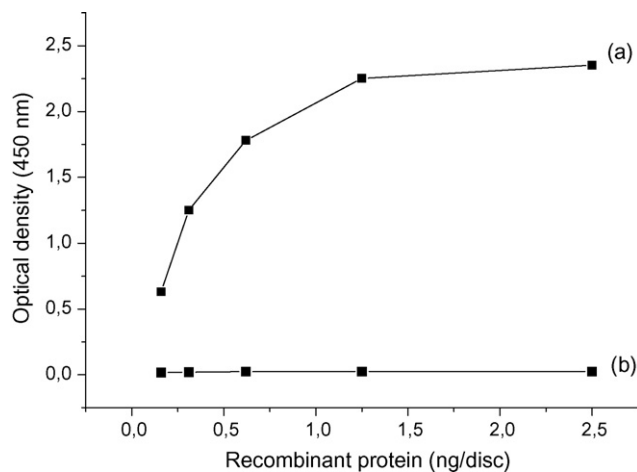


Fig. 3. Optimization of concentration of GST–HCV–core protein using siloxane–poly(propylene oxide) discs (PPO). The conjugate and serum dilutions were 1:10,000 and 1:40, respectively (a), and Control–PBS (b).

ture reported composites synthesized by sol–gel techniques have been used for covalent binding the antigen to this matrix [17] or incorporate the antigen into this matrix [15,18]. However, there are no investigations regarding the ELISA test involving the proposed siloxane–poly(propylene oxide) disc. Therefore, in the present work, this recombinant protein was immobilized on siloxane–poly(propylene oxide) discs and used to detect HCV antibodies.

The PPO 300 hybrid discs with diameter of 3 mm prepared using the sol–gel method were rigid, transparent and weighed between 5 and 10 mg. The physical adsorption of GST–HCV–core onto these discs was evaluated using the ELISA immunoassay. Fig. 3 shows the relationship between the different concentrations of GST–HCV–core immobilized on the PPO 300 discs and the absorbance obtained when using fixed values of conjugate (1:10,000) and serum dilution (1:40). The curve obtained (Fig. 3a) shows the reaction of the antigen–antibody complex according to the enzyme–substrate complex formed. In absence of core protein (PBS only), the absorbance values were seen to be close to 0 (Fig. 3b). These results demonstrate that, considering fixed dilutions of conjugate and serum, 1.25 ng of protein per disc were sufficient to standardize this ELISA methodology for the screening of the serum samples. The absorbance average values of 20 individual negative controls were 0.204 and 0.236, respectively, for the conventional ELISA and PPO–ELISA. The reactivity threshold was calculated by using twice standard deviation plus absorbance average of negative controls. A sample is considered non-reactive when the current intensity is equal or lower than 0.313 and 0.386 nm, respectively, for the conventional ELISA and PPO–ELISA, and reactive when values were above those absorbance values. PPO–ELISA was applied for the detection of anti-HCV antibodies in samples from HCV-infected patients and the results obtained from this method were compared to those obtained with ELISA using the direct adsorption of proteins on polystyrene microplates. The comparison between these methods is presented in Table 1. Significant decreasing absorbance values were observed when comparing negative and positive sera. Under

Table 1

Comparison of ELISA using siloxane–poly (propylene oxide) discs and polystyrene as solid phases (antigen concentration 1.25 ng/disc, sera and conjugate diluted to 1:40 and 1:10,000, respectively)

Negative sera		Positive sera	
Polystyrene	PPO disc	Polystyrene	PPO disc
0.260 ± 0.06	0.345 ± 0.01	3.32 ± 0.02	4.26 ± 0.07
0.155 ± 0.03	0.268 ± 0.05	1.77 ± 0.03	2.26 ± 0.03
0.231 ± 0.02	0.375 ± 0.02	1.53 ± 0.02	1.90 ± 0.08
0.167 ± 0.03	0.325 ± 0.06	1.16 ± 0.03	1.60 ± 0.02
0.174 ± 0.05	0.298 ± 0.03	0.88 ± 0.05	1.04 ± 0.05
0.247 ± 0.09	0.402 ± 0.12	1.33 ± 0.08	1.74 ± 0.09
0.158 ± 0.10	0.196 ± 0.09	1.58 ± 0.01	2.05 ± 0.04
0.102 ± 0.02	0.138 ± 0.05	1.07 ± 0.01	1.56 ± 0.04
0.163 ± 0.06	0.191 ± 0.09	1.87 ± 0.09	2.24 ± 0.05
0.201 ± 0.09	0.233 ± 0.24	2.51 ± 0.21	2.97 ± 0.04
0.101 ± 0.07	0.148 ± 0.03	1.79 ± 0.06	2.16 ± 0.02
0.132 ± 0.06	0.154 ± 0.09	1.99 ± 0.01	2.91 ± 0.05
0.142 ± 0.12	0.193 ± 0.02	2.21 ± 0.10	2.97 ± 0.12
0.278 ± 0.06	0.297 ± 0.06	2.58 ± 0.01	3.06 ± 0.08
0.159 ± 0.01	0.191 ± 0.08	2.08 ± 0.01	2.55 ± 0.02

$n = 2; A = 450\text{nm}$.

conditions established (antigen concentration 1.25 ng/disc, sera and conjugate diluted to 1:40 and 1:10,000, respectively), the ELISA using PPO discs as solid phase and the recombinant core antigen was able to efficiently detect HCV antibodies, with results comparable to those obtained for ELISA that utilizes the adsorption of the antigen on polystyrene microplates. Furthermore, the ELISA using siloxane–poly(propylene oxide) discs as a matrix for immunodetection was able to distinguish positive and negative sera samples. The immunoassay using the sol–gel discs indicated interactions between recombinant protein and hybrid PPO 300. Possibly, this is due to balance of forces associated with Van der Waals interaction, hydrophilic and hydrophobic. These interactions were sufficient to maintain the biomolecule immobilized on the solid support during several ELISA washing steps. Those results showed that recombinant core protein were successfully adsorbed onto the PPO 300 hybrids.

4. Conclusions

The present work shows that the precursor 3-(isocyanatopropyl)triethoxysilane and *O,O'* bis(2-aminopropyl)poly(propylene oxide) having a molecular weight of 300 g mol^{-1} are suitable for HCV core protein immobilization. A new methodology to detect HCV antibodies was herein proposed using this PPO 300 precursor. This method may prove to be important for the diagnosis and screening of blood donations.

The performance of the PPO 300 discs as solid phase for immunoassay were seen to have the additional advantages of being easy to synthesize and having good reproducibility for commercial application. In addition, the immobilization of biomolecule onto this hybrid organic–inorganic composite permits its application in automated processes used in clinical assays and could be potentially a key role in the manufacturing of immunosensors.

Acknowledgements

We thank Dr. C.V. Santilli and Dr. K. Dahmouche for technical assistance and FAPESP for financial support (CBME-CEPID, Process 98/14138-2). Tagliavini, S.A. thanks the fellowship from CAPES, Brazil.

References

- [1] W.P. Hofmann, V. Dries, E. Herrmann, B. Gartner, S. Zeuzem, C. Sarrazin, *J. Clin. Virol.* 32 (2005) 289.
- [2] Q.L. Choo, K.H. Richman, J.H. Han, K. Berger, C. Lee, C. Dong, C. Gallegos, D. Coit, R. Medina-Selby, P.J. Barr, *Proc. Natl. Acad. Sci. U.S.A* 88 (1991) 2451.
- [3] Q.L. Choo, G. Kou, A.J. Weiner, L.R. Overby, M. Houghton, *Science* 244 (1989) 359.
- [4] M. Hijikata, N. Kato, Y. Ootsuyama, M. Nakagawa, K. Shimotohno, *Proc. Natl. Acad. Sci. U.S.A* 88 (1991) 5547.
- [5] A. Grakoui, C. Wychowski, C. Lin, S.M. Feinstone, C.M. Rice, *J. Virol.* 67 (1993) 1385.
- [6] H. Okamoto, S. Okada, Y. Sugiyama, K. Kurai, H. Iizuka, A. Machida, Y. Miyakawa, *J. Gen. Virol.* 72 (1991) 2697.
- [7] C. Jolivet-Reynaud, P. Dalbon, F. Viola, S. Yvon, G. Paranhos-Baccala, N. Piga, L. Bridon, M.A. Trabaud, N. Battail, G. Sibai, M. Jolivet, *J. Med. Virol.* 56 (1998) 300.
- [8] S.S. Alam, T. Nakamura, A. Naganuma, A. Nozaki, K. Nouse, H. Shimomura, N. Kato, *Acta Med. Okayama* 56 (2002) 141.
- [9] F. Sanger, S. Nicklen, A.R. Coulson, *Proc. Natl. Acad. Sci. USA* 74 (1977) 5463.
- [10] U.K. Laemmli, *Nature* 227 (1970) 680–685.
- [11] H. Towbin, T. Staehelin, J. Gordon, *Proc. Natl. Acad. Sci. USA* 76 (1979) 4350.
- [12] K. Dahmouche, C.V. Santilli, S.H. Pulcinelli, A.C. Craievich, *J. Phys. Chem. B* 103 (1999) 4937.
- [13] C.S. Riccardi, K. Dahmouche, C.V. Santilli, P.I. Costa, H. Yamanaka, *Talanta* 70 (2006) 638.
- [14] E.P. Lopes, C.H. Granato, V. Lanzoni, L. Granero, G. Paranhos-Baccala, H. Tomiyama, A.E. Silva, M.L. Ferraz, *Mem. Inst. Oswaldo Cruz* 95 (2000) 717.
- [15] H.S. Mansur, R.L. Oréfice, W.L. Vasconcelos, Z.P. Lobato, L.J.C. Machado, *J. Mater. Sci. Mater. Med.* 16 (2004) 333.
- [16] A.C. Pierre, *Biocatal. Biotransform.* 22 (2004) 145.
- [17] R.A.L. Coelho, H. Yamasaki, E. Perez, *Mem. Inst. Oswaldo Cruz* 98 (2003) 391.
- [18] E.F. Reis, F.S. Campos, A.P. Lage, R.C. Leite, L.G. Heneine, W.L. Vasconcelos, Z.I.P. Lobato, H.S. Mansur, *Mater. Res.* 9 (2006) 185.

Development and validation of a screening procedure for the assessment of inhibition using a recombinant enzyme

Pierre Van Antwerpen^{a,*}, Patrick Moreau^a, Karim Zouaoui Boudjeltia^b,
Sajida Babar^b, François Dufrasne^a, Nicole Moguevsky^c,
Michel Vanhaeverbeek^b, Jean Ducobu^d, Jean Nève^a

^a *Laboratory of Pharmaceutical Chemistry, Institute of Pharmacy, Université Libre de Bruxelles, Brussels, Belgium*

^b *Laboratory of Experimental Medicine (Unit ULB 222), CHU Charleroi, Université Libre de Bruxelles, Montigny-le-Tilleul, Belgium*

^c *Technology Transfert Office, FUNDP, Namur, Belgium*

^d *Department of Internal Medicine, CHU Tivoli, Université Libre de Bruxelles, La Louvière, Belgium*

Received 10 September 2007; received in revised form 14 November 2007; accepted 14 November 2007

Available online 22 November 2007

Abstract

Myeloperoxidase (MPO, E.C. 1.1.1.7) is a heme-containing enzyme that catalyses the synthesis of hypochlorous acid (HOCl) in the presence of hydrogen peroxide (H₂O₂) and chlorine anions. The production of HOCl is kept under strict control of neutrophils. However, in several pathological conditions, MPO is leaked in the extracellular fluid, which involves an over-production of reactive oxygen species like HOCl and promotes the damages caused by neutrophils. As a consequence, the inhibition of MPO by various agents has been investigated and a variety of molecules have been evaluated for this activity in different models. The present study aims to describe and validate a rapid screening method based on the taurine assay and using a recombinant MPO. After validation of the stock solutions used during the experiments, the amount of MPO for the completion of the reaction was measured and fixed to an optimal value. The inhibiting concentration at 50% of flufenamic acid (taken as a reference molecule) was then assessed in both a simple tube test and a microplate test and delivered similar results ($1.3 \pm 0.2 \mu\text{M}$ vs $1.4 \pm 0.2 \mu\text{M}$, $P = 0.2$). Finally, different molecules able to inhibit MPO were evaluated in this rapid assay system providing results comparable to literature. The high throughput screening is undoubtedly a first line assessment method which affords the selection of inhibitors and permits to reduce the number of candidates for a further elucidation of the mechanism of MPO inhibition.

© 2007 Elsevier B.V. All rights reserved.

Keywords: Myeloperoxidase; Screening; Inhibitor; Taurine assay

1. Introduction

Myeloperoxidase (MPO, E.C. 1.1.1.7) is a heme-containing enzyme that catalyses the synthesis of hypochlorous acid (HOCl) in the presence of hydrogen peroxide (H₂O₂) and chlorine anions (Fig. 1). The particular interaction of the heme with the protein moiety of the enzyme confers to the system redox properties that allow the rapid oxidation of MPO in compound I by H₂O₂ ($k_s \sim 10^7 \text{ M}^{-1} \text{ s}^{-1}$). The high reduction potential

($E'^{\circ} = 1.16 \text{ V}$) of the redox couple ‘compound I/MPO’ results in the oxidation of chloride in HOCl ($k_s \sim 10^4$). This species is a powerful oxidant that is extremely cytotoxic and rapidly reacts with most biological molecules [1,2].

The production of HOCl is kept under strict control of neutrophils as MPO is present in the azurophilic granules of the cells and the enzyme is poured out in the phagolysosome after the phagocytosis process. However, in conditions such as chronic inflammatory syndromes, MPO is leaked in the extracellular fluid during a phase called ‘oxidative burst’. The main consequence of this is the over-production of reactive oxygen species like HOCl that promote the inflammatory damage caused by neutrophils [3]. Moreover, the organism has to deal with a ‘circulating MPO’ that can be adsorbed on electronegative

* Corresponding author at: Bd du triomphe, Campus Plaine CP 205/5, 1050 Brussels, Belgium. Tel.: +32 26505263; fax: +32 26505249.

E-mail address: pvantwer@ulb.ac.be (P. Van Antwerpen).

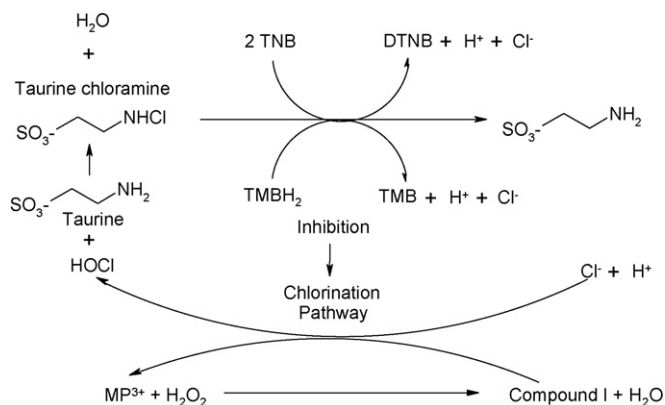


Fig. 1. Schematic representation of the chemical reactions involved in the assay.

macrostructures like cell surfaces or lipoproteins, increasing the potential oxidative damage of MPO [4,5]. For this reason, MPO is often mentioned as a contributing factor in conditions such as atherosclerosis, chronic inflammatory syndromes, neurodegenerative disease or End-Stage Renal Disease [6–9].

As a matter of fact, some authors pointed out that the development of efficient MPO inhibitors could be of interest [10]. Such compounds would permit to surround the real impact of the enzyme in the different mentioned pathological conditions and become interesting therapeutic agents. As a consequence, the inhibition of MPO by various agents has been deeply investigated and a wide variety of molecules have been evaluated in different models. For example, Ximenes et al. tested the inhibiting effect of several indolic compounds while Van Antwerpen et al. investigated anti-inflammatory drugs in a simple taurine assay [11,12]. Jantchko et al. (2005) focused on tryptamine derivatives in a stop-flow system assessment [13] and also evaluated the inhibiting effect of melatonin or betalanin compounds by this system [14,15]. In some studies, H₂-receptor antagonists were also tested [16]. However, due to the use of many methods, it is difficult to properly compare the activity of the different molecules. In order to optimize the candidate examination and selection in a therapeutical approach, it could be of interest to dispose of an efficient screening method that rapidly and adequately discriminates inactive compounds from good candidates. In addition, such an assay system would considerably simplify a rational drug design process.

In the present paper, a rapid screening method based on the taurine assay and using a recombinant MPO is described and validated [17,18]. By comparing different systems and controlling stock solutions, the protocol is optimized in order to test a large number of compounds and decrease the consumption of both MPO and other reagent quantities.

2. Experimental

2.1. Materials

High purified recombinant MPO was prepared as previously described [18]. Each batch solution was characterized by its protein concentration (mg/ml), its activity (U/ml) and its spe-

cific activity (U/mg). The chlorination activity was determined according to Hewson and Hager [19].

Hydrogen peroxide as a 30% solution and hypochlorous acid as a 13% active chlorine solution were respectively obtained from VWR (Leuven, Belgium) and Acros (Geel, Belgium). The solutions were kept in the dark at 4 °C. Taurine, dithio-bisnitrobenzoic acid (DTNB), NaBH₄, KI and bovine catalase were purchased from Sigma (Boornem, Belgium). Na₂S₂O₃ (1 M), acetic acid (99%, m/m), H₂SO₄ (96%, m/m), HCl (32%, m/m), KBrO₃, NaCl, KH₂PO₄, Na₂H₂EDTA, KOH, KMnO₄ and starch were obtained from VWR (Leuven, Belgium) while tetramethylbenzidine (TMB) and HgI₂ were provided by Acros (Geel, Belgium). Boiled MilliQ water was used to prepare the solutions and during all experimentations.

The starch solution was prepared by triturating 1 g in 5 ml of water and then by adding 100 ml of boiling water containing 10 mg of HgI₂. A 0.1 M solution of Na₂S₂O₃ was prepared daily by diluting the stock solution. The concentration was then determined by using the diluted Na₂S₂O₃ solution to assay a mixture containing 40 ml of water, 10.00 ml of 0.033 M KBrO₃ solution and 10 ml of KI solution (16.7%, m/v). The equivalence was detected by addition at the end of the assay of the starch solution and by observing the disappearance of the blue color. A 0.02 M KMnO₄ solution was prepared by dissolving 3.2 g of KMnO₄ in 1 L of water. The solution was boiled during 1 h and then filtered. The concentration was measured by assaying, with the 0.1 M solution of Na₂S₂O₃, a mixture of 20.00 ml of the KMnO₄ solution with 2 g of KI and 10 ml of 1 M H₂SO₄ solution. The equivalence was detected by addition at the end of the starch solution and by observing the disappearance of the blue color. Finally, a solution of 2-nitro-5-thiobenzoate (TNB) was prepared daily as previously described [20] and diluted to 0.45 mM after determination of concentration, using an extinction coefficient of 13,600 M⁻¹ cm⁻¹ at 412 nm [20]. The drugs used during the experimentations were dissolved daily in water or ethanol (96%, v/v) at a concentration of 2.0 mM. They were purchased from different well-established manufacturers.

The different UV–vis absorbances were measured with a diode-array spectrophotometer (Agilent 8453, Palo Alto, CA, USA) at the mentioned wavelengths. However, the measurements of the absorbances in the 96-well plate were performed with a diode array microplate reader (Synergy HT, BioTek, Winooski, VT, USA).

2.2. Methods

2.2.1. The validation process

To determine the concentration of stock solutions on the basis of volumetric or spectrometric measurements, the initial dilution was repeated five times and each diluted solution was measured five times. Moreover, this process was repeated on three consecutive days. The different methods were simultaneously carried out in order to properly compare the results. Concerning the calibration curves, the initial dilution of the stock solution was made five times per day and the five different points of the calibration curves were made for each diluted solution. Finally, each calibration point was measured five times. This delivered a total

of 150 measurements including the zero concentration point. The concentrations of the calibration points were simultaneously determined by measuring the concentration of the stock solution. Finally, sigmoid curves were independently plotted with nine concentrations repeated three times per day during three consecutive days to determine the inhibiting concentration at 50%.

2.2.2. Hypochlorous acid assay

The NaOCl concentration was assayed according three different protocols using the iodometric method as a reference [21]: in this procedure, 50.0 ml of water, 1.0 g of KI and 1.50 ml of diluted acetic acid (12%, m/m) were first mixed (solution A). A volume of 10.00 ml of HOCl stock solution was then taken and diluted to 100.0 ml of water (solution B). A volume of 10.00 ml of B was then added to A and the resulting solution was assayed with 0.1 M Na₂S₂O₃ solution in the presence of the starch solution until disappearance of the blue color. The second method consisted in the measurement of the absorbance at 290 nm of a diluted NaOCl solution (50 µl in 50.0 ml) using 350 M⁻¹ cm⁻¹ as the molar extinction coefficient [22]. The third method involved the spectrophotometric determination of the amount of I₂ formed by the addition of NaOCl solution. In a 10.0 ml flask, 500 µl of a 2000 times diluted NaOCl stock solution adjusted at pH 6.2 with H₂SO₄ were added to 2.5 ml of a 20 mM KI solution and the volume was adjusted with water. The NaOCl concentration (in M) was calculated by measuring the absorbance of the solution at 350 nm using 22,900 M⁻¹ cm⁻¹ as the molar extinction coefficient [23].

2.2.3. Hydrogen peroxide assay

The concentration of H₂O₂ was determined by two methods using the manganometric procedure as a reference [21]. In the first assay, the H₂O₂ stock solution was diluted by adding 900.9 µl in 100.0 ml of water. A volume of 10.00 ml of this solution was assayed after addition of 20.00 ml of a 1 M H₂SO₄ solution, using the 0.02 M KMnO₄ solution which was added until the appearance of a pink color. The second method consisted in the measurement of the absorbance at 240 nm of a diluted H₂O₂ stock solution (60 µl/50.00 ml of water). The concentration (in M) was calculated using 43.6 as the molar extinction coefficient [24].

2.2.4. Taurine assay

Taurine is commonly used to measure the production of HOCl by the formation of taurine chloramines. These were presently measured by two different methods. In both procedures, the reaction mixture contained the following reagents in a final volume of 1.00 ml at the final concentrations indicated between brackets: PBS Buffer pH 7.4 (PO₄³⁻ 10 mM/NaCl 300 mM), taurine (15 mM), NaOCl (0–100 µM). The temperature was maintained at 37 °C during the whole experiment. The curves were constructed according to the validation procedure (Section 2.2.1) with 10, 30, 60, 80 and 100 µM of NaOCl. To determine the amount of taurine chloramines produced, the following reagents were used and added after 5.0 min: thionitrobenzoic acid (TNB) or tetramethylbenzidine (TMB) [17,25]. On the one hand, 750 µl

of 0.45 mM solution of TNB were added and the volume adjusted to 4.00 ml. Then, the absorbance of the solutions was measured at 412 nm and the curve of the absorbance as a function of NaOCl concentration was plotted. On the other hand, 250 µl of a TMB solution (31.3 mg/50.0 ml) and 50 µl of a 2 M HCl solution were added before adjusting the volume to 4.00 ml. The absorbance of the solutions was then measured at 451 nm and the curve of the absorbance as a function of NaOCl concentration was plotted.

2.2.5. Myeloperoxidase assay

The MPO assay was constructed to determine in a first step the amount of MPO necessary to produce 60 µM of HOCl in 5.0 min at 37 °C. Briefly, the reaction mixture contained the following reagents at the concentrations stated between brackets, in a final volume of 1.00 ml: pH 7.4 phosphate buffer (PO₄³⁻ 10 mM/NaCl 300 mM), taurine (15 mM) and different volumes of the recombinant MPO batch solution diluted five times (0, 20, 40, 60, 80 and 100 µl). When necessary, the volume was adjusted to 900 µl with water. The mixture was incubated at 37 °C and the reaction initiated with 100 µl of H₂O₂ (100 µM). After 5.0 min, the reaction was stopped by the addition of 100 µl of catalase (4 U/µl). Finally, the quantity of taurine chloramine was measured as described in the previous section (Section 2.2.4). Using both the TMB and TNB methods according to the first protocol of the validation procedure, the amount of MPO necessary to produce 60 µM of HOCl in 5.0 min at 37 °C was calculated by interpolating the absorbance value obtained with 60 µM solution of HOCl on the calibrating curves obtained with the different volumes of the MPO batch solution. The measurement of the inhibition of MPO chlorinating activity was therefore assessed as previously described [17]. The method quantified the amount of taurine chloramine produced by the MPO/H₂O₂/Cl⁻ system in the presence of several concentrations of a specified inhibitor. The reaction mixture contained the following reagents, at the concentrations stated between brackets, in a final volume of 1.00 ml: pH 7.4 phosphate buffer (PO₄³⁻ 10 mM/NaCl 300 mM), taurine (15 mM) and the inhibitor (0–20 µM). The fixed amount of recombinant MPO (66 µl of MPO batch solution diluted five times, ~40 nM) was added and when necessary, the volume was adjusted to 900 µl with water. The mixture was incubated at 37 °C and the reaction initiated with 100 µl of H₂O₂ (100 µM). After 5 min, the reaction was stopped by the addition of 100 µl of catalase (4 U/µl). Finally, the quantity of taurine chloramine was measured as described in the previous section (Section 2.2.4).

The significance of the mean inhibitory curve for the inhibition in the MPO-chlorinating activity assay was tested by fitting the curve with a three parameters sigmoid model (Sigmastat[®]). Results were considered as statistically significant at $P < 0.05$ and the concentrations of drugs that inhibited 50% of HOCl production (IC₅₀) were measured from the dose-effect curves by taking the absence of the inhibitor as the 0% of inhibition and the absence of H₂O₂ as the 100% of inhibition.

2.2.6. Screening procedure

The screening method is an adaptation in a 96-well plate suitable for spectrophotometric detection (Sarstedt, Essen, Bel-

Table 1
Measurement of the HOCl stock solution concentration by three different methods

Method	Mean \pm S.D. (M)	CV (%)	Recovery (%)
Iodometry (reference method) ^a	1.36 \pm 0.01	0.7	–
UV measurement of NaOCl (290 nm) ^b	1.440 \pm 0.008	0.5	105.8
UV–vis measurement of I ₂ (350 nm) ^c	1.21 \pm 0.06*	4.5	87.9

^a European Pharmacopoeia, fifth edition [21].

^b Zavodnik et al. [22].

^c Gressier et al. [23].

* Significantly different from the reference method ($P < 0.05$, Bonferroni *t*-test).

gium) of the classical tube method. Briefly, the reaction mixture contained the following reagents, at the concentrations stated between brackets, in a final volume of 200 μ l: pH 7.4 phosphate buffer (PO₄³⁻ 10 mM/NaCl 300 mM), taurine (15 mM), the inhibitor (0–20 μ M) and the fixed amount of the recombinant MPO (6.6 μ l of MPO batch solution diluted 2.5 times, \sim 40 nM). When necessary, the volume was adjusted with water. The mixture was incubated at 37 °C and the reaction initiated with 10.0 μ l of H₂O₂ (100 μ M). After 5 min, the reaction was stopped by the addition of 10 μ l of catalase (8 U/ μ l). To determine the amount of taurine chloramines produced, 50 μ l of 1.35 mM solution of TNB were added and the volume adjusted to 300 μ l. Then, the absorbance of the solutions was measured at 412 nm with a microplate reader and the curve of the absorbance as a function of the inhibitor concentrations was plotted. When the inhibitor was dissolved in ethanol, the solution was gradually diluted to add a constant volume of 2 μ l for each concentrations of the sigmoid curve. The controls also contained 2 μ l of ethanol.

The significance of the mean inhibitory curve for the inhibition in the MPO-chlorinating activity assay was tested by fitting the curve with a three parameters sigmoid model (Sigmastat[®]). Results were considered as statistically significant at $P < 0.05$ and the concentration of drugs that inhibited 50% of HOCl production (IC₅₀) were measured from the dose-effect curves by taking the absence of the inhibitor as the 0% of inhibition and the absence of H₂O₂ as the 100% of inhibition.

Concerning the high throughput screening, a variety of inhibitors were selected and tested 5 times by the described screening procedure at the relevant concentration of 1 μ M. The percentage of inhibition at this concentration was calculated by using the absence of the inhibitor as the 0% of inhibition and the absence of H₂O₂ as the 100% of inhibition.

3. Results and discussion

3.1. Hypochlorous acid assay

The determination of the concentration of the HOCl stock solution concentration is crucial for the whole screening process. Indeed, a fixed amount of MPO has to be selected for the procedure. As each batch solution of the recombinant enzyme is characterized by its protein concentration (mg/ml), its activity (U/ml) and its specific activity (U/mg), the amount of MPO necessary to ensure the production of the proper HOCl quantity must be defined for each batch solution using the HOCl stock solution as a reference. To this purpose, three methods were

compared for the measurement of HOCl concentration including the reference method (described in the Pharmacopoeia [21]) and two other procedures taken from the literature [22,23]. The reference method using the iodometric procedure delivered a concentration of 1.36 \pm 0.01 M for the examined solution with an acceptable coefficient of variation (Table 1). However, both spectrophotometric methods gave a poor recovery of 105.8 and 87.9% as compared to the reference method (Table 1). Moreover, the third assay was characterized by an increasing variability (Table 1). The last two spectrophotometric procedures appeared as not suitable to recover the concentration found with the reference method. An alternative procedure would consist in the definition of a proper molar extinction coefficient for HOCl solution followed by the re-analysis of the recovery of the spectrophotometric methods, but the turnover of the MPO solution is relatively slow and the volume of the batch solution to be used is rather large. Therefore, the reference method was preferably selected in order to avoid an over-consumption of the enzyme.

3.2. Hydrogen peroxide assay

The reference volumetric method using KMnO₄ provided a concentration of H₂O₂ in the stock solution of 10.29 \pm 0.05 M, which is equivalent to 31.5 \pm 0.1% (m/m). The UV measurement simultaneously performed and using 43.6 M⁻¹ cm⁻¹ as a molar extinction coefficient [24], provided a concentration of 9.81 \pm 0.02 M with a recovery of 95.3% (Table 2). Both measurements were statistically different ($n = 4$, $P < 0.001$, Dunnett's *post-hoc* test, Sigmastat[®]) and the recovery was not satisfactory according to the procedure described in the literature. As the H₂O₂ solution has to be used daily and must be freshly prepared, the volumetric reference method appeared as not suitable for the screening as it consumes both time and a large volume of solution. For this reason, it was necessary to redefine the molar extinction coefficient at 240 nm (Table 2). Using repeated calibration curves, a value of 39.8 \pm 0.3 M⁻¹ cm⁻¹ was finally derived, which was comparable to the value used by Nelson et al. [26] (Table 3). With this new experimental value, the concentration of the H₂O₂ solution could be directly and daily measured for the screening procedure.

3.3. Taurine assay

After having selected the control methods for stock solutions, the detection method for the product of the reaction between HOCl and taurine was checked. Performances of two methods

Table 2
Measurement of the H₂O₂ stock solution concentration by two different methods

Methods	Mean ± S.D. (M)	CV (%)	Concentration (% m/m)	Recovery (%)
Manganometry (reference method) ^a	10.29 ± 0.05	0.4	31.5	–
UV measurement of H ₂ O ₂ 240 nm ^b	9.81 ± 0.02	0.6	30.1	95.3

^a European Pharmacopoeia, fifth edition [21].

^b Noble et al. [24].

Table 3
Determination of the molar extinction coefficient of H₂O₂ calculated from the slope of the linear relationship between the H₂O₂ concentration and the absorbance at 240 nm

Curve day	Slope (M ⁻¹)	Intercept	Correlation coefficient
1	39.68	0.011	0.999
2	40.09	0.006	0.999
3	39.63	0.008	0.999
Mean ± S.D.	39.8 ± 0.3		

The reference method was used daily to determine the concentration of the H₂O₂ stock solution.

were then compared for the detection of a gradient of taurine chloramines produced by several concentrations of HOCl in a range between 0 and 100 μM. As shown in Fig. 1, the oxidation of TNB in DTNB has been frequently used to measure the production of taurine chloramines [17,23,25]. More recently, the oxidation of TMB was pointed out to be more sensitive in the detection of chloramines (Fig. 1) [25]. Both assays showed a satisfactory reproducibility of the slope, but, as illustrated by Table 4, the TMB method carried out in an acidic medium was two times more sensitive than the TNB assay ($P < 0.001$, Dunnett's *post hoc* test, Sigmastat[®]). Actually, the detection by TMB was firstly conducted in a neutral medium in the presence of iodide with a higher specificity for taurine chloramines towards taurine bromamines and iodamines [25]. However, a precipitate appeared after reaction in the final volume of 4.0 ml, decreasing the reproducibility (data not shown). To avoid this interference, a less specific acidic medium was then selected but remained perfectly suitable as only chloramines were produced in our experiments [25].

3.4. Myeloperoxidase assay

The amount of MPO was previously fixed to produce, in pH 7.4 PBS buffer, 60 μM of HOCl with 100 μM of H₂O₂ in 5 min at 37 °C. Working with a fixed amount of MPO was a deliberate

choice while Allegra et al., Jantchko et al., Van Zyl et al. and Ximenes et al. worked with MPO concentration (10–20 nM) [11,13,14,16]. This allows to work with a MPO activity and to compare the results obtained with different MPO batches. Moreover, the purpose is to select a MPO inhibitor efficient in extracellular fluids and a pH 7.4 PBS buffer is more suitable than pH 7.0 or 5.0 as previously described [13,14].

Consecutively, the detection of taurine chloramines with TMB was firstly chosen to measure the production of HOCl by the MPO/H₂O₂/Cl⁻ system in the selected range of 0–100 μM. The first step consisted in the investigation of the gradient production of chloramines as a function of the MPO batch solution volume. The volume of MPO necessary was further calculated by interpolating the absorbances of a 60 μM HOCl solution that chlorinates taurine in similar conditions. Fig. 2A illustrates the production of taurine chloramines as a function of the volume of MPO solution. However, the absorbance related to the production of 60 μM of HOCl could never be reached, which is not in accordance with previous results (Section 3.3). In order to document this phenomenon, the stability of the signal was studied as a function of the volume of HCl solution added. It was found that the addition of 50 μl of a 7 M HCl solution was suitable to the assay as the maximum of the signal was rapidly reached and that it remained stable during at least 25 min (Fig. 3A). Different hypothesis for this effect were then explored and a major interference between catalase and TMB was identified as the absorbance at 451 nm rapidly decreased in the presence of catalase (Fig. 3B). On the contrary, the method using TNB had a lesser sensitivity but did not suffer from interferences, permitting to calculate the volume of MPO solution that produces 60 μM of HOCl and to measure the production of taurine chloramine in the selected range. A linear gradient was obtained in the range of 0–100 μM of HOCl and the curve actually passed through the absorbance measured with the 60 μM HOCl solution (Fig. 2B). As a correlation could be found between the production of taurine chloramines by MPO and the absorbance, the volume of MPO was fixed according to the TNB method as indicated in Table 5. The absorbance with 60 μM of HOCl was taken

Table 4
Measurement of the taurine chloramines gradient obtained from the reaction of taurine with HOCl at several concentrations (0–100 μM)

Method		Slope (μM ⁻¹)	Mean ± S.D. (μM ⁻¹)	CV (%)
TMB in HCl	Day 1	0.01451	0.0145 ± 0.0002	1.08
	Day 2	0.01438		
	Day 3	0.01469		
TNB	Day 1	–0.00702	–0.0070 ± 0.0001	–1.06
	Day 2	–0.00693		
	Day 3	–0.00708		

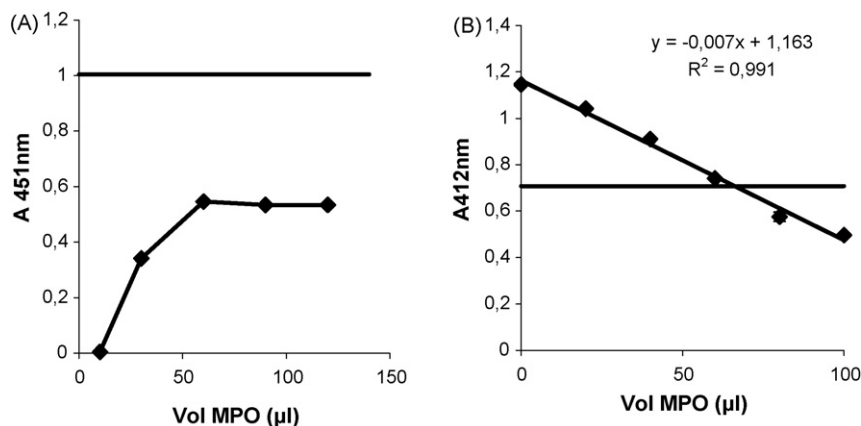


Fig. 2. Graphs of the relationship between the absorbance and the gradient of MPO volume (μl) obtained by the TMB method (A) and the TNB method (B). The absorbance obtained with $60 \mu\text{M}$ of HOCl in the same conditions is represented by the solid horizontal black line.

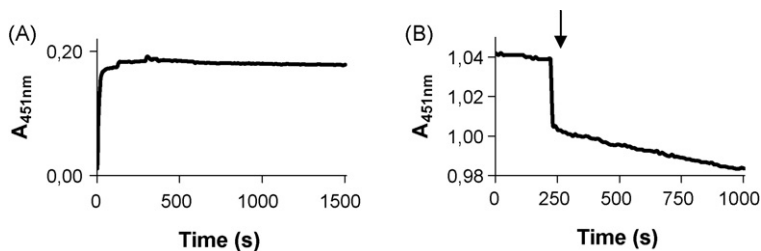


Fig. 3. Kinetics of TMB oxidation after the addition of $50 \mu\text{l}$ of diluted HCl (A) and decrease of the absorbance after the addition of catalase (\downarrow) (B).

from the curve and corresponded to the volume of MPO necessary during the screening. According to the above-described procedure, the interpolated volume corresponded to $66 \pm 8 \mu\text{l}$. However such a procedure is time and reagents consuming (150 tubes and 1.5 ml of MPO solution) and should ideally be simplified. By comparing the whole validation procedure to a running test that consists in a curve constructed with only 18 points (18 tubes and $180 \mu\text{l}$ of MPO solution), it was demonstrated that the rapid test delivered identical results, even with less variability (Table 5).

As all the previously described reactions were performed in single tubes, we decided to transpose the reaction and the study of the MPO inhibition in a microplate system to reduce the time

of analysis and the amount of MPO used during the test. The activity of flufenamic acid on MPO inhibition is well described and frequently handled in our laboratory for different investigations [12]. Therefore, this anti-inflammatory drug was selected to compare the classical method to the transposed microplate method. Actually, the inhibition of MPO by flufenamic acid was performed and compared in both a simple tube test and in a 96-well plate. The results obtained from the construction of sigmoid curves with flufenamic acid concentrations between 0 and $20 \mu\text{M}$ permitted to obtain comparable IC_{50} values both with the screening method in water and in a diluted ethanolic solution (Table 6, $P = 0.2$, one-way ANOVA test, Sigmastat®). This last observation is interesting for the investigation of molecules

Table 5
Determination of the amount of MPO necessary to produce $60 \mu\text{M}$ of HOCl with $100 \mu\text{M}$ of H_2O_2 at 37°C and in 5 min

Method	Interpolated volume of MPO (μl)	Mean \pm S.D. (μl)	CV (%)
Validation procedure ^a	74.11	66 ± 8	12
	58.77		
	60.25		
	71.4		
Running test ^b	66.09	66 ± 2	3
	64.17		
	67.50		

The curves represent the relationship between the volume of MPO added and the absorbances at 412 nm. The interpolated volume is the volume of MPO corresponding to the absorbance obtained in the same conditions with a solution containing $60 \mu\text{M}$ of HOCl.

^a The validation procedure consisted in the establishment of the curves as described in the second protocol of the validation procedure section (Section 2.2.1).

^b The running test used a simplified protocol where only three points per concentration were measured daily.

Table 6

Comparison between the classical tube test and the screening method for the MPO/H₂O₂/Cl⁻ system inhibition by flufenamic acid

Methods		IC ₅₀ (μM)	Mean ± S.D. (μM)	CV (%)
Classical tube (water)	Day 1	0.985	1.3 ± 0.2	19
	Day 2	1.384		
	Day 3	1.417		
96-well plate (water)	Day 1	1.155	1.4 ± 0.2	17
	Day 2	1.630		
	Day 3	1.493		
96-well plate (ethanol)	Day 1	1.631	1.6 ± 0.1	8
	Day 2	1.475		
	Day 3	1.614		

that have a poor water-solubility. However, the percentage of ethanol in the final solution must be carefully handled and do not exceed 1% (v/v).

3.5. Screening procedure

The microplate method was finally adapted to rapidly assess the inhibiting effect of several molecules (examined at 1.0 μM concentration) that were previously shown as MPO inhibitors in the view of a high throughput screening. The conditions of the assay have been set as to select MPO inhibitors having a minor scavenging effect. Indeed, the ratio drug/HOCl (1:60) has been chosen in favor of HOCl in order to observe an enzyme inhibiting effect rather than a scavenging effect. A molecule that inhibits the MPO activity at 50% (30 μM HOCl produced) at a 1 μM

concentration can be assumed to be an enzyme inhibitor. In this context, Table 7 gives the results obtained and compared them to those of literature. Among water soluble molecules, tryptamine derivatives were the most efficient inhibitors, which is consistent with the values obtained by Jantschko et al. [13]. Concerning non-steroidal anti-inflammatory drugs, flufenamic acid and nimesulide were the most efficient molecules although ibuprofen and the oxicams were ineffective. Comparing to the IC₅₀ values recently obtained [12,27], these results are highly comparable. Sodium azide and cimetidine are well known inhibitors of MPO such as attested by the screening procedure that showed an inhibition higher than 50% for 1 μM [16,28]. Other molecules like hydralazine, cinnamic acid and methylthiouracyl had no activity at 1 μM as already reported in the literature [29,30]. When molecules were dissolved in ethanol, the results were also satis-

Table 7

Percentages of inhibition of the MPO/H₂O₂/Cl⁻ system at 1.0 μM for several molecules able to inhibit MPO

Molecules at 1 μM	Mean ± S.D. (%)	Value of the literature	Remark
5Cl-tryptamine	91.1 ± 1.2	0.79 μM ^a	IC ₅₀ at pH 7.0
5F-tryptamine	90.7 ± 2.0	0.73 μM ^a	IC ₅₀ at pH 7.0
Flufenamic acid	43 ± 13	1.1 ± 0.1 μM ^b	IC ₅₀ at pH 7.4
Nimesulid	30.9 ± 6.7	2.1 ± 0.3 μM ^b	IC ₅₀ at pH 7.4
Tenoxicam	2.2 ± 1.6	10 ± 2 μM ^b	IC ₅₀ at pH 7.4
Piroxicam	3.1 ± 5.5	12 ± 4 μM ^b	IC ₅₀ at pH 7.4
Meloxicam	11.5 ± 9.5	11 ± 1 μM ^b	IC ₅₀ at pH 7.4
Ibuprofen	1.2 ± 7.3	400 μM ^c	IC ₅₀
Cimetidine	20.4 ± 9.5	<3 μM ^d	IC ₅₀ at pH 7.4
Sodium azide	27.9 ± 4.6	25 μM ^e	IC ₅₀ at pH 7.0
Hydralazine	-5.1 ± 1.8	57% ^f	% of inhibition at 130 μM
Cinnamic acid	4.8 ± 5.8		
Methylthiouracyl	-1.3 ± 4.6		
Indolylacetate*	72.9 ± 1.3		
Dapsone*	59.9 ± 2.5	0.42 ± 0.05 μM	IC ₅₀ at pH 7.4
Flufenamic acid*	43.0 ± 0.9		
Propylthiouracyl*	-0.9 ± 5.3	~20 μM ^h	IC ₅₀ at pH 7.0

The mean ± S.D. is the result of five measurements.

^gKettle and Winterbourn [31].

^a Jantschko et al. [13].

^b Van Antwerpen et al. [12].

^c Pekoe et al. [27].

^d van Zyle et al. [16].

^e Davies and Edwards [28].

^f Nässberger [29].

^h Lee et al. [32].

* The molecules were dissolved in ethanol.

factory. Indeed, indoxylacetate had a high inhibiting effect which is comparable to the effect of indolic compounds as demonstrated by Ximenes et al. [11]. Dapsone and flufenamic acid could be considered as potent MPO inhibitors with an inhibition higher than 50%, confirming the values obtained in the present study for flufenamic acid and in the literature for dapsone [31]. Finally, propylthiouracyl had no inhibiting effect at 1 μM in the screening test with an IC_{50} around 25 μM [32].

4. Conclusions

The validated screening procedure here described is a convenient method both to select potent inhibitors of the $\text{MPO}/\text{H}_2\text{O}_2/\text{Cl}^-$ system and to measure the IC_{50} value in water or ethanolic solution. For each MPO batch solution used, the amount of MPO necessary for completion of the reaction was calculated with the running test and according to the HOCl stock solution, the concentration of which was measured by the iodometric method. A solution of H_2O_2 was made daily and its concentration measured by a direct spectrophotometric method using $39.8 \text{ M}^{-1} \text{ cm}^{-1}$ as molar extinction coefficient. In conditions where a large number of molecules is available for the screening procedure, their percentage of inhibition at 1.0 μM could be assessed in the microplate assay and molecules that inhibit the MPO activity at more than 50% can be considered as enzyme inhibitors. Thereafter, these potent inhibitors have to be further characterized by their IC_{50} value. The velocity of the assessment is one of the advantages of the present screening procedure that can also evaluate poorly water-soluble molecules with the measurements performed in a 1% (v/v) ethanolic solution. Moreover, the quantity of MPO used in the microplate assay system is rather low. However, some limitations must be highlighted like the interferences of molecules highly absorbing in the range of TNB absorption ($\sim 412 \text{ nm}$). Moreover, thiol-containing molecules and strong reducing agents cannot be evaluated by this method as they react with TNB and DTNB. Obviously, the method does not aim to elucidate the mechanism of inhibition towards MPO which can be investigated by the accumulation of compound II or by the measurement of the rate constant of the reaction between the inhibitor and compound I and II of the enzyme [12,13]. In this context, the high throughput screening is undoubtedly a first line assessment method which affords the selection of inhibitors and permits to reduce the number of candidates for a further elucidation of the mechanism of action.

Acknowledgments

We thank Professor J.-P. Dehaye (Laboratory of Biochemistry and Cellular Biology from the Institute of Pharmacy, Université Libre de Bruxelles) who made possible the measurements on the microplate reader.

References

- [1] P.G. Furtmüller, M. Zederbauer, W. Jantschko, J. Helm, M. Bogner, C. Jakopitsch, C. Obinger, *Arch. Biochem. Biophys.* 445 (2006) 199–213.
- [2] P.G. Furtmüller, U. Burner, W. Jantschko, G. Regelsberger, C. Obinger, *FEBS Lett.* 484 (2000) 139–143.
- [3] S.J. Klebanoff, *J. Leuk. Biol.* 77 (2005) 598–625.
- [4] A.C. Carr, M.C. Myzak, R. Stocker, M.R. McCall, B. Frei, *FEBS Lett.* 487 (2000) 176–180.
- [5] N. Moguilevsky, K. Zouaoui Boudjeltia, S. Babar, P. Delrée, I. Legssyer, Y. Carpentier, M. Vanhaeverbeek, J. Ducobu, *Biochem. Biophys. Res. Commun.* 323 (2004) 1223–1228.
- [6] E. Malle, G. Waeg, R. Schreiber, E.F. Gröne, W. Sattler, H.J. Gröne, *Eur. J. Biochem.* 267 (2000) 4495–4503.
- [7] H.L. Nurcombe, R.C. Bucknall, S.W. Edwards, *Ann. Rheum. Dis.* 50 (1991) 237–242.
- [8] D.-K. Choi, S. Pennathur, C. Perier, K. Tieu, P. Teismann, D.-C. Wu, V. Jackson-Levis, M. Vila, J.P. Vonsattel, J.W. Heinecke, *J. Neurosci.* 25 (2005) 6594–6600.
- [9] Y. Maruyama, B. Lindholm, P. Stenvinkel, *J. Nephrol.* 17 (2004) S72–S76.
- [10] E. Malle, P.G. Furtmüller, W. Sattler, C. Obinger, *Br. J. Pharmacol.* 152 (2007) 838–854.
- [11] V.F. Ximenes, I.M.M. Paino, O.M.M. de Faria-Oliveira, L.M. da Fonseca, I.L. Brunetti, *Braz. J. Med. Biol. Res.* 38 (2005) 1575–1583.
- [12] P. Van Antwerpen, F. Dufrasne, M. Lequeux, K. Zouaoui Boudjeltia, I. Legssyer, S. Babar, P. Moreau, N. Moguilevsky, M. Vanhaeverbeek, J. Ducobu, J. Nève, *Eur. J. Pharmacol.* 570 (2007) 235–243.
- [13] W. Jantschko, P.G. Furtmüller, M. Zederbauer, K. Neuschwandtner, I. Lehner, C. Jakopitsch, J. Arnhold, C. Obinger, *Biochem. Pharmacol.* 63 (2005) 1149–1157.
- [14] M. Allegra, P.G. Furtmüller, G. Regelsberger, M.L. Turco-Liveri, L. Tesoriere, M. Perretti, M.A. Livrea, C. Obinger, *Biochem. Biophys. Res. Commun.* 282 (2001) 380–386.
- [15] M. Allegra, P.G. Furtmüller, W. Jantschko, M. Zederbauer, L. Tesoriere, M.A. Livrea, C. Obinger, *Biochem. Biophys. Res. Commun.* 332 (2005) 837–844.
- [16] J.M. van Zyl, A. Kriegler, B.J. van der Walt, *Biochem. Pharmacol.* 45 (1993) 2389–2397.
- [17] J. Nève, N. Parij, N. Moguilevsky, *Eur. J. Pharm.* 417 (2001) 37–43.
- [18] N. Moguilevsky, L. Garcia-Quintana, A. Jacquet, C. Tournay, L. Fabry, L. Pierard, A. Bollen, *Eur. J. Biochem.* 197 (1991) 605–614.
- [19] W.D. Hewson, L.P. Hager, *J. Biol. Chem.* 254 (1979) 3175–3181.
- [20] T.L. Ching, J. De Jong, A. Bast, *Anal. Biochem.* 218 (1994) 377–381.
- [21] *European Pharmacopoeia*, 5th ed., Drukerei C.H. Beck, Nördlingen, 2004.
- [22] I.B. Zavodnik, E.A. Lapshina, L.B. Zavodnik, M. Soszynski, G. Bartosz, M. Bryszewska, *Bioelectrochemistry* 58 (2002) 127–135.
- [23] B. Gressier, N. Lebegue, C. Brunet, M. Luyckx, T. Dine, M. Cazin, *J.C. Cazin, Pharm. World Sci.* 3 (1995) 76–80.
- [24] R.W. Noble, Q.H. Gibson, *J. Biol. Chem.* 245 (1970) 2409–2413.
- [25] J.M. Dypbukt, C. Bishop, W.M. Brooks, B. Thong, H. Eriksson, A.J. Kettle, *Free Radic. Biol. Med.* 39 (2005) 1468–1477.
- [26] D.P. Nelson, L.A. Kiesow, *Anal. Biochem.* 49 (1972) 474–478.
- [27] G. Pekoe, K. Van Dyke, D. Peden, H. Mengoli, D. English, *Agents Actions* 12 (1982) 371–376.
- [28] B. Davies, S.W. Edwards, *Biochem. J.* 258 (1989) 801–806.
- [29] L. Nässberger, *Biochem. Pharmacol.* 42 (1991) 1844–1847.
- [30] Y. Kato, A. Nagao, J. Terao, T. Osawa, *Biosci. Biotechnol. Biochem.* 67 (2003) 1136–1139.
- [31] A.J. Kettle, C.C. Winterbourn, *Biochem. Pharmacol.* 41 (1991) 1485–1492.
- [32] E. Lee, Y. Miki, H. Katsura, K. Kariya, *Biochem. Pharmacol.* 39 (1990) 1467–1471.

Quantitative determinations of SiC and SiO₂ in new ceramic materials by Fourier transform infrared spectroscopy

E. Vereda Alonso*, A. García de Torres,
M.T. Siles Cordero, J.M. Cano Pavón

Department of Analytical Chemistry, University of Málaga, Campus de Teatinos s/n, 29071 Málaga, Spain

Received 1 August 2007; received in revised form 31 October 2007; accepted 8 November 2007

Available online 22 November 2007

Abstract

Silicon carbide-based biomorphic ceramics have been fabricated by the pyrolysis and infiltration of natural wood (mukali and pine) with molten silicon. The results of the process of synthesis have been studied in this and other biomorphic ceramics using thermogravimetric analysis (TGA), X-ray photoelectron spectroscopy (XPS) analysis and scanning electron microscopy (SEM). For evaluating the yield of the synthesis, a new method by Fourier transform infrared spectrometry (FTIR) has been developed for the direct determination of SiC and the simultaneous determination of SiC and SiO₂ by absorbance measurements in KBr pellets. The procedure was based on the use of the ratio between the absorbance of the characteristic band of silicon carbide or silica and those of an acetate internal standard added to samples. A multivariate calibration strategy based on inverse least squares and the standard addition approach were employed for quantification. The results obtained for all biomorphic ceramics studied and synthetic samples prepared by mixing pyrolyzed wood with pure SiC were satisfactory. The relative standard deviation for all samples was lower than 2.9%.

© 2007 Elsevier B.V. All rights reserved.

Keywords: Fourier transform infrared spectroscopy; Multivariate calibration; Ceramic materials; Silicon carbide; Silica

1. Introduction

In recent years, a new type of porous ceramic materials with specific functional properties and structures by mimicking the hierarchical cellular structure of wood has attained particular interest. These ceramic materials, called biomorphic ceramics, show at low density excellent mechanical properties such as high-strength, stiffness, toughness, good oxidation and corrosion resistance, high-thermal conductivity, and good thermal shock resistance. The applications of this type of porous ceramics are increasing and include heat and acoustic insulating structures, medical implants and microelectronics components. The synthesis of these new materials is based on the infiltration of the pyrolyzed wood template with silicon; there are several ways of synthesis: infiltration with molten silicon [1–4], chemical Si contained vapor infiltration (CVI) [5,6], infiltration–pyrolysis of metallic-alkoxide [7], polymeric precursors [8], sol–gel infil-

tration/carbothermal reduction [9–11], etc. Among them, the chemical vapor infiltration produces SiC ceramics with very good properties; however, the cost is higher compared with the infiltration with molten silicon. In this last technique, biomorphic SiC ceramics are manufactured by a two-step process: a controlled pyrolyzation of the wood followed by a rapid controlled reactive infiltration of the carbon preform with molten silicon. The result is a Si/SiC composite that replicates the highly interconnected microstructure of the wood with SiC, while the remaining unreacted Si fills most of the wood channels. The diversity of wood species provides a wide choice of materials, in which the density and the anisotropy are the critical factors of the final microstructure and hence the mechanical properties of the material. This manufacturing process presents several advantages over others: lower cost because the temperatures of process and the use of additives or high-purity powders are reduced and faster, because the time and the synthesis rates are reduced.

For the evaluation of the quality of the process of synthesis of these biomorphic ceramics the quantitative determination of SiC and SiO₂ is very interesting. As there are no adequate certified reference materials available for the calibration of analytical

* Corresponding author. Tel.: +34 952131883; fax: +34 952132000.
E-mail address: eivereda@uma.es (E. Vereda Alonso).

methods for the characterization of this new class of compounds no direct methods could be used. Inductively coupled plasma atomic emission spectrometry (ICP-AES) is the most widely used technique for the determination of Si in advanced ceramics [12]. However, for the chemical analysis of these refractory and chemical resistant materials by ICP-AES, complete dissolution of the sample with extreme chemical treatments must be performed. This has been realized by two general procedures: acid decomposition and alkaline fusion. These dissolution procedures, which are a major source of errors and difficulties, present several serious disadvantages. Acid decomposition procedures are time-consuming, often require the use of potentially hazardous acids and can lead to systematic errors such as contamination and incomplete digestions. Alkaline fusion procedures although efficient and relatively rapid, are laborious, requiring constant supervision during operation, and can also lead to the aforementioned systematic errors. Additionally, the analysis of the solutions by atomic spectroscopic techniques produces matrix effects owing to high-salt loading. In view of these drawbacks direct solid sampling techniques offer advantages. Our investigations have shown that Fourier transform infrared spectroscopy (FTIR) and X-ray photoelectron spectroscopy (XPS) are the more useful devices to obtain fast information about the content of silicon carbide in the sample [13].

FTIR is potentially a good tool for the structural studies of these types of materials, however up to now it has not been widely used, only Quian et al. [9,10,14] have employed this technique to investigate the carbothermal conversion of the charcoal silica composites into SiC in the final step of the synthesis. These authors registered the FTIR spectra of charcoal/silica composite and porous SiC ceramic, the absorption bands of the charcoal/silica composite at 1090, 800 and 466 cm^{-1} were attributed to antisymmetric and symmetric stretching vibrations of Si–O–Si bond, respectively. Compared with the porous SiC ceramic spectrum, the above-mentioned absorption bands nearly disappear, and at the same time, a new intense broad band centered at 825 cm^{-1} was observed, which was ascribed to the Si–C fundamental stretching vibration and a low intensity broad band located between 1250 and 1000 cm^{-1} was assigned to the presence of a small fraction of silica that was negligible at the X-ray diffraction (XRD) sensitivity. This would imply that silica hardly remains in the porous SiC ceramic. In XPS studies realized by us [13], the presence of silica in this type of biomorphic materials was evidenced too.

FTIR is a rapid analytical technique that provides information about the qualitative composition of samples. However, quantitative analysis by FTIR requires the use of cells of known thickness and, in general, a previous dilution of the samples with a suitable solvent, limitations which often preclude the general application of this technique to quantitative determinations. In recent years, a series of simple models for carrying out quantitative determinations from infrared data, which do not require the use of a known absorption pathlength, have been described [15–19]. These models are based on the use of the ratio of the absorbances at two well-defined wavenumbers, however the use of the ratio of the characteristic bands of two compounds in a

mixture does not permit the determination of the concentration of each component, and only the proportion of the two compounds considered was obtained. This problem can be solved if the concentration of one of the compounds is known; thus it is possible when this compound is an adequate internal standard [20].

The aim of this paper has been the development of simple strategies which could be used for routine determination of SiC and SiO₂ in biomorphic ceramics based on the use of FTIR absorbance measurements in KBr pellets. The simplest procedure was based on the use of the ratio between the absorbance of the characteristic band of SiC at 847 cm^{-1} and three intense bands at 1560, 1420 and 650 cm^{-1} of an internal standard (barium acetate) added to samples. A multivariate calibration strategy based on inverse least squares and standard additions approach was employed for quantification. Due to the good results of this calibration strategy, the method was also applied to the simultaneous determination of SiC and SiO₂ using the quotients between the characteristic band of SiC (847 cm^{-1}) and the characteristic band of SiO₂ (1090 cm^{-1}) on the same three intense bands of the selected internal reference and the same calibration strategy.

2. Experimental

2.1. Reagents and samples

Different kinds of biomorphic ceramics derived from natural woods (oak, eucalyptus, beech, sapelli, Swedish pine and mukali) were used. Samples were supplied by the Departments of Condensed Matter of the University of Seville, Spain and Materials Science, Glass and Ceramics of the University of Erlangen-Nuremberg, Germany except Swedish pine and mukali that were synthesized by us.

Analytical reagent grade chemicals were used throughout. Potassium bromide, and barium acetate were purchased from Merck (Darmstadt, Germany) and pure silicon, silicon carbide and silicon dioxide (99.999%, w/w) from Aldrich Chemie (Steinheim, Germany). All these reagents were dried at 48 °C for 24 h and after conserved into a desiccator.

2.2. Instrumentation

The infrared spectroscopic measurements were carried out using a Shimadzu Model 8300 Fourier transform infrared spectrometer. The spectra were recorded in the range 2000–500 cm^{-1} with a resolution of 2 cm^{-1} . Potassium bromide pellets were used to obtain the IR spectra of the samples. The pellets with 13 mm diameter and 0.4 mm thickness were pressed at 8 tonnes for 10 min in an evacuated pellet die from 90.0 mg mixture of sample, barium acetate and potassium bromide, and dried to remove water. For the mass measurements it was used an AND GR-202 balance was used with a precision of ± 0.01 mg. Multivariate calibration data treatment was carried out using Statgraphics Plus 6.0 professional software [21].

A Lenton Tube furnace, model LTF 16/180, was employed for the synthesis of biomorphic ceramics.

Thermogravimetric analysis (TGA) and differential thermal analysis measurements were made with a Rigaku Thermoflex TG 8110; the temperature was increased to 1200 °C at 10 °C min⁻¹ in a dry atmosphere.

XPS analysis was performed with a Physical Electronics 5700 instrument with a Mg K α X-ray excitation source ($h\nu = 1253.6$ eV); binding energies (BE) were determined with respect to the position of the C 1s peak corresponding to Si–C bond at 282.4 eV [22]. The residual pressure in the analysis chamber was maintained below 3×10^{-9} Torr during data acquisition.

The cellular microstructures of the biomorphic ceramics were observed by scanning electron microscopy (SEM, JEOL, JFM 840) operated at 20 kV.

2.3. Material preparation

Rectangular specimens (3 mm \times 1 mm \times 0.6 mm) of the carbon preform were prepared by pyrolyzing the dried (70 °C, 15 h) wood (pine or mukali) in argon-atmosphere in a carbon-heated furnace. A slow heating rate of 1 °C/min was applied up to 500 °C where the organic biopolymers have been completely decomposed to carbon followed by an accelerated rate of 5 °C/min up to the peak temperature. The specimens were hold at 1500 °C for 4 h, resulting in a porous biocarbon template (charcoal). The charcoal pieces were packed in silicon powder and heated together at 1500 °C for 4 h with the same temperature program in a vacuum furnace to allow complete reaction of silicon with the carbon structure to form β -SiC. Unreacted silicon remained in part of the pore channels so that a cellular Si-containing SiC composite material finally was obtained. The fabrication process is shown in Fig. 1.

2.4. Preparation of standard addition calibration set for SiC determination

KBr pellets were prepared by mixing different accurately weighted amounts from 0.00 to 2.00 mg (± 0.01 mg) of SiC, 1.00 mg (± 0.01 mg) biomorphic ceramic (previously grounded and homogenized), 1.00 mg (± 0.01 mg) internal standard (barium acetate), and KBr to complete a total amount of 200.0 mg (± 0.1 mg). The mixture was homogenized for 5 min in an agate mortar, and then 90.0 mg (± 0.1 mg) of this were weighted for the pellets preparation.

For the background spectrum, a pellet was prepared by mixing an accurately weighted amount of 1.00 mg (± 0.01 mg) charcoal and 199.0 mg (± 0.1 mg) KBr, after the 5 min homogenization, 90 mg (± 0.1 mg) of the mixture were weighed. Else six blanks were prepared in the same form but mixing 1.00 mg (± 0.01 mg) charcoal, 1.00 mg (± 0.01 mg) barium acetate and 198.0 mg (± 0.1 mg) KBr.

Table 1
Baselines established for integrating areas

$\bar{\nu}$ (cm ⁻¹)	X_{\min} (cm ⁻¹)	X_{\max} (cm ⁻¹)
1559.34	1465.80	1739.67
1420.51	1383.83	1465.80
1091.63	1033.70	1247.20
847.65	792.69	971.09
650.93	628.75	672.93

The spectra were recorded from 2000 to 500 cm⁻¹, using a nominal resolution of 2 cm⁻¹ and accumulating 100 scans for spectrum. Peak area measurement corresponding to SiC band (847 cm⁻¹) was divided by data corresponding to the 1560, 1420 and 650 cm⁻¹ acetate bands, using the baselines given in Table 1, and SiC determined by multivariate calibration strategy of inverse least squares, using the standard addition approach as a function of added mg of the SiC, from absorbance quotient data of six blanks prepared as described above. The baselines were chosen with the pellet spiked with a 1 mg SiC.

2.5. Preparation of standard addition calibration set for simultaneous SiC and SiO₂ determination

The simultaneous determination of SiC and SiO₂ was carried out by the same procedure described above. KBr pellets were prepared by mixing different accurately weighed amounts from 0.00 + 0.00 to 2.00 + 2.00 mg (± 0.01 mg) of SiC + SiO₂, 1.00 mg (± 0.01 mg) biomorphic ceramic (previously grounded and homogenized), 1.00 mg (± 0.01 mg) internal standard (barium acetate), and KBr to complete a total amount of 200.0 mg (± 0.1 mg). The mixture was homogenized for 5 min in an agate mortar, and then 90.0 mg (± 0.1 mg) of this were weighed for the pellets preparation. For the background and six blanks spectra, the pellets were prepared in the same form as described for the individual SiC determination, and the spectra were recorded using the aforementioned instrumental conditions.

For the simultaneous determination of SiC and SiO₂, the peaks area corresponding to SiC (847 cm⁻¹) and to SiO₂ (1090 cm⁻¹) were divided by data corresponding to above-mentioned three barium acetate bands at 1560, 1420 and 650 cm⁻¹, and SiC and SiO₂ determined in the same pellet by multivariate calibration strategy of inverse least squares using the standard addition approach from absorbance quotient data of six blanks.

2.6. Standard addition analysis using an internal standard and multivariate calibration strategy by inverse least squares

For samples containing mixtures of different compounds, which present their characteristics absorption bands at differ-

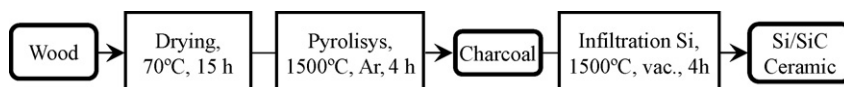


Fig. 1. Processing scheme of manufacturing Si/SiC ceramics from wood.

ent wavenumbers, it can be established a relationship between the absorbance at two wavenumbers (each of one corresponding to each compound), considered for a same spectrum, which will be independent on the bandpass, b , and will depend on the proportion between the concentrations of the two compounds.

$$\frac{A_{\text{SiC}}}{A_{\text{BaAc}_2}} = \frac{\varepsilon_{\text{SiC}} b [\text{SiC}]}{\varepsilon_{\text{BaAc}_2} b [\text{BaAc}_2]} \Rightarrow \frac{A_{\text{SiC}}}{A_{\text{BaAc}_2}} = \frac{\varepsilon_{\text{SiC}} [\text{SiC}]}{\varepsilon_{\text{BaAc}_2} [\text{BaAc}_2]}$$

The addition of different amounts of the analyte to be determined to a series of fixed aliquots of the sample to be analyzed provides a typical standard addition expression, in our case

$$\frac{A_{\text{SiC}}}{A_{\text{BaAc}_2}} = \frac{\varepsilon_{\text{SiC}} [\text{SiC}]_{\text{sample}}}{\varepsilon_{\text{BaAc}_2} [\text{BaAc}_2]} + \frac{\varepsilon_{\text{SiC}} [\text{SiC}]_{\text{added}}}{\varepsilon_{\text{BaAc}_2} [\text{BaAc}_2]}$$

being ε_{SiC} and $\varepsilon_{\text{BaAc}_2}$ the absorption coefficient of the analyte, SiC, and the internal standard, barium acetate, at the considered wavenumbers. From the quotient between the intercept, $a = (\varepsilon_{\text{SiC}} [\text{SiC}]_{\text{sample}}) / (\varepsilon_{\text{BaAc}_2} [\text{BaAc}_2])$ and the slope, $m = \varepsilon_{\text{SiC}} / (\varepsilon_{\text{BaAc}_2} [\text{BaAc}_2])$. The concentration of the analyte in the sample can be obtained. This value can be obtained with more exactitude if a blank is measured, then

$$[\text{SiC}]_{\text{sample}} = \frac{a - (A_{\text{SiC}}/A_{\text{BaAc}_2})_{\text{blank}}}{m}$$

being $(A_{\text{SiC}}/A_{\text{BaAc}_2})_{\text{blank}}$ the signal measured of the blank.

In multivariate calibration strategy by inverse least squares, several instrumental responses ($r_1, r_2, r_3, \dots, r_n$) can be used and the analyte concentration can be calculated as

$$[\text{SiC}]_{\text{sample}} = b_0 + b_1 r_1 + b_2 r_2 + b_3 r_3 + \dots + b_n r_n$$

where b_0, b_1, b_2, b_3 and b_n are the regression coefficients.

In our case the instrumental responses are the quotients between the peak area corresponding to SiC (847 cm^{-1}) divided by the peak areas corresponding to the 1560, 1420 and 650 cm^{-1} acetate bands:

$$r_1 = \frac{A_{847}}{A_{1560}}; \quad r_2 = \frac{A_{847}}{A_{1420}}; \quad r_3 = \frac{A_{847}}{A_{650}}$$

So, an equation with four unknowns (b_0, b_1, b_2, b_3) is obtained. If I added samples for measurement, there will be a system of I equations with four unknowns. Obviously, must be made at least four additions. When the regression coefficients are calculated, the determination of SiC in the sample is done in the same form rather than in standard additions with univariate calibration, by means of the measurement of a blank.

In the same form is operated for the determination of $[\text{SiO}_2]$, being in this case the instrumental responses

$$r_1 = \frac{A_{1090}}{A_{1560}}; \quad r_2 = \frac{A_{1090}}{A_{1420}}; \quad r_3 = \frac{A_{1090}}{A_{650}}$$

3. Results and discussion

3.1. Characterization of the biomorphic ceramics

3.1.1. TGA analysis

Thermogravimetric curves of the biomorphic ceramics show in general a slight increase of mass between 200 and $1200 \text{ }^\circ\text{C}$;

Table 2
Analysis of biomorphic samples by XPS

Biomorphic ceramics from	C 1s (%)		O 1s (%)		Si 2p (%)	
	Atomic	Mass	Atomic	Mass	Atomic	Mass
Oak	26.63	17.00	41.32	35.85	32.06	46.86
Beech	22.40	13.88	42.32	34.96	32.28	51.16
Sapeli	20.85	13.13	46.89	39.35	32.26	47.52
Pine	53.66	41.16	31.44	32.12	14.90	26.72
Mukali	23.52	15.73	44.88	39.99	25.93	40.56
Eucalyptus	31.93	19.93	30.69	25.52	37.39	54.55

these increases are comprised between 2 and 6%, and can be attributed to the oxidation of unreacted silicon to SiO_2 . As unreacted carbon must be present in all samples, the loss of mass due to C oxidation (to CO and CO_2) must be appreciable lesser; this fact indicates that excess of silicon is habitual in the synthetic procedures used for to obtain these ceramic composites.

3.1.2. XPS analysis

XPS has been used for the study of the composition of the samples. For this study the biomorphic materials were powdered and homogenized in an agate mortar. Measurements were performed on samples mounted in a cup ($1 \text{ mm} \times 3.5 \text{ mm}$ i.d.) and pressed manually. The atomic concentration calculation is expressed as a percentage in a tabular form based on the area under the peak, multiplied by the sensitivity factor for each element, and provides a ratio of a single element to the sum of the others elements present [23] (Table 2). The error of the method is approximately of 10%.

Deconvolution of the Si 2p peak has been carried out for determining the percentage of Si, SiC and SiO_2 (in % of total area). In Fig. 2 can be seen the deconvolution of the Si 2p peak for biomorphic eucalyptus and mukali, the percentage of Gaussian employed in the deconvolution was 90%. With these data and those given in Table 2 for Si 2p, it is possible to calculate the percentages of these species in the samples approximately. The results of these analyses are given in Table 3.

3.1.3. SEM analysis

Fig. 3 shows the cellular microstructures of biomorphic ceramics from beech (Fig. 3A and B) and oak woods (Fig. 3C and D). During the reactive infiltration processing, silicon infiltrates through the pores and channels of the pyrolyzed wood structure and reacts with the carbon. Some of the large pores (black

Table 3
Results of the deconvolution of the Si 2p peak

Biomorphic ceramics from	Si 2p (in % total area)			Si 2p (in % samples)		
	SiO_2	SiC	Si	SiO_2	SiC	Si
Oak	21.76	52.89	25.35	21.81	35.38	11.88
Beech	22.40	42.32	35.28	24.51	30.90	18.05
Sapeli	20.10	51.97	28.82	20.43	34.64	13.70
Pine	9.39	82.8	7.81	5.37	31.58	2.09
Mukali	43.19	26.56	30.25	37.48	15.37	12.27
Eucalyptus	16.45	46.12	34.25	19.20	35.91	18.68

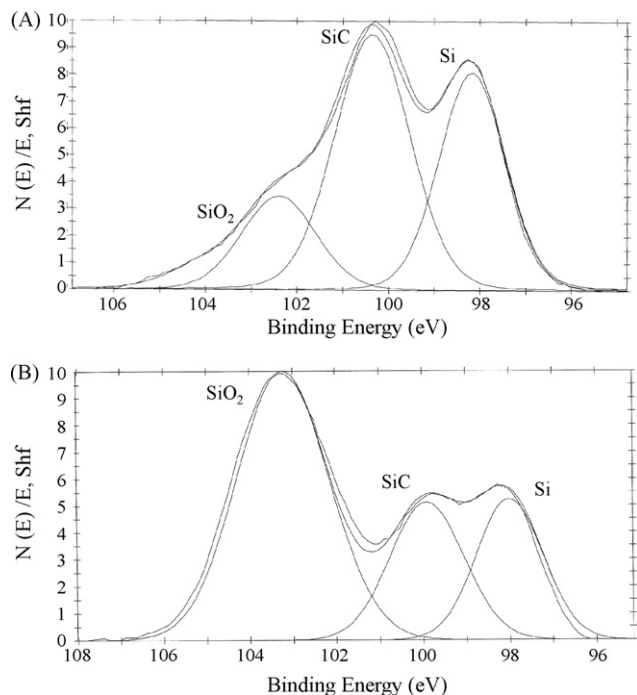


Fig. 2. Deconvolution of the Si 2p peak obtained from some powdered biomorphic ceramics for XPS; the percentage of Gaussian employed in the deconvolution was 90%. (A) Eucalyptus and (B) mukali.

area in the micrographs) have not been completely filled with silicon. The gray blocks in the micrographs are silicon carbide grains from the Si–C reaction. The white blocks are free silicon not reacted. The microstructure of the wood charcoal shows hollow channels of various diameters that originate from tracheid

cells that are parallel to the axis of the tree. The channels can be classified into two groups, depending on their cross-sectional area: large channels and small channels. The SEM micrographs of the resulting biomorphic ceramic (Fig. 3) shows a bimodal grain-size distribution consisting on both micron-sized grains (μ -SiC) and nanometric grains (n-SiC). SiC grains in the micron range are only found inside channels where Si is majoritary (residual crystalline Si with white blocks in SEM micrographs, Fig. 3D). Normally a layer of μ -SiC is formed where carbon walls previously existed surrounding the large channels. Inside small channels μ -SiC grains are found closing the pores. Surrounding these μ -SiC and towards the unreacted C, n-SiC grains can be found (Fig. 3B). So, the struts of the biomorphic ceramic are composed of SiC particles with typical diameter of about 2 μ m, and some nanometer SiC grains that can be observed in cellular pores.

3.2. FTIR determination of SiC and SiO₂

3.2.1. Selection of the appropriate bands for the FTIR measurement of SiC and SiO₂

Fig. 4 shows the FTIR spectra of KBr pellets of pure SiC, sodium carbonate and barium acetate. As can be seen in the case of pure SiC, an absorption band at 847 cm^{-1} is found. For barium acetate three bands are located at 1560, 1420 and 650 cm^{-1} . These bands were attributed to antisymmetric and symmetric stretching vibrations of C–O bond and to symmetric twisting of O–C–O, respectively [24], not overlapping with the band of the SiC, however the carbonate band localized at 875 cm^{-1} produces interferences in the SiC band. So the acetate bands are the most appropriate to be employed for SiC determination in

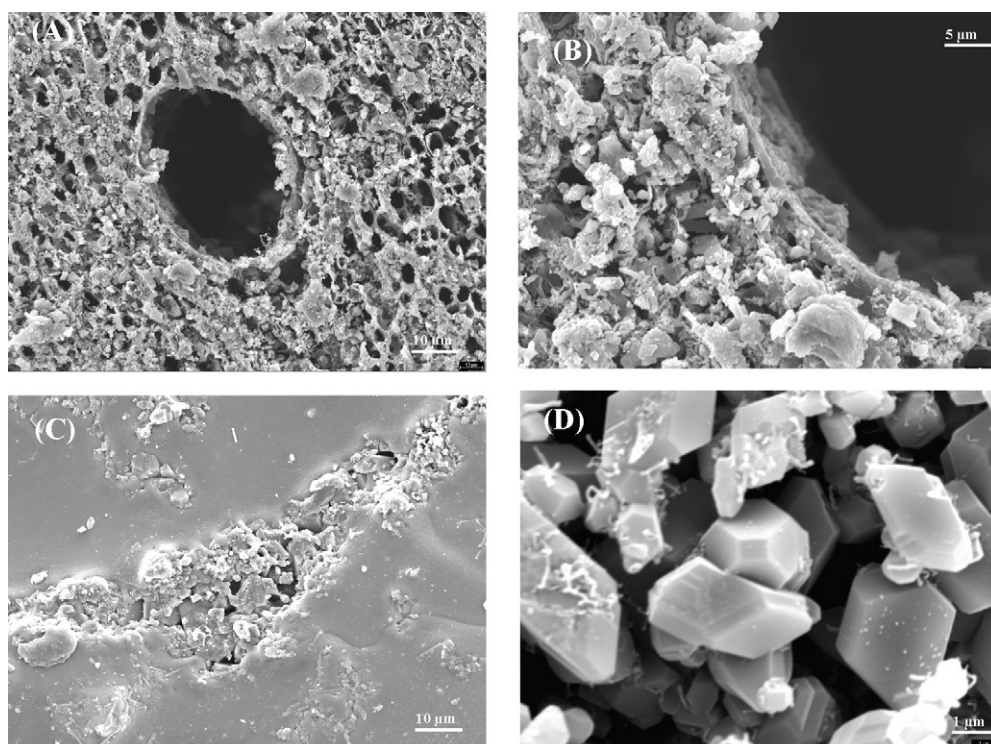


Fig. 3. SEM micrographs of some biomorphic ceramics. (A and B) Beech and (C and D) oak (white, Si; grey, SiC; black, pores).

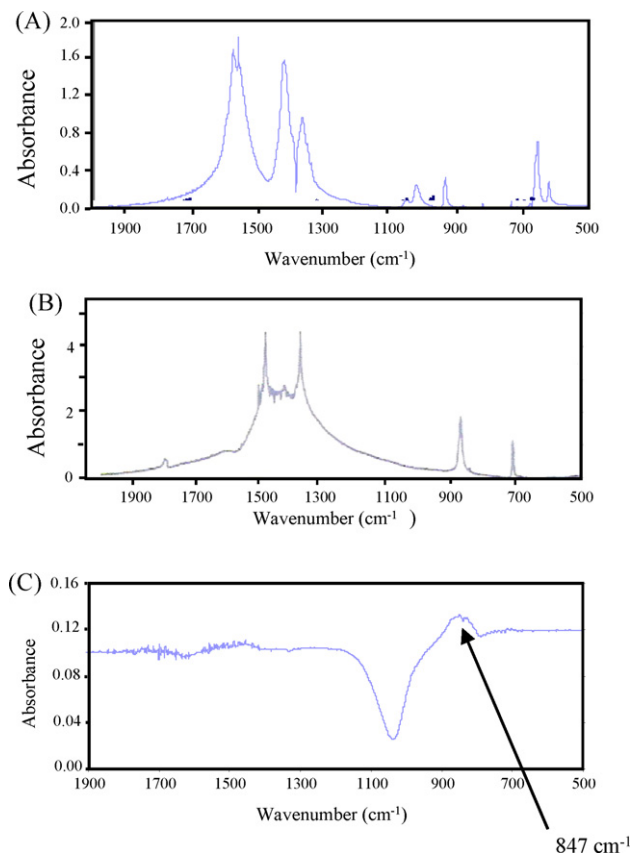


Fig. 4. FTIR spectra of KBr disks of barium acetate (A), sodium carbonate (B) and pure SiC (C).

order to avoid the problems related to establish quantitative data in conditions for which it is difficult to fix the bandpass.

Fig. 5 shows the FTIR spectrum of a KBr disk with 0.5% of biomorphic ceramic plus 0.5% of barium acetate. As can be seen, in the spectrum appear the three characteristic bands of barium acetate and the broad band centered at 847 cm^{-1} ascribed to the Si–C fundamental stretching vibration according to the literature for SiC materials [25–27]. In addition, the band centered at 1090 cm^{-1} is assigned to the presence of a small fraction of silica (this would imply that silica hardly remains in the porous SiC ceramic, according to the XPS study). This peak was used for the determination of the silica in the biomorphic ceramics.

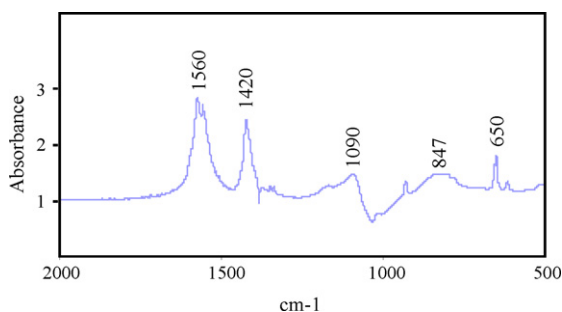


Fig. 5. FTIR spectrum of a KBr disk with 0.5% of biomorphic ceramic plus 0.5% of barium acetate.

3.2.2. Selection of the instrumental parameters and conditions of measurement

Absorbance measurements in the solid phase are usually affected by levels of noise larger than those found in homogeneous solution due to the presence of the solid support, which causes a strong attenuation of the light intensity reaching the detector. Thus, a careful study of the instrumental parameters and conditions of measurement was carried out in order to obtain as good as possible signal-to-noise ratio, which would then ensure satisfactorily reproducible data.

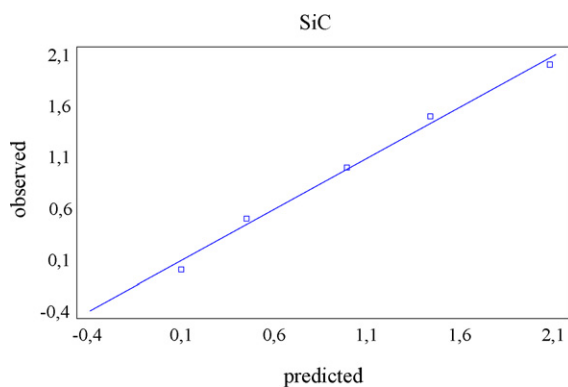
The SiC band at 847 cm^{-1} , the SiO_2 band at 1090 cm^{-1} and the barium acetate bands at 1560, 1420 and 650 cm^{-1} were used in this study. Heights were measured at these wavenumbers and areas were calculated by drawing the baselines shown in Table 1. The ratios of the band heights (or areas) were used, obtaining the best results with the areas ratios.

A systematic study of the effect of the nominal resolution and the number of cumulated scans was performed under the aforementioned conditions. The number of accumulated scans per spectrum was changed from 50 to 150, and the nominal resolution varied from 1 to 16 cm^{-1} . An increase in the number of cumulated scans has no influence on the ratio of the bands (heights or areas) but it reduces the background drastically. So 100 scans were established as suitable FTIR measurements in order to ensure a compromise between measurement frequency and precision values. On the other hand, the more intense signals were found for a 2 cm^{-1} nominal resolution, this value also corresponding to the best repeatability.

3.2.3. Quantitative analysis of FTIR data

The choice of the calibration method is imposed by the nature of the sample, the KBr disks of the biomorphic ceramics are darker than those of pure SiC, and so a method of external calibration could not be possible, being necessary use standard additions. On the other hand, due to the darkness of the KBr disks of the biomorphic ceramics, the amount of ceramic for preparing the disk and the total weight of the pellet had to be optimized; the amount of biomorphic ceramic was varied from 1 to 10 mg maintaining the total weight of the mix in 200 mg and taking 90 mg of the homogeneous mix for preparing the pellet; the most transparent pellet and so with more intense signal at the interest bands was that with 1 mg of biomorphic ceramic (0.5% in biomorphic ceramic), with this concentration in biomorphic ceramic the total weight of the disk was varied from 60 to 100 mg. A decrease in the weight of the disk produces more transparent disks, but more fragile, so 90 mg were established for suitable FTIR measurements in order to ensure resistant KBr disks.

Simple linear regression (SLR) for the standard addition calibration was proved with each of the three ratios of areas chosen between the analyte and the internal standard, obtaining low regression correlation coefficients, so multiple linear regression (MLR) that has the advantage to work on signals at more than one wavelength was used. Then, under the aforementioned instrumental conditions, calibration lines were prepared by addition of 0.00 to 2.00 mg of SiC. The peak area values of the interest bands were calculated using the baselines given in Table 1. The



$$[\text{SiC}] = -0.305358 - 1.00643 \cdot \frac{A_{847}}{A_{650}} - 2.48777 \cdot \frac{A_{847}}{A_{1420}} + 21.3073 \cdot \frac{A_{847}}{A_{1560}}$$

R-squared = 99,125 percent
 R-squared (adjusted for d.f.) = 96,5001 percent
 Standard Error of Est. = 0,1479

Fig. 6. The observed vs. predicted graph and the equation of the fitted model for the biomorphic ceramic from oak for SiC determination.

Table 4

Results of the determination of SiC and SiO₂ in biomorphic ceramic by XPS and FTIR

Biomorphic ceramics from	XPS		FTIR (SiC) FTIR (SiC and SiO ₂)		
	%SiC	%SiO ₂	^a %SiC	^a %SiC	^a %SiO ₂
Oak	35.4	21.8	35.7 ± 0.2	33.6 ± 0.2	23.0 ± 0.1
Beech	30.9	24.5	44.6 ± 0.1	47 ± 1	23.9 ± 0.6
Sapeli	34.6	20.4	31.2 ± 0.1	26.4 ± 0.1	24.9 ± 0.4
Pine	31.5	5.3	30.7 ± 0.1	31.2 ± 0.1	6.9 ± 0.2
Mukali	15.4	37.5	17.7 ± 0.3	14.3 ± 0.4	34.3 ± 0.5
Eucalyptus	35.9	19.2	35.2 ± 0.2	35.2 ± 0.2	27.9 ± 0.1

^a Results obtained from six different blanks ± standard deviations.

observed versus predicted graphs and the equation of the fitted model for the biomorphic ceramic from oak for SiC determination and simultaneous SiC and SiO₂ determination are given in Figs. 6 and 7, respectively.

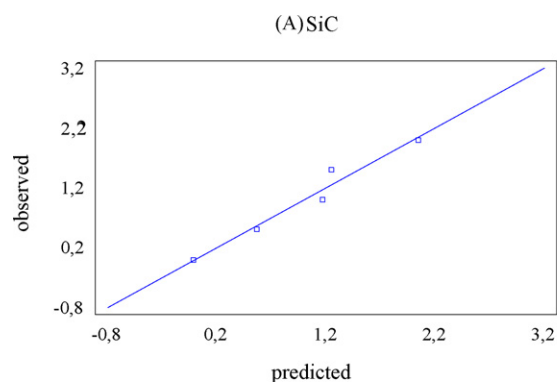
The results obtained for all biomorphic ceramics studied (Table 4) were satisfactorily compared with those obtained by XPS analysis although this last technique produces semiquantitative results. To test the applicability of the method, synthetic samples were prepared by mixing pyrolyzed wood with pure SiC and were analyzed by the proposed method. The results shown in Table 5 indicated good recovery in all instances. As can be seen the relative standard deviation for all samples was lower than 2.9%.

Table 5

Results of the determination of SiC and SiO₂ for synthetic samples

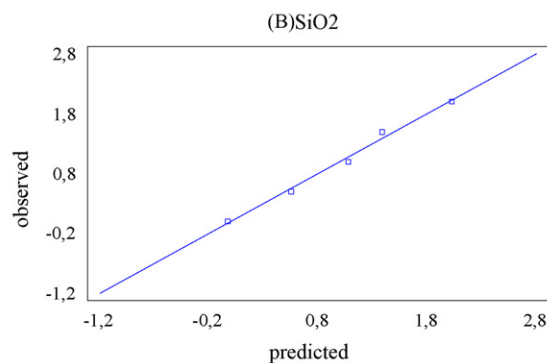
Content of the synthetic samples		FTIR analysis	
%SiC	%SiO ₂	^a %SiC	^a %SiO ₂
40	–	41.4 ± 0.3	–
60	–	61.5 ± 0.3	–
40	20	40.2 ± 0.1	21.8 ± 0.1
60	30	58.5 ± 0.3	30.7 ± 0.7

^a Results obtained from six different blanks ± standard deviations.



$$[\text{SiC}] = -0.333726 \cdot \frac{A_{847}}{A_{650}} + 1.42487 \cdot \frac{A_{847}}{A_{1420}} - 68.3212 \cdot \frac{A_{847}}{A_{1560}}$$

R-squared = 96,1099 percent
 R-squared (adjusted for d.f.) = 84,4394 percent
 Standard Error of Est. = 0,311855



$$[\text{SiO}_2] = -0.150005 + 1.14486 \cdot \frac{A_{1090}}{A_{650}} + 7.90381 \cdot \frac{A_{1090}}{A_{1419}} - 31.7735 \cdot \frac{A_{1090}}{A_{1560}}$$

R-squared = 99,0597 percent
 R-squared (adjusted for d.f.) = 96,2388 percent
 Standard Error of Est. = 0,153321

Fig. 7. The observed vs. predicted graphs and the equations of the fitted models for the biomorphic ceramic from oak for simultaneous SiC (A) and SiO₂ (B) determinations.

4. Conclusions

The results presented for SiC and SiO₂ in biomorphic ceramics show that FTIR using the ratio of absorbance peak areas between the analyte and a reference compound, provides accurate results for the determination of each compound in the samples without the need to use sample cells with a known optical pathlength. This method can be used satisfactorily in the evaluation of the quality of the processes of synthesis of these new materials because the preparation of these samples as KBr pellets is the simplest and the most rapid form to realize these analyses; so as to allow its applicability in the industrial field, where short times are always a priority.

Acknowledgments

The authors thank the Spanish Ministerio de Ciencia y Tecnología (MCyT) for supporting this study, project no. CTQ 2006-00735, and also FEDER funds and the Junta de Andalucía.

References

- [1] P. Greil, T. Lifka, A. Kaindl, *J. Am. Ceram. Soc.* 83 (1998) 825.
- [2] C. Zollfrank, H. Sieber, *J. Eur. Ceram. Soc.* 24 (2004) 495.
- [3] M. Presas, J.Y. Pastor, J. Llorca, A.R. Arellano López, J. Martínez Fernández, R. Sepúlveda, *Int. J. Refrac. Met. Hard Mater.* 24 (2006) 49.
- [4] A.I. Shelykh, I.A. Smirnov, A.R. Arellano López, J. Martínez Fernández, F.M. Varela-Feria, *Phys. Solid State* 48 (2006) 216.
- [5] E. Vogli, J. Mukerji, C. Hoffman, R. Kladny, H. Sieber, P. Greil, *J. Am. Ceram. Soc.* 84 (2001) 1236.
- [6] J.M. Quian, J.P. Wang, G.Y. Hou, G.J. Quiao, Z.H. Jin, *Scripta Mater.* 53 (2005) 1363.
- [7] T. Ota, M. Imaeda, H. Takase, M. Kobayashi, N. Kinoshita, T. Hirashita, et al., *J. Am. Ceram. Soc.* 83 (2000) 1521.
- [8] C. Zollfrank, R. Kladny, H. Sieber, P. Greil, *J. Eur. Ceram. Soc.* 24 (2004) 479.
- [9] J. Quian, J. Wang, G. Quiao, Z. Jin, *J. Eur. Ceram. Soc.* 24 (2004) 3251.
- [10] J. Quian, J. Wang, Z. Jin, *Mater. Sci. Eng. A371* (2004) 229.
- [11] C.R. Rambo, J. Cao, O. Rusina, H. Sieber, *Carbon* 43 (2005) 1174.
- [12] S. Mann, D. Geilenberg, J.A. Broekaert, M. Yansen, *J. Anal. Atom. Spectrom.* 12 (1997) 975.
- [13] J.M. Cano Pavón, E. Vereda Alonso, M.T. Siles Cordero, A. García de Torres, *Anal. Chim. Acta* 528 (2005) 129.
- [14] J. Quian, Z. Jin, *J. Eur. Ceram. Soc.* 26 (2006) 1311.
- [15] M. de la Guardia Cirugeda, J.L. Carrión Domínguez, J. Medina Escriche, *Analyst* 109 (1984) 457.
- [16] J.L. Carrión Domínguez, S. Sagrado, M. de la Guardia Cirugeda, *Anal. Chim. Acta* 185 (1986) 101.
- [17] Z.A. Benzo, C. Gómez, S. Menéndez, M. de la Guardia Cirugeda, A. Salvador, *Microchem. J.* 40 (1989) 271.
- [18] J.V. Julián Ortiz, M. de la Guardia Cirugeda, *Can. J. Spectrosc.* 25 (1990) 44.
- [19] S. Garrigues, M. de la Guardia Cirugeda, *Analyst* 116 (1991) 1159.
- [20] S. Garrigues, M. de la Guardia Cirugeda, *Anal. Chim. Acta* 242 (1991) 123.
- [21] Statgraphics Plus Versión 6.0, Referente Manual, Manugistics Rockwille, MD, 1992.
- [22] B.A. De Angelis, C. Rizzo, S. Contarini, S.P. Howlett, *Appl. Surf. Sci.* 51 (1991) 177.
- [23] Physical Electronics, Multitechnique ESCA Referente manual for the PC-ACCES Software Versión 6.0, Physical Electronics, Minneapolis, USA, 1995.
- [24] A.W. Musumeci, R.L. Frost, E.R. Waclawik, *Spectrochim. Acta A* 67 (2007) 649.
- [25] H. Preiss, L.M. Berger, M. Braun, *Carbon* 33 (1995) 1739.
- [26] M.I. Baraton, M.S. El-shall, *Nanostruct. Mater.* 6 (1995) 301.
- [27] E. Ermer, W.S. Ptak, *Vibr. Spectrosc.* 29 (2002) 211.

Organotin speciation in textile and plastics by microwave-assisted extraction HPLC–ESI-MS

Xiupin Wang, Haiyan Jin, Lan Ding, Huarong Zhang,
Hanqi Zhang, Chenling Qu, Aimin Yu*

College of Chemistry, Jilin University, Changchun 130012, PR China

Received 29 August 2007; received in revised form 19 November 2007; accepted 19 November 2007

Available online 9 January 2008

Abstract

The HPLC coupled with electrospray ionization mass spectrometry (ESI-MS) was applied for the determination of tributyltin chloride (TBT), triphenyltin chloride (TPhT), triethyltin chloride (TET) in textile and plastic samples. The separation was performed in the isocratic mode on ion exchange SCX column with a mobile phase containing methanol–ammonium acetate (50 mmol l^{-1})–acetic acid (90/9.98/0.02, v/v/v). Sensitive detection of three organotin compounds by ESI-MS was performed on the basis of multiple reaction monitoring (MRM) mode. Limits of detection were 0.4, 20, 4 ng ml^{-1} for TBT, TPhT, and TET, respectively. Microwave-assisted extraction (MAE) of organotin compounds was finished in 60% (v/v) methanol aqueous solution. Under the experimental conditions used, recoveries of three organotin compounds obtained for spiked textile and plastic samples are in the range of 55–95% and the R.S.D.s are 3–9%.

© 2007 Elsevier B.V. All rights reserved.

Keywords: Speciation analysis; Organotin compounds; Microwave-assisted extraction; HPLC–ESI-MS; Textile; Plastic

1. Introduction

The organotin compounds (OTs) are used worldwide as insecticides, fungicides, bactericides, acaricides, preservatives, stabilizers, antifouling agents, water repellents, fire retardants for woolen, cotton fabrics, moth proofing of textiles, disinfectors of hospitals and clothing, and UV-oxidation resistance stabilizers, therefore found in numerous compartments such as water, plastic, textile. Organotins can elicit a wide range of endocrine and nervous-system effects, particularly tri-substituted species, are recognized to be very toxic to marine organisms [1]. For instance, organotins may cause neural degeneration in fetal rat cell cultures and induction of diabetes in hamsters [2,3]. In recent years, the many studies about sediment and biotic samples have been reported [4,5], but the scientists seldom pay attention to research of textile and plastic samples. Therefore, analysis of textile and plastic samples is particularly important because they and the health of person are vitally related.

Come to light, reliable and practical extraction methods for the determination of OTs in complex natural matrices are of considerable interest. The microwave-assisted extraction (MAE) has advantages of lower volumes of organic solvent, simplicity, increase of sample throughput and reduction of extraction time compared with conventional sample preparation techniques. Donard et al. studied butyl- and phenyltin-derivatives in the sediments by MAE using capillary gas chromatography with flame photometric detection (GC-FPD) [6]. High recovery values (80–100%) were obtained for all butyl and phenyltin compounds (BTs and PTs). However, the poor precision (20–30%) obtained for monobutyltin is partly due to derivatization agent (NaBEt_4) leaded into its ethylation after leaching. Pereira et al. used MAE method to extract butyl- and phenyltin compounds from biological materials and the compounds were determined by GC-atomic emission detection (GC-AED) and GC-FPD [7]. Yang et al. used MAE-high performance liquid chromatography-inductively coupled plasma mass spectrometry (HPLC–ICPMS) to investigate butyltin compounds from sediment, but monobutyltin (MBT) was hardly recovered, because of using acetic acid as the extraction medium [8].

Traditional methods of detection of organotins mainly include GC-FPD [9,10], isotope dilution-GC-ICPMS [11,12],

* Corresponding author. Tel.: +86 431 5168399; fax: +86 431 5112355.
E-mail address: juanzimumu@email.jlu.edu.cn (A. Yu).

HPLC–ICP-MS [4,5,8,11,13–16], and HPLC–electrospray-MS (HPLC–ES-MS) [12,17]. When the GC was applied, either hydrolysis or derivatization of the organotin compounds before analysis was required. Although ICP-MS is very sensitive, structure information of OTs was not obtained. Wu et al. attempted to use HPLC–ES-MS to detect butyltin compound in aqueous samples and environmental samples, but only detection of tributyltin was achieved [18]. Jones-Lepp and Varner described a new method that a micro-HPLC–ES-MS (μ -HPLC–ES-MS) was applied to the detection of dibutyltin from water polluted by potable-water polyvinyl chloride (PVC) pipe [19]. Toledo et al. [17] achieved solid phase extraction HPLC–ES-MS (SPE-LC–ES-MS) method using selected-ion monitoring (SIM) mode to detect TBT and TPhT in natural waters, but SPE was not used to extract solid samples. When the multiple reaction monitoring (MRM) mode was used to quantify OTs, the specific pairs were used as monitoring ions and the disturbed effect was decreased compared with SIM mode.

In this work the MAE-HPLC–ESI-MS was developed to detect tributyltin chloride (TBT), triphenyltin chloride (TPhT), and triethyltin chloride (TET) in textile and plastic samples. The application of the MAE for the extraction of OTs was evaluated and the affect of microwave extraction temperature, extraction solvent and extraction time were examined. The separation of tri-OTs in a SCX column with a suitable mobile phase was investigated, and ES-MS detection conditions for the organotin compounds under positive ion detection mode were studied.

2. Experimental

2.1. Chemicals and reagents

Analytical grade methanol and ammonium acetate were purchased from Beijing Chemical Factory (China). HPLC grade methanol was obtained from Fisher Scientific (USA). Ultra-pure water obtained with Milli-Q (Millipore, 21 Molheim, France) was used throughout. TBT, TPhT, and TET were purchased from Sigma Products (USA). Stock OT standard solutions ($1000 \mu\text{g ml}^{-1}$) were prepared separately by adding each OT compound into methanol. Working standard solutions ($1 \mu\text{g ml}^{-1}$) were prepared weekly by diluting the stock solutions in a methanol.

2.2. Instrument and analytical conditions

A WR-3C microwave sample preparation system (MicheM, Beijing, China) equipped with ten extraction vessels was used for closed-vessel MAE of organotins from the textile and plastic samples. The extraction vessel consists of a vessel body and a liner vessel. Separations were performed using a ZORBAX 300-SCX strong cation exchange column ($200 \text{ mm} \times 4.6 \text{ mm i.d.}$, $5 \mu\text{m}$, Agilent, USA) with a guard column of the same material. Optimal separation was achieved in isocratic mode with a mobile phase containing methanol–ammonium acetate (50 mmol l^{-1})–acetic acid (90/9.98/0.02, v/v/v) mixture at a flow-rate of 1 ml min^{-1} .

Table 1

Pairs of monitored ions of three OTs in the MRM mode and corresponding MS condition

Compound	Parent ion (m/z)	Product ion (m/z)	Declustering potential (V)	Collision energy (eV)
TBT	291.1	179.0	50	20
TPhT	351.1	197.0	70	40
TET	237.1	179.0	50	20

All HPLC–MS experiments were carried out on an Agilent Technologies 1100 HPLC system (Palo Alto, CA, USA) coupled with an ESI mass spectrometer. Mass spectra were obtained from ABI Q-Trap mass spectrometer (Applied Biosystems Sciex, Foster City, USA) equipped with ESI source. The instrument was connected with a computer running Applied Biosystems Analyst Version 1.4 software. Mass spectrum data were obtained with Bio-Analyst software (Applied Biosystems, Sydney, Australia). The ESI-MS detection conditions were: curtain gas, N₂; nebulizer gas, N₂ (40 psi); ionization mode, positive; curtain gas, “high”; entrance potential, 10 v; dwell time, 100 ms. The quantification for three OTs was achieved in the MRM mode. Pairs of monitoring ions of three OTs, and corresponding declustering potential, and collision energy are shown in Table 1.

2.3. Sample preparation

2.3.1. Preparation of spiked sample

After cutting the textile and plastic into pieces, the three OTs standard solutions were added to submerge 5 g of the textile and plastic pieces above mentioned, respectively. After an equilibration time of 48 h, the solvent was eliminated with a gentle stream of nitrogen. The concentrations of OTs in the spiked sample, for TBT was 0.5, 1, $2 \mu\text{g g}^{-1}$, for TPhT was 2, 4, $8 \mu\text{g g}^{-1}$, and for TET was 1, 2, $4 \mu\text{g g}^{-1}$, respectively. The spiked samples were stored at $+4 \text{ }^\circ\text{C}$ in the dry brown bottle. Blank samples were prepared in the same way except that the standard solution containing OT was not added.

2.3.2. Preparation of mimetic real sample

The three OTs working standard solutions were prepared by dilution with acetone from the stock solutions. Ten ml of working standard solutions and the plastic sample, polymethyl methacrylate, with certain weight ($\sim 1 \text{ g}$) were added into a 25 ml glass beaker. The concentrations of OTs in the plastic sample, for TBT was 0.5, 1, $2 \mu\text{g g}^{-1}$, for TPhT was 2, 4, $8 \mu\text{g g}^{-1}$, and for TET was 1, 2, $4 \mu\text{g g}^{-1}$, respectively. The glass beaker was sealed with a stopper and shaken on a platform shaker operating at 200 rpm for 30 min. The plastic sample was dissolved fully and equilibrated for 72 h in the dark. The acetone solution containing plastics and OTs was spread on weighed glass slide. The glass slide loading sample was dried at room temperature for 5 min to remove acetone and weighed. Based on the weight data, the weight of mimetic real sample was calculated. This procedure ensures that the OTs were not only deposited on the surface of the plastic, but also were uniformly dispersed in the bulk of the plastic.

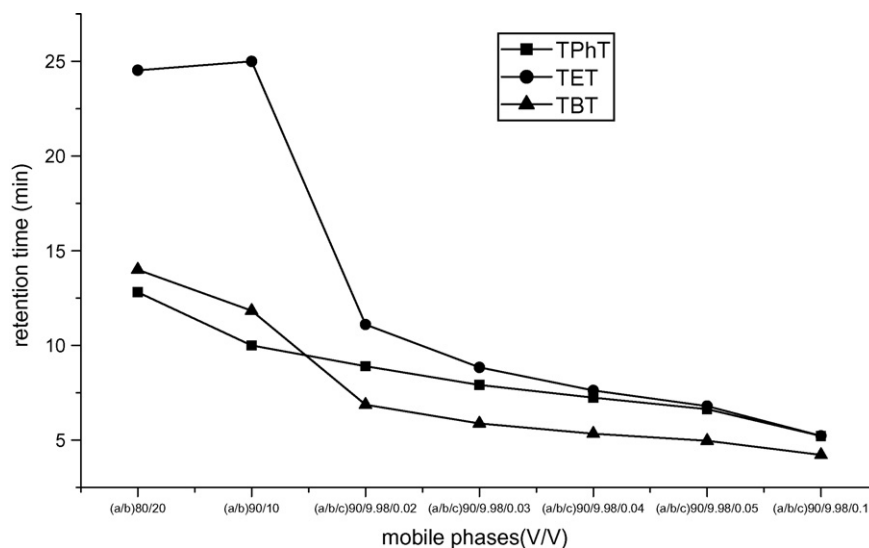


Fig. 1. Retention time of three organotin compounds in different mobile phase. (a) Methanol, (b) ammonium acetate aqueous solution, (c) acetic acid.

2.4. Extraction

0.5 g of spiked textile or plastic sample or 5 g of glass slide loading mimetic real sample was added into the liner vessel of extraction vessel tubes, into which 4.5 ml (for spiked sample) or 30 ml (for glass slide loading mimetic real sample) of 60% (v/v) methanol aqueous solution was added. The liner vessel was put into the vessel body. The closed extraction vessels were put into microwave sample preparation system and subjected to microwave irradiation at 90 °C for 5 min. The extract from MAE was concentrated to a volume of about 2 ml with rotary evaporator under reduced pressure at 40 °C and diluted to 8 ml using the mobile phase. The diluted sample solution was filtered through a 0.45 μm membrane and directly injected into the HPLC–ESI–MS system.

3. Results and discussion

3.1. Separation of OTs by HPLC

The separation of TBT, TPhT, and TET was carried out on a SCX column due to its compatibility with ES–MS detection. Because too high concentration of ammonium acetate has a significant effect on the degree of ionization, the ammonium acetate was added in methanol–water. As shown in Fig. 1, methanol–ammonium acetate aqueous solution mobile phases proved to be satisfactory for the separation of TBT, TPhT, and TET, but too long retention time of TET affects the detection speed. Therefore, an acetic acid is added in above mobile

phases, and the effect of acetic acid concentration on the separation was studied. The use of acetic acid in ammonium acetate aqueous solution mobile phase greatly shorten the retention times of TET, but too high concentration of acetic acid affects the chromatographic separation. Methanol–ammonium acetate (50 mmol l⁻¹)–acetic acid (90/9.98/0.02, v/v/v) can give the good resolution between the three OTs in less than 13 min.

Isocratic elution was employed using methanol–ammonium acetate (50 mmol l⁻¹)–acetic acid (90/9.98/0.02, v/v/v) as the mobile phase at a flow rate of 1 ml min⁻¹ and the column temperature was kept at 30 °C. The retention times of TBT, TPhT, and TET are about 6.98, 8.902, and 11.27 min, respectively. The regression equations, correlation coefficients, and concentration range for determination of TBT, TPhT, and TET, are listed in Table 2.

3.2. Detection of OTs by MS

3.2.1. Electrospray mass spectra of OTs

To optimize the ES–MS parameters for each of the compounds, direct sample injection was used. The three OTs studied usually provide cation (Cat) and anion (An) in the first-order mass spectra without protonated molecules or molecular adducts. Thereby, [Cat]⁺ and its fragment ions were studied in positive ion detection mode [20]. ES mass spectra of TBT (Fig. 2a), TPhT (Fig. 2b), and TET (Fig. 2c) were initially obtained under positive ion detection mode, respectively. The mass spectra of the organotins are very characteristic. Because

Table 2
Calibration curves of three organotin compounds

Compound	Pairs of monitoring ions	Calibration curves	Correlation coefficient R^2	Linearity range (μg ml ⁻¹)
TBT	[Cat] ⁺ /[Cat-2Bt+2H] ⁺ (m/z 291/179)	$Y = 1.34 \times 10^5 x - 88.1$	0.9998	0.001–15
TPhT	[Cat] ⁺ /[Sn ^{II} +Ph] ⁺ (m/z 351/197)	$Y = 1.01 \times 10^6 x - 5.17 \times 10^3$	0.9991	0.05–25
TET	[Cat-Et+Ac] ⁺ /[Cat-2Et+2Me] ⁺ (m/z 237/179)	$Y = 1.19 \times 10^4 x - 41.1$	0.9993	0.01–40

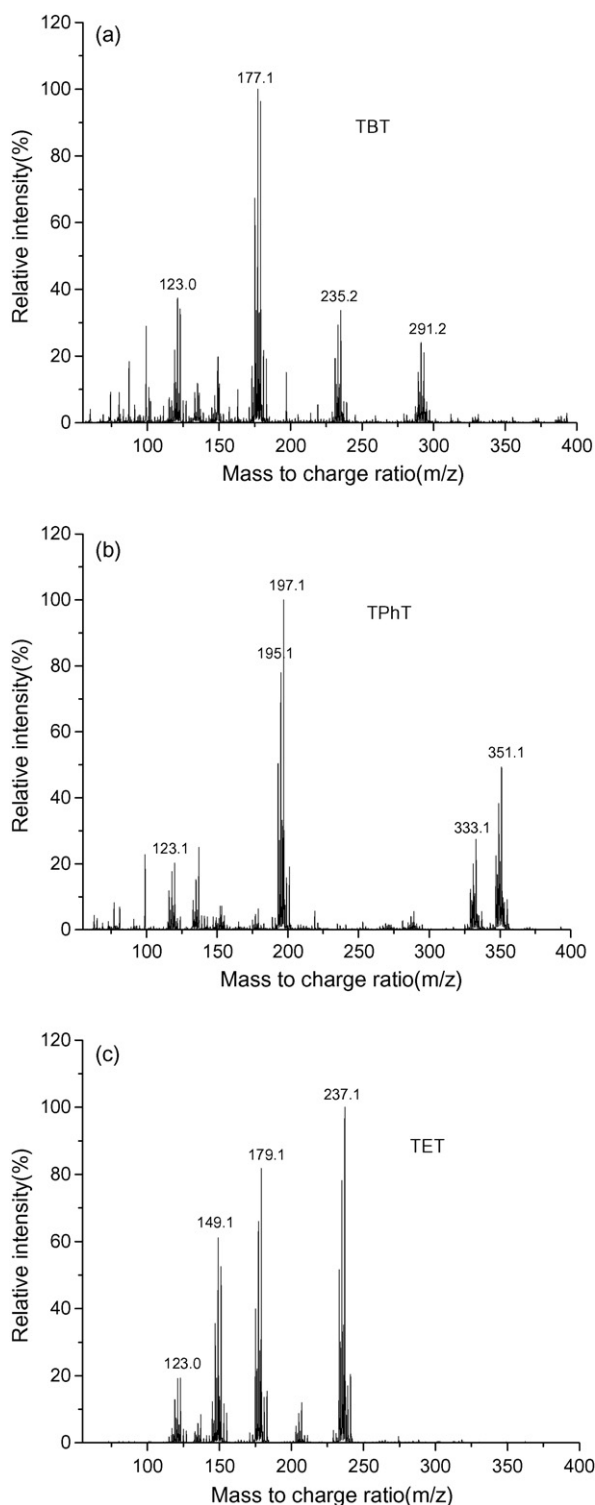


Fig. 2. Full scan mass spectra of (a) TBT, (b) TPhT, and (c) TET.

tin has ten isotopes, thereby in subsequent discussion of the mass spectra, only the most abundant ion of the isotope cluster, based on ^{120}Sn , will be mentioned. The use of ammonium acetate as an additive in the mobile phase helped to stabilize the predominant ions of the organotin formed during the electrospray process. The mass spectra for TBT, TPhT, and TET exhibited intense $[\text{Cat-Bt} + \text{Ac}]^+$ (m/z 293), $[\text{Cat-Ph} + \text{Ac}]^+$ (m/z

Table 3
Typical fragments ions of three OTs

Compound	M_r	m/z	Tentative assignation
TBT	291 + Cl	293	$[\text{Cat-Bt} + \text{Ac}]^+$
		291	$[\text{Cat}]^+$
		235	$[\text{Cat-Bt} + \text{H}]^+$
		179	$[\text{Cat-2Bt} + 2\text{H}]^+$
		177	$[\text{Sn}^{\text{II}} \text{Bt}]^+$
TPhT	351 + Cl	351	$[\text{Cat}]^+$
		333	$[\text{Cat-Ph} + \text{Ac}]^+$
		197	$[\text{Sn}^{\text{II}} \text{Ph}]^+$
		123	$[\text{Cat-3Ph} + 3\text{H}]$
TET	207 + Cl	237	$[\text{Cat-Et} + \text{Ac}]^+$
		207	$[\text{Cat}]^+$
		179	$[\text{Cat-2Et} + 2\text{Me}]^+$
		151	$[\text{Cat-2Et} + 2\text{H}]^+$
		149	$[\text{Sn}^{\text{II}} \text{Et}]^+$
		123	$[\text{Cat-3Bt} + 3\text{H}]^+$

333), and $[\text{Cat-Et} + \text{Ac}]^+$ (m/z 237) ion cluster, respectively. The main ions with their corresponding tentative assignations are shown in Table 3. The fragment ions (m/z 177 of TBT, m/z 197 of TPhT, m/z 149 of TET) are experimentally attributable to $[\text{Sn}^{\text{II}} \text{Bt}]^+$, $[\text{Sn}^{\text{II}} \text{Ph}]^+$, and $[\text{Sn}^{\text{II}} \text{Et}]^+$, respectively. The presence of tin (II) ions is not unexpected, similar results were also obtained by other researchers [17].

3.2.2. Optimization of the MS parameters

Among these MS parameters, the collision energy and the declustering potential were most important. The effects of the two parameters on the electrospray processes were studied. Collision energy (or fragmentor voltage) influences the fragmentation of the charged species and the transmission of ions. Thus, in order to establish the optimum condition for the determination of three OTs, standard solutions were injected at collision energy from 0 to 130 eV and the mass spectra were recorded in full scan mode. Fig. 3 shows the relationship of the normalized relative abundances of the fragment ions of TBT (Fig. 3a), TPhT (Fig. 3b), and TET (Fig. 3c) and the collision energy values. The effect of the collision energy on the peak distribution in mass spectrum is clearly seen. High collision energy leads to decomposition of the organotin species into elemental tin. At collision energy values lower than 20 eV the mass spectra obtained for the three compounds exhibit intense $[\text{Cat}]^+$ ion cluster, and the formation of the $[\text{Cat-Ph} + \text{Ac}]^+$ (m/z 333, Fig. 3b), and $[\text{Cat-Et} + \text{Ac}]^+$ (m/z 237, Fig. 3c) adduct. However, there is an exception for Fig. 3a that fragment ion $[\text{Cat-2Bt} + 2\text{H}]^+$ (m/z 179) and $[\text{Cat-3Bt} + 3\text{H}]^+$ (m/z 123) become predominant because TBT can be disintegrated more easily. The fragment ions of the three compounds almost disappear at collision energy values higher than 70 eV. Therefore, the optimum collision energy value for the analysis of the three compounds was found to be between 10 and 40 eV (Table 1).

The effect of the declustering potential on the abundances of the three compounds parent ions and their respective frag-

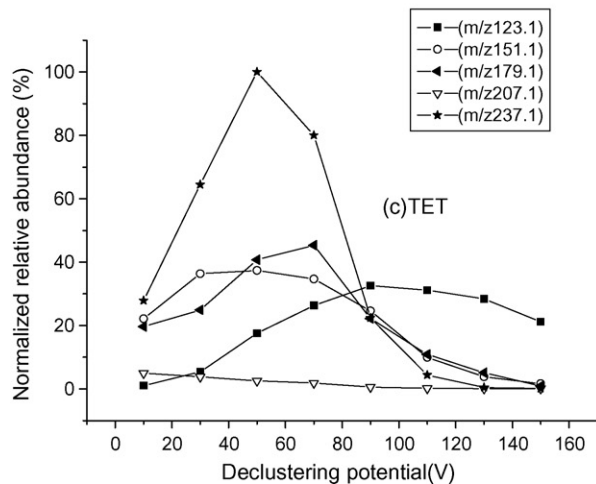
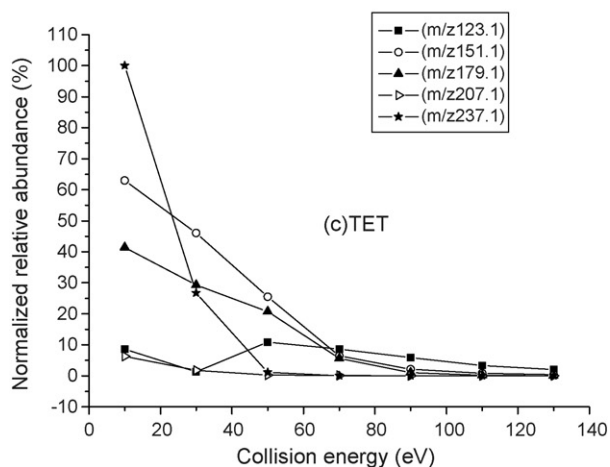
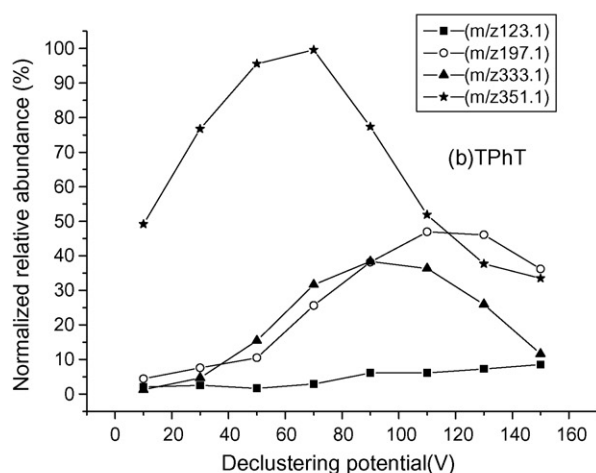
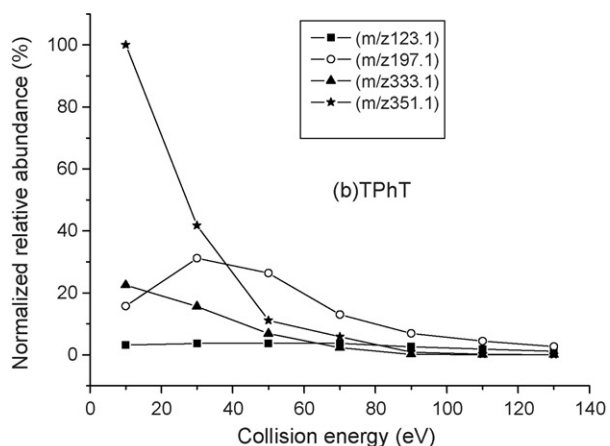
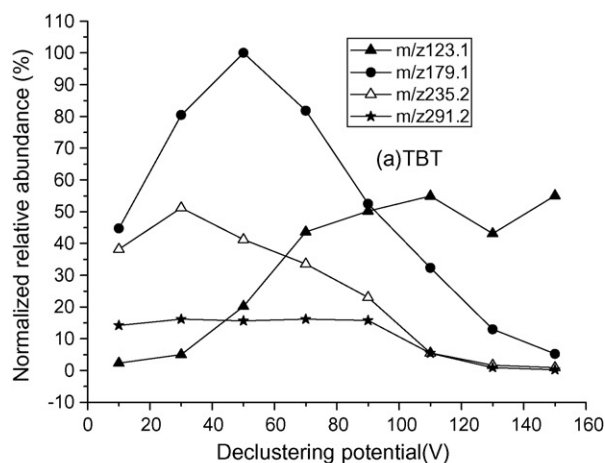
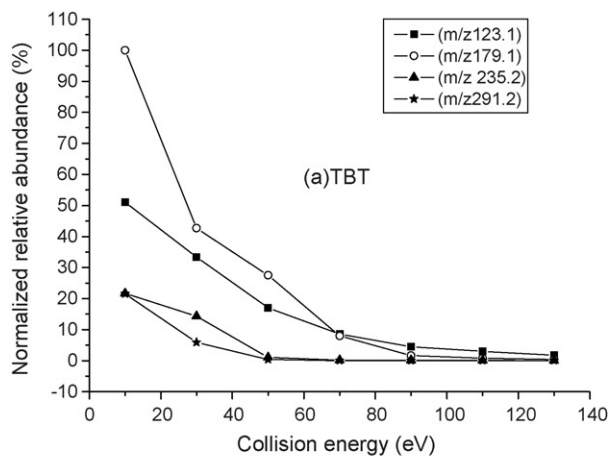


Fig. 3. Variation of the normalized relative abundances (%) of the fragments ions vs. collision energies for (a) TBT, (b) TPhT, and (c) TET.

mentation products was studied at potential range between 10 and 150 V. Fig. 4 shows the change of the normalized relative abundances of the fragment ions of TBT (Fig. 4a), TPhT (Fig. 4b), and TET (Fig. 4c) with the declustering potential. Clearly, the $[\text{Cat}]^+$ of TBT (Fig. 4a) and TPhT (Fig. 4b) dominate at lower declustering potential, but the $[\text{Cat-Et} + \text{Ac}]^+$ (m/z 237) of TET (Fig. 4c) dominates at lower declustering potential rather than the $[\text{Cat}]^+$. Contrastively, decreasing of the abundance of the $[\text{Cat}]^+$ is accompanied with the increasing of the

Fig. 4. Variation of the normalized relative abundances (%) of the fragments ions vs. declustering potential for (a) TBT, (b) TPhT, and (c) TET.

abundance of the elemental tin at higher declustering potential.

3.2.3. The selection of monitoring ion pairs

For analytical practice to choose the appropriate a pair of monitoring ion is important for quantification in the MRM. To

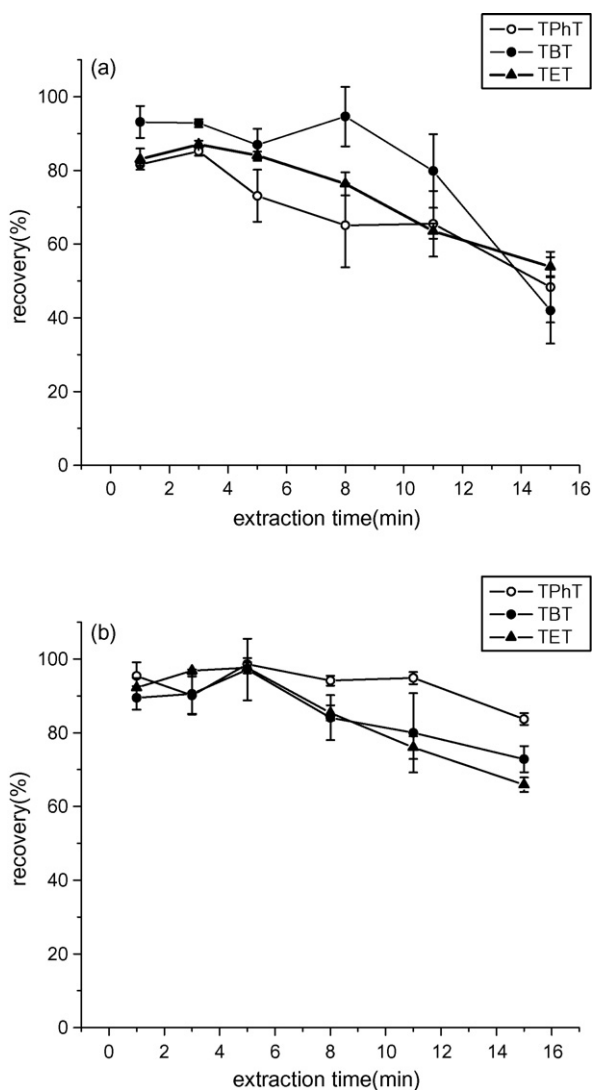


Fig. 5. Effect of extraction time on the recoveries of three organotin compounds in textile (a) and plastic (b). Extraction solution: 60% (v/v) methanol aqueous solution; extraction temperature: 90 °C. Error bars represent standard deviation of three measurements.

achieve maximum sensitivity, normalized relative abundance of the parent ions would be the highest. As shown in Fig. 4b, the $[\text{Cat}]^+$ (m/z 351) of TPhT shows the highest normalized relative abundance at 70 V declustering potential. Then the $[\text{Cat}]^+$ of TPhT undergoes collision again and gives rise to product ions $[\text{Sn}^{\text{II}}\text{Ph}]^+$ (m/z 197) which have the highest normalized relative abundance. For the TBT (Fig. 4a) and TET (Fig. 4c), the experimental results obtained were similar to that for TPhT. The appropriate a pair of monitoring ion for TBT and TET at declustering potential of 50v are $[\text{Cat}]^+ / [\text{Cat}-2\text{Bt} + 2\text{H}]^+$ (m/z 291/179) and $[\text{Cat}-\text{Et} + \text{Ac}]^+ / [\text{Cat}-2\text{Et} + 2\text{Me}]^+$ (m/z 237/179), respectively.

3.3. Microwave-assisted extraction

3.3.1. Extraction solvent

The results reported previously [21] indicated that the MAE by using acetic acid–methanol as extraction solvent showed

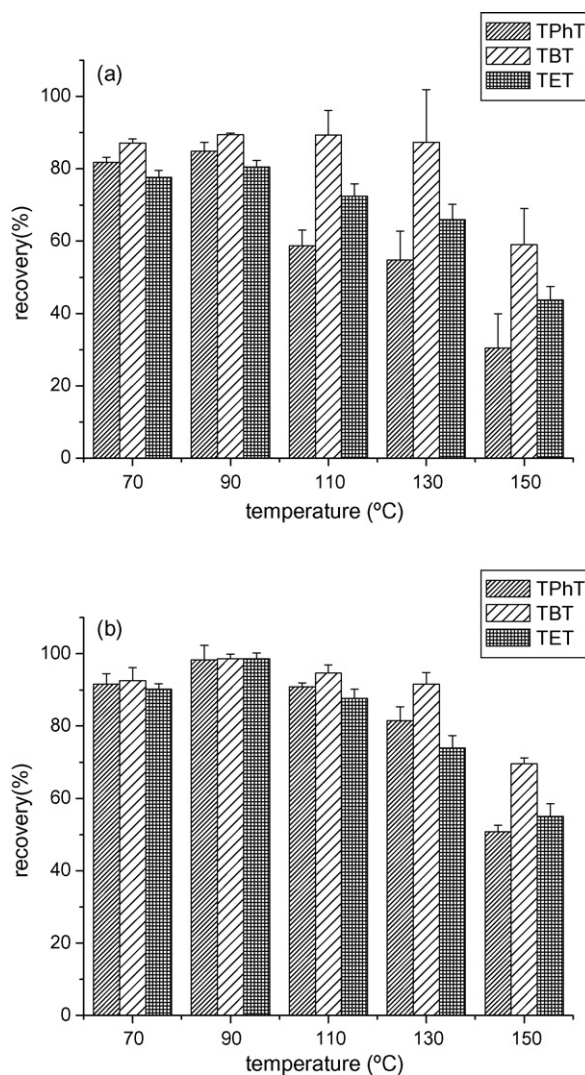


Fig. 6. Effect of extraction temperature on the recoveries of three organotin compounds from textile (a) and plastic (b). Extraction solution: 60% (v/v) methanol aqueous solution; extraction time: 3 min (textile) and 5 min (plastic). Error bars represent standard deviation of three measurements.

poor recovery values for extraction of TET. In the paper four different concentration of methanol aqueous solution: 20, 40, 60 and 80%, were used as extraction solvents for the extraction of three OTs from a spiked textile and plastic samples (data not shown). The recovery values of three OTs increase with the increase of methanol concentration from 20 to 60%, probably due to insufficient liberation of the analytes from the sample matrices. When methanol concentration in extraction solvent is higher than 60%, the recovery values of three OTs decrease. Optimal methanol content was found to be 60%. The 60% (v/v) methanol aqueous solution was used in the following experiments.

3.3.2. Extraction time and temperature

The extraction time is an important factor for the MAE. Fig. 5 shows that for a given microwave temperature the recovery changes significantly with extraction time, and reaches a maximum at 3 min for OTs from spiked textile sample

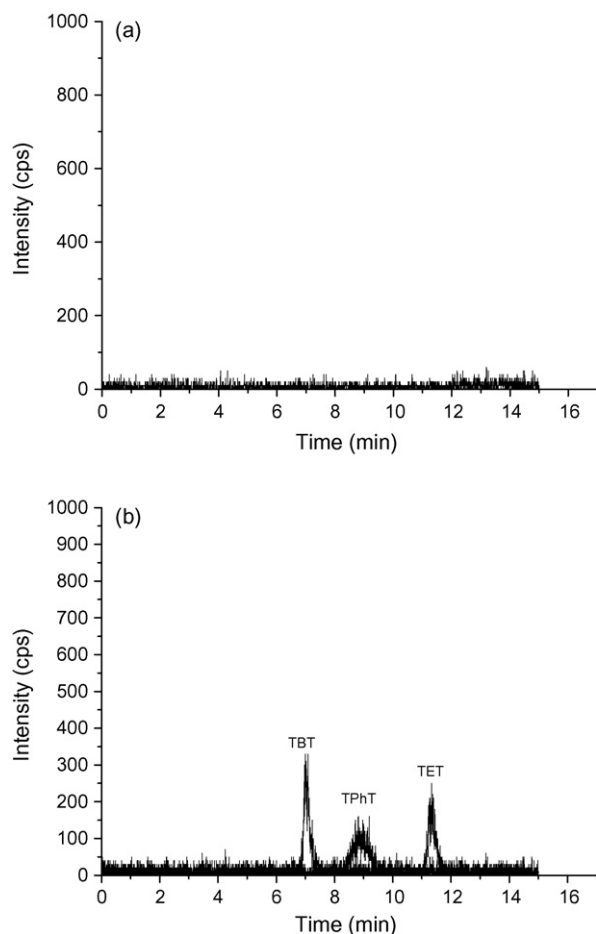


Fig. 7. The chromatograms of the blank sample (a), and spiked textile sample (b). Mobile phase: methanol–50 mmol l⁻¹ ammonium acetate aqueous solution–acetic acid=90/9.98/0.02 (v/v/v). Flow ratio: 1 ml min⁻¹. The concentrations of TBT, TPhT, and TET in the spiked textile sample are 0.5, 2, and 1 μg g⁻¹, respectively.

(Fig. 5a) and at 5 min for OTs from spiked plastic sample (Fig. 5b). Increasing the extraction time usually results in high recovery. However, too long extraction time may be not favourable for enhanced recovery because of degradation of OTs [22].

The extraction temperature affects the partition of the analytes between the sample and the solvent. Fig. 6 shows the effect of the extraction temperature on the extraction efficiency. This experiment was carried out by exposing spiked samples to a microwave field at temperature ranging from 70 to 150 °C for 3 min for spiked textile sample, 5 min for plastic. The results indicated that the recovery values of three OTs increase with the increase of MAE temperature from 70 to 90 °C. The highest recovery values are obtained at 90 °C. If MAE temperature is higher than 90 °C, the recovery values of three OTs decrease with the increase of MAE temperature because trisubstituted OTs is degraded to disubstituted and unsubstituted OTs, and inorganic tin [22]. However, percentage recovery of TBT shows almost non-significant change, and rapidly decreases at temperature higher than 130 °C. This result indicates that TBT is more stable than TPhT and TET at higher extraction temper-

Table 4
Recoveries of three OTs in spiked textile sample, plastic sample, and mimetic real sample (n=3)

Analyte	Added (μg g ⁻¹)	Found from textile (μg g ⁻¹)	Recovery ± R.S.D. from textile (%)	Found from plastic (μg g ⁻¹)	Recovery ± R.S.D. from plastic (%)	Found from mimetic real sample (μg g ⁻¹)	Recovery ± R.S.D. from mimetic real sample (%)
TBT	0.5	0.45 ± 0.036	90 ± 8	0.49 ± 0.010	98 ± 2	0.39 ± 0.033	78 ± 7
	1.0	0.93 ± 0.037	93 ± 4	0.96 ± 0.038	96 ± 4	0.87 ± 0.031	87 ± 3
	2.0	1.90 ± 0.057	95 ± 3	1.82 ± 0.091	91 ± 5	1.68 ± 0.064	84 ± 3
TPhT	2.0	1.82 ± 0.164	91 ± 9	1.98 ± 0.099	99 ± 5	1.10 ± 0.099	55 ± 5
	4.0	3.76 ± 0.188	94 ± 5	3.88 ± 0.116	97 ± 3	2.68 ± 0.182	67 ± 5
	8.0	7.36 ± 0.221	92 ± 3	7.50 ± 0.15	95 ± 2	5.04 ± 0.246	63 ± 3
TET	1.0	0.94 ± 0.065	94 ± 7	0.97 ± 0.029	97 ± 3	0.82 ± 0.095	82 ± 9
	2.0	1.84 ± 0.092	92 ± 5	1.88 ± 0.113	94 ± 6	1.58 ± 0.077	79 ± 4
	4.0	3.64 ± 0.109	90 ± 3	3.64 ± 0.182	91 ± 5	3.56 ± 0.236	89 ± 6

ature. Extraction temperature of 90 °C was optimal for three OTs.

3.4. Analytical performances

Data were obtained in MRM mode on the basis of the ^{120}Sn , which provided a higher signal than the other isotopes. The calibration curves were constructed by comparing peak area versus concentrations of OTs. As shown in Table 2, a good linear relationship was obtained for three OTs. The limits of detection (LODs) and the limits of quantitation (LOQs) were calculated using a signal-to-noise ratio of 3 and 10, respectively. The detection limits, for a 20 μl injection volume, are 0.4, 20, 4 ng ml^{-1} for TBT, TPhT, and TET, respectively. The LOQ values are 0.001, 0.05, 0.01 $\mu\text{g ml}^{-1}$, respectively. The RSDs of seven replicates were calculated. At the 1 $\mu\text{g ml}^{-1}$ concentration level of three OTs, the RSDs for determination of OTs are between 3 and 9%.

3.5. Analysis of samples

In the work, the applicability of the proposed method was evaluated for determining OTs in real textile and plastic samples, whereas none of them contains measurable amounts of three OTs (Fig. 7a). The spiked textile and plastic samples were analyzed. Fig. 7b shows chromatograms of three OTs in the spiked textile sample. The extraction recoveries of three OTs from spiked textile samples, plastic samples, and mimetic real plastic samples are shown in Table 4, respectively. It is obvious from the experimental results that good recoveries (90–95%) and R.S.D.s (3–9%) were obtained for the spiked textile and plastic samples. However, low recoveries are obtained and the results are still satisfactory for the quantitative analysis for the mimetic real samples. The low recovery may be because the analytes in the bulk of the plastics is difficult to be extract completely.

4. Conclusions

This study demonstrates the organotin speciation in the textile and plastic samples by MAE-HPLC–ES-MS. The experimen-

tal conditions for MAE, chromatographic separation and mass spectrometric detection were examined. The proposed method allows to simultaneously obtain speciation information of TBT, TPhT, and TET. The three kinds of organotin compounds in textile and plastic samples were determined and the results obtained are satisfactory.

References

- [1] R.J. Maguire, *Appl. Organomet. Chem.* 1 (1987) 475.
- [2] F. Monnet-Tschudi, M.G. Zurich, B.M. Riederer, *Neurotoxicology* 16 (1995) 97.
- [3] S. Ohhira, H. Matsui, *Toxicol. Lett.* 85 (1996) 3.
- [4] C. Rivas, L. Ebdon, E.H. Evans, S.J. Hill, *Appl. Organomet. Chem.* 10 (1996) 61.
- [5] R. Wahlen, T. Catterick, *J. Chromatogr. B* 783 (2003) 221.
- [6] O.F.X. Donard, B. Lalere, F. Martin, R. Lobinski, *Anal. Chem.* 67 (1995) 4250.
- [7] I.R. Pereiro, V.O. Schmitt, J. Szpunar, O.F.X. Donard, R. Lobinski, *Anal. Chem.* 68 (1996) 4135.
- [8] L. Yang, J.W.H. Lam, *J. Anal. At. Spectrom.* 16 (2001) 724.
- [9] T. Zuliani, G. Lespes, R. Milačič, J. Ščančar, *J. Chromatogr. A* 1132 (2006) 234.
- [10] C.H. Tang, W.H. Wang, *Anal. Chim. Acta* 581 (2007) 370.
- [11] J.R. Encinar, P.R. Gonzalez, J.I.G. Alonso, A.S. Medel, *Anal. Chem.* 74 (2002) 270.
- [12] P.R. Gonzalez, J.I.G. Alonso, A.S. Medel, *J. Anal. At. Spectrom.* 20 (2005) 1076.
- [13] H.J. Yang, S.J. Jiang, Y.J. Yang, C. Hwang, *Anal. Chim. Acta* 312 (1995) 141.
- [14] S. White, T. Catterick, B. Fairman, K. Webb, *J. Chromatogr. A* 794 (1998) 211.
- [15] S. Chiron, S. Roy, R. Cottier, R. Jeannot, *J. Chromatogr. A* 879 (2000) 137.
- [16] P.R. González, J.I.G. Alonso, A.S. Medel, *J. Anal. At. Spectrom.* 20 (2005) 1076.
- [17] E.G. Toledo, R. Compano, M.D. Prat, M. Granados, *J. Chromatogr. A* 946 (2002) 1.
- [18] J. Wu, Z. Mester, J. Pawliszyn, *J. Anal. At. Spectrom.* 16 (2001) 159.
- [19] T.L. Jones-Lepp, K.E. Varner, *Appl. Organometal. Chem.* 15 (2001) 933.
- [20] M. Holčapek, L. Kolarova, *Anal. Chem.* 78 (2006) 4210.
- [21] X. Wang, L. Ding, H. Zhang, *J. Chromatogr. B* 843 (2006) 268.
- [22] A. Praet, C. Dewaele, L. Verdonck, *J. Chromatogr.* 507 (1990) 427.

Surface-enhanced Raman scattering from surfactant-free 3D gold nanowire networks substrates

Tie Wang^{a,b}, Xiaoge Hu^{a,b}, Jianlong Wang^{a,b}, Shaojun Dong^{a,b,*}

^a State Key Laboratory of Electroanalytical Chemistry, Changchun Institute of Applied Chemistry, Chinese Academy of Sciences, Changchun, Jilin 130022, People's Republic of China

^b Graduate School of The Chinese Academy of Sciences, Beijing 100039, People's Republic of China

Received 26 July 2007; received in revised form 8 November 2007; accepted 9 November 2007

Available online 21 November 2007

Abstract

A useful method for the fabrication of three-dimensional gold nanowire networks based on the chemical reduction of HAuCl_4 with trisodium citrate was presented. The coverage of the 3D gold nanowire networks was tunable by altering precursor concentration. The as-prepared 3D gold nanowire networks could be used as surface-enhanced Raman scattering (SERS) substrates and examined by 4-aminothiophenol (4-ATP) as a probe molecules. Since the proposed strategy is simple, cost-effective and reproducible for the mass production of network-like gold films irrespective of the kinds of the underlying substrates, it is expected to play an important role in the development of surface plasmon-based analytical devices. © 2007 Elsevier B.V. All rights reserved.

Keywords: Gold nanowire networks; SERS spectra; Gold nanoparticles; 4-Aminothiophenol

1. Introduction

Noble metallic nanostructures exhibit a phenomenon known as surface-enhanced Raman scattering (SERS) in which the intensity of Raman spectroscopy are dramatically enhanced through adsorbing the molecules onto metal surfaces [1,2]. SERS has been proven to be a powerful tool in research and application in the field of analytical chemistry, biochemistry and catalysis [3,4]. The aggregate of noble metal particles is prerequisite for stronger SERS enhancement [5,6]. This is due to the existence of so-called “hot spots” having intense local electromagnetic fields in which highly efficient Raman scattering can be obtained [7]. It is necessary for the SERS-active substrate to be stable, reproducibly prepared, inexpensive, and easy to make [8]. However, the acceptance of SERS as a general analytical tool has been hindered by the SERS-active substrate lacking in stability and/or reproducibility [9]. It is difficult to control

the extent of aggregation of colloidal sols, and is not reproducible to sedimentate aggregated sols onto solid substrates [10]. Vacuum-evaporated metal island films can be prepared to obtain enormous SERS enhancement; the system requires expensive and specialized apparatus [11].

Among the conventional methods of synthesis of gold nanoparticles by chemical reduction of gold(III) derivatives, the most popular one for a long time has been that using citrate reduction of HAuCl_4 in water [12]. This method is very often used even now when a rather loose shell of ligands is required around the gold core [13]; however, up to now, these investigations are mainly focused on the fabrication of spherical gold nanoparticles in solution. Nonspherical nanoparticles, such as gold nanorods and nanocubes, are of significant interest as SERS substrates because of their longitudinal plasmon bands and the “lightning rod” effect on surface enhancement [14]. Previous strategy to control the growth of nonspherical gold nanoparticles generally involved surfactants or polymer [15]. The removal of softer template requires multiple washing, yet some residues are still bound on the surfaces of nanoparticles. The presence of surface-bound residues may be a significant interferent or increase the adsorbed difficulty of analyte at the surfaces of nanoparticles for application in SERS analysis that

* Corresponding author at: State Key Laboratory of Electroanalytical Chemistry, Changchun Institute of Applied Chemistry, Chinese Academy of Sciences, Changchun, Jilin 130022, People's Republic of China. Tel.: +86 431 85262101; fax: +86 431 85689711.

E-mail address: dongsj@ciac.jl.cn (S. Dong).

obtains vibrational information on molecules adsorbed on the surfaces of metal nanoparticles [16,17]. Therefore, controlled organization of metal nanostructures with as “clean” surfaces as possible represents a requirement for sensing application.

In present work, we demonstrate a one-step route to prepare three-dimensional (3D) gold nanowire networks in the absence of surfactants and polymer, attempting to prepare gold nanostructures with “clean” surfaces [17]. The network-like gold films can be reproducibly and directly fabricated on solid substrates at moderate temperatures. Comparing to conventional chemical method for synthesizing nanostructures, the fabricated process elides additional self-assembling technology. The coverage of the 3D gold nanowire networks on solid substrates is tunable by altering the concentration of citrate and HAuCl_4 . The results demonstrate that the as-prepared 3D gold nanowire networks with “clean” surfaces could be used as good SERS-active substrates with 4-aminothiophenol (4-ATP) as probe molecule, and the Raman enhancement ability can increase with the increasing coverage of the 3D gold nanowire networks. The network-like gold films prepared in this way are expected to present a new type of substrate material for developing SERS as an ultrasensitive analytical tool.

2. Experimental

In a typical direct-heating synthesis, a 0.5 mL aqueous solution of HAuCl_4 (25.0 mM) was quickly added to 0.5 mL aqueous trisodium citrate solution (25.0 mM) under vigorous

stirring at room temperature with 1:1 molar ratio of trisodium citrate/ HAuCl_4 . A drop (20 μL) of the solution was coated on a silicon slide. Next, the silicon slide coated with the solution was heated at 90 °C in air for 30 min. Immediately, the product was carefully washed with water to remove the excess reagents, and then kept in a desiccator to dry for characterization.

The products were imaged by an XL30 ESEM FEG field emission scanning electron microscopy (SEM, FEI Company with 20 kV operating voltage) equipped with energy-dispersive X-ray (EDX). The Raman instrument includes a FT-Raman spectrometer (Thermo Nicolet 960) equipped with an InGaAs detector and a Nd/ VO_4 laser (1064 nm) as an excitation source. The laser power used was about 400 mW at the samples. All FT-SERS were recorded by averaging 512 scans. X-ray photoelectron spectroscopy (XPS) measurement was performed on an ESCALAB-MKII spectrometer (VG Co., U.K.) with an Al $\text{K}\alpha$ X-ray radiation as the X-ray source for excitation. X-ray diffraction (XRD) analysis was carried out on a D/Max 2500 V/PC X-ray diffractometer using Cu (50 kV, 250 mA) radiation.

3. Results and discussion

The morphology of as-prepared products was characterized by scanning electron microscopy (Fig. 1). The lower magnification image (Fig. 1A) shows the presence of macroscopic interconnected networks, while the higher magnification image (the inset of Fig. 1A) clearly reveals that the frames of networks are composed of branched gold nanoparticles

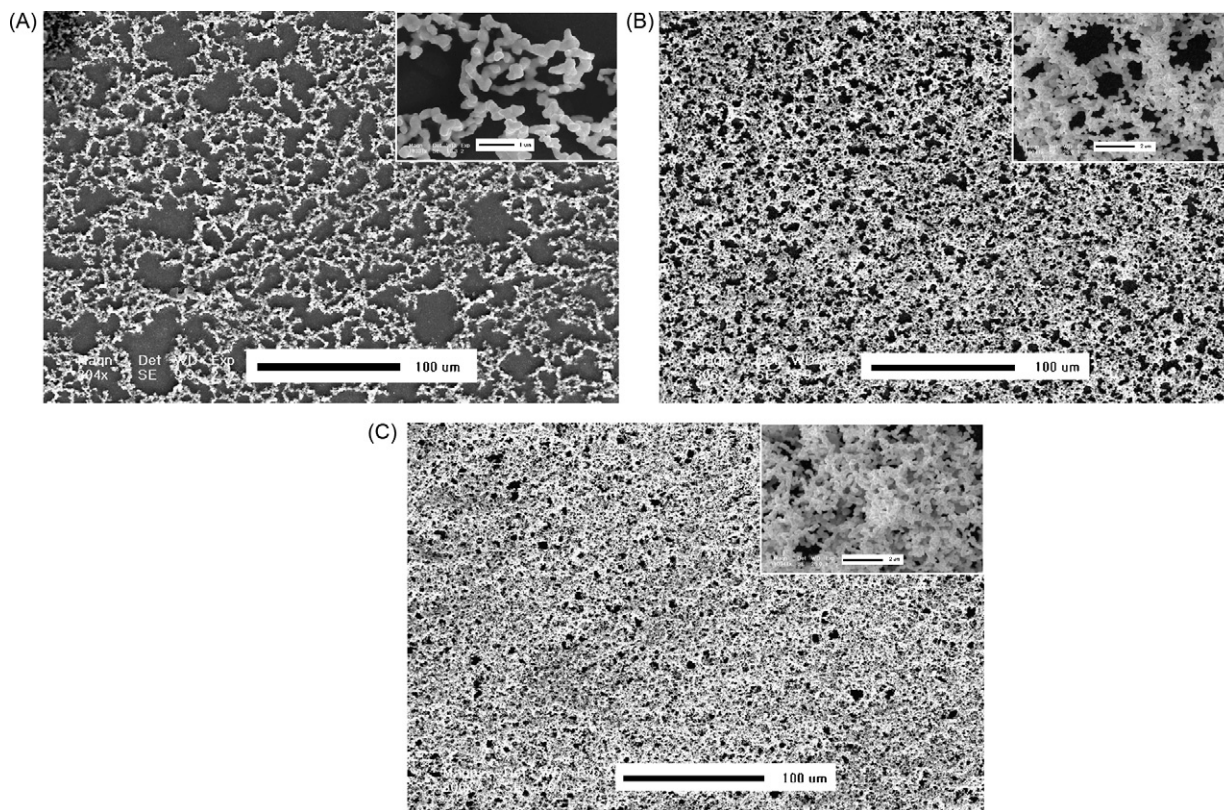


Fig. 1. Top-view SEM images of 3D gold nanowire networks. (A–C) Low-magnification SEM images of 3D gold nanowire networks obtained with the concentrations of trisodium citrate and HAuCl_4 12.5, 30.0, and 50.0 mM, respectively. The inset showing corresponding higher magnification SEM images.

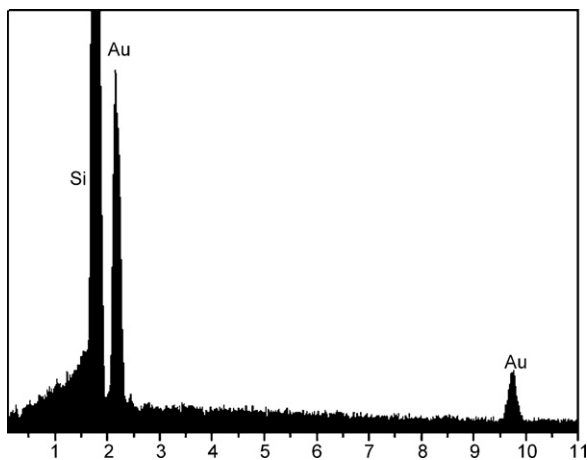


Fig. 2. EDX spectrum of as-prepared products on silicon slides.

with approximately 200 nm in average diameter. These network nanostructures can extend to a surface area of several square millimeters. When we changed the concentration of HAuCl_4 from 12.5 to 50.0 mM while kept the molar ratio (R) of trisodium citrate to HAuCl_4 invariable, the coverage of the 3D gold nanoparticle networks is changed. SEM studies indicate that the increasing coverage of the 3D gold nanoparticle networks is associated with the increasing concentration of HAuCl_4 (Fig. 1A–C). At higher HAuCl_4 concentrations, the branched nanoparticles are linked relatively compactly and there are fewer interstices in the networks (Fig. 1C) than that in Fig. 1A. In addition, it should be noted that different substrates (ITO, gold and glass slides) used in our experiments have no obviously effect on the morphology of 3D gold nanoparticle networks from SEM observation.

The chemical compositions of the as-prepared products on the silicon slides were confirmed with EDX. As an example, the EDX spectrum obtained from Fig. 1A reveals the presence of Au and Si elements (Fig. 2). Si peak originates from silicon substrate. Although there may be a small number of residual citrate molecules serving as a rather loose shell of ligands adsorbed on gold nanostructures, traces of carbon, oxygen, and sodium (from trisodium citrate molecules) are not detected, which demonstrate that a majority of citrate molecules have been washed off from solid substrates. Therefore, the products are pure metallic gold.

The crystal structure and phase composition of the 3D gold nanowire networks were characterized with XRD. Fig. 3A shows a typical XRD pattern of the as-prepared product. Five peaks can be observed, corresponding to diffraction from the (1 1 1), (2 0 0), (2 2 0), (3 1 1), and (2 2 2) planes of face-centered cubic (fcc) gold, respectively. This indicates that as-prepared product is composed of pure crystalline Au. The oxidation state of 3D gold nanowire networks was determined by XPS as shown in Fig. 3B. The XPS spectrum of the product shows the Au $4f_{7/2}$ and $4f_{5/2}$ doublet with the binding energies of 84.0 and 87.8 eV, respectively, corresponding to Au^0 state.

Since understanding the growth mechanism of the gold networks depends on the revelation of the intermediate steps involved in the growth process, the products at various stages are studied by SEM. Fig. 4 shows the evolution of the 3D

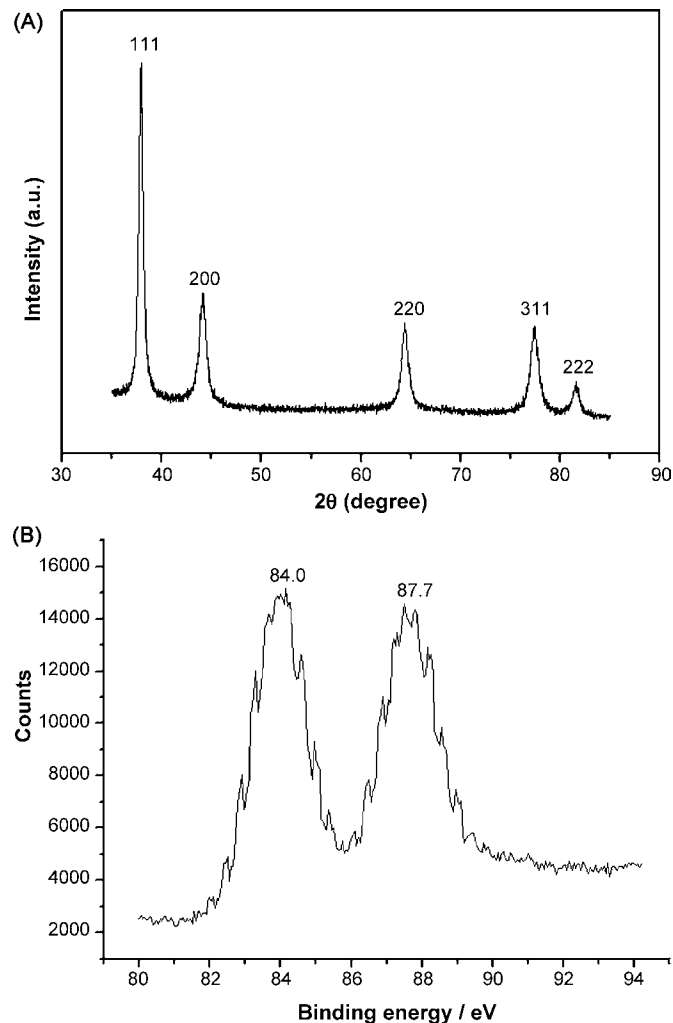


Fig. 3. (A) XRD patterns recorded for 3D gold nanowire networks. (B) XPS spectrum of Au 4f of the 3D gold nanowire networks.

gold nanowire networks as a function of reaction time. SEM observation of the product heating for only 1 min reveals that gold nanoparticles with diameter in the range of 30–60 nm are randomly scattered on the solid substrate (Fig. 4A). Besides gold nanoparticles, a spot of agglomerated gold clusters are also observed as indicated by white arrows in Fig. 4A. With increasing of reaction time to 3 min, the size of the gold cluster become obviously larger, showing increased reduction of HAuCl_4 (Fig. 4B). A large percentage of gold nanoparticles are coalesced, resulting in the formation of branched nanowires with an average diameter of about 60 nm. The growth of nanowires by extending the reaction time to 5 min is clearly seen from SEM image (Fig. 4C), and the average diameter of branched gold nanowires is approximately 100 nm. The branched gold nanowires are connected in a network structure and the discrete nanoparticles are decreased evidently. The products obtained after reaction for 30 min are shown in Fig. 1A, where the average diameter of the branched nanowires is 200 nm accompanying with disappearing gold nanoparticles. When the reaction time is further increased to 60 min, no evident difference of morphology compared to the products with 30 min reaction is observed.

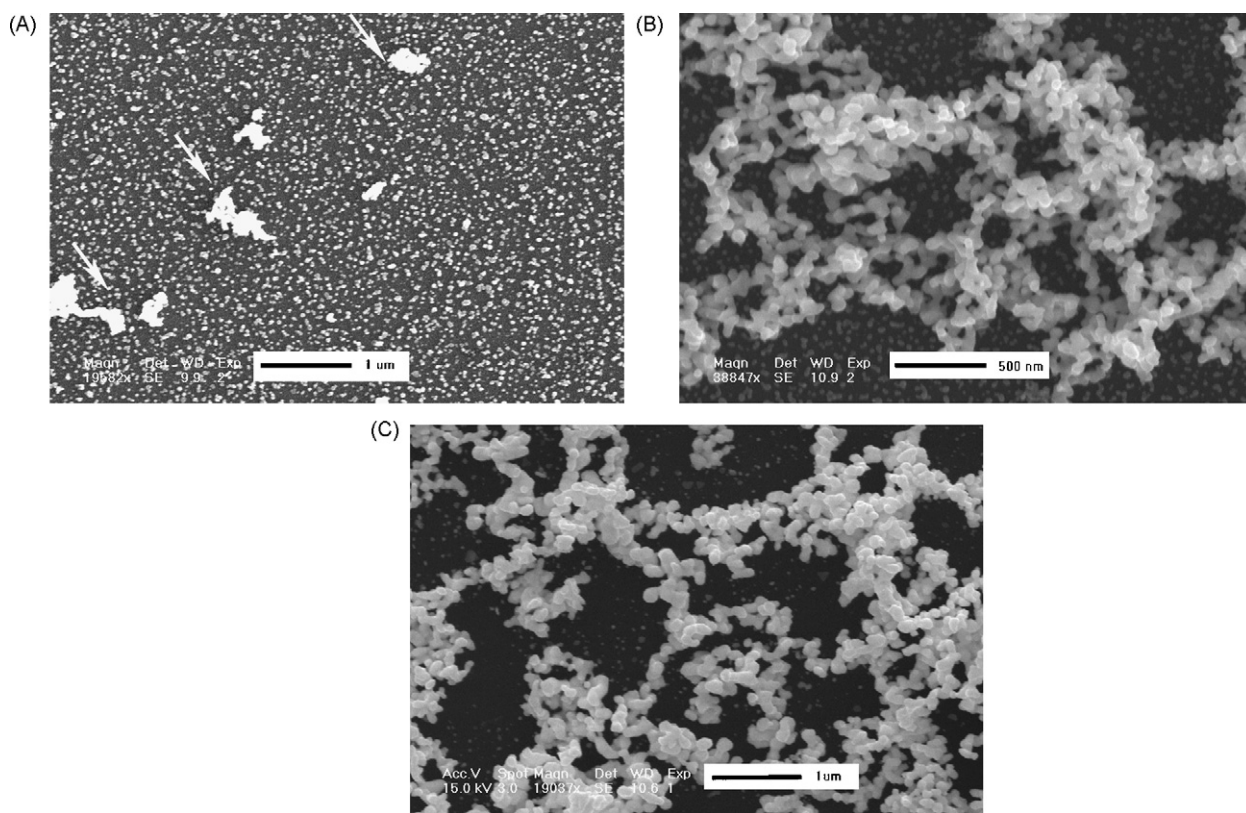


Fig. 4. SEM images of 3D gold nanowire networks at various stages. (A) 1, (B) 3, and (C) 5 min, respectively.

Based on the above investigations, it can be concluded that the mechanism for the formation of the gold nanowire networks is correlated with the growth and coalescence of the gold nanoparticles. First, a portion of AuCl_4^- is reduced, and the reduction of the gold ion results in gold nanoparticles at the initial reaction stage, in which trisodium citrate not only acts as a reducing agent but also as a capping agent in the reduction reaction [18]. The nanoparticles will act as seeds for the growth of larger nanoparticles and formation of nanowire networks. Second, as reported by Zukoski and co-workers [19], AuCl_4^- can be preferentially adsorbed onto the surfaces of gold nanoparticle even in the presence of excess citrate ions. The adsorption reduces the surface charge, increasing the van der Waals attractive interaction between the gold surfaces, and resulting in the attractive interaction [20]. The attraction among gold nanoparticles acts as driving factors for the fusing process. Third, the anisotropic coalescence of these nanoparticles forms the 3D nanowire networks. A drop (20 μL) on a silicon slide is dried at 90 °C after about 7 min, which can be easily observed by naked eyes. But when the reaction time is less as 1, 3, or 5 min, the reactant is not dried during the process of reaction, wherein the gold nanoparticles randomly move by Brownian motion and approach adjacent particles in solution, attaching to other particles driven by the van der Waals attractive force [21]. Meanwhile, the volatilization of solution on the solid substrate results in increasing concentration of nanoparticles. The gold nanoparticles in higher concentration have been reported to show a tendency to fuse [22]. These nanoparticles hit and stick together very rapidly and drastically, followed by deposition of

newly formed gold atoms onto surfaces of nanoparticles and the concave region of the connected particles, following a hit-to-stick-to-fusion model [20]. Because of the random hit between nanoparticles, these particles are preferably held together in a 3D fashion [23–25]. The nondirectional growth of nanowires results in branched gold nanowires, that is, enlargement in length and diameter, and formation of a 3D network structure. While at the lower concentration, the coalescence between nanoparticles is difficult, showing a relatively good stability. Moreover, the content of gold nanoparticles in products is obviously decreased with the reaction processing, which indicates that the formation of gold nanowire networks is also relative with the Ostwald ripening at the expense of small gold particles. Finally, when the reaction time is further prolonged, AuCl_4^- is completely exhausted, and no change of nanowire networks morphology was observed.

The above-mentioned 3D gold nanowire networks films are very suitable as SERS substrates [26]. 4-ATP was selected as the probing molecule. Fig. 5a–c displays the FT-SERS spectrum of 4-ATP collected from difference coverage of the 3D gold nanowire networks. SERS spectra of 4-ATP are comparable to those reported previously for 4-ATP adsorbed onto gold substrates. Characteristic bands, including νCS (1072 cm^{-1}) and νCC (1580 cm^{-1}), are observed in the SERS spectra of 4-ATP [27]. The predominance of a_1 modes in the FT-SERS spectrum, may imply that the enhancement via an electromagnetic (EM) mechanism is significant [28,29]. The band at 389 cm^{-1} can be assigned to one of the vibrational modes of the C–S bond [27].

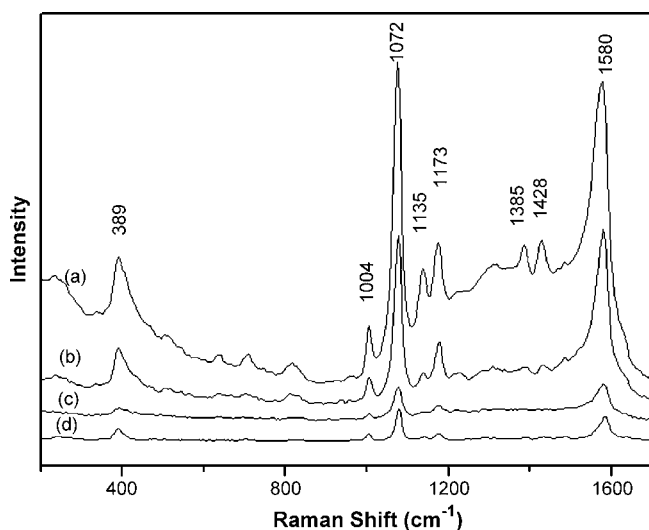


Fig. 5. FT-SERS spectra of 4-ATP on different substrates: (a–c) collected from 3D gold nanoparticle networks obtained with the concentrations of trisodium citrate and HAuCl_4 50, 30.0, and 12.5 mM, respectively; (d) obtained from gold island film.

It has been well-recognized that the junctions of aggregated nanoparticles possess SERS-active sites [7]. Therefore, the great Raman enhancement of 4-ATP on these nanowire networks may originate from the coalesced gold nanostructures. The 4-ATP Raman signals have an obvious trend that the enhancement ability dramatically increases with the increasing coverage of the 3D gold nanowire networks. The SERS spectra, in fact, show that the intensity of the band at 1072 cm^{-1} in Fig. 5a and b being enhanced 11-fold and 5-fold, respectively, compared to that in Fig. 5c. The area of SERS-active substrate is increased by bringing the nanowire networks closer and minimizing the voids on the gold film, which allow more molecules to adsorb. Taking into account the sensitivity of SERS for the junctions, the increasing intensities of SERS signal may originate from the huge number of Au–Au nanoparticle junctions and 4-ATP molecules, as a result of the high-coverage nanowire networks. Moskovits and co-worker proposed that the source of the largest SERS signals is the nanoparticle dimers and clusters, which rests upon the well-established role of SERS hot spots in the interstices between nanoparticles [30]. Previous theoretical and experimental studies have indicated that the control of gaps between nanostructures in the sub-10 nm regime is likely to be critical for the fabrication of a SERS-active substrate with uniformly high enhancement factors [31]. The electromagnetic hot spots tend to be gap modes in the interstice between closely spaced metallic nanostructures [32]. As the particles approach each other, there is a dramatic enhancement factor increase based on the theory of interparticle-coupling-induced Raman enhancement [33]. Intense EM field enhancement is expected for the high-coverage nanowire networks, in which there are the most sub-10 nm gaps, that is, high-coverage increase SERS-active sites. Aside from the aforementioned factors, the surface plasmon resonance is affected by electromagnetic coupling between the nanostructures. In the case of the close-packed nanostructures, the decreased spacing may makes the plasmon peak red

shift to the far-red and near-infrared light region [34]. The high SERS intensities generally occur when the exciting wavelength is near the surface plasmon band [14]. Therefore, the high-coverage gold nanowire networks show a dramatic enhancement in the SERS signal. In a parallel experiment, about 60% of samples get SERS enhancement. In addition, gold island film gave comparable SERS intensities of low coverage nanostructure film, but was far lower than that from high-coverage nanostructure film, which indicated that the strategy in prepared SERS substrate was effective.

4. Conclusion

In summary, via heating a drop of HAuCl_4 /trisodium citrate aqueous solution on solid substrates, we obtained stably and reproducibly 3D gold nanowire networks with tunable coverage by altering the precursor concentration. The method represents a convenient, low-cost approach that is suitable for the mass production of network-like gold films irrespective of the kinds of the underlying substrates. In addition, due to the existence of so-called “hot spots”, the 3D gold nanowire networks have been demonstrated to be a SERS-active substrate for probing 4-ATP, which will be useful in the development of plasmon-based analytical devices, specifically SERS-based biosensors.

Acknowledgment

This work was supported by the National Natural Science Foundation of China (Nos. 20575064 and 20427003).

References

- [1] X. Li, W. Xu, J. Zhang, H. Jia, B. Yang, B. Zhao, B. Li, Y. Ozaki, *Langmuir* 20 (2004) 1298.
- [2] M. Fleischmann, P. Hendra, A. McQuillan, *Chem. Phys. Lett.* 26 (1974) 163.
- [3] J. Zhang, Y. Gao, R. Alvarez-Puebla, J. Buriak, H. Fenniri, *Adv. Mater.* 18 (2006) 3233.
- [4] A. Michales, J. Jiang, L. Brus, *J. Phys. Chem. B* 104 (2000) 11965.
- [5] J. Hu, B. Zhao, W. Xu, Y. Fan, B. Li, Y. Ozaki, *J. Phys. Chem. B* 106 (2002) 6500.
- [6] B. Nikoobakht, M. El-Sayed, *J. Phys. Chem. A* 107 (2003) 3372.
- [7] M. Suzuki, Y. Niidome, Y. Kuwahara, N. Terasaki, K. Inoue, S. Yamada, *J. Phys. Chem. B* 108 (2004) 11660.
- [8] S. Lee, K. Kim, *Chem. Commun.* (2003) 212.
- [9] X. Zhang, J. Zhao, A. Whitney, J. Elam, R. Duynes, *J. Am. Chem. Soc.* 128 (2006) 10304.
- [10] H. Park, J. Yoon, K. Kim, *Langmuir* 22 (2006) 1626.
- [11] S. Chaney, S. Shanmukh, R. Dluhy, Y. Zhao, *Appl. Phys. Lett.* 87 (2005) 31908.
- [12] J. Turkevitch, P. Stevenson, J. Hillier, *Discuss. Faraday Soc.* 11 (1951) 55.
- [13] M. Daniel, D. Astruc, *Chem. Rev.* 104 (2004) 293–346.
- [14] C. Orendorff, A. Gole, T. Sau, C. Murphy, *Anal. Chem.* 77 (2005) 3261.
- [15] T. Hassenkam, K. Nørsgaard, L. Iversen, C. Kiely, M. Brust, T. Bjørnholm, *Adv. Mater.* 14 (2002) 1126.
- [16] M. Schulz-Dobrick, K. Sarathy, M. Jansen, *J. Am. Chem. Soc.* 127 (2005) 12816.
- [17] K. Caswell, C. Bender, C. Murphy, *Nano Lett.* 3 (2003) 667.
- [18] N. Jana, L. Gearheart, C. Murphy, *J. Phys. Chem. B* 105 (2001) 4065.
- [19] S. Biggs, P. Mulvaney, C. Zukoski, F. Grieser, *J. Am. Chem. Soc.* 116 (1994) 9150.
- [20] L. Pei, K. Mori, M. Adachi, *Langmuir* 20 (2004) 7837.

- [21] J. Wall, F. Grieser, C. Zukoski, *J. Chem. Soc. Faraday Trans.* 93 (1997) 4017.
- [22] C. Kiely, J. Fink, M. Brust, D. Bethell, D. Schiffrin, *Nature* 396 (1998) 444.
- [23] B. Enüstün, J. Turkevich, *J. Am. Chem. Soc.* 85 (1963) 3317.
- [24] M. Maillard, L. Motte, A. Ngo, M. Pileni, *J. Phys. Chem. B* 104 (2000) 11871.
- [25] R. Jin, S. Egusa, N. Scherer, *J. Am. Chem. Soc.* 126 (2004) 9900.
- [26] L. Lu, I. Randjelovic, R. Capek, N. Gaponik, J. Yang, H. Zhang, A. Eychmüller, *Chem. Mater.* 17 (2005) 5731.
- [27] J. Zheng, X. Li, R. Gu, T. Lu, *J. Phys. Chem. B* 106 (2002) 1019.
- [28] J. Zheng, Y. Zhou, X. Li, Y. Ji, T. Lu, R. Gu, *Langmuir* 19 (2003) 632.
- [29] M. Osawa, N. Matsuda, K. Yoshii, I. Uchida, *J. Phys. Chem.* 98 (1994) 12702.
- [30] M. Schierhorn, S. Lee, S. Boettcher, G. Stucky, M. Moskovits, *Adv. Mater.* 18 (2006) 2829.
- [31] H. Wang, C. Liu, S. Wu, N. Liu, C. Peng, T. Chan, C. Hsu, J. Wang, Y. Wang, *Adv. Mater.* 18 (2006) 491.
- [32] S. Lee, A. Morrill, M. Moskovits, *J. Am. Chem. Soc.* 128 (2006) 2200.
- [33] Y. Lu, G. Liu, L. Lee, *Nano Lett.* 5 (2005) 5.
- [34] T. Wang, R. Zheng, X. Hu, L. Zhang, S. Dong, *J. Phys. Chem. B* 110 (2006) 14179.

A new method for the HPLC determination of gamma-hydroxybutyric acid (GHB) following derivatization with a coumarin analogue and fluorescence detection

Application in the analysis of biological fluids

Constantinos K. Zacharis^a, Nikolaos Raikos^b, Nikolaos Giouvalakis^a, Helen Tsoukali-Papadopoulou^b, Georgios A. Theodoridis^{a,*}

^a *Laboratory of Analytical Chemistry, Department of Chemistry, Aristotle University, 541 24 Thessaloniki, Greece*

^b *Laboratory of Forensic Medicine and Toxicology, Medical School, Aristotle University, 541 24 Thessaloniki, Greece*

Received 19 July 2007; received in revised form 25 October 2007; accepted 7 November 2007

Available online 17 November 2007

Abstract

A new method of the determination of gamma-hydroxybutyric acid (GHB) in human biological fluids cerebrospinal fluid (CSF) and saliva after off-line derivatization is described. The proposed method was based on the reaction of 4-bromomethyl-7-methoxy coumarin (Br-MMC) with GHB in the presence of dibenzo-18-crown-6-ether (acting as reaction catalyst) to produce a fluorescent derivative. The formed derivative was monitored fluorimetrically at $\lambda_{\text{ext.}} = 330$ nm and $\lambda_{\text{em.}} = 390$ nm. The effect of derivatization parameters such as the concentration of Br-MMC, reaction time and the temperature was investigated in order to achieve the maximum method's sensitivity. The separation was achieved by use of a C₁₈ analytical column (Kromasil[®] 250 mm × 4 mm i.d., 5 μ m) while the injected sample volume was set to 25 μ L. A binary gradient elution program of methanol versus phosphate buffer (40 mM, pH 3) was selected for the quantitative analysis of GHB. The method showed satisfactory linearity ($R^2 = 0.9979$) in a linear range from 2.4×10^{-6} to 7.2×10^{-5} M. Ultrafiltration method was employed for the pre-treatment of the cerebrospinal fluid (CSF) prior to the analysis of GHB. The limit of detection (LOD) of the method was 3×10^{-7} M in saliva and 2×10^{-7} M in CSF samples, respectively, while the limit of quantitation (LOQ) was 1×10^{-6} M for both specimens. The proposed protocol offers sensitivity comparing with the existing HPLC analytical methods or the CE indirect UV methods and can function as an attractive alternative to be used in clinical and toxicological analysis.

© 2007 Elsevier B.V. All rights reserved.

Keywords: Derivatization; Gamma-hydroxybutyric acid; HPLC; Cerebrospinal fluid; Saliva

1. Introduction

Gamma-hydroxybutyric acid (GHB) was originally developed as an anesthetic drug and is still used as a licensed medicine in some States. It acts as a central nervous system depressant and hypnotic and is chemically related to the brain neurotransmitter gamma-aminobutyric acid (GABA). GHB is known by a variety of street names: “liquid ecstasy”, “gamma-OH”, “oxybate”, “somatomax”, “happiness drops”, “liquid loving” and others. GHB is also known as a “rave drug” or “rape drug” because

it has been widely used in rave parties and has been associated with sexual crimes. Although the commercial distribution and use of GHB and analogues is restricted, these drugs are commonly sold on the Internet. GHB is mostly found in the illicit market in the form of tablets, powder or liquid consumed with beverages (typically dissolved or diluted into beverages) [1–3].

The molecule of GHB is very small and polar and the chromatographic analysis proves problematic in most of the cases. The same molecular properties make GHB a “problem molecule” for the development of extraction assays. A highly sensitive and selective detection method is required for biological and biomedical investigations of this compound. Further to this the intrinsic UV absorbance of the carboxylic group, even

* Corresponding author. Tel.: +30 2310997718; fax: +30 2310997719.
E-mail address: gtheodor@chem.auth.gr (G.A. Theodoridis).

at low wavelengths (e.g. 210 nm), is not sufficient to provide adequate detection sensitivity.

In the literature, a variety of analytical methods for the determination of GHB in biological fluids have been reported including: (A) gas chromatography (GC) with FID, MS or MS–MS detection [4–15], (B) liquid chromatography (LC) with UV [16] or MS [16–20], (C) capillary electrophoresis (CE) with indirect UV detection [21,22] and (D) ^1H NMR spectroscopy [23,24]. Chromatographic techniques which comprise MS detection have proved powerful tools providing sensitive and reliable analysis of GHB. On the other side, these techniques bear high instrumentation cost and complexity and also need highly trained personnel. Furthermore, the analysis with GC is problematic due to the anionic and polar character of GHB molecule and its thermal instability. LC–UV techniques utilize common instrumentation but provide low sensitivity which does not reach the concentration levels needed in the analysis of biological samples. Furthermore unambiguous detection of GHB in biological matrices cannot be ascertained due the poor specificity of the UV detection at the low wavelength range. Electrodriven techniques (e.g. CE) with indirect UV detection employ a chromophore compound in electrolyte solution while the non-absorptive compound is detected as negative peak (or converted positive peak). The main limitation of this type of detection is the high relatively LODs which can be achieved.

Derivatization is one of the most popular approaches today to enhance the sensitivity and selectivity of a chromatographic method. In the case of carboxylic acids, chemical derivatization of the carboxyl moiety with an appropriate tagging reagent giving chromophore, fluorophore or electrophore properties is the most commonly used approach. Several derivatization approaches for GHB determination have been published. Typical derivatizing reagents prior to GC analysis include hexylchloroformate [25], *N*-methyl-*N*-trimethylsilyltrifluoroacetamide (MSTFA) [26], *N,O*-bis(trimethylsilyl)trifluoroacetimidetriethylchlorosilane (BSTFA) [27,28] prior to the analysis by GC or GC–MS and 3-bromomethyl-6,7-dimethoxy-1-methyl-1,2-dihydroquinoxaline-2-one (Br-DMEQ) [29] for LC with UV detection. Recently, a review has been published focusing on the application of derivatizing reagents to the analysis of carboxylic-group containing compounds using various techniques and detection schemes [30]. One of the most advantageous and popular reagent in such type of analysis is 4-bromomethyl-7-methoxycoumarin (Br-MMC) which produces highly fluorescent derivatives and is therefore commonly applied prior to LC analysis of carboxylic-containing analytes such as [31].

Regarding the determination of GHB in CSF and saliva, only two methods have been reported previously [34,35]. These methods employ ^1H NMR [33] and GC–MS [34] as analytical techniques. The scope of the present work was the development of a derivatization method to enable sensitive detection of GHB in biological samples with the use of HPLC and fluorescence detection. To the best of our knowledge this is the first method reporting the LC determination of GHB after derivatization coupled to fluorescence detection. The method provides satisfactory

specificity and sensitivity and has proven robust and reliable thus providing an attractive alternative to GC and GC–MS analysis.

2. Material and methods

2.1. Solutions and materials

Sodium gamma-hydroxybutyrate was obtained through the United Nations (Office on drugs and crime) International Quality assurance program (IQAP). Anthracene, used as internal standard (IS) was provided from Sigma (St. Louis, MO, USA). The derivatizing reagent 4-bromomethyl-7-methoxy coumarin, the catalyst dibenzo-18-crown-6-ether was obtained from Sigma and all other chemicals were of analytical or higher grade and were provided by Merck (Darmstadt, Germany). A Milli-Q[®] water purification system (Millipore) was utilized to obtain ultra-pure water. Methanol and acetonitrile were of HPLC grade and all organic solvents used were obtained from Carlo Erba (Milan, Italy) or Merck.

Stock solution of GHB (9.6×10^{-4} M) was prepared in *N,N*-dimethylformamide (DMF) and stored at 4 °C. Working standards were prepared by appropriate dilutions of the stock solution in DMF. Anthracene solution was prepared in acetonitrile at 2.8×10^{-4} M. Standard solutions of Br-MMC were prepared on a daily basis to avoid the decomposition of the reagent due to exposure to light. Dibenzo-18-crown-6-ether and Br-MMC solutions were prepared in acetonitrile.

All the mobile phases were filtered through 0.2 μm membrane filters (Schleicher & Schuell, Dassel, Germany) and degassed with helium for 10 min prior to use. Helium spargers were employed for continuous degassing of eluents.

A Centrex UF-0.5 ultra-filter (10,000 M_r cut-off) was used for the pretreatment of human cerebrospinal fluid (CSF) in order to remove existing macromolecules. Molecular sieves employed as dehydrators of samples were provided from Aldrich. These sieves were pre-heated at 200 °C in order to regenerate and activate the surface.

2.2. Instrumentation

Liquid chromatographic analysis was carried out using an LCP 5020 gradient pump (INGOS, Czech Republic). GHB separations were accomplished at constant flow at 1.3 mL min^{-1} on a 250 mm \times 4.6 mm i.d. C_{18} Kromasil 4 μm analytical column from MZ-Analysentechnik (Mainz, Germany) protected by a guard column (3 mm \times 1.0 mm i.d. packed in the lab with 10 μm C_{18} bonded silica). The derivative was introduced to the HPLC analytical column through a six port injection valve Rheodyne 7010 (Cotati, CA, USA) equipped with a 25 μL sample loop. The Shimadzu RF-535 spectrofluorimetric detector was operated at $\lambda_{\text{ex}} = 330 \text{ nm}$ and $\lambda_{\text{em}} = 390 \text{ nm}$. The response signal of the detector was acquired digitally and the data were saved in ASCII format for further manipulation (peak height/area measurement, digital filtering, etc.) using a home-made software programmed by Prof. P. Nikitas (Laboratory of Physical Chemistry, Department of Chemistry, Aristotle University Thessaloniki), running in Visual Basic[®]

6.0. All measurements were performed at ambient temperature.

2.3. Samples pre-treatment

2.3.1. Saliva

A 500 μL of human saliva was evaporated to dryness at 30 $^{\circ}\text{C}$ using a gentle stream of nitrogen over the surface of the liquid. The residue was reconstituted to solution with 200 μL of DMF (for blank measurements) or with 200 μL of standard solutions of GHB in DMF (for spiked/fortified measurements). Pre-heated molecular sieves were next added and remained in the vial for 30 min in order to remove the water traces. Finally, a 100 μL of the resulted mixture was used for the derivatization.

2.3.2. Cerebrospinal fluid

Post-mortem human CSF was collected during autopsy from left and right ventricles. Hundred microlitres of CSF was collected and ultra-filtrated using a membrane filter with 10 kDa cut-off. The sample was centrifuged at 12,000 rpm (8000 $\times g$) for 30 min and the filtrate was diluted 10-fold and stored at -5°C prior to use. An aliquot of the ultrafiltrated sample was evaporated to dryness at 30 $^{\circ}\text{C}$ using a stream of nitrogen and was next treated as described above for saliva.

2.4. Derivatization protocol

Derivatization was performed under non-aqueous conditions. A hundred microlitres of standard solution or sample were mixed with 200 μL of dibenzo-18-crown-6-ether (1.4 $\times 10^{-3}$ M in acetonitrile) in dark tube. The mixture was vortexed for 1 min and then 200 μL of Br-MMC at 1.3 $\times 10^{-3}$ M was added. The final mixture was left to react for 70 min in a water bath at 70 $^{\circ}\text{C}$. After heating, 100 μL of anthracene solution (2.8 $\times 10^{-4}$ M in acetonitrile) was added and the final mixture was diluted up to 1 mL with acetonitrile. All the reaction tubes were protected from light. Finally, 25 μL of the derivative was injected to the analytical column.

2.5. HPLC conditions—elution program

Several gradient elution protocols were tested to facilitate adequate elution and separation of the GHB and the external standard from the peak of the excess derivatizing reagent. Finally, a binary elution system consisted of mobile phase A

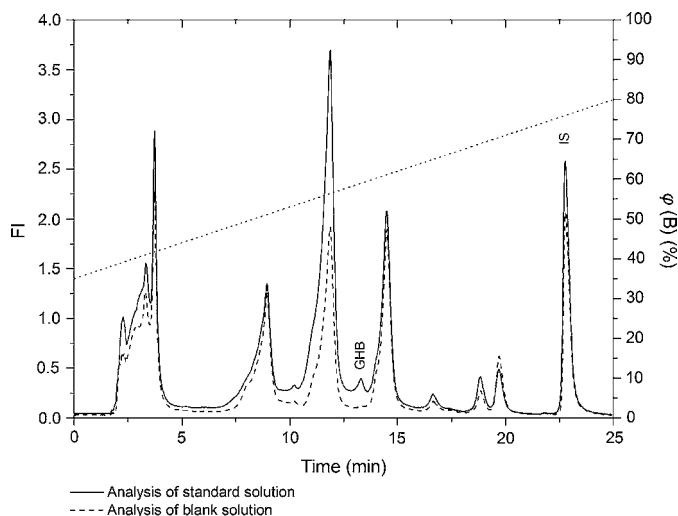


Fig. 1. Representative chromatogram of a blank and standard solution of GHB (9.6×10^{-6} M) following derivatization with Br-MMC, where IS is the internal standard (anthracene) and FI the fluorescence intensity. The right vertical axis represents to percentage of methanol in the gradient elution program. Chromatographic conditions are described in the text.

(40 mM phosphate buffer, pH 3 adjusted with H_3PO_4) and mobile phase B (CH_3OH) was chosen and applied. Linear gradient elution started at 35% of B until 80% at the end of 25 min. The flow rate was maintained at 1.3 mL min^{-1} , while all separations were performed in ambient temperature. Three replicates were made in all instances.

Under the selected separation conditions the retention times were 13.3 min for the GHB derivative and 22.7 min for the internal standard anthracene. Representative chromatograms of the injection of a blank solution and a standard solution of GHB after derivatization are depicted in Fig. 1.

3. Results and discussion

3.1. Investigation of derivatization conditions

The reaction between the carboxylic group of GHB and Br-MMC is of $\text{S}_{\text{N}}2$ type and proceeds in aprotic solvents (e.g. acetone, acetonitrile, DMF and dichloromethane). Furthermore the addition of a catalyst phase transfer agent (e.g. 18-crown-6-ether) is necessary in the reaction mixture in order to improve the reaction yield [32]. As shown in Fig. 2, the crown ether acts as catalyst and its role is to capture and seclude the Na^+ ion.

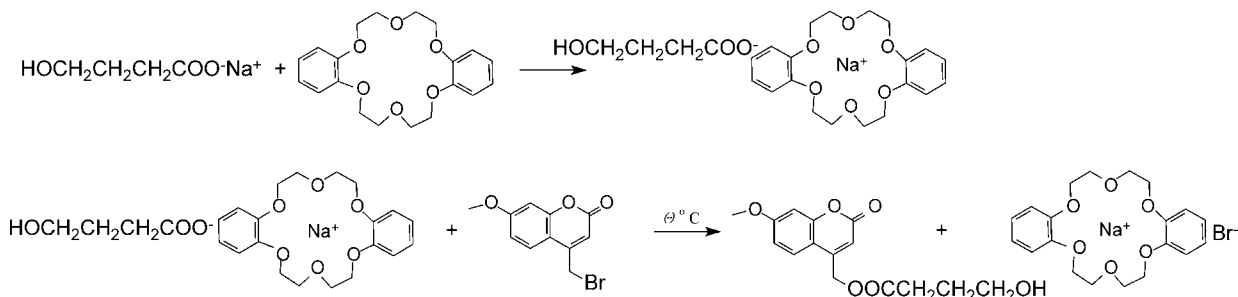


Fig. 2. Scheme of the reaction of GHB with Br-MMC using dibenzo-18-crown-6-ether as reaction catalyst.

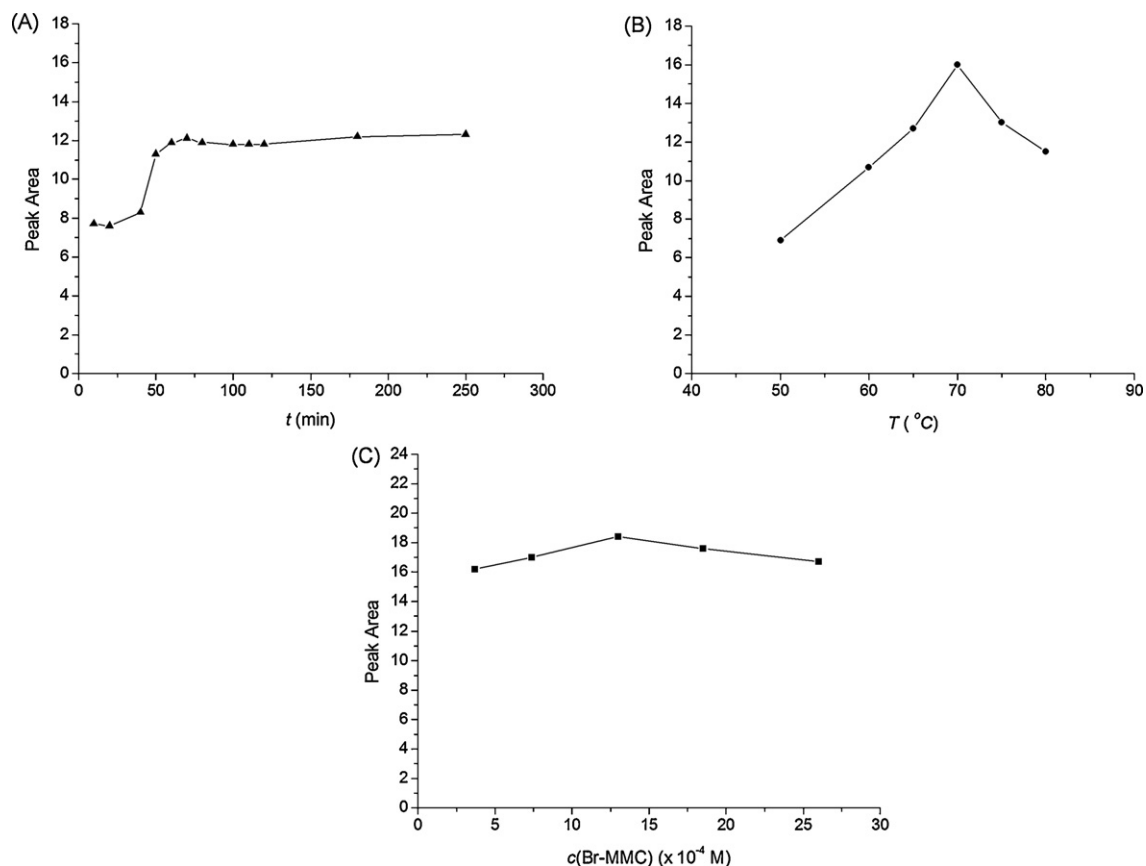


Fig. 3. Study of derivatization parameters on peak area of GHB: effect of time of the derivatization (A), temperature (B) and concentration of Br-MMC (C).

This would liberate the carboxylic anion which could then take part in the derivatization reaction.

Analytical parameters have been studied in order to enhance sensitivity. This was measured from the absolute peak area of the analyte derivative. In order to obtain the maximum fluorescence intensity critical parameters such as the reaction time, the temperature, and the concentration of Br-MMC were studied. It should be noted that the initial concentrations of GHB, Br-MMC and 18-crown-6-ether were $c(\text{GHB}) = 4.8 \times 10^{-5}$ M, $c(\text{Br-MMC}) = 7.4 \times 10^{-4}$ M and $c(18\text{-crown-6-ether}) = 1.4 \times 10^{-3}$ M.

3.1.1. Investigation of derivatization time

Reaction time is an important parameter which affects the sensitivity of the method to a great extent. In general this type of reaction is performed by heating at around to 60 $^{\circ}\text{C}$ for 30–60 min [25]. For this reason, 65 $^{\circ}\text{C}$ was selected as initial temperature. The reaction time was studied in the range of 20–250 min. A high increase of the peak signal (derivative peak area) was observed close to 50 min. The peak area did not increase significantly even with the increase of reaction time until 250 min. A graph exhibiting the results of this study is given in Fig. 3A. Therefore the time of 70 min was chosen for the rest of the study because it provided satisfactory detection sensitivity and adequate sample throughput. It should be noted that the formed derivative was stable for a relatively long period (longer than 4 h).

3.1.2. Investigation of temperature

Temperature is a fundamental parameter for derivatization. Generally, an increase in temperature can increase the derivatization yield. In order to determine the effect of temperature in the reaction yield, a series of standard solution of GHB (4.8×10^{-5} M) was heated for 70 min at increasing temperatures in the range from 50 to 80 $^{\circ}\text{C}$. It was found that the peak area of the GHB derivative increased in the elevated temperatures till 70 $^{\circ}\text{C}$ (see Fig. 3B). Further heating may cause decomposition of derivative and consequently the value of 70 $^{\circ}\text{C}$ was selected for further studies.

3.1.3. Investigation of Br-MMC concentration

The concentration of Br-MMC was studied in the range of 3.7×10^{-4} to 2.6×10^{-3} M. Proportionally, the increase of concentration of alkylating agent caused higher detector signals until the concentration of 1.3×10^{-3} M. Fig. 3C shows the influence of the variation of the concentration of Br-MMC on the analyte signal. The increase of reagent concentration to values higher than 1.3×10^{-3} M did not result in signal enhancement due to rise of the background (baseline). Therefore, the concentration of 1.3×10^{-3} M was selected for further experiments.

3.1.4. Investigation of 18-crown-6-ether concentration

Another parameter studied was the concentration of 18-crown-6-ether. We found that the variation of concentration did

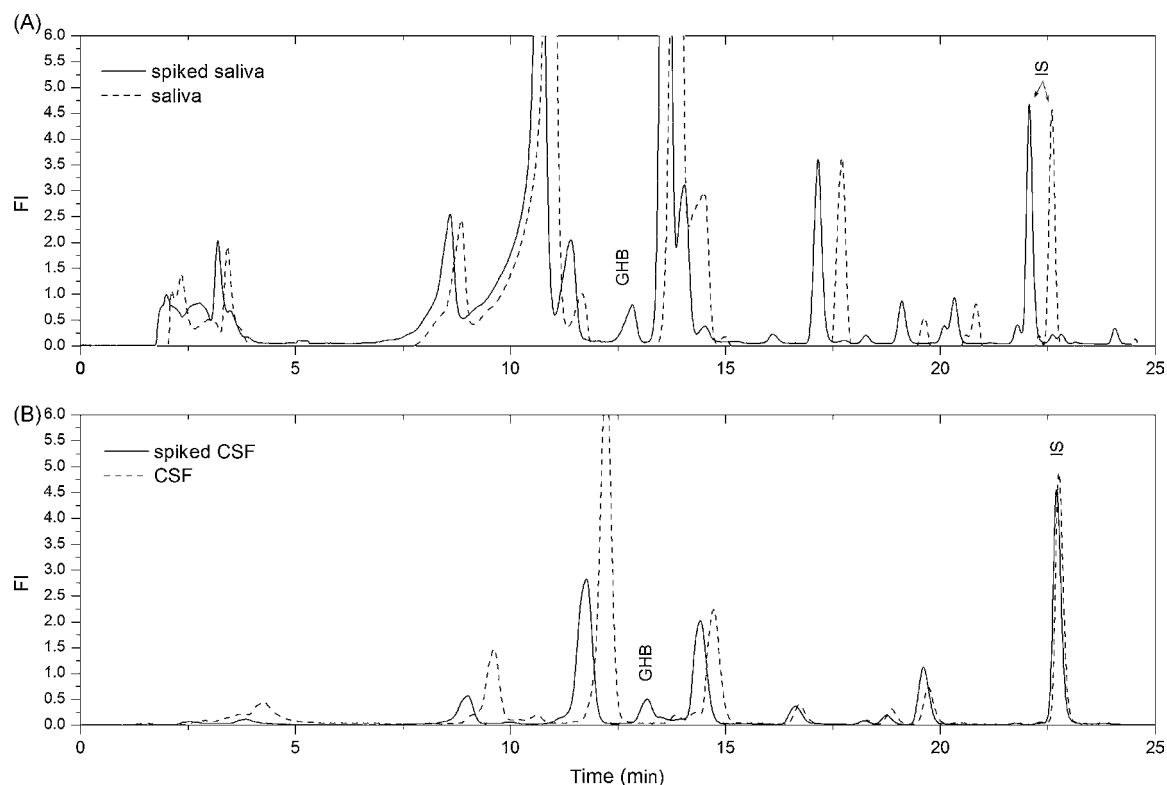


Fig. 4. Chromatographic analysis of (A) blank and spiked saliva (1.92×10^{-5} M GHB and 2.8×10^{-4} M IS) and (B) blank and spiked CSF (1.44×10^{-5} M GHB and 2.8×10^{-4} M IS). Dotted lines and solid lines represent the blank and the spiked biological samples, respectively (Note that the time-axis of the dotted chromatograms is shifted to improve the presentation perspective). Experimental conditions are described in the text.

not affect the reaction yield. This result was expected because the crown is used as catalyst in the specific reaction [33]. In Table 1 the range of each parameter investigated and the selected value is shown.

3.2. Analytical data

Under the selected derivatization conditions a calibration curve for GHB was constructed by measuring seven different concentrations. The calibration curve was linear in the range of 2.4×10^{-6} to 7.2×10^{-5} M and described by the following equation:

$$R_p = (3811 \pm 78) c(\text{GHB}) + (0.052 \pm 0.003) \quad \text{with} \quad R^2 = 0.9979,$$

where R_p is the ratio of peak areas of GHB derivative to internal standard— $c(\text{IS}) = 2.8 \times 10^{-4}$ M in all instances and $c(\text{GHB})$ is the concentration of GHB derivative.

The within-day relative standard deviation s_r varied between 6.7 and 7.5% at 4.8×10^{-6} to 1.92×10^{-5} to 3.84×10^{-5} M

Table 1
Study of derivatization parameters

Parameter	Studied range	Optimum value
Derivatization time (min)	20–250	70
Temperature ($^{\circ}\text{C}$)	50–80	70
$c(\text{Br-MMC})$ (M)	3.7×10^{-4} to 2.6×10^{-3}	1.3×10^{-3}

GHB ($n = 5$). The within-day accuracy of the developed protocol also proved to be satisfactory as the recoveries of the above-mentioned GHB concentrations were in the range 104–106%. The inter-day precision of the method was verified by measuring the same concentrations at seven consecutive days ($n = 7$). The between-day precision of the GHB measurements revealed that the s_r was varied between 5.9 and 8.4% and the recoveries were from 92 to 104% ($n = 3$).

3.3. Analysis of biological samples

The derivatization with the coumarin analogue provided a specific and sensitive method for the determination of GHB in biological fluids. Blank saliva and CSF samples were treated as described in the Section 2.3.1 and were spiked with six different concentration of GHB in the range of 1.92×10^{-5} to 1.44×10^{-3} M and 1.44×10^{-5} to 9.60×10^{-4} M, respectively. In all cases the concentration of the internal standard was kept constant at 2.8×10^{-4} M.

Typical chromatograms of blank and spiked saliva and CSF are shown in Fig. 4(A) and (B). As seen in the figures no interferences were observed and the GHB derivative peak was clearly separated from peaks of the matrix. The obtained calibration graphs were linear and described by the regression equations:

$$R_{p(\text{saliva})} = (2635 \pm 49) c(\text{GHB}) + (0.032 \pm 0.028) \quad \text{with} \quad R^2 = 0.9991,$$

Table 2
Analysis of biological samples

Sample	Added GHB ($\times 10^{-5}$ M)	Found GHB ^a ($\times 10^{-5}$ M)	R ^b
Saliva	–	ND ^c	–
	9.60	8.83	92
	24.0	25.5	106
	96.0	98.9	103
CSF	–	ND	–
	9.60	10.3	107
	24.0	22.7	95
	96.0	94.5	98

^a Mean of three replicates.

^b Percent recovery.

^c Not detected.

$$R_{p(\text{CSF})} = (2159 \pm 102) c(\text{GHB}) - (0.155 \pm 0.077) \quad \text{with} \quad R^2 = 0.9993,$$

where R_p is the ratio of peak areas of GHB derivative to external standard and $c(\text{GHB})$ is the concentration of the analyte. The detection limit (at the $S/N=3$ level) was 3×10^{-7} M in saliva and 2×10^{-7} M in CSF samples, respectively.

The accuracy of the proposed method was evaluated by recovery experiments of known amounts of GHB spiked in the real samples. The obtained results are shown in Table 2 in which the recoveries were in the range 92–107% in all cases.

4. Concluding remarks

In the present paper we reported the development of a derivatization protocol for the determination of GHB in biological fluids. The carboxylic acid moiety is more challenging to derivatize than, e.g. the primary amines. Nevertheless the analytical interest for carboxylic acids is immense as these are numerous and are present in samples of diversifying origin (biological samples, foods, etc.). The proposed method provides a simple, sensitive and efficient assay for the quantitative determination of GHB in CSF and saliva samples.

References

- [1] G. Estievenart, Report on the risk assessment of GHB in the framework of the joint action on new synthetic drugs, European Monitoring Centre for Drugs and Drug Addiction, 2002.
- [2] C.S. Hornfeldt, K. Lothridge, J.C.U. Downs, *Forensic Sci. Commun.* 4 (2002) 1.

- [3] A. Gonzalez, D.J. Nutt, *J. Psychopharmacol.* 19 (2005) 195.
- [4] G. Frison, L. Tedeschi, S. Maietti, S.D. Ferrara, *Rapid Commun. Mass Spectrom.* 14 (2000) 2401.
- [5] A.A. Elian, *Forensic Sci. Int.* 128 (2002) 120.
- [6] M. Villain, V. Cirimele, B. Ludes, P. Kintz, *J. Chromatogr. B* 792 (2003) 83.
- [7] S.P. Elliott, *Forensic Sci. Int.* 133 (2003) 9.
- [8] F.J. Couper, B.K. Logan, *J. Anal. Toxicol.* 28 (2004) 481.
- [9] P. Kintz, M. Villain, V. Cirimele, B. Ludes, *Forensic Sci. Int.* 143 (2004) 177.
- [10] R. Brenneisen, M.A. Elsohly, T.P. Murphy, J. Passarelli, S. Russmann, S.J. Salamone, D.E. Watson, *J. Anal. Toxicol.* 28 (2004) 625.
- [11] P. Richard, L. Tsanaclis, R. Kingston, A. Berry, A. Guwy, *J. Anal. Toxicol.* 30 (2006) 375.
- [12] D. Richard, B. Ling, N. Authier, T.W. Faict, A. Eschalier, F. Coudore, *Anal. Chem.* 77 (2005) 1354.
- [13] R. Paul, L. Tsanaclis, R. Kingston, A. Berry, A. Guwy, *J. Anal. Toxicol.* 30 (2006) 375.
- [14] M.A. LeBeau, M.L. Miller, B. Levine, *Forensic Sci. Int.* 119 (2001) 161.
- [15] M.A. LeBeau, M.A. Montgomery, M.L. Miller, S.G. Burmeister, *J. Anal. Toxicol.* 24 (2000) 421.
- [16] C.A.d. Vriendt, D.K.V. Sassenbroeck, M.T. Rosseel, E.J.V.D. Velde, A.G. Verstraete, Y.V. Heyden, F.M. Belpaire, *J. Chromatogr. B* 752 (2001) 85.
- [17] M.Z. Mesmer, R.D. Satzger, *J. Forensic Sci.* 43 (1998) 489.
- [18] M. Wood, M. Laloup, N. Samyn, M.R. Morris, E.A.D. Bruijn, R.A. Maes, M.S. Young, V. Maes, G.D. Boeck, *J. Chromatogr. A* 1056 (2004) 83.
- [19] H.-L. Fung, E. Haas, J. Raybon, J. Xu, S.-M. Fung, *J. Chromatogr. B* 807 (2004) 287.
- [20] E. Kaufmann, A. Alt, *Forensic Sci. Int.* 168 (2006) 133.
- [21] A. Baldacci, R. Theurillat, J. Caslavská, H. Pardubská, R. Brenneisen, W. Thormann, *J. Chromatogr. A* 990 (2003) 99.
- [22] F. Bortolotti, G.D. Paoli, R. Gottardo, M. Trattene, F. Taliaro, *J. Chromatogr. B* 800 (2004) 239.
- [23] M. Grootveld, D. Algeo, C.J.L. Silwood, J.C. Blackburn, A.D. Clark, *Biofactors* 27 (2006) 121.
- [24] S. Del, G. Anthony, M. McGregor, B.P. Cho, *J. Forensic Sci.* 50 (2005) 81.
- [25] S.D. Brown, D.J. Rhodes, B.J. Pritchard, *Forensic Sci. Int.* 171 (2007) 142.
- [26] K. Berankova, K. Mutnanska, M. Balikova, *Forensic Sci. Int.* 161 (2006) 158.
- [27] J.W. Mercer, L.S. Oldfield, K.N. Hoffman, D.M. Shakleya, S.C. Bell, *J. Forensic Sci.* 52 (2007) 383.
- [28] P. Kintz, M. Villain, A.-L. Pelissier, V. Cirimele, G. Leonetti, *J. Anal. Toxicol.* 29 (2005) 582.
- [29] K. Matsuda, N. Asakawa, M. Iwanaga, A. Gohda, S. Fukushima, Y. Ishii, H. Yamada, *Forensic Toxicol.* 24 (2006) 41.
- [30] T. Toyo'oka, *Anal. Chim. Acta* 465 (2002) 111.
- [31] J.H. Wolf, J. Korf, *J. Chromatogr.* 436 (1988) 437.
- [32] A. Hulshoff, A.D. Forch, *J. Chromatogr.* 220 (1981) 275.
- [33] H.D. Durst, M. Milano, E.J. Kikta, S.A. Connelly, E. Grushka, *Anal. Chem.* 47 (1975) 1797.
- [34] M. Grootveld, D. Algeo, C.J.L. Silwood, J.C. Blackburn, A.D. Clark, *Biofactors* 27 (2006) 121.
- [35] P. Kintz1a, J.-P. Gouille, V. Cirimele, B. Ludes, *Clin. Chem.* 47 (2001) 2033.

Chromium(III)-imprinted silica gel for speciation analysis of chromium in environmental water samples with ICP-MS detection

Nan Zhang, Jibrin Sabo Suleiman, Man He, Bin Hu*

Department of Chemistry, Wuhan University, Wuhan, Hubei Province 430072, PR China

Received 8 August 2007; received in revised form 13 November 2007; accepted 16 November 2007

Available online 4 December 2007

Abstract

A new chromium(III)-imprinted 3-(2-aminoethylamino) propyltrimethoxysilane (AAPT)-functionalized silica gel sorbent was synthesized by a surface imprinting technique and was employed as a selective solid-phase extraction material for speciation analysis of chromium in environmental water samples prior to its determination by inductively coupled plasma mass spectrometry (ICP-MS). The prepared Cr(III)-imprinted silica gel shows the selectivity coefficient of more than 700 for Cr(III) in the presence of Mn(II). The static adsorption capacity of the ion-imprinted and non-imprinted sorbent for Cr(III) were 30.5 mg g⁻¹ and 13.4 mg g⁻¹. It was also found that Cr(VI) could be adsorbed at low pH by the prepared imprinted silica gel, and this finding makes it feasible to enrich and determine Cr(VI) at low pH without adding reducing reagents. The imprinted silica gel sorbent offered a fast kinetics for the adsorption and desorption of both chromium species. Under the optimized conditions, the detection limits of 4.43 pg mL⁻¹ and 8.30 pg mL⁻¹ with the relative standard deviations (R.S.D.s) of 4.44% and 4.41% ($C = 0.5 \text{ ng mL}^{-1}$, $n = 7$) for Cr(III) and Cr(VI) were obtained, respectively. The proposed method was successfully applied to the speciation of trace chromium in environmental water samples. To validate the proposed method, two certified reference materials were analyzed and the determined values were in a good agreement with the certified values. The developed method is rapid, selective, sensitive and applicable for the speciation of trace chromium in environmental water samples. © 2007 Elsevier B.V. All rights reserved.

Keywords: Chromium speciation; Ion-imprinted silica gel sorbent; Surface imprinting technique; Environmental water samples; ICP-MS

1. Introduction

Chromium is widely used in various industries, such as plating, tanning, paint and pigment production and metallurgy, which could possibly contaminate the environmental waters and enter human body through intake of water. In environmental waters, chromium exists predominantly in two chemical forms: Cr(III) and Cr(VI).

It is well known that the toxicological and biological properties of most elements depend upon their chemical forms. Cr(III) is an essential component having an important role in the glucose, lipid and protein metabolism, whereas Cr(VI) has a definite adverse impact on living organisms. Cr(VI) can easily penetrate the cell wall and exert its noxious influence in the cell itself, being also a source of various cancer diseases [1,2]. Therefore, the speciation of chromium in environmental samples is of significance.

The speciation of chromium in environmental waters could be realized by combining high efficient separation techniques with element-specific detection technique [3]. Of all element-specific detection techniques, ICP-MS has been considered to be one of the most efficient and robust element-specific techniques due to its low detection limit, wide linear range and isotope capability [4]. Various separation techniques, especially different chromatographic separation techniques, combined with ICP-MS have become one of the most powerful techniques for elemental speciation [5]. The most widely used separation methods for chromium speciation include: solid-phase extraction [6–15], high-performance liquid chromatography [16], ion chromatography [17] and capillary electrophoresis [18]. Among the above methods, solid-phase extraction (SPE) is the most commonly used separation technique for the speciation of chromium in environmental waters due to the following advantages [19]: (1) absence of emulsion; (2) high enrichment factors; (3) flexibility and (4) easy of automation. Since the adsorption materials play a very important role in SPE, the current researches in SPE are mainly focused on the development of new sorbents. Silica gel especially immobilized with various organic compounds

* Corresponding author. Tel.: +86 27 68752162; fax: +86 27 68754067.
E-mail address: binhu@whu.edu.cn (B. Hu).

with metal chelating ability has received great attention. It is stable under acidic conditions and nonswelling inorganic material, and has fast and quantitative sorption and elution, high mass exchange and capacity characteristics and very high thermal resistance [20]. However, the basic disadvantage of the traditional solid sorbents is the lack of specific metal ion selectivity [21].

Molecular imprinting is a technique for preparing polymeric materials that are capable of high molecular recognition. Molecular-imprinted polymers (MIPs) are synthesized by polymerization of functional monomers in the presence of template and excess of crosslinker. The imprint molecule is leached out after polymerization and leaved the memory of the analyte. Thus MIPs are capable of recognizing and rebinding the desired target analyte with a high affinity and selectivity [22]. Ion-imprinted polymers (IIPs) are similar to MIPs, but they can recognize metal ions after imprinting and retain all the virtues of MIPs [23,24]. A particularly promising application of IIPs is the solid-phase extractive preconcentration of analytes present in low concentration or the separation from other coexisting ions or complex matrix. In view of the above reasons, ion-imprinted polymers for solid-phase extraction are a fast developing area for the application of ion imprinting technology [25]. Surface molecular imprinting technique is one of the important types of molecular imprinting. Imprinted polymers prepared by this technique show many advantages including high selectivity, more accessible sites, fast mass transfer and binding kinetics [26,27] because it avoids high embedment and retain a better site accessibility to the target molecules.

Up-to-date, many ion-imprinted polymers have been prepared by using surface imprinting technique, which include Pd [28], Ni [21,29], Fe [20], Cd [30,31], Zn [32], Cu [33] and Dy [34]. However, there are few publications on the speciation of elements using imprinted material. Due to the presence of the functional group $\text{-NH-CH}_2\text{-CH}_2\text{-NH}_2$, 3-(2-aminoethylamino) propyltrimethoxysilane has been used as a silylating reagent to synthesis hierarchically imprinted sorbents via sol-gel method to extract Cu^{2+} from aqueous solutions [35] and anchored to silica surface for adsorption isotherms studies of Co^{2+} , Ni^{2+} , Cu^{2+} and Zn^{2+} in ethanol and acetone solution [36].

In this study, AAPTS was used as functional monomer and Cr(III)-imprinted modified silica gel sorbent was prepared by a surface molecular imprinting technique. The imprinted material shows good selectivity to Cr(III) in the existence of Mn(II) and could also absorb Cr(VI) at low pH. The prepared sorbent was used as microcolumn packing material for solid-phase extraction and ICP-MS determination of Cr(III) and Cr(VI) in environmental water samples.

2. Experimental

2.1. Instruments and apparatus

The experiment was performed by a quadrupole (Q) ICP-MS (Model Agilent 7500a, Hewlett-Packard, Yokogawa Analytical Systems, Tokyo, Japan) with a Babington nebulizer and

Table 1
Optimum operating condition for ICP-MS

ICP-MS plasma	
Rf power	1200 W
Plasma gas flow rate	15 L min ⁻¹
Auxiliary gas flow rate	0.1 L min ⁻¹
Carrier gas flow rate	1.08 L min ⁻¹
Sampling depth	7.0 mm
Sampler/skimmer diameter orifice	Nickel 1.0 mm/0.4 mm
Time-resolved data acquisition	
Scanning mode	Peak-hopping
Dwell time	0.1 s
Points per spectral peak	1
Isotopes	⁵⁰ Cr

the optimum operation conditions are summarized in Table 1. The pH values were controlled with a Mettler Toledo 320-S pH meter (Mettler Toledo Instruments Co. Ltd., Shanghai, China) supplied with a combined electrode. FT-IR spectra (4000–400 cm⁻¹) in KBr were recorded using a 170SX FI-IR (NICOLET, USA). A HL-2 peristaltic pump (Shanghai Qingpu Huxi Instrument Factory, Shanghai, China) was used for the separation/preconcentration process. A home-made PTFE microcolumn (20 mm × 3.0 mm i.d.) with end caps was used in the experiment and a minimum length of PTFE tubing with an i.d. of 0.5 mm was used for all connections in order to minimize the dead volume.

2.2. Standard solutions and reagents

CrCl₃·6H₂O (A.R.), K₂Cr₂O₇ (A.R.) and MnCl₂·4H₂O (A.R.) were purchased from Shanghai Reagent Factory, Shanghai, China. 3-(2-Aminoethylamino) propyltrimethoxysilane was obtained from Wuhan University Chemical Factory, Wuhan, China. HNO₃ (A.R.) was further purified by sub-boiling distillation prior to use. All other chemicals were of analytical reagent grade. The stock solution of Cr(III), Cr(VI) and Mn(II) were prepared using standard methods. Standard solution and test solution were obtained by diluting the stock solution with 2% (v/v) HNO₃. All stock standard solutions were stored in polyethylene bottles in refrigerator held at 4 °C. All glassware were kept in 10% nitric acid for at least 24 h and washed three times with high purity deionized water before use. The pH of the solution was adjusted using nitric acid for pH 0 and 1, sodium acetate/nitric acid for pH 2 and 3, and sodium acetate/acetic acid for pH 4–8. The high purity deionized water (18.2 MΩ cm⁻¹) obtained from a Labconco system (Kansas City, MO, USA) was used throughout this work.

2.3. Contamination control

All laboratory wares were made of polyethylene or polypropylene material and thoroughly cleaned by soaking in 10% nitric acid for at least 24 h. Immediately prior to use, all acid-washed wares were rinsed with high purity deionized water.

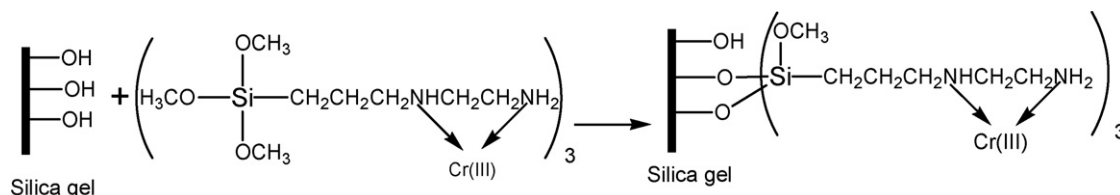


Fig. 1. Scheme for preparation of Cr(III)-imprinted APTS modified silica gel.

2.4. Synthesis of Cr(III)-imprinted silica gel sorbent

The commercially available silica gel (80–120 mesh size), was activated by refluxing with 6 mol L⁻¹ hydrochloric acid for 8 h. It was then filtered, washed with high purity deionized water until free from acid, dried in a furnace at 393 K for 12 h and finally degassed at 373 K under vacuum for 8 h.

To prepare the Cr(III)-imprinted APTS functionalized silica gel sorbent, 1.3325 g of CrCl₃·6H₂O was dissolved in 30 mL of methanol under stirring and then mixed with 3.5 mL of APTS. The solution was stirred and refluxed for 1 h, to which 8 g of activated silica gel was added. After 20 h of stirring and refluxing the mixture, the product was recovered by filtration and then washed with ethanol. Then 50 mL of 6 mol L⁻¹ HCl was used for eluting the Cr(III). The final product was recovered by filtration, washed with high purity deionized water up to the eluent pH 6 and dried under vacuum at 80 °C. The scheme of the reaction is shown in Fig. 1. For comparison, the non-imprinted functionalized silica gel sorbent was also prepared using an identical procedure, but without the addition of CrCl₃·6H₂O.

2.5. General procedure for preconcentration/separation

2.5.1. Static adsorption test

A portion of sample solution containing Cr(III) was transferred into a 50 mL polypropylene tube. After the sample solution was adjusted to the desired pH value with buffer solution, it was diluted to 20 mL with high purity deionized water. Then 20 mg of imprinted silica gel was added, and the mixture was shaken vigorously for 30 min to facilitate adsorption of the metal ions onto the ion-imprinted sorbent. After the solution was centrifuged, the supernatant liquid was diluted and detected by ICP-MS. The adsorption rate of the elements was calculated by subtraction of the concentration between initial sample and the supernatant liquid.

2.5.2. Dynamic adsorption test

A total of 40 mg of imprinted sorbent was filled into the PTFE microcolumn plugged with a small portion of glass wool at both ends. Prior to use, methanol and high purity deionized water were passed through the column in sequence in order to clean it. The column was then conditioned to the desired pH with buffer solution. Test solutions were adjusted to pH 7 for preconcentration/separation total chromium and pH 2 for preconcentration/separation Cr(VI). The amount of Cr(III) was calculated by subtracting total chromium from Cr(VI). The blank solution and the series of standard solution were prepared using the same procedure.

2.6. Constant

The extraction percentage, the distribution ratio, the selectivity coefficient and the relative selectivity coefficient were calculated by the following equations:

$$E(\%) = \frac{C_0 - C_e}{C_0} \times 100, \quad D = \frac{C_0 - C_e}{C_e},$$

$$S = \frac{D_{Cr}}{D_{Mn}}, \quad Sr = \frac{Si}{Sn}$$

$E(\%)$ represents the extraction percentage, C_0 and C_e are the initial and equilibrium concentration of Cr(III), D is the distribution ratio, S represents the selectivity coefficient, D_{Cr} and D_{Mn} represent the distribution ratios of Cr(III) and Mn(II), Sr is the relative selectivity coefficient, and Si and Sn represent the selectivity factor of imprinted sorbent and non-imprinted sorbent, respectively.

2.7. Sample preparation

Tap water was collected in our laboratory. Well water was collected in local temple, Wuhan, China. Lake water was collected from East Lake, Wuhan, China. Immediately after sampling, all water samples were filtered through a 0.45 μm membrane (Tianjing Jinteng Instrument Factory, Tianjin, China) and stored in precleaned polypropylene bottles in a refrigerator at 4 °C until analysis of chromium. The Environmental Water Reference Materials ERMs, GSBZ 50009-88 and GSBZ 50027-94 were provided by the Institute for Reference Materials of Sepa, Beijing, China. Prior to use, the ampoule was broken carefully at the neck and 10 mL of the sample was pipetted into 250 mL volumetric flask and bring to volume using high purity deionized water according to the instructions by the supplier. The sample was further diluted and adjusted to desired pH for analysis.

The blank sample was also prepared by the same procedure described above except that no analytes were added.

3. Results and discussion

3.1. Preparation of the Cr(III)-imprinted APTS modified silica gel sorbent

At the surface of silica gel sorbent, the structure terminates in either siloxane group (≡Si–O–Si≡) with the oxygen atom on the surface, or one of the several forms of silanol groups (≡Si–OH). The silanol groups facilitate the modification of organic groups which covalently bind to the silica surface. Because commercial

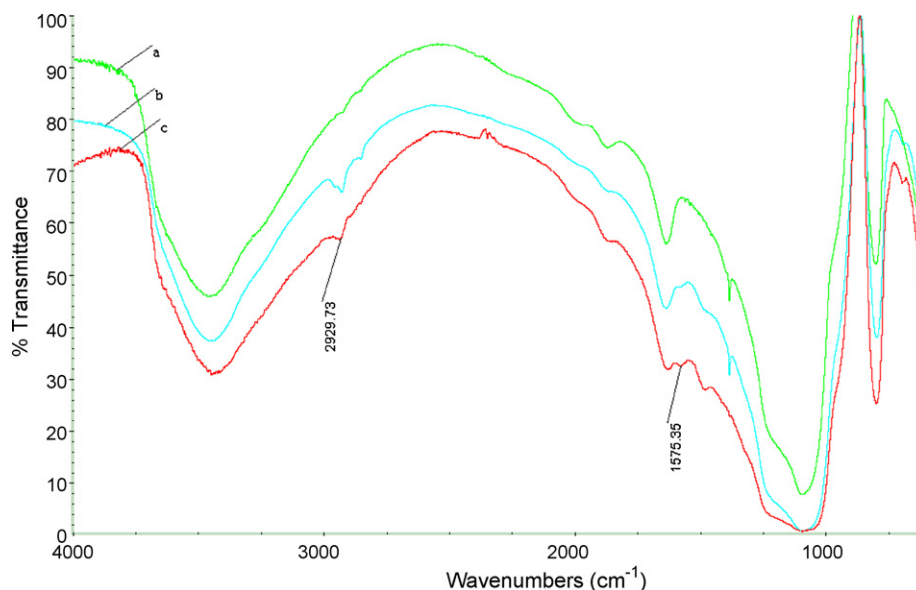


Fig. 2. Infrared spectra of activated silica gel (a), non-imprinted silica gel (b) and Cr(III)-imprinted AAPTS-modified silica gel (c).

silica gel contains a low concentration of surface silanol groups, in this work, concentrated hydrochloric acid was used for the activation of silica gel and increased the silanol groups [37].

In this method, the complex was formed between Cr(III) and AAPTS in methanol solution before cohydrolyzing and cocondensing with the silanol groups. The key of this methodology was to make sure that the activated silica gel surface was grafted with the complex of Cr(III) and AAPTS rather than just the AAPTS. After the remnant Cr(III) and AAPTS were removed by concentrated HCl and methanol, tailor-made cavities for Cr(III) were left on the surface of silica gel sorbent.

3.2. Characteristic of the IR spectra

To ascertain whether AAPTS has been successfully grafted onto the surface of activated silica gel, FT-IR was employed to characterize silica gel (a), non-imprinted silica gel (b) and Cr(III)-imprinted AAPTS modified silica gel (c). As shown in Fig. 2, the different features of the imprinted and non-imprinted sorbents when compared with activated silica gel were N–H band around 1575.35 cm^{-1} and C–H band around 2929.73 cm^{-1} , which indicated that AAPTS has been successfully immobilized to silica gel surface, and both imprinted and non-imprinted sorbents possessed similar component.

3.3. Evaluation of static adsorption

Mn(II) was chosen as the competitive ion with Cr(III) because they were close elements in periodic table and had very similar

ionic radius. In their binary mixture, the pH of solution was adjusted to 7, these two metal ions had the same concentration of $5\text{ }\mu\text{g mL}^{-1}$ and the sorbent was 20 mg. Table 2 summarized the percentage extraction, distribution ratios, selectivity coefficients and relative selectivity coefficient of Cr(III) and Mn(II) using non-imprinted and Cr(III)-imprinted sorbents. It is obvious that the distribution ratios and selectivity coefficients of imprinted sorbent are much higher than that of non-imprinting sorbent for Cr(III). The results indicated that the imprinted modified silica gel sorbent had higher selectivity for Cr(III) in the presence of Mn(II).

To measure the static adsorption capacity, 40 mg of imprinted or non-imprinted sorbent was equilibrated with 50 mL of various concentrations of Cr(III) solutions at pH 7. The adsorption capacity increased as the initial Cr(III) concentration was increased until the plateau were obtained. The static adsorption capacities of the ion-imprinted and non-imprinted sorbent for Cr(III) were 13.4 mg g^{-1} and 30.5 mg g^{-1} , respectively. The results indicated that the ion-imprinted sorbent has a higher static adsorption capacity for Cr(III) than non-imprinted sorbent.

3.4. Effect of pH

The effect of pH on the retention of Cr(III) and Cr(VI) on imprinted sorbent were investigated separately with the microcolumn operation mode. 20 mL of Cr(III) and Cr(VI) solutions with concentration of 5 ng mL^{-1} were prepared separately and pH values of sample solutions were adjusted to a range of 0–8 with buffer solution and passed through the

Table 2

Percentage extraction, distribution ratios, selectivity coefficients and relative selectivity coefficient of non-imprinted and leached Cr(III)-imprinted silica gel sorbent

Elements	<i>E</i> (%)		<i>D</i>		<i>S</i>		<i>Sr</i>
	Non-imprinted	Imprinted	Non-imprinted	Imprinted	Non-imprinted	Imprinted	
Cr	96.1	99.8	24.64	499	–	–	16.5
Mn	34.6	39.4	0.53	0.65	46.49	767.69	

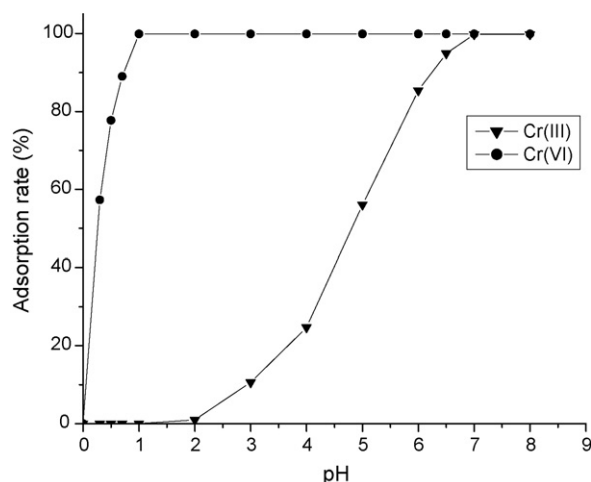


Fig. 3. Effect of pH on the adsorption percentage (%) of Cr(III) and Cr(VI). Sample volume: 20 mL. Cr(III) and Cr(VI) concentration: 5 ng mL⁻¹.

microcolumn. The retained ions were stripped off from the column by 1 mol L⁻¹ HNO₃ and determined by ICP-MS as described in the recommended procedure. Fig. 3 was the effect of pH on the adsorption percentage of Cr(III) and Cr(VI). As can be seen, there is almost no adsorption of Cr(III) when the pH was below 2, the absorption of Cr(III) was increased with the increase of the sample pH from 2 to 6.5 and quantitative adsorption (>95%) could be obtained in the pH range of 6.5–8. For the absorption of Cr(VI), its adsorption percentage was increased sharply with the increase of pH from 0.3 to 0.8 and the absorption percentage remained constant (>95%) with further increase of pH to 8. The different pH trend made it possible to separate Cr(III) and Cr(VI) at low pH. In this work, a pH of 2 was selected for determination of Cr(VI) and a pH of 7 was selected for determination of total chromium. The amount of Cr(III) was obtained by subtracting total chromium of Cr(VI).

The result could be explained by the different absorption mechanism of the Cr(III) and Cr(VI) on imprinted silica gel sorbent. At low pH values, Cr(III) exists as its kinetically inert aquacomplex Cr(H₂O)₃³⁺. As the pH increases, the coordinated water is displaced by the more reactive OH⁻ [38], rendering the former complex to a more labile form (Cr(H₂O)₂OH²⁺ or Cr(H₂O)(OH)²⁺), which allows for better reactivity with chelating group of -NHCH₂CH₂NH₂ on the surface of imprinted sorbent. In the pH range of 1–8, the -NHCH₂CH₂NH₂ is abundant of positive charge and is similar to weak-base anion-exchange resin, thus most of the Cr(VI) could be retained on the surface of imprinted silica gel by electrostatic effect. Because in such pH range, Cr(VI) exist in the form of CrO₄²⁻ or HCrO₄⁻ and can be adsorbed by -NHCH₂CH₂NH₃⁺. If the pH was further decreased, the HCrO₄⁻ would further transform to H₂CrO₄, which cannot be retained on the sorbent.

By these mechanisms, the speciation analysis of chromium was feasible while no reduction/oxidation reagent was required.

3.5. The optimization of elution conditions

From Fig. 3, it could be concluded that the adsorption of Cr(III) below pH 2 could be negligible. HNO₃ is a recom-

mended acid for ICP-MS detection and the functional group of -NHCH₂CH₂NH₂ is stable at least in 1 mol L⁻¹ HNO₃ [35]. For this reason, 0.5 mL of various concentrations of HNO₃ were studied independently for the desorption of adsorbed Cr(III) and Cr(VI). The results indicated that 0.1 mol L⁻¹ HNO₃ and 1.0 mol L⁻¹ HNO₃ was sufficient for complete elution of Cr(III) and Cr(VI). Furthermore, imprinted sorbent can withstand as high as 2 mol L⁻¹ HNO₃ with a satisfactory recovery for the target analyte. Therefore, 1.0 mol L⁻¹ HNO₃ was chosen as eluent in subsequent experiments.

3.6. Elution volume and elution flow rate

The effect of elution volume for quantitative elution of the studied chromium species was investigated separately. It was demonstrated that 0.5 mL of elution solution containing 1.0 mol L⁻¹ HNO₃ was sufficient to recover both Cr(III) and Cr(VI) quantitatively.

The effect of elution flow rate on recovery of both analytes was investigated by keeping the elution volume of 0.5 mL, 1.0 mol L⁻¹ HNO₃. The result indicated that both species of chromium could be recovered quantitatively (above 90%) at flow rate range of 0.5–1.5 mL min⁻¹. Consequently, elution flow rate of 1.0 mL min⁻¹ was selected in this experiment.

3.7. Sample flow rate and sample volume

The sample flow rate should be optimized to ensure quantitative retention along with minimization of the time required for sample processing. It was found that, with the increase in flow rate from 0.5 mL min⁻¹ to 2.0 mL min⁻¹, the recoveries of both chromium species decrease slowly, but still above 95%. In this work, sample flow rate of 2.0 mL min⁻¹ was selected.

In order to investigate the breakthrough volume, the sample solutions of 10 mL, 20 mL, 30 mL, 40 mL and 50 mL containing 0.1 µg of Cr(III) or Cr(VI) were prepared and then operated according to the general procedure. It was found that the analytes could be quantitatively retained (above 90%) when sample volumes were less than 30 mL. To trade-off the enrichment factor and analytical speed, a sample volume of 20 mL and an elution volume of 0.5 mL were used, so that an enrichment factor of 40 was obtained in this work.

3.8. Effect of coexisting ions

The effects of common coexisting ions were investigated. In these experiments, solutions of 5 ng mL⁻¹ of Cr(III) or Cr(VI) and the added interfering ions were treated according to the procedure described in dynamic adsorption test. The tolerance of the coexisting ions, defined as the largest amount making the recovery of the studied elements less than 90%, are given in Table 3. It can be seen that the presence of major cations and anions have no obvious influence on the determination of both Cr(III) and Cr(VI) under the selected conditions, which shows that the Cr(III)-imprinted APTS modified silica gel sorbent has a good selectivity for Cr(III) and is suitable for the analysis of samples with complicated matrix.

Table 3
Tolerance of the coexisting ions

Coexisting ions	Tolerance limit of ions ($\mu\text{g mL}^{-1}$)	
	Cr(III)	Cr(VI)
K^+ , Na^+	10,000	2000
Ca^{2+} , Mg^{2+}	1000	1000
Al^{3+}	800	800
Zn^{2+}	1000	1000
Fe^{3+}	100	100
Cl^-	10,000	2000
NO_3^-	2000	1000
H_2PO_4^-	1000	1000
CH_3COO^-	1000	1000
SO_4^{2-}	3000	1000

There are three possible factors for the selectivity of Cr(III) [30]. One is the functional group inherent selectivity; double amino group of $-\text{NHCH}_2\text{CH}_2\text{NH}_2$ has good affinity toward Cr(III). The second is the hole-size selectivity. That is, the size of Cr(III) exactly fits the cavity of the Cr(III)-imprinted silica gel sorbent. The third is the coordination-geometry selectivity because the Cr(III)-imprinted sorbent can provide the ligand groups arranged in a suitable way required for coordination of Cr(III) ion. For Cr(VI), it could be interpreted that weak-base anion-exchange resin which have functional group of $-\text{NH}_2$, have better affinity for CrO_4^{2-} than other anion such as NO_3^- and Cl^- [39]. Moreover, the imprinted sorbent possessed high adsorption capacity for CrO_4^{2-} and thus Cr(VI) could be quantitative recovered in complicated matrix which was validated by further experiment on adsorption capacity.

3.9. Dynamic adsorption of Cr(III) and Cr(VI) by the imprinted silica gel sorbent

The adsorption capacity is an important factor, because it determines how much imprinted sorbent is required to quantitatively concentrate the analytes from a given solution. The capacity study method used was adapted from that recommended by Maquieira et al. [40]. 50 mL aliquots of a series of concentrations were adjusted to the appropriate pH, then pre-concentrated and eluted. The eluent were diluted and determined by ICP-MS. The amount of Cr(III) and Cr(VI) adsorbed at each concentration level were determined and the adsorption capacity of imprinted sorbent for Cr(III) and Cr(VI) were 33.4 mg g^{-1} and 11.7 mg g^{-1} , respectively. Table 4 is the comparisons of adsorption capacity for Cr(III) and Cr(VI) obtained by different SPE materials. As could be seen, the adsorption capacity for Cr(III) and Cr(VI) obtained by Cr(III)-imprinted AAPTS modified silica gel sorbent is comparable with that obtained by other reported SPE materials [6,13–15].

3.10. Figures of merit for the imprinted sorbent

The main isotopes of chromium are ^{50}Cr (4.35%), ^{52}Cr (83.79%), ^{53}Cr (9.50%) and ^{54}Cr (2.36%). Although a much higher sensitivity can be obtained when using ^{52}Cr or ^{53}Cr , the interference caused by $^{40}\text{Ar}^{12}\text{C}$, $^{40}\text{Ar}^{13}\text{C}$, $^{36}\text{Ar}^{16}\text{O}$, $^{36}\text{Ar}^{17}\text{O}$,

Table 4
Comparisons of adsorption capacity of different SPE materials for Cr(III) and Cr(VI)

SPE material	Adsorption capacity		Reference
	Cr(III) (mg g^{-1})	Cr(VI) (mg g^{-1})	
Chromium(III)-imprinted silica gel	33.4	11.7	This work
Cr(III)-imprinted polymeric beads	69.28	–	[6]
Multiwalled carbon nanotubes	–	9.50	[13]
Crosslinked chitosan-bound FeC nanoparticles	10.5	–	[14]
Immobilized moss	11.5	–	[15]

$^{35}\text{Cl}^{17}\text{O}$ and $^{35}\text{Cl}^{18}\text{O}$ cannot be ignored because they have mass-to-charge ratio of 52 and 53. Therefore, the mass 50 was used for the quantification of the analyte and the study of the values of interest.

Compared to reported Cr(III)-imprinted polymeric beads sorbent in literature [6], the adsorption time was shortened from 30 min to 10 min and desorption time was greatly shortened from 2 h to 30 s. The detection limit of Cr(III) was also improved from 1.2 ng mL^{-1} to 4.43 pg mL^{-1} and the detection limit of Cr(VI) was 8.30 pg mL^{-1} (calculated by 3 s of the blank value). The precision (R.S.D.) for seven-replicate solid-phase extractions of 0.5 ng L^{-1} Cr(III) and Cr(VI) were 4.44% and 4.41%, respectively. The imprinted silica gel sorbent also offered good linearity ($R^2 = 0.9994$) for solid-phase extraction of trace chromium. Table 5 is the comparison of the detection limits of this work with other literature works on the speciation of chromium [6–12] in environmental water samples. As could be seen, the detection limit obtained by this work is the lowest one for both Cr(III) and Cr(VI). It should be noted that most sorbents in these literatures can only adsorb one chromium species and thus some reduction/oxidation reagent was needed. Compared with these literature works which take 1 h or so for complete reduction/oxidation, the proposed method does not require any reduction/oxidation and the total time for speciation of chromium is reduced.

The regeneration is one of the key factors in evaluating the performance of the adsorption material. The column packed with imprinted sorbent can be reused for more than 100 times when the concentration of HNO_3 in the eluting agent is 1.0 mol L^{-1} , which indicates that the material has good stability under acidic conditions.

3.11. Validation and applications

In order to establish the validity of the proposed procedure, the method has been applied to the determination of total chromium content and Cr(VI) in certified reference materials (GSBZ 50009-88 and GSBZ 50027-94) and the results are listed in Table 6. As could be seen, a good agreement between determined values and the certified values were obtained. Furthermore, the proposed method was successfully applied to the speciation of chromium in environmental water samples and the results are given in Table 7.

Table 5
Comparisons of analytical technique, detection limit and samples for speciation analysis of chromium.

Analytical technique	SPE material	Sample volume (mL)	Enrichment factor	Detection limit (ng mL ⁻¹)		Application	Reference
				Cr(III)	Cr(VI)		
ICP-MS	Cr(III)-imprinted silica gel	20	40	0.004	0.008	Lake/tap/well water	This work
FAAS	Cr(III)-imprinted polymeric beads	100	267	1.2	–	Environmental/industrial water	[6]
Spectrophotometry	Sawdust	250	100 and 80	50	40	Lake/river water	[7]
ICP-MS	Minodiacetate resin	7	11.5	0.02	–	Seawater	[8]
ETAAS	Activated carbon	10	35	0.003	–	Drinking water	[9]
ICP-OES	Activated carbon	25	70	0.029	–	Parenteral solution	[10]
Spectrophotometry	Polystyrene anion exchange resin	12	26.5	–	0.05	Surface water	[11]
ICP-OES	Iminodiacetate resin	5	10	0.08	0.15	River/tap/waster water	[12]

Table 6
Analytical results of chromium in certified materials of GSBZ 50009-88 and GSBZ 50027-94 (mean ± S.D., *n* = 3)

Sample	Element	Certified (μg mL ⁻¹)	Determined (μg mL ⁻¹)	<i>t</i> -Test ^a
GSBZ 50009-88	Cr (total)	1.49 ± 0.06	1.47 ± 0.09	0.57
GSBZ 50027-94	Cr(VI)	0.12 ± 0.005	0.12 ± 0.001	0.00

^a *t*_{0.05,2} = 4.30.

Table 7
Analytical results of chromium speciation in three environmental water samples (mean ± S.D., *n* = 3)

Samples	Total Cr (ng mL ⁻¹)	Cr(VI) (ng mL ⁻¹)	Cr(III) ^a (ng mL ⁻¹)
Tap water	0.86 ± 0.02	0.39 ± 0.03	0.47 ± 0.02
Lake water	1.49 ± 0.03	0.64 ± 0.02	0.85 ± 0.02
Well water	0.80 ± 0.01	0.32 ± 0.01	0.48 ± 0.01

^a Cr(III) is calculated as the difference between the concentration of total chromium and Cr(VI).

4. Conclusions

In this paper, a simple procedure for the synthesis of Cr(III)-imprinted AAPTS modified silica gel sorbent was developed by a surface imprinting technique. The prepared imprinted sorbent exhibits better selectivity for Cr(III) than Mn(II) and could also enrich Cr(VI) at a low pH, which make it feasible for the speciation of Cr(III) and Cr(VI) without adding any reduction/oxidation reagent. Moreover, it shows other good characteristics such as good stability under acidic conditions, fast adsorption and desorption kinetics, large adsorption capacity and good tolerance to foreign ions, making it an ideal solid-phase extraction sorbent for the speciation analysis of chromium in environmental water samples.

Acknowledgments

The authors would like to thank Science Fund for Creative Research Groups of NSFC (no. 20621502), National Nature Science Foundation of China (no. 20575048), NCET-04-0658, MOE of China for their financial support.

References

- [1] C. Barnowski, N. Jakubowski, D. Stuewer, J. Anal. Atom. Spectrom. 12 (1997) 1155.
- [2] R.A. Gil, S. Cerutti, J.A. Gásquez, R.A. Olsina, L.D. Martínez, Talanta 68 (2006) 1065.
- [3] V. Gómez, M.P. Callao, Trends Anal. Chem. 25 (2006) 1006.
- [4] X.L. Pu, B. Hu, Z.C. Jiang, C.Z. Huang, Analyst 130 (2005) 1175.
- [5] O.T. Butler, J.M. Cook, C.F. Harrington, S.J. Hill, J. Rieuwerts, D.L. Miles, J. Anal. Atom. Spectrom. 22 (2007) 187.
- [6] E. Birlik, A. Ersöz, E. Açikkalp, A. Denizli, R. Say, J. Hazard. Mater. 140 (2007) 110.
- [7] S.Q. Memon, M.I. Bhangar, M.Y. Khuhawar, Anal. Bioanal. Chem. 383 (2005) 619.
- [8] S. Hirata, K. Honda, O. Shikino, N. Maekawa, M. Aihara, Spectrochim. Acta B 55 (2000) 1089.
- [9] R.A. Gil, S. Cerutti, J.A. Gásquez, R.A. Olsina, L.D. Martínez, Talanta 68 (2006) 1065.
- [10] R.A. Gil, S. Cerutti, J.A. Gásquez, R.A. Olsina, L.D. Martínez, Spectrochim. Acta B 60 (2005) 531.
- [11] H. Cui, R.H. He, J.H. Wang, Talanta 70 (2006) 139.
- [12] T. Sumida, T. Ikenoue, K. Hamada, A. Sabarudin, M. Oshima, S. Motomizu, Talanta 68 (2005) 388.
- [13] M. Tuzen, M. Soylak, J. Hazard. Mater. 147 (2007) 219.
- [14] Y.W. Wu, Y.Y. Jiang, D.Y. Han, F. Wang, J.X. Zhu, Microchim. Acta 159 (2007) 333.
- [15] M.V. Balarama Krishna, K. Chandrasekaran, S.V. Rao, D. Karunasagar, J. Arunachalam, Talanta 65 (2005) 135.
- [16] Y. Martínez-Bravo, A.F. Roig-Navarro, F.J. López, F. Hernández, J. Chromatogr. A 926 (2001) 265.
- [17] M. Derbyshire, A. Lamberty, P.H.E. Gardiner, Anal. Chem. 71 (1999) 4203.
- [18] I.I. Stewart, J.W. Olesik, J. Chromatogr. A 872 (2000) 227.
- [19] C.F. Poole, Trends Anal. Chem. 22 (2003) 362.
- [20] X.J. Chang, N. Jiang, H. Zheng, Q. He, Z. Hu, Y.H. Zhai, Y.M. Cui, Talanta 71 (2007) 38.
- [21] N. Jiang, X.J. Chang, H. Zheng, Q. He, Z. Hu, Anal. Chim. Acta 577 (2006) 225.
- [22] K. Haupt, Analyst 126 (2001) 747.
- [23] T.P. Rao, S. Daniel, J.M. Gladis, Trends Anal. Chem. 23 (2004) 28.
- [24] S.Y. Bae, G.L. Southard, G.M. Murray, Anal. Chim. Acta 397 (1999) 173.
- [25] S. Daniel, P.E.J. Babu, T.P. Rao, Talanta 65 (2005) 441.
- [26] J. Na, X.J. Chang, Z. Hong, H. Qun, H. Zheng, Anal. Chim. Acta 577 (2006) 225.
- [27] D.M. Han, G.Z. Fang, X.P. Yan, J. Chromatogr. A 1100 (2005) 131.
- [28] H. Zheng, D. Zhang, W.Y. Wang, Y.Q. Fan, J. Li, H.P. Han, Microchim. Acta 157 (2007) 7.
- [29] A. Ersöz, R. Say, A. Denizli, Anal. Chim. Acta 502 (2004) 91.
- [30] G.Z. Fang, J. Tan, X.P. Yan, Anal. Chem. 77 (2005) 1734.
- [31] F. Li, H.Q. Jiang, S.S. Zhang, Talanta 71 (2007) 1487.

- [32] Q. He, X.J. Chang, H. Zheng, N. Jiang, Z. Hu, Y.H. Zhai, *Chem. Anal.* 51 (2006) 715 (Warsaw, Poland).
- [33] I. Fujiwara, A. Uchiyama, Y. Sasaki, M. Maeda, M. Takagi, *Bunseki Kagaku* 52 (2003) 147.
- [34] N. Zhang, B. Hu, C.Z. Huang, *Anal. Chim. Acta* 597 (2007) 12.
- [35] S. Dai, M.C. Burleigh, Y.H. Ju, H.J. Gao, J.S. Lin, S.J. Pennycook, C.E. Barnes, Z.L. Xue, *J. Am. Chem. Soc.* 122 (2000) 992.
- [36] C. Airoidi, Y. Gushikem, J.G.P. Espínola, *Colloids Surf.* 17 (1986)317.
- [37] P.K. Jal, S. Patel, B.K. Mishra, *Talanta* 62 (2004) 1005.
- [38] G.Z. Tsogas, D.L. Giokas, A.G. Vlessidis, N.P. Evmiridis, *Spectrochim. Acta B* 59 (2004) 957.
- [39] J.A. Dean, *Analytical Chemistry Handbook*, Science Press, 2003, pp. 4.72–4.76.
- [40] A. Maquieira, H.A.M. Elmahadi, R. Puchades, *Anal. Chem.* 66 (1994) 3632.